

Sandra Raquel de Sousa Monteiro

LOAD DISTRIBUTION ON TIMBER-CONCRETE COMPOSITE FLOORS

PhD Thesis in Civil Engineering, branch of Structures, supervised by Professor Alfredo Manuel Pereira Geraldes Dias and by Professor Sérgio Manuel Rodrigues Lopes and submitted to the Faculty of Sciences and Technology of the University of Coimbra

July, 2015



UNIVERSIDADE DE COIMBRA

Sandra Raquel de Sousa Monteiro

LOAD DISTRIBUTION ON TIMBER-CONCRETE COMPOSITE FLOORS

PhD Thesis in Civil Engineering, branch of Structures, supervised by Professor Alfredo Manuel Pereira Geraldes Dias and by Professor Sérgio Manuel Rodrigues Lopes and submitted to the Faculty of Sciences and Technology of the University of Coimbra

July, 2015



UNIVERSIDADE DE COIMBRA

Á minha família.

“In the entire history of the human race, every truth began as a blasphemy, and no one has ever made a contribution of any real worth without self-sacrifice, personal suffering and sometimes even death.”

Martin Sheen

ABSTRACT

The main objective of this research is the analysis of timber-concrete composite slabs, with particular focus on the transversal distribution of internal forces and stresses when concentrated external loads are applied to these structures. More specifically, the essential aim of this work is to understand the manner in which a load, particularly a concentrated load, applied to a slab is transmitted to each supporting element across the main beams of the slab.

Although concentrated, point or line loads are common load cases in slabs, consequence of heavy items, such as furniture or equipment or walls parallel to the beams longitudinal axis, their effects are not completely understood, with few studies available in literature. Concerning timber-concrete composite slabs, the knowledge is even more scarce. Hence, the importance of investigating these aspects of the structural behavior and developing technical design rules is evident.

This doctoral research was based in numerical modeling and in experimental tests. Three numerical models, based on different finite elements were developed and their results were compared. The numerical results were also compared with those obtained from some preliminary experimental tests complemented with the computational work using the analytical method developed by Guyon-Massonnet, known as Distribution Coefficients Method. Through this procedure, the models were validated and the most adequate one was chosen to perform the parametric study.

Experimental tests were performed on specimens at real scale. For this purpose, five composite specimens with different characteristics were built. A different parameter whose effect on the load distribution was intended to be analyzed was associated to each one of them. The parameters that were studied were the influence of the concrete type (normal weight *vs.* light-weight), the span length and the thickness of the concrete layer. The experimental specimens were subjected to concentrated loads at different positions one at a time. The point loads were applied at mid- and quarter-span of the beams and the line loads were applied aligned with the longitudinal direction of the beams.

Beyond the increasing of the knowledge on the transversal distribution of load, this investigation intended to develop an expedite tool that would reflect the correct behavior of this kind of structures under concentrated loads. Through the numerical and experimental results it was possible to identify the parameters with the greatest effect on the transversal distribution of concentrated loads on these floors and subsequently an analysis of sensitivities was also carried out. This led to the development and the suggestion of a simplified equation

ABSTRACT

capable of predicting the percentage of load received by each beam in timber-concrete composite slabs when subjected to concentrated loads. This percentage is a function of the span, the beam position at the slab and the thickness of the concrete layer.

The developments from this investigation can be applied in the design of timber-concrete composite structures under concentrated loads. It is expected that the rules proposed here can be adopted in design codes, such as Eurocode 5. Since these kind of structures and loading are rather frequent in rehabilitation works, an improving on the knowledge will be reflected on the price of the final work. Naturally, the lack of knowledge on the behavior of structures under a certain circumstances will force to solve the problem by considering the least favorable approach, therefore corresponding to expensive solutions. If more knowledge is available, the design can be optimized, therefore, more economical.

Keywords: Timber-concrete composite floors; Point and line loads; Transversal distribution of point and line loads; Experimental tests; Numerical modeling.

RESUMO

O objectivo principal da presente investigação centra-se na análise de lajes mistas madeira-betão, com particular enfoque na distribuição transversal de esforços internos e tensões nestas estruturas quando sujeitas a forças concentradas. Mais especificamente, o objectivo essencial deste trabalho consiste em compreender a forma como uma carga, especificamente uma carga concentrada, aplicada a uma laje é transmitida para cada elemento de apoio através das vigas principais da laje.

Apesar dos carregamentos concentrados, pontuais ou de faca, serem casos de carga comuns em lajes, consequência de elementos pesados, tais como, mobiliário, equipamentos ou paredes paralelas ao eixo longitudinal das vigas, os efeitos decorrentes não se conhecem completamente, com escassos estudos que lhes digam respeito. Estes estudos são ainda mais escassos quando se considera o tipo de elemento misto em estudo. Como tal, torna-se evidente a importância de esclarecer e investigar estes aspectos do comportamento da estrutura e desenvolver regras de dimensionamento.

Esta investigação baseou-se essencialmente na modelação numérica e em ensaios laboratoriais. Três modelos numéricos, baseados em diferentes elementos finitos foram desenvolvidos e os respectivos resultados comparados entre si. Estes foram ainda comparados com resultados de alguns ensaios experimentais preliminares e complementados com trabalho computacional usando os resultados do método analítico desenvolvido por Guyon-Massonnet, também conhecido como Método dos Coeficientes de Distribuição. Este procedimento permitiu validar e escolher o modelo com o qual se procedeu posteriormente ao estudo paramétrico.

Os ensaios experimentais foram realizados em provetes à escala real. Para tal, construíram-se cinco pavimento mistos com diferentes características cujo efeito na distribuição de cargas se pretendia apurar, nomeadamente o tipo de betão (regular vs. leve), o vão e a espessura da camada de betão. Os provetes foram sujeitos a cargas concentradas, pontuais e de faca, localizadas em diferentes posições, meio ou quarto de vão ou alinhadas com a direcção longitudinal das vigas, respectivamente.

Além de aumentar o conhecimento acerca da distribuição transversal de cargas, esta investigação pretende desenvolver uma ferramenta expedita capaz de reflectir correctamente o comportamento deste tipo de estruturas quando sujeitas a cargas concentradas. Assim, através dos resultados numéricos e experimentais obtidos foi possível identificar os parâmetros com maior influência sobre a distribuição transversal de cargas concentradas nestes pavimentos e

subsequentemente efectuar uma análise de sensibilidades. Tal permitiu desenvolver e sugerir uma equação simplificada de avaliação da percentagem de carga recebida por cada viga em lajes mistas madeira-betão sujeitas a cargas concentradas. Esta percentagem é função do vão, da posição da viga na laje e da espessura da camada de betão.

Os desenvolvimentos desta investigação podem ser utilizados no dimensionamento de estruturas mistas madeira-betão sujeitas a carregamentos concentrados. Espera-se que as propostas aqui sugeridas possam ser adoptadas na regulamentação de dimensionamento, como é o caso do Eurocódigo 5. Sendo este tipo de estruturas e carregamento bastante frequentes em trabalhos de reabilitação, o aumento do conhecimento nesta área reflectir-se-á no preço final da construção. A falta de conhecimento acerca do comportamento das estruturas sujeitas a determinadas circunstâncias terá como consequência a adopção de abordagens menos favoráveis por parte do projectista, e consequentemente ao aumento dos custos das soluções correspondentes. Se o conhecimento disponível for maior, o dimensionamento poderá ser optimizado tornando-se, consequentemente, mais económico.

Palavras-chave: Pavimentos mistos madeira-betão; Cargas concentradas: pontuais e de faca; Distribuição transversal de cargas concentradas; Ensaios experimentais; Modelação numérica.

ACKNOWLEDGEMENTS

I would like to express my sincerest gratitude to my scientific supervisors without whom this work could not be produced. To Prof. Alfredo M. P. G. Dias for his involvement in the investigation, his capacity to challenge and put questions to me, and by his altruism and friendship. To Prof. Sérgio M. R. Lopes by his involvement in the investigation, assistance and friendship.

I would also like to thank the colleagues Mr. Carlos Martins, Mr. André Marques, Dr. Joao Nuno Rodrigues and Mr. Pedro Santos by their valuable help during the experimental program. They were always available after hours, on weekends and on holidays. I would also like to thank their friendship. To the laboratorial technicians Mr. Edmundo Pais, Mr. José António Lopes, Mr. Ilídio Santos I would like to thank their assistance and help during the laboratorial tasks. I would also like to extend my thanks to Prof. Fernando Branco by providing cork residues used in the light-height aggregate concrete and, together with Prof. Rui Simões for borrowing some equipment to the experimental investigation. Thanks also to Mr. Hugo Caetano, Mr. Rafael Campos, Mr. Rui Ferreira and Mr. Luís Gaspar by their assistance and fellowship at the laboratory.

I also wish to thank Mr. Luís Moreira and Mr. Noel Varela by providing the cement and the concrete needed to build the experimental specimens, on behalf of *SECIL*; Mr. Nelson Batista by providing the steel mesh and rods, in representation of *Fapricela*; Mr. Pedro Sousa by providing the mold release agent, in representation of *Sika*.

I would also like to thank the sponsors of this research work: the Portuguese Foundation for Science and Technology (*FCT*), the Operational Program for Science and Innovation and the *COMPETE* – Operational Program for Competitiveness Factors both co-financed by the European Union Fund *FEDER* through the research projects FCOMP-01-0124-FEDER-PTDC/ECM/099833/2008 and Pest-C/EME/UI0285/ 2013, respectively.

By their inestimable help in many tasks during the development of this work, I want to show my gratitude to Dr. Telmo Morgado, Mr. Nuno Almeida, Mrs. Anabela Reis, Mrs. Isabel França, Prof. Ana Amaro Martins and all the persons that made this work possible.

Particularly to my family in the persons of my parents and sister, I wish to thank the education and the values they have passed me, which together with the love that unite us made the journey possible. During the thesis they have always encouraged me. And lastly, to my beloved husband and colleague, always encouraging me and supporting me as a friend and as a researcher, thank you very much.

ACKNOWLEDGEMENTS

SYMBOLS
Latin upper case letters

A_i	Cross-sectional area of the part i
B	Half width of the slab
B_i	Beam number i
C	Denotes the strength of normal weight concrete
C_{slab}	Total compressive force in the slab
D	Thin plate flexural rigidity
DF_i	Distribution factor at the beam i , with $i = ext$ for external beams and $i = int$ for internal beams
D_{med}	Mean diameter
E	Modulus of elasticity
E_c	Tangent modulus of elasticity of normal weight concrete at a stress of $\sigma_c = 0$ and at 28 days
E_i	Modulus of elasticity in major axis for the i element
$E_{m,g}$	Global modulus of elasticity in bending
E_x	Modulus of elasticity in major axis
E_y	Modulus of elasticity in minor axis
EI	Bending stiffness
F	Force
Fx	Fixed support
F_{beam}	Maximum load effect (moment or shear) in a single member
F_{max}	Ultimate load, Failure load
F_{system}	Maximum load effect (moment or shear) in the system
G	Bending stiffness parameter
H	The greatest height of a non-prismatic beam
I	Second moment of area, moment of inertia
K	Shear stiffness
$K(y)$	Transversal distribution coefficient, function of the y coordinate
K_α	Transversal distribution coefficient defined as a function of α
K_i	Transversal distribution coefficient when $\alpha = i$
K_8	Load sharing factor

SYMBOLS

L	Span length
LC	Denotes the strength of light-weight concrete
LCi	Load cell at point i
L_e	Equivalent span
Ln	Linear load
L_p	Distance between the nearest support of the slab and the center of the loaded area
M_{beam}	Bending moment in a beam representing a plate
$M_{comp,i}$	Bending moment in the composite girder i
$M_{max,beam}$	Maximum bending moment in a beam representing a plate
M_{sd}	Maximum sagging bending moment
$MVDi$	Mid-span vertical displacement at point i
N_L	Number of traffic lanes
P, Pt	Point load
Pr	Polynomial approximation of the distribution percentage associated with the loaded beam
$QVDi$	Quarter-span vertical displacement at point i
R	Correlation coefficient
R^2	Coefficient of determination
S	Distance between stringers
SDi	Slip displacement at point i
UPi	Uplift displacement at point i
W	Deflection
$W(y)$	Deflection, function of the y coordinate
W_0	Average deflection
Y	Yielding force
Z_i	Value of the parameter variation curve for the point i
\bar{Z}	Average of the values to approximated

Latin lower case letters

a	Initial stiffness
a_i	Coefficients of the polynomial approximation, $a_i = \{a_0, a_1, a_2, \dots, a_{11}, a_{12}\}$
a_m	Length over which the concentrated load is assumed to be distributed
a_p	Length of the rectangular ($a_p \times b_p$) loaded area
b	Width
b_{eff}	Total effective width

$b_{eff,i}$	Partial effective width of the concrete flange on each side of the web, with $i = e$ at left and $i = d$ at right, i can also take the value 1 or 2 associated with each side of the web
b_{em}	Effective width of a composite slab considering angular dispersion through the slab layers
b_i	Half distance between the beam axis and the adjacent beam
b_{ic}	Distance from the beam axis to the slab end
b_l	Beam location
b_m	Width over which the concentrated load is assumed to be distributed
b_p	Width of the rectangular ($a_p \times b_p$) loaded area
b_{slab}	Sum of two b_i on each side of the beam
b_t	Width of the timber beam
$b_{t,i}$	Width of the timber beam at the section i
b_w	Web width
$b_{w,p}$	Width of the loaded area on the contact surface of the deck plate
$b_{w,p,middle}$	Width of the loaded area referred to the middle plane of the deck plate
b_0	Distance between the centers of the outstand shear connectors
c	Relation between the numerical vertical displacements at three quarters of span and at mid-span
c_{fi}	Coefficient associated with the Pr polynomial with $i = \{bm, vd, sr\}$
c_0	Distance between the m principal longitudinal beams
d_{eff}	Distribution width
d_{iso}	Distribution width ignoring the timber panel orthotropy
d_{ortho}	Distribution width considering the timber panel orthotropy
d_p	Distance between the centroidal axis of the profiled steel sheeting and the extreme fiber of the composite slab in compression
dy	Infinitesimal change in y
e	Eccentricity
e	Neper number
$f_{c,cube,max}$	Compressive strength of concrete cube at failure
f_{cm}	Mean value of concrete cylinder compressive strength
$f(x)$	Function of x
g	The lowest height of a non-prismatic beam
h	Slab thickness; Cross section height; Homogeneous (when associated with the strength of glued laminated timber)
h_c	Thickness of concrete above the main flat surface of the top of the ribs of the

SYMBOLS


	sheeting or above the beams
h_f	Thickness of finishes
h_i	Thickness of the interlayer
hK	High slip modulus
h_p	Overall depth of the profiled steel sheeting excluding embossments
h_t	Height of the timber beam
$h_{t,i}$	Height of the timber beam at the section i
i	Element number, $i = 1, 2, \dots, n$;
j	Coefficient associated with the calculation of the effective width, depending on effort type (vertical shear or bending) and on the span type (exterior, interior...)
k	Ratio between the simple shear stiffness and the connector spacing
k_s	Shear connection modulus
k_{sys}	System strength factor
lK	Low slip modulus
l_0	Distance between the n secondary/bracing beams
m	Number of principal longitudinal beams
mK	Medium slip modulus
m_{plate}	Bending moment in a plate per unit length
$m_{max,plate}$	Maximum bending moment in a plate
n	Total number of elements; Number of secondary/bracing beams
$p(x)$	Distributed line load acting parallel to the XX axis, function of the x coordinate
$p_0(x)$	Uniformly distributed load over the all width of the slab, function of the x coordinate
p_1	Constant related with the load $p(x)$
q	Force per unit width of slab
r	Distance between the midplanes of the concrete slab and the timber beam
s	Mean spacing between connectors
s_b	Beams spacing
t	Thickness of the plate or sheathing
$t_{c,slab}$	Total slab thickness subjected to compression
u	Hardening
vd_i	Experimental vertical displacement at point i
vd_{ni}	Numerical vertical displacement at point i
x_i	Variable of the polynomial approximation, with x_1 - the span length, x_2 - the beam location and x_3 - the concrete thickness
z	Value given by the polynomial approximation

z_i	Value given by the polynomial fit for the point i
z_0	Distance between the concrete slab top and the concrete slab centroid
$w(x, y)$	Vertical displacement of a point on the structure under the effect of $p(x)$, function of the x and y coordinates (sinusoidal shaped deformation)
$w_0(x)$	Vertical displacement associated with the same point as $w(x, y)$, but under the effect of $p_0(x)$, function of the x coordinate (cylindrical shaped deformation)

Greek lower case letters

α	Torsion parameter
α_i	Parameter depending on the partial effective width and the equivalent span
β_i	Dispersion angle for concentrated loads in layer i
β_M	Effective width factor from a moment-curvature relationship for a beam
β_{MG}	Reduction factor due to bending stresses
β_{NG}	Reduction factor due to normal stresses
β_{st}	Effective width factor from a consideration of membrane stress distribution
γ	Specific weight
γ_E	Torsional strength of the secondary beams/bracing per unit length
γ_P	Torsional strength of the principal beams per unit length
δ	Slip
δ_0	Initial slip
θ	Angle; Bracing parameter
λ	Shear influence number
ν	Poisson's coefficient
ρ	Density
ϱ_E	Bending stiffness of the secondary beams/bracing per unit length
ϱ_P	Bending stiffness of the principal beams per unit length
σ	Normal stress
$\sigma_{c,max}$	Maximum slab compressive stress
$\sigma_{c,min}$	Minimum slab compressive stress
σ_{max}	Maximum normal stress
ω	Ratio between bending stiffness of the joist and the slab

Graphical symbols

\emptyset	Diameter
	Circular/Round cross-section

SYMBOLS



I-shape cross-section



Rectangular cross-section

$\%_i$

Percentage associated to the element i

ABBREVIATIONS AND ACRONYMS

AASHTO	American Association of State Highway and Transportation Officials
AB	Adjacent beam
ABNT	Associação Brasileira de Normas Técnicas
af	After failure
AF&PA	American Forest & Paper Association
AITC	American Institute of Timber Construction
ASCE	American Society of Civil Engineers
<i>bm</i>	Longitudinal bending moment
BRE	Building Research Establishment
BS	British Standard
BSI	British Standard Institute
<i>Bs</i>	Base simulation
BSp	Base specimen
CEN	European Committee for Standardization
CLT	Crossed laminated timber
CSGL	Composite slab with glued laminated beams
CSTL	Composite slab with timber logs
DEC	Departamento de Engenharia Civil (Department of Civil Engineering)
DF	Distribution Factor
DIN	Deutsches Institut für Normung (German Institute for Standardization)
dof	Degrees of freedom
DLM	Direct Load Model
EC	Eurocode
EN	European Standard
<i>EPP</i>	Elastic Perfectly Plastic
f	Failure
FCT	Fundação para a Ciência e a Tecnologia (Portuguese Foundation for Science and Technology)
FCTUC	Faculdade de Ciências e Tecnologia da Universidade de Coimbra (Faculty of Sciences and Technology of the University of Coimbra)
FE	Finite Element
FEM	Finite Element Method

ABBREVIATIONS AND ACRONYMS

FRP	Fiber Reinforced Polymer
GA	Grillage analogy
GL, Glulam	Glued laminated timber
<i>Il</i>	Imposed load
LB	Loaded beam
LDF	Load Distribution Factor
LE	Linear Elastic
LEMEC	Laboratório de Estruturas, Mecânica Estrutural e Construções (Laboratory of Structures, Structural Mechanics and Constructions)
<i>lin</i>	Linear load
LRFD	Load and Resistance Factor Design
LRM	Lever Rule Model
LVL	Laminated veneer lumber
LWAC	Light-weight aggregate concrete
MOE	Modulus of Elasticity
NCHRP	National Cooperative Highway Research Program
NP	Norma Portuguesa (Portuguese Standard)
OSB	Oriented Strand Board
<i>Ov</i>	Oversized
<i>Rt</i>	Rectangular
RC	Regular concrete; Normal weight aggregate concrete
Sae	Simply supported in all ends
Sc	Support conditions
SDI	Steel Deck Institute
SH	Series or harmonic method
SLLM	Slab Lateral Load Model
SLS	Serviceability Limit State
<i>sr</i>	Support reactions
<i>Ss</i>	Simply supported
STEP	Structural Timber Education Program
<i>sw</i>	Self-weight
TxDOT	Texas Department of Transportation
ULS	Ultimate Limit State
<i>Un</i>	Undersized
UNESCO	United Nations Educational Scientific and Cultural Organization
US	United States
<i>vd</i>	Vertical displacement

TABLE OF CONTENTS

ABSTRACT i

RESUMO iii

ACKNOWLEDGEMENTS v

SYMBOLS vii

ABBREVIATIONS AND ACRONYMS..... xiii

LIST OF FIGURES xix

LIST OF TABLES xxvii

1. INTRODUCTION 1

 1.1 Background..... 1

 1.2 Aims of the work and methodologies..... 2

 1.3 Basic concepts 4

 1.4 Organization of the thesis 6

2. LITERATURE REVIEW 9

 2.1 Introduction 9

 2.2 Effective width 9

 2.2.1 Historical introduction 9

 2.2.2 Steel-concrete composite structures..... 13

 2.2.3 Timber-concrete composite structures 22

 2.3 Distribution of concentrated loads..... 26

 2.3.1 Preliminary notes 26

 2.3.2 Steel-concrete composite structures..... 26

 2.3.3 Timber and timber based structures 38

 2.4 System effect 45

 2.4.1 Preliminary notes 45

TABLE OF CONTENTS

2.4.2 Timber structures.....	47
2.4.3 Timber-concrete structures.....	50
2.4.4 Steel structures	53
2.5 Portuguese situation in terms of timber floors.....	54
2.6 Final remarks.....	56
3. MODEL DEVELOPMENT: PRELIMINARY STUDIES	59
3.1 Introduction.....	59
3.2 Preliminary experimental tests.....	60
3.3 Base numerical model.....	69
3.4 Analytical model.....	76
3.5 Numerical model validation.....	80
3.5.1 Experimental results.....	80
3.5.2 Numerical vs. CSGL experimental results	86
3.5.3 Modeling analysis.....	90
3.5.4 Additional remarks	105
3.6 Preliminary numerical analysis.....	106
3.7 Definition of the experimental program.....	109
4. EXPERIMENTAL ANALYSIS	113
4.1 Introduction.....	113
4.2 Test specimens: properties and geometry	113
4.3 Test setup	125
4.4 Experimental results.....	136
4.4.1 Vertical displacements	137
4.4.2 Support reactions.....	150
4.4.3 Slip displacements.....	161
4.4.4 Uplift displacements.....	163
4.4.5 Strains.....	163
4.4.6 Failure tests.....	168

4.4.7 Parametric study of the tests	174
4.5 Experimental vs. numerical results	182
4.5.1 Vertical displacements	182
4.5.2 Support reactions	187
4.5.3 Stresses.....	192
4.6 Summary.....	196
5. SENSITIVITY ANALYSIS	197
5.1 Introduction	197
5.2 Parametric study	197
5.3 Development of an expeditious tool.....	223
5.4 Summary.....	248
6. SUMMARY AND CONCLUSIONS.....	251
6.1 Summary.....	251
6.2 Conclusions	252
6.3 Recommendations for future work.....	256
7. REFERENCES	257
APPENDICES.....	265

TABLE OF CONTENTS

LIST OF FIGURES

Fig. 1.1 – Concept of effective width, <i>ad.</i> (Amadio <i>et al.</i> 2004)	5
Fig. 1.2 – Organizational flowchart of the thesis’ chapters.....	7
Fig. 2.1 – Effective flange width parameters, <i>ad.</i> (EN1992 2004)	14
Fig. 2.2 – Lateral dispersion of concentrated load in steel-concrete slabs, <i>ad.</i> (EN1994 2004)	15
Fig. 2.3 – Critical perimeter for punching shear, <i>ad.</i> (Johnson 1994).....	15
Fig. 2.4 – Effective width of composite slab for point load, <i>ad.</i> (Johnson 1994).....	17
Fig. 2.5 – Distribution of strain across the slab, <i>ad.</i> (Evans and Wright 1988)	19
Fig. 2.6 – Determination of effective flange width for positive moment section at SLS, <i>ad.</i> (Chiewanichakorn <i>et al.</i> 2004)	21
Fig. 2.7 – Effective width in a steel-concrete slab, <i>ad.</i> (Miotto 2009).....	22
Fig. 2.8 – Dispersion of concentrated load from contact area width $b_{w,p}$, in timber laminated deck plates, <i>ad.</i> (EN1995 2004b)	23
Fig. 2.9 – Example of bending moment distribution in the plate for determination of the effective width, <i>ad.</i> (EN1995 2004b).....	23
Fig. 2.10 – Twin girder steel bridge floor system, <i>ad.</i> (Pennings <i>et al.</i> 2000).....	33
Fig. 2.11 – Direct load model for load distribution, <i>ad.</i> (Pennings <i>et al.</i> 2000).....	33
Fig. 2.12 – Lever rule model for load distribution, <i>ad.</i> (Pennings <i>et al.</i> 2000).....	34
Fig. 2.13 – Slab lateral load distribution model, <i>ad.</i> (Pennings <i>et al.</i> 2000).....	34
Fig. 2.14 – Influence surface for floor beam mid-span moment, <i>ad.</i> (Pennings <i>et al.</i> 2000)....	36
Fig. 2.15 – Load sharing behavior in a slab-girder bridge, <i>ad.</i> (Harris 2010).....	37
Fig. 2.16 – Vertical section of a load-bearing partition supported by a timber joisted floor, <i>ad.</i> (Ozelton and Baird 2006)	43
Fig. 2.17 – Timber-concrete bridge with timber truss beams, <i>ad.</i> (Moraes 2007).....	45
Fig. 3.1 – Geometrical characteristics, plan view: a) CSGL and b) CSTL	60
Fig. 3.2 – Cross section: a) CSGL beam (AA’ line); and b) L1 beam in CSTL (BB’ line).....	61
Fig. 3.3 – Test setup – CSGL	63

LIST OF FIGURES

Fig. 3.4 – Test setup scheme, plan view: a) CSGL and b) CSTL	63
Fig. 3.5 – Test setup detail – CSGL: slip displacement transducers.....	64
Fig. 3.6 – Test setup detail – CSGL: vertical displacement transducers	65
Fig. 3.7 – Test setup detail – CSGL: load cells	65
Fig. 3.8 – Acquisition unit	66
Fig. 3.9 – Test setup detail – CSTL: slip displacement transducers.....	66
Fig. 3.10 – Test setup detail – CSTL: load cells.....	67
Fig. 3.11 – Test setup – CSTL	68
Fig. 3.12 – Composite T-beam obtained from the CSGL slab	68
Fig. 3.13 – Beam (GL7) obtained from the CSGL slab subjected to a load test	69
Fig. 3.14 – Connection properties.....	71
Fig. 3.15 – Grid model scheme	71
Fig. 3.16 – FE mesh schemes (top view): a) Grid model; b) Frame+Shell model; c) Solid model.....	73
Fig. 3.17 – Frame+Shell model scheme.....	74
Fig. 3.18 – Solid model scheme.....	76
Fig. 3.19 – Guyon-Massonnet model: simplified slab and load scheme	77
Fig. 3.20 – CSGL: support reaction distribution when loaded at $\frac{1}{2}$ and at $\frac{1}{4}$ span	82
Fig. 3.21 – CSTL: support reaction distribution when loaded at $\frac{1}{2}$ and at $\frac{1}{4}$ span.....	83
Fig. 3.22 – CSGL: vertical displacement at $\frac{1}{2}$ and $\frac{1}{4}$ span when loaded at $\frac{1}{2}$ (left) and $\frac{1}{4}$ span (right).....	84
Fig. 3.23 – CSTL: vertical displacement at $\frac{1}{2}$ and $\frac{1}{4}$ span when loaded at $\frac{1}{2}$ (left) and $\frac{1}{4}$ span (right).....	85
Fig. 3.24 – Numerical vs. experimental CSGL support reactions for B3 $\frac{1}{2}$	88
Fig. 3.25 – Numerical vs. experimental CSGL support reactions for B3 $\frac{1}{4}$	88
Fig. 3.26 – Numerical vs. experimental CSGL vertical displacements at mid-span for B3 $\frac{1}{2}$	89
Fig. 3.27 – Numerical vs. experimental CSGL vertical displacements at quarter-span for B3 $\frac{1}{4}$	89
Fig. 3.28 – CSGLi loaded at $\frac{1}{2}$ L: support reactions	92
Fig. 3.29 – CSGLi loaded at $\frac{1}{4}$ L: support reactions	92

Fig. 3.30 – CSGLi loaded at $\frac{1}{2}$ L: vertical displacements at each beam $\frac{1}{2}$ L	93
Fig. 3.31 – CSGLi loaded at $\frac{1}{4}$ L: vertical displacements at each beam $\frac{1}{4}$ L	93
Fig. 3.32 – Theoretical analysis – load at $\frac{1}{2}$ L: vertical displacements at each beam $\frac{1}{2}$ L	95
Fig. 3.33 – Theoretical analysis – load at $\frac{1}{4}$ L: vertical displacements at each beam $\frac{1}{4}$ L	96
Fig. 3.34 – Theoretical analysis: percentage distribution of vertical displacement	98
Fig. 3.35 – Theoretical analysis – load at $\frac{1}{2}$ L: support reactions	100
Fig. 3.36 – Theoretical analysis – load at $\frac{1}{4}$ L: support reactions	101
Fig. 3.37 – Theoretical analysis – load at $\frac{1}{2}$ L: longitudinal bending moment at $\frac{1}{2}$ L cross section	103
Fig. 3.38 – Theoretical analysis – load at $\frac{1}{4}$ L: longitudinal bending moment at $\frac{1}{4}$ L cross section	104
Fig. 3.39 – <i>Bs</i> modeling: geometrical characteristics	107
Fig. 4.1 – Plan view scheme: specimens S1 to S3	115
Fig. 4.2 – Casting of the test specimens	116
Fig. 4.3 – Testing of prismatic concrete specimens: a) MOE; and b) failure	118
Fig. 4.4 – MOE static test	118
Fig. 4.5 – Connectors: a) steel rod $\varnothing 8$ mm; and b) SFS VB 48-7.5 \times 100 screw	119
Fig. 4.6 – Placing of the steel rods: marking, drilling and positioning	120
Fig. 4.7 – SFS VB 48-7.5 \times 100 screw scheme: geometrical characteristics	121
Fig. 4.8 – SFS VB 48-7.5 \times 100 screws application scheme	121
Fig. 4.9 – Placement of the SFS screws on specimen S3	122
Fig. 4.10 – Geometrical characteristics, plan view of the specimens: a) S1; b) S4; c) S5	123
Fig. 4.11 – Geometrical characteristics, plan and side views of specimen S3	124
Fig. 4.12 – Cross section of a beam at specimens: a) S1 (CC' line); b) S5 (DD' line) and c) S3 (EE' line)	124
Fig. 4.13 – Test setup scheme, plan view: a) S1; b) S4 and c) S5	125
Fig. 4.14 – Test setup: $\frac{1}{2}$ point load (S5-L=6.00m)	126
Fig. 4.15 – Test setup: $\frac{1}{4}$ point load (S4-L=2.00m)	127
Fig. 4.16 – Test setup: four-point load at S1-BSp	128
Fig. 4.17 – Test setup: line load regularization layer detail (S5-L=6.00m)	128

LIST OF FIGURES

Fig. 4.18 – Test setup: line load at a 4.00 m span specimen (S3-hc=0.03m)	129
Fig. 4.19 – Test setup: line load at the 2.00 m span specimen (S4-L=2.00m).....	129
Fig. 4.20 – Test setup: line load at the 6.00 m span specimen (S5-L=6.00m).....	130
Fig. 4.21 – Displacement transducers: a) timber-concrete slip; and b) vertical displacement	131
Fig. 4.22 – Uplift displacement transducers: positioning detail	131
Fig. 4.23 – Strain gauges setup detail	132
Fig. 4.24 – Test setup detail: bottom view	132
Fig. 4.25 – Test setup detail: load cells.....	133
Fig. 4.26 – Acquisition unit	133
Fig. 4.27 – Test setup: equipment designation.....	137
Fig. 4.28 – S1-BSp: vertical displacement at $\frac{1}{2}$ L and $\frac{1}{4}$ L when loaded at B4 lin and B4 4P	138
Fig. 4.29 – S1-BSp: vertical displacement at $\frac{1}{2}$ L and $\frac{1}{4}$ L when loaded at B1 $\frac{1}{2}$	139
Fig. 4.30 – Vertical displacement at $\frac{1}{2}$ L and $\frac{1}{4}$ L when loaded at B2 $\frac{1}{4}$: S1-BSp and S2-LWAC.....	139
Fig. 4.31 – S4-L=2.00m: vertical displacement at $\frac{1}{2}$ L and $\frac{1}{4}$ L when loaded at B3 $\frac{1}{4}$	141
Fig. 4.32 – Vertical displacement at $\frac{1}{2}$ L and $\frac{1}{4}$ L when loaded at B5: S4-L=2.00m (B5 lin) and S5-L=6.00m (B5 $\frac{1}{2}$)	142
Fig. 4.33 – Vertical displacement at $\frac{1}{2}$ L and $\frac{1}{4}$ L when loaded at B3 $\frac{1}{2}$: S3-hc=0.03m and S4-L=2.00m.....	142
Fig. 4.34 – Vertical displacement vs. highest displacement for the loaded beam in S1-BSp: a) all load cases; b) disregarding 4P load case.....	143
Fig. 4.35 – Vertical displacement vs. highest displacement for the loaded beam in S2 to S5	144
Fig. 4.36 – Slab deflections: B3 $\frac{1}{2}$	146
Fig. 4.37 – S4-L=2.00m B2 deflections.....	147
Fig. 4.38 – S5-L=6.00m B4 deflections.....	148
Fig. 4.39 – S2-LWAC B4 and B5 deflections	148
Fig. 4.40 – S3-hc=0.03m B1 and B3 deflections.....	149
Fig. 4.41 – S1-BSp B5 deflections.....	150
Fig. 4.42 – Support reaction distribution in S4-L=2.00m.....	153
Fig. 4.43 – Support reaction distribution in S1-BSp and S5-L=6.00m.....	154

Fig. 4.44 – Support reaction distribution in S2-LWAC and S3-hc=0.03m.....	156
Fig. 4.45 – Support reaction distribution for S1-BSp.....	157
Fig. 4.46 – Support reaction distribution S2-LWAC vs. S1-BSp, point load at B3 and B5...	158
Fig. 4.47 – Support reaction distribution S2-LWAC vs. S1-BSp: line loading.....	159
Fig. 4.48 – Support reaction distribution S3-hc=0.03 vs. S1-BSp, point load in B5.....	159
Fig. 4.49 – Support reaction distribution for S4-L=2.00m, S5-L=6.00m and S1-BSp, point loading	160
Fig. 4.50 – Support reaction distribution for S4-L=2.00m, S5-L=6.00m and S1-BSp, line loading	161
Fig. 4.51 – Strain distribution for the loaded beam, by load case	167
Fig. 4.52 – S1-BSp failure test: a) B3-GL13; b) B3-GL13 failure detail and c) B4-GL1.....	169
Fig. 4.53 – Failure sections.....	170
Fig. 4.54 – Load-stress curves for B3 at failure	171
Fig. 4.55 – S3-hc=0.03m B4-GL5 failure	172
Fig. 4.56 – Distributions of vertical displacements for the loaded beam, by load case	175
Fig. 4.57 – Distribution of support reactions for the loaded beam, by load case	176
Fig. 4.58 – Distribution of deflections when the specimens where loaded at B3	177
Fig. 4.59 – Transversal distribution of vertical displacements for the loaded beam.....	180
Fig. 4.60 – Transversal distribution of vertical displacements vs. timber beam MOE	181
Fig. 4.61 – Experimental and numerical vertical displacements: S1 when loaded at B3 and B4	184
Fig. 4.62 – Experimental and numerical vertical displacements when loaded at B3: S2 and S3	185
Fig. 4.63 – Numerical vertical displacements: S5 when loaded at B2	186
Fig. 4.64 – Numerical modeling deformed shape for the central beam loaded at mid-span..	187
Fig. 4.65 – S2: experimental and numerical support reaction distribution.....	189
Fig. 4.66 – S3: experimental and numerical support reaction distribution.....	190
Fig. 4.67 – Numerical distribution of support reactions for the loaded beam, by load case ..	192
Fig. 4.68 – Stresses at each beam mid-span for load tests at B1 ½ L, B2 ½ L and B 3½ L ..	194
Fig. 4.69 – Stresses at each beam in failure test (loading at B3).....	195

LIST OF FIGURES

Fig. 5.1 – <i>Bs</i> modeling scheme	200
Fig. 5.2 – First phase analysis: <i>vd</i> received by the central beam when a point load acts over it	204
Fig. 5.3 – First phase analysis: <i>sr</i> received by the center beam when a point load acts over it	205
Fig. 5.4 – First phase analysis: <i>bm</i> associated with the center beam when a point load acts over it	206
Fig. 5.5 – First phase analysis: <i>vd</i> , <i>sr</i> and <i>bm</i> distributions for self-weight and imposed load cases; a) by load case; b) by beam	208
Fig. 5.6 – Parameters with higher effect in the studied quantities (maximum deviation percentages)	211
Fig. 5.7 – Distribution of <i>vd</i> for the point load case by concrete thickness	213
Fig. 5.8 – Distribution of <i>vd</i> for the point load case by span	214
Fig. 5.9 – Second phase: distribution of <i>vd</i> by percentage at the loaded beam	215
Fig. 5.10 – Distribution of <i>sr</i> for the point load case by concrete thickness	216
Fig. 5.11 – Distribution of <i>sr</i> for the point load case by span	217
Fig. 5.12 – Second phase: distribution of <i>sr</i> by percentage at the loaded beam	218
Fig. 5.13 – Distribution of <i>bm</i> for the point load case by concrete thickness	219
Fig. 5.14 – Distribution of <i>bm</i> for the point load case by span	220
Fig. 5.15 – Second phase: distribution of <i>bm</i> by percentage at the loaded beam	221
Fig. 5.16 – Beam location scheme	223
Fig. 5.17 – Parameter variation curves for the various sets	228
Fig. 5.18 – <i>Bs</i> set parameter variation curves and 2 nd degree polynomial fit for $\frac{1}{2} L$, $\frac{1}{4} L$ and <i>lin</i>	233
Fig. 5.19 – <i>Bs</i> set parameter variation curves and <i>Pr</i> polynomial	234
Fig. 5.20 – <i>Un</i> , EC5 and <i>Ov</i> parameter variation curves and <i>Pr</i> polynomial	239
Fig. 5.21 – Bridge geometrical characteristics: a) plan view; b) cross section	240
Fig. 5.22 – Distribution of <i>bm</i> for $\frac{1}{2} L$, $\frac{1}{4} L$ and <i>lin</i> loadings in the bridge example	241
Fig. 5.23 – Experimental <i>vd</i> $\frac{1}{2} L$ and <i>vd</i> $\frac{1}{4} L$ vs. <i>Pr</i> distribution for S1 to S5	243
Fig. 5.24 – Distribution of <i>sr</i> for S1 to S5 when loaded with $\frac{1}{2} L$, $\frac{1}{4} L$ and <i>lin</i>	244
Fig. 5.25 – Experimental <i>vd</i> $\frac{1}{2} L$ and <i>vd</i> $\frac{1}{4} L$ vs. <i>cfvd</i> · <i>Pr</i> distribution for S1 to S5	245

Fig. 5.26 – Experimental sr vs. $cfsr \cdot Pr$ distribution for S1 to S5	246
Fig. 5.27 – Experimental $vd \frac{1}{2} L$ and $vd \frac{1}{4} L$ vs. $cfvd \cdot Pr$ distribution for CSGL and CSTL	247
Fig. 5.28 – Experimental sr vs. $cfsr \cdot Pr$ distribution for CSGL and CSTL.....	248

LIST OF FIGURES

LIST OF TABLES

Table 3.1 – Geometrical properties CSTL beams	61
Table 3.2 – CSGL and CSTL material properties	62
Table 3.3 – Experimental connection stiffnesses CSGL	69
Table 3.4 – Load cases and applied loads during the experimental test.....	81
Table 3.5 – Studied parameters	91
Table 3.6 – Summary of the parameters with higher effect in the quantities studied	109
Table 3.7 – Parameters to test in the experimental specimens	110
Table 4.1 – Experimental specimens: variation parameters	114
Table 4.2 – Characteristics of the experimental specimens.....	114
Table 4.3 – Cork-concrete composition	116
Table 4.4 – Concrete properties (mean values)	117
Table 4.5 – Timber beams of each specimen	119
Table 4.6 – Connection properties.....	134
Table 4.7 – Loads applied during the experimental tests for the several load cases.....	135
Table 4.8 – Support reaction distribution [%]	151
Table 4.9 – Support reaction spreading summary [%]	155
Table 4.10 – Maximum and minimum experimental slip displacements.....	162
Table 4.11 – Extreme slip displacements for the loaded beams [mm].....	162
Table 4.12 – Maximum and minimum experimental uplift displacements [mm].....	163
Table 4.13 – Maximum and minimum experimental strains [$\mu\epsilon$].....	164
Table 4.14 – Maximum stresses [MPa]	164
Table 4.15 – Strain gauge pairs differences [$\mu\epsilon$].....	166
Table 4.16 – Loads and strains at failure.....	171
Table 4.17 – Strain distribution at failure and immediately after [%].....	173
Table 4.18 – Vertical displacement vs. maximum vertical displacement at the loaded beam	178

LIST OF TABLES

Table 4.19 – Numerical support reaction spreading summary [%]	191
Table 5.1 – First phase parameters.....	199
Table 5.2 – <i>Bs</i> modeling characteristics.....	201
Table 5.3 – First phase modeling: description and variation	201
Table 5.4 – First phase: parameters with higher effect in the mid-span vertical displacement	209
Table 5.5 – First phase: parameters with higher effect in the support reactions.....	209
Table 5.6 – First phase: parameters with higher effect in the mid-span longitudinal bending moment	210
Table 5.7 – Second phase modeling.....	212
Table 5.8 – Transversal spreading [%] between the concrete height of 0.02 and 0.10 m	221
Table 5.9 – Transversal spreading [%] between the span length of 2.00 and 12.00 m.....	222
Table 5.10 – <i>bm</i> received by the beam when loaded at $\frac{1}{2} L$, <i>lin</i> and $\frac{1}{4} L$	224
Table 5.11 – Polynomial coefficients to approximate the parameter variation curves.....	230
Table 5.12 – Comparison between coefficients of the polynomial fit for <i>Bs</i>	232
Table 5.13 – <i>bm</i> percentages predicted for <i>Bs</i> : numerical vs. <i>Pr</i> polynomial	235
Table 5.14 – <i>bm</i> percentages predicted for <i>Un</i> , EC5 and <i>Ov</i> : numerical vs. <i>Pr</i> polynomial .	237
Table 5.15 – Bridge material properties.....	241
Table 5.16 – Numerical vs. <i>Pr</i> polynomial predictions for <i>bm</i> : bridge example	242
Table 5.17 – Average partial differences: experimental vs. <i>Pr</i> for S1 to S5	244
Table 5.18 – <i>cfi</i> coefficients	245
Table 5.19 – Average partial differences: experimental vs. <i>cfi</i> · <i>Pr</i> for S1 to S5	246
Table 5.20 – Average partial differences: experimental vs. <i>cfi</i> · <i>Pr</i> for CSGL and CSTL..	248

1. INTRODUCTION

1.1 Background

The use of timber-concrete composite structures is relatively new with the first records dating back from the 20's and 30's of the last century (Linden 1999). These structures emerged as a consequence of the steel shortage that occurred in the period between World Wars. However, scientific studies on structures composed by timber and concrete are recent, with almost no studies published until the 70's of the last century. Thereafter, many studies on the subject took place in an attempt to develop knowledge and solutions (Dias 2005, Etournaud 1998, Godycki *et al.* 1984, Gutkowski *et al.* 2000, Gutkowski *et al.* 2010, Mettern 2003, Piazza and Turrini 1983, Timmermann and Meierhofer 1993, Werner 1992, Yeoh *et al.* 2008, Yttrup 1996).

Although timber-concrete composite structures were originally intended for rehabilitating or strengthening timber floors, they started to be used in the construction of new buildings (in floors and in walls) and in bridge decks (Bathon *et al.* 2006, Dias *et al.* 2011, Lukaszewska *et al.* 2006, NTC 2002, Poštulka 1997, RILEM 1992). The concept behind those structures is the same associated to reinforced concrete, with the timber playing the role of the steel by taking the tension forces, leaving the compression forces to the concrete. This takes the most advantages of the dual materials solution. In floors/decks structures, when the dual material solution is compared with a floor made by timber alone, some advantages can be listed, such as, higher in-plane stiffness and strength, higher fire resistance and sound insulation, less vibration, to mention only a few of them. Comparatively with the solution made by concrete alone, the composite solution is lighter, faster to build, less formwork consuming, and consequently cheaper (Ceccotti 2002, Dias 2012, Stojić and Cvetković 2001).

The increasing use of this type of structures motivated the investigation on them, for instance with regard to the development of models that would define the structural behavior and its characteristics. These studies comprised analyses based on experimental results and theoretical modeling in order to approach several conditions, such as: loading type, second order effects, long-term behavior and geometry (Fragiacomo *et al.* 2007, Girhammar and Gopu 1991, Natterer and Hoefl 1987, Werner 1992). Nevertheless, all those studies were focused on analyzing the behavior of timber-concrete composite structures according to the longitudinal direction of timber elements. In general, the studied elements were composed by a “T” beam to simulate a part of the structure that is repeated. When a greater width

(multiple “T”) is tested the loading is applied to the whole width. As far as standards are concerned, the model proposed by Eurocode 5 – EC5 (EN1995 2004a, EN1995 2004b) is also only valid in these situations. There are a great number of studies on the topic of connections aiming to attain connections able to guarantee an efficient composite behavior (Deam *et al.* 2008, Dias *et al.* 2007b, Kuhlmann and Michelfelder 2004). In parallel, there are many studies focused on connection modeling (Dias 2005, Dias 2012, Dias *et al.* 2007a, Fernández-Cabo *et al.* 2008, Fragiacomio *et al.* 2006, Lukaszewska *et al.* 2010, Monteiro *et al.* 2010, Monteiro *et al.* 2011, Monteiro 2008, Oudjene *et al.* 2013, Piazza and Ballerini 2000, Smilovic *et al.* 2013). In building rehabilitation, available connections respond to the inherent needs of these specific situations.

Studies about the behavior of timber-concrete composite structures in the width direction of the timber beams (transversal direction) are scarce, particularly when associated with concentrated loads (point or line loads acting parallel to the longitudinal direction of the beam). However, there are some studies which deal with these issues in structures composed by the combination of others materials rather than timber-concrete, namely steel-concrete composite structures, concrete composite structures and timber structures. From the results of such studies it is possible to notice some differences in behavior when composite structures of various types of materials are compared with each other. Timber-concrete composite structures have specificities which make their analysis quite different from other combination of materials, namely the timber brittle behavior, the size of the compressed and tensioned elements, the part of concrete element that is likely to crack, or the existence of an intermediate layer with bearing capacity in the transversal direction.

1.2 Aims of the work and methodologies

As presented before, point loads and linear loads are very common in floors, especially in floor rehabilitations. It is therefore of great interest to understand how the load will be distributed to the various timber elements, in order to optimize the design solution. Although the floors may be idealized as a series of repeatable elements, placed side by side, and calculated associating the action of a point load only to the element where it is applied, this is not entirely correct since other beams are also affected by the load. The way of the distribution of internal forces and stresses occurs for various elements geometries and material properties, as well as different loads configurations is the essential goal of this doctoral research. Thus, this thesis aims to analyze and to develop solutions for problems associated with the design and construction of timber-concrete composite structures on the rehabilitation of timber floors. This study focusses on the distribution of internal forces and stresses in these structures, namely on the distribution in the transversal direction. The

phenomenon to be investigated is the way a load applied to a slab is directed to each supporting element/beam in the orthogonal direction, taking the longitudinal axis of the main beams as reference.

To attain the goals of this research, a comprehensive literature review is essential, not only for giving an overview of the research works that could be related with the topic of this thesis, but also to know the various concepts and phenomena associated with the distribution of internal forces and stresses in the transversal direction in slab structures composed either by timber and concrete or by different materials. The methodologies adopted by the various authors in their investigations are naturally of utmost importance. Some studies are based essentially on experimental tests, such as those by (Daniels 1990, Etournaud 1998, Luttrell 1995, Moreira 2001, Mullenex 1993, Porter and Ekberg-Jr. 1977, Thomas 2003); whereas others are based essentially on numerical modeling, such as those by (Chiewanichakorn *et al.* 2004, Gara *et al.* 2009, Nie *et al.* 2008, Simon 2008). However, the combined use of the two approaches enables the comparison between results and, at the same time, the validation of the model (Dahl *et al.* 2006, Daniels and Crisinel 1993, Gutkowski *et al.* 2010, Ilharco 2008, Kearley and Carruthers 1991, Moreira 2001). This is also the intention of this doctoral research. Thus, two approaches were used, a numerical one and an experimental one from which the behavior of this type of structures was analyzed. Numerical models, categorized by some authors as an important tool to optimize and compare results (Dias *et al.* 2007a, Lopes *et al.* 2012, Oliveira 2002) are an essential part of this work. Beyond predicting the behavior of test slabs, they also allow to study the effects that a great number of parameters may have on their behavior. These models were developed and validated based on the results of theoretical models and experimental tests performed in real-scale test specimens subjected to point loads and line loads parallel to the timber elements. After validated, they allow parametric studies to be performed, aiming at evaluating the ability of transverse distribution of loads, assessing the features established for the study, for all types of geometries, material properties and loads configurations that are likely to be found in real structures. The purpose was to obtain a quick evaluation model to be applied together with the behavior models specified in applicable standards (EN1995 2004a).

This study aims at improving the current knowledge on the behavior of timber-concrete floor systems subjected to concentrated loads, concerning the transversal distribution of load, contributing to the establishment of rules to reflect the actual functioning, and to the development of adequate structural solutions. This, together with the proposed simplified evaluation model will make the use of timber-concrete floors feasible in wider set of rehabilitation situations.

1.3 Basic concepts

Associated with the subject of transversal distribution of loads there are some concepts that are extremely important to be identified in order to clarify the following analyses. This is the case of the effective width, the distribution of concentrated loads and the system effect.

The *effective width* is associated with the stress distribution and the fact that it is not always uniform. Thus, this is a concept that is intrinsic to the shear lag phenomenon which, due to shear deformation, leads to a non-uniform transversal stress distribution in certain areas when the slab or the beam is subjected to bending. Thereby, the concept of effective width arises from the simplified consideration of the shear lag and it is obtained by defining a smaller width on which the stress distribution can be assumed as uniform taken as the maximum stress value, corresponding to the same resultant force as that of the non-uniform stress distributed, integrated over the whole actual width, Fig. 1.1. The definition of the effective width allows the use of the elementary bending analysis. The Euler-Bernoulli's hypothesis is valid and the increased complexity of a rigorous analysis is avoided.

$$b_{eff} = b_{eff,1} + b_{eff,2} + b_0 \quad (1)$$

$$b_{eff,i} = \int_{b_0/2}^{b_i} \sigma dy / \sigma_{max} \quad i=1,2 \quad (2)$$

where: b_{eff} is the total effective width;

$b_{eff,i}$ is the partial effective width associated with the concrete flange, on each side of the web;

b_0 is the width of the connection zone, distance between the centers of the outstand shear connectors;

b_i is the half distance between the beam axis and the adjacent beam;

d_y is the infinitesimal change in y ;

σ is the normal stress in the concrete slab; and

σ_{max} is the maximum normal stress in the concrete slab; defined according to Fig. 1.1.

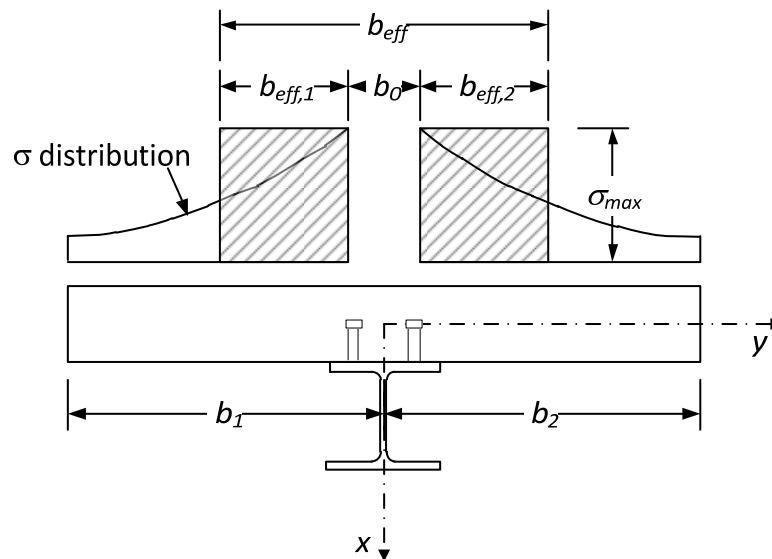


Fig. 1.1 – Concept of effective width, *ad.* (Amadio *et al.* 2004)

Considering that a sole concentrated load is acting on a timber floor composed by identical timber joists with the same stiffness and equally spaced, connected through sheathing, the joist immediately below the load will receive the bigger proportion of load and the adjacent joists the remaining part of the load. That happens as consequence of shear transfer through the connectors to the sheathing, from the loaded beam to the adjacent ones and this mechanical transfer is then known as the *distribution of concentrated loads*. Associated with this concept it is common to see an “effective width” with a different meaning than the presented before, in this case intending to represent the width in which the load distribution is assumed to exist. This is why, from now on, this width will be identified as “distribution width”.

However, in common structures, the joists’ stiffness is not equal. Considering a situation similar to the previous one but where the joists have different stiffnesses, advantage can be taken from the correlation between the stiffness and strength of the joists. Knowing that:

- the stiffer members, usually the stronger ones, tend to receive a portion of load higher than the flexible ones; and
- the less stiff the joist, the higher the associated deformation;

the existence of an effective load distribution system, compared with a structural arrangement without this system, reduces the deformation at the same time that lead to a more efficient distribution of load, since the stiffer joists can support part of the load that would be associated with the flexible ones. To cover this kind of situations the concept of *system effect* was introduced.

1.4 Organization of the thesis

Beyond the *Introduction* to the investigation under consideration, it is essential to define the boundaries of the study, as well as the scientific background. The latter is presented in Chapter 2, *Literature Review*, separated in three essential points: effective width, distribution of concentrated loads and system effect. Among these groups, the state of the art distinguishes the materials used in each study in order to evaluate how other studies might contribute for the investigation. The standardization approaches to each theme were also covered. Also, in each subsection the chronological appearance was taken into consideration.

Chapter 3, *Model development: Preliminary studies*, describes all the approaches chosen to evaluate the load distribution in the transversal direction of timber-concrete floors. Three numerical models were developed and an analytical method, developed by Guyon-Massonnet (Bareš and Massonnet 1966) was used to simulate the composite floor behavior. These four theoretical models were validated using the results from some preliminary experimental tests and those associated with each other. This led to a Finite Element (FE) numerical model capable to describe the phenomena related with the transversal distribution of load in the floors under consideration. Through a preliminary numerical analysis some of the parameters that most affect the behavior of such composite elements were identified. Subsequently, the experimental program could be established.

The experimental specimens were assembled and tested in the Laboratory of Structures, Structural Mechanics and Constructions (LEMEC), at the Department of Civil Engineering (DEC) of the Faculty of Sciences and Technology of the University of Coimbra (FCTUC). By changing material or geometrical characteristics, five specimens were created and tested subjected to point loads, at mid- and quarter-span, and line loads along specimens' beams, applied one at a time to the various specimens and beams. The consequences of the load type and position and also of the parameters considered at each specimen in the load distribution were presented and discussed. Chapter 4 summarizes all the information associated with the experimental program.

After the experimental program, an extensive numerical analysis was performed. Chapter 5, *Sensitivity Analysis*, exposes the parametric study and the development of a simplified equation capable to simplify the achievement of the load distribution, aiming at a prompt design solution, for the composite elements in consideration.

Chapter 6 summarizes the essential conclusions of this research and points out some ways to follow in future researches based on this one.

Finally, a list of the scientific literature consulted and cited along the text is gathered in *References*, followed by the *Appendices*, where the experimental and numerical results are widely exposed.

Fig. 1.2 outlines the essential organization of this thesis.

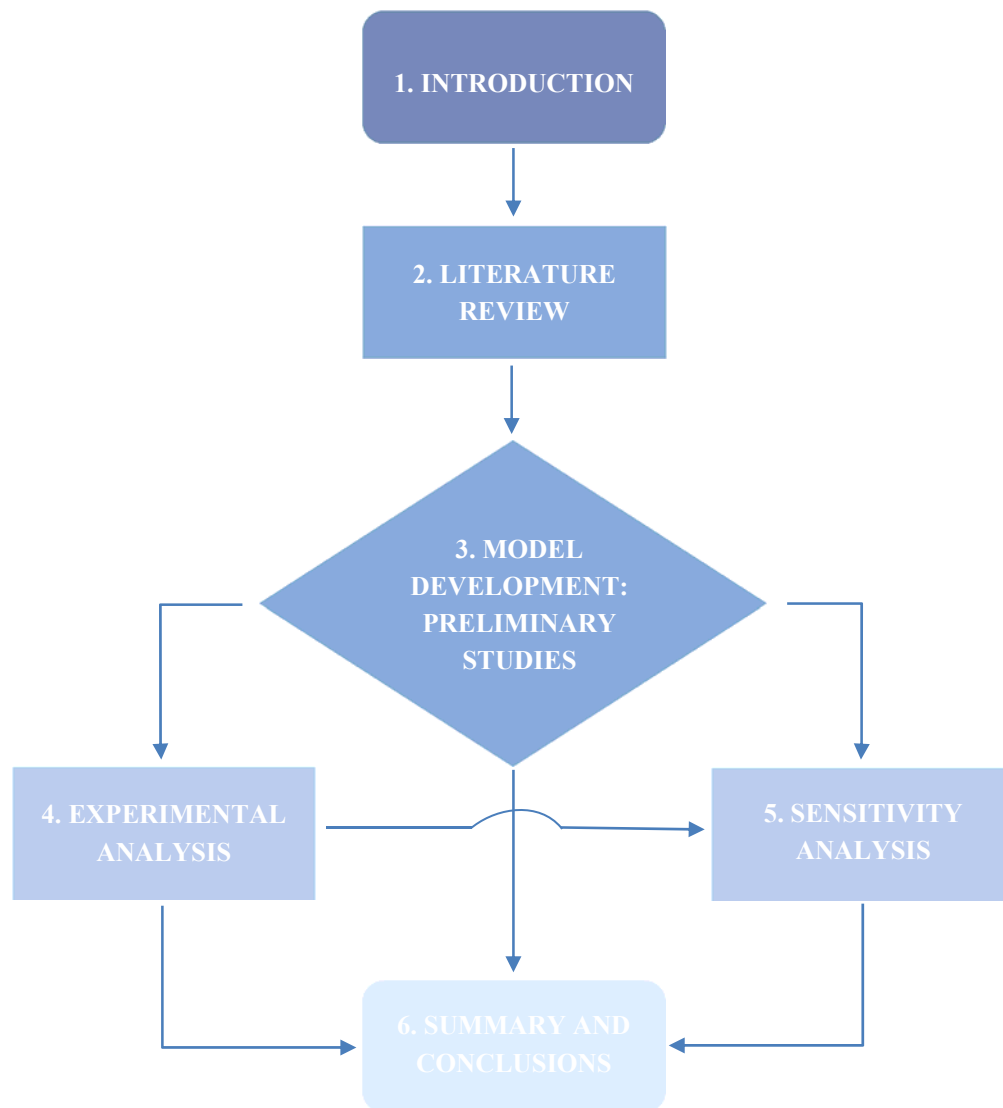


Fig. 1.2 – Organizational flowchart of the thesis' chapters

2. LITERATURE REVIEW

2.1 Introduction

The investigation on load distribution in timber-concrete composite floors is very scarce. However, this topic was relatively well studied for structures made by other materials, either those made by a single material such as concrete or steel structures or other comprising more than one material, such as steel-concrete composite structures. Taking into account that different materials lead to different mechanical behaviors, the studies on load distribution in structures made by materials different from the timber-concrete combination are certainly very interesting as a starting point for the study on timber-concrete composite floors. Therefore, they are described in this literature review.

Independently of the choice of materials, different concepts were used in the various research works found in the literature, namely the effective width, the distribution of concentrated loads and the system effect. As explained before, these concepts cover different phenomena and they will be considered separately. Indeed, some authors defend that a clear distinction between the concept of load sharing and the lateral dispersion of a concentrated load applied to a floor or roof should be made (Kearley and Carruthers 1991). This is a consequence of the lack of information, essentially in codes and standards, for both situations: load transfer from a loaded joist to adjacent joists of different stiffness, and for the lateral dispersion of a concentrated load applied to that part of a laminar material spanning between joists.

Thus, the literature review was grouped in sections with the same denomination of the concepts. Both technical/scientific articles/thesis/books or standards were referred in the individual sections. In addition, a section considering the use of timber floors in Portugal is also presented. This exposes the building solutions commonly used at national level.

2.2 Effective width

2.2.1 Historical introduction

The concept of effective width was always associated with the shear lag phenomenon, which was related with the non-uniform stress distribution in specific areas. This variability

on the stress distribution affects the area that actually contribute to the bending stiffness and the strength of the cross-section (Moreira 2001, Segundinho 2005).

The earliest record of this concept dates back to the first third of the 20th century, with the first research works being on homogeneous structures and in composite structures later (Castro *et al.* 2007). According to these authors, the first scientific paper on composite structures belongs to Miller¹ and was published in 1929. Other authors, as Evans and Wright (Evans and Wright 1988), ascribe primacy to Von Karman *et al.*², with a study based on an intense experimental work. However this study was only published in 1932. Von Karman has proposed to replace the analysis over the entire slab width subjected to a complex stress pattern due to the buckling by that of a simple beam analysis by adopting a width on which a uniform longitudinal stress would take place. According to the same authors, in 1947 Winter³ followed the same line of research and suggested a modification of the method proposed by Von Karman. By its turn, in 1952 Marguerre⁴ used the effective width to develop an equation to determine the cross-section effective stiffness in steel constructions (Moreira 2001).

According to Oliveira (Oliveira 2002), the concept of effective width applied to timber structures is in current use since, at least 1966, after the publication of the *Timber construction manual, AITC*⁵. At that time only boundary values were proposed, both for interior and edge beams. They were based on the beam span, on the distance between beams' centers and on the slab thickness.

With regard to the composite structures, the decade of the 60's is considered the decade when the first research works were published. However, timber-concrete structures were not the first structures to be studied, and the first works were indeed focused in steel-concrete composite beams. The article by Castro *et al.* (Castro *et al.* 2007) listed several studies covering the shear lag effects. The study by Adekola (Adekola 1968) is one of them. It considered the computation of the effective width associated with simply supported steel-concrete beams through the use of analytical solutions derived, years before, by Allen

¹ Miller, AB., The effective width of a plate supported by a beam. Selected engineering papers. The Institution of Civil Engineers, Paper no. 83, 1929.

² Karman, T. Von, Sechler, E. E. and Donnel, L. H., The strength of thin plates in compression, Trans. ASCE, 54, 53, 1932.

³ Winter, G., Strength of thin steel compression flanges, Trans. ASCE, 112, 1947.

⁴ K. von Marguerre, Über die Beanspruchung von Plattenträgern. Der Stahlbau 8 (in English, *About the stress of cantilever panel. Steel construction*), 1952.

⁵ Timber construction manual, 1^o. ed., American Institute of Timber Construction (AITC), Washington, 1966.

and Severn⁶. (Ansourian 1975) is also referred as the first study where the finite element method was used to perform elastic analysis on fixed composite beams.

For timber-concrete structures design is based on standards, however some lacks still persist when concerning to the effective width definition. Essentially, standards as DIN 1052⁷ or NBR-7190⁸ suggest the use of similar procedures as those for reinforced concrete structures or even steel-concrete composite structures. Besides that, the standards recommendations only consider flexible connections between materials for composite structures (Oliveira 2002).

The behavior of the materials and the connection in composite members, such as those of steel-concrete beams, were initially defined in an approximate way. According to Adekola (Adekola 1974b), studies on shear lag in composite beams began without taking into account the contribution of the shear connection (through studs or dowels). Later, such connection began to be considered in some studies which attempted to investigate its effect on the shear lag in composite prismatic beams and “isotropic” concrete plates. In fact, in one of his previous studies (Adekola 1974a), Adekola demonstrated the direct dependence between the effective width and the interaction degree, with the effective width increasing with the degree of interaction.

Some studies presented a definition for the concept of “effective width” and a list of parameters on which it is dependent on. According to Adekola, the effective width is defined as the “width of slab that would sustain a force equal to the force in the slab assuming that the longitudinal stress is constant across the width of slab at the peak stress takes place in the slab at the center line plane of the web of the steel joist” (Adekola 1968). Some parameters affecting the effective width were identified in many studies (Adekola 1968, Castro *et al.* 2007, Chiewanichakorn *et al.* 2004, Chiewanichakorn *et al.* 2005, Cosenza and Zandonini 1999, Daniels 1990, El-Lobody 2002, Evans and Wright 1988, Lind *et al.* 1976, Macorini *et al.* 2006, Miotto 2009, Natterer and Hoefft 1987, Nie *et al.* 2008, Oliveira 2002, Sedlacek and Bild 1993, Segundinho 2005, Simon 2008, Vallenilla and Bjorhovde 1985):

⁶ Allen DNdG and Severn RT., Composite action between beams and slabs under transverse load. *The Structural Engineer*; 39 (Part I):149–54, 1961.

⁷ DIN 1052 Entwurf, Berechnung und Bemessung von Holzbauwerken – Allgemeine Bemessungsregeln und Bemessungsregeln für den Hochbau (in English, *DIN 1052 Design, calculation and dimensioning of timber structures - General rules and rules for building construction*): 1988, Deutsches Institut für Normung (DIN), Berlin.

⁸ NBR-7190 Dimensionamento de estruturas de madeira (in English, *Design of timber structures*): 1997, Associação Brasileira de Normas Técnicas (ABNT), Rio de Janeiro.

- beam: span, sectional dimensions (slab thickness to beam depth ratio, span to beam spacing ratio \equiv side ratio), plan dimensions, equivalent length, variation of the bending moment distribution over the beam length (hogging or sagging moments);
- slab: sectional dimensions, width to thickness ratio, total width of the slab to beam length ratio;
- beam spacing/clear distance to the adjacent beam;
- web: stiffness;
- flange element: stiffness, span-width ratio, ratio of longitudinal and shear stiffnesses of the flange;
- connection between slab and beam: number of shear connectors and degree of interaction;
- boundary conditions (essentially on the transversal direction);
- loading type, magnitude and location;
- behavior range: elastic or plastic;
- material properties: modulus of elasticity (ratio between the modulus of elasticity of the beam to the slab), yield strength, ultimate strength, inhomogeneity, anisotropy or orthotropy;
- neutral axis position;
- section location;
- flexural cracking;
- transverse reinforcement;
- shrinkage;
- stress level;
- geometric imperfections, eccentricity and stress imperfections (initial or residual stress).

Several studies tried to develop a model for the effective width simpler or more accurate than the existent at the time, some of them aimed at comparing it with the existing ones, especially to those proposed by the standards. Several techniques and approaches were used, from theoretical: through analytical deductions, mathematical or finite elements models; to statistic and experimental ones. Hence, the methods found for the computation of the effective width are quite different with regard to the use of the stress curve over the width of the concrete slab or the resolution of harmonic series, regression equations combining membrane and bending stress effects or equilibrium equations, concerning forces and moments and the neutral axis location (Adekola 1974b, Amadio *et al.* 2004, Ansourian 1975, Chen 1995a, Chiewanichakorn *et al.* 2004, Daniels 1990, Natterer and Hoefl 1987). Also the use of models based on FE formulation computer programs is very common. In this case with a variety of goals related with the effective width or the stress distribution (closely correlated), and modeling options such as: 2D vs. 3D analysis, non-linear behavior, full composite action,

concrete cracking consideration, among others. Some of the FE models were used to perform parametric studies in order to analyze the way in which the effective width was affected by some characteristics as, for example, the span length, the slab depth or the beam cross-section.

With respect to the experimental studies, several approaches were adopted depending on the specific aim of the investigation. Some researches aimed at comparing the experimental results with the values obtained from the standard recommendations. For these, the common experimental procedure passed through the reproduction of the standard conditions, with the application of concentrated loads at specific locations over the beams. Other researches focused on the evaluation of the influence that several parameters may have on the effective width value, performing cross-sectional and connection degree variations.

Some authors chose, exclusively, to compare several researches with each other, listing the experimental conclusions in order to better characterize the effective width of composite steel members. The studied parameters were essentially the following: type of load (concentrated *vs.* distributed load), girder spacing, load magnitude, boundary conditions (simple *vs.* continuous span beams), negative moment regions of continuous composite beams with continuous slab reinforcement, and span length (with different values for end spans, interior spans or cantilever spans).

Clearly, there is a significant amount of information about effective width proceeding from different sources, as scientific texts or structural design standards, covering structures composed by various materials. Therefore, it was considered very important to present the literature review on the effective width separately, using the structural materials in which the literature was based as criterion to perform that separation. Steel-concrete and timber-concrete composite structures are, thereafter presented in two subsections. As mentioned before, a large number of parameters and phenomena affect the effective width, many of them of material nature. The importance in presenting separately the findings associated with the different materials is evident. The perspective of the standards was included in these groups due to their importance in providing design guidelines and because some of the studies were based on the existing regulations.

2.2.2 Steel-concrete composite structures

Concerning the current standards and restricting the analysis to the European zone, the concept of effective width is usually connected with the shear lag phenomenon, hence associated to the stress distribution, as in codes EC2 (EN1992 2004), EC3 (EN1993 2005, EN1993 2006) and EC4 (EN1994 2004, EN1994 2008) which deal with concrete, steel and steel-concrete structures, respectively. As mentioned before, the shear lag phenomenon is associated with bending, whether a concentrated or a uniformly distributed load is acting.

However, the type of load is one of the factors referred as affecting the effective width value. Besides the loading type, also the web and flange dimensions, the span length and type (external, internal, cantilever), the support conditions and the transverse reinforcement are listed in EC2 (EN1992 2004), as being the factors on which the effective flange width depend on.

Both Eurocodes which refer to concrete (EN1992 2004) and steel (EN1993 2006) structures suggest an equation in order to compute an effective width, depending on parameters as the effective length of the continuous beam or the web and flange widths, among others. The part 1-1 of EC4 (EN1994 2004), referring to steel-concrete composite structures, besides suggesting equations to compute the effective width (3), also states a specific simplification for beams on buildings: the assumption of constant effective widths over two particular zones, the whole region in sagging bending of each span and the whole region in hogging bending on both sides of an intermediate support. Anyhow, the effective width value is limited to a value specifically related with the distance between adjacent beams, Fig. 2.1. This implies that the effective width is, at most, equal to the sum of half the distances between the beam and the adjacent beams, considered for each side.

$$b_{eff} = b_0 + \sum \alpha_i b_{eff,i} \quad (3)$$

where: b_0 is the distance between the centers of the outstand shear connectors, which may be taken as zero for analysis of building structures;

α_i is a parameter, unitary at mid-span or internal supports, otherwise is given by $\alpha_i = (0.55 + 0.025 L_e / b_{eff,i}) \leq 1.0$ (with L_e - the equivalent span); and

$b_{eff,i}$ with $i = 1, 2$, is the value of the partial effective width of the concrete flange on each side of the web or beam.

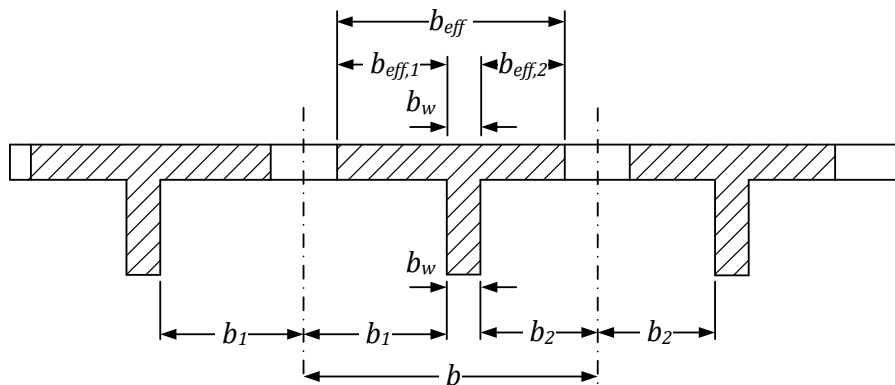


Fig. 2.1 – Effective flange width parameters, *ad.* (EN1992 2004)

In EC4 (EN1994 2004) it is possible to find the concept of effective width associated with steel-concrete composite slabs subjected to concentrated loads, Fig. 2.2. This code states that this type of loads should be considered as being distributed over an effective width measured at the up level of the sheeting ribs. Separate considerations are presented for situations where the loads are acting parallel or perpendicular to the slab span.

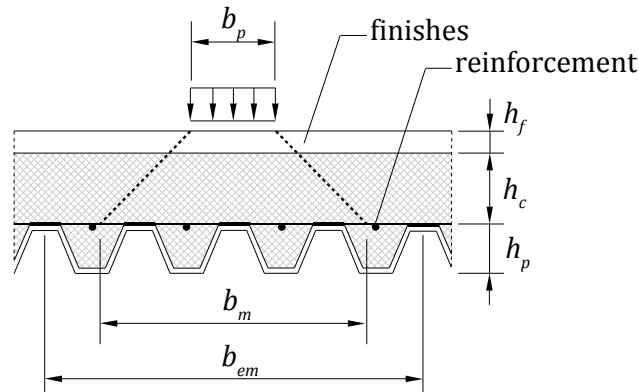


Fig. 2.2 – Lateral dispersion of concentrated load in steel-concrete slabs, *ad.* (EN1994 2004)

Concerning to standards, there are some authors which concentrated their work to make easy the use of standard rules, explaining the basic concepts and the proper manner to use them. This is the case of Johnson, in his book *Composite Structures of Steel and Concrete*, (Johnson 1994). This author discussed, among other subjects on steel-concrete structures, the specific situation of simply-supported steel-concrete composite slabs and beams when subjected to concentrated loads. One of the studied topics was the punching shear, and the slab resistance to it, as a possible critical point. In this case, the failure is assumed to occur on a “critical perimeter” which is defined for reinforced concrete slabs by assuming a 45° spreading through the top layer, Fig. 2.3.

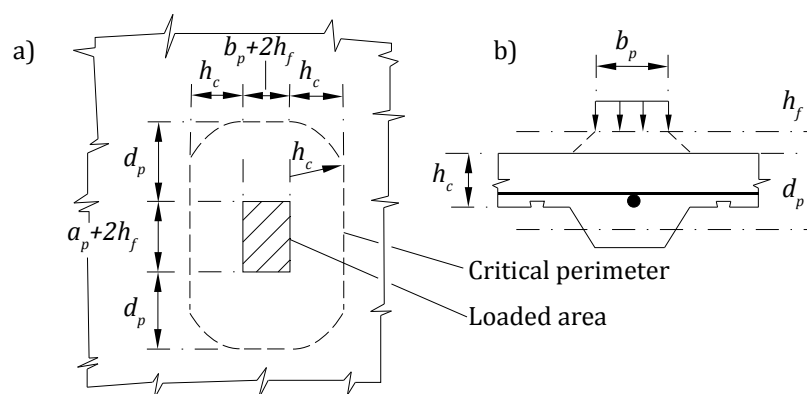


Fig. 2.3 – Critical perimeter for punching shear, *ad.* (Johnson 1994)

With regard to the action of point and line loads in composite slabs span in one direction only, as are heavy machinery or partition walls, European codes, as EC4, define effective widths for bending and for vertical shear resistance, as functions of the shape and size of the loaded area. According to Johnson, these rules were essentially obtained gathering knowledge from simplified analyses, test data, and experience. Once again, those widths can be found considering a 45° line of distribution, from the application surface up to a certain depth in the slab, and also the width of application and the thickness of concrete and finishes, if any, Fig. 2.3. Johnson considers reasonable to assume the same rule in the spanwise direction, despite this to be omitted in the codes. By its turn, the width of slab assumed to be effective for global analysis (for continuous slabs only) and for resistance is obtained through the Equation (4).

$$b_{eff} = b_m + j \cdot L_p \cdot \left[1 - \frac{L_p}{L} \right] \leq \text{width of the slab} \quad (4)$$

where: b_{eff} is the effective width of the composite slab;

b_m is the width of the composite slab over which a load is distributed,
 $b_m = b_p + 2 \cdot (h_f + h_c)$ with: b_p - width of the concentrated load; h_f - thickness of the finishes; and h_c - thickness of slab above the sheeting, see Fig. 2.3;

j is a coefficient taken as: 1 for vertical shear; 2 for bending and longitudinal shear, except for and interior spans of continuous slabs, for which 1.33 should be taken;

L_p is the distance between the nearest support of the slab and the center of the loaded area, see Fig. 2.4 a); and

L is the span of the slab.

For a simply-supported slab subjected to point load, the sagging moment per unit width depends on this effective width. Thus, the variation of the effective width with the distance between the nearest beam axis and the center of the loaded area tends to be that on Fig. 2.4 a). The load is assumed to be uniformly distributed along line BC, whereas the resistance is distributed along line AD, so there is a sagging bending along AD. The maximum sagging bending moment is at E, and is given by

$$M_{sd} = P \frac{b_{eff} - b_m}{8} \quad (5)$$

where: M_{sd} is the maximum sagging bending moment;

P is the point load;

b_{eff} is the effective width of the composite slab; and

b_m is the width of the composite slab over which the load is distributed, Fig. 2.4.

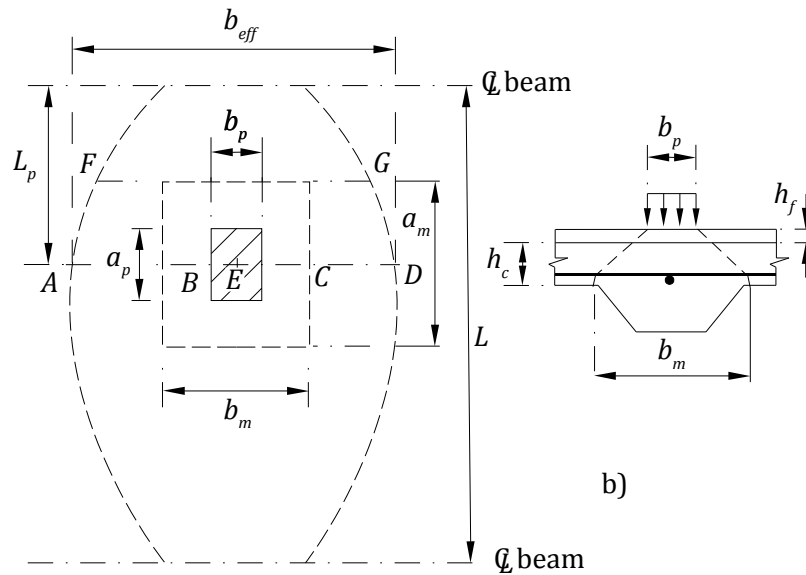


Fig. 2.4 – Effective width of composite slab for point load, *ad.* (Johnson 1994)

Concerning the scientific literature specifically focusing on steel-concrete structures, it was found to be quite extensive, contrary to other materials. Thus, only that aiming at studying the concept of effective width and considered very important for the current investigation will be cited.

The work by Adekola (Adekola 1974b) was one of the first to be published on this topic and presents a study on orthotropic composite beams. This study focus specifically on the interaction between steel non-prismatic beams and orthotropic concrete plates, based upon the linearized theories of the bending and tension of thin plates. Adekola analyzed the consequences of varying the elastic shear connection, given by the shear connection modulus (k_s) and the flexural rigidity of the steel beams (through g/H) on the effective width. The influence of those characteristics was qualitatively evaluated through their effects in the so-called effective width factors. These factors were defined for the membrane stresses (β_{st}) and for the moment-curvature relationship for a beam (β_M). The effective width factor for the membrane stresses was defined through the comparison between the membrane stress distribution of the available contributing width, *i.e.* the joists spacing, at constant maximum longitudinal stress, and the force equal to the interacting axial forces. As for β_M , the effective width was obtained by comparing the moment-curvature relationship for a steel beam alone subjected to a given loading situation with that for the composite assembly under the same

load and support conditions. The author also studied structures with continuous beams, aiming at considering more common typical non-prismatic profiles of continuous bridges.

Through its qualitative evaluation, Adekola found that a partial interaction in continuous non-prismatic beam concrete deck systems had some influence on the shear lag. Also, the values of deflection were closely related with k_s , diminishing with the increase of the shear connection, with similar conclusions relatively to slip. Concerning β_M , it tended to decrease as g/H diminished, similarly to k_s . He also noted that the stiffening effect of the concrete plate on the steel beams varied with the shear connection modulus with the ratio of deflection of the interacting elements to that of the steel beam.

Ansourian presented a study on steel-concrete composite slabs in the elastic range (Ansourian 1975). The study focused on the differences associated with the use of T-beams instead of the whole slab. He intended to represent the composite slab knowing that the behavior of both type of structures was not similar, especially when considering stress combination associated with a concrete slab or an isolated T-beam. The author emphasized the fact that, generally the distribution of membrane stress across the slab did not coincide with that developed in an isolated beam and that the stresses caused by bending of the slab were a more complicated problem. Ansourian performed a theoretical analysis using two different widths for the composite T-beam, and an FE analysis of a composite slab, using thin plate and line elements to represent the membrane and the joists, respectively. He has assumed a rigid connection between the continuous concrete slab and the top flange of the parallel I-joists spanned between rigid columns. The slabs were subjected to two types of loads: uniform load over the whole slab and uniform load along the line of each joist, intended to estimate the error arising from the assumption that the entire slab was applied directly to the joist. The total load applied to the floor was the same in both loading cases.

Based on previous researches, the author defined as “principal variable” of the study the ratio between bending stiffness of the joist and the slab given by Equation (6). The values adopted for ω ranged from 0.24 to 6.00, values obtained with $h = 150$ mm, $I = 44.3 \times 10^6$ mm⁴ and $I = 1132 \times 10^6$ mm⁴, covering the range from a light to a very stiff joist.

$$\omega = (EI)_{joist} / (D \cdot b_{eff}) \quad (6)$$

where: ω is the ratio between bending stiffness of the joist and the slab;

$(EI)_{joist}$ is the bending stiffness of the joist, with E - bending modulus of elasticity (MOE) of the joist and I - moment of inertia of the joist;

D is the thin plate flexural rigidity, $D = (Eh^3)_{slab} / (12(1 - \nu^2))$ with E - bending

MOE of the slab, h - slab thickness and ν - Poisson's coefficient; and b_{eff} the effective width of the slab.

Thus, by comparing results obtained from the theoretical and numerical analyses and also from experimental results obtained on a composite beam to column connection it was found that ω would affect not only the axial load distribution along the joist, but also the bending moment, both in the joist and in the concrete slab in almost every locations. Concerning the choice among analyzing the whole slab or a T-beam, the author stated that the use of the T-beam theory generally estimates conservatively the stresses if using an effective width whose value was limited by the distance s_b between parallel joists (when evaluating joists stresses) and a quarter of the span (when evaluating slab stresses).

Evans and Wright (Evans and Wright 1988) obtained the slab width that might be effectively carrying the compression in the system by checking the strain measurements. The ratio between the strain across the slab and at the centerline was found to vary very little due to shear lag (even for low ratios of span to slab breadth: Fig. 2.5). The slab was simply supported and subjected to a four-point loading system to represent the uniformly distributed load. After, a preliminary cycling test performed in order to eliminate any chemical bond that might exist between the steel and the concrete, the testing program with beams loaded to failure was carried out. Several parameters were changed during the program, namely the type of concrete (to light-weight concrete), the embossment pattern and the slab span and depths.

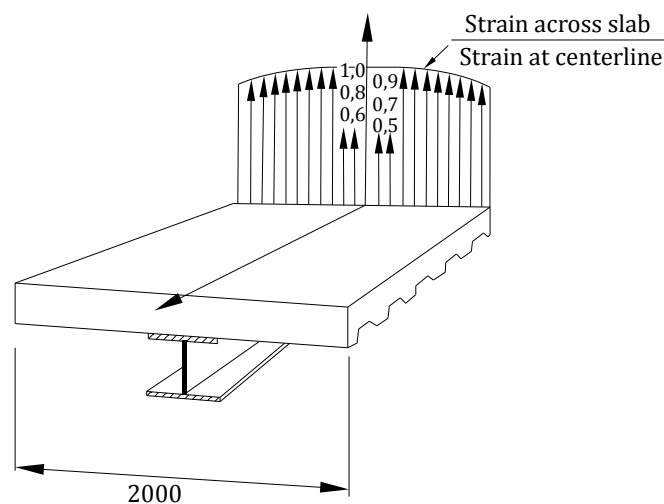


Fig. 2.5 – Distribution of strain across the slab, *ad.* (Evans and Wright 1988)

Although, the concept of effective width has a commonly accepted theoretical definition, there are authors who think that a different definition is needed. This is the case of Chiewanichakorn *et al.* (Chiewanichakorn *et al.* 2004). These authors proposed a new definition for the effective width, for a particular structure type and range of behavior: steel-concrete composite bridge girders at the Serviceability Limit State (SLS) (elastic behavior). In elastic stress analysis, the theoretical effective width was already defined as the width where a constant stress distribution, equal to σ_{max} , can be assumed. However, since the stress is not constant over the slab thickness, it is considered as reference the distribution at the central fiber of the concrete slab. While for thin plates it reveals very simple, for thick plates it can be a problem. This is one of the reasons pointed out for the need of a new definition for the effective width. Another reason is intimately related with the structures analyzed by these authors, steel-concrete bridges. According to Chiewanichakorn *et al.* the effective width associated with these structures depends essentially on the girders span and spacing between them (girder size and deck thickness had insignificant effects), whether for thin or thick plates. Thus, through the Finite Element Method (FEM) using non-linear finite element analysis, validated based on experimental results, Chiewanichakorn *et al.* developed a new and, as described by the authors, “more versatile” effective flange width definition for simple-span bridges, Fig. 2.6:

$$b_{eff} = \frac{C_{slab}}{q} = \frac{C_{slab}}{0.5t_{c,slab} \cdot (\sigma_{c,max} + \sigma_{c,min})} \quad (7)$$

where: b_{eff} is the total effective slab width for one girder;

C_{slab} is the total compressive force in the slab, $C_{slab} = \sum_{i=1}^n \sigma_i \cdot A_i$ with n - total number of slab elements in compression; i - deck element number, $i = 1, 2, \dots, n$;

σ_i - deck element normal stress; A - deck element cross-sectional area;

q is the force per unit width of slab;

$t_{c,slab}$ is the total slab thickness subjected to compression;

$\sigma_{c,max}$ is the maximum slab compressive stress; and

$\sigma_{c,min}$ is the minimum slab compressive stress.

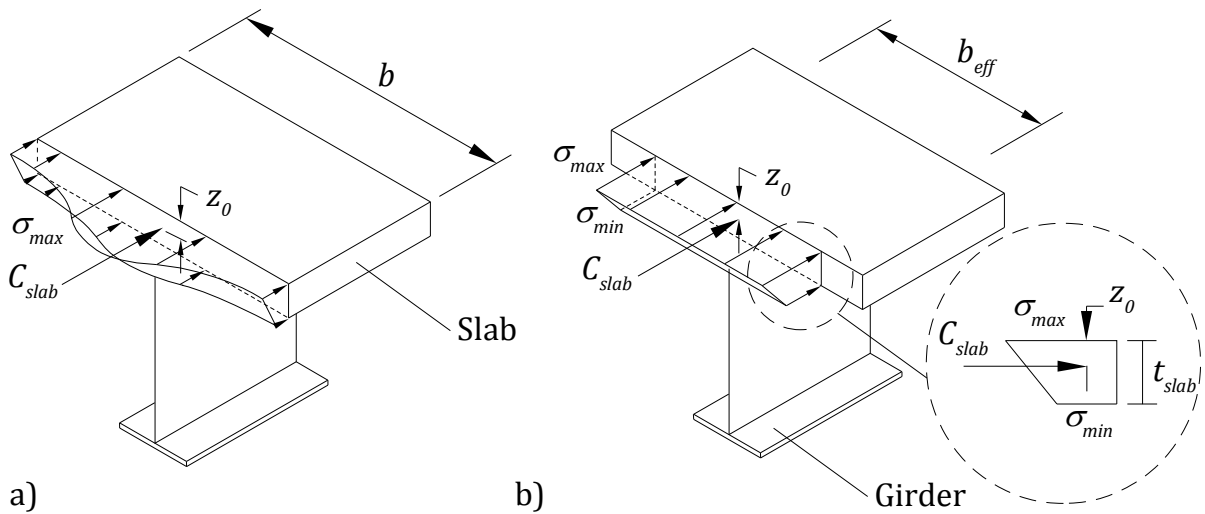


Fig. 2.6 – Determination of effective flange width for positive moment section at SLS, *ad*.
(Chiewanichakorn *et al.* 2004)

Through the presentation of a numerical example, Chiewanichakorn *et al.* showed the simplicity and accuracy of their proposal. According to them, this method suggests that a larger effective flange width could be used when compared to the rules provided by the United States (US) bridge design specifications.

According to Miotto (Miotto 2009), based on the work developed by Chiewanichakorn *et al.* and presented in (Chiewanichakorn *et al.* 2004), the FE studies presented to quantify the effect of several parameters on the effective width led to the definition of this magnitude as the sum of the partial effective widths, $b_{ef,e}$ and $b_{ef,d}$. By their turn, these were defined for simply supported beams through the Equation (8). The effective slab width showed to tend to the slab dimension, Fig. 2.7, whereas the ratio $2b_i/L$ nears zero.

$$\begin{cases} \text{If } \frac{2b_i}{L} \leq 1; \frac{b_{eff}}{b_i} = 1 - 0.6 \frac{2b_i}{L} \\ \text{If } \frac{2b_i}{L} > 1; b_{eff} = 0.2L \end{cases}, \text{ with } b_{eff} \leq b_i \text{ or } b_{eff} \leq b_{ic} \quad (8)$$

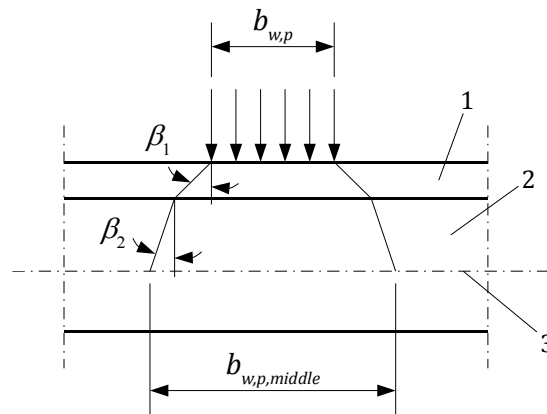
where: $b_{eff,e}$ and $b_{eff,d}$ are the partial effective widths (see Fig. 2.7);

b_i is the half distance between the beam axis and the adjacent beam;

L is the beam span; and

b_{ic} is the distance from the beam axis to the slab end.

subjected to a concentrated load, Fig. 2.8. This code sets out some specifications considering an effective contact area at the middle plan of the deck, obtained based on the width of the applied load and on the materials that compose the deck, pavement and timber deck plate. Concerning the Ultimate Limit States (ULS), the effective width must be computed based on the ratio between two bending moments: the maximum obtained in the beam representing the plate and the maximum obtained for the plate, by performing a plate analysis, Fig. 2.9.



Key: 1 - Pavement; 2 - Timber deck plate; 3 - Reference in middle of timber deck plate

Fig. 2.8 – Dispersion of concentrated load from contact area width $b_{w,p}$, in timber laminated deck plates, ad. (EN1995 2004b)

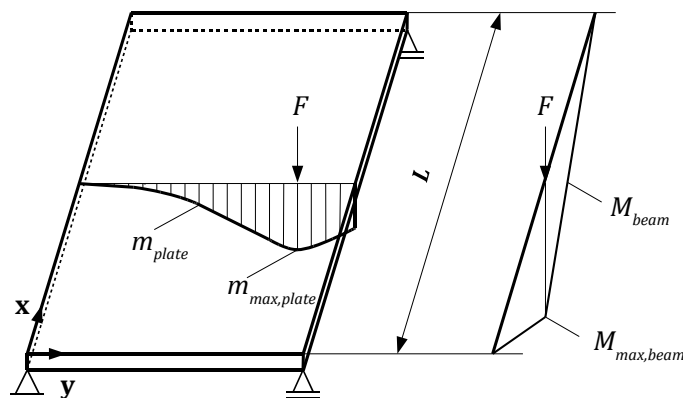


Fig. 2.9 – Example of bending moment distribution in the plate for determination of the effective width, ad. (EN1995 2004b)

As previously mentioned, the use of timber-concrete composite structures dates back to the beginning of the last century, especially in the period between Wars, due to the steel scarcity. Since then, the studies about those structures have continued, attempting to characterize the essential points of the structural behavior with a special emphasis on the

conditions and constructions that may be used in practical applications. Few researches were found to deal with the effective width of these composite structures, although some had used this parameter in their investigations. This is the case of (Moreira 2001), whose investigation focused on the bending design of timber-concrete composite beams. In this study, the effective width was associated to the connection effectiveness using essentially steel-concrete composite structures scientific background, (Timoshenko and Goodier⁹ 1951; Marguerre¹⁰ 1952; Johnson and Lewis¹¹ 1966; Adekola 1968; Gjelsvik¹² 1991; Vallenilla and Bjorhovde 1985). Miotto (Miotto 2009) studied timber-concrete composite structures constituted by glued laminated timber beams, with glass fiber reinforcement, and a concrete deck. Their focus was on the design method of this type of structures, especially on the parameters that may affect their behavior, and particularly the effective width definition. Miotto based his research in studies covering several material compositions, including timber-concrete structures. However concerning the definition of the effective width, due to the lack of knowledge for these composite structures, he based his work essentially on the study by Chiewanichakorn *et al.* (Chiewanichakorn *et al.* 2004), reported above.

One of the most relevant investigations on this topic associated to timber-concrete composite structures was authored by Julius Natterer and Michael Hoefft. In 1987 these authors published a report (Natterer and Hoefft 1987) where the structural behavior of timber-concrete composite structures was studied. The study focused on proving the validity of the behavior of such structures using the general theory of elasticity (theory of elastic composite). To attain that, a beam subjected to the most common load cases (point load, uniformly distributed load and sinusoidal load) was considered. The study also covered the problems associated to the effective width of timber-concrete composite slabs, adjusting the analysis with the theory of elastic composites to consider the consequent effects.

These authors developed and proposed a method for the effective width based on definition of reduction factors. By using a theoretical approach, they related the normal force/stress integrated in the width of the cross-section and the simple beam theory for various loading conditions (point load at mid-span, uniformly distributed and sinusoidal), and obtained a definition of the corresponding reduction factor. This made the authors state that a

⁹ Timoshenko, S.P., and J.N. Goodier. *Theory of Elasticity*. McGraw-Hill, 1951.

¹⁰ K. von Marguerre, Über die Beanspruchung von Plattenträgern. *Der Stahlbau* 8 (in English, *About the stress of cantilever panel. Steel construction*), 1952.

¹¹ Johnson, J.E., and A.D.M. Lewis. Structural Behavior in a Gypsum Roof-Deck System. *Journal of the Structural Division-ASCE* 92, ST2 (April): 283-296, 1966.

¹² Gjelsvik, A., Analog-Beam Method for Determining Shear-Lag Effects. *Journal of Engineering Mechanics - ASCE* 117, 7: 1575-1594, 1991.

weighted sum of the terms associated with the reduction factor was enough to obtain the effective width associated to it. Thus, knowing the strong influence of the loading type on the effective width, the reduction factors were obtained for point loads and uniformly distributed loads. Another parameter that significantly affects the value of the effective width is the type of internal forces to which the composite cross-section is subjected. Consequently, besides the pure normal stress, also the pure bending stress was considered and the reduction factors obtained in a similar manner.

Reduction factors due to the bending stresses:

$$\left\{ \begin{array}{l} \text{For uniformly distributed loading: } \beta_{MG} = 1 \\ \text{For point load at mid-span: } \beta_{MG} = 1 - 0.25 \cdot \left(\frac{2b_i}{L}\right) \cdot \frac{\lambda}{(1 + \lambda)} \end{array} \right. \quad (10)$$

Reduction factors due to the normal stresses:

$$\left\{ \begin{array}{l} \text{For uniformly distributed loading: } \beta_{NG} = 1 - 1.4 \cdot \left(\frac{2b_i}{L}\right)^2 \cdot \frac{\lambda}{(1 + \lambda)} \\ \text{For point load at mid-span: } \beta_{NG} = 1 - 1.4 \cdot \left(\frac{2b_i}{L}\right)^2 \cdot \frac{\lambda}{(1 + \lambda)} - 0.8 \cdot \left(\frac{2b_i}{L}\right) \cdot \frac{\lambda}{(1 + \lambda)} \end{array} \right. \quad (11)$$

where: $2b_i$ is the distance between two adjacent beams;

L is the beam span; and

λ is the shear influence number, defined by $\lambda^2 = G^2 \cdot L^2$, where $G^2 = \frac{(E_1 \cdot A_1 + E_2 \cdot A_2) \cdot k}{E_1 \cdot A_1 \cdot E_2 \cdot A_2} + \frac{k \cdot r^2}{(E_1 \cdot I_1 + E_2 \cdot I_2)} = W^2 + \frac{k \cdot r^2}{(E_1 \cdot I_1 + E_2 \cdot I_2)}$ with $k = \frac{K}{s}$, K being the simple shear stiffness, s - the mean spacing between connectors, E_i - MOE along major axis of the part i of the cross-section and A_i - cross-sectional area of the part i , W - beam deflection.

Although as part of a preliminary study, also (Simon 2008) analyzed the effective width of the composite element. From the reduction factors calculated based on the study of Natterer and Hoefl (Natterer and Hoefl 1987) and on the DIN FB 102¹³ standard, Simon presented the relationship between the effective width and the ratio between the support width and the beam

¹³ DIN-Fachbericht 102: Betonbrücken (in english, *DIN-Technical Report 102: Concrete Bridges*), 2003.

span. Comparing these results with those obtained by Natterer and Hoefft she found that, for the chosen cross-section geometry, an exact solution could be obtained. Providing that the span length is equal or higher than 15 m and the acting load is a moment load or a uniformly distributed load. To smaller spans the solution is on the safe side, and combined with point loads, the effective width is significantly reduced.

From the above descriptions, it is noted that the researches on timber-concrete structures about effective width and the associated phenomena are very scarce and this topic needs more investigation.

2.3 Distribution of concentrated loads

2.3.1 Preliminary notes

This section presents the relevant studies, as well as some normative guidelines to clarify how the distribution of load between the various elements of the floor/slab structure occurs when subjected to a concentrated load. Associated with this phenomenon, the concept of *distribution width* is very important. It defines the width in where the influence of the concentrated load is effective. As for the effective width, also the methods used to consider the distribution width and the associated phenomena are quite different either by performing a grillage or FE analysis, or by carrying out field or laboratory tests (Araujo 2009, Mullenex 1993, Nie *et al.* 2008, Thomas 2000). Although the investigation on this topic has been performed not so comprehensively as for the effective width, some authors listed several parameters that may affect the distribution width. A few of them were listed in (Thomas 2003, Thomas 2004b) for the specific case of wood-based isotropic sheathings, namely: the span for the near practical range of properties these materials; the thickness; the degree of fixity at the supports and the anisotropy or orthotropy of the material.

Thus, as in the previous section, the literature review associated with the distribution of concentrated loads was separated for the different materials, specifically, to steel-concrete composite structures and timber and timber based structures where timber-concrete composite structures are included. The standards considerations were also considered.

2.3.2 Steel-concrete composite structures

Enclosed in a larger program of theoretical and experimental research on steel-deck-reinforced floor slabs, Porter and Ekberg Jr. (Porter and Ekberg-Jr. 1977) presented the essential conclusions obtained from five full-scale tests performed in two-way simply supported floor slabs. According to them, the usual approach to analyze and design steel-deck-reinforced floor slabs by considering a one-way floor slab system is not the most

appropriate. Knowing that there is a distribution of forces in the direction transverse to the deck corrugations, this must be considered in design. Thus, the authors studied the two-way behavior of this slab system when subjected to point loads (as those from a fork-lift truck).

The tested specimens were simply supported on the sides transversally to the steel corrugations, and along the corrugated sides ball-bearing-ball caster bearing supports. Only for the first slab, the corners were restrained in order to prevent vertical uplift to occur. Three of the tested slabs had supplementary reinforcement in the form of welded wire fabric, one of the remaining had supplementary reinforcing transverse to the deck corrugations in the form of deformed wire uniformly spaced and the other had no supplementary reinforcement at all. Also the steel deck section was different for the five composite slabs, according to the previous groups presented (the first three, the fourth and the fifth). Concerning the concrete, all the specimens were composed by different compressive strength concretes. The first slab had been loaded from zero to ultimate and the others from zero to about 64 % of the ultimate load and then cyclically unloaded/load until ten cycles had occurred. In all the slab specimens four concentrated loads were applied, simulating the action of a fork-lift truck. 229 mm (\cong 9 in) square pads were used to transmit the load to the slab top. Results showed that most of the load flow through the so-called "strong" direction (parallel to corrugations), 72 to 78 %. However, these load distribution changes as the load nears to the ultimate value, becoming quite marked the one-way action of the main load-carrying element of the slabs. At that time the load percentage supported by the "strong" direction reached 97 % of the total load. The maximum edge reactions in the weak direction usually occurred when the live load was about 50 % ultimate, or roughly equivalent to the design load.

Mullennex (Mullennex 1993) developed an investigation about the load distribution, and the associated distribution width, in steel-concrete composite slabs, constituted by a normal concrete slab over steel trapezoidal sheets, when subjected to concentrated loads. According to the author, some characteristics inherent to this slab type, as the spacing and the geometry of the ribs, are essential considerations in the design of these slabs, since they affect their behavior. The goals of this work were essentially attained by experimental tests on specimens using two different cross-sections, simply supported and subjected to concentrated loads applied across and along the slab, using a 40.6 \times 40.6 cm (\cong 16 \times 16 in) grid. Aiming at obtaining a criterion of loading distribution for light gage composite steel slabs several parameters were recorded, such as crack patterns, load-displacement behavior and failure loads. The specimens were tested firstly by applying a usual load value, recording the vertical deflections, and later, the same slabs were loaded at the absolute center, recording the deflections at the axe, until failure.

The gathered data was used to characterize the behavior and to develop an approximate theory allowing the understanding of the real loading distribution. To do so, Mullennex

compared the experimental results with those obtained with the theoretical design equations and also with the standard recommendations. Although established as a common practice, the assumption of a “strip width”, over which the load is acting, was considered by Mullenex as non-realistic. This parameter is proposed by the *Steel Deck Institute* (SDI)¹⁴ for slabs acted by concentrated loads, based on the basic concrete theory of a 45 degree angle for distribution. However, when comparing it with the distribution width obtained from the experimental tests, the author found that the latter are nearly two times higher. Concerning to the theoretical equations, for wide slabs with short spans subjected to concentrated loads, by associating them to a sinusoidal shape assumed for the slab deflections, an adequate prediction of the ultimate load could be obtained. The comparison with the experimental results proved the adequacy of these equations in the design. Also the theoretical distribution width either along or across the span showed to agree with the experimental deflection results. The width along half of the theoretical span was effective, which was in accordance with the theory. The actual slab showed to be completely effective over the transversal direction, diverging from the one-way slab theory used in the design of composite slabs. This conclusion was also corroborated by the study by Roeder (Roeder 1981) who observed that the loaded panel only supported 50 % of the load with the remaining being distributed by the adjoining ones. Despite these conclusions, Mullenex highlighted a set of parameters whose effect in the distribution width should be studied before design guidelines would be established, as the deck type, the concrete depth, the width, the span length and the number of spans.

The study by Chen (Chen 1995a) focuses on the prediction of the lateral load distribution in bridges, with a particular structural characteristic, unequally spaced I-shaped girders. To attain this goal, distributions factors were determined based on FEM for bridge analysis. The author defined two models differing in the elements chosen to the I-shape girder: the beam model, simple and more practical, and the plate model, complex and allowing different steel grades to be considered. While in the first, standard beam elements were defined, in the second the web and flanges of the I-beam were defined using plate elements. Nevertheless, both used shell elements to define the slab. Simply-supported bridges were studied in this work, assuming hinges at one end and rollers at the other. Due to its lower redundancy, these structures represent the most critical cases. The slab and the girder were connected through rigid link elements, defined between their centers of gravity. Constraints imposing equal vertical displacement were defined at the two nodes of a rigid element. Aiming at obtaining

¹⁴ Steel Deck Institute Design Manual for Composite Decks, Form Decks, Roof Decks, and Cellular Metal Floor Deck With Electrical Distribution, Canton, Ohio: SDI, 1989.

the maximum live-load distribution factors (DF) associated with the maximum bending and shear efforts, Chen considered two particular loading conditions: moment loading condition, which produces maximum flexural effects; and shear loading condition, which leads to the maximum shear effects on the girders. The live loads were assumed to move on the bridge deck longitudinally and transversely until maximum bending or shear effects of girders are reached. When the locations of wheel loads did not match the nodes of the shell element in the bridge deck, the author considered a “tributary area” in order to estimate the equivalent nodal loads.

The distribution factor obtained using a refined FEM can be computed based on the number of loaded traffic lanes (N_L), the composite girder moment ($M_{comp,i}$) and the total composite girder moment ($\sum M_{comp,i}$), through $DF_i = (N_L \cdot M_{comp,i}) / \sum M_{comp,i}$. To obtain the composite girder moment the author presented two different procedures, the beam theory and the plate theory, nonetheless both had associated the concept of distribution width. In the former procedure, the effective width was based on American Association of State Highway and Transportation Officials (AASHTO) standard recommendations¹⁵ and depended on the span length, the average spacing of three consecutive beams or the center-to-center spacing between the exterior and interior girders, and the slab thickness. In the latter, the distribution width was, theoretically, used as integration range to compute the slab bending moment at the slab center of gravity, unless some simplifications were considered.

Chen implemented this method to obtain the live-load distribution factors and compared them with the simplified methods to estimate the distribution factors, (Chen 1995b). According to the author, the material formulation of the plate (elastic plate or orthotropic plate) in a linear analysis with the beam model showed to have almost no influence in the value of the maximum DF. This allows the choice of an elastic plate for the deck modeling, instead of a complex one.

Concerning the maximum DF, the plate model showed to predict slightly higher values than the beam model (between 4.2 and 3.6 %, for the interior and exterior girders, respectively). The nonlinear analysis, by its turn led to slightly lower values than the linear ones (± 8 %). However, the forces and moments of girders computed from this analysis were decreased at significantly higher rates, resulting in a more economical bridge design. From the

¹⁵ AASHTO, Standard Specifications for Highway Bridges. American Association of State Highway and Transportation Officials, Washington, DC (1991).

analyzed simplified methods, the one proposed in NCHRP 12-33¹⁶ is the one which gave the best estimation of the maximum DF. The following equations describe this simplified method based the bridge span (L) and the center-to-center girder spacing (s_b):

$$DF_{ext} = f(DF_{int}) \quad (12)$$

$$DF_{int} = 0.5[0.15 + (s_b/3)^{0.6}(s_b/L)^{0.2}] \quad (13)$$

According to this author, simplified methods for estimating live-load DF showed that, generally, they would not be suitable for bridges with unequal girder spacing, besides to be too conservative for bridges with uniform girder spacing. He suggested a revision and the incorporation of the results from the refined analysis proposed on his the study. As for the refined methods (the FE method; the grillage analogy (GA) method; and the series or harmonic (SH) method) to estimate the live-load DF, beam model or plate model, the author listed the most important parameters which were considered to give an accurate prediction (in ascending order): diaphragms; material strength; span length; transverse distribution of girder stiffness; girder spacing and pattern; bridge skew; and analysis type. The approach through refined methods was categorized as more rational, very effective and efficient, and capable of handling a general bridge system. However, further investigation, by performing parametric studies, is recommended.

Luttrell (Luttrell 1995) performed a study on the transverse distribution of non-uniform loads on steel-concrete composite slabs. The main goals were to evaluate the behavior of these structures and to develop a design method adequate to this slab type when subjected to non-uniform loads. Thus, in spite of the difficulties to simulate the real conditions, six full-scale tests were performed in composite slabs subjected to concentrated point and line loads. The corresponding deflections, steel strains and failure modes were analyzed. To attain the second objective, the author proposed a new model, reflecting the actual behavior of composite beams subjected to the considered loads. This was achieved by defining an equation which describes the actual distribution width of the slab, with a fairly high degree of accuracy, based on the relative magnitude of the strain in the center of each unit width. When there is the need to analyze a complex problem, the usual application of simplified procedures not always represent the real behavior. That is why the author mentioned the researches by

¹⁶ National Cooperative Highway Research Program (NCHRP), Development of comprehensive bridge specifications and commentary. Report NCHRP 12-33, Transport Research Board, Majeski-Masters, PA (1993).

Porter¹⁷, on simply supported beams and by Heagler¹⁸ on slabs with multiple panels, and also the researches by Roeder (Roeder 1981) considering the blocking action of shear studs and the action of concentrated loads and that by Mullenex (Mullenex 1993) on transverse distribution of load in composite slabs.

The author was particularly interested in the relationship between the transverse curvature and the load distribution on the loaded test slab. Thus, the experimental specimens were established considering some factors that might affect this curvature and, consequently, the distribution of the applied load. Six slab specimens were built differing in reinforcement and deck (steel and concrete), but with some common construction details. All of them were composed by a steel deck and a concrete slab poured over the connected steel panels, totaling 2.74×3.05 m ($\cong 9 \times 10$ ft). The point loads were applied over a steel plate of 30.5×45.7 cm ($\cong 1 \times 1.5$ ft) and the line loads along steel beams measuring 10.2 cm ($\cong 4$ in) wide and separated from the concrete surface through a layer of soft particle board to minimize localized stress concentrations.

Panels with different depth and patterns of embossment were used to build the specimens. Also different reinforcement was used in the specimens. The first four slabs were reinforced in both faces, using steel rebar on the bottom and welded mesh wired rebar on the top. In the first two slabs only half of it was reinforced, while in the remaining slabs, the entire top surface was reinforced. The slabs five and six only had welded wire mesh. All the slabs were tested until complete failure, with the load applied in one or several stages. Four of the slabs were loaded with point loads, in various positions, and two with line loads. The first two slabs were loaded at different positions according to the cross-section reinforcement, the location relatively to the slab transverse dimension (transverse third or quarter point) and the physical behavior (elastic, plastic). The next two slabs were loaded only at the central point of the slab. The last two slabs were loaded with a line load along the longitudinal centerline of the slab. Due to the differences among the slab specimens: steel panel, dimensions and loading type; failure modes and crack patterns were somewhat different for each of them. However, no punch failure was observed in any of the tested slabs.

In order to define a method which accurately predicts the distribution width associated with the composite slabs, the author started with the observation of the experimental results. The first equation resulted from the attempt to mathematically define the strain experimental

¹⁷ Porter, M. L., Analysis of two-way acting composite slabs, *Journal of Structural Engineering*, January, Vol. 111, pp. 1-17, 1985.

¹⁸ Heagler, R. B., Luttrell, L. D., and Easterling, W. S., "The steel deck institute method for composite slab design", Spring, 1993 Steel Deck Institute design seminar, pp. 1-5, 1993.

curves and related the relative magnitude of the strain, in the center of each unit width, with the affected transverse width of the slab (d_{eff}), and the transverse distance from the center of the load point. The affected transverse width showed to depend on the load. Through an iterative process, relating the theoretical uniform load moments with the observed failure loads, d_{eff} could be obtained for the slabs loaded with concentrated loads. Taking into account that this width showed to depend on the slab depth (h) and the concrete layer thickness (h_c), the author tried to obtain the values found with the experimental tests.

$$d_{eff} = 22 \left(\frac{h_c}{h} \right) \text{ (ft)} \quad (14)$$

The theoretical distribution width was found to be greater than the actual width, for all the tested slabs. This led Luttrell to believe that the whole slab width was involved, for each case. When applying the same equations to the slabs loaded with a concentrated line load, the author found that theoretical and actual distribution widths were relatively close. Most of the slabs tested showed results in agreement with the theoretical ones.

The author found, through his analysis, the existence of transverse load distribution in steel-concrete composite slabs subjected to concentrated loads. The inadequacy of the predictions proposed by the *American Society of Civil Engineers (ASCE)* and SDI also became clear. The method proposed by Luttrell, by its turn, predicted the slab distribution width with a fairly high degree of accuracy, for slabs with relatively shallow depths of concrete cover. For slabs with a thicker concrete layer, the method proposed by the author seems to slightly deviate from the real behavior. Taking into account the increasing use of this composite system, the author suggested the adequacy of design codes to more realistically reflect their behavior. One of the suggestions involves the revision of the limit imposed by the punching failure considered in the distribution width definition, for this composite system. The use of reinforced concrete design standards rules in the design of composite slabs was considered as overly conservative.

Pennings *et al.* (Pennings *et al.* 2000) produced a report whose main goal was to investigate the lateral load distribution on transverse floor beams in twin girder steel bridges, Fig. 2.10. To attain that it was evaluated, essentially through the use of Finite Element Models (FEM), the load received by those floor beams when applying a concentrated point load over the concrete layer, in the steel-concrete composite bridge deck. The authors intended to achieve a more accurate method to obtain the bending moment associated to each floor beam. To understand the moment in the floor beams it is essential to understand the load path, so they started by evaluating the load distribution in the floor beams. The structural system as,

for instance, the existence of contact between the slab and the beam, affects the bending moment associated with the floor beams.

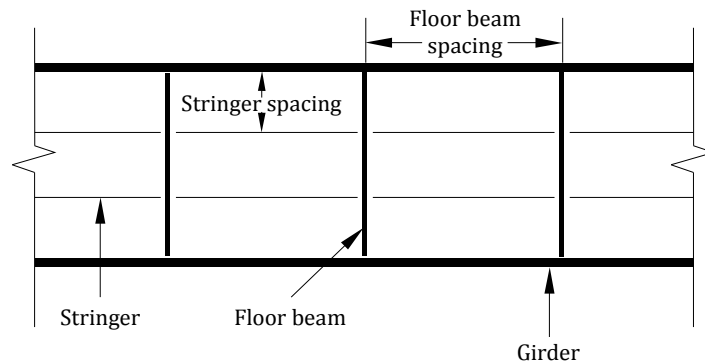


Fig. 2.10 – Twin girder steel bridge floor system, *ad.* (Pennings *et al.* 2000)

In order to study the load distribution on the floor beams caused by truck loads on the floor system, the authors also used three different methods: the Direct Load Model (DLM), the Lever Rule Model (LRM), and Slab Lateral Load Model (SLLM). The first method is adopted by some US entities, namely the AASHTO and Texas Department of Transportation (TxDOT). Both the DLM and the LRM assume the stringers and floor beams as simply supported and ignore the moment carried by the slab while the SLLM assumes contact between slab and the floor beams.

The DLM is characterized by a static longitudinal load distribution between the adjacent beams, without a lateral distribution. This means that the point load, applied in the middle of the bridge, is assumed as a point load on each of the adjacent floor beams, Fig. 2.11. The authors found with this method a conservative estimate for the load on the floor beam, since a point load will produce the maximum moment.

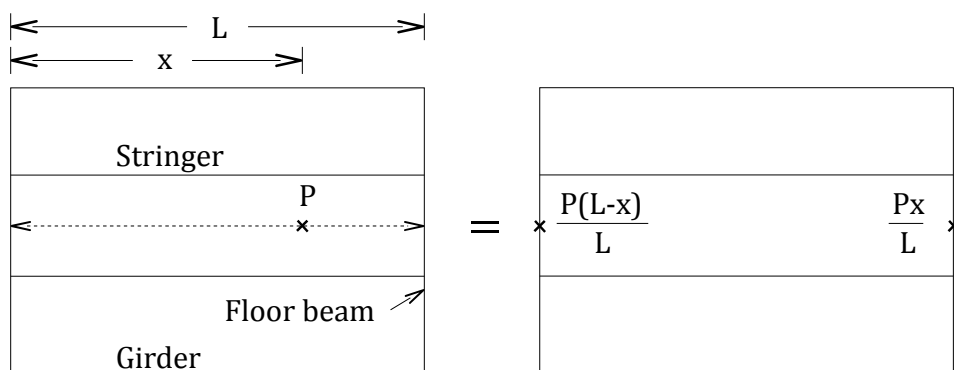


Fig. 2.11 – Direct load model for load distribution, *ad.* (Pennings *et al.* 2000)

The LRM assumes the slab as simply supported between the stringers, distributing the load to each stringer, Fig. 2.12. It results in two point loads associated with each floor beam at the location of the stringers. The authors classified this method as less conservative than the previous method and better in modeling the load path, with the load transferred from the slab to the floor beam through the stringers. Besides to be simple to use, if there is no contact between the floor beam and the slab, it was found to be a good model of the floor system.

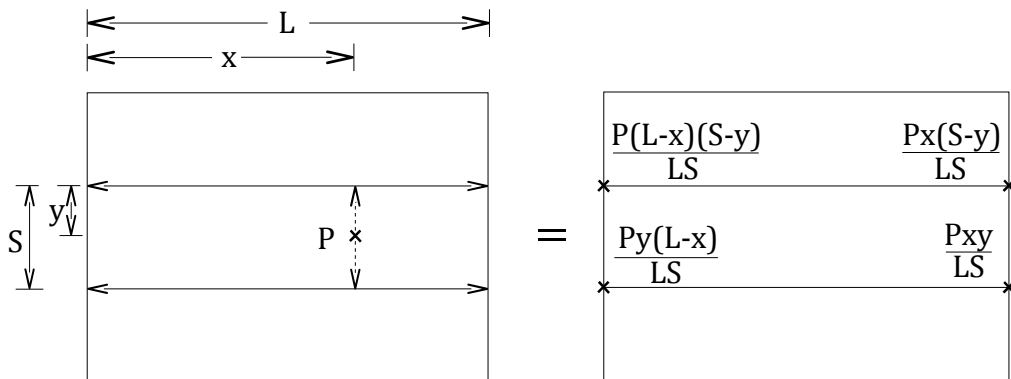


Fig. 2.12 – Lever rule model for load distribution, *ad.* (Pennings *et al.* 2000)

By its turn, in the SLLM the load flows from the slab to the stringers and subsequently to the floor beams, Fig. 2.13. At the same time, as this method considers the contact between the slab and the floor beams, the slab also transfers the load directly to the floor beams. However, this load is transmitted as a distributed load, instead of punctual. This distributed load implies a different moment distribution over the floor beam, leading to a lower maximum moment. This method became less simple than the previous because the distribution of load in the transversal direction depends on several parameters, as are the spacing of the system or the stiffness of the members. Consequently, the authors used a finite element model to analyze the bridge floor system.

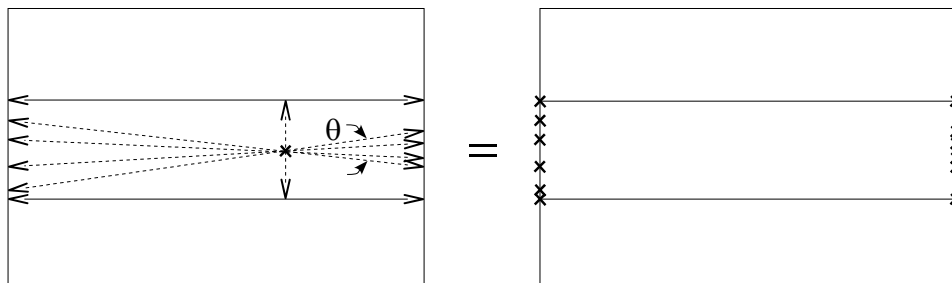


Fig. 2.13 – Slab lateral load distribution model, *ad.* (Pennings *et al.* 2000)

By comparing the moment diagram obtained with each method, assuming the action of a point load at the center of the simple span, the authors found that the boundary results were given above by the Distribution Load Method and below by the Lever Rule Method. The maximum bending moment obtained with the latter represented 77 % of the former.

The authors used the SAP2000 program to model a floor system, a twin-girder steel bridge. This floor system was composed by girders supporting the transverse floor beams, which in turn support the stringers and with the concrete slab resting on the stringers. The FE model was defined using frame and shell elements; stringers were released at the floor beams joints and the influence of the model size upon the results was studied. They concluded from the FE modeling of the floor system that the relationship between the moment of inertia of the floor beam and that of the concrete slab is the only parameter that affected the bending moment of the floor beam. The higher moment of inertia of the floor beam, the higher bending moment the floor beam will carry. These results led the authors to find a correlation between the floor beam to slab bending stiffness (EI) ratio and the percent reduction of the floor beam moment. Pennings *et al.* also analyzed an actual bridge using the FE models, the Llano Bridge, where experimental tests were already performed by a different author. Their modeling was performed using similar FE models to calculate the moments in the bridge. The models analyzed were a single-span model with two floor beams, a 2-span model (3 floor beams), and a 4-span model (5 floor beams). The two-span and four-span models were modeled with the slab continuous and cracked over the floor beam. However, no difference was found when the slab was modeled as cracked defining more than two stringer spans.

Following the FE analysis, Pennings *et al.* introduced the concept of “influence surface” defining it as a useful tool for evaluating FE models. This surface predicts the effect of a 4.45 kN (1 kip) load placed at any location on the floor system over a selected stress resultant. It also provides a “picture” for the effect that the wheel of each truck has on the moment and can easily show the differences between models, Fig. 2.14. According to the authors, their most effective use is to generate surfaces that normalize the moment generated in an FE model at each location by the moment generated at the same location using the DLM, the longitudinally distributed load placed directly on the floor beam.

The authors used the available experimental results of the floor beam moments due to a truck load on the bridge and compared them with those obtained with the load distribution method and those of the finite element models. It was found that either the DLM or the FE models overestimate, significantly, the actual moments. The authors attributed that fact to the fixity of the floor beam to truss connections and to the underestimation of slab stiffness in the finite element model.

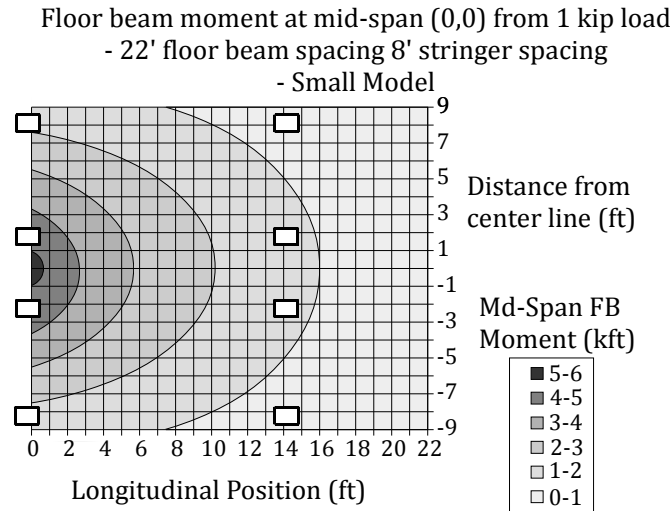


Fig. 2.14 – Influence surface for floor beam mid-span moment, *ad.* (Pennings *et al.* 2000)

Thus, in spite of still being conservative relatively to the bending moment values obtained with the FE analysis, the LRM was recommended to be used when the floor beam does not contact with the slab. Otherwise, the load is transferred in a more complex manner. In that case, the authors suggested the computation of the moment by using an equation, whose results are closer to the actual ones. The proposed equation should predict the percentage of moment taken by the floor beam and the slab, depending on the ratio of floor beam stiffness to slab stiffness.

According to Harris (Harris 2010), recent studies were developed on the lateral load distribution. The author associated this rising interest with the transition between US standard recommendations, namely from the traditional “s-over” approach (AASHTO¹⁹) to the semi-empirical based approach of the AASHTO Load and Resistance Factor Design (LRFD), AASHTO LRFD²⁰. Previous investigations included the assessment of the stringer bridges behavior, the development of methods, some through simplified equations, to determinate the load distribution, and the evaluation of parameters that could affect it. This knowledge is essential for both design and load rating of this bridge type, since the magnitude of this load

¹⁹ AASHTO, Standard specifications for highway bridges. 17th ed. Washington (DC): American Association of State Highway and Transportation Officials, 2002.

²⁰ AASHTO LRFD bridge design specifications. 4th ed. Washington (DC): American Association of State Highway and Transportation Officials, 2007 [with 2008 interim revisions].

distribution determines the resistance that must be provided by the primary load carrying members.

The lateral load distribution is a concept associated with the simplified computation of the design loads for a primary load carrying member. This is attained through the definition of distributions factors (DF). Several methods considering the lateral load distribution use these factors, but they do not share the same definition for the DF. According to the author, the methods proposed by the AASHTO Standard and LRFD specifications serve nothing but as a conservative approximation of load distribution behavior that can be used for design. Aiming to find a method adequate for analysis purposes, two of them were used by the author to determine load distribution factors (LDF) for slab–girder bridges. The beam-line method and the load fraction method, commonly used in field testing and for analytical methods, respectively, were the chosen ones. The beam-line method, in an attempt to simplify the complex interaction between the deck and the stringers, characterizes the load transference through the association of a load fraction to the primary load carrying members, or stringers, (Fig. 2.15). These load fractions allow the primary structural members to be designed, without a complex numerical analysis of the structure. This method computes the DF through the ratio between the maximum load effect (*i.e.* moment or shear) in the system (F_{system}) with the maximum load effect in a single member subjected to the same loading configuration (F_{beam}), see Equation (15). Given its practical nature, usually used in the field where the load effects cannot be measured, the load fraction approach uses the member response (*i.e.* deflection and strain). Thus, the ratio between the relative member response and the total system response is used to compute the DF. According to the author, the challenge lies in how these are related with each other and with the design, and in the choice of the proper location for measurement.

$$DF = F_{system}/F_{beam} \quad (15)$$

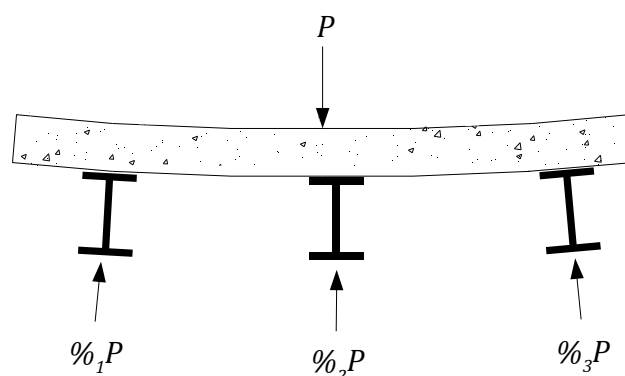


Fig. 2.15 – Load sharing behavior in a slab-girder bridge, *ad.* (Harris 2010)

Besides the referred methods, Harris also used a validated FEM to evaluate the member response and the correspondent LDF, using variations of the two methods. Through the FE analysis, the author found that parameters such as the boundary restraints and the composite action, as well as the effects of the analysis approach (beam-line vs. load fraction) significantly affect the lateral load distribution response of the system. Those parameters can be added to those that are commonly accepted as affecting the load distribution, namely the girder spacing, pointed as having the most impact, the span length, the longitudinal stiffness and the deck thickness.

Harris found that, although parameters such as secondary members or the relationships of member load effects were not defined consensually, the boundary conditions and the internal member load effects must be properly considered otherwise potential errors may arise. Secondary members showed to affect the load sharing in the bridge, in a direct way on the beam-line method, but not explicitly on the load fraction method. Besides, the two approaches showed opposite conclusions about the effect of boundary conditions. While the load fraction method obtained little effect of this parameter on the DF, the beam-line method found it. According to the author, higher restraints led to a reduction in member response, and consequently to a reduction in load distribution. This proves the need to correctly consider the actual boundary restraints and their effect on member response, when analyzing the load distribution in these bridges.

Nevertheless, both methods, load fraction and beam-line, have demonstrated their effectiveness in determining LDF. However, the proper selection and use of appropriate member response variables showed to be of extreme importance. Otherwise, DF can be incorrectly determined and may result in an underestimation of member capacity requirements, with the analytical methods, as the FEM, particularly affected. Also, the consideration of the composite action showed to be essential in the computation of load distribution, under penalty of a significant portion of internal forces and moment, transferred from the deck and the girders, would be ignored. From this may result an underestimation of the primary member load sharing response and potentially an underestimation of the applied load.

2.3.3 Timber and timber based structures

Once again, due to the lack of scientific publications aiming at studying timber and timber based structures, it was decided to present them in the same section, with the particularity of all the studies presented for the timber structures have been developed by a single author, Wilfred H. Thomas. This author developed several investigations about timber floors/decks on which he studied the effect of concentrated loads, most of the times

considering the use of Oriented Strand Board (OSB) floor decking. According to him guidance for using structural-grade OSB panels, namely deflection, safe load or safe span, was essentially provided by the manufacturers until the late 1990's, (Thomas 2000). He also highlighted the point-load deflection of wood-based floor decking in terms of the structural properties as an important amount to obtain a design method based on the mechanical properties of OSB. Although there is an equation for the deflection at the center of an orthotropic sheathing for specific support conditions, quoted by the Structural Board Association, USA, there is no guaranty that it applies to OSB sheathing, since it is expressed only in terms of the bending moduli of elasticity which, according to the author, has no direct correlation proven between the planar shear moduli of rigidity and that property. He stated that shear and flexural deflection equations expressed in terms of the shear and flexural properties would be desired. By means of a parametric study, Thomas (Thomas 2000) focused on determining the maximum shear and flexural deflections of simply supported and continuous rectangular plate models of joisted OSB floor sheathing with full edge support under concentrated load. Thus, considering the effects of decking continuity, orthotropy in bending, planar and panel shear stiffnesses and Poisson's ratio were evaluated by using an FEM. Flexural deflection showed to be significantly influenced by the level of orthotropy in bending stiffness, in contrast with the Poisson's ratio which moderately influenced it. Also support conditions showed to affect the flexural deflection, with the value of the continuous decking being about 0.8 times that of the single-span decking of the same material and span. Concerning the maximum shear deflections, support conditions (single-span *vs.* continuous span) for orthotropic plate models with the same span and material properties, showed to be practically equal. This implies that the total deflection for both support conditions considered be deemed to be roughly equal.

In 2003, the same author presented a work about the determination of models for the concentrated load performance assessment of isotropic wood joist floor sheathings, (Thomas 2003). Due to the importance of the distribution width, defined as the minimum width of one-way spanning panel that practically supports a concentrated load, a parametric study was performed. From this parametric study it was found that mechanical properties of the timber sheathing have almost no influence on the distribution width. On the other hand, it depended directly on the span for the near practical range of properties of wood-based isotropic sheathings, and inversely on the thickness and restraint at the supports. Thomas found that the distribution widths of the corresponding continuous and fixed models, composed by the same material and with identical span and thickness, were roughly 0.9 and 0.6 times the distribution width of the simply supported model, respectively. Also the load position at the panel showed to affect the distribution width, assuming dimensions of the same order as those of the loaded area. As the load moves or is moved away from the joist, the distribution width increases due

to the dispersion of the load in the plane of the panel, reaching a maximum value when the load is near the center of the area of panel between the joists. The corresponding distribution width is the minimum width of floor panel to use in modeling the concentrated load performance of wood joist floor panels. The following equation was developed by the author to compute the distribution width of the models when simply supported, $d_{eff}/L = 1.2 + 0.021 L/t$, where d_{eff} , L and t are the distribution width, the span and the thickness of the plate sheathing, respectively.

Knowing the distribution width also leads to check if the blockings (in which the floor panel is supported, along with timber joists) will contribute to the load carrying capacity and stiffness of a panel. This means that a one-way or a two-way spanning behavior would depend on the relative values of the spacing of the blockings and the distribution width of the one-way plate model. When the distribution width, for wood joist floor sheathing with full edge supports, is greater than the spacing between blockings (or width of an individual panel), the floor sheathing is effectively two-way spanning. Otherwise, the floor sheathing is effectively one-way spanning and geometric models defined by the ratio of distribution width to span are the minimum aspect ratio of the floor sheathing required in concentrated load performance tests. When the influence of the blockings on the concentrated load performance is neglected, the wood joist floor panels are effectively one-way spanning long rectangular plates, (Kearley and Carruthers 1991).

In 2004 Thomas presented a study about *Modelling the influence of boundary conditions on the concentrated load performance of oriented strand board floor decking* (Thomas 2004a). The author performed a series of laboratory tests to failure. Concentrated load performance on one-way single-span simply supported, screwed and bolted OSB panels, loaded at the center of each panel were carried out. The short-term tests were performed on panels where the span to thickness ratios were 16.7 and 25.0 (spans of 300 mm and 450 mm) using different types of supports in order to analyze how the boundary conditions affect the stiffness, failure mode and load capacity of the panels. Results showed that only the stiffness depends on both joint slip and support fixity, load capacities and mode of failure (punching shear) of the panels are almost independent of the boundary conditions.

In the same year, this author published the results of an investigation on the size of the test-piece in the performance assessment of wood floor panels subjected to uniformly distributed and concentrated load, (Thomas 2004b). The results obtained showed that the distribution width depends on the span to thickness ratio, on the degree of restraint at the support (fixed, continuous and simply supported) and on the relation E_x/E_y . As opposed, Poisson's coefficient and planar shear stiffness showed to be negligible.

Regarding to Thomas' work (Thomas 2003), where an equation for the distribution width was presented in terms of the span and thickness for simply supported and isotropic panels,

an upgraded equation, associated with some simplifications, was presented for the same quantity but for orthotropic panels. That implied the consideration of mechanical properties, besides the span and thickness. The equation proposed for a simply supported panel is $d_{ortho}/L = d_{iso}/(0.9 + 0.13 E_x/E_y) = (1.2 + 0.021 L/t)/(0.9 + 0.13 E_x/E_y)$, where E_x and E_y are the bending MOE in major axes and in minor axes, respectively. Knowing that the distribution width changes with the distance of the load to the joist and the position relatively to the panel, the author refers the existence of a critical width beyond which further increases in width result in negligible changes in the stiffness or load carrying capacity of the plate. The critical width is referred to as the effective or participating width in bending, *i.e.* the minimum width of the decking required in concentrated and uniformly distributed load tests.

Thomas (Thomas 2004b) used two different methods to obtain the distribution width, and consequently the distribution width to span ratio, a stiffness method and a reactive force method. Both allow obtaining the distribution width of each model subjected to a concentrated load at the center of the span, the first through the variation of the center stiffness with width of the panel, with the center stiffness taken as the load per unit deflection under the load. The second uses the distribution of reactive forces at the supports. When the curve of cumulative reactive forces *vs.* width of plate becomes asymptotic to a horizontal line, *i.e.* parallel to the width of plate axis, the distribution width has been reached. The same happen when using the stiffness method, considering the curve of stiffness *vs.* of the plate. Thus, it was possible to obtain an upper bound to the distribution width, for the three considered support conditions. For a panel with a near upper bound of ratio of span to thickness of forty, the values varied from a distribution width near 2.0 times the span, when the panel is isotropic and simply supported, to about the value of the span in the case of fixed supports. Therefore, the author considered, as an adequate value for the uniform and concentrated load performance assessment, a panel width of twice the span. The use of widths of eight times the span recommended in American and European standards were avoided.

On standardization, only the studies whose investigation focused in standard analysis will be presented, as those developed by Kearley and Carruthers (Kearley and Carruthers 1991) or Ozelton and Baird (Ozelton and Baird 2006), concerning timber and timber based structures. Kearley and Carruthers presented a report (Kearley and Carruthers 1991) which summarize the considerations of various standards about the concentrated loads, namely: the reason for the dimensions of the concentrated area; the relative importance given to concentrated loads in the design calculations, as opposed to uniformly distributed loads; the types, the number and loads duration; among others. Concerning the distribution of concentrated load the British

standard BS 5268 – part 2²¹ is referred. This British Standard provides considerations about the load sharing between primary structural members of a floor or roof built up from joists and rafters, with a defined spacing and covered with a sheet material such as plywood or particleboard. According to Kearley and Carruthers there was a common point of view, the design of a timber based roof or floor element would rarely be controlled by the concentrated load rather than by the distributed load, though local effects on the board materials themselves can often be controlled by concentrated loads. Let us consider the simplest situation, with a concentrated load applied in the mid-span of a joist, which is far from an edge of the slab. Concerning the bending stress, it is difficult to define the width of the board parallel to the joist which should be used in the calculation as the applied concentrated load is gradually dispersed in this direction. BS 5268 gives a simple solution that considers the width equal to the span, which, despite to not have supporting data, has been confirmed to some degree by work on plywood in North America. Being so, the authors considered extremely important to analyze this assumption and to restructure the method of describing the bending moment.

Ozelton and Baird presented several considerations about concentrated loads, in *Timber Designer's Manual* (Ozelton and Baird 2006). This type of load was presented either as medium term or as short term loading, caused by walls and partitions, in the first case or caused by a person, in the second. According to the authors, the consideration of concentrated load in UK codes is intended to simulate the loading of a person (particularly for roof structures), or the foot of a piece of furniture or equipment or a trolley wheel. The area assumed for the concentrated load must be proportional to the load in question. Usually, squares of 50 mm and 125 mm are taken, for furniture and equipment or for footfall loads, respectively.

Ozelton and Baird stated that, the first introduction of concentrated imposed loads in place of the equivalent slab loading raised the question about the ability of these structures to distribute the load through the construction. However, tests performed at the Forest Products Research Laboratory, incorporated in the Building Research Establishment – BRE, in England, on typical timber and deck sheathing floors, confirmed that it should not be a concern. The sheathing proved to be capable of providing significant distribution of the concentrated load from the point of application to the adjacent joists. Assuming that 50 % of the load is taken by the joist immediately beneath the applied load and the adjacent joists equally loaded with 25 % each. According to the authors, the distribution of concentrated load

²¹ British Standard BS 5268 - Structural Use of Timber, Part 2: 1991, Code of Practice for Permissible Stress Design Materials and Workmanship, British Standard Institute (BSI), London.

will usually give a less onerous design condition when compared to the corresponding uniformly distributed load (but for ceiling constructions).

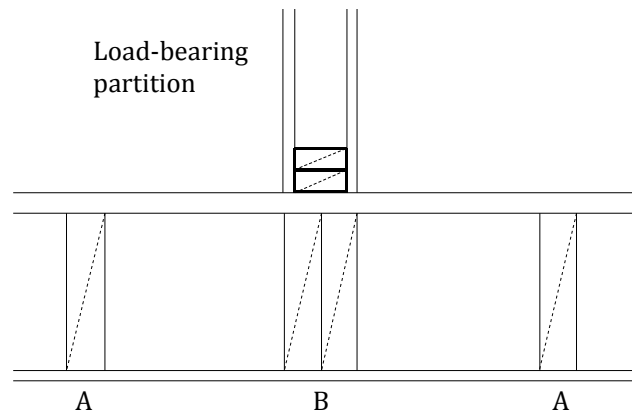


Fig. 2.16 – Vertical section of a load-bearing partition supported by a timber joisted floor, *ad.* (Ozelton and Baird 2006)

These authors also referred special considerations to concentrated loads from partitions. The case illustrated in Fig. 2.16 can raise some questions, namely, if joists B, supporting the partition should or should not be designed using the mean MOE on the assumption that they are part of a load-sharing system and if the two joists A will or will not carry a share of the load from the partition. The authors defended as a good hypothesis to assume that joists B support the total weight of the partition and a share of the floor loading, since this assumption will not lead to significant differential deflection between joists A and B. In this case, any imposed loading under the “footprint” of the partition should be excluded and a consistent MOE must be adopted. According to them “it is prudent to carry out an additional deflection check to ensure that under dead loading only the deflections of joists A and B are similar and that any difference is unlikely to be noticeable.”

Concerning the timber-concrete composite structures, two researches deserve some attention, namely the one developed by Etournaud (Etournaud 1998) in the Colorado State University (USA), and that developed by Moraes (Moraes 2007) in Universidade Estadual Paulista (Brazil). Etournaud (Etournaud 1998) studied timber-concrete decks connected by anchored notches through glued dowels. His work aims were to measure the degree of composite action of the decks’ cross-section under point loads and to infer about the effectiveness of the distribution of the point load. Experimental tests, namely with an elastic point loading, cyclic, creep and failure tests were performed in deck specimens. Two bridge specimens with different geometries, rectangular and skewed, were tested with and without the concrete layer, aiming to infer about the load distribution, associated with the existence of

the concrete layer. The decks were subjected to an increasing point load, on an elastic range in the case of timber decks and until failure in the case of the timber-concrete decks. The loads were consecutively positioned at four and six different locations, on the rectangular and on the skewed decks, respectively. That enable to obtain the vertical deflections (measured at mid-span and quarters, of clear span), as well as the slip between the timber and concrete layers at the ends. The results showed that point load position affects the deflection reduction factor, found between the deflections obtained with timber decks and timber-concrete composite decks. A great increase in composite action was also found when using the glued dowel with the notch, as well as increase in stiffness, when comparing deflections on bare wood and in composite decks. Slip between timber and concrete showed to be negligible, evidencing the efficiency of the composite connection.

By his turn, Moraes (Moraes 2007) presented a study about timber-concrete composite bridges, constituted by timber truss beams and a concrete deck. He studied the wheel load distribution on the transversal direction, considering a 16 m span bridge with one traffic lane and two sidewalks for pedestrian walkway, Fig. 2.17. The analytic methods commonly used to evaluate the load distribution in decks with multiple beams on reinforced or pre-stressed concrete were listed, namely the methods by Engesser-Courbon and Leonhardt which disregard the beam torsional stiffness and the ones by Guyon-Massonnet and Homberg-Trenks which do not. According to this author, in spite of being developed for decks constituted by concrete beams, an extension can be made to a composite structure constituted by timber truss beams and a concrete deck. Based on the simplicity of application and the good representation of the proposed deck model, substantiated by other authors (Segundinho 2005, Souza 2004), Moraes choose the Engesser-Courbon method. This method assumes that transversal secondary beams, considered to be simply supported by the stringers and to behave as rigid bars, remaining with straight axes after the deformation of the set. The studies developed by Souza (Souza 2004) and Segundinho (Segundinho 2005) corroborate such choice, especially for the cases where the loading is applied near the deck's end. In both investigations, the transversal stiffness of the deck specimens was given by the concrete slab and the spacing between the longitudinal beams, without requiring transversal ones. In this manner, the transversal load distribution among stringers could be determined by computing the support reactions due to force acting on a rigid beam on elastic supports. The deck was 5.76 m wide (with 4.00 m of traffic road), and it was composed by five timber truss beams spaced by 1.40 m with a cross-section of 0.16×2.04 m, the concrete slab was 0.20 m depth.

Moraes found that the Engesser-Courbon distribution method leads to satisfactory results when the load is applied close to the bridge end. Concerning the transversal displacements, the method showed to be slightly conservative at the same time that, the essential assumption of a linear profile of displacements in the transversal direction, was not completely fulfilled.

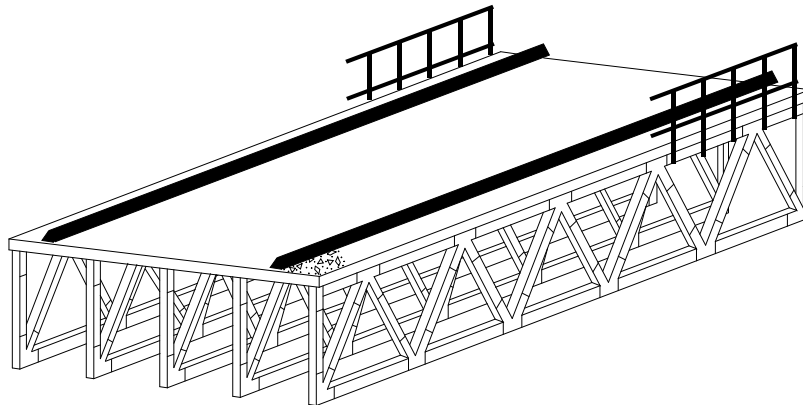


Fig. 2.17 – Timber-concrete bridge with timber truss beams, *ad.* (Moraes 2007)

Again, by comparison with the number of studies associated with steel-concrete composite structures, it is clear that there exist a lack of researches focused on timber-concrete structures concerning the distribution of concentrated loads. Consequently more studies need to be performed.

2.4 System effect

2.4.1 Preliminary notes

As presented before, the concept of system effect is associated with the phenomena which take place when the load is distributed considering the different stiffnesses of the joists composing the floor system. Given the close correlation between the stiffness and strength of the joists and the existence of an effective load distribution system, advantage can be taken from the tendency of the stiffer members, usually stronger, to receive a higher share of load. At the same time, they partially support the less stiff members, which receive a proportional, and consequently, smaller share of load. Therefore, this system tends to distribute the load from the flexible members, generally the weaker members, to the stiff ones (Cramer and Drozdek 2000, Cramer *et al.* 2000). When the structure is no longer behaving linearly, the stiffer members that would be associated with higher loads in the elastic range, may suffer plastic deformations and its stiffness will start to decrease. From this moment on, the load will tend to be redistributed to the remaining members within the assembly, and the damaged member can continue to contribute to the total load supported. This contribution will depend on the plastic deformation capacity of the damaged member (Blass 1995, Linden 1999).

The consideration of the system effect, and consequently the load sharing, arose associated with timber structures and the first records date back from the early sixties (Cramer *et al.* 2000).

As in the previous sections, the way in which the several authors and standards consider the system effect is not exactly the same. The standards tend to approach it by assuming a simplification: the use of a factor that intends to increase the elements performance. This factor has many denominations such as system strength factor, system factor, load-sharing factor and also repetitive member factor, and depends on several parameters such as the stiffnesses of the load distribution system and the support elements, the modulus of elasticity of the last and their relation with the bending strength (Blass 1995). The scientific studies usually define load-sharing factors, which intend to associate to each beam, the load that it will support according to the structure's properties. Linden (Linden 1999) draws some attention to the existence of various studies on the system effect phenomenon, and consequently, several definitions for the system factors, that may lead to describe the same phenomenon by factors with different values. Hence, the need to study and characterize the load-sharing factor is obvious. Some of the differences found by Linden include material models, considered as linear or nonlinear; the consideration of failure, assumed to happen when the first local failure occurs or at total collapse of the structure; and even the consideration of sheathing contribution to obtain the load-sharing factors. Consequently, several parameters affecting the load sharing could be collected (Araujo 2009, Clayton and Stephens 2010, Linden 1999, Simon 2008, Tucker and Fridley 1999), such as:

- the number of elements;
- the beam span;
- the coefficient of variation of the bending strength;
- the slab geometry;
- the beam spacing;
- the ratio between the global torsional stiffness and the bending stiffness;
- the bending stiffness of a principal beam;
- the ratio of girder stiffness to diaphragm stiffness;
- the composite action (partial); and
- the sheathing thickness.

Thereby, this section will describe the relevant scientific knowledge, expressed through studies and standards. Compared with the previous sections, which cover the effective width and the distribution of concentrated loads, the found studies about the system effect were mostly on timber and timber based structures. Thus, the literature review associated with it is presented first for these structures, since they were the base of the investigations performed thereafter in structures composed by other material.

2.4.2 Timber structures

As mentioned before, the concept of system effect was firstly investigated associated with timber structures. This section intends to list some of the most relevant research works, together with the standardization covering the system effect in floor structures, either listed in standards or in scientific studies.

This system effect concept does not exist in standards of other materials, as composite steel-concrete structures, for instance. Therefore, only EC5 (EN1995 2004a), was considered in this section. Also the studies performed by Blass (Blass 1995) and Ozelton and Baird (Ozelton and Baird 2006) were found relevant for the knowledge on this topic.

EC5 part 1-1 (EN1995 2004a), in the section dedicated to the ULS, introduces the concept of “system strength”, associated with structural systems composed by similar elements, equally spaced and laterally connected. When this connection is made by a continuous system, ensuring the load distribution, one can consider the advantageous correlation between strength and stiffness of the timber elements, as well as the fact that it is unlike that the weakest elements would be exactly in the zones where the stresses are the maximum ones (underneath the loads), (Blass 1995). The load sharing system allows that a higher amount of applied load to be supported by the stiffer elements, while the flexible elements support a minor amount, creating an “homogenized” deck, allowing the loads to be distributed in proportion to the element’ stiffness.

Considering that a sole concentrated load is acting on a timber floor composed by timber joists with the same stiffness, connected through sheathing, the joist immediately below the load will receive the larger proportion of load, and the adjacent joists the remaining part of the load. However, in common structures, the joists’ stiffness is not equal, with the stiffer joist tending to deform less and the less stiff to deform more. Nevertheless, the existence of a continuous element, capable of sharing the load, provides a more uniform deformation of the joists, compared with a structural arrangement without this system, reducing deformation and consequently the load to support, (Criswell²² 1983).

When there is a load sharing system, EC5 (EN1995 2004a) recommends to use a system strength factor, k_{SYS} , with a value larger than one, that should be multiplied by the strength properties of the timber elements, increasing their values. This code recommends the value of 1.10 for this factor, unless it is a laminated timber deck, for which several values are defined (from 1.00 to 1.20), depending on the number of loaded laminations and how they are

²² Criswell, M. E., New floor design procedures. Proc. 7317, Wall and Floor Sys: Des. and Perf. of Light-Frame Struct., Forest Products Research Society, Madison, Wis., 63–86, 1983.

connected. Blass (Blass 1995) studied this factor and presented the structure characteristics that may influence it, namely: the ratio between the stiffness of the load distribution system and the average member' stiffness; the modulus of elasticity of the member and their correlation with the bending strength.

According to Ozelton and Baird (Ozelton and Baird 2006), the British Standards also consider the existence of a load-sharing system, and depending on it, BS 6399²³ allows concentrated load to be disregarded on the design of supporting members of a floor. With such a system, the lateral distribution of load will reduce the effect on any member, particularly if the decking is quite thick and the effect can 'spread' (sideways and along the span) through the thickness of the decking. Ozelton and Baird underlined the fact that, even the load being quoted in codes and standards as the load per unit area, this uniformly distributed load is far from uniform in its distribution. Another pointed reason is associated with the fact that the load sharing implies loads coming from a larger area than that on a single element of the structure and hence the probability that the average load per element will be lower. Despite the lack of a consensual criterion, the load sharing phenomenon should be considered on the designing methods, with the simplest option being to consider a "10 % increase" in the enhancement of performance under load, through the consideration of the load sharing factor, K_8 .

Concerning the research performed on this subject, the works developed by (Wolfe and Moody²⁴1979; Foschi *et al*²⁵ 1989) and (Mtenga *et al.* 1995) are commonly referred by other authors as providing the bases for their investigations on system effect behavior. A simplified manner to consider the phenomena associated with the system effect is to adopt a load-sharing factor, as explained in the standardization section. Although it is assumed as a constant value used in design, this factor may assume different values according to the sheathing material, as recommend by the standards. However, several parameters can affect its value and some of the researchers tried to investigate which of them has more influence. Chasten *et al.* (Chasten *et al.* 1992) focused their research in the load-sharing effects on members in metal-plate-connected timber trusses. To attain that, structural analysis and analytical modeling was performed, together with Monte Carlo simulations, covering for various timber stiffness and strength properties and truss configurations (with a random selection of the

²³ BS 6399 Loading for Buildings Part 1: 1996 Code of Practice for Dead and Imposed Loads, BSI London.

²⁴ Wolfe, Ronald W. and Moody, Russel C., Bending strength of vertically glued laminated beams with one to five plies. FPL Research Paper 333, 1979.

²⁵ Foschi, R.O., Folz, B.R. and Yao, F.Z., Reliability-based design of wood structures. Structural Research Series, Report No. 34. Dept. of Civil Engineering. University of British Columbia, Vancouver, Canada. 1989.

timber member properties). Aiming at quantifying the load-sharing effects in the system, the assemblies were analyzed with and without attached sheathing. The mean ratios of the critical member *combined stress index*²⁶ for an unsheathed assembly in relation with an identical sheathed assembly were taken as load-sharing factors. Results showed that the value recommended by the design code at the time was slightly conservative. The authors also stated that load-sharing factors were applicable to tension and compression resistances of chords as well as to the bending resistances of wood members.

Tucker and Fridley (Tucker and Fridley 1999) studied light-frame timber structures (structures constituted by parallel members with a limited spacing, covered by a structural sheathing system, and relying on walls and floors), specifically the effect that uniform vs. concentrated load cases may have on the load-sharing behavior. The authors constructed and tested eight floor systems, subjected to a concentrated load at quarter- and mid-span of the floor separately, in order to evaluate the load-sharing behavior. With the experimental support reactions and mid-span deflections associated with previous FE results, design adjustment factors were developed, accounting for the load conditions. These factors were incorporated in design equations for a single joist, to obtain the maximum moment and deflection. Therefore, Tucker and Fridley found that, the load sharing associated with the joist directly subjected to a concentrated load tends to present moment and displacement substantially smaller.

In Portugal, Ilharco presented a study on timber floors in old buildings (Ilharco 2008), specifically in diagnosis and structural intervention, following the guidelines proposed by Eurocode 5 and other authors, such as Blass and others in the Structural Timber Education Program (STEP) publications (STEP1 1995), e.g. Lectures B2²⁷ and B16²⁸, and Foschi²⁹ *et al.* 1989. This work focuses essentially in assessing the behavior of existing timber floors and in their rehabilitation and/or reinforcement solutions. To do so, experimental load tests were performed, to understand the load distribution to the adjoining elements and the behavior of

²⁶ Combined stress index – parameter that relates compressive or tensile stress and strength with bending stress and strength according to equations (3) and (4) in (Cramer *et al.* 2000).

²⁷ Blass, H. J., Aune, P., Cjoo, B. S., Edlund, B. – Tension and compression. Timber Engineering - STEP 1. Lecture B2, Almere Centrum Hout, Holanda, 1995.

²⁸ Blass, H. J., Load Sharing. Timber Engineering - STEP 1. Lecture B16, Almere Centrum Hout, Holanda, 1995.

²⁹ Foschi, R. O., Folz, B. R. and Yao, F. Z., Reliability-Based Design of Wood Structures. Structural Research Series, Report No. 34, Department of Civil Engineering. University of British Columbia Vancouver, Canada, 1989.

the structural elements of the timber floor when subjected to loading. Also numerical model through FE aiming to predict the mechanical behavior of these floors were developed.

The experimental tests were performed in situ in a timber floor, belonging to an old building, isolated from its degraded areas through sawing of beams and bridge joints. According to the author, in this way, the assessment of the bidirectional behavior of the involved structural elements was more accurate. The tested specimen comprised seven timber beams and was laterally supported by two stone walls, despite these floors to be usually supported on the four sides. In the first test, only the central beam was loaded in order to assess the effectiveness of the load transmission to other beams through the bridge joints and the plank floor – load distribution factor. The loading was performed with three overlaid tanks filled with water, totaling 1.65 ton (roughly 16.5 kN). To ensure that the load was applied in the influence width of the central beam a timber structure was created to support the tanks. In order to guarantee the test sequence, the loading was performed assuring that the structural elastic behavior was not exceeded. To perform the second test the bridge joints were removed, and instead of one, two beams were loaded, allowing estimating the timber average modulus of elasticity.

Vertical displacements were measured in the timber ribbing at different points (depending on the beam and on the test). Ilharco obtained a similar load distribution with the two tests: about 0 % on the exterior beams, 10 % in the adjoining ones, 20 % in the closer to the central beam and 40 % in the central beam; showing that the plank floor was the main factor for the load transmission between the floor elements.

2.4.3 Timber-concrete structures

Concerning the timber-concrete composite structures, few relevant studies on this topic were found, and those presented by Linden (Linden 1999) and Simon (Simon 2008) are rare exceptions. This fact highlights once again the importance of the ongoing research. Linden (Linden 1999) investigated timber-concrete composite floor systems, and one of his research focus was the derivation of load-sharing factors. The concept of load-sharing factor was already studied by other researchers and is even used by several standards (U. S., Canadian and European). According to the author, most of the authors obtain the load-sharing factors by relating the system behavior with the behavior of a single member. By their turn, the mentioned standards define the factors based on studies about timber structures, and each of them adopts different values. However, the higher stiffness of the concrete slab when compared to that of the floor-boards, or of the sheeting, commonly used in timber floor structures leads to a higher load redistribution and consequently to an expected higher value

for the load-sharing factor. This makes it worthwhile to be studied for timber-concrete floor systems.

Linden defined the load-sharing factor as “the ratio of the characteristic strength of the system to the characteristic strength of a single element of that system regarding a uniformly distributed load.” The sharing of load was presented as caused by two consecutive effects. The first when the structure behaves elastically, and load distribution occurs depending on the element stiffness and the second when its behavior is no longer linear. According to Linden the load-sharing associated with the non-linearly behavior is not easily obtained, suggesting the use of models considering the system plasticity and cracking.

Based on simulations and tests, the author found that timber-concrete beams can experience much plasticity before the collapse. Thus, by adopting an approach using a finite element program (DIANA) he simulated tests to failure of the systems considered. He also performed Monte Carlo simulations on which the material properties were randomly assigned to the timber beams, but the concrete and the connectors properties were kept constant. In spite of adopting constant properties for the connectors, twelve configurations were simulated, in series of a hundred simulations of a single T-beam and a hundred simulations of a floor system composed by five beams. Linden also simulated five configurations for floor systems composed by ten beams. In those configurations the parameters varied were the distance between the timber beams, the thickness of the concrete slab and the stiffness and strength of the joints between the concrete slab and the timber beams.

In (Linden 1999) the load-sharing factors derived for composite systems have limited validity for not brittle joints.

The author performed a parametric study in order to evaluate the sensitivity of the load sharing factor to the system characteristics, changing one at a time with the others remaining fixed. Some characteristics were found to hardly influence the load sharing, as the sheeting thickness, the coefficient of variation of the modulus of elasticity and the correlation between the modulus of elasticity and the bending strength. Conversely, parameters as: the number of elements, the span of the timber member, and on a smaller extent, the coefficient of variation of the bending strength, showed to have great effect on the sharing of load for the studied structures. The connection showed no significant influence at ‘normal’ stiffnesses, but if the connection were considered as rigid the load-sharing increases about 20 %, in specific comparative conditions. The span variation (3.30 - 3.84 m) significantly affected the load-sharing factor, on about 25 %, when both the beam depth and width were kept constant.

When analyzing the load-sharing factor for timber systems proposed by the European code (EN1995 2004a) Linden affirmed that the value set, 1.10, might be tolerable for specific series. Nevertheless, when comparing the equivalent results for floors systems composed by ten beams and those for single T-beams, that value might seem too high for timber-concrete

composite systems in general, even with a maximum difference obtained being quite small, 9 %. The reduction associated with the load-sharing factors for these composite systems relatively to those associated with timber systems is justified with the prevention of the plasticity of the timber in the compression zone. Linden found through different simulations that especially this plasticity enables a higher load sharing. Although the decreasing in the strength of the connections led to an increase of plasticity of the timber, the amount associated with the timber compression zone was considered of no interest, due to its value comparatively to the bending strength (< 0.8). In the same manner, the amount of plasticity associated to the connections could not always be synonymous of load-sharing.

Within his parametric study, specifically, on the effects caused by the concrete on the strength and stiffness of a timber-concrete beam, Linden also analyzed the effective width of the concrete slab. For building floors with spans of, at least, five times greater than the distance between the beams and subjected to uniform loads, it corresponds to the distance between the timber beams. For beams in which point loads are applied, the effective width tends to diminish (8 % was the value found by Natterer and Hoefft (Natterer and Hoefft 1987) when the point load was applied at mid-span of the beam).

More recently, Antje Simon published a study about the behavior of timber-concrete composite road bridges (Simon 2008). Her work was essentially centered in developing design guidelines and in establishing characteristic values for the design of timber-concrete composite structures. She also studied the load distribution over the cross-section. First of all, the direct loading on the principal beam was found not to be stored according to the load deformation. Instead, it is a function of the bending and the torsional stiffness of the group, and depends on the second principal beam, to share the bearing capacity. The transversal load distribution was defined as depending on the span geometry, the spacing between the principal beams and their materials' properties, specifically on the ratio between the global torsional stiffness and the bending stiffness. When geometrical conditions are constant, the load is distributed uniformly as the torsional stiffness of the principal beams increases and their bending stiffness decreases.

The geometrical conditions under study caused an increasing of the total torsional stiffness, a decreasing on the cross-sectional deformations relationship and, consequently, a better distribution of the load.

The lateral load distribution for the timber-concrete composite section, as function of the span and the cross-sectional stiffness, was compared with that for sole concrete cross-section. The load distribution for the concrete cross-section showed to be significantly better than the obtained for the composite cross-section. This was justified by the higher torsional stiffness of the concrete cross-section. With the increase of the spans, the beam deformations increase, and consequently the loads will be distributed over the principal beams more uniformly. For

minor spans the transversal distribution showed to be marginal. To compute the global bending stiffness, the higher stiffness of the composite element was considered. However, the author did not consider it for the torsional stiffness. As a consequence, the transversal distribution decreased with the increasing of the composite element stiffness.

The parametric study the load distribution on the transversal direction was analyzed for the higher value of stiffness of the composite element, since this represents the least favorable design situation. The transversal distribution associated with the beam cross-section for flexible beams showed to be non-linear.

2.4.4 Steel structures

Once the timber structures were the base to the system effect consideration, it was difficult to find studies on structures composed by different materials. Concerning to steel structures, Clayton and Stephens (Clayton and Stephens 2010) presented the results of their research on cold-formed steel framing system. Since this is a repetitive structure, the authors compared the design procedure with that adopted for timber structures with similar characteristics (repetitive members covered by a sheathing system), specifically the use of a load-sharing factor. The reason lies in the simplified manner in which this factor is used in the increase of the design bending strength, while for the cold-formed steel repetitive members this is not an accepted procedure. Thus, the authors intend to conclude about the validity of a load-sharing factor applied to a cold-formed steel framing system.

The work developed by Clayton and Stephens (Clayton and Stephens 2010) is based on the knowledge already collected for timber structures, namely design values, composite action, load sharing and residual capacity (related with the ability of a system to not collapse after the failure of an element), in literature and standards. With this information and assuming the same principles used to define the load-sharing factors in timber structures, given the similarities with the cold-formed steel, the authors found that a the load-sharing factor would be feasible for cold-formed steel when the values are based only on load-sharing and full composite action. They also state that, for timber repetitive systems, the residual capacity could be added to the considerations used in the (AF&PA³⁰ 2005) methods for the calculation of the load-sharing factor – partial composite action load sharing – due to their positive effects on the flexural capacity.

³⁰ AF&PA, National Design Specification for Wood Construction. Washington, DC: American Forest & Paper Association, 2005.

The concept of “system effect” is, therefore, commonly approached using “load-sharing factors” or “system factors”, either by standards or research works, aiming at taking advantage of this effect. Nevertheless, investigation still can be performed, not only by the number of parameters involved in the phenomena associated, but also as a matter of uniformity, in order to enable to adopt coherent factors when describing the same effect, (Linden 1999).

2.5 Portuguese situation in terms of timber floors

It is known that Portugal has little tradition in constructions performed exclusively with timber. However, this material is used for some centuries, usually associated with masonry, to perform part of the buildings, as: the floors, through bearing systems and sheathing, roofs' structures or even walls. In Portugal there are few investigations in this field.

The main focus of this section is the use of timber in building floors, proving an overall perspective of the Portuguese scenario, while allowing foreseeing the possibilities for intervention in the rehabilitation area.

Despite the limited number of studies, there is one that worth to be presented, namely that developed by Vicente (Vicente 2008). This author collected an important set of information about the Coimbra's downtown buildings, in where about 800 buildings were inspected with different techniques (eye inspection, photography and filling in of inspection forms). Despite focusing on the buildings of Coimbra, it also provides information on the country constructions. Considering that the structural concepts are generally the same, the structural solutions will be rather similar, varying only the materials used to produce them.

This work identified some particular characteristics in specific areas, as for instance, the constructive solutions used or the applied wood species. According to Vicente, in Coimbra' downtown, the buildings have various architectural typologies and constructive solutions depending on the size and the heritage of the buildings, with some of them having recently been classified by UNESCO as having a World Heritage status. Most of the inspected buildings were residential and had simple structural schemes: stone masonry walls, floors and roofs in timber structures. Resisting walls showed to be composed by small and medium-size irregular stone masonry (dolomitic limestone) and their thickness varies in height, on average, from 70.0 cm on the base to 26.0 cm on the top.

Concerning to floors (structure and cladding), roofs and panel interior walls were found to be commonly constructed using timber. Most of the plank floors were nailed to the beams and their connection to the walls was commonly made by inserting the beams in openings arranged in the wall with the same dimensions as the beam cross-section, without a real connection. As outlined above, the wood species employed to build the floors was one of the

studied points. Maritime pine (softwood), Portuguese oak and chestnut (hardwoods) are the most commonly used in beams. With smaller representation he found Spruce (Whitewood) and Pine (Redwood), Poplar and Eucalyptus, with the last two being less suitable to structural functions. Most of the floors were composed by parallel timber beams on which the timber planks are laid and connected through nails. Spacing between beams axis depends on the floor span, varying between 30.0 cm to 40.0 cm for spans among 3.00 m and 4.00 m, and the beams cross-sections had an average width and height of 10.0 cm and 18.0 cm, respectively. For spans of 6.00 m the cross-sections increased to 12.0 × 20.0 cm, and for spans between 6.00 m and 15.00 m to about 25.0 – 33.0 × 25.0 – 40.0 cm. For the last spans, great principal beams are usually placed perpendicularly to the floor ribbing on where the planks are nailed, in some cases, bridging joists and secondary floors were found. Besides the variability of the beams sizes, it was found that, most of the beams were non squared poles, this means, poles without rectangular section, sometimes only poles to which the bark was removed.

Vicente affirms that, the relation among the spacing between the beams and bridging joists width reflects the good or bad quality of the housing, in most cases 1:3 or 1:4. The conservation of the supports is intimately related with the floor covering, with particularly evidence for the floors cover by timber planks. Timber floors act like diaphragm stiffeners of the structures on masonry buildings and decrease the instability risk of the masonry walls with great slenderness, especially in higher floors of tall buildings. The most common pathologies found on timber floors were aging problems and biological attacks, as well as deformations on the supports, cambering, water action and cracking. Some areas showed greater damages on the floors. In terms of structural problems excessive deformations and weaknesses of the beam's connections near the walls were found.

As said before, the simplest connection between the timber floors and the masonry walls is the fitting of the beams on holes in the walls, without an element capable to distribute the load like a timber ground sill in order to avoid stress concentration in that zone. The connection between these two elements is critical since the transfer of static and dynamic loads is warranted or conditioned by the degree of connection.

During the study, several floors were found to be reinforced in order to control the deformation and increase the load carrying capacity: insertion of steel profiles on the longitudinal and transversal directions of the bridging joists; introduction of columns to act like intermediate supports, replacement of some beams and introduction of cooperating formwork. The problems on timber floors are usually associated with the nature of the material and aggravated by their aging, degradation and creep effect. One of the major anomalies that were found was the excessive deformation described as a pronounced deformation of floors with great deflections between the beams of the support structure. This can had been caused by:

- an insufficient beam cross-section and excessive spacing between them, characteristic of these buildings, affecting the floor durability in long-term;
- natural aging of timber, warping associated to non-controlled drying processes, suppression of structural walls where the floors are supported, lack of horizontal bridging joists of the principal ribbing in order to improve the membrane effect and the stiffness of the timber floors;
- the presence of water and the xylophages' attacks.

The interruption of structural elements and the introduction of excessive load can lead to excessive deformation of the timber floors. Adapting the building to new requirements in terms of loading, which can be excessive sometimes, can lead to non-recoverable deformation levels, accelerating the long-term deformation effects. In the analyzed region, buildings with basement are rare and very often the floors above the ground floor serve as storage for the shops installed on the ground floor. In many of these cases reinforcements were added (beams doubling, introduction of new timber elements and/or steel profiles) after visible deformations of the existent ribbing.

2.6 Final remarks

As the previous sections show, the action of concentrated loads over floor/deck structures is an important issue whose effects in terms of structural behavior must be known.

This chapter highlights the essential concepts associated with the phenomena of transversal distribution of load and the way in which they are considered. The notions of effective width, distribution of concentrated loads and system effect were given, and the approaches to these concepts by various authors and their considerations in standards rules were presented.

In the literature, several parameters were found to affect the effective width, associated with the shear lag phenomenon; the distribution width, related to distribution of concentrated loads; and also the load distribution factors, usually associated with the system effect considerations. Among those were, most of the times, geometrical and material properties, and sometimes the manner in which they were modeled or considered in the study. Despite they were associated with different concepts, it was possible to find some common parameters among the listed ones, such as: the span, the boundary conditions, the number of beams and the spacing between them. This can be a good starting

The structures under consideration in the scientific works and standardization were composed by a sole material, as steel, timber or timber based materials, or using a dual materials solution, as steel-concrete and timber-concrete composite structures. Studies on shear lag refers essentially to steel and steel-concrete composite structures. In turn, those

associated with the system effect focus on timber and timber based structures. In general, studies on timber-concrete structures are very scarce, regardless of the concept in question, hence the need to perform more studies on this area.

The collected information, as the phenomena and the associated behaviors, the way in which the studies were performed and the parameters affecting the quantities associated with the load distribution, provided the basis to initiate the investigation on the matter of this thesis. Thus, in the following chapters the approaches adopted in order to enhance the knowledge on load distribution across the support elements of timber-concrete floors will be presented.

3. MODEL DEVELOPMENT: PRELIMINARY STUDIES

3.1 Introduction

This work aims at investigating the load distribution on the direction perpendicular to the longitudinal axis of the beams in timber-concrete slabs subjected to concentrated loads. As explained before, the essential goals of this investigation are attained by using experimental and numerical approaches, with a special focus on FE modeling. The definition of the experimental program, as well as the choice of the numerical model to study these structures was based in a preliminary analysis.

This chapter presents essentially the development of an FE numerical model capable of characterizing the mechanical behavior of the composite slab structures subjected to a given loading. Numerical models have a great importance when the research aims at optimizing and comparing results. There must be a guarantee that they really reflect the actual behavior of the phenomena under study. The so called validation of the numerical model is of utmost importance. In the present research the chosen option was to validate the numerical models using experimental results. Therefore, aiming at predicting accurately the mechanical behavior of timber-concrete floors in the orthogonal direction, a base FE numerical model was established and, previously to the main experimental program, two preliminary experimental tests were performed. The experimental results permitted to confirm the validity of the results obtained with the numerical model validation, opening the possibility of further analyses with different location of the loads.

The validated base model allowed a numerical preliminary analysis, aiming at establishing the essential parameters that would affect the mechanical behavior of the composite floors subjected to the load cases under consideration. One of the main concerns of this phase was to define the experimental program, namely:

- i) the characteristics of the test slabs;
- ii) the number of specimens, their geometrical and material properties; as well as
- iii) the load types, their locations and magnitudes; and
- iv) the support conditions.

To attain that, the effects that some parameters may have on the transverse distribution of loads on commonly used floors systems must be evaluated.

Aiming to analyze its validity on the study of transversal load distribution, an analytical model was used to predict the behavior of timber-concrete composite floors subjected to

concentrated loads. It was also considered as a further element for comparison with the numerical models.

The following paragraphs describe the work in more detail.

3.2 Preliminary experimental tests

The preliminary experimental tests were performed in the DEC-FCTUC at the LEMEC laboratory. They include the testing of two timber-concrete composite floor real scale specimens. The first floor specimen was a timber-concrete composite slab with glued laminated timber (glulam, GL) beams, from now on designated as CSGL. The CSGL was composed by five rectangular glulam beams, a timber floorboards interlayer and a concrete top flange, Fig. 3.1 a) and Fig. 3.2 a). The second specimen was a timber-concrete slab with timber logs, CSTL, composed by seven timber logs and a concrete layer performed with light-weight concrete, Fig. 3.1 b), Fig. 3.2 b) and Table 3.1. Beyond different geometric characteristics, the specimens also had different material properties. The connection system, used to connect the concrete and timber elements, was chosen to be identical in both specimens.

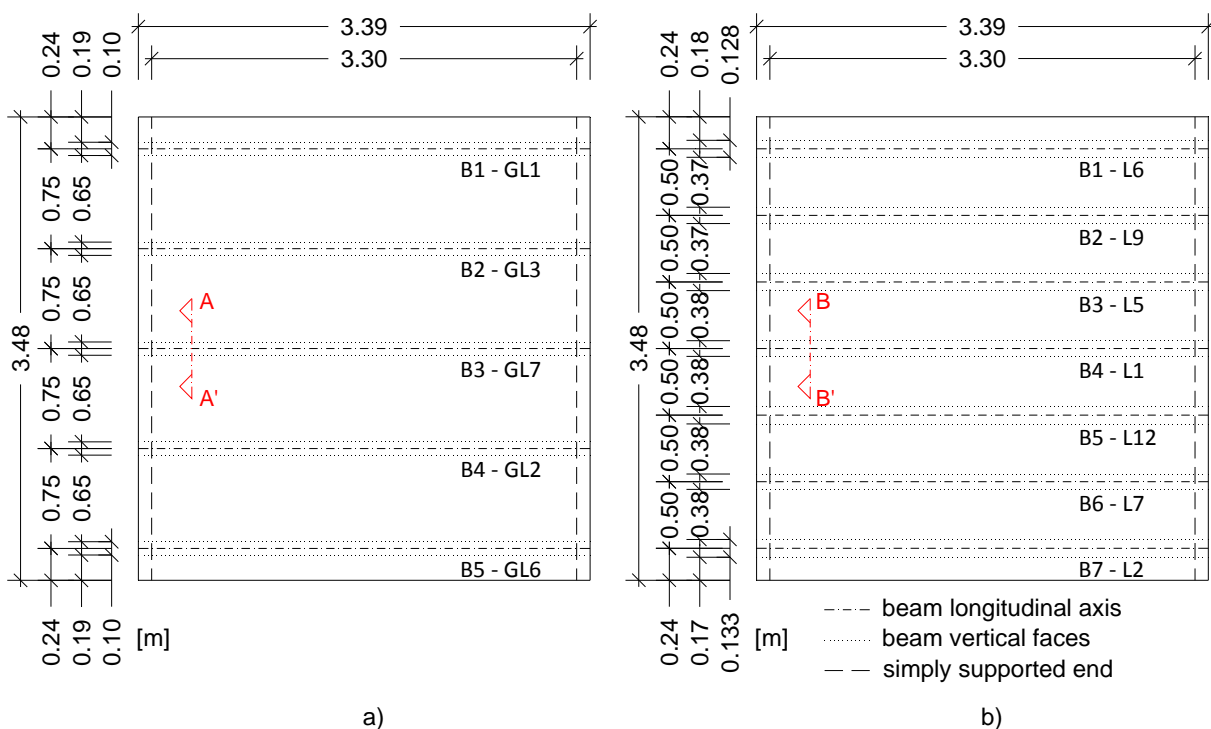


Fig. 3.1 – Geometrical characteristics, plan view: a) CSGL and b) CSTL

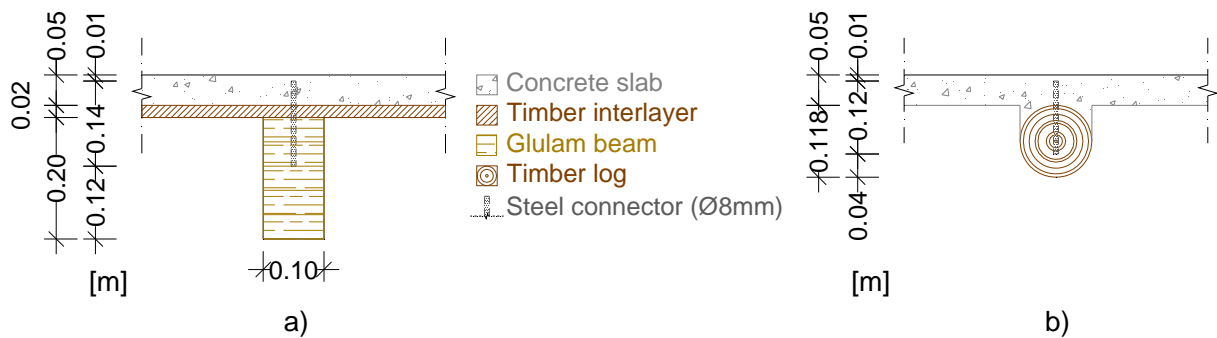


Fig. 3.2 – Cross section: a) CSGL beam (AA' line); and b) L1 beam in CSTL (BB' line)

Table 3.1 – Geometrical properties CSTL beams

Log designation	Mean diameter
	D_{med} [m]
L6	0.12800
L9	0.12300
L5	0.12850
L1	0.11825
L12	0.13075
L7	0.11525
L2	0.13300

Both the slab specimens were designed according to EC5 (EN1995 2004a, EN1995 2004b), for the loads required by EC1 (EN1991 2001). They were simply supported at two opposite ends with a span of 3.30 m (Fig. 3.1). The top concrete flange was 0.050 m thick performed on normal strength concrete on the CSGL specimen, for the CSTL light-weight concrete was used. For the CSGL specimen, the 0.020 m thick interlayer was achieved by Pine timber boards. Five rectangular section (0.100 × 0.200 m) glulam *Abies alba* beams, placed 0.750 m apart, were also part of the whole CSGL composite slab (Fig. 3.2 a)). The CSTL by its turn was composed by seven round, non-squared, *Pinus pinaster* logs, placed 0.500 m apart (Fig. 3.2 b)), whose diameter ranged between 0.11525 m and 0.13300 m, Table 3.1.

The concrete slab was provided with a wire mesh (A500NR), with diameter of 5 mm and 0.10 m of mesh spacing, in order to diminish tension effects. Each timber beam was connected to the concrete slab through 8 mm diameter reinforced concrete steel rods (A500NR) spaced by 0.10 m. Each stud in both CSGL and CSTL specimens, 0.140 m and 0.120 m long, respectively, was inserted on a predrilled hole crossing all the interlayer thickness (0.020 m) in the case of the CSGL slab, and having an embedment length of

0.080 m in the wooden beam. The remaining 0.040 m was left off the timber beams/boards system and the timber logs, respectively, Fig. 3.2, to be embedded in the concrete layer, which was to be poured later. The connection system was chosen by weighing some aspects, such as, the simplicity of application, the economy and the efficiency, namely by ensuring a good link between timber and concrete.

To characterize the materials used in the slab, some tests and measurements were carried out before assembly, namely, the weight, the global modulus of elasticity (according to the European Standard (EN408 2010)), the concrete compressive strength at 28 days. The results are summarized on Table 3.2.

Table 3.2 – CSGL and CSTL material properties

Timber beams							
Beam position	Beam designation		Global MOE		Density		
			$E_{m,g}$		ρ		
			[MPa]		[kg/m ³]		
	CSGL	CSTL	CSGL	CSTL	CSGL	CSTL	
B1	GL1	L6	12732.6	10954.3	419.88	615.19	
B2	GL3	L9	12860.3	11164.0	410.36	507.34	
B3	GL7	L5	13982.0	15784.9	425.11	663.53	
B4	GL2	L1	13401.4	16752.1	429.88	673.00	
B5	GL6	L12	12511.0	13985.2	424.16	614.63	
B6	-	L7	-	13753.6	-	545.93	
B7	-	L2	-	9888.7	-	622.91	
Concrete slab							
				MOE		Mean compressive strength	
				E_c		f_{cm}	
				[MPa]		[MPa]	
				CSGL	CSTL	CSGL	CSTL
				30000.0	14300.0	24.43	11.50

The floor specimens were subjected to a sole concentrated point load, Fig. 3.3. The CSGL floor specimen was the first to be tested. The test had some repetitions with the load applied in a different location and with a different load magnitude, Fig. 3.4. The load was applied on each beam at mid- and quarter-span, with values near the service loads, considered to be approximately 40 % of the ultimate load. This load level was assumed to be high enough to represent the service loads, but low enough to avoid the risk of inducing some kind of damage or permanent deformations. The prediction of this ultimate load was numerically estimated and will be presented ahead in this chapter.

The mechanical performance of each floor was recorded using displacement transducers and load cells. The displacement transducers were used to measure the slip between the concrete slab and each end of the timber beams and also the vertical displacement at every beam mid- and quarter-span, Fig. 3.4.

Ten displacement transducers were placed at the ends of each timber beam, with the help of steel plates screwed to each beam top. They were placed aligned with the beams' longitudinal axis with their rod near the timber-concrete interface (on a regular surface), Fig. 3.5. Concerning the vertical displacement, five displacement transducers were placed below each beam at the point corresponding to the intersection of the mid-span and the beam longitudinal axis and five others at the points corresponding to the intersection of the quarter-span and the beam longitudinal axis (since symmetry was assumed, only half of the slab was instrumented), Fig. 3.6. The load cells recorded the load supported by each beam, Fig. 3.3. They were placed under each floor beam with the help of steel plates, placed between the cell and the timber beam, avoiding damage of load concentration, and leveling devices, ensuring a beam span of 3.30 m, Fig. 3.7.

All the measuring devices were connected to a data acquisition unit and recorded every three seconds, Fig. 3.8.

Following a similar procedure, the CSTL floor specimen was instrumented with the same aims as the CSGL one: recording the slip between the concrete slab and the timber logs, recording the vertical displacements at mid- and quarter-span of each log beam, and recording the load supported by each beam. Therefore, fourteen displacement transducers were placed at the ends of each timber log, aligned with their longitudinal axes and with their rod near the timber-concrete interface, Fig. 3.9.



Fig. 3.5 – Test setup detail – CSGL: slip displacement transducers



Fig. 3.6 – Test setup detail – CSGL: vertical displacement transducers

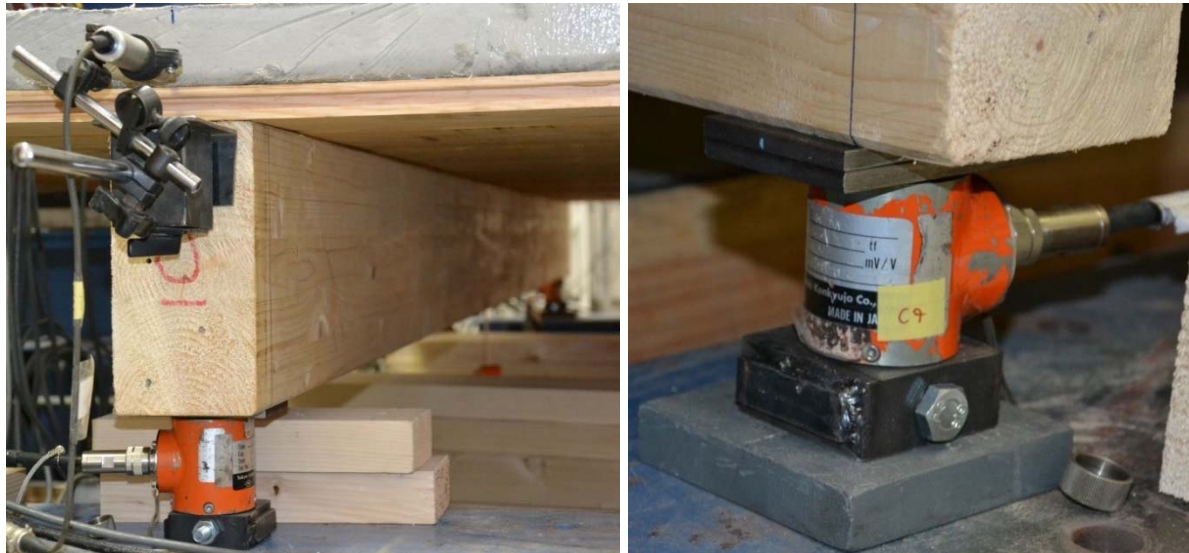


Fig. 3.7 – Test setup detail – CSGL: load cells

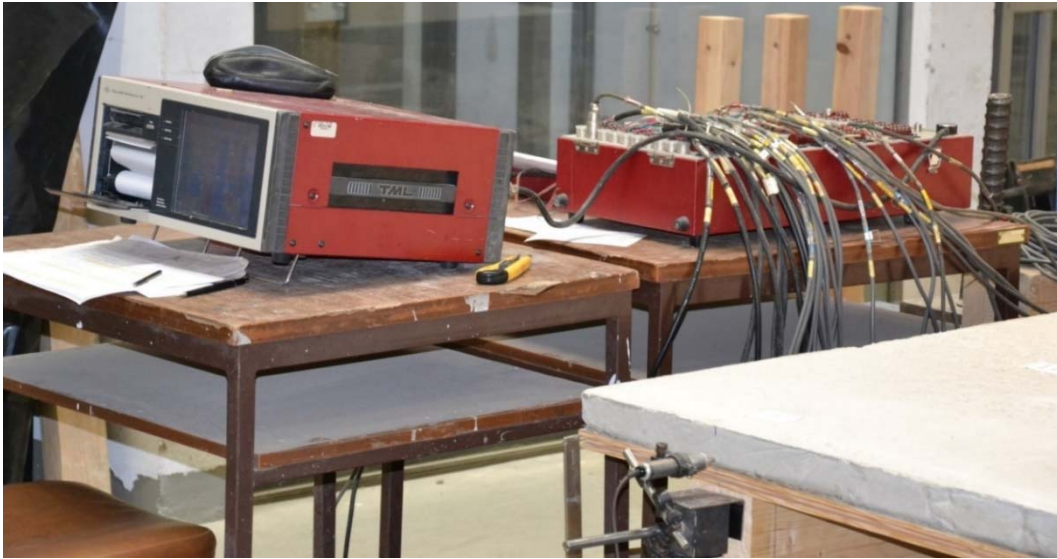


Fig. 3.8 – Acquisition unit

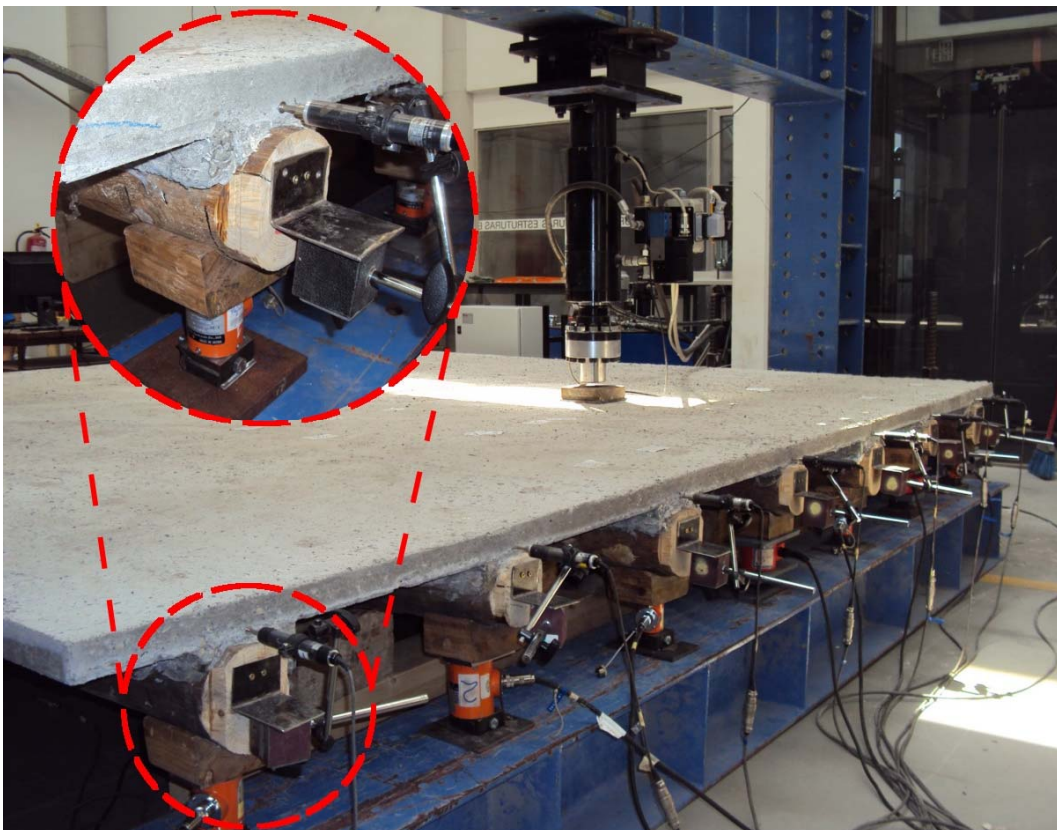


Fig. 3.9 – Test setup detail – CSTL: slip displacement transducers

Other fourteen displacement transducers were placed below the beams for recording their vertical displacement: seven at the point corresponding to the intersection of the mid-span and the beam longitudinal axis, and seven others at the points corresponding to the intersection of the quarter-span and the beam longitudinal axis. As well as for the CSGL specimen, symmetry was assumed and, consequently, only half of the slab was instrumented. The load cells recorded the load supported by each beam, Fig. 3.10. They were placed under each log beam with the aid of half-round timber pieces which created a flat surface to guarantee a complete contact between the steel plates and the load cell. The steel plates had the same function as in the CSGL specimen, placed between the cell and the timber pieces, they avoid damage of load concentration, and leveling devices, ensuring a beam span of 3.30 m, Fig. 3.10.



Fig. 3.10 – Test setup detail – CSTL: load cells

Ten loading tests were performed in the CSGL specimen: five with the load located, one at a time, at the mid-span of the beam immediately below (Fig. 3.4 – points B1 1/2 to B5 1/2, where, e.g., B4 1/2 means: beam 4 with load at mid-span), and five others at quarter-span of the beam immediately below (Fig. 3.4 – points B1 1/4 to B5 1/4 where, e.g., B5 1/4 means: beam 5 with load at quarter-span). In a similar manner, fourteen loading tests were performed in the CSTL specimen: seven with the load located, one at a time, at the mid-span of the beam immediately below and seven others at quarter-span of the beam immediately below. The load was applied, at constant rate, to the concrete surface through a $0.20 \times 0.20 \times 0.04$ m steel plate using a hydraulic jack, Fig. 3.3 and Fig. 3.11.



Fig. 3.11 – Test setup – CSTL

After testing both floor specimens, the CSGL floor was cut into five strips, giving way to five individual composite beams, Fig. 3.12. Three of those beams were then subjected to a concentrated load at mid-span, Fig. 3.13, up to 40 % of the ultimate load level. Based in the tests' results, load and slip, and by using the procedure recommended at the Annex B - EC5 (EN1995 2004a), to compute the effective bending stiffness of mechanically joined cross section beams, it was possible to obtain the joint stiffness associated with each beam, Table 3.3.



Fig. 3.12 – Composite T-beam obtained from the CSGL slab



Fig. 3.13 – Beam (GL7) obtained from the CSGL slab subjected to a load test

Table 3.3 – Experimental connection stiffnesses CSGL

Slab specimen	Connection		
	Beam position	Beam designation	K [kN/m]
CSGL	B3	GL7	1223.12
	B4	GL2	952.33
	B5	GL6	1358.13

3.3 Base numerical model

To obtain the adequate numerical model, capable of predicting the mechanical behavior of the structures that are intended to be studied, specifically the transversal load distribution in timber-concrete floor specimens subjected to point loading, several FE models were defined using different finite element types. Their results were compared with each other and with some existing experimental tests, which permitted to obtain a validated FE numerical model.

Therefore, three different FE models were created using commercial FE programs. A Grid model, composed by frame elements, and a Composite model, *Frame+Shell*, composed by frame and shell elements, were developed using the SAP2000 software (CSI 2004). Also a Solid model composed by solid elements was developed, this one using the AbaqusCAE software (Simulea 2011). The three were firstly validated through experimental tests and later compared to each other.

A timber-concrete composite slab with glulam beams, identical to the first specimen considered in the preliminary experimental tests, CSGL, was considered. The geometric

characteristics of the specimen were already presented in Fig. 3.1 a) and Fig. 3.2 a) and the material properties were listed in Table 3.2.

To characterize the materials used in the floor specimen some tests and measurements were done before assembly. Each timber beam was weighed, measured and statically tested in order to obtain the global modulus of elasticity (MOE), according to (EN408 2010). To obtain the concrete compressive strength, three concrete cubic specimens were tested 14 days after pouring and other three specimens were tested 28 days after pouring. The connection properties were obtained based on results of several four point bending tests, (Domingues 2012), carried out according to (EN26891 1991). These tests were performed in timber-concrete composite beams with the same connection system. With these results and assuming an adjustment to the load-slip curve, linear or nonlinear, the connection properties were set. In the first case, that adjustment was performed through a linear approach to the experimental load-slip curves. The linear stiffness was set as the corresponding average stiffness. As for the nonlinear properties, the adjustment was performed according to the Foschi's law (16) (Dias 2010):

$$F = (Y + u \cdot (\delta - \delta_0)) \cdot \left(1 - e^{\left(\frac{-a \cdot (\delta - \delta_0)}{Y}\right)}\right) \quad (16)$$

where: F is the load;

Y is the “yielding” force; when $u \neq 0$ the interception between the line defined by $F = u \cdot \delta$ and the load axis gives an approximation of the yielding load of the joint (when $u = 0$ this interception gives the ultimate carrying capacity of the joint);

u is the hardening, given by the slope of the load-slip curve after the joint yielding;

δ is the slip;

δ_0 is the initial slip;

a is the initial stiffness, given by the tangent to the load-slip curve in the origin.

Despite the tests performed by (Domingues 2012) were on composite beams with timber logs, therefore using materials with different properties and different cross-sections, their connection properties were considered to be an acceptable approximation. These properties are presented in Fig. 3.14.

The Grid model, Fig. 3.15, was defined by frame elements arranged in two orthogonal directions, corresponding to the beams longitudinal axis and to the orthogonal direction. Link elements were defined to connect the elements representing beams and slab. Since the timber interlayer does not contribute to the structural behavior (Dias *et al.* 2010), its consideration

was only reflected on the gap between the elements representing the beam and those representing the concrete slab.

Connection properties		
Linear	Non-linear (multi-linear)	
K	F	d
[kN/m]	[kN]	[m]
6723.34	-27.000	-5.429×10^{-3}
	-17.306	-0.754×10^{-3}
	0.000	0.000
	17.306	0.754×10^{-3}
	27.000	5.429×10^{-3}

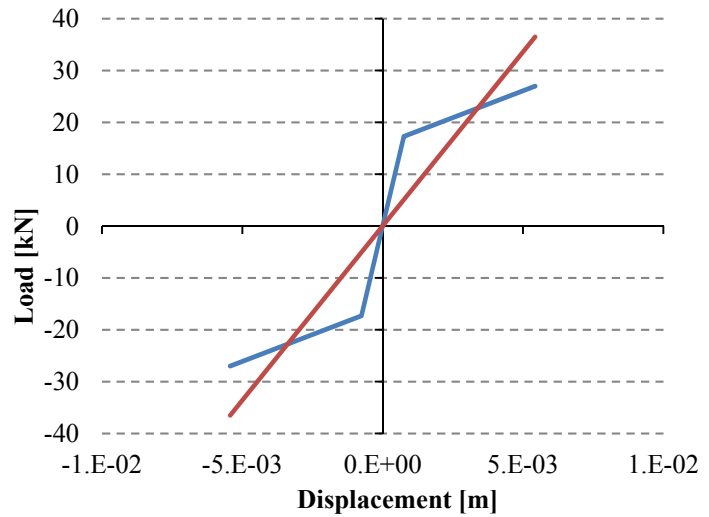


Fig. 3.14 – Connection properties

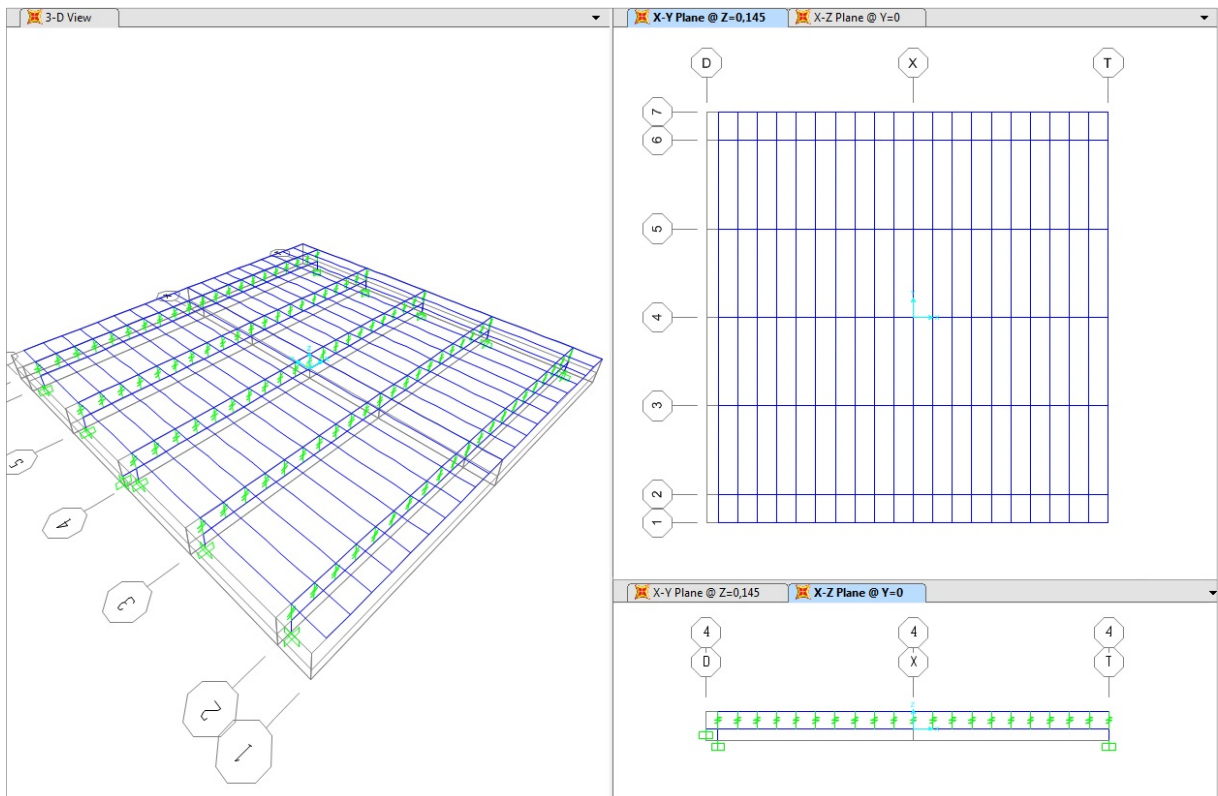


Fig. 3.15 – Grid model scheme

According to the SAP Manual (CSI 2004), frame elements, defined as a straight line connecting two points, can be used to model beams in structures such as three-dimensional frames, planar frames or planar grillages, which makes them suitable for the model of this investigation. These elements consider six degrees of freedom (dof) at both its connected joints. In terms of analysis, they use a general, three-dimensional, beam-column formulation which includes the effects of biaxial bending, torsion, axial deformation, and biaxial shear deformations. Link elements were the second type of elements considered in the Grid model. These elements enable the connection between two joints, using six deformational dof (axial, shear, torsion, and pure bending), for linear elastic and non-linear analysis, such as proposed in (Dias 2012).

Frame prismatic elements were used to model the beams. They were defined according to the longitudinal axis of each beam. The dimensional values were those of the test slab. For simplicity, a linear and isotropic material behavior was adopted. This assumption is supported by some studies, as is the one developed by Chen (Chen 1995b). According to this author, when the transversal load distribution is under consideration, the material formulation of the plate in a linear analysis showed to have almost no influence in the results. The numerical model was considered simply supported, to reflect the support conditions of the actual slab.

To model the concrete slab, an orthogonal Grid of frame prismatic elements was defined. In the longitudinal direction, the frame elements were placed 0.750 m apart in order to coincide with the position of the beams, Fig. 3.16. The cross section, 0.750×0.050 m, was considered homogeneous with the proper concrete properties. In the longitudinal direction twenty 0.165 m long elements were defined both for the frames representing the beams and for the slab in that direction. In the transversal direction, the frame elements were placed 0.165 m apart, in order to allow a perfect match between all the elements to be connected. A 0.165×0.050 m cross section was adopted for these elements. At the ends of both directions, to model the geometrical conditions, frames with different cross sections were defined. This led to 0.495×0.050 m (beams) and to 0.120×0.050 m (“slab”) cross sections in the longitudinal direction, and to 0.0825×0.050 m (“slab”) cross sections in the transversal direction.

To connect those elements, a linear elastic behavior connector was adopted, using the properties listed in the table at Fig. 3.14.

The loads were defined as point loads acting at the slab top surface.

The Frame+Shell model, Fig. 3.17, was defined using frame elements to model the timber beams and shell elements to model the concrete slab. Link elements were also defined to model the connection between beams and slab.

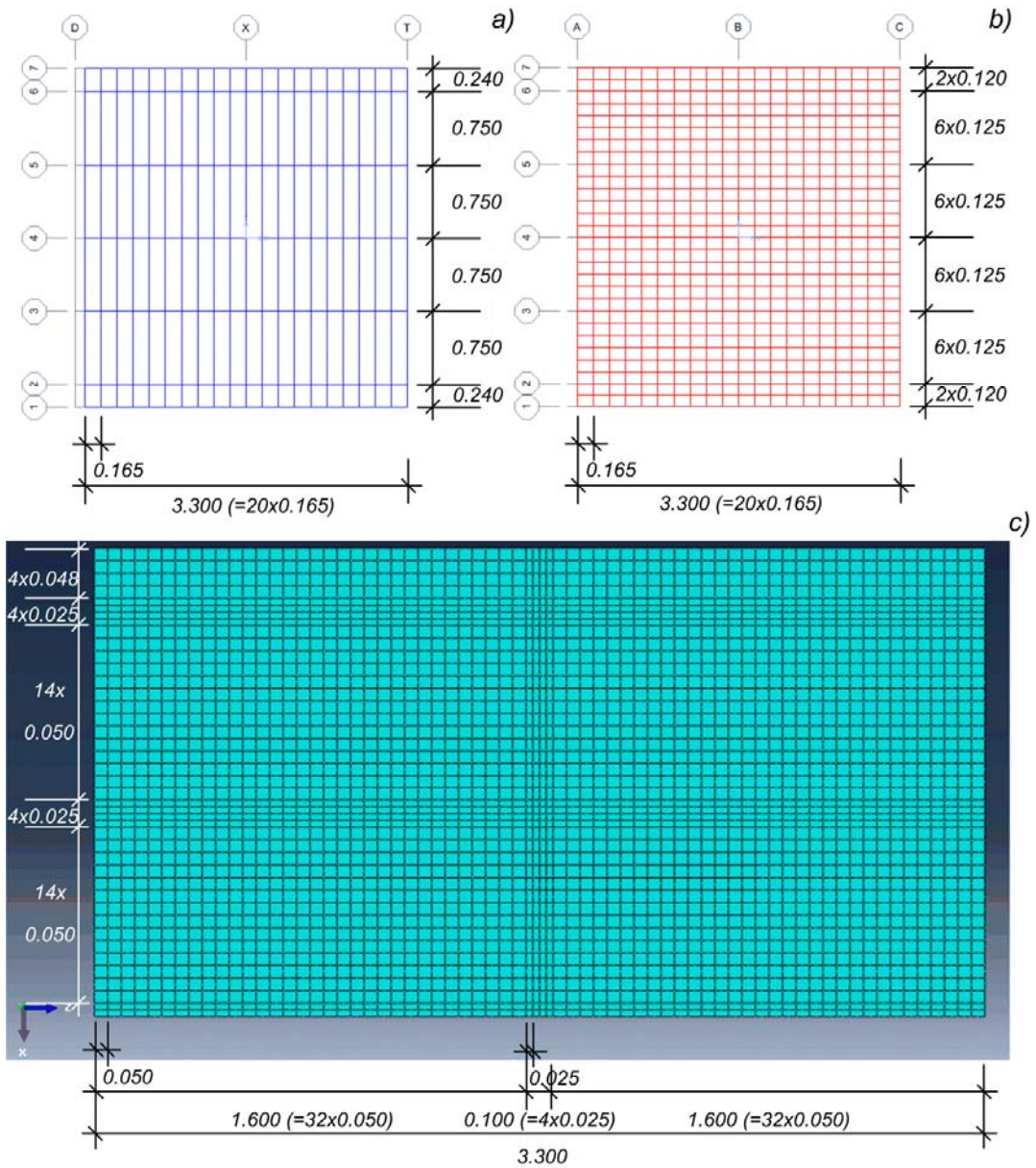


Fig. 3.16 – FE mesh schemes (top view): a) Grid model; b) Frame+Shell model; c) Solid model

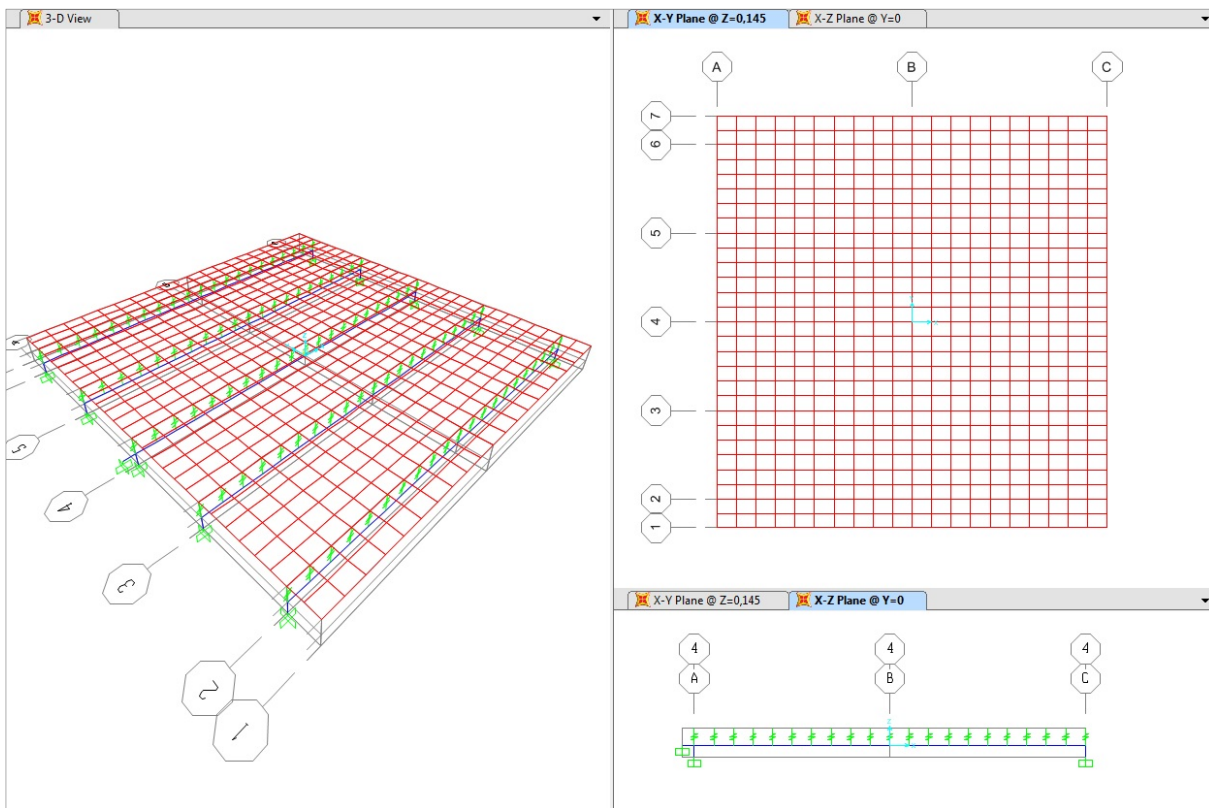


Fig. 3.17 – Frame+Shell model scheme

According to the SAP Manual (CSI 2004), shell elements are area objects which use translational and rotational dof, six at each its connected joints. These elements can model several structural elements as floors, walls and bridge decks. The adequate behavior should be selected: plate, membrane or shell. The full shell behavior combines membrane and plate behavior, implying that the element can develop internal forces and moments.

In terms of analysis, the numerical formulation can be a three- or four-node formulation, with the stresses and internal forces and moments being evaluated at the 2-by-2 Gauss integration points and extrapolated to the joints of the element. The thickness formulation implies the choice of a thick-plate (Mindlin/Reissner) formulation or a thin-plate (Kirchhoff) formulation, which, respectively, considers or neglects the effects of transverse shear deformations.

Beams were defined through frame prismatic elements, and the slab was modeled by shell elements with homogenous thickness. For simplicity, in both cases, a linear and isotropic material behavior was assumed. Sectional properties were defined based on the actual ones. Due to the fact that timber beams are essentially subjected to forces along its longitudinal (grain) direction, the assumption of isotropic material behavior turns out to be an acceptable

approximation. Since the concrete thickness is very small compared to the span, transverse shear deformation was neglected. Therefore, a shell behavior with a thin-plate formulation was chosen.

To connect frame to shell elements, connectors were defined using the linear properties listed in the table at Fig. 3.14.

In the longitudinal direction both the Grid and the Frame+Shell models had equal dimensions and the same number of elements. In the transversal direction, the shell elements were 0.125 m wide in the zone between the beams and 0.120 m wide in the concrete outer flanges, Fig. 3.16.

All the beams were considered to be simply supported. The loads were defined as point loads acting at the top surface of the shell element.

To deal with the Solid model, Fig. 3.18, AbaqusCAE software (Simulea 2011) was used. The components of the composite slab were defined using 3D solid deformable elements, with exception of the timber interlayer which was considered as a 0.020 m clear space between the slab bottom and the beams top surfaces. A “20-node quadratic brick” element with reduced integration was chosen. Using a reduced integration means that a lower-order integration to form the element stiffness is used. This option leads to a reduction in running time, especially in three-dimensional analyses. In this specific case, this element type with reduced integration has 8 integration points which compares to 27 of the full integration. In fact, according to AbaqusCAE documentation (Simulea 2011), the element assembly becomes about roughly 3.5 times less costly than that of full integration, for this particular element. According to the same reference, the use of second-order reduced-integration elements generally leads to more accurate results than the corresponding fully integrated elements.

The values of the cross sections were defined based on the real values, and the materials were those presented in Table 3.2. The materials were considered as homogeneous, isotropic and with a linear elastic behavior. For simplicity, the slab was considered symmetrical about the longitudinal axis and only half of the slab was modeled, the half containing Beams 1, 2 and 3.

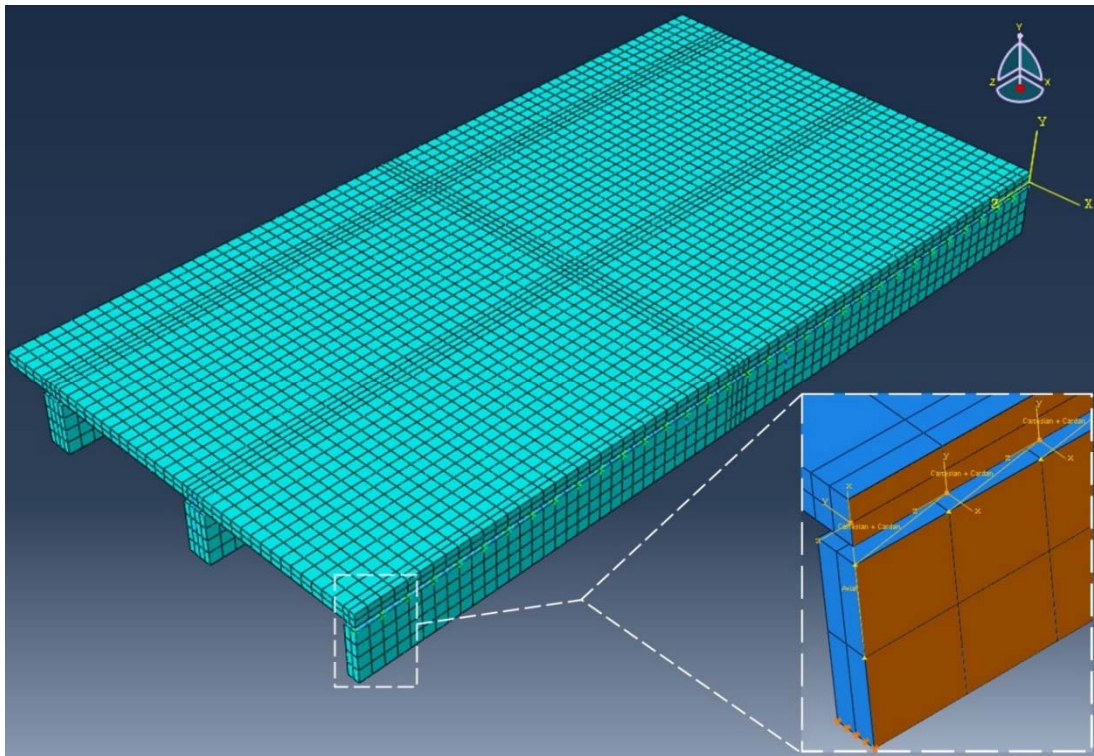


Fig. 3.18 – Solid model scheme

The connection between timber beams and concrete slab was guaranteed through the inclusion of connectors. These elements were defined through connector features, 0.100 m apart, which linked a concrete point to a timber point. The connector was defined in terms of translational and rotational displacements. In this case, the rotational displacements were considered rigid, as adopted in the previous models, and the translational displacements were considered to have a linear elastic behavior according to the values given in the table at Fig. 3.14. The FE mesh was defined essentially through square elements (0.050×0.050 m), Fig. 3.16, except for the areas where timber and concrete elements would interact with each other, where a finer mesh was adopted (0.050×0.025 m). Since the 3D model for solid elements did not allow point loads, the load was distributed in a small area of 0.050×0.050 m on the top surface of the concrete slab, aligned to the beam's mid-span. This area was fixed in accordance with the recommendations by EC1 (EN1991 2001) for concentrated loads.

3.4 Analytical model

The Analytical model adopted in this work was that proposed by Guyon-Massonnet (Bareš and Massonnet 1966), also known as Distribution Coefficients Method. It is an approximate method that was developed in order to be used in the practical design of

reinforced concrete slabs. At the time it was created, computing equipment was very scarce and expensive and approximate procedures of manual computing were consequently very useful in design.

This method was established for grid structures, commonly composed by two sets of orthogonal beams connected to a top slab, by applying the orthotropic plate theory. Assuming that, most of the grid structures are composed by a beam grid and a slab with average thickness, their behavior would be intermediate between that of an anisotropic plate (associated with a thick slab) and that of a simple grid structure (with no slab associated). Therefore, by comparing the deflections relations, in the form of the slab differential equation, for the two fundamental systems: orthotropic plates and simple grids (with orthogonal beams), Bareš and Massonnet stated the findings for what they call “general” grid structures. These structures were assumed to be constituted by m principal longitudinal beams, c_0 apart, and n secondary/bracing beams, l_0 apart, composed by the same material and rigidly connected to each other at the common nodes.

The method is essentially based in the following assumptions: the actual non-homogenous structure is replaced by an orthotropic slab with constant (average) values for the bending and torsional stiffnesses; the “equivalent slab” is simply supported at two opposite edges, corresponding to the principal beams ends, with the two remaining edges free; the actual load is replaced by an equivalent sinusoidal shaped load distributed along the XX axis of the structure (coincident with the beams longitudinal axis). This equivalence is set from the deformations of both situations (Fig. 3.19). The Poisson’s coefficient of the material, considered as homogenous, is taken as zero ($\nu = 0$). This last assumption is justified in the light of the main objective of the method, which was the computing of the distribution of internal forces, (Calgaro and Virlogeux 1988). Knowing that they do not vary significantly with the Poisson’s Coefficient, the errors associated with it can be considered negligible.

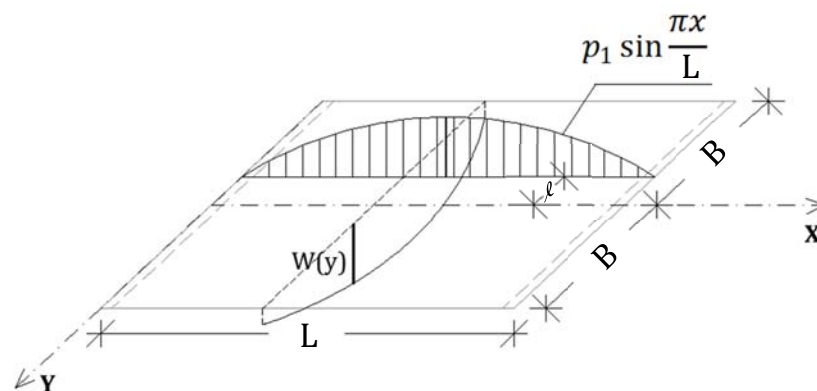


Fig. 3.19 – Guyon-Massonnet model: simplified slab and load scheme

Boundary conditions are essential to solve the slab fundamental equation, and despite Bareš and Massonnet had analyzed various support conditions, they focused in bridge slabs with two opposite ends simply supported and the remaining ends free. Nevertheless, the method is still applicable even when the deck/floor is statically indeterminate (continuous), by replacing the actual span by one simply supported at the two ends, belonging to a fictitious slab with the same elastic deflection as the real slab when subjected to a concentrated load applied at mid-span.

Therefore, the method assumes a distributed line load $p(x) = p_1 \cdot \sin(\pi x/L)$ acting parallel to the XX axis with an eccentricity e (p_1 is a constant related with the load and L is the span along the XX axis). This load leads to a sinusoidal shaped deformation: $w(x, y) = W(y) \cdot \sin(\pi x/L)$, where $W(y)$ is the deflection shown in Fig. 3.19. If the load was considered to be uniformly distributed in the structure (width = $2B$) maintaining the sinusoidal shape of the load in the XX direction, the resulting deformed shape will be cylindrical and expressed by $w_0(x) = W_0 \cdot \sin(\pi x/L)$, where W_0 is the average deflection. Consequently, the transversal distribution coefficient $K(y)$ is obtained from the ratio between $w(x, y)$ and $w_0(x)$, *i.e.*

$$K(y) = w(x, y)/w_0(x) = W(y)/W_0 \quad (17)$$

where: $w(x, y)$ is the vertical displacement of a point on the structure under the effect of a line load $p(x)$; and

$w_0(x)$ is the vertical displacement associated with the same point, but under the effect of a uniformly distributed load $p_0(x)$ over the all width of the slab.

This coefficient depends on several dimensionless factors, namely:

- the bracing parameter θ , deduced by Guyon neglecting the torsion in grids, and which relates the width with the length of the slab and also depends on the bending stiffnesses of the longitudinal and transversal beams, and is given by:

$$\theta = \frac{B}{L} \sqrt[4]{\frac{\varrho_P}{\varrho_E}} \quad (18)$$

where: B is half width of the slab;

L is the slab span; and

ϱ_P and ϱ_E are the bending stiffness, per unit length, of the principal beams and of the secondary beams/bracing, respectively;

- the torsion parameter α , which relates the bending and torsional stiffnesses, and is given by:

$$\alpha = \frac{\gamma_P + \gamma_E}{2 \cdot \sqrt{\varrho_P \varrho_E}} \quad (19)$$

where: γ_P and γ_E are the torsional strength, per unit length, of the principal beams and of the secondary beams/bracing, respectively;
 ϱ_P and ϱ_E are the bending stiffness, per unit length, of the principal beams and of the secondary beams/bracing, respectively;

- the relative eccentricity of the line load e/B ; and
 - the relative ordinate of the point considered y/B .

Since the transversal distribution coefficient K is related with the torsion parameter α , an equation to compute K_α was developed. This procedure avoids separate calculations for each of the α values using complex equations. The equation for K_α resulted from the resolution of the differential equations of a fictitious slab developed in Fourier series. Equations (20) - (22) give K_α as a function of θ :

$$K_\alpha = K_0 + (K_1 - K_0) \cdot \alpha^{0.05} \quad 0 < \theta \leq 0.1 \quad (20)$$

$$K_\alpha = K_0 + (K_1 - K_0) \cdot \alpha^{\left(1 - e^{\frac{0.065 - \theta}{0.663}}\right)} \quad 0.1 < \theta \leq 1 \quad (21)$$

$$K_\alpha = K_0 + (K_1 - K_0) \cdot \sqrt{\alpha} \quad \theta > 1 \quad (22)$$

with K_0 and K_1 being the values of the distribution coefficient when $\alpha = 0$ and $\alpha = 1$, respectively.

This model has some limitations. For instance, it only considers symmetrical slabs, the beams need to be identical among their category, principal or secondary, and an interlayer with no structural function is not possible. Also the stiffness of both beams is “distributed” along and across at the “equivalent slab”. The method is, therefore, the most effective the greater the number of secondary beams, since the approximation of the stiffness “distribution” decreases, (Sieffert 2004).

The computation of bending moments and deflections considers the Fourier series development truncated at the first term, which implies losing about 10 % of the remaining

terms contribution, (Samartin and Martinez 1974). To cope with this difference, the computations of the mentioned quantities may be affected by a factor of 1.1.

3.5 Numerical model validation

As already presented, the use of a numerical model capable to characterize the mechanical behavior of the composite floor structures in consideration, when subjected to concentrated loading is essential. Especially when considering their behavior in the orthogonal direction. Therefore, beyond comparing the experimental results and those from the numerical models several structural situations were modeled using the four theoretical models, in order to achieve a more comprehensive validation.

3.5.1 Experimental results

As presented earlier, both experimental specimens were subjected to a point load applied one at a time in different locations, with a magnitude of about 40 % of the ultimate load, for that specific location. The ultimate load level expected for each load position was estimated through an FE analysis, using the Frame+Shell Model, presented in the section 3.3 *Base numerical model*. The model was created using geometrical and material properties already shown, Fig. 3.1 to Fig. 3.3 and Table 3.2. A multi-linear elastic behavior was assumed for the connector elements, and the non-linear connection properties listed in the table at Fig. 3.14 were used. To attain a value for each loaded beam and location, a stress analysis was performed for the ultimate load levels by modeling some previous experimental tests (Domingues 2012). By analyzing the stress levels numerically obtained when modeling these tests, for the ultimate load, and assuming that the preliminary experimental specimens will behave the same way, the reverse procedure was adopted. Developing a model of each of the experimental slabs and using an iterative procedure of load application *vs.* stress analysis, for the various loading locations, the load applied was changed until reaching the average stress level found for the tests performed by (Domingues 2012). This procedure allowed obtaining a prediction for the experimental ultimate loads and led to the definition of a test protocol for any position of the load. The load values that were actually applied to the slab are listed in Table 3.4.

As can be seen, the load values applied to the CSTL specimen were slightly lower than those applied to the CSGL. This is consequence of the fragile failure associated with timber log beams. After the tests at mid-span of the beams near the center of the slab (B3 and B4) was considered safer to reduce the level of load applied. That is why in the following tests, the load applied was lower, about 30 %.

Table 3.4 – Load cases and applied loads during the experimental test

Floor specimen	Load case	Applied Load	Applied Ultimate ^a
		[kN]	[%]
CSGL	B1 ½	31.8	40
	B2 ½	49.9	43
	B3 ½	57.5	50
	B4 ½	44.6	39
	B5 ½	32.1	40
	B1 ¼	34.8	40
	B2 ¼	51.7	40
	B3 ¼	51.7	40
	B4 ¼	50.6	40
	B5 ¼	35.2	40
CSTL	B1 ½	24.5	30
	B2 ½	29.7	27
	B3 ½	39.2	40
	B4 ½	38.2	40
	B5 ½	32.0	30
	B6 ½	28.4	30
	B7 ½	25.7	29
	B1 ¼	23.2	26
	B2 ¼	30.9	25
	B3 ¼	32.3	30
	B4 ¼	31.1	30
	B5 ¼	35.1	30
	B6 ¼	24.1	23
	B7 ¼	29.0	30

^a - Estimated based on the numerical modeling

½ - mid-span; ¼ - quarter-span

The results obtained from the several tests can be found in *APPENDIX A, A.1 Results from the preliminary experimental tests* (Fig A.1 to Fig A.36). The following figures show a summary of those results, considering the load applied one at a time over the beams B1, B2 and B3 of the CSGL and over the beams B1, B3 and B4 of the CSTL. Fig. 3.20 and Fig. 3.21 show the results in terms of support reactions, while Fig. 3.22 and Fig. 3.23 show the results in terms of vertical displacements.

3. MODEL DEVELOPMENT: PRELIMINARY STUDIES

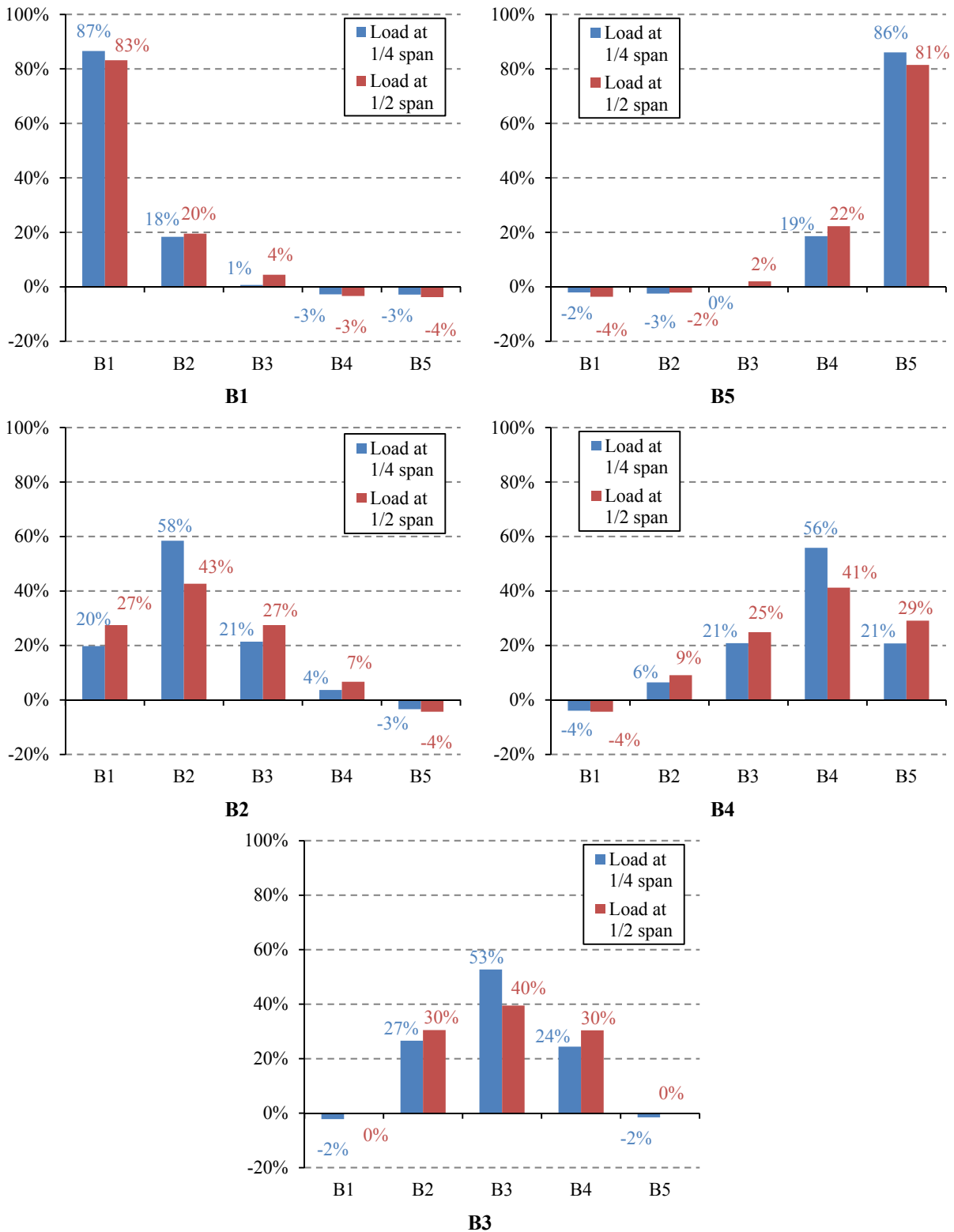


Fig. 3.20 – CSGL: support reaction distribution when loaded at 1/2 and at 1/4 span

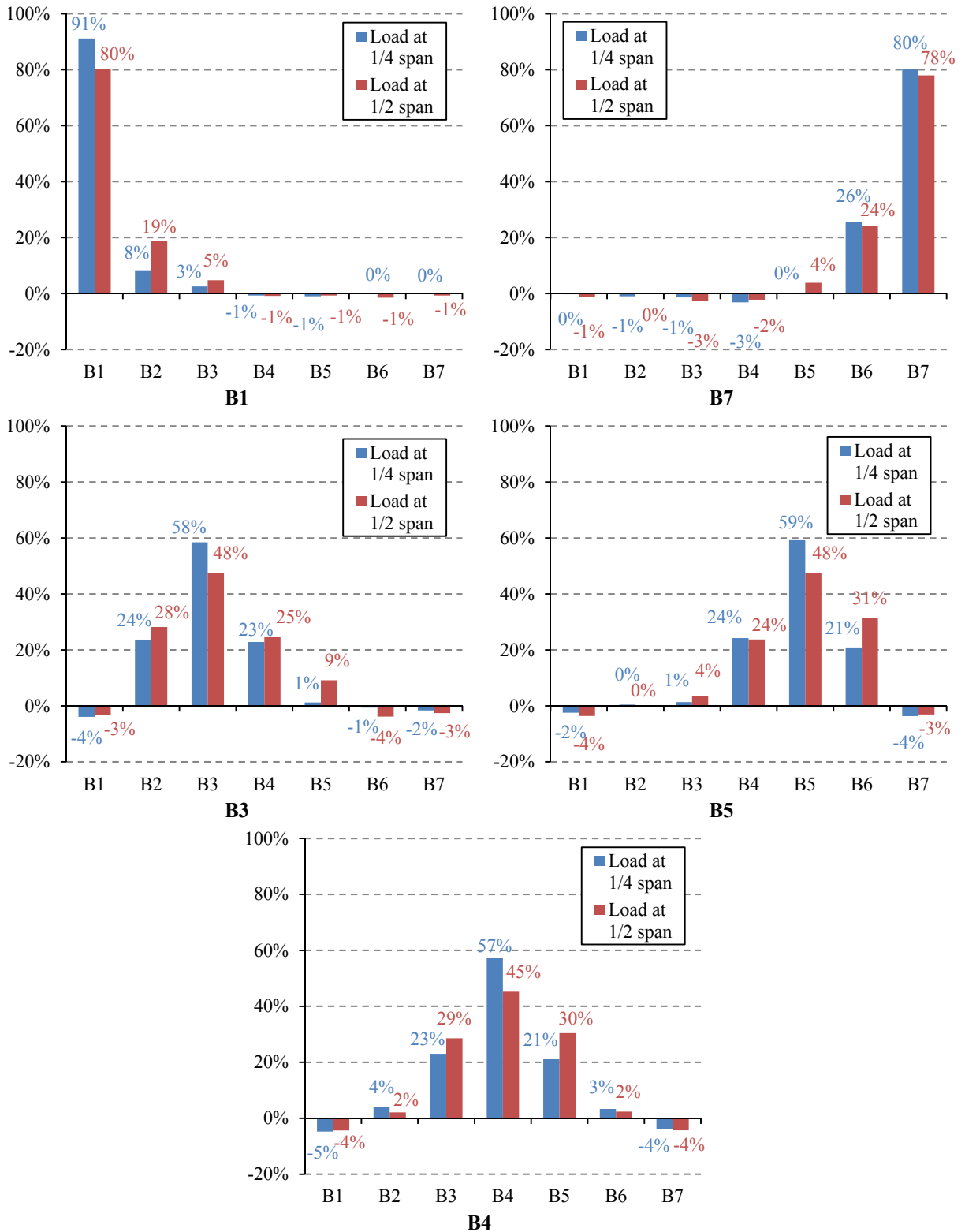


Fig. 3.21 – CSTL: support reaction distribution when loaded at 1/2 and at 1/4 span

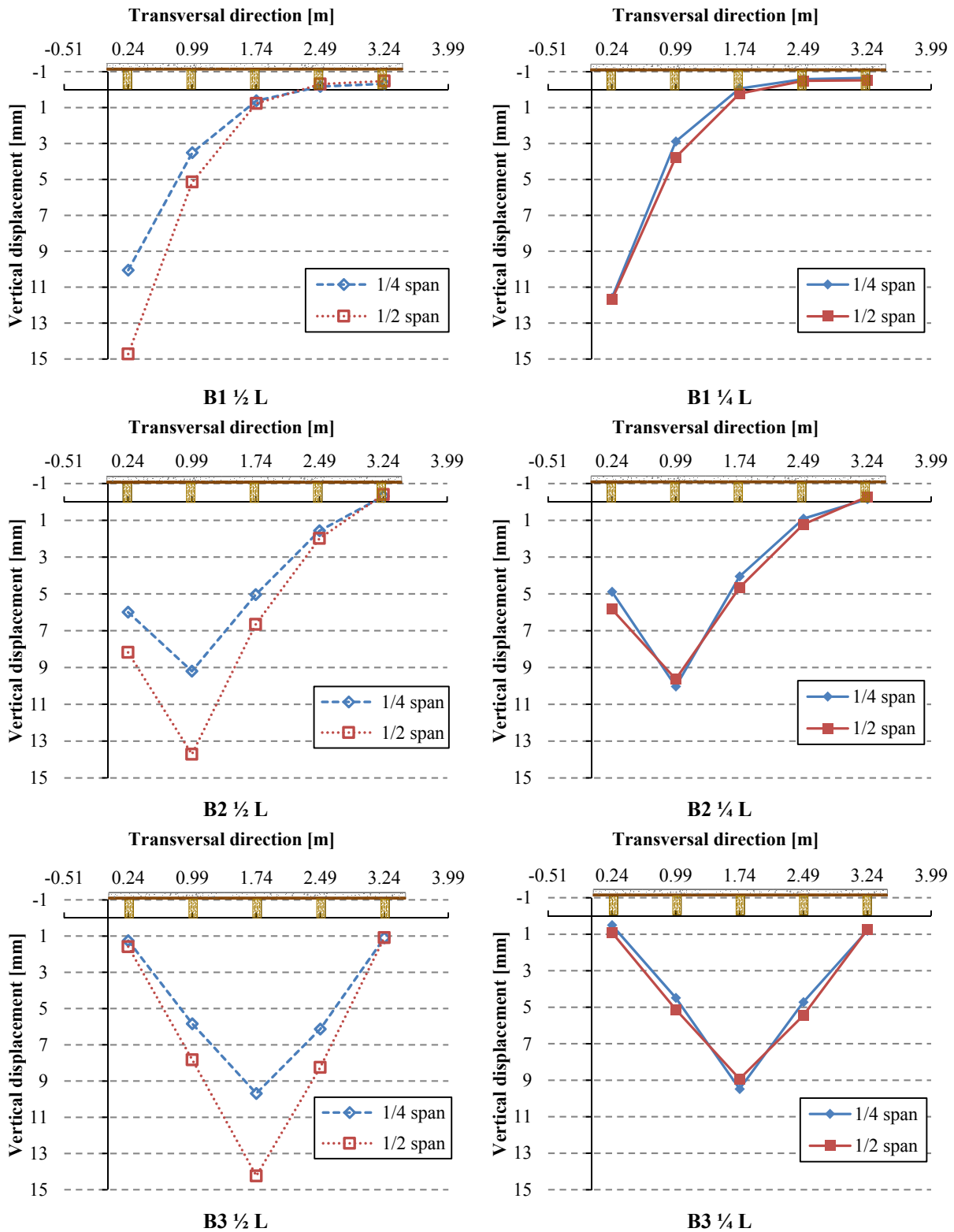


Fig. 3.22 – CSDL: vertical displacement at 1/2 and 1/4 span when loaded at 1/2 (left) and 1/4 span (right)

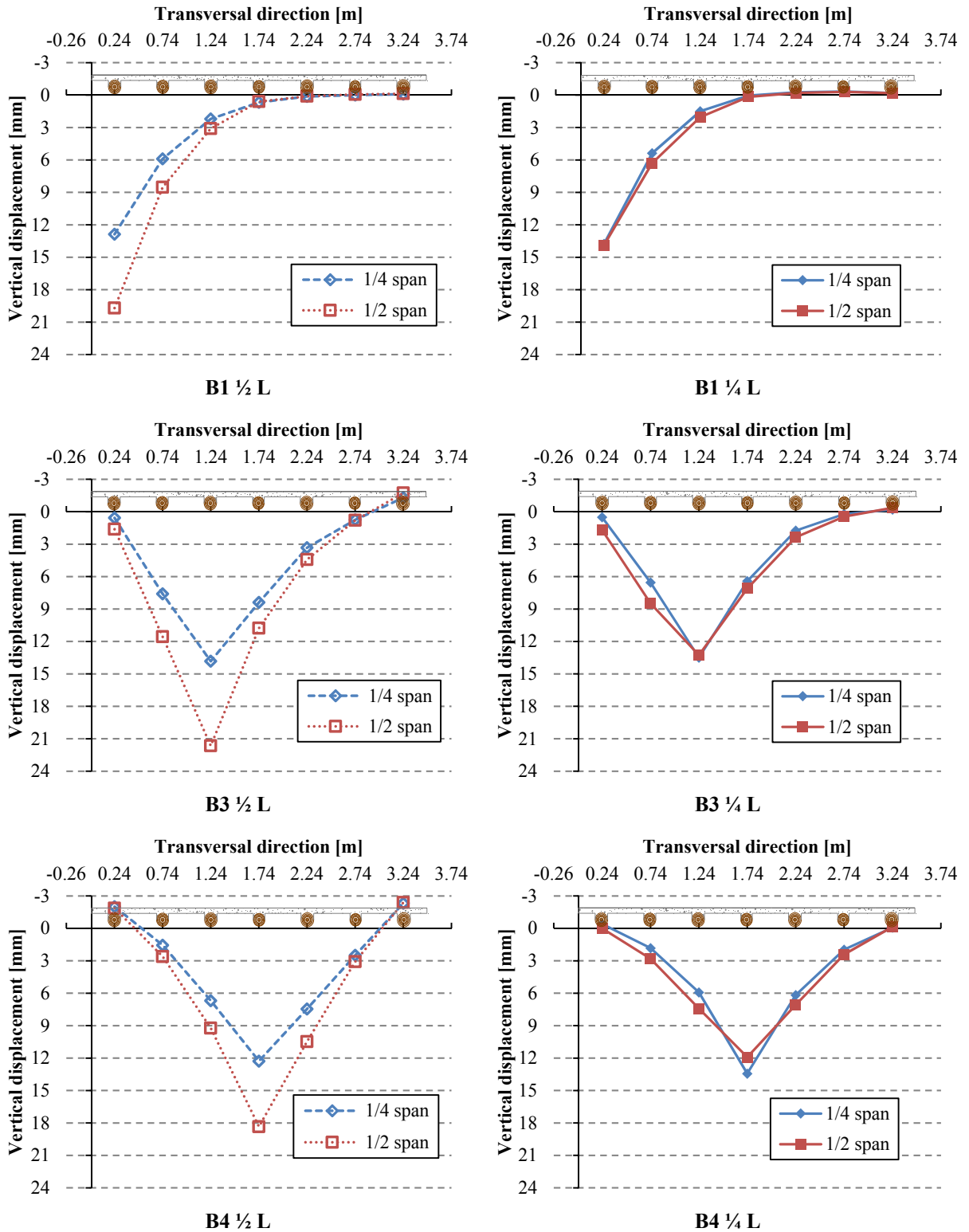


Fig. 3.23 – CSTL: vertical displacement at 1/2 and 1/4 span when loaded at 1/2 (left) and 1/4 span (right)

These results clearly show that the transverse load distribution in timber-concrete composite floors can be significant. Indeed, for the case where the load is applied at mid-span of a border beam, at least 17 % of the load applied above the timber beam is redistributed for the adjacent ones. This percentage increases as the loaded beam moves away from the border beam. When the load is applied at mid-span of the central beam at least 55 % of it was found to be redistributed for the adjacent beams. Meaning that, only 45 % of the applied load was received by the beam immediately below.

According to (Dias *et al.* 2013), also the structural bending stiffness affects the load distribution. Taking into account that the structural system under consideration has a small to medium stiffness, the transference of load is significantly higher for systems with stiff concrete decks (e.g. bridge deck with a concrete slab 0.20 m thick).

Analyzing the results when the load is applied at quarter-span, it was found a higher load percentage supported by the loaded beam, relatively to the immediately adjacent ones and also to that found for the mid-span loading cases. Consequently, the load distribution shows to be the more effective the farther the applied load is to the supports. Design can take advantage from this load transfer, especially if the bending moments are an important issue. Since they are often maximum at mid-span, for loads applied at the mid-span, the loaded beam receives only a share of the applied load, and the bending moment in that beam will be lower than that caused by the whole load. There is not so much a benefit if the key issue are the support reaction induced stresses, usually maximum at the supports.

The vertical displacement values as well as the values in terms of support reactions follow the expected behavior, with the major displacement associated with the loaded beam. Moreover, it is important to emphasize the non-linearity in graphs representing the displacements in the transverse direction, with a clear inversion of the slope for both the central and the adjacent beams. This is a good indication of the system stiffness in the transverse direction which has a significant influence in the load transference among adjacent beams.

3.5.2 Numerical vs. CSGL experimental results

As exposed in the section 3.3 *Base numerical model* the numerical models, Grid, Frame+Shell and Solid were created and Analytical was computed in order to perform a comparison between their results and those experimentally obtained. In this first phase only the CSGL specimen was modeled. The characteristics used to define the models were those already presented for this specimen, geometrical (Fig. 3.1 a) and Fig. 3.2 a)) and material (Table 3.2). In terms of connection properties, the values obtained through the tests performed in the three T-beams resulting from the cut of the slab into five stripes, Table 3.3, were used,

assuming by simplicity that the connection properties were symmetrical relatively to the central beam.

The comparison between the experimental and the numerical results was performed considering only the loading cases where the concentrated load is applied to the central beam, at mid- and quarter-span, CSGL - B3 $\frac{1}{2}$ and B3 $\frac{1}{4}$. The load value was considered to be the same as that applied in the preliminary experimental test, 57.5 kN and 51.7 kN, respectively.

Fig. 3.24 and Fig. 3.25 show the relationship between the support reactions of each beam and the applied load for the CSGL specimen. In turn, Fig. 3.26 and Fig. 3.27 show the vertical displacement of every beam for the load cases analyzed. For the central beam loaded at mid-span, the plotted displacements referred to the mid-span of each beam. As for the central beam loaded at quarter-span, displacements at quarter-span in each beam were considered.

Analyzing the load distribution, numerically and experimentally, for both loading cases, the loaded beam presented the highest support reaction, as it would be expected. The predicted values that are the closest to the real ones are those for the immediately adjacent beams. The mean differences were lower than 3.0 % for both loadings, ranging between 0.7 % (Frame+Shell) and 8.8 % (Analytical) for the loading at mid-span, and between 0.5 % (Grid) and 4.3 % (Analytical) for the loading at quarter-span. These beams were also the ones for which the predictions tended to be more uniform, with the models showing relatively similar percentages. This is more evident when the load was applied at quarter-span. In general, the analytical model tended to predict a more even participation of all the beams in the load distribution, deviating from the experimental results, more than the remaining theoretical models. This trend is accentuated in the loading at quarter-span. Conversely, Frame+Shell estimations seem to be the closest to the experimental results, for both load cases in analysis, with maximum differences of -2.7 % (loaded beam) and 1.6 % (adjacent beam) for loading at mid- and quarter-span, respectively. Concerning the loaded beam, the theoretical predictions ranged, in absolute terms, between 2.7 % (Frame+Shell) and 8.7 % (Solid) for the loading at mid-span, and between 0.8 % (Frame+Shell) and 21.7 % (Solid) for the loading at quarter-span.

As for the vertical displacements, despite the numerical estimations to be in accordance with those measured experimentally, they tended to underestimate the displacements at the loaded beam, between 22.4 % (Solid) and 28.7 % (Analytic) when the load was applied at the beam mid-span and between 32.5 % (Analytic) and 49.3 % (Solid) when the load was applied at quarter-span. The higher experimental deformations were probably caused by cracking of the concrete member, which was quite significant already before the load test was performed. This cracking was mostly consequence of the fact that the specimens used to perform the preliminary tests had been casted in a laboratory different from the one where they were statically tested, requiring transportation. Previously to the static tests, they were also

subjected to acoustic tests, which may also have contributed to some extra cracking and therefore to increase the differences found for deformation. As expected, the maximum vertical displacements were found immediately below the loaded point, and once more the immediately adjacent beams were those for which the theoretical estimations were close to each other and in this case, also close to the experimental results, for both load cases (mean differences lower than 13 % for $\frac{1}{2} L$ and lower than 20 % for $\frac{1}{4} L$).

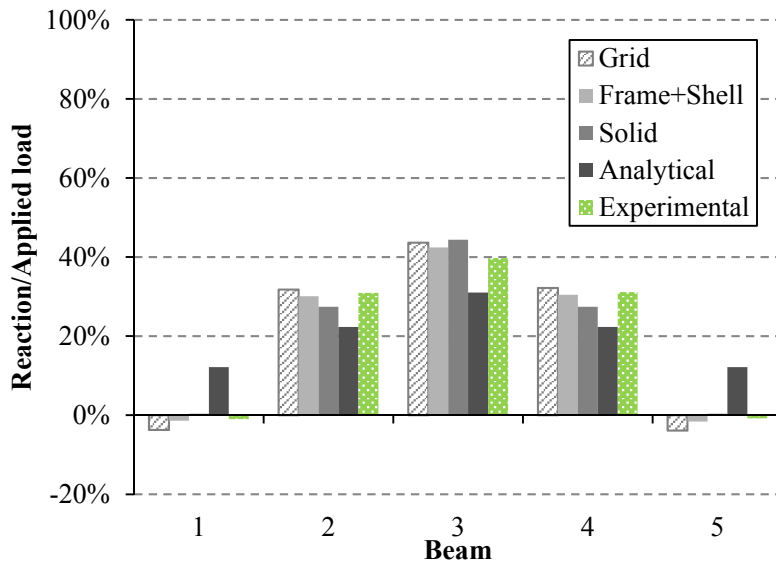


Fig. 3.24 – Numerical vs. experimental CSGL support reactions for B3 1/2

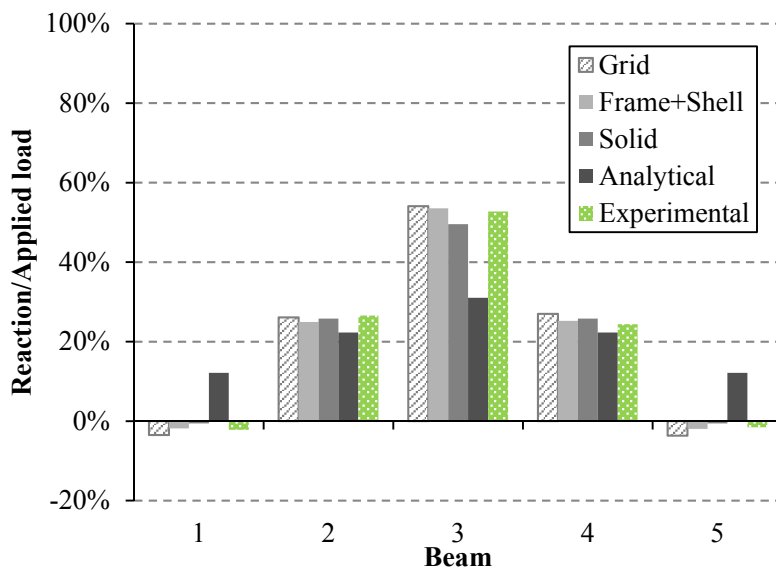


Fig. 3.25 – Numerical vs. experimental CSGL support reactions for B3 1/4

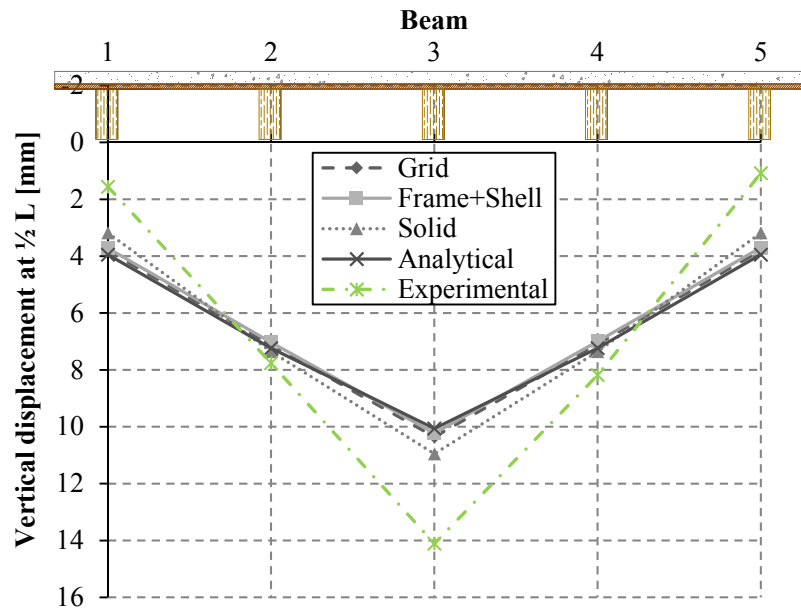


Fig. 3.26 – Numerical vs. experimental CSGL vertical displacements at mid-span for B3 1/2

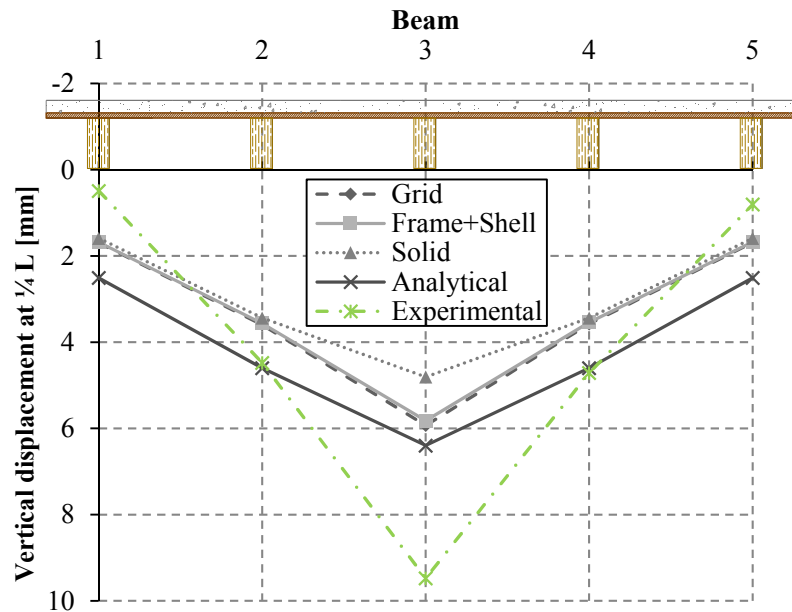


Fig. 3.27 – Numerical vs. experimental CSGL vertical displacements at quarter-span for B3 1/4

The modeling of CSGL slab and the comparison between their results and the experimental ones, in terms of support reactions and vertical displacements at the load location, allowed the validation of the numerical models. Although there are some differences between the experimental and the numerical results, a similar behavior pattern was clearly

observed. This is particularly evident when the experimental results are compared with those of the Frame+Shell model.

Therefore, in the light of the experimental results, it can be concluded that the numerical predictions, besides being in line with the experimental results, led to good approximations also making clear the existence of transversal load distribution.

Thus, the analysis of the support reactions and of the deflections at the load location of a timber-concrete slab modeling provides the information for a more efficient design. The fact that the beam under the load does not take 100 % of the load, but only part of it must be taken into account in practical design. If a beam supports a lower load, the associated stresses will be smaller, and consequently the required section will be smaller too. Hence, a more efficient design can be performed, by avoiding the over estimation of the beam section. By performing an analysis considering the load at various positions (different beams and different load locations), one at a time, can provide an overall view of the behavior of these composite floors.

In this way, the use of numerical models to assess the transversal load distribution contribute to improve the knowledge in this area and are at the same time an advantage that design practice can take advantage.

3.5.3 Modeling analysis

After validating the numerical models with the experimental results, a set of further modeling tasks was defined. Varying the values of some parameters, the theoretical predictions were compared with each other. This helped to extend the validation of the models to other situations.

Timber-concrete composite structures can be used in several applications such as floors rehabilitation or bridge decks. In their wide range of applications, several parameters can vary. This is the case of the connector stiffness, the cross sectional dimensions of the beams or even their span, among others. A good choice of these parameters can cover a wide range of practical applications. With this idea in mind, a set of parameters was established and analyzed with the various models under study (Grid, Frame+Shell, Solid and Analytical). The following parameters were considered: the elimination of the timber interlayer, different stiffnesses for the connection, different analysis types, and different cross sections and spans. This information is summarized in Table 3.5.

These parameters were varied from those of the CSGL specimen, maintaining the material properties of both concrete slab and timber beams unchanged. Also the load was applied at mid- and quarter-span of the central beam (B3), and was kept constant at every new modeling: 57.5 kN at B3 $\frac{1}{2}$ and 51.7 kN at B3 $\frac{1}{4}$. Therefore, the base modeling was

designated as *CSGL* and the results associated with each load case considered are those already presented: Fig. 3.24 and Fig. 3.26 for B3 ½, and Fig. 3.25 and Fig. 3.27 for B3 ¼.

Table 3.5 – Studied parameters

Modeling denomination	Model characteristics				
	Analysis	Connection	Timber interlayer	Beam cross section	Beam span
CSGL	Linear	$K = 6723.34 \text{ kN/m}$	0.020 m thickness	0.100 × 0.200 m	3.30 m
CSGLi			No		
CSGLnla	Non-linear	See Fig. 3.14	0.020 m thickness		
CSGL-lK	Linear	Low stiffness; $K = 3000 \text{ kN/m}$			
CSGL-mK		Medium stiffness; $K = 10000 \text{ kN/m}$			
CSGL-hK		High stiffness; $K = 100000 \text{ kN/m}$			
CSGLsb		$K = 6723.34 \text{ kN/m}$			
CSGLjb				Juxtaposed $3 \times (0.750 \times 0.200 \text{ m})$	
CSGLl			0.100 × 0.200 m	6.60 m	

There were two cases where the modeling with the Analytical model was not possible to perform. One was the non-linear analysis; in fact the method of Guyon-Massonnet is not capable of taking that into consideration. The other was the consideration of juxtaposed beams because the beams cross section had such geometrical properties that did not guarantee the method requirements. As presented before, this model cannot cope with the consideration of the interlayer; thus all the modeling tasks with the Analytical model were performed considering the non-existence of a timber interlayer.

The predictions obtained from the numerical and the analytical models, as well as the results from the experimental tests were compared and analyzed.

Aiming at comparing all the theoretical models, the following figures, Fig. 3.28 to Fig. 3.31, show their results concerning the absence of interlayer between the timber beams and the concrete layer, for both loading cases. Fig. 3.28 and Fig. 3.29 present the relationship between the support reactions of each beam and the applied load. In turn, Fig. 3.30 and Fig. 3.31 show the vertical displacement of every beam at mid- and quarter-span, for the load applied at the mid- and quarter-span of the central beam, respectively.

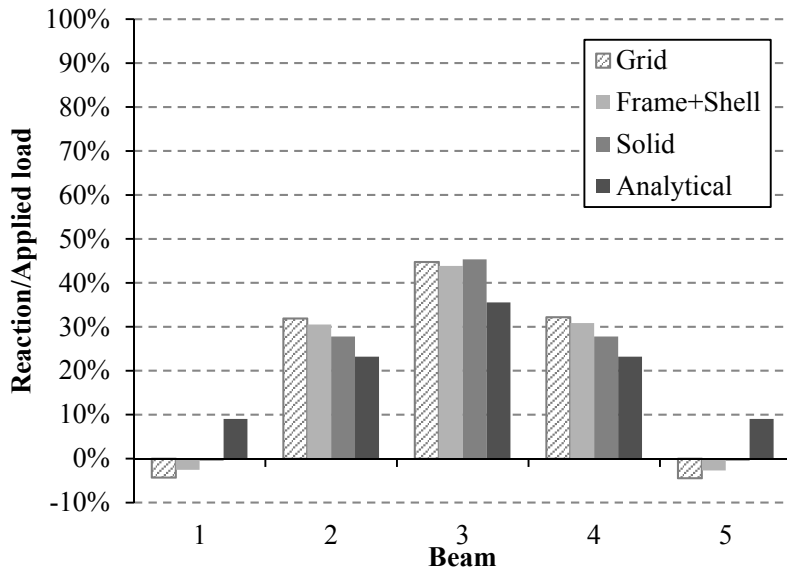


Fig. 3.28 – CSDLi loaded at 1/2 L: support reactions

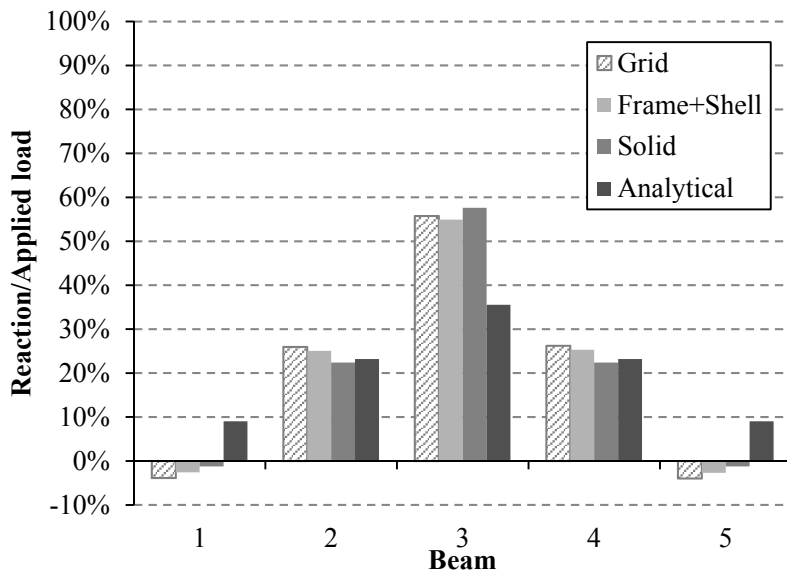


Fig. 3.29 – CSDLi loaded at 1/4 L: support reactions

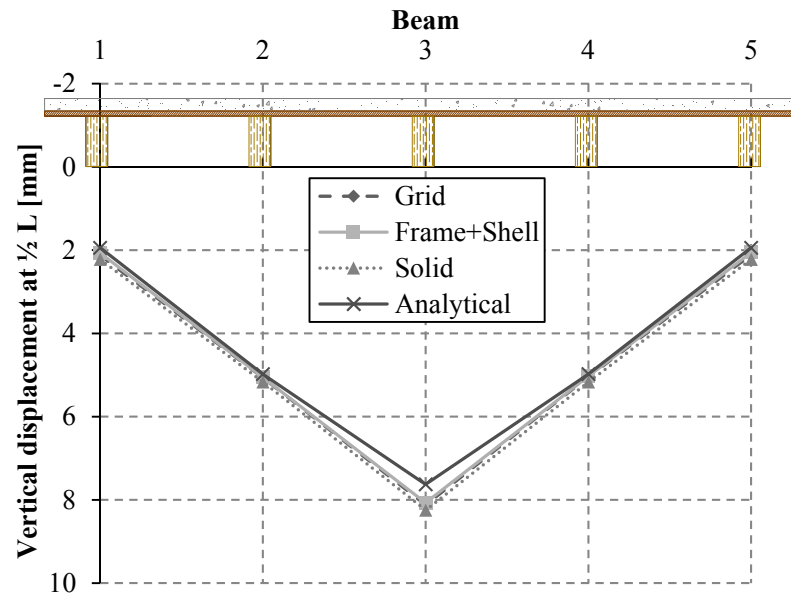


Fig. 3.30 – CSGLi loaded at $\frac{1}{2} L$: vertical displacements at each beam $\frac{1}{2} L$

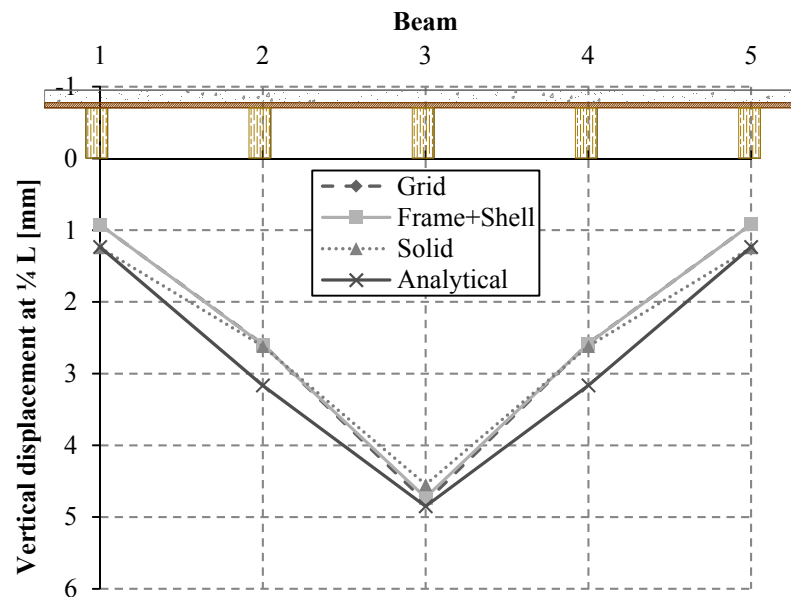


Fig. 3.31 – CSGLi loaded at $\frac{1}{4} L$: vertical displacements at each beam $\frac{1}{4} L$

The results show that the loaded beam and the adjacent ones tend to support the entirety of the applied load. The percentage received by the loaded beam when the load is applied at quarter-span tended to be higher than that found for the loading at mid-span. The extremity beams tend to have negative reactions, which means that they tend to move up from the supports. A similar trend can be observed in terms of vertical displacements. The manner in

which the beams suffer deflection under the action of a centered load in contrast with the action of a decentered one is clearly shown in Fig. 3.30 and Fig. 3.31. Whereas the “curves” associated with the loading at mid-span show an almost constant slope, for the loading at quarter-span this does not apply. For the latter load case, the beams adjacent to the loaded one tend to be less affected for the applied load.

Nevertheless, the development of transverse load distribution in timber-concrete composite floors is clearly evidenced. For the decentered load over the central beam approximately 42 % of the load is redistributed to the beams aside of the central one, Fig. 3.29, as for a centered action the percentage rises to 55 %, Fig. 3.28.

Once more, beyond some differences, the theoretical models’ results present a general behavior pattern clearly similar.

According to the list presented in Table 3.5, a detailed analysis was performed using only the theoretical models. This analysis focus specifically on the vertical displacements in each beam at mid- and quarter-span, according to the load location, the support reactions in individual beams and their relative weight when compared to the total load (which is the same as the sum of the support reactions of all the beams), and the longitudinal bending moment at the cross section at mid- and quarter-span of each beam compared with the sum of the moments of the five beams. The following paragraphs summarize its inferences. All the graphical comparisons of the theoretical results can be found in *APPENDIX A, A.2 Results from the theoretical analysis*.

In general, concerning the vertical displacements when the load was applied at mid-span of the central beam, Fig. 3.32, all the models presented very similar results and very consistent behaviors. In fact, the Grid and Frame+Shell models presented almost coincident results. Nevertheless, there are slight differences when comparing models with each other. For instance, the Solid model in the CSGLnla, or the Analytic model in CSGL-hK or CSGLI. This is a consequence of the characteristics inherent to each model and it is closely related with the simplifications. The greater the number of simplifications, the greater the tendency of the results, associated with a method, to deviate from the experimental results. As for the Analytical model there is a tendency to overestimate the displacements, which, despite deviating from the experimental values, leads to a safe prediction (predicting a displacement higher than the real one). Concerning the Solid model, differences seem to be consequence of the model complexity, by using tridimensional FE. Also nonlinear problems solving process can be another reason for the differences. As AbaqusCAE solve these problems through an iterative process using the Newton Raphson method, SAP2000 tries, at first, a constant-stiffness iteration approach. If that does not lead to convergence, a tangent-stiffness (Newton Raphson) approach is used next, and if this fails, the program reduces the step size, and the process is repeated.

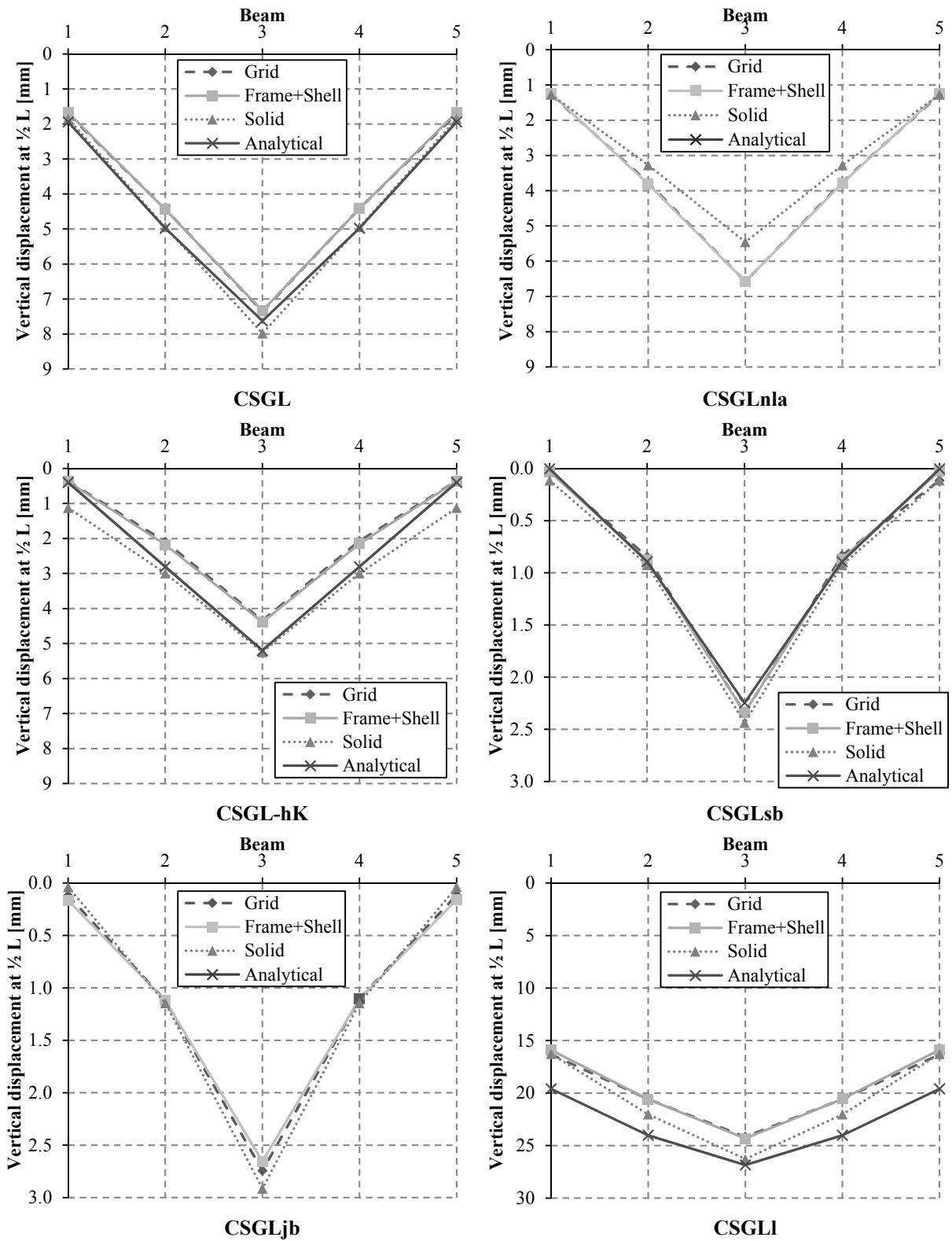


Fig. 3.32 – Theoretical analysis – load at $\frac{1}{2}L$: vertical displacements at each beam $\frac{1}{2}L$

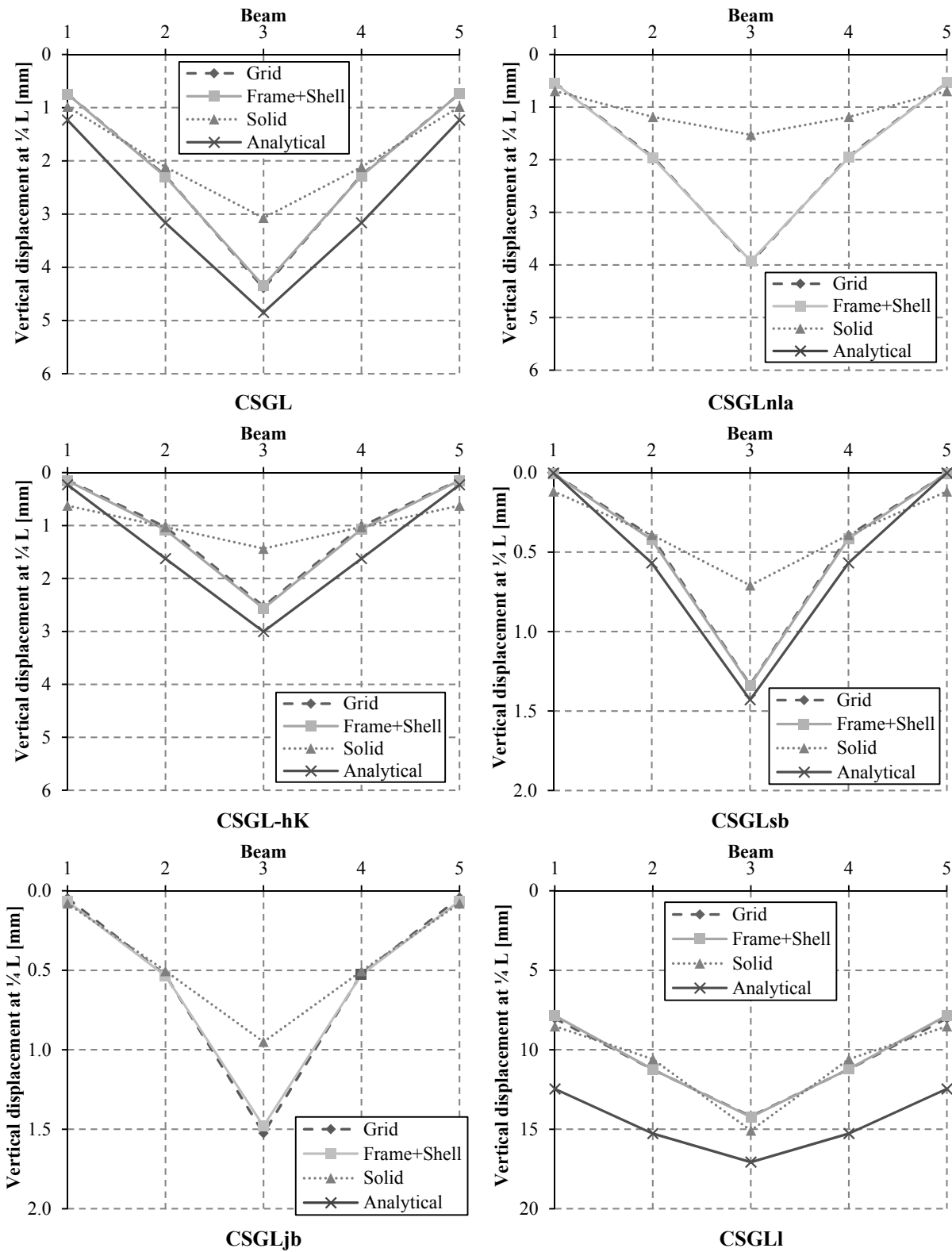


Fig. 3.33 – Theoretical analysis – load at $\frac{1}{4}L$: vertical displacements at each beam $\frac{1}{4}L$

The same tendency is observed for the decentered load in some modeling tasks, even in a more obvious manner. In fact, the Analytical model tends to overestimate the vertical displacement when the load is applied at quarter-span, maintaining however the same trend as the Grid and Frame+Shell models. As for the Solid model, a clear tendency to deviate from the remaining models can be observed, most of the times underestimating the displacement at the loaded beam. Once more the inherent characteristics of the model are expressed in the results obtained.

Thus, by comparing the numerical models in the light of the hypotheses associated with each one of them, it was possible to understand why their results deviated from the experimental ones. In fact, the way the slab is modeled was found to be of great importance. While the Frame+Shell model uses shell elements to model the slab, the Grid model uses a set of orthogonal prismatic elements. Despite the differences in the results not to be significant, it was expected that the first led to results nearer the real ones, given the simplifications associated with the consideration of the slab as a grid instead of a thin continuous element. The Solid model, by its turn, uses solid elements to model the concrete slab, a structural part that had a much smaller thickness, compared with its depth and width. This means that, given its geometrical characteristics, this element would behave in a manner much closer to a shell FE than to a solid one. Therefore, it was expected that the Solid model showed a stiffer response than the real one. This tendency is particularly noticeable for the decentered load action, Fig. 3.33. As far as the Analytical model is concerned, it is a simplified method which leads to a greater deviation of results when compared with the numerical ones, mostly for the decentered load. The sinusoidal load transformation certainly contributes to this, but the model has further limitations, such as the imposed symmetry and the impossibility of the interlayer option.

In terms of percentage, computed relating the vertical displacement at a beam with the sum of displacements found for the five beams at the same location as the loading applied, the models predicted for CSGL that about 37 % of the displacement is found right below the load position, for the centered load, ranging between 36 % (Analytical) and 38 % (Frame+Shell). When the load was decentered, although the mean percentage was close to the previous, 36 %, there was no such uniformity in the predictions which varied between 33 % (Solid) and 42 % (Grid). For the remaining modeling tasks, the maximum percentage of displacement reached 56 % and 55 % for the modeling where the beams were slender than those of CSGL (CSGLsb), for mid-span ($\frac{1}{2} L$) and quarter-span ($\frac{1}{4} L$) loadings, respectively. The minimum percentages, 25 % and 26 %, correspondingly to $\frac{1}{2} L$ and $\frac{1}{4} L$ loadings, were found for the modeling where the span was twice that of CSGL (CSGLI).

Concerning the beam loaded at mid-span, results found with the various modeling tasks tended to be relatively close, differing between 0 % (CSGLi) and 8 % (CSGL-hK),

considering the difference between the maximum and the minimum percentages found with the four models for the same modeling task. When the load was applied at quarter-span these differences ranged between 4 % (CSGLi) and 22 % (CSGL-hK). For both loading cases and modeling tasks, these boundary percentages were found when comparing the values obtained with the Solid model (lower percentage) and the Grid model (higher percentage), Fig. 3.34.

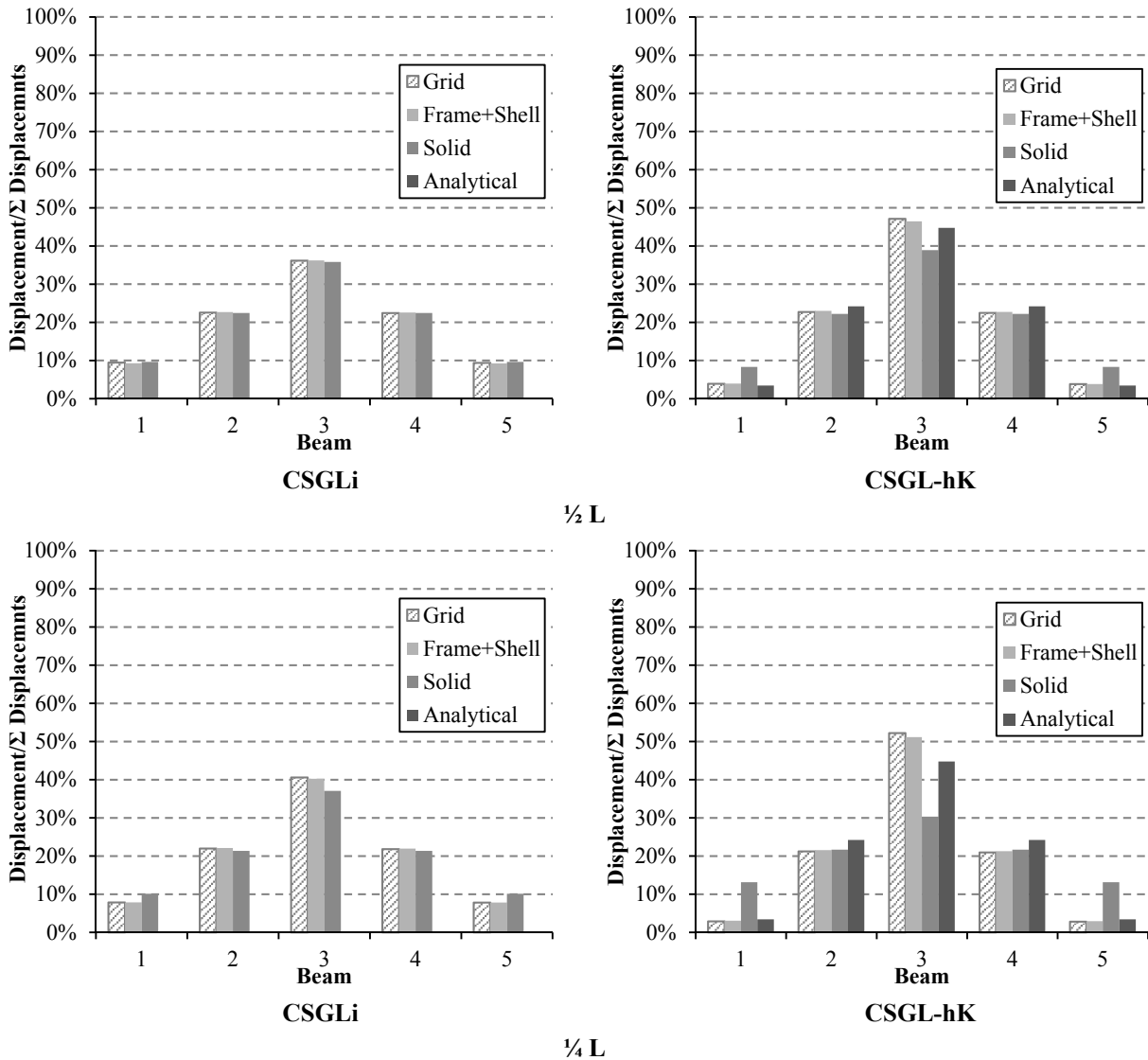


Fig. 3.34 – Theoretical analysis: percentage distribution of vertical displacement

When considering the beams immediately adjacent to the loaded one, for the whole modeling tasks, very similar percentages ($\cong 22\%$) were found among the theoretical models, with maximum percentage differences of 2 % (CSGLsb) and 4 % (CSGLjb), for loadings at

mid- and quarter-span. As for the extremity beams, the percentages also varied little among the theoretical models, with maximum differences of 5 % and 10 %, for centered and decentered loading, both for CSGL-hK modeling. For these beams, displacement percentages ranged, on average, between 1 % (CSGLjb) and 16 % (CSGLi), for the loading at mid-span; and between 2 % (CSGLjb) and 16 % (CSGLi), for the loading at quarter-span.

Considering the overall responses in terms of vertical displacement, it was found that the modeling without interlayer (CSGLi) was the one for which the predictions of the various models were more similar, with mean differences of about 0 % (centered load) and 2 % (decentered load). By opposed is CSGL-hK modeling with mean differences of 5 % (centered load) and 12 % (decentered load).

With regard to the load distribution, specifically to the ratio between the support reactions of individual beams and the applied load, Fig. 3.35 and Fig. 3.36, the various modeling tasks showed a similar behavior. As found for the displacements, the Grid and the Frame+Shell models showed results very close to each other, although not coincident (differences between 0 % and 4 %). However, the values of the different slab configurations seemed a little more dispersed in terms of support reactions when compared to displacements.

In general, the Analytical model presented a more uniformed distribution of load over the five beams when compared to the numerical models. As for the Solid model the opposite happens, with its tendency to predict a higher percentage of load to be supported by the loaded beam. Thus, for the loaded beam, the modeling associated with the lowest differences between theoretical models was the one without interlayer, CSGLi. Supporting, on average, about 45 % of the centered load and 56 % of the decentered load, this modeling was associated with a mean difference of less than 3 %, found between the predictions of the Solid and the Frame+Shell models. In contrast, a difference of 15 % was found between the same models when a nonlinear analysis was performed (CSGLnla), considering a centered load applied. As for the load applied at quarter-span, a maximum difference of 25 % was found for CSGL-mK, between the Analytical and the Grid models. In fact, in what concerns to the decentered loading, the percentages found with the Analytical model tended to deviate from those numerically predicted. When considering the whole models, an average difference of 16 % was obtained, whereas only the numerical models were considered this value decreases to 5 %.

The adjacent beams were, once more, those for which the predictions of the various models were more consistent, leading to lower differences between them. Therefore the differences between the percentages obtained with the various models varied between 4 % (CSGLi) and 10 % (CSGLnla), among the Solid and the Grid models, when the load is centered; and between 2 % (CSGL) and 9 % (CSGLi), among the Analytical and the Grid models, when the load was decentered.

3. MODEL DEVELOPMENT: PRELIMINARY STUDIES

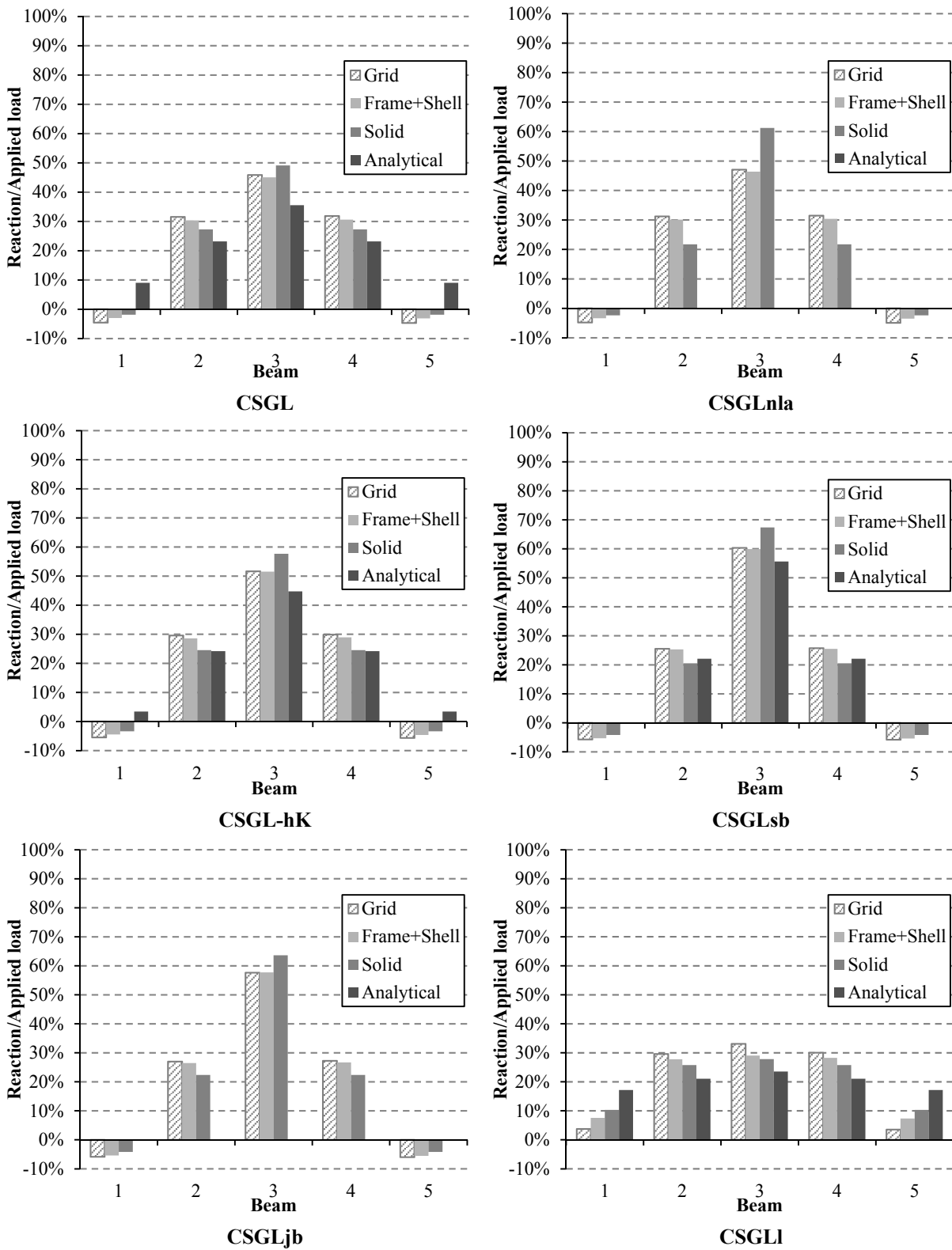


Fig. 3.35 – Theoretical analysis – load at 1/2 L: support reactions

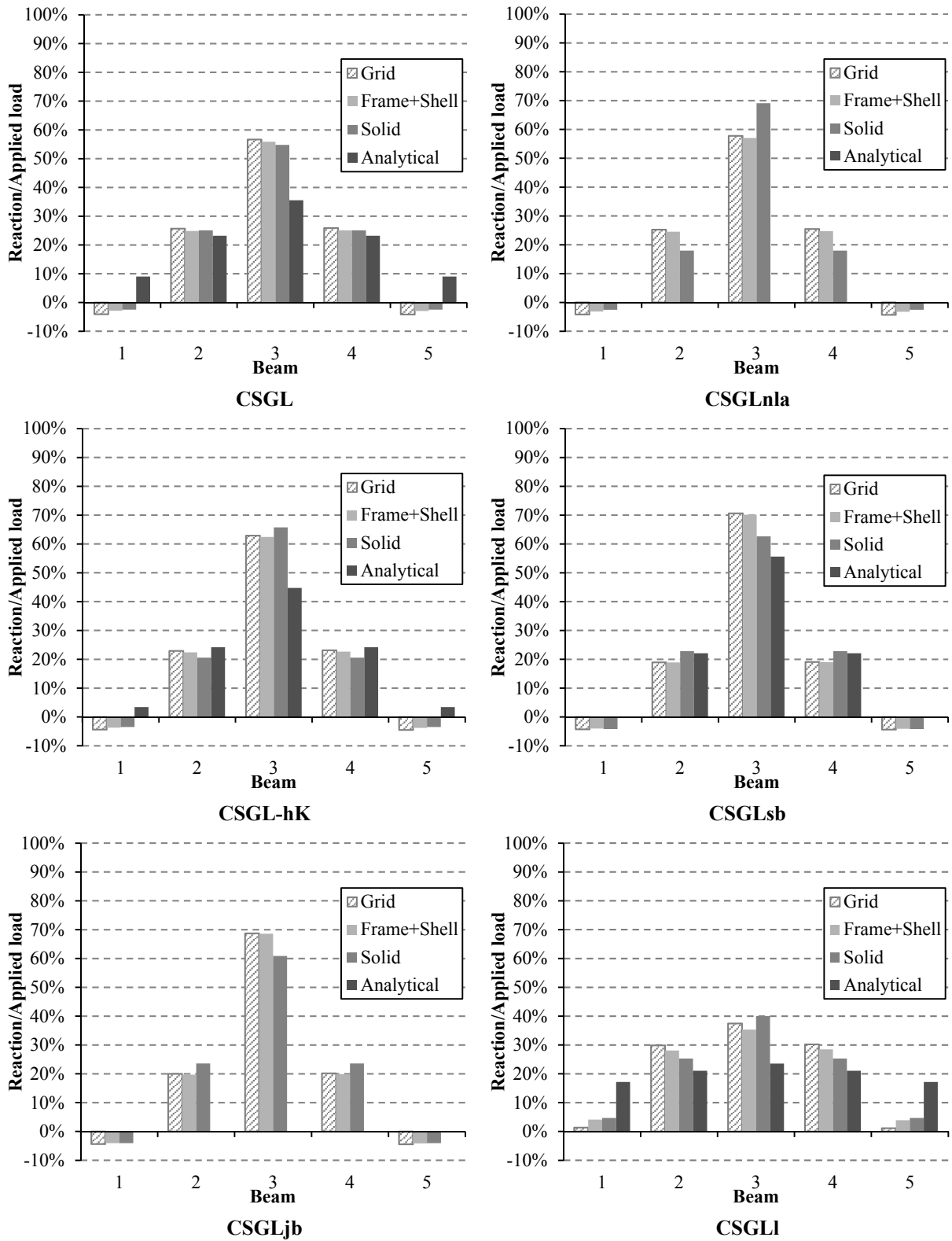


Fig. 3.36 – Theoretical analysis – load at 1/4 L: support reactions

As for the extremity beams, the differences between the models' predictions ranged between 0 % (CSGLjb) and 15 % (CSGL-mK), for both loading cases.

Thus, in general, the modeling without interlayer (CSGLi) was the one for which the percentages predicted with the various models were more similar, with mean differences of about 4 %, for both load cases. In contrast, the CSGL, for the centered load and the CSGLI, for the decentered load were those where the predictions of the various models were less consistent, with differences of 12 % and 13 %, respectively.

The longitudinal bending moment was computed individually for the mid-span cross section of each beam and compared to the sum of moments of the five, for the centered load. In a similar manner, for the decentered load case, the longitudinal bending moment was computed for the quarter-span cross section of each beam and compared to the sum of moments of all the beams. Fig. 3.37 and Fig. 3.38 present some of those results.

From the three aspects that were studied, vertical displacement, support reactions and bending moments, the last one appeared to be the most heterogeneous. In fact, when Grid, Frame+Shell, Solid and Analytical models are compared to each other, the differences are higher for bending moments when compared to those of the displacements and support reactions. However, the same general pattern is maintained; the central beam receiving the highest amount of the bending moments and the other beams receiving small portions of those moments. As it was found in the analysis of the vertical displacements, the Grid and the Frame+Shell models showed a very close agreement.

The analytic model distinguishes itself from the numerical models because it tend to predict a greater distribution of longitudinal bending moments, mainly for CSGLI, Fig. 3.37 and Fig. 3.38. In this case, beams are subjected to more even moments, varying between 17 % and 24 % of the sum of moments.

In general, for the centered load, the Solid model presented a higher value for the bending moment associated with the central beam than the remaining models. The only exceptions are associated with CSGLnla and CSGL-hK, on which the Frame+Shell model showed a higher value when compared with the others. Concerning the decentered load, except for the CSGLI, in which this trend was maintained, for the remaining modeling the Grid model assumed this role.

For the beam loaded at mid-span, the bending moment received represented 40 % (CSGLI) to 65 % (CSGLsl) of the sum of moments in all the beams. When the beam was loaded at quarter-span, the loaded beam received between 42 % (CSGLI) and 70 % (CSGLjb). Thus, for the loaded beam, the differences found among the modeling predictions varied between 2 % (CSGLnla) and 28 % (CSGLI), for the centered loading; and 5 % (CSGLjb) and 12 % (CSGLi), for the decentered loading.

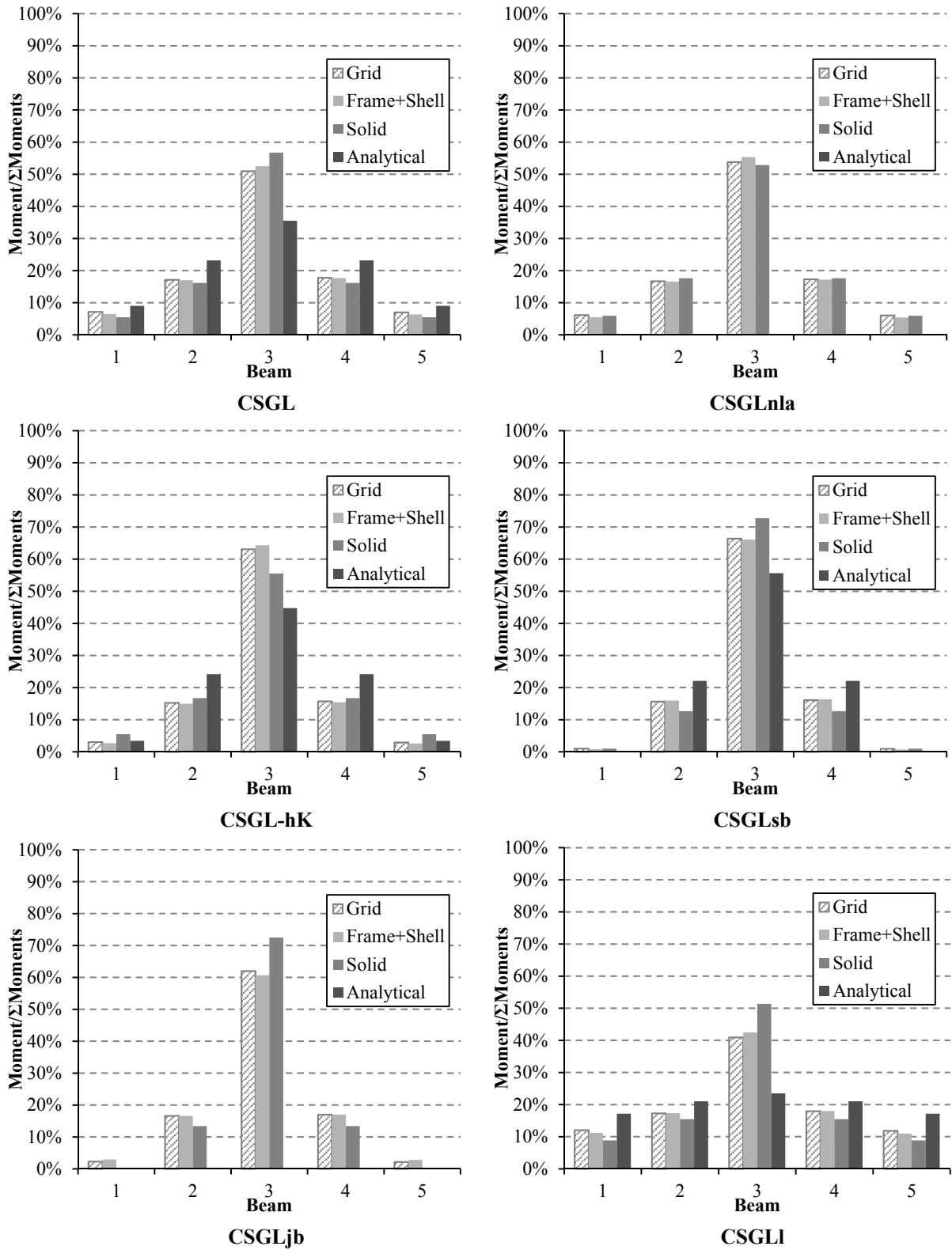


Fig. 3.37 –Theoretical analysis – load at 1/2 L: longitudinal bending moment at 1/2 L cross section

3. MODEL DEVELOPMENT: PRELIMINARY STUDIES

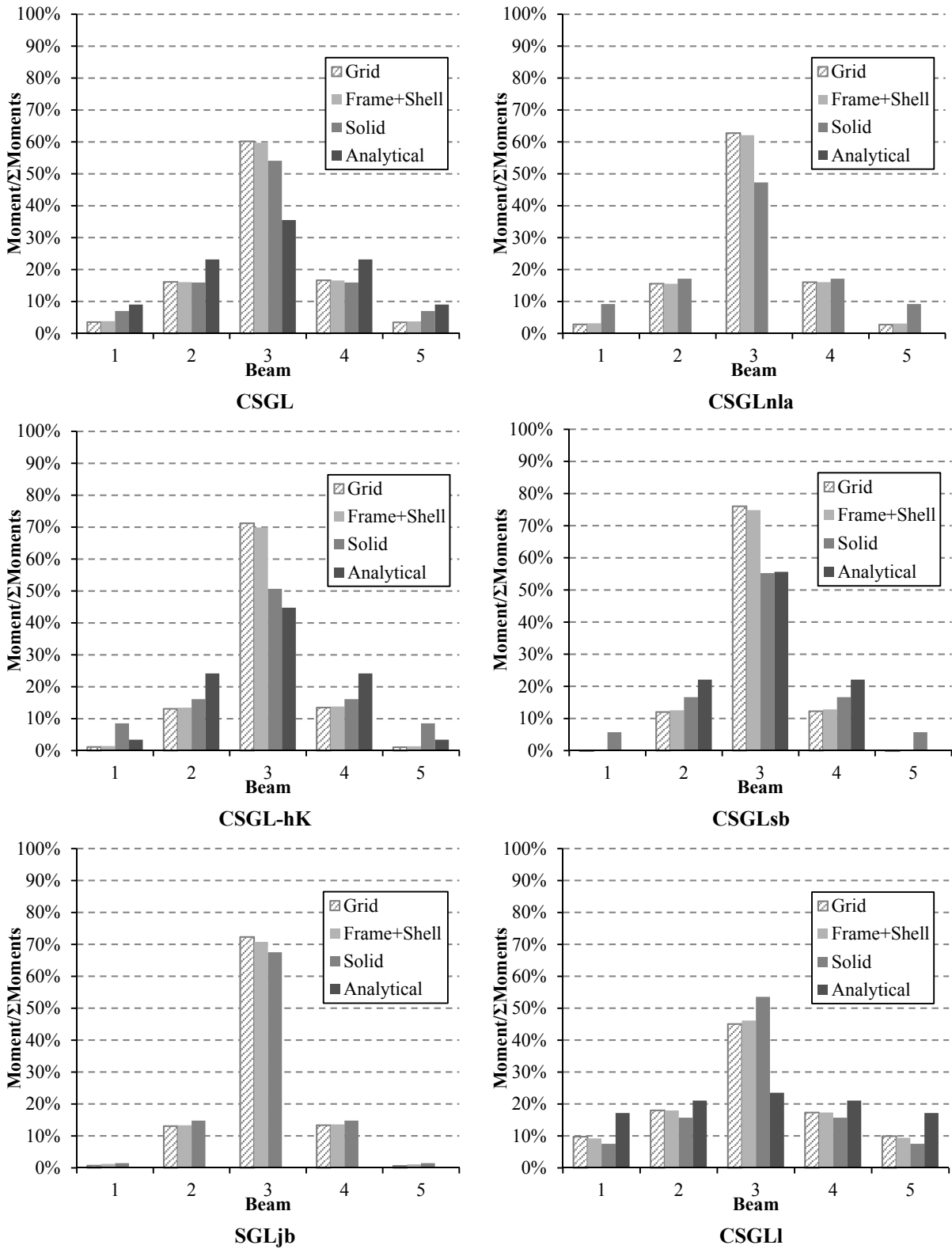


Fig. 3.38 –Theoretical analysis – load at ¼ L: longitudinal bending moment at ¼ L cross section

As well as was found for the support reactions, when only the numerical predictions were considered, the mean differences among the relation of bending moments decrease by about half: from 18 % to 9 %, when the load was applied at mid-span; and from 20 % to 11 % when the load was applied at quarter-span.

Concerning the beams adjacent to the loaded one, the same trend as for the previous quantities was observed: predictions obtained with the various models tended to be closer than for other beams. Therefore, for the centered loading, differences ranging between 0 % (CSGLnla) and 9 % (CSGLsl) were obtained among the Frame+Shell and the Solid models, and among the Solid and the Analytical models, respectively. For the decentered loading, the differences ranged between 1 % (CSGLnla) to 11 % (CSGL-hK), among the same theoretical models. As for the extremity beams, the differences between the models' predictions varied between 1 % (CSGLnla) and 8 % (CSGLl), among the Frame+Shell and Grid models and among the Solid and the Analytical models, respectively. When the load was applied at quarter-span these differences varied between 0 % (CSGLi) and 16 % (CSGL-hK), among the Grid and Frame+Shell models and among the Grid and Solid models, respectively.

In summary, for the three quantities that were analyzed, the Solid and the Analytical models, separately or together, stood out by presenting a behavior somehow different from the remaining. Most of the times this meant that the differences were obtained considering the prediction of one of them as extreme. The Analytical model tended to predict a more uniform contribution of all the beams, which led their predictions to deviate from the numerical ones. Consequently, when considering only the numerical models, very close predictions were found, with mean differences below 10 %. In general, the loading at quarter-span led to predictions less uniform, when comparing the four models, while for the centered load the trend was to obtain more regular predictions. As for the analyzed quantities, the vertical displacements and the support reactions presented relatively homogeneous results. Concerning the various modeling tasks, the one without interlayer (CSGLi) showed to be the one for which the differences among predictions were lower, when considering the whole theoretical models. By opposition, but without the same regularity, the modeling with the highest connector stiffness (CSGL-hK) tended to be for which the differences between theoretical predictions was higher.

3.5.4 Additional remarks

In this section it was intended to validate the developed numerical models in order to analyze the transversal load distribution on timber-concrete composite floors. Therefore, the approach adopted was to compare the predictions of the theoretical models, numerical and analytical, with experimental results for timber-concrete composite slabs under concentrated

loads. Such comparative work was carried out in terms of vertical displacements and distribution of support reactions of the timber beams. This comparison allowed the statement that the predictions from the theoretical models lead to sufficiently close results to validate the theoretical models.

Grid and Frame+Shell models showed, in most of the cases, a great concordance, while the Solid and the Analytical models are sometimes a little apart from the rest of models. The Analytical model tends to predict more even distributions, either for loading or bending moments. On the other hand, the Solid model tends to predict a less even distribution.

In general, the use of these four models to predict the behavior of timber-concrete composite bi-dimensional systems showed to be satisfactory. However, it should be noted that, the Analytical model is an approximate method with several simplifications, and it might be used with precaution in the structural design of such composite systems. From the comparison with the experimental results and as confirmed by the modeling of different conditions, the Frame+Shell model was found to be the most adequate for the ongoing investigation. This model, besides being the closest to the experimental results, is simple to apply and implies less time consumption when compared to the Solid model. Comparing with the Grid model, the Frame+Shell model can simulate the overall behavior more efficiently, especially in the cases where the interaction between the timber beams and the concrete slab is important, including the ones associated with the numerical models validation. Consequently, it was the model chosen to perform the numerical analysis in the ongoing study of the transversal load distribution.

3.6 Preliminary numerical analysis

According to (Oliveira 2002), besides predicting the behavior of test slabs, the use of numerical models also allows the study of the effects that a great number of parameters may have on their behavior. Therefore, after developing and validating the model, a numerical preliminary analysis was performed in order to establish the experimental program.

Based on the validation of the numerical models and on the conclusions associated with it, the Frame+Shell model was chosen to perform the concerned analysis. Besides its ability to more efficiently simulate the overall behavior when compared with the Grid model and its simple application and less time consumption when compared to the Solid model, this model showed the closest results when compared to the experimental ones.

Primarily, a group of parameters, whose effects might have a great importance when considering the action of a concentrated load and the consequent transverse load distribution in timber-concrete floors, was collected. Thus, considering the actual characteristics of

timber-concrete composite floors, as the materials, the geometry, the support conditions, and also the loading conditions, the following were chosen to be analyzed:

- width and span;
- relative heights of the resistant elements, concrete slab and the timber beams, and their mechanical properties;
- connection between timber beams and concrete slab: stiffness and behavior;
- existence of interlayer (pre-existing timber floorboards);
- load type and location; and
- support conditions.

By studying this group in the light of the commonly used floors systems and acting loads, a set of parameters was established to perform the study, as well as the *base simulation* (*Bs*). This modeling is the one to which the remaining were compared, serving as base modeling. Thus, the *Bs* modeled a simply supported (*Ss*) square floor with a value of 4.00 m for the width (b_{slab}) and for the span (L), with a timber interlayer 0.02 m (t_i) thick and a concrete layer with a thickness of 0.07 m (t_c). Also seven rectangular (*Rt*) cross-section timber beams, 0.10×0.20 m ($t_t \times h_t$), placed 0.60 m (s_b) apart from each other, composed the floor, Fig. 3.39. A more detailed description can be found in 5.2 *Parametric study*.

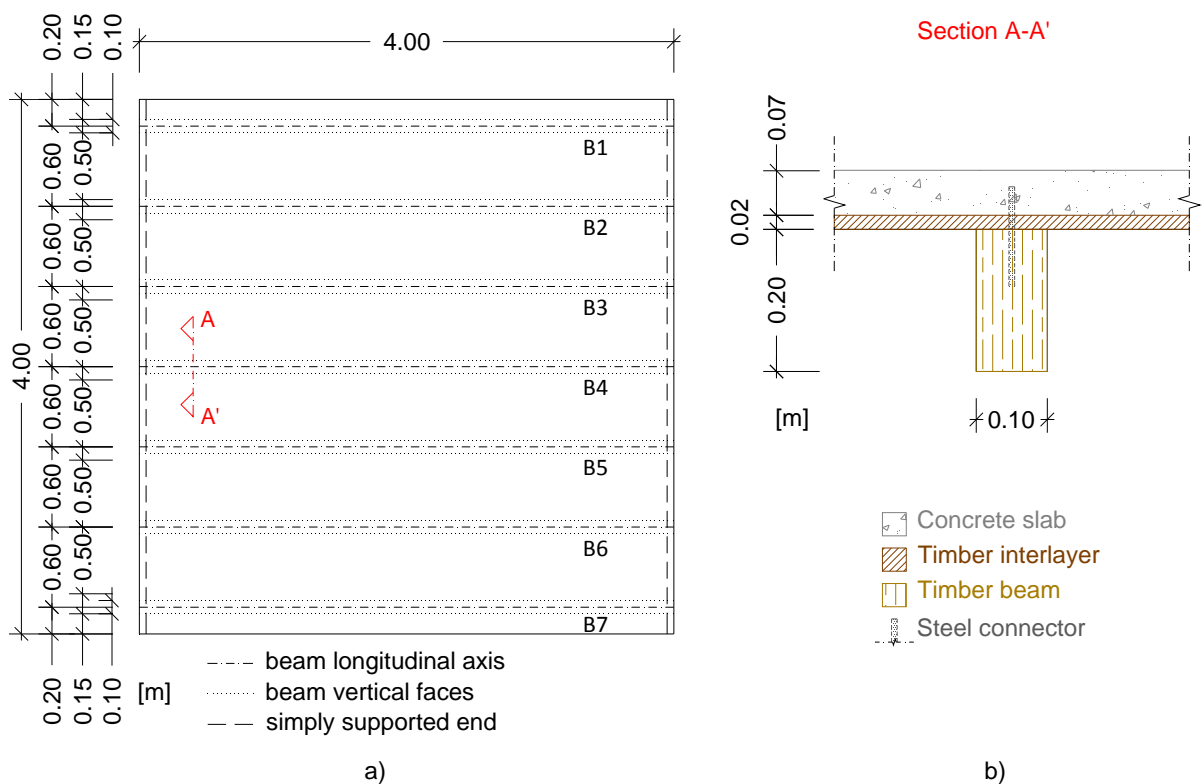


Fig. 3.39 – *Bs* modeling: geometrical characteristics

Starting from the *Bs* modeling based in the parameters listed before and trying to vary only one parameter, as possible, the remaining modeling were established. By analyzing the obtained results, among all parameters, some showed to affect the behavior of the composite floors in study. The analysis was focused in the vertical displacement at mid-span of the each beam compared to the sum of displacements of all the beams, in the support reactions in each beam and their relative weight when compared to the sum of reactions, and in the longitudinal bending moment at mid-span cross section of each beam compared with the sum of the moments of all the beams. With each modeling, several load cases were considered allowing an analysis for each concentrated load applied to all the beams, one at a time (the self-weight or the imposed load, was considered uniformly distributed over the slab surface).

Aiming at finding the parameters that most affect the transversal distribution of load in the composite floor systems under consideration, a comparative analysis was performed. Therefore, the values of *Bs* were compared with those of the remaining modeling, searching for the major differences, maximum and minimum. This procedure was adopted individually for the quantities listed before for each of the concentrated loads acting at each beam considering always the loaded beam.

Table 3.6 compiles the final results of the preliminary numerical study, identifying the parameters with the highest influence in the distribution of vertical displacements, support reactions and bending moments. The parameter and the range of variation computed based on the results for the loaded beam considered at *Bs* were identified together with the load case corresponding to the highest percentage.

Analyzing these results it is clear the effect that the support conditions have in the distribution of the three comparative parameters, either considering or not the existence of a lower deck in crossed laminated timber (CLT) (varying between 10 and 75 %). There follows the thickness of the concrete layer. This parameter present a deviation between 18 and 31 %.

The use of a CLT deck rather than a lower layer composed by juxtaposed beams also show a great influence, 27 %, specifically in the distribution of support reaction. The span of the slab and the type of the concrete are the following with deviations of about 20 %.

Table 3.6 – Summary of the parameters with higher effect in the quantities studied

	Variation with higher effect	Highest deviation [%]	Load Case	Maximum variation found between
	Vertical displacements	Concrete thickness, h	31	Ln B1
21			Bs + $h = 0.03$ m and Bs ($h = 0.07$ m)	
CLTdeck supports		26	Bs + CLTdeck (Ss) and Bs + CLTdeck + Sae	
Span, L		19	Bs + $L = 2.00$ m and Bs ($L = 4.00$ m)	
Concrete		17	Bs + LC16/18 and Bs (C25/30)	
$L = 6.00$ m + $h = 0.05$ m		11	Bs + $h = 0.05$ m ($L = 4.00$ m) and Bs + $h = 0.05$ m + $L = 6.00$ m	
Support conditions		10	Pt B1	Bs (Ss) and Bs + Fx
Support reactions	Support conditions	75	Pt B1	Bs (Ss) and Bs + Sae
	CLTdeck supports	70		Bs + CLTdeck (Ss) and Bs + CLTdeck + Sae
	Concrete thickness, h	31	Pt B2	Bs + $h = 0.02$ m and Bs ($h = 0.07$ m)
		18		Bs + $h = 0.03$ m and Bs ($h = 0.07$ m)
	CLTdeck vs. Juxtaposed beams	27	Pt B1	Bs and Bs + CLTdeck
	Span, L	22	Pt B2	Bs + $L = 2.00$ m and Bs ($L = 4.00$ m)
	Concrete	14	Ln B2	Bs + LC16/18 and Bs (C25/30)
	$L = 6.00$ m + $h = 0.05$ m	11	Pt B2	Bs + $h = 0.05$ m ($L = 4.00$ m) and Bs + $h = 0.05$ m + $L = 6.00$ m
Beam spacing, s_b	10	Pt B1	Bs + $s_b = 0.40$ m and Bs ($s_b = 0.60$ m)	
Bending moments	Support conditions	36	Ln B1	Bs (Ss) and Bs + Sae
	Concrete thickness, h	31		Bs + $h = 0.02$ m and Bs ($h = 0.07$ m)
		19		Bs + $h = 0.03$ m and Bs ($h = 0.07$ m)
	CLTdeck supports	23	Pt B1	Bs + CLTdeck + Supports in all ends
	Span, L	18	Ln B1	Bs + $L = 2.00$ m and Bs ($L = 4.00$ m)
	Concrete	16		Bs + LC16/18 and Bs (C25/30)
	CLTdeck vs. Juxtaposed beams	14	Pt B4	Bs and Bs + CLTdeck
$L = 6.00$ m + $h = 0.05$ m	10	Ln B1	Bs + $h = 0.05$ m ($L = 4.00$ m) and Bs + $h = 0.05$ m + $L = 6.00$ m	

3.7 Definition of the experimental program

After analyzing the results of the previous section the plan for the experimental program was established. Based in the gathered information together with the design practice and taking into account the limitations associated to the laboratory work, the following conclusions were stated.

The experimental tests should be carried out in real-scale test specimens, subject to point loads and line loads parallel to the timber elements.

The number of different configurations to test must be able to cover most, or all, of the parameters whose effects in the transversal distribution of load were numerically significant. Therefore, it would be interesting to consider:

- different support conditions;
- specimens with different thicknesses of concrete;
- the use of a CLT deck and individual beams;
- different spans for the beams; and
- different types of concrete.

Due to the time available to use the laboratory it was stated that five would be the number of specimens to produce and test. Given the restraints in laboratory space, also the maximum span to use was set in 6.00 m. The costs and time associated to the delivery of a CLT deck made it inadequate to the intended experimental analysis. In turn, the setting of support conditions different from those corresponding to the simply supported at the beams' ends was considered unfeasible. This is consequence of the lack of equipment able to guarantee fixed ends, by completely avoiding the rotation and translational displacements at the beams' ends. Also the conditions where all the slab sides would be simply supported were unachievable at the available place and equipment in the laboratory.

The use of a rectangular plant, rather than a square one, was considered to make a more comprehensive analysis. Therefore, a base test specimen was defined with 3.00 m width and 4.00 m span. A common regular concrete, as C25/30, was chosen, as well as an intermediate thickness for this layer, 0.05 m.

Hence, the parameters stated to vary relatively to the *Base specimen* are set as the following: the use of a light-weight aggregate concrete (LWAC); the definition of a different concrete height; and different slab spans. This information is summarized in Table 3.7.

Table 3.7 – Parameters to test in the experimental specimens

Description	Variation	Span	Concrete height	Concrete type
		L	h	
		[m]	[m]	
Base specimen	-	4.00	0.05	RC
Base specimen + LWAC	Concrete		< 0.05	LWAC
Base specimen + h_c	h_c	< 4.00	0.05	RC
Base specimen + short L	L	> 4.00; max = 6.00		
Base specimen + long L				

Relatively to the LWAC, based in the inferences of the previous section, it must have a lower MOE and strength relatively to the one used in the *Base specimen*. Properties shown by the numerically modeled LC16/18, relatively to the C25/30. As for the concrete height, a thickness smaller than the one set in the *Base specimen* (< 0.05 m). This is justified with the deviation pattern found in *3.6 Preliminary numerical analysis*. In fact, the deviation found between the smaller thicknesses was higher than the one found between the greater ones, showing the greater influence of the former.

Concerning the change in the span, two different values were set, a smaller and a bigger than that of the base test specimen. This, as the preceding parameters, also follow the findings in the previous section.

Beyond the parameters that should be considered in the experimental analysis, also the load to apply has an important role. As already mentioned, two types of concentrated loads were considered: point and line loads. Although, the preliminary numerical analysis considered the mid-span of each beam as action position for the point loads, also the quarter-span was considered relevant for the study. This option was taken by considering the already performed preliminary experimental tests. Locations as the space between beams, in the central area and near the extremity beam were also weighed. However, they were disregarded due to punching shear which *per se* would require a specific investigation which was not the goal of this thesis. Therefore the point loads should be applied to mid- and quarter-span, over all the beams, one at a time. As for the line loads, the positions chosen were along each beam, one at a time.

The loads to be applied will be numerically estimated, as previously presented. The load level to be applied will be defined aiming to be high enough to represent the service loads, but low enough to avoid the risk of inducing some kind of damage and permanent deformations, as not to compromise the following tests.

The following chapter presents a detailed description of the experimental tests performed and of the specimens' characteristics.

4. EXPERIMENTAL ANALYSIS

4.1 Introduction

The use of experimental tests to support an investigation is a common practice. Several studies were essentially based on experimental tests, such as those by (Daniels 1990, Etournaud 1998, Luttrell 1995, Mullenex 1993, Porter and Ekberg-Jr. 1977, Thomas 2003). However, the combined use of the two approaches enables the comparison between results, and, at the same time, the model to be validated (Dahl *et al.* 2006, Daniels and Crisinel 1993, Gutkowski *et al.* 2010, Ilharco 2008, Kearley and Carruthers 1991, Moreira 2001, Smilovic *et al.* 2013). This is also the intension with the present doctoral research.

The experimental program of this thesis, which included preliminary tests, was performed in DEC-FCTUC at the LEMEC laboratory. A set of tests on timber-concrete composite floor real scale specimens was carried out to find out how the load would be distributed in the transversal direction. To achieve this goal, different types of concentrated loads were applied at different locations.

Some parameters, identified in the previous chapter as affecting the composite floor behavior, were experimentally analyzed. The degree these parameters would interfere in the transversal distribution of load was sought. To do so, the values of displacements at different locations and with different directions, support reactions and strains were measured and analyzed.

With the numerical Frame+Shell model, already presented, the tested specimens were modeled and the corresponding results evaluated in the light of the experimental results. The conclusions are presented in the following sections.

4.2 Test specimens: properties and geometry

The experimental analysis intends to investigate the transversal load distribution in timber-concrete composite slabs. To do so, it is extremely important to define a sample that characterizes the composite slabs under consideration and at the same time is able to capture the phenomenon under study. Thus, based on the conclusions of the preliminary parametric study which led to the identification of this means, the parameters whose influence in the distribution of load was worthy to be studied, five specimens were defined.

As previously presented, parameters as the span, the concrete strength or the thickness of the concrete layer shown to have a great influence the way in which the load is distributed transversally to the slab supports. Parameters as the slab width, the beam spacing, the timber strength and section were chosen to be fixed in all the specimens.

Table 4.1 and Table 4.2 summarize the characteristics of each specimen and the parameter which differ relatively to the *Base specimen* (BSp). This specimen was defined and designed considering usual dimensions and materials commonly applied in such composite slabs. The properties associated with the *Base specimen*, as the span or the thickness of the upper layer, were designated preceded by the term “*base*” (e.g. *base span*). The five specimens were numbered and the designation adopted based on it, namely S1 to S5.

Table 4.1 – Experimental specimens: variation parameters

Specimen designation	Characteristics			Variation
	Span [m]	Concrete thickness [m]	Concrete type -	
S1	4.00	0.05	RC	Base specimen
S2			LWAC	Concrete
S3		0.03	RC	Concrete thickness
S4	2.00	Span		
S5	6.00			

Table 4.2 – Characteristics of the experimental specimens

Specimen designation	Geometrical characteristics						Material characteristics		
	Span	Width	Concrete thickness	Timber interlayer	Beam section	Beam spacing	Concrete layer		Timber beams
	L [m]	b_{slab} [m]	h_c [m]	h_i [m]	$(b_t \times h_t)$ [m]	s_b [m]	Strength class	Aggregate	
S1	4.00	3.00	0.05	No	0.12×0.24	0.60	C25/30	Limestone	Homogeneous Picea Abies Glulam, GL 24h
S2				Yes (0.02)			LC16/18	Cork	
S3			No	C25/30			Limestone		
S4	2.00	0.05	No	0.12×0.32	0.60	C25/30	Limestone		
S5	6.00								

All the floor specimens were composed by five glulam beams linked together by a top concrete layer of different thicknesses and properties. The width was fixed to 3.00 m and the beam spacing to 0.60 m. Parameters as the beam section, connector type or timber interlayer

were also intended to be fixed, however they had to be changed as consequence of the structural design requirements or for practical feasibility reasons.

As the previously tested specimens, these five specimens were structurally designed according to EC5 (EN1995 2004a) for the loads required by EC1 (EN1991 2001). They were also simply supported at two opposite ends with a *base span* of 4.00 m (Fig. 4.1). The *base thickness* of the concrete layer was 0.05 m and was composed by normal strength concrete. For all the specimens but S2, a C25/30 ready-mix concrete was used, according to EC2 (EN1992 2004). For S2 floor, a cork light-weight concrete was used, and the mixture was prepared at the laboratory. This kind of concrete was already studied (Dias and Martins 2012), and proved to have a good performance in timber-concrete composite slabs solutions. Associated with an ecological aspect because of the use of cork waste material, it also decreases the slab weight and improve the thermal insulation relatively to a timber-concrete common solution. Table 4.3 summarizes the composition of the concrete produced and used in S2.

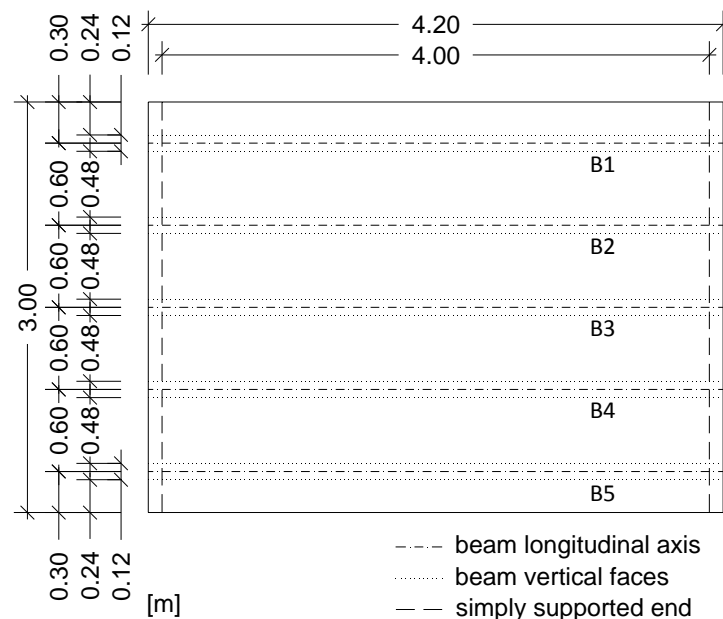


Fig. 4.1 – Plan view scheme: specimens S1 to S3

Table 4.3 – Cork-concrete composition

Material		Quantity
		[kg/m ³]
Sand		375.0
Coarser aggregate		670.0
Cork	0/3	13.0
	3/10	10.0
Cement		242.0
Water		134.0
Superplasticizer		1.9

The five specimens were cast in the same place where they were assembled and tested, the LEMEC laboratory, Fig. 4.2. In order to optimize the ready-mix concrete supply, taking into account the quantity needed for the several specimens, it was decided to cast separately specimens S1 and S5, and S3 and S4 together.

**Fig. 4.2 – Casting of the test specimens**

In all the concrete pouring, some 0.15 m cubes and 0.15 × 0.15 × 0.60 m prisms were also cast in order to determine the strength and MOE of the concrete. The following table presents the mean properties associated with the concrete used for the several specimens. Except for the MOE, the remaining properties were evaluated for several ages, yet the values presented in Table 4.4 correspond to the age closest to the testing day. Detailed exposition can be found in the *APPENDIX B, B.1 - Material characteristics, B.1.1 - Concrete*.

Table 4.4 – Concrete properties (mean values)

Specimen designation	Concrete		
	Density	MOE	Mean compressive strength
	ρ	E_c	f_{cm}
	[kg/m ³]	[MPa]	[MPa]
S1	2318	26456	18.15
S2	1777	13717	12.46
S3	2302	23341	16.20
S4			17.00
S5	2315	28648	23.46

The mean compressive strength was obtained based in the compression tests performed to the cube specimens, according to the Portuguese standard (NP-EN12390 2012). The mean modulus of elasticity (MOE) was obtained through static tests performed in the prismatic concrete specimens, according to (E397 1993), Fig. 4.3. This specification implies the assumption of a compressive strength for the concrete. The used values correspond to those found for the cube specimens. After the prismatic specimens have been tested to compressive failure the value obtained for the compression strength must be compared with the one that was assumed. For the cases where the difference between both values is superior to 20 %, the Standard suggests that this aspect should be referred in the test report. Despite not to be a Standard request, it was decided to disregard the value of MOE of the prism for which the difference between compressive strength was greater than 20 %, assuming that the remaining would represent better the property in question.

In order to reduce tension effects, the concrete layer was provided with a steel wire mesh (A500NR) with a diameter wire of 3 mm and 0.10 m of mesh spacing.

The timber beams were constituted by homogenous *Picea Abies* glued laminated timber. The class requested, GL 24h according to (NP-EN1194 2002), was the same for all the twenty-five beams that composed the specimens. All of them were numbered, weighted and measured in several sections. The global modulus of elasticity was obtained through static tests according to (EN408 2010), Fig. 4.4. Table B.5 and Table B.6, in Section *B.1.2* –

4. EXPERIMENTAL ANALYSIS

Timber, APPENDIX B, summarize geometric and material properties measured or computed for each beam.



Fig. 4.3 – Testing of prismatic concrete specimens: a) MOE; and b) failure

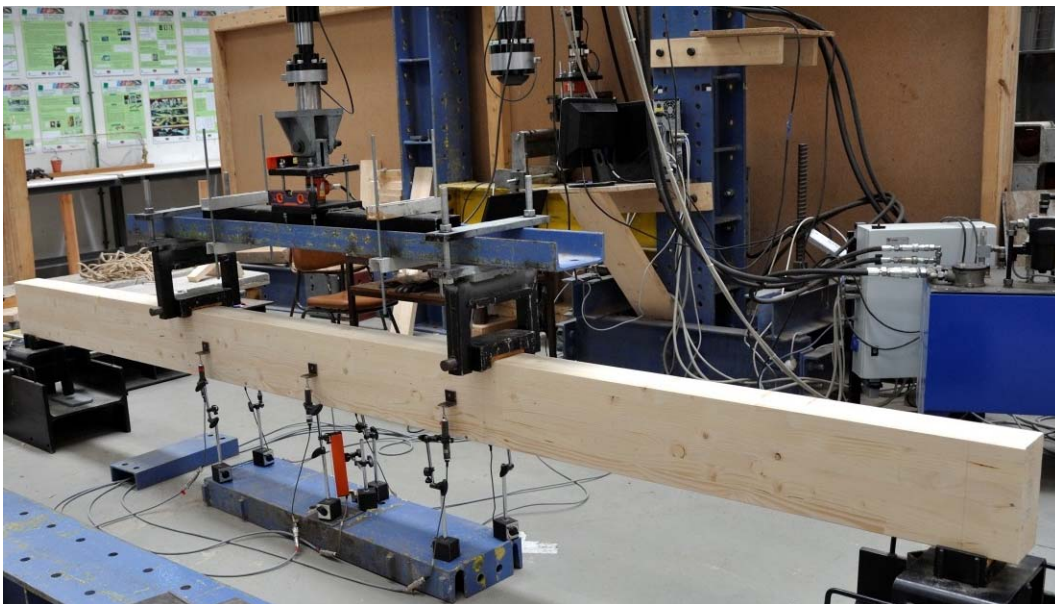


Fig. 4.4 – MOE static test

To define which beams would be associated with each specimen the combinations at Table 4.5 were created. The sets were gathered based on the beams MOE, aiming to obtain, as possible slab specimens with uniform timber material properties and at the same time symmetry relatively to the central beam.

Table 4.5 – Timber beams of each specimen

Specimen designation	Beam position	Beam designation	Global MOE	Specimen designation	Beam position	Beam designation	Global MOE
			$E_{m,g}$				$E_{m,g}$
			[MPa]				[MPa]
S1	B1	GL3	7851.0	S4	B1	GL17	6118.1
	B2	GL9	10248.8		B2	GL20	7959.9
	B3	GL13	8927.0		B3	GL19	7092.2
	B4	GL1	10164.8		B4	GL18	7467.2
	B5	GL8	8225.1		B5	GL16	6332.6
S2	B1	GL4	8312.8	S5	B1	GL23	9309.5
	B2	GL10	9674.8		B2	GL24	8643.4
	B3	GL11	9846.0		B3	GL22	10697.8
	B4	GL14	9520.5		B4	GL25	8931.4
	B5	GL15	8331.4		B5	GL21	9170.6
S3	B1	GL6	8387.8				
	B2	GL12	8651.1				
	B3	GL2	11059.2				
	B4	GL5	8981.4				
	B5	GL7	8571.3				



Fig. 4.5 – Connectors: a) steel rod $\varnothing 8$ mm; and b) SFS VB 48-7.5x100 screw

4. EXPERIMENTAL ANALYSIS

Based on the same reasons as before, simplicity of application, economy and efficiency, a connection system similar to the one used in the preliminary test specimens was chosen to joint each timber beam with the concrete layer. 0.140 m long reinforced concrete steel rods (A500NR) with 8 mm diameter, Fig. 4.5 a), were placed along the beams 0.10 m apart. Each stud was inserted on a predrilled hole through the timber height, with an embedment length of 0.10 m in the wooden beam. The remaining 0.04 m was left off the timber beams upper surface, to be embedded in the concrete slab, which was to be poured later, Fig. 4.6.



Fig. 4.6 – Placing of the steel rods: marking, drilling and positioning

In specimen S3 the parameter whose interaction with the load distribution were intended to be analyzed was the thickness of the concrete layer. This led to define a 0.03 m height for this top flange. For constructive reasons, a permanent formwork was used in the form of 0.02 m thick timber interlayer, achieved by Pine timber boards. As mentioned before, the connection system, and consequently the connector, were supposed to be the same for the five floor specimens. However, given the thickness of the slab, it was necessary to use a different connector type: one guarantying an efficient cover and assembly between timber and concrete. The choice was based on the mechanical characteristics of several connections, namely their slip modulus, and the overall behavior of the composite slab when they were used. A set of two SFS VB 48-7.5×100 screws, inclined at 45 degrees and with an “X” configuration, spaced 0.20 m along the beams span was chosen (Fig. 4.5 b), Fig. 4.7 to Fig. 4.9).

The screws were placed so that the same cover as in the remaining floor specimens (0.01 m) had to be guaranteed together with a symmetrical arrangement relatively to each beam mid-span, Fig. 4.8.

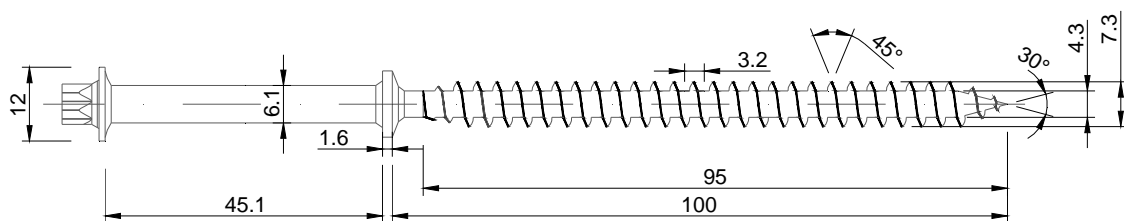


Fig. 4.7 – SFS VB 48-7.5×100 screw scheme: geometrical characteristics

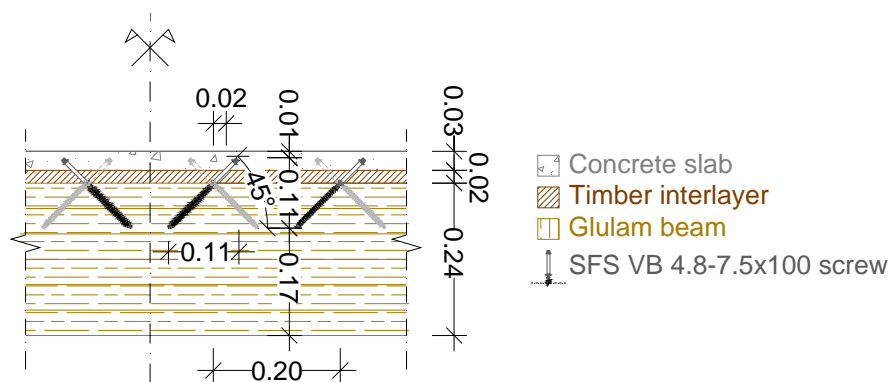


Fig. 4.8 – SFS VB 48-7.5×100 screws application scheme

In all the specimens, a plastic film was applied to the timber beams top surface, or in the case of specimen S3 to the timber interlayer top surface, providing moist protection from the fresh concrete and avoiding friction between timber and concrete.

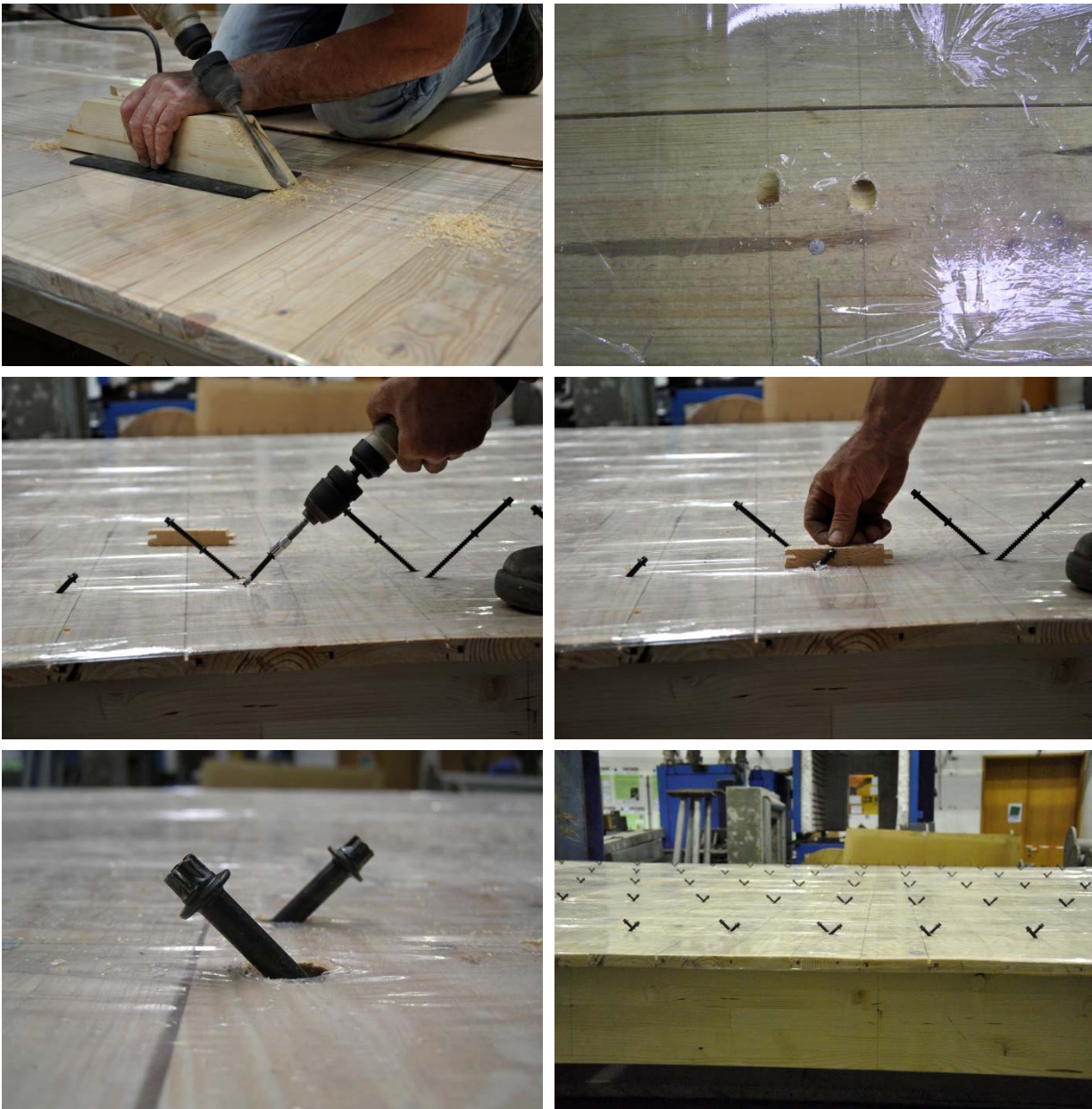


Fig. 4.9 – Placement of the SFS screws on specimen S3

Both specimens S4 and S5 intend to analyze the effects of the beams' span in the load distribution of the composite floors considered. The former was defined with a shorter span equal to half the span of the *Base specimen* (4.00 m), 2.00 m. Despite being an oversized section for the span in question, it was decided to maintain the same beam cross section as for the previous specimens. In turn, specimen S5 was defined with 6.00 m span, 1.5 times the span of the *Base specimen*. The design requirements led to define a different cross section for

the glulam beams, 0.12×0.32 m instead of 0.12×0.24 m. This introduced a change in the beams cross section, besides the beams span, relatively to the *Base specimen*.

The geometrical characteristics associated with each test specimen are gathered in the following figures, Fig. 4.10 to Fig. 4.12.

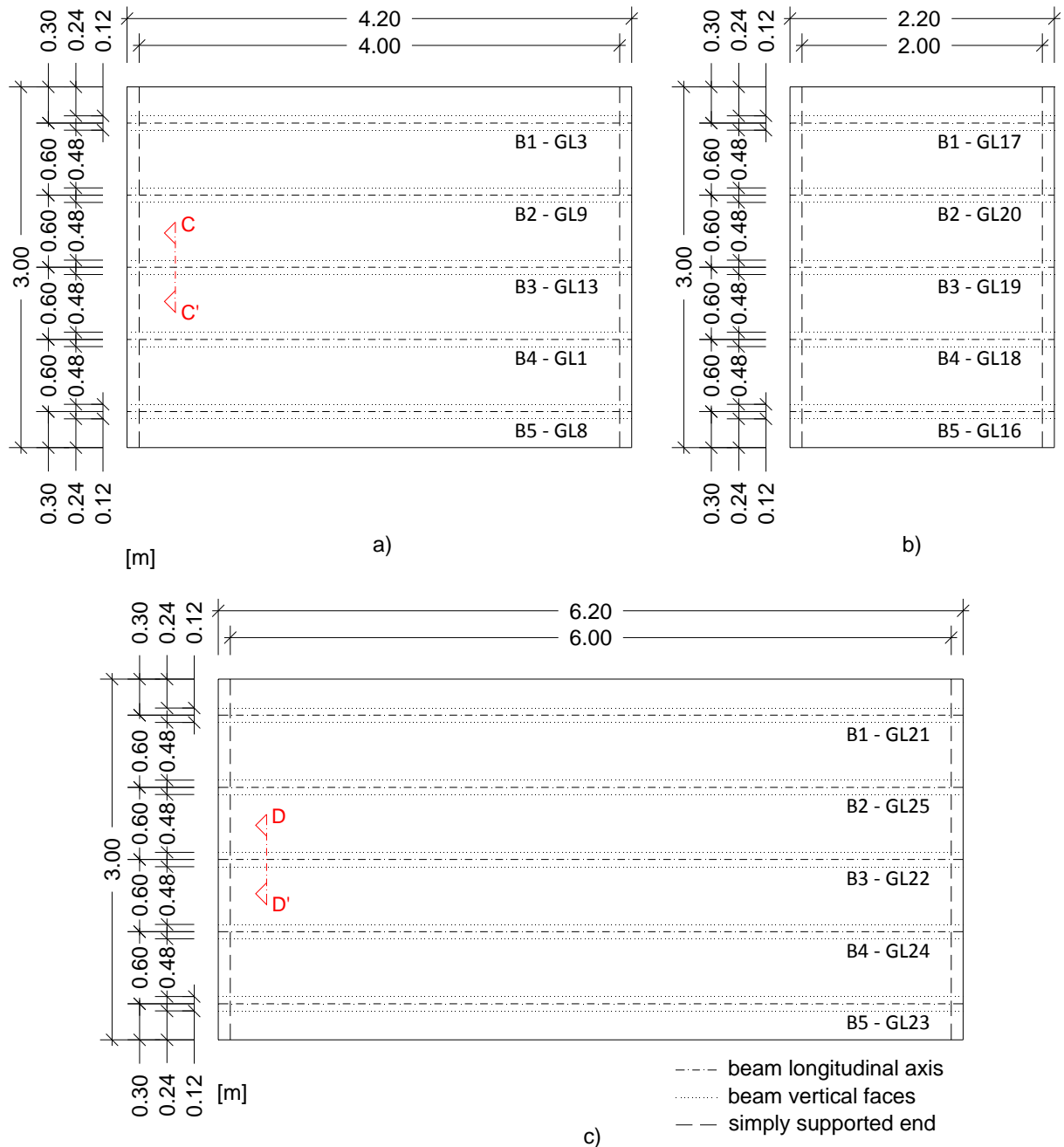


Fig. 4.10 – Geometrical characteristics, plan view of the specimens: a) S1; b) S4; c) S5

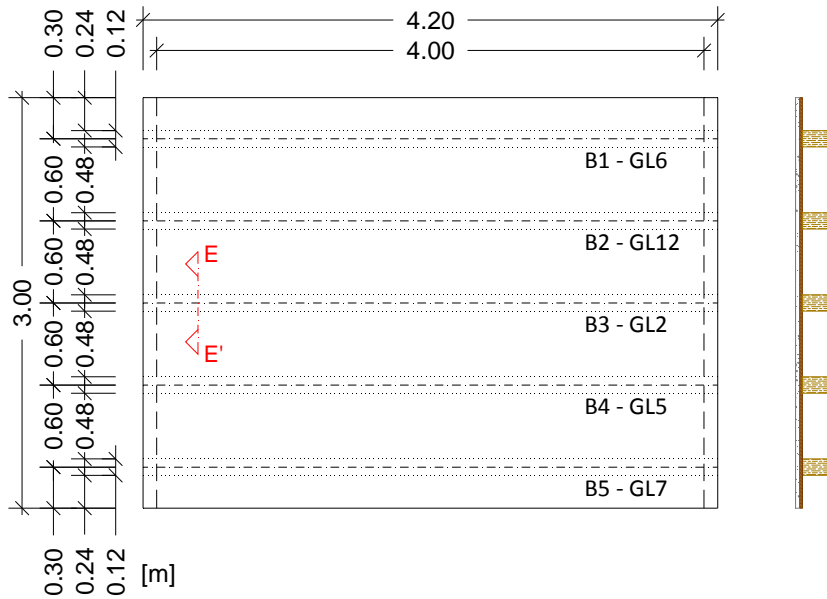


Fig. 4.11 – Geometrical characteristics, plan and side views of specimen S3

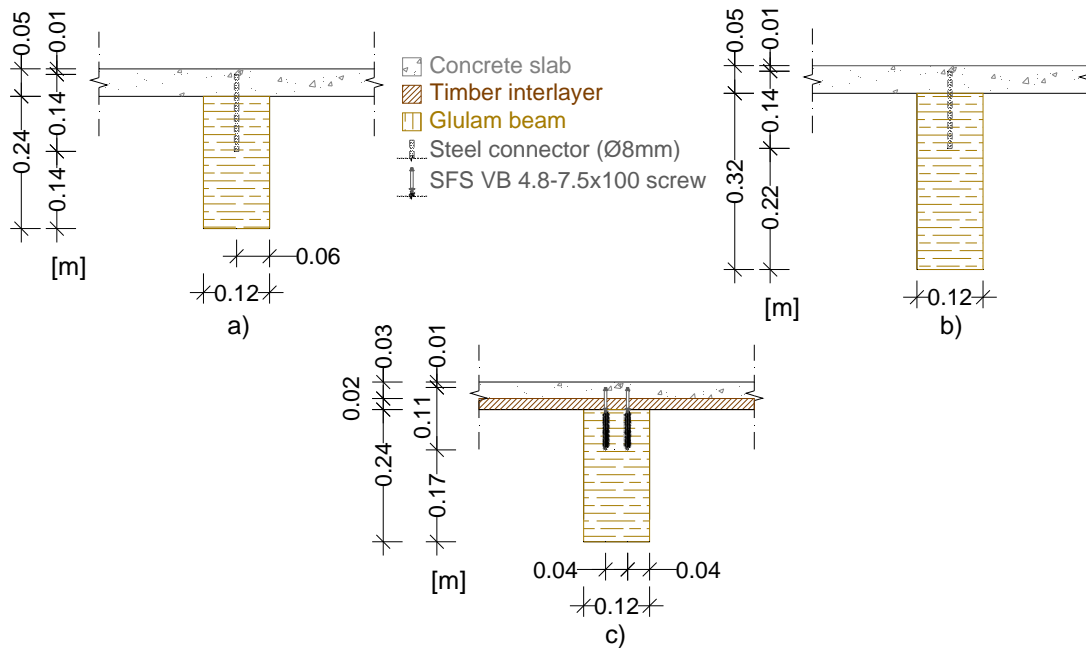


Fig. 4.12 – Cross section of a beam at specimens: a) S1 (CC' line); b) S5 (DD' line) and c) S3 (EE' line)

4.3 Test setup

The floor specimens were subjected to a sole concentrated point load at mid- and quarter-span, one at a time. Thereafter, they were subjected to a concentrated line load acting along each beam longitudinal axis, one at a time. The test setup is summarized in Fig. 4.13.

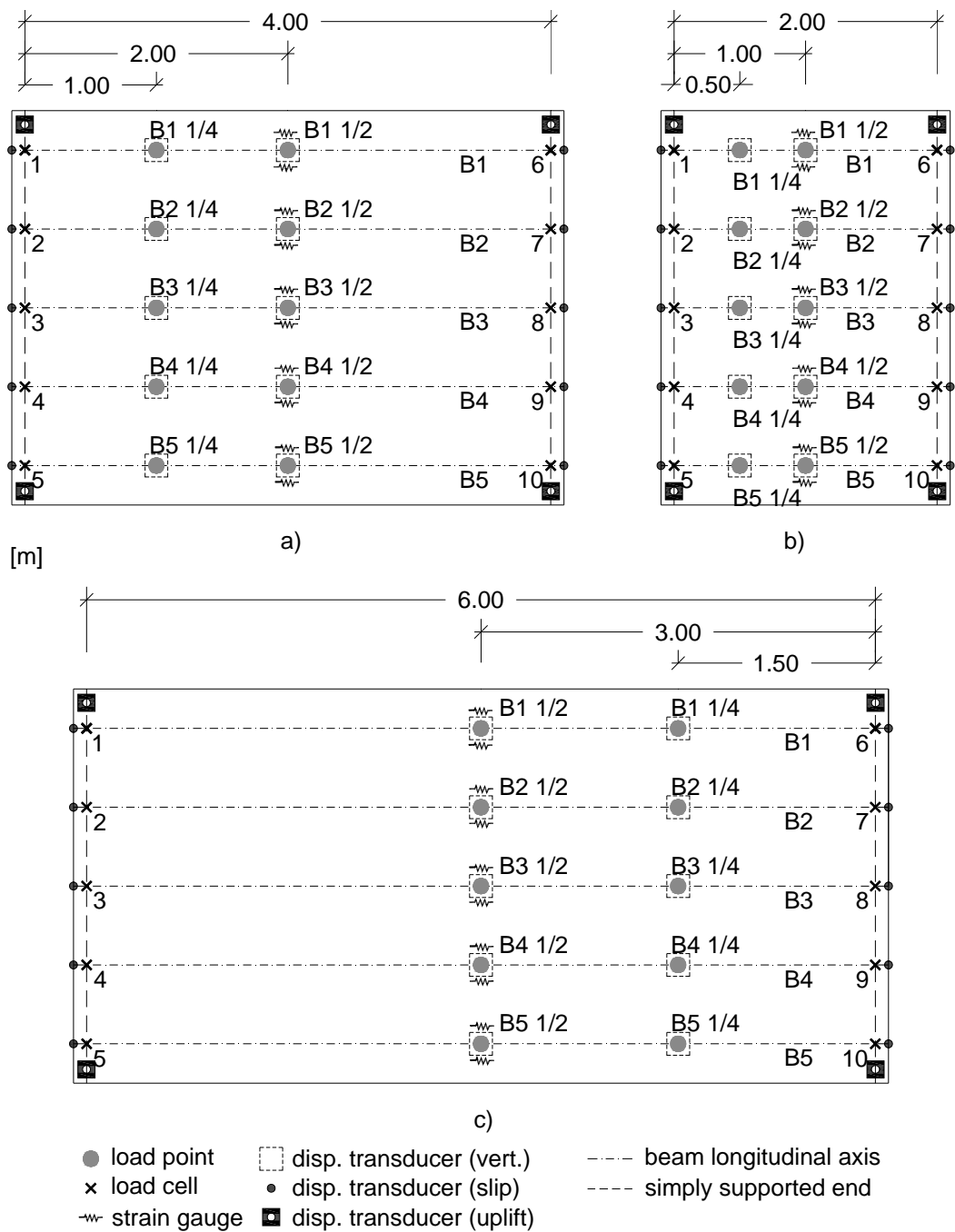


Fig. 4.13 – Test setup scheme, plan view: a) S1; b) S4 and c) S5

The loading procedure was repeated ten times per specimen to perform all the point load locations, and five times to perform the different line load positions (which coincide with the beams' longitudinal axis), Fig. 4.13.

The values for the loads were numerically predicted following the same procedure presented in 3.5.1 *Experimental results*. As stated in 3.2 *Preliminary experimental tests*, the values of load to apply in each test were intended to be near the service loads. Since several tests were intended to be performed in the same specimen, the load level to which it should be subjected was set in order to avoid the risk of inducing some kind of damage or permanent deformation. Thus, it was assumed that the point loads would be around 40 % of the predicted ultimate load in the case of the concentrated point loads. For the line load cases, as a preventive measure, the level of applied load was set near 20 % of the predicted ultimate load. This last level was adjusted and established based on the vertical displacements associated the loaded beam, for the first tested specimen. Therefore, the value defined correspond to approximately the same displacement verified for the loaded beam when loaded with 40 % of the ultimate point load.

The load was applied to the specimens through a 100 kN hydraulic jack. All the specimens were marked at the points where the concentrated point loads were to be applied. For the point load cases, Fig. 4.14 and Fig. 4.15, a steel plate with a square base of 0.05 x 0.05 m was placed between the jack and the slab surface. The steel plate section was selected according to the EC1 size recommendations for point loads. Also, a load cell was placed between the jack head and the steel plate.



Fig. 4.14 – Test setup: ½ point load (S5-L=6.00m)

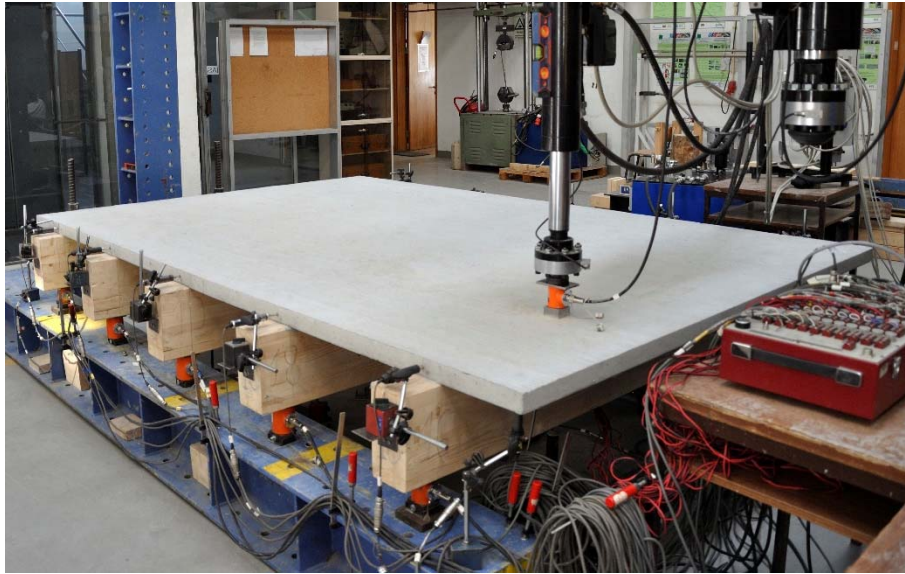


Fig. 4.15 – Test setup: $\frac{1}{4}$ point load (S4-L=2.00m)

For the linear loads, instead of the steel plate, a set of two C-section (UPN) steel beams was placed between the jack and the slab surface. In all the specimens, except for S4, two UPN 300 steel beams 4.30 m long were used. In the case of S4 a set of two UPN 200 steel beams 2.00 m long was used.

The specimens were tested in the same order as they were presented, with the first being S1 and the last S5. In all the specimens, the first loading to apply was the point load, at quarter- or mid-span. Only after, the line load was applied. The order in which the beams were tested was determined by practical matters, in order to minimize the use of resources and save time.

In the case where the line load was applied to the first specimen, S1, the load system did not performed as it was predicted. After subjecting the central beam to the “line” loading, it was found that between the concrete top surface and steel beams bottom surfaces the contact was not perfect, with some zones with no contact at all. In fact, although the slab surface had been leveled when the concrete was poured it is hard to obtain a completely horizontal surface. This implied that there was no guarantee that the applied load was uniformly distributed or symmetrical. Even so, two more beams were tested with the same system. Since an even contact was not achieved, a different load system was used: a 4-point load was considered to simulate the line load, despite some limitations. Given the materials and the equipment available in the laboratory, a system composed by several tubular and C-section steel profiles was used to apply the load in four points, Fig. 4.16. All S1 beams were tested with this system. As Fig. 4.16 shows, it is far from perfectly represent a 4.00 m line load, as intended. However, this system allowed to apply a symmetrical loading.



Fig. 4.16 – Test setup: four-point load at S1-BSp

As the second system did not overcome completely the problem, a different approach was adopted for the remaining line loading tests. Using the same beam system and prior to placing them over the slab, a layer of sand with about 20 mm thick and the width of the timber beam was put over the concrete top surface, Fig. 4.17. When compared with the first attempts this regularization layer allowed that the load transfer to the specimen was closer to the intended, uniformly distributed along the beam span.



Fig. 4.17 – Test setup: line load regularization layer detail (S5-L=6.00m)

As referred before, the line load whose effects were intended to be studied in this investigation represents the existence of a wall aligned with the beam longitudinal axis. For that it was assumed that the load applied had to have the same length as the beam span, Fig. 4.18 and Fig. 4.19. For specimen S5, with a 6.00 m span, this was not possible to achieve,

since the longer steel beams, of the laboratory were those 4.30 m long. These beams were the longest ones, with adequate characteristics to apply the intended load. Therefore, for specimen S5 the line load applied was 4.30 m long, Fig. 4.20.

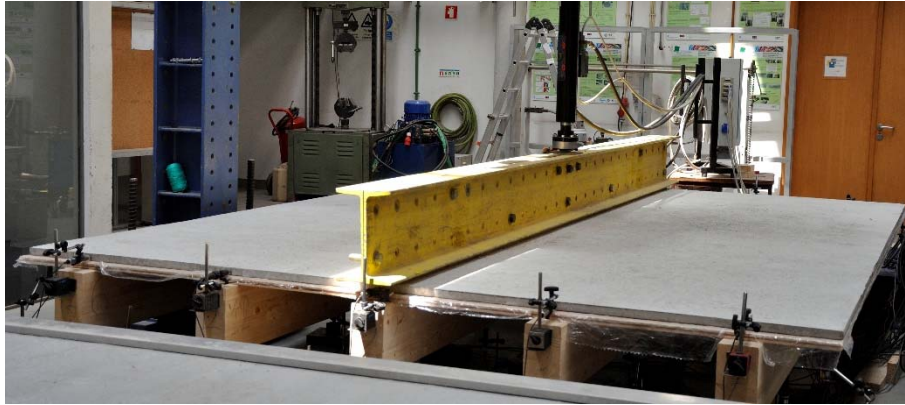


Fig. 4.18 – Test setup: line load at a 4.00 m span specimen (S3-hc=0.03m)



Fig. 4.19 – Test setup: line load at the 2.00 m span specimen (S4-L=2.00m)



Fig. 4.20 – Test setup: line load at the 6.00 m span specimen (S5-L=6.00m)

The mechanical performance of each floor specimen was recorded using displacement transducers, strain gauges and load cells. The displacement transducers were used to measure the slip between the concrete slab and each end of the timber beams, the vertical displacement at every beam mid- and quarter-span and also the uplift at the concrete layer corners. In each of the tested specimens, ten displacement transducers were placed at the ends of each timber beam, with the aid of steel plates screwed to each beam top. Their rod was horizontally aligned with the beams longitudinal axis and their tip placed near the timber-concrete interface (on a regular surface), Fig. 4.21 a). For the vertical displacements, ten displacement transducers were placed vertically under the points corresponding to the mid- and quarter-span of each beam. Following the same procedure as presented in Section 3.2, and assuming the existence of symmetry, five were placed below the mid-span and five other below the quarter-span. They were placed with the aid of heavy steel plates to where the magnetic bases were connected, Fig. 4.21 b). The uplift was recorded by four displacement transducers, one at each corner. They were placed at the point 0.05 m away from each side of the concrete top layer, Fig. 4.22. In all the cases, the transducers' rods were aligned with the required points using a level.

In this experimental program, the measurement of strains at the mid-span section of the timber beams was also considered. A pair of strain gauges were glued at every beam mid-span cross section, amounting ten strain gauges per specimen. The strain gauges used had the same resistance, $120 \pm 0.3 \Omega$, but for different specimens, they had different lengths according to the availability at the time of instrumentation. For S1 to S3 60 mm length strain gauges were used

(PL-60-11 model from TML), as for the remaining they had 90 mm (PL-90-11 model from TML). The strain gauges were placed only at the bottom surface, at 0.04 m of the beams vertical faces, Fig. 4.23. The beams instrumentation was performed when the specimens where assembled, guaranteeing a better access to the sections and an adequate adhesive drying. Besides the strain recording, these gauges collected extra data to characterize the beam mechanical behavior. Fig. 4.24 shows an overall bottom view of the test setup.

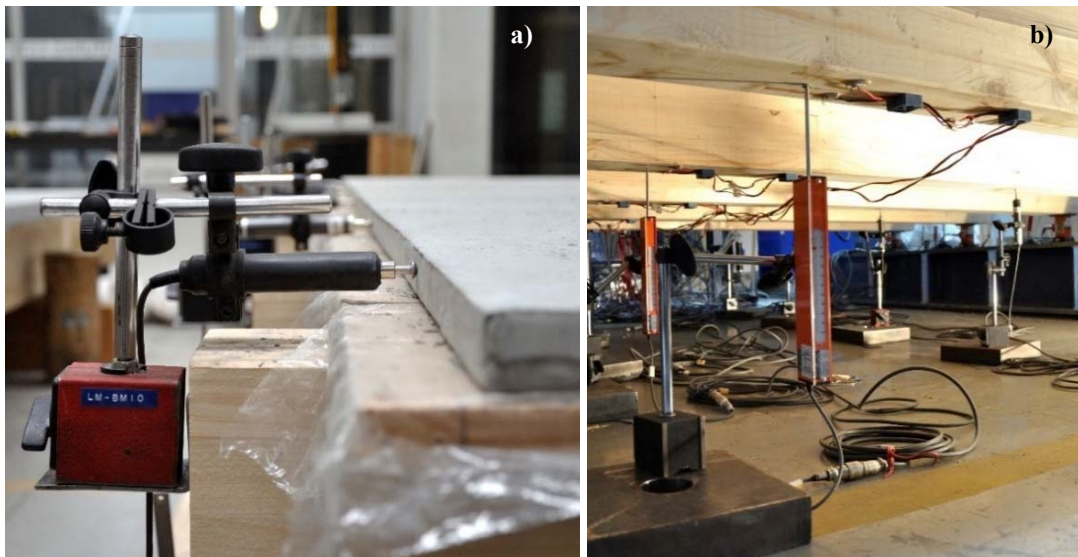


Fig. 4.21 – Displacement transducers: a) timber-concrete slip; and b) vertical displacement

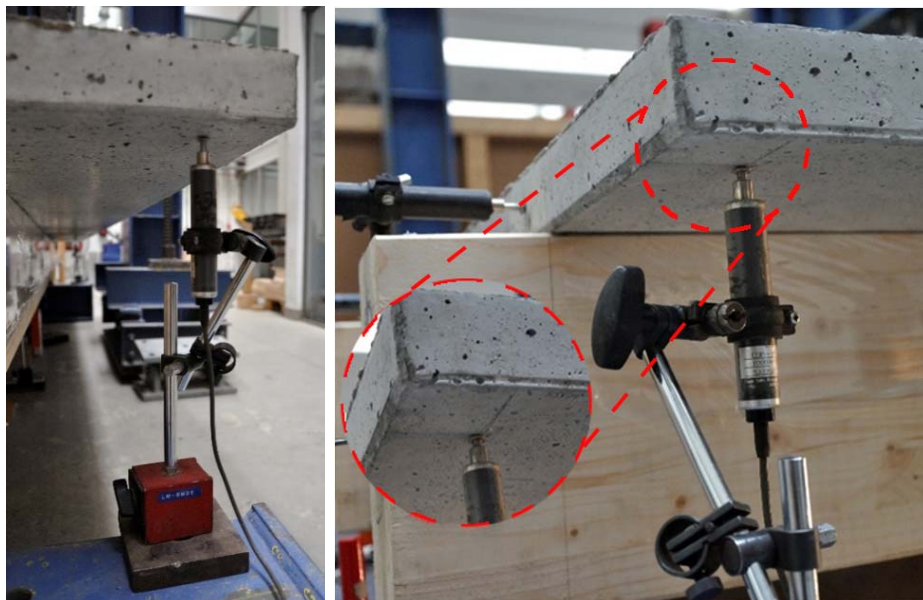


Fig. 4.22 – Uplift displacement transducers: positioning detail

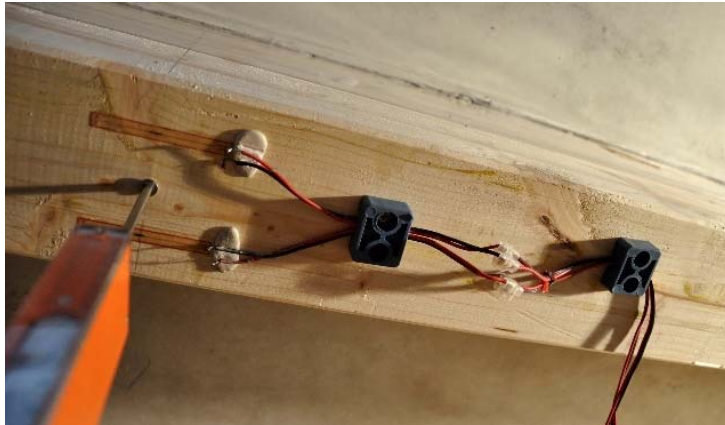


Fig. 4.23 – Strain gauges setup detail

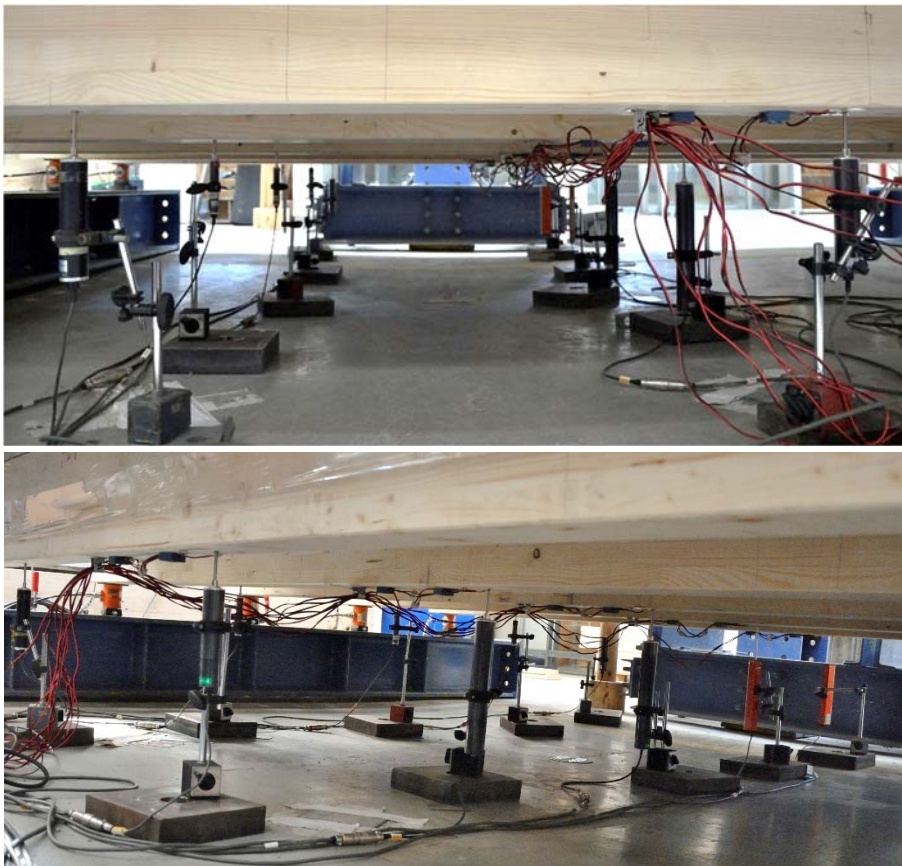


Fig. 4.24 – Test setup detail: bottom view

As previously, the load cells were used to record the load supported by each beam. Therefore, following the same assumptions as before, they were placed under each floor beam with the aid of steel plates, placed between the cell and the timber beam. Damage of load

concentration was carefully avoided, and leveling devices were used to ensure the required beam span (4.00 m for S1 to S3, 2.00 m for S4 and 6.00 m for S5), Fig. 4.25. All the measuring devices were connected to a data acquisition unit and recorded, Fig. 4.26.



Fig. 4.25 – Test setup detail: load cells



Fig. 4.26 – Acquisition unit

Ten point loading tests were performed in specimen S1: five with the load located, at every mid-span of the beam immediately below (Fig. 4.13 – points B1 1/2 to B5 1/2, using the same nomenclature as for the preliminary tests, *i.e.*, B3 1/2 means: beam 3 loaded at mid-span), and five others at quarter-span of the beam immediately below (Fig. 4.13 – points B1 1/4 to B5 1/4 where, *e.g.*, B4 1/4 means: beam 4 loaded at quarter-span). This experimental program was followed by five line loading tests. For the specific case of this specimen three of the beams were loaded with linear load and then all of them were loaded with a 4-point load (associated from now on with the designation *4P*, in tables and graphs).

Thereafter, the specimen was tested until failure by applying a point load at the mid-span of the central beam. At this time, the specimen was no longer recorded for slip, displacements or support reactions, but only to strains at the bottom mid-span section of the timber beams and applied load. In the cases where there was a local collapse other beams were also tested until failure. The same experimental program was adopted for the remaining specimens.

Once again, following the same procedure as presented for the preliminary experimental tests, the ultimate load level expected for each load position was estimated through an FE analysis. By using the Frame+Shell Model the several specimens were modeled and an iterative procedure of load application *vs.* stress analysis was performed until the ultimate load levels. As the material properties were not completely known when modeling was carried out, some of them were assumed. This was the case of the concrete properties for which the ones listed in the standard (EN1992 2004) were used to characterize the regular concrete (considered C25/30). For the case of the LWAC, the properties used in the modeling were those obtained for a concrete already studied in a previous investigation (Martins *et al.* 2015), and whose properties were the ones intended for the specimen S2. Regarding the connection properties, the values presented in Table 4.6 were used assuming a linear elastic behavior for the connector elements. These values were obtained in previous investigations using the same connection system and similar connected materials (Dias 2005, Dias and Martins 2012, Linden 1999).

Table 4.6 – Connection properties

Specimen	K
	[kN/m]
S1, S4 and S5	6469
S2	7350
S3	12900

This procedure led to the definition of a test protocol for any position of the load. The load values that were actually applied to the slab are listed in Table 4.7. Although not all were point loads, the values presented for the applied loads correspond to the resulting load and also the value applied by the hydraulic jack. For the first specimen the two sets of loads associated with the different systems used to apply the line load are presented.

Table 4.7 – Loads applied during the experimental tests for the several load cases

Floor specimen	Load case	Applied Load	Applied Ultimate ^a	Floor specimen	Load case	Applied Load	Applied Ultimate ^a
		[kN]	[%]			[kN]	[%]
S1	B1 ½	20.3	40	S4	B1 ½	28.4	40
	B2 ½	25.5	40		B2 ½	34.4	40
	B3 ½	29.5	40		B3 ½	37.8	40
	B4 ½	25.4	40		B4 ½	35.5	40
	B5 ½	19.8	40		B5 ½	27.7	40
	B1 ¼	21.9	40		B1 ¼	33.1	40
	B2 ¼	27.8	40		B2 ¼	38.8	40
	B3 ¼	31.4	40		B3 ¼	40.8	39
	B4 ¼	28.1	40		B4 ¼	39.3	39
	B5 ¼	21.4	40		B5 ¼	31.9	39
	B1 4P	25.7	20		B1lin	31.5	20
	B2 4P	37.5	20		B2lin	43.4	20
	B3lin/4P	48.5/48.8	20		B3lin	49.5	20
	B4lin/4P	37.9/38.1	20		B4lin	45.5	20
B5lin/4P	25.3/25.3	20	B5lin	30.8	20		
S2	B1 ½	22.8	40	S5	B1 ½	21.5	37
	B2 ½	30.4	40		B2 ½	34.2	39
	B3 ½	32.4	40		B3 ½	32.8	39
	B4 ½	30.9	40		B4 ½	33.3	39
	B5 ½	22.8	40		B5 ½	23.6	41
	B1 ¼	25.0	40		B1 ¼	24.6	39
	B2 ¼	34.1	40		B2 ¼	37.7	39
	B3 ¼	36.0	40		B3 ¼	35.5	39
	B4 ¼	34.5	40		B4 ¼	37.2	39
	B5 ¼	25.0	40		B5 ¼	25.2	40
	B1lin	28.4	20		B1lin	21.7	20
	B2lin	44.5	20		B2lin	39.8	20
	B3lin	51.2	20		B3lin	38.9	20
	B4lin	45.2	20		B4lin	38.9	20
B5lin	28.6	20	B5lin	21.6	20		
S3	B1 ½	14.1	40				
	B2 ½	20.0	40				
	B3 ½	18.2	40				
	B4 ½	19.8	40				
	B5 ½	14.0	40				
	B1 ¼	16.1	40				
	B2 ¼	21.0	40				
B3 ¼	19.6	40					

Table 4.7 – Load cases and applied loads during the experimental test (cont.)

Floor specimen	Load case	Applied Load	Applied Ultimate ^a	Floor specimen	Load case	Applied Load	Applied Ultimate ^a
		[kN]	[%]			[kN]	[%]
S3	B4 ¼	21.0	40				
	B5 ¼	16.0	40				
	B1lin	16.5	20				
	B2lin	29.7	20				
	B3lin	25.5	20				
	B4lin	28.8	20				
	B5lin	16.4	20				

^a - Estimated based on the numerical modeling

½ - mid-span; ¼ - quarter-span; lin - line load; 4P - 4-point load

Analyzing Table 4.7, it is possible to find similar load values for S1, S2 and S5 for the various load cases. The values for specimen S3 are slightly lower than average, while for S4 they appear to be greater. In fact, for similar material properties and geometry, as found in specimens S1 and S4, the shorter the span, the stiffer the floor and consequently the greater the associated ultimate load. Similarly, it would be expected that a longer span in specimens with similar material properties and geometrical characteristics, the opposite would occur. However, when comparing the ultimate loads levels found for S1 and S5, they seem to be quite similar. In fact, in spite of the span of S5 is 3/2 the span of S1, their beams' sections are higher, justifying the similarity of ultimate loads for both specimens. In the case of specimen S3, the thinner concrete slab affects the structure stiffness, making it smaller and affecting the ultimate load levels in the same direction.

4.4 Experimental results

This section presents the results obtained from the experimental tests in terms of:

- support reactions;
- vertical displacements at mid- and quarter-span;
- slip displacements between timber beams and concrete slab;
- uplift at the concrete slab corners; and
- strains at the bottom mid-span cross section of the timber beams.

The following sections report a summary of the results found for the several quantities during the experimental tests. Despite a comprehensive list of results to be presented in *APPENDIX B, B.2 - Results from the experimental analysis*, a condensed exposition of the results from all the experimental tests are presented here.

Aiming at simplifying the results understanding, the equipment designation was used in the results exposition. Fig. 4.27 summarizes this information.

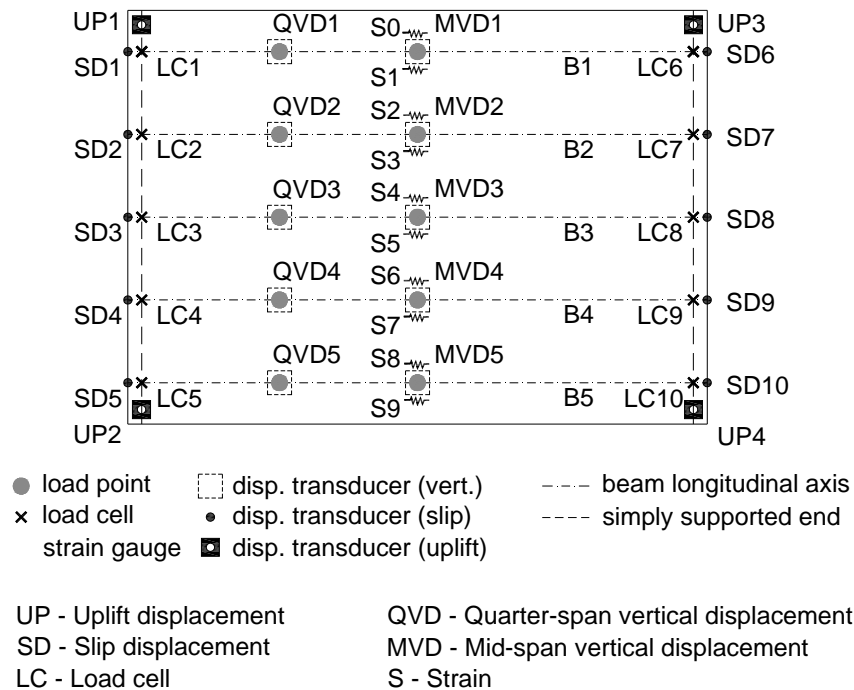


Fig. 4.27 – Test setup: equipment designation

Despite it may sound a little awkward, in the following sections, the word “distribution” will be used aiming at designating a pattern associated with the various quantities and the manner in which they vary across the floor slabs. In the same context, the term “spreading” was used to define the difference between the sum of all the distribution percentages for a load case in a specific beam (100 %) and the distribution percentage associated with the loaded beam. When concerning the load distribution, the associated spreading would represent the percentage of load that would not be supported by the loaded beam, and consequently would have to be spread for the remaining ones.

4.4.1 Vertical displacements

A complete set of results obtained from the several load tests performed in the five floor specimens can be found in *B.2.1 – Vertical displacements (APPENDIX B)*. The graphs of this section were chosen to highlight a common behavior or a specific characteristic that would deserve to be analyzed and discussed.

Analyzing the results obtained for the vertical displacements at mid- and quarter-span for the several load cases in each floor specimen tested, the following conclusions could be drawn. For specimen S1, comparing the responses for the three loading cases, assuming that *lin* and *4P* intend to simulate both a linear load case, Fig. B.1 to Fig. B.5, the last stands-out by presenting the greatest magnitudes (ex.: Fig. 4.28 for B4-GL1). This is followed by the mid-span point load response, while the one corresponding to the line load case tends to present the lowest magnitudes. On the other hand, displacements at mid-span showed to be higher than those obtained at quarter-span (ex.: Fig. 4.29 for B1 ½). Exception is observed for the load applied at quarter-span. In this case, both displacements, at mid- and quarter-span, have similar values but there is a trend for the second to be greater, specifically when the loaded beam is concerned (ex.: Fig. 4.30 for B2-GL9).

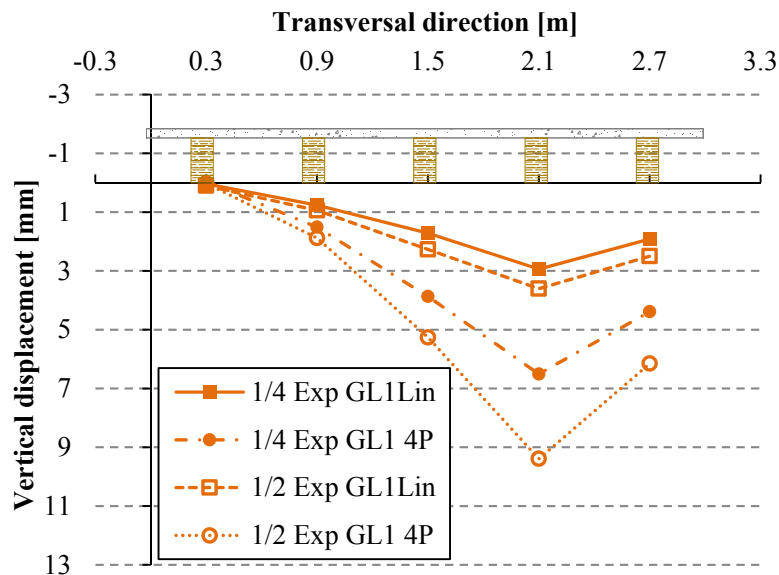


Fig. 4.28 – S1-BSp: vertical displacement at ½ L and ¼ L when loaded at B4lin and B4 4P

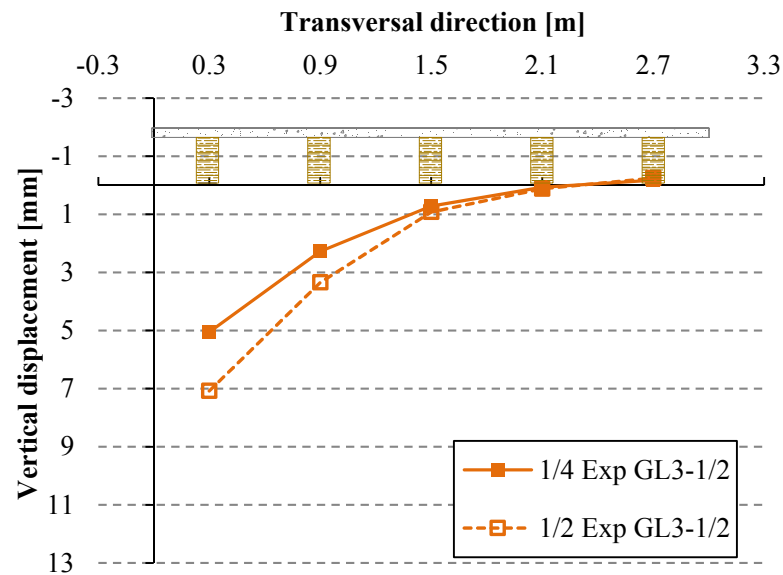


Fig. 4.29 – S1-BSp: vertical displacement at $\frac{1}{2} L$ and $\frac{1}{4} L$ when loaded at B1 $\frac{1}{2}$

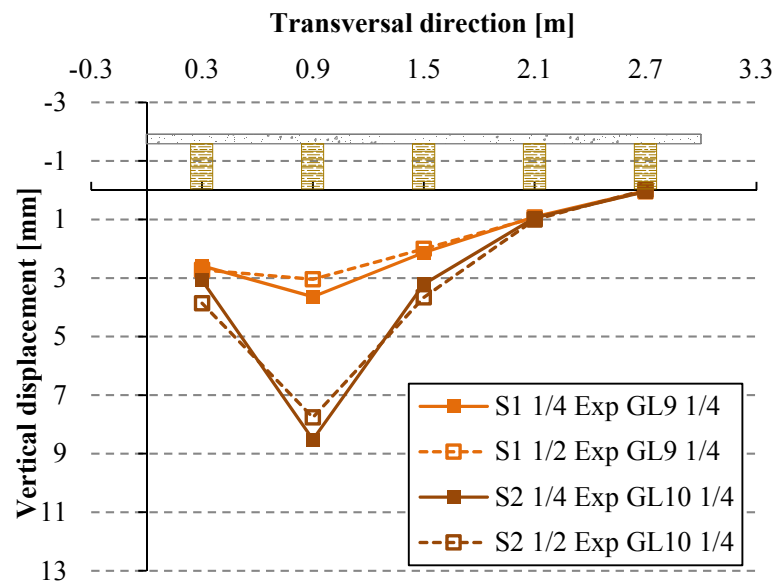


Fig. 4.30 – Vertical displacement at $\frac{1}{2} L$ and $\frac{1}{4} L$ when loaded at B2 $\frac{1}{4}$: S1-BSp and S2-LWAC

The percentage of distribution of vertical displacements was computed for the several load cases at mid- and quarter-span, Table B.7. These percentages were obtained by comparing the displacement in question with the sum of displacements for the same load case at the same location in all the beams.

Thus, concerning the loaded beam, similar displacement pattern was found for the three loading cases. The maximum absolute differences between the percentages associated with the central beam were about 8 % when considering the point load at quarter-span and the linear load. For the 4P load the maximum difference (about 10 %) was found when the central beam was loaded, between this load case and that of the point load at quarter-span. In general, for the several load cases, a significant spreading of displacements between the five beams was found, varying between 30 % ($\frac{1}{4}$ B1 4P) and 66 % ($\frac{1}{2}$ B4 $\frac{1}{4}$). The designation used together with the percentages, e.g. “ $\frac{1}{4}$ B1 4P”, intends to identify the measuring location, the beam number and the load case for which the vertical displacement is being considered. Therefore, “ $\frac{1}{4}$ B1 4P” means: vertical displacement measured at quarter-span when the 4P load is applied at B1. In turn, “ $\frac{1}{2}$ B4 $\frac{1}{4}$ ” means: vertical displacement measured at mid-span when the point load is applied at quarter-span of B4.

As Fig. B.3 to Fig. B.5 show, the displacements obtained for the 4P load case are much larger than those obtained with the linear loading. The system used to apply the four point load was not long enough to simulate a 4.00 m long line load, concentrating its influence in the central portion of the beam. The same load distributed in a smaller length results in great displacements in its vicinity.

As for specimen S2, the response found for the point load at mid-span of each beam appeared to be the one with greater magnitude, with the one found for the line load case with the minor magnitude. In terms of individual response of the loaded beam, the mid-span displacement appear to be greater than the one measured at quarter-span for all the responses of the three loading cases. This happens even when the load is applied at quarter-span, with the displacement at mid-span showing a greater magnitude in almost all the beams. The exception is observed for the loaded beam (ex.: Fig. 4.30 for B2-GL10) with the displacement at quarter-span overtaking the value of displacement found for the same beam at the mid-span. Regarding the percentage distributions, when the loaded beam is considered, similar values were found for the three loading cases. The maximum absolute differences are similar to those found for the previous specimen, about 9 %. In spite of existing a clear spreading of displacements between the beams, it was found to be lower than the one found for specimen S1. In this case it varies between 25 % ($\frac{1}{2}$ B5 $\frac{1}{2}$) and 56 % ($\frac{1}{2}$ B2lin). With a difference between 5 % and 10 % relatively to S1.

Specimen S3 showed a trend identical to that found for S2, except for the magnitude of the response. In this case the displacements tend to be lower. The maximum absolute differences are about 9 % and the spreading of displacements between the beams varies between 21 % ($\frac{1}{4}$ B1 $\frac{1}{4}$) and 61 % ($\frac{1}{2}$ B3lin). In this case, relatively to S1 which showed a wider spreading, the difference is about 9 % in the inferior limit and 5 % in the superior one.

For specimen S4 a behavior similar to those of specimens S2 and S3 was found: the response for the point load at mid-span was the one with greater magnitude and response for the line load case the one with a lower magnitude; the mid-span displacement for the several load cases and load locations tend to be higher than the displacement at quarter-span, except for the quarter-span load. In this case, displacements at quarter-span were greater than those measured at mid-span, not only for the loaded beam, Fig. 4.31. In a general manner, as expected, the magnitude of the measured displacements is lower than the remaining, consequence of the stiffness characteristics of the floor specimen, Fig. 4.32. In percentage terms, the distributions of displacements when the loaded beam is considered, presented the same trend as the previous specimens. However for S4 the maximum absolute differences found between the percentages associated with the same beam for the three loading cases were greater than those of the previous specimens, about 14 %. This difference is associated with a trend to the uplifting of the extremity beams when the central beam was loaded, Fig. 4.33. This specimen also showed the minor displacement spreading between the beams, varying between 20 % ($\frac{1}{4}$ B5lin) and 46 % ($\frac{1}{4}$ B3lin). Comparatively to the specimen S1, the difference is about 10 % in the inferior limit and 20 % in the superior one.

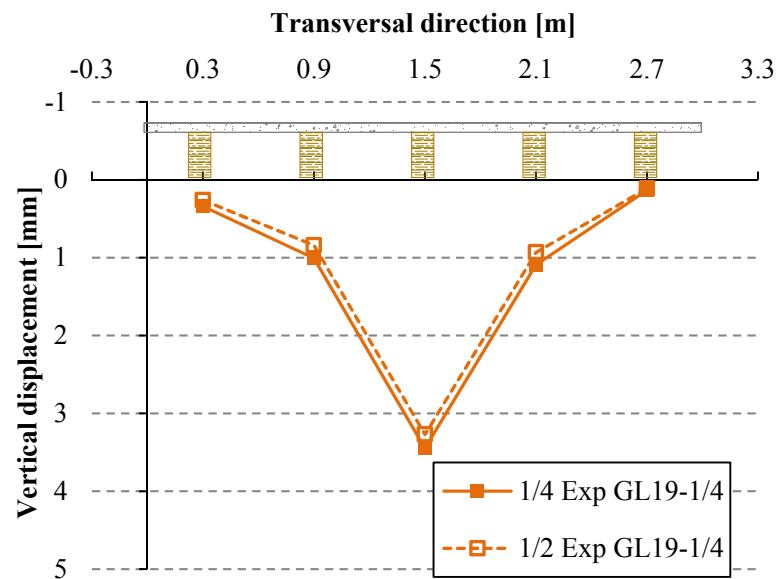


Fig. 4.31 – S4-L=2.00m: vertical displacement at $\frac{1}{2}$ L and $\frac{1}{4}$ L when loaded at B3 $\frac{1}{4}$

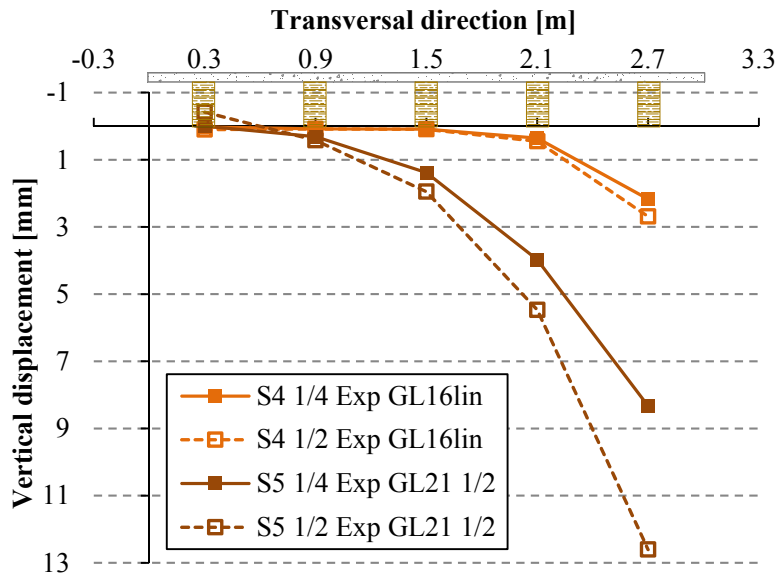


Fig. 4.32 – Vertical displacement at $\frac{1}{2} L$ and $\frac{1}{4} L$ when loaded at B5: S4-L=2.00m (B5lin) and S5-L=6.00m (B5 $\frac{1}{2}$)

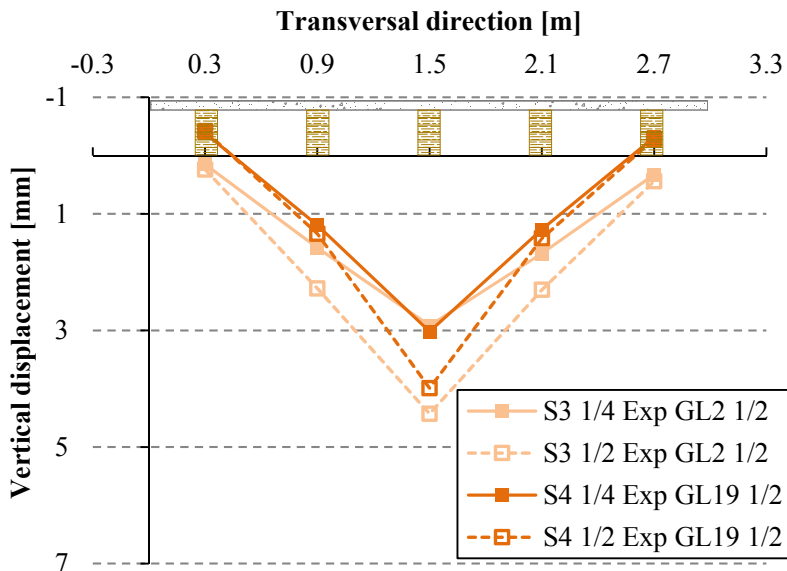


Fig. 4.33 – Vertical displacement at $\frac{1}{2} L$ and $\frac{1}{4} L$ when loaded at B3 $\frac{1}{2}$: S3-hc=0.03m and S4-L=2.00m

As expected, specimen S5 showed the greatest displacement magnitude, Fig. 4.32. As the previous, the mid-span load case led to the greatest displacements, as the line load case led to the lowest displacements. In terms of deformation, considering the responses of all the specimens and load cases, S5 showed a similar trend as the remaining, except for S4. The

displacements measured at mid-span tend to be higher than those measured at quarter-span. However, when the load is applied to quarter-span, displacements at mid- and quarter-span are very similar (with their graphical curves crossing each other) and the displacement at this location in the loaded beam showed to be greater than the measured at mid-span. As for the spreading of displacements between the beams, S5 appeared to have a more effective behavior with percentages of 36 % ($\frac{1}{4} B5 \frac{1}{4}$) and 68 % ($\frac{1}{2} B3 \frac{1}{4}$). Although very close, these values exceed the ones found for specimen S1.

A different perspective of the vertical displacement distribution is achieved when considering the highest displacement recorded for a specific beam, among all the load cases. Thus, by comparing the displacement of a beam, at mid- or quarter-span, with the highest magnitude found for that same beam it was possible to find the load case and location to which it happened and to relate its magnitude with those found for the remaining loading cases. These results were gathered for each specimen in Fig. B.26 to Fig. B.31. Fig. 4.34 and Fig. 4.35 summarize those percentages for the percentages associated with the loaded beams. Except for S1, for which the higher vertical displacements were recorded for the 4P load case, for the remaining specimens they were recorded for the point load at mid-span. As presented, the 4P load case was an alternative solution to the line load case, but it did not lead to the same structural behavior. Therefore, if 4P load would not be taken into account, the point load at mid-span would be the load case leading to the highest vertical displacement. This way this specimen has a behavior like the remaining ones, all following therefore a common pattern, Fig. 4.34.

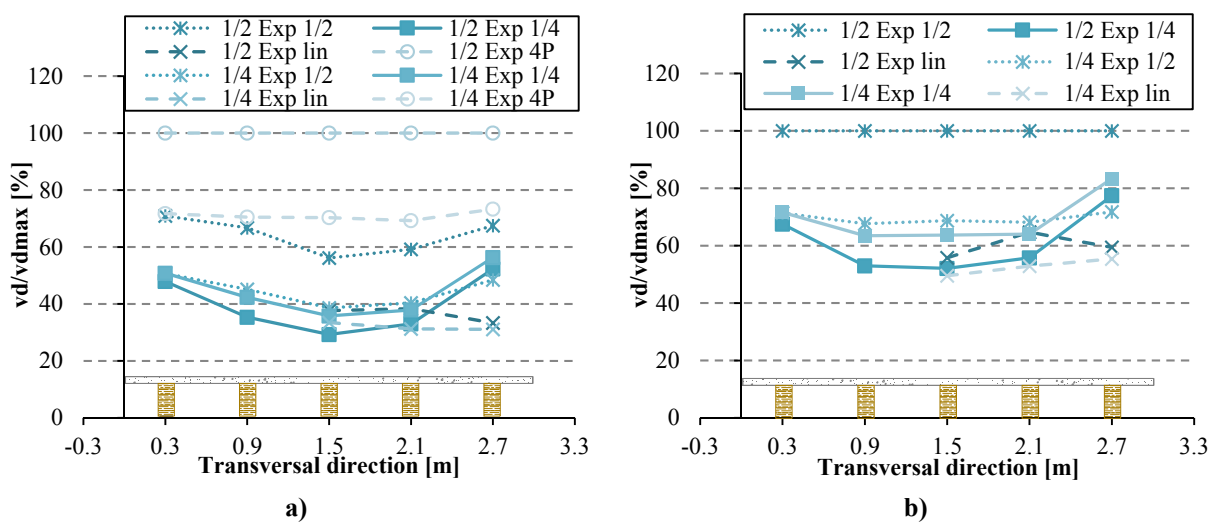


Fig. 4.34 – Vertical displacement vs. highest displacement for the loaded beam in S1-BSp: a) all load cases; b) disregarding 4P load case

4. EXPERIMENTAL ANALYSIS

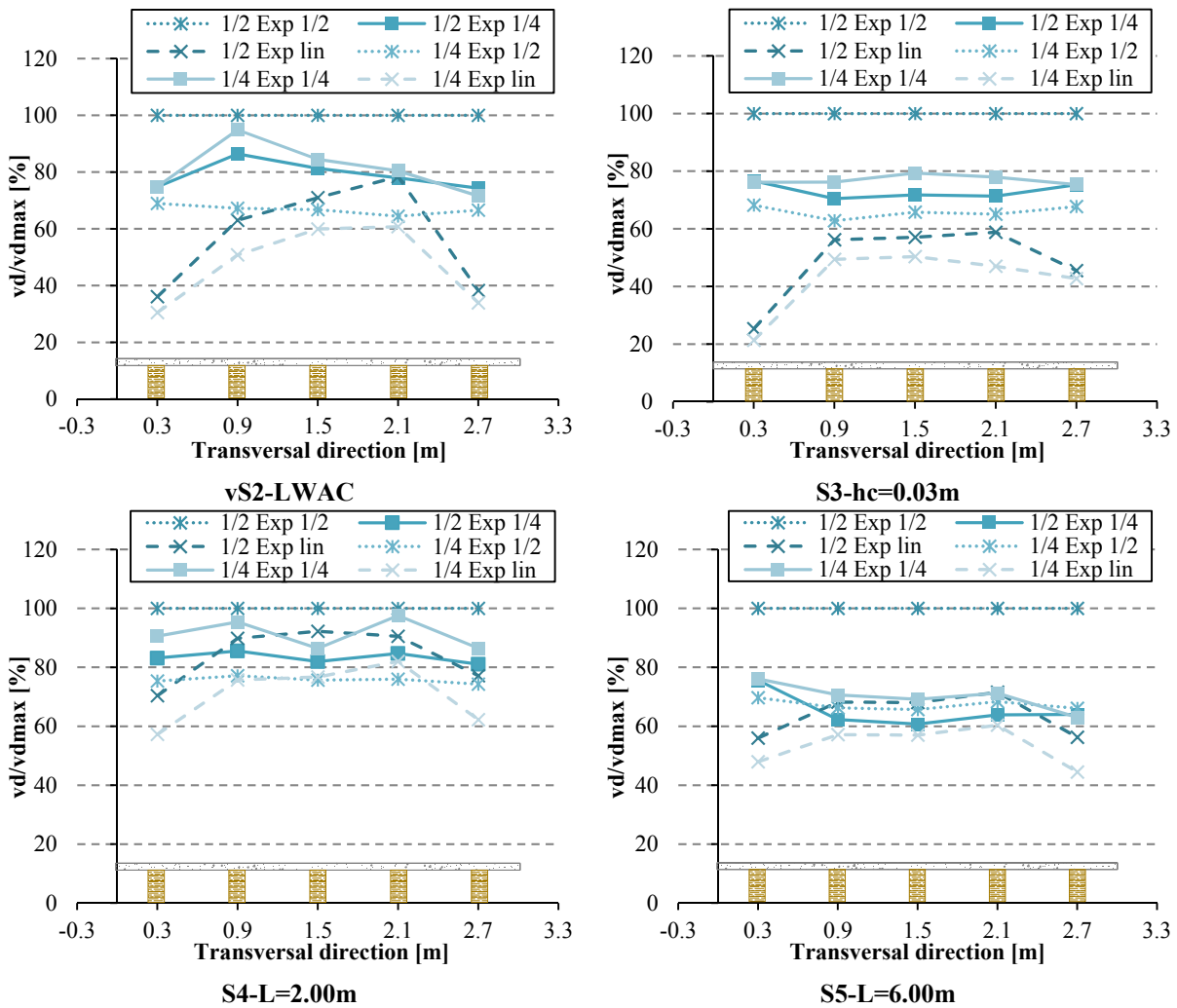


Fig. 4.35 – Vertical displacement vs. highest displacement for the loaded beam in S2 to S5

By analyzing these distributions for the five specimens, considering the loaded beam and disregarding the 4P load case, the following conclusions can be drawn. In general, vertical displacements associated with the line load case presented the lowest percentages, about 58 % of the maximum recorded displacement (min: 21 % (S3), max: 92 % (S4)). On the other hand, displacements associated with loading at quarter-span tend to appear just below the highest displacements (100 %) with an average value of 75 %, (min: 52 % (S1), max: 98 % (S4)). Displacements associated with the loading at mid-span measured at quarter-span range between 63 % and 77 % of those measured right below the load.

For S4, the percentages found were all very similar and high, with the displacements varying between 57 % and 98 % of the maximum that was recorded. A similar behavior was found for S5, with a tendency to uniformity, but with slightly lower percentages, 44 % to

76 %. In both cases, this behavior means that vertical displacements were not too different from the maximum ones. In fact, for S4 the vertical displacements for the loaded beam (situation under consideration) tend to have close magnitudes, regardless of the load case. S2 and S3, in turn, showed the opposite behavior with a broader variation of percentages. With variations of 31 % - 95 % and 21 % - 79 %, respectively. For all the specimens the range boundaries were found for the same load case, with the minimum associated with the line load and the maximum with the loading at quarter-span.

Also the deflection of the beams was studied. In a more extensive way Fig. B.32 to Fig. B.53 show the results obtained for each specimens beam. Here, Fig. 4.36 to Fig. 4.41 summarize the main findings, allowing the comparison between specimens' behaviors.

The first figure give a general view of the specimens' tridimensional deflection when the central beam was loaded at mid-span. To achieve this figure the vertical displacements measured at mid- and quarter-span were used, assuming that the displacements at three quarters-span were symmetric of those found at quarter-span. Equivalent figures were created for the remaining load cases acting over the same beam, Fig B.37 to Fig. B.46. For the loading at quarter-span, only the measured displacements, at mid- and quarter-span, were used to create the graphs (Fig. B.37 to Fig. B.41). These figures make it clear the different behaviors of the five specimens under each action. The trend to concentrate the vertical displacement below the point of application stands out for the mid-span loading. For the point load at quarter-span this is not that clear, due to the lack of displacements measured at three quarters-span. On the other hand, also the trend to distribute the displacement over the loaded beam when a line load was applied is highlighted in Fig. B.44.

Fig. 4.37 to Fig. 4.41, present the deflections along the longitudinal direction of a specific beam for the three loading cases. A presentation for all the specimens can be found in *APPENDIX B*, Fig. B.47 to Fig. B.51. Concerning the symmetrical load cases, and since symmetry was assumed from the beginning by measuring only half floor slab, the displacement at three quarters of span was considered to be equal to the one obtained for quarter-span. As for the load at quarter-span, displacements at three quarters of span of the loaded beam were computed based on the displacements at mid-span and on a constant obtained based on numerical predictions of these floors' behavior (23).

$$Vd_{3/4L} = c \cdot Vd_{1/2L} \quad (23)$$

with Vd_i the vertical displacement at point i and c the relation between the numerical vertical displacements at three quarters of span and at mid-span, $c = \frac{Vd_{n3/4L}}{Vd_{n1/2L}}$, where Vd_{ni} is the numerical vertical displacement at point i .

4. EXPERIMENTAL ANALYSIS

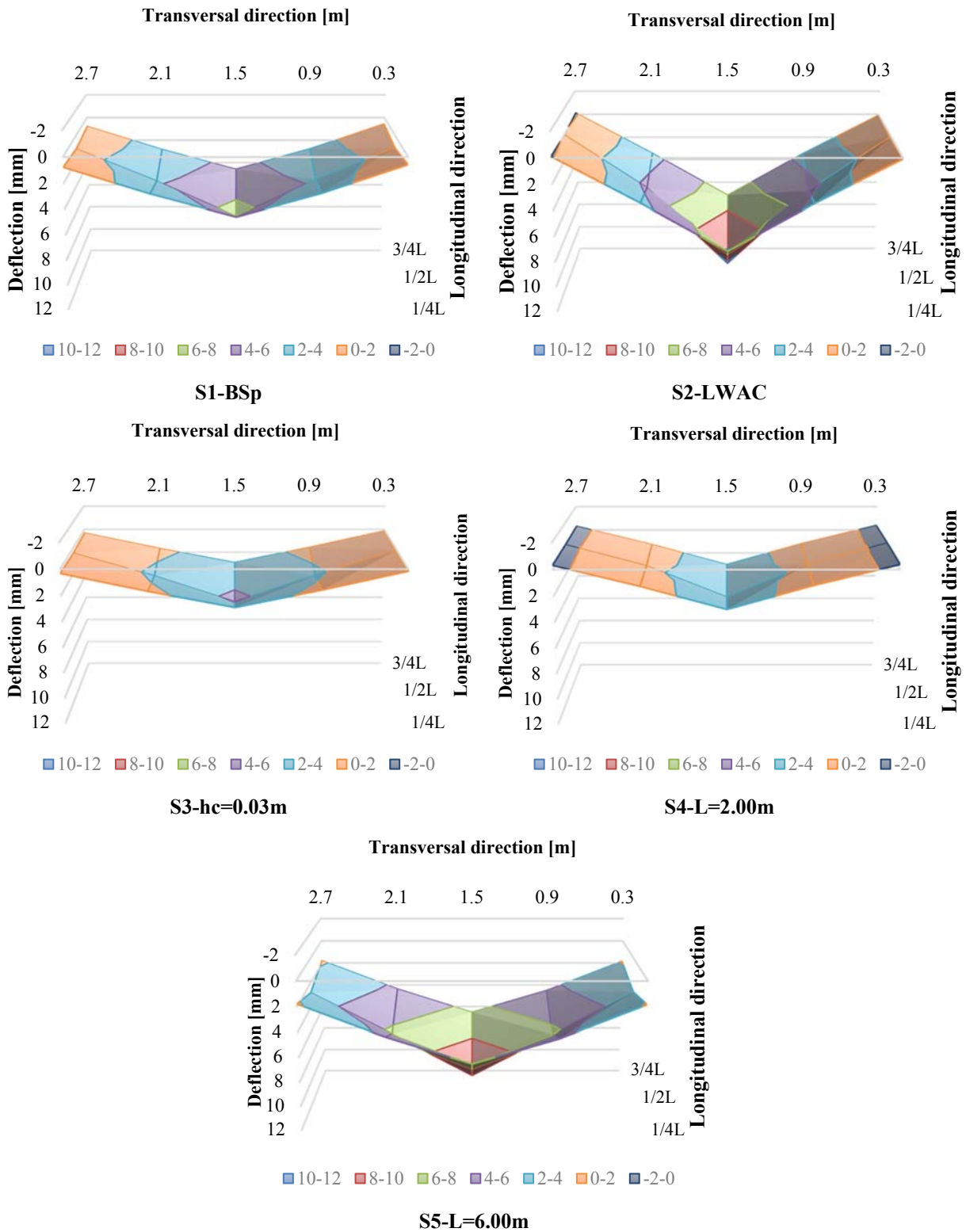


Fig. 4.36 – Slab deflections: B3 ½

In general, S2-LWAC shows to be the specimen that most deform, by opposition to S3-hc=0.03m. S5-L=6.00m seems to be the specimen with the great ability to mobilize the all slab under the concentrated action considered, followed closely by the *Base specimen*, S1. S4-L=2.00m, as found before, presents the opposite behavior.

Without focusing on displacements' magnitudes, widely explained, the shape of the deflection curves express the manner in which the beam “participate” in the load spreading. Thus, for S4, deflections tend to be almost coincident for the three load cases, presenting a flattened shape considerable more evident than for others specimens, Fig. 4.37. The concentrated load over the beams of this specimen tend to be slightly “felt” along their longitudinal axis. This behavior is in line with the already found for S4, showing a great stiffness and consequent low deformation capacity. By opposition, deflections associated with S5 tend to have a pronounced curvature, with the load spreading to the supports throughout the beam span, Fig. 4.38. In addition to the point immediately beneath the point load to be associated with the highest displacement magnitude (for that beam and load case), displacements in the adjacent measuring points showed to be relatively close to that one. For the line load case this is, in fact, a common characteristic for all the specimens, consequence of the symmetrical and uniform nature of this load case.

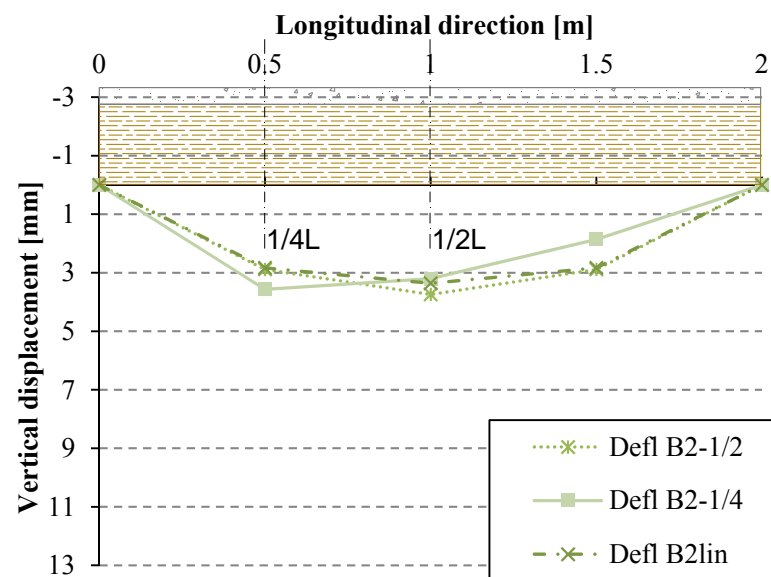


Fig. 4.37 – S4-L=2.00m B2 deflections

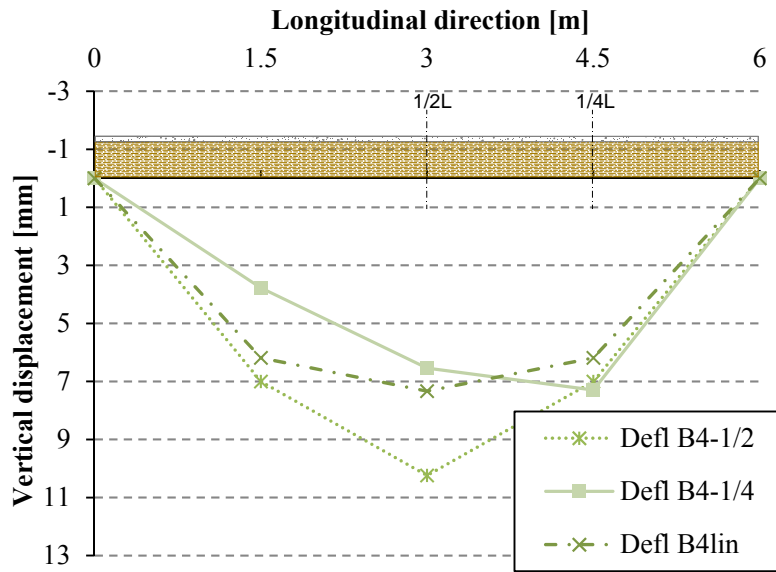


Fig. 4.38 – S5-L=6.00m B4 deflections

S2 deflection curves also showed a pronounced curvature, result of its more flexible nature. Nevertheless, for the line load case this is not a constant in the transversal direction. This means that when analyzing the behavior of the five beams, deflections associated with the line load case tend to be less pronounced for the exterior beams (*i.e.*, B1 and B5), Fig. 4.39.

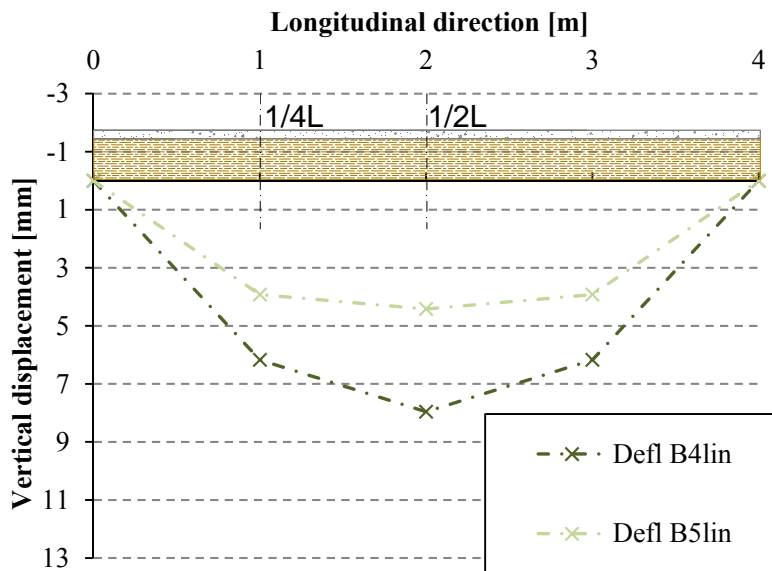


Fig. 4.39 – S2-LWAC B4 and B5 deflections

In turn, S3 tend to present an intermediate behavior, but somehow closer to that of S4. When compared to the remaining specimens, S3 presented a particular characteristic: deflections recorded at mid- and quarter-span for the line loading are very close, turning the associated curve flatter than those found for S4, Fig. 4.40. Concerning to S1, deflection curves associated with 4P load case divert from those found for the line load case, as already mentioned. This is clearer for the cases in which both loadings were applied, Fig. 4.41. Indeed, besides the greater magnitude, the shape of the deflection curves associated with 4P loading tends to be similar to that found for mid-span point loading.

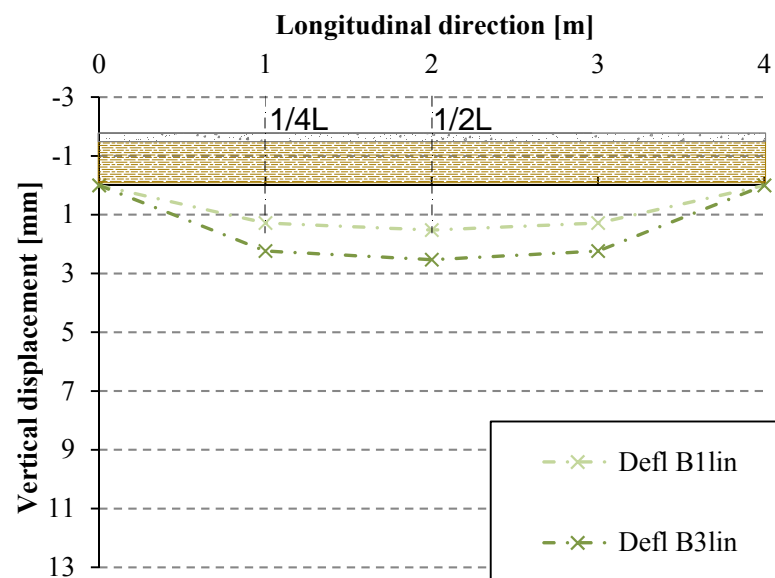


Fig. 4.40 – S3-hc=0.03m B1 and B3 deflections

Therefore, in general, the vertical displacements showed to be higher for the loaded beam, decreasing from it to the farthest beams, for both measuring locations and all the load cases. For mid-span and line loading cases the displacement at mid-span showed to be higher than the measured at quarter-span. When the load was applied at quarter-span, displacements measured at mid- and quarter-span were very close to each other, and at the loaded beam the second tends to be higher than the first.

With the deflection curves it is possible to evaluate the degree each beam is involved in the load distribution along its span. The stiffer the beam/structure, the flatter the deflection curve and the closer the deflection curves are for different load cases.

All the parameters whose effects in the behavior of these timber-concrete composite floors were analyzed proved to have some influence on the mechanical behavior of such structures. A LWAC and a thinner concrete slab led to a lower “displacement distribution”. This means

that the displacement occurs essentially at the loaded beam and in its vicinity. Also a shorter span led to a lower “displacement distribution”.

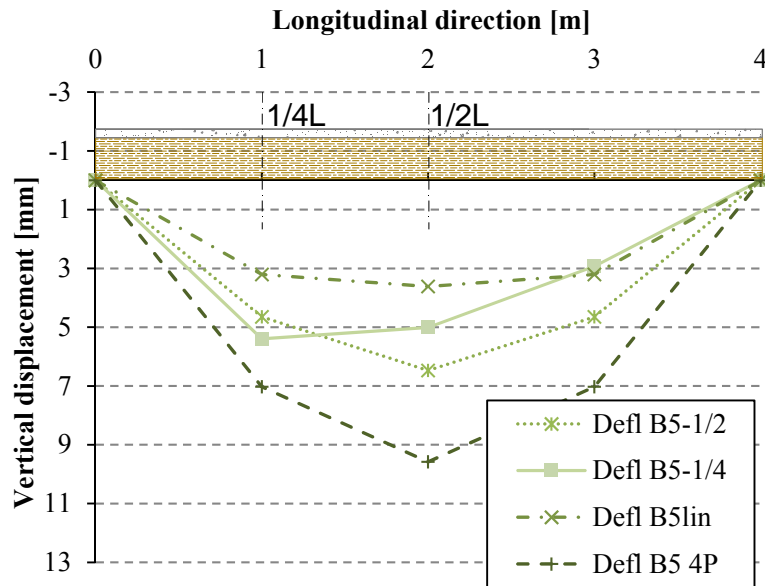


Fig. 4.41 – S1-BSp B5 deflections

4.4.2 Support reactions

As in the previous section, the discussion about the experimental results of support reactions is based in the overall collected data. These results are included in a graphical form in the *B.2.2 – Support reactions (APPENDIX B)*. However, only the figures whose characteristics may be relevant to the discussion were chosen to be presented in this section. Nevertheless, it was found interesting to collect the support reaction distribution, in percentage, for all the load cases considered in Table 4.8. These percentages were obtained by comparing the support reaction of the beam in question with the sum of loads transferred to the supports at the specific load case considered.

In general a very similar behavior was found: the loaded beam is the one that receives the highest percentage of support reaction. The adjacent beams receive the second highest portion and together with the loaded beam they totalize between 93 % and 116 % of the applied load. Thereby, as the beams are farther away from the loaded one, their participation in the support reaction distribution tends to decrease. This behavior becomes clearer for some specific specimens. This is the case of S4, where the beams to which the load is applied support more

than 73 % of the applied load, with a maximum of 96 % for the exterior beams and 86 % for the remaining.

Table 4.8 – Support reaction distribution [%]

Floor specimen	Load case	Beam position					LB + AB	Floor specimen	Load case	Beam position					LB + AB		
		B1	B2	B3	B4	B5				B1	B2	B3	B4	B5			
S1-BSp	B1 ½	76	29	5	-3	-7	105	S4- L=2.00m	B1 ½	94	9	-1	-1	0	103		
	B2 ½	27	46	22	13	-7	94		B2 ½	8	79	16	-2	-1	104		
	B3 ½	-2	34	37	35	-3	105		B3 ½	-5	18	73	19	-5	110		
	B4 ½	-6	13	20	46	27	93		B4 ½	-2	1	15	77	9	102		
	B5 ½	-5	-3	2	24	81	105		B5 ½	-1	0	-1	8	94	102		
	B1 ¼	82	23	3	-3	-5	105		B1 ¼	94	10	-3	-1	0	104		
	B2 ¼	25	49	22	9	-5	96		B2 ¼	6	84	14	-3	-1	104		
	B3 ¼	1	27	43	29	0	99		B3 ¼	-3	10	83	13	-3	106		
	B4 ¼	-4	10	20	48	26	95		B4 ¼	-1	-2	14	82	6	103		
	B5 ¼	-4	-3	2	20	84	105		B5 ¼	0	-1	-2	8	95	103		
	B1 4P	82	23	0	-2	-3	106		B1lin	95	7	-1	0	0	102		
	B2 4P	25	49	21	10	-5	95		B2lin	5	86	11	-2	0	103		
	B3lin	-3	19	69	18	-3	106		B3lin	-2	11	82	12	-2	105		
	B3 4P	-5	31	49	29	-4	109		B4lin	0	-2	11	86	6	102		
	B4lin	-3	5	16	68	14	98		B5lin	0	-1	-1	6	96	102		
	B4 4P	-6	9	22	53	22	97										
	B5lin	-2	-2	-1	22	84	105										
	B5 4P	-4	-4	1	28	79	107										
	S2-LWAC	B1 ½	88	15	2	-2	-3		103	S5- L=6.00m	B1 ½	80	19	8	-1	-7	100
		B2 ½	26	46	25	9	-6		97		B2 ½	31	34	29	11	-5	94
B3 ½		-8	33	51	32	-8	116	B3 ½	2		28	39	28	3	95		
B4 ½		-5	6	25	53	21	99	B4 ½	-6		12	26	38	31	94		
B5 ½		-3	-2	1	17	88	104	B5 ½	-7		-1	8	20	81	101		
B1 ¼		89	14	1	-3	-1	103	B1 ¼	81		19	7	-1	-7	100		
B2 ¼		17	63	19	3	-2	99	B2 ¼	29		41	25	8	-4	95		
B3 ¼		-4	23	63	22	-4	108	B3 ¼	3		25	43	25	4	93		
B4 ¼		-4	4	20	65	15	100	B4 ¼	-5		9	23	45	27	96		
B5 ¼		-2	-2	-1	17	88	105	B5 ¼	-8		0	7	21	80	101		
B1lin		93	9	-1	-1	-1	103	B1lin	84		18	4	-2	-4	102		
B2lin		14	72	14	1	-2	100	B2lin	25		47	26	6	-3	97		
B3lin		-3	16	75	15	-3	106	B3lin	1		25	48	25	1	98		
B4lin		-2	2	15	73	12	100	B4lin	-4		7	23	52	23	97		
B5lin		-1	-1	-2	8	95	103	B5lin	-5		-1	5	17	85	102		

Table 4.8 – Support reaction distribution [%] (cont.)

Floor specimen	Load case	Beam position					LB + AB	Floor specimen	Load case	Beam position					LB + AB
		B1	B2	B3	B4	B5				B1	B2	B3	B4	B5	
S3- hc=0.03m	B1 ½	85	18	2	-1	-4	103								
	B2 ½	23	51	25	5	-4	99								
	B3 ½	-1	30	45	26	0	101								
	B4 ½	-4	4	29	47	24	100								
	B5 ½	-5	-4	4	26	78	104								
	B1 ¼	89	14	1	-2	-2	104								
	B2 ¼	17	64	21	1	-2	101								
	B3 ¼	-1	23	58	19	1	100								
	B4 ¼	-3	3	23	61	17	101								
	B5 ¼	-3	-3	2	22	83	105								
	B1lin	95	7	0	-1	-1	102								
	B2lin	11	76	14	1	-1	101								
	B3lin	0	17	69	15	0	101								
	B4lin	-1	1	15	72	13	101								
	B5lin	-2	-1	0	13	90	103								

½ - mid-span; ¼ - quarter-span; lin - line load; 4P - 4-point load; LB - loaded beam; AB - Adjacent beams

By analyzing the responses found for S1, the percentages associated with the line load case seemed to be the highest, closely followed by the ones associated with the four point (4P) and quarter-span load cases. The load case with the point load applied at mid-span is the one which provides the widest load spreading, which results from a lower magnitude of support reaction associated with the loaded beam when compared with the other load cases. This is also a common behavior found for the several specimens analyzed. The higher or lower degree in which it manifests varies. For specimen S4 it occurs in the lowest degree, with the percentages associated with the three load cases being very close, despite of those associated with the mid-span load case being slightly lower than the remaining. By opposition, specimen S5 clearly shows a wider load spreading associated with this specific load case.

Thus, comparing the response of S2 with that obtained for S1 it was found that, similarly, the line load case is the one associated with the higher percentages. In the same way, the mid-span load case was associated with the lower ones. The percentages found for the quarter-span load case were not so close to those found for the line load as for S1.

S3 presented a response very similar to that found for S2. For specimen S4 the capacity to distribute loads to the beams besides the loaded one is noticeably smaller, Fig. 4.42. In the

case of S5 the behavior is the opposite, with the trend to mobilize more beams for the load spreading, Fig. 4.43.

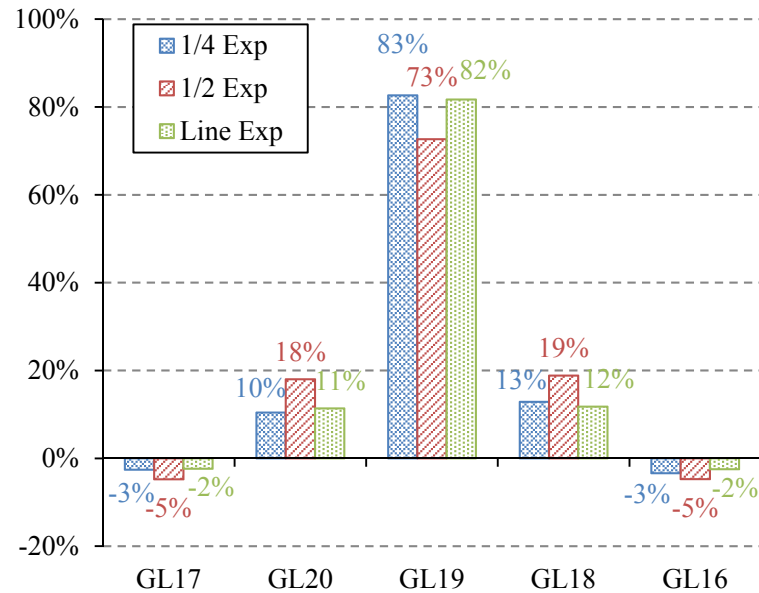


Fig. 4.42 – Support reaction distribution in S4-L=2.00m

In percent terms, a significant load spreading can be observed in specimen S1 with percentages varying between 16 % (B5 ¼) and 63 % (B3 ½), Table 4.9. S2 and S3 presented relatively close spreading behavior. Compared with the values found for S1, the spreading percentages tend to decrease: 5 % (B5lin) and 54 % (B2 ½) for S2; and 5 % (B1lin) and 55 % (B3 ½) for S3. Specimen S4 is the one with the lower load spreading, varying between 4 % (B5lin) and 27 % (B3 ½). By its turn, S5 presented the higher percentage of load spreading which varied between 15 % (B5lin) and 66 % (B2 ½). This results seem to be rather in line with the ones obtained for the vertical displacements.

Regarding the capacity to distribute the load applied to the supports under each beam, the slab with the shorter span is the most limited while the one with the longest span is the most effective. When comparing the limit values of spreading found for S1 and S5 they seemed to be very close 16 % vs. 15 % and 63 % vs. 66 %. Nevertheless, when comparing the global behavior of these two specimens S5 denotes a better ability to mobilize all the beams of the slab, Fig. 4.43. These is true for all the load cases considered, but clearer to the point load applied at mid-span. Also between specimens S2 and S3, despite the proximity of the spreading limits the global behavior shows some differences, Fig. 4.44. Specimen S2 denotes a slight trend to concentrate the load over the loaded beam when compared with specimen S3, which tends to delegate the load to the remaining beams.

4. EXPERIMENTAL ANALYSIS

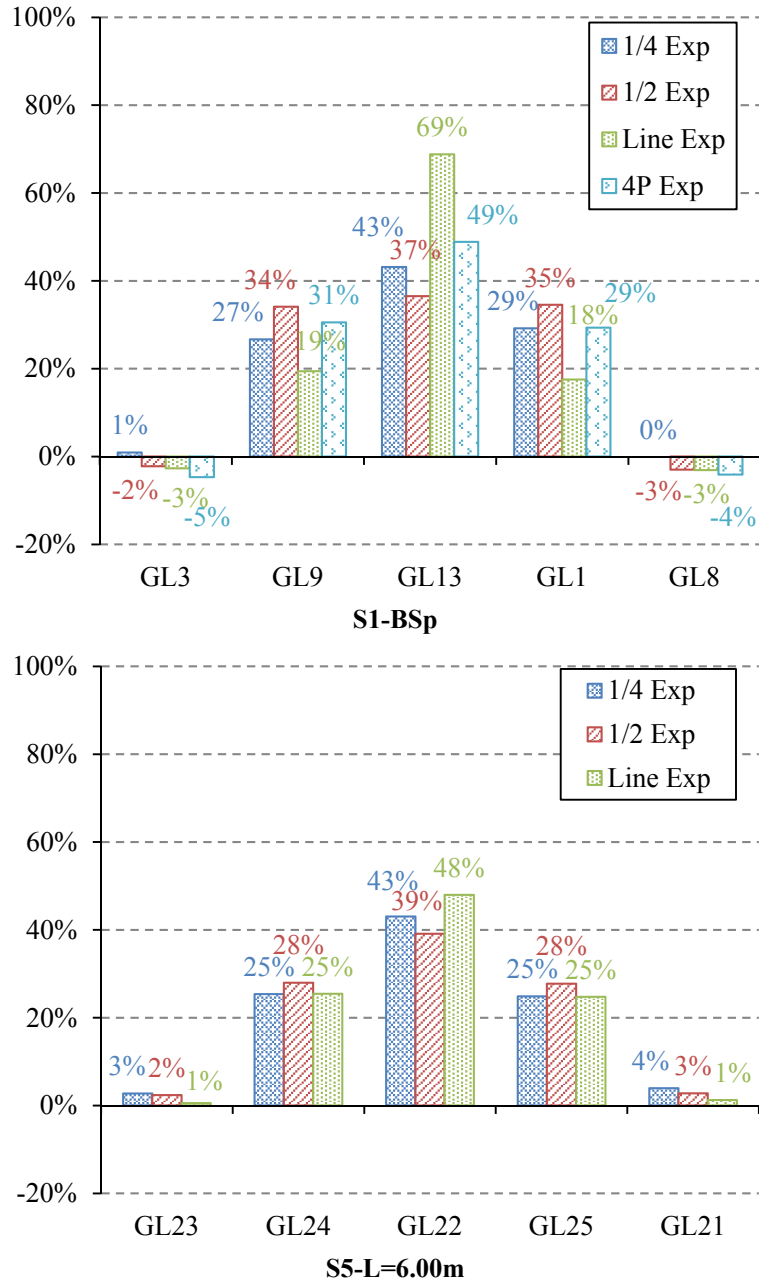


Fig. 4.43 – Support reaction distribution in S1-BSp and S5-L=6.00m

Table 4.9 – Support reaction spreading summary [%]

Floor specimen	Extreme	Load case		
		$\frac{1}{2}$	$\frac{1}{4}$	<i>lin</i>
S1-BSp	max	63	57	51
	med	43	39	34
	min	19	16	16
S2-LWAC	max	54	37	28
	med	35	26	18
	min	12	11	5
S3-hc=0.03m	max	55	42	31
	med	39	29	20
	min	15	11	5
S4-L=2.00m	max	27	18	18
	med	17	12	11
	min	6	5	18
S5-L=6.00m	max	66	59	53
	med	46	42	37
	min	19	19	15
Average spreading		36	30	24

From the three load cases considered, the one providing the widest load spreading is the point load at the mid-span (36 % on average), varying between 6 % (S4 - B1 $\frac{1}{2}$) and 66 % (S5 - B2 $\frac{1}{2}$). Conversely, the line load case is the one for which the lower load spreading was found (24 % on average), varying among 5 % (S3 - B1 $_{lin}$) and 53 % (S5 - B2 $_{lin}$).

Gathering these distributions by load type, Fig. B.79 to Fig. B.81, it becomes clearer that line load tend to be concentrated over the loaded beam, in a more pronounced manner than for the remaining load cases. Fig. 4.45 presents the graphs obtained for the *Base specimen*. On the other hand, loading over the beam mid-span led to the higher distributions. All the three load cases are consistent in behavior and in line with the presented before. The extreme opposite behavior belongs to S4 and S5. S4 showed the already noticed tendency to concentrate the support reactions over the loaded beams, with the extremity ones receiving above 90 % and the central above 70 %. For S5, the second beam is the one supporting to the lowest share of load, above 30 % but below 50 %, and the extremity ones tend support about 80 % of the applied load. For more information see Section B.2.2 – *Support reaction*, in APPENDIX B.

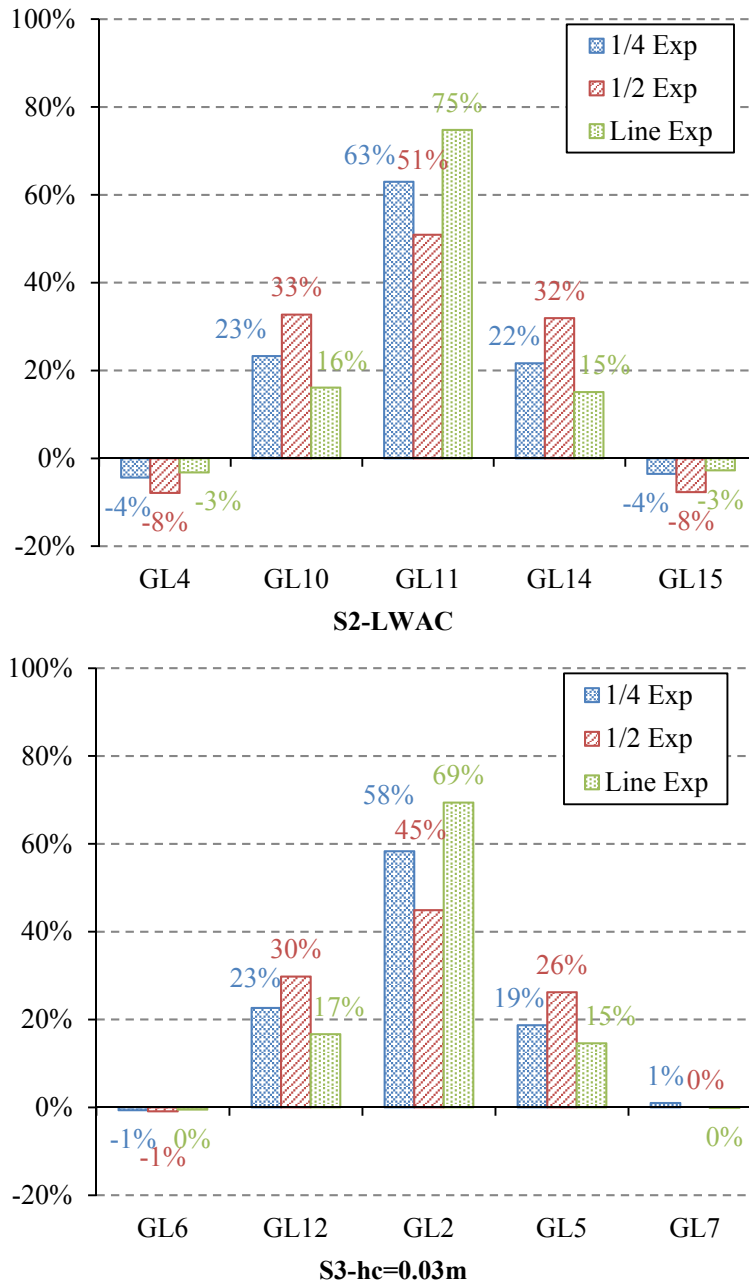


Fig. 4.44 – Support reaction distribution in S2-LWAC and S3-hc=0.03m

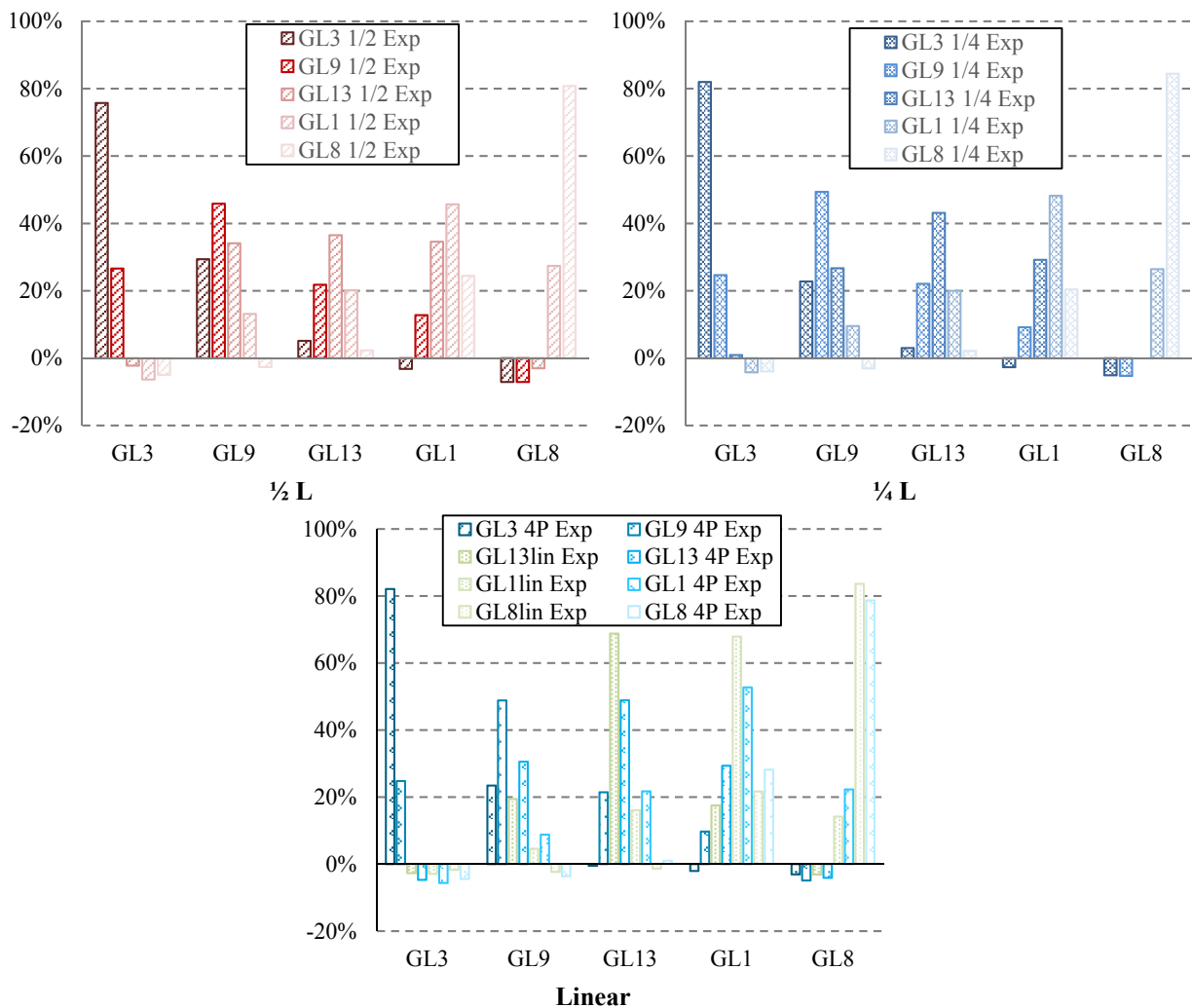


Fig. 4.45 – Support reaction distribution for S1-BSp

In order to relate the support reaction distribution with the parameter changed relatively to the *Base specimen*, the responses associated with the different parameters were gathered by beam and load case (Fig. B.82 to Fig. B.90). When comparing the behavior of S1, the *Base specimen*, with S2, associated with the use of a LWAC layer instead of a regular concrete very similar behavior was found when the load was applied at mid-span of B2 and B5. However for B3 loaded at mid-span the support reaction distribution of these two specimens tend to deviate. Analogous conclusions can be drawn when the load was applied at quarter-span, Fig. 4.46. For the line load case, considering the beams of S1 for which it was possible to apply the line load, distributions for both specimens are almost coincident, especially when concerning B3 and B4, Fig. 4.47. As for the distributions associated with 4P

loading, they tend to deviate from the line load distributions, with a response closer to those found for point loads.

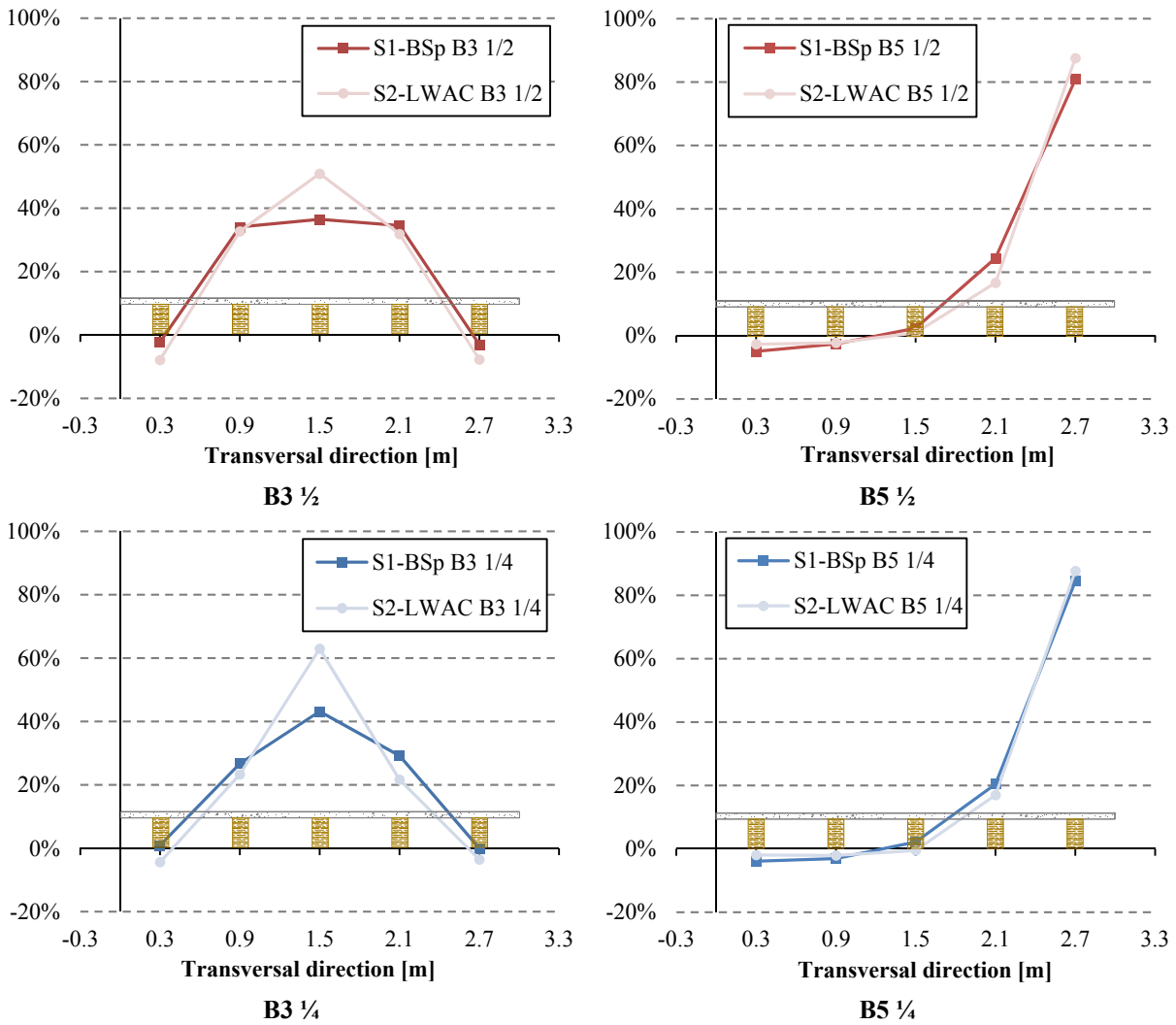


Fig. 4.46 – Support reaction distribution S2-LWAC vs. S1-BSp, point load at B3 and B5

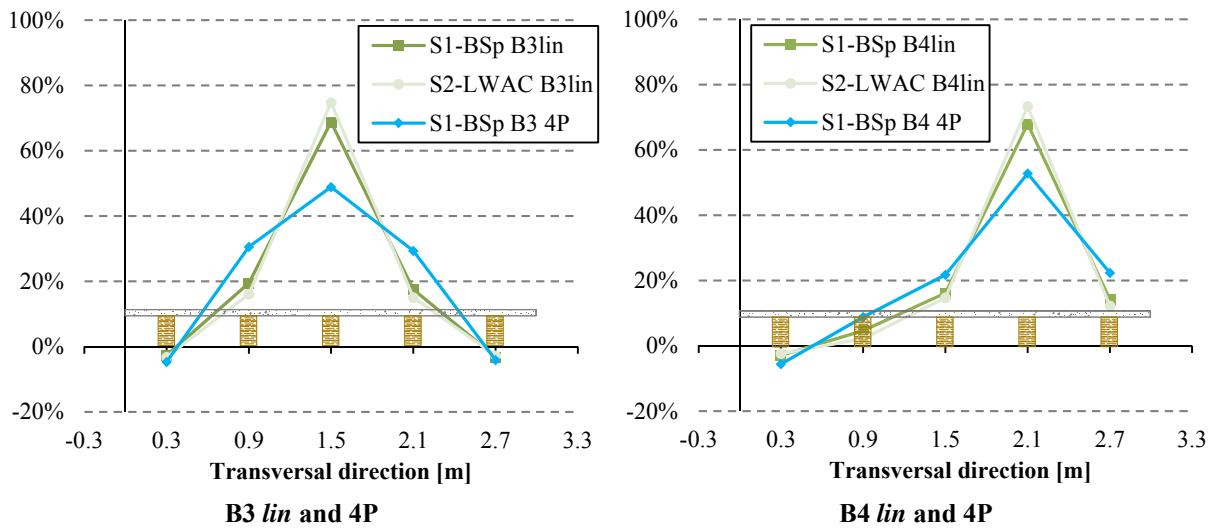


Fig. 4.47 – Support reaction distribution S2-LWAC vs. S1-BSp: line loading

When comparing distributions associated with S1 to those of S3, in where a 0.03 m thick layer of concrete was used in opposition to the 0.05 m thick used in S1, the same tendencies were found. A particular close behavior was found when the load was applied over B5, with the distribution for both specimens being almost coincident when the load was applied at quarter-span, Fig. 4.48. As for the comparison between S1 and S2, also the distributions found for S1 and S3 seem to be much closer when the line loading is considered, in comparison with the remaining concentrated loads. In general, S2 and S3 differ from S1 through a tendency to associate a higher support reaction with the loaded beam, which results into a reduced ability to mobilize the remaining beams to participate in the load distribution.

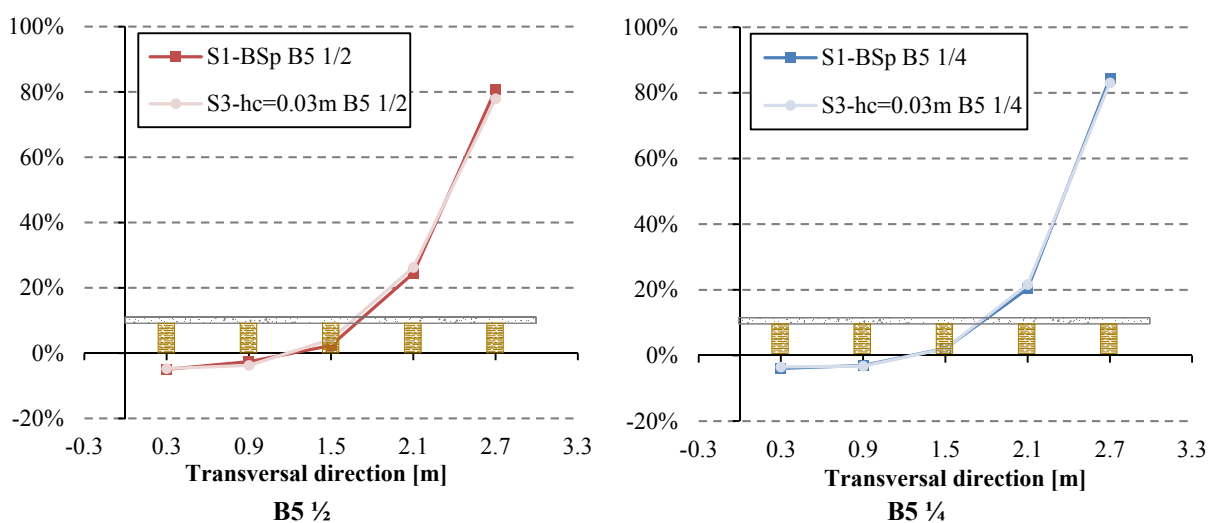


Fig. 4.48 – Support reaction distribution S3-hc=0.03 vs. S1-BSp, point load in B5

4. EXPERIMENTAL ANALYSIS

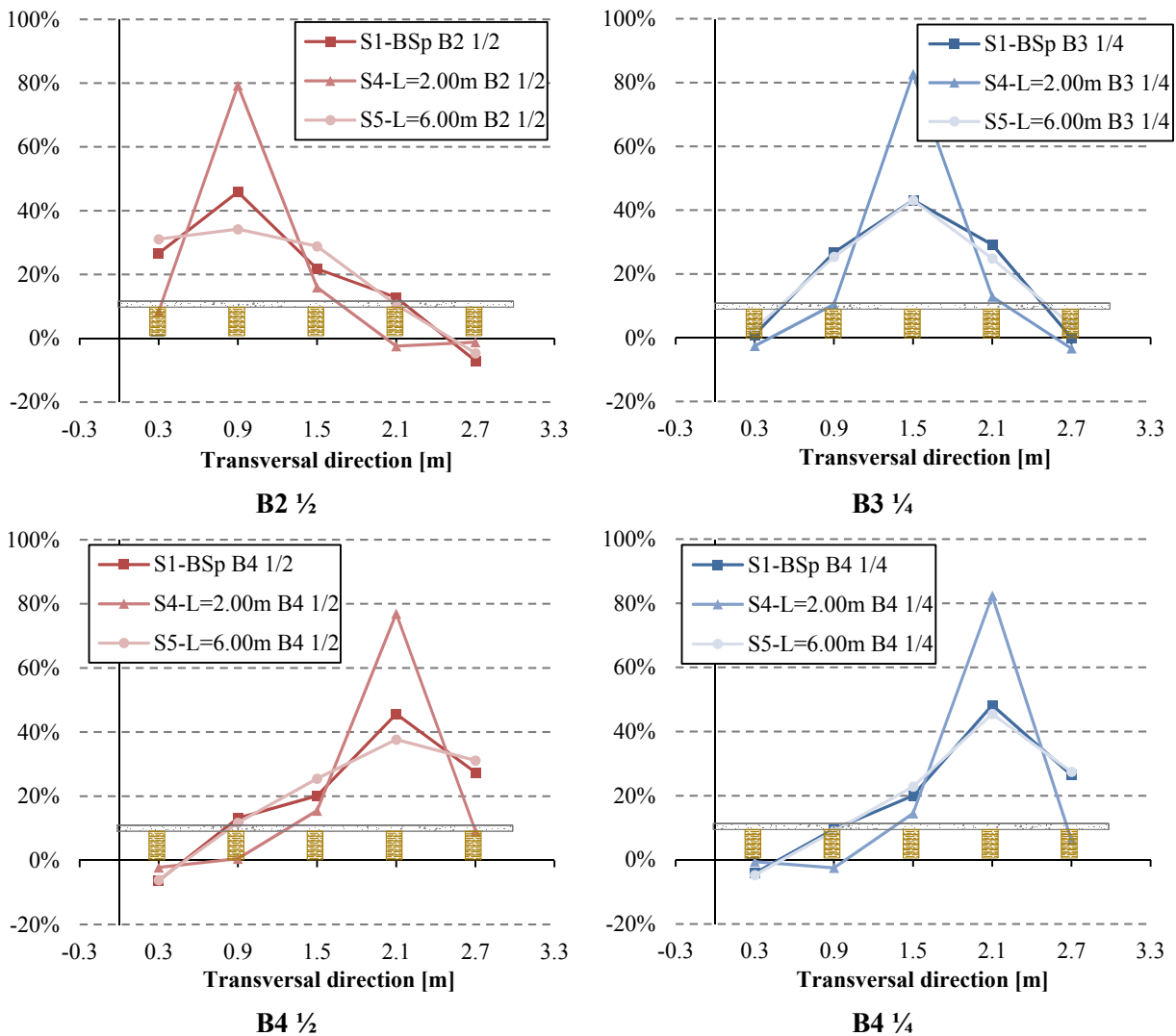


Fig. 4.49 – Support reaction distribution for S4-L=2.00m, S5-L=6.00m and S1-BSp, point loading

Concerning the span, comparing S4 (2.00 m span) with S5 (6.00 m span) and S1 (4.00 m span) generally the specimen with the longest span show even distributions. This behavior is clearer for B2 and B4 than for the remaining beams, Fig. 4.49. This no longer applies for the loading on quarter of the span, for which S5 and S1 present behavior even closer. For S4, the tendency for both point loading is to show a distribution of support reactions deviating for the other two specimens, guiding the load mainly to the supports of the beam to which it was applied, Fig. 4.49. Analyzing the line loading distributions it was noted that S5 *lin* is closer to S1 4P than to other specimen loaded with a line load. This is particular true for B4, where those distributions almost do not differentiate from each other, Fig. 4.50. For this parameter, S1 *lin* seems to have an intermediate behavior, limited above by S4 and below by S1 4P. As

presented before, the tendency to a wider distribution is a characteristic of the specimen with the longest span, presenting flatter distribution “curves” when compared to those of the shortest span. The shorter the span, the more angular will be the distribution “curves” and the highest will be their peaks, corresponding to the loaded beam position.

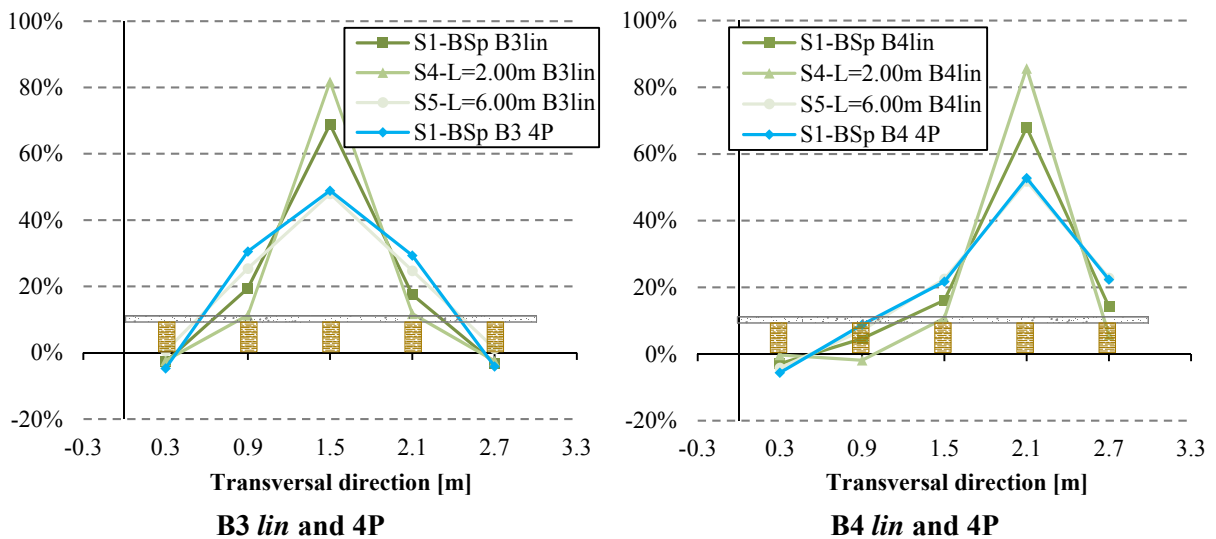


Fig. 4.50 – Support reaction distribution for S4-L=2.00m, S5-L=6.00m and S1-BSp, line loading

4.4.3 Slip displacements

Similarly to what was found for the preliminary tests, the slip between timber beams and concrete slab was very small for the several tests (Table B.8). The recorded values varied between -1.390 mm and 0.146 mm, found for S1 and S2 respectively. For more information see Section B.2.3 – *Slip displacements*. Table 4.10 sums up the extreme values, maximum and minimum, for each specimen found with the various load tests. By its turn, Table 4.11 presents the extremes considering only the response of the loaded beam in each specimen.

For the load cases to which the structure responds symmetrically, as the mid-span and the line load cases, the slip tend to follow such symmetry either for the pairs of transducers along a beam (SD1-5 vs. SD6-10, Fig. 4.27) or transversally for the different beams of the slab (B1 and B2 vs. B4 and B5). A few exceptions were found, and these exceptions are associated with specific cases. When comparing the pairs of transducers, different slips at opposite ends of a beam were found for some tests. This could be consequence of some uncontrolled connection characteristics, as friction between the steel connector and the concrete aggregates or the steel mesh, or even friction between the connector and some glued joint or knot in the glulam beam, which can cause different behavior between beam ends. In the case when line

load was applied, a possible unevenness could persist, despite the best efforts to avoid it. When comparing symmetrically disposed beams, the small differences ($SD_i - SD_{i+5}$) can result from the fact that the beams did not have exactly the same material properties when compared to each other or even when compared different zones of the same beam. However, it should be remembered that the magnitude of the values under consideration is quite low, which greatly reduces the importance of these differences.

Table 4.10 – Maximum and minimum experimental slip displacements

Floor specimen	Extreme	Load case	Slip
			[mm]
S1-BSp	Max	B2 4P	0.028
	Min	B4 4P	-1.390
S2-LWAC	Max	B3 ¼	0.146
	Min		-1.200
S3-hc=0.03m	Max	B2 ½	0.006
	Min	B1 ¼	-0.473
S4-L=2.00m	Max	B3 ½	0.015
	Min	B1 ¼	-0.554
S5-L=6.00m	Max	B5 ¼	0.021
	Min		-0.766

½ - mid-span; ¼ - quarter-span; 4P - 4-point load

Table 4.11 – Extreme slip displacements for the loaded beams [mm]

Floor specimen	Extreme	Load case					
		½		¼		lin/4P	
S1-BSp	Max	-0.288	B3	-0.040	B3	-0.167	B5lin
	Min	-0.569	B5	-0.606	B5	-1.390	B4-4P
S2-LWAC	Max	-0.530	B2	-0.358	B2	-0.322	B1
	Min	-0.772	B4	-1.200	B3	-0.738	B4
S3-hc=0.03m	Max	-0.148	B4	-0.114	B3	-0.134	B5
	Min	-0.334	B5	-0.473	B1	-0.290	B4
S4-L=2.00m	Max	-0.350	B3	-0.268	B3	-0.300	B3
	Min	-0.536	B1	-0.554	B1	-0.538	
S5-L=6.00m	Max	-0.360	B4	-0.130	B4	-0.349	B1
	Min	-0.702	B5	-0.766	B5	-0.586	B2

½ - mid-span; ¼ - quarter-span; lin - line load; 4P - 4-point load

4.4.4 Uplift displacements

The uplift displacements (UP) were measured in each corner of the slabs at the bottom face of the concrete layer, or at the timber interlayer in the case of S3. The positive value corresponds to an upwards displacement. The values recorded are summarized in Table B.9.

As found before in the preliminary tests, this quantity is relatively small in magnitude, varying between -3.100 mm and 1.753 mm, for S2 and S1 respectively. Table 4.12 summarizes the extreme values, maximum and minimum, for each specimen and load case.

In general, loading of the extremity beams, *i.e.* the closest to the uplift measuring locations, led to lowering in the corresponding transducers. This means that when the load was applied to B1 the trend was UP1 and UP3 to show negative displacements, while for the loading of B5, the transducers that showed that trend were UP2 and UP4, Fig. 4.27. For the loading of the central beams the trend was for the transducers to present positive values, meaning that the slab tend to uplift in all the corners when loaded in this beam. For loading in the adjacent beams the trend was not as clear as for the remaining. In this case the values recorded were either negative or positive, varying with the load case and the floor stiffness. For S1, S3 and S5 the trend was for the closer transducers to show a lowering.

Table 4.12 – Maximum and minimum experimental uplift displacements [mm]

Floor specimen	Extreme	Load case								
		½		UP	¼		UP	lin/4P		UP
S1-BSp	Max	0.649	B3 ½	UP1	0.283	B3 ¼	UP1	1.753	B3 4P	UP3
	Min	-2.165	B5 ½	UP2	-2.390	B5 ¼	UP2	-3.074	B1 4P	
S2-LWAC	Max	1.048	B3 ½	UP2	1.368	B4 ¼	UP2	0.864	B4lin	UP4
	Min	-2.591	B5 ½		-3.100	B5 ¼		-2.008	B5lin	UP2
S3-hc=0.03m	Max	0.210	B3 ½	UP3	0.338	B2 ¼	UP1	0.250	B2lin	UP1
	Min	-1.386	B1 ½		-1.848	B1 ¼		-1.114	B1lin	UP4
S4-L=2.00m	Max	1.327	B3 ½	UP3	1.068	B2 ¼	UP1	0.924	B2lin	UP3
	Min	-2.130	B1 ½	UP1	-2.497	B1 ¼		-2.112	B1lin	UP1
S5-L=6.00m	Max	0.378	B4 ½	UP1	0.268	B3 ¼	UP3	0.296	B4lin	UP1
	Min	-1.574	B5 ½	UP2	-2.218	B5 ¼	UP4	-1.346	B5lin	UP2

½ - mid-span; ¼ - quarter-span; lin - line load; 4P - 4-point load; UP – Uplift displacement

4.4.5 Strains

The strain results gathered from the several load tests are presented in *B.2.5 – Strains (APPENDIX B)*. This section presents the essential conclusions in terms of absolute value and in terms of distribution over the slab specimens for the several load cases. Aiming at complementing the information, also the stress values will be presented in the current section,

where deemed appropriate. Since the load level was established in order to avoid any risk of inducing some kind of damage or permanent deformations, the stresses were computed assuming a linear elastic behavior and therefore obtained simply by multiplying the strain value by the MOE of the corresponding beam.

Table 4.13 summarizes the extreme values (highlighted in bold) found for the strains in each specimen for the various load cases. Since the strains were measured with two strain gauges at each measuring section, the values found with each pair are presented. In turn, Table 4.14 presents the corresponding stresses.

Table 4.13 – Maximum and minimum experimental strains [$\mu\epsilon$]

Floor specimen	Extreme	Load case								
		$\frac{1}{2}$			$\frac{1}{4}$			lin/4P		
S1-BSp	Max	871.7	563.0	B1	319.8	210.6	B1	845.8	963.3	B3 4P
	Min	-24.0	-17.2		-20.1	-15.3		-17.2	-12.4	B5 4P
S2-LWAC	Max	1122.9	1086.4	B5	476.2	439.9	B5	361.4	362.9	B4
	Min	-16.3	-31.6		-12.5	-24.9		-11.4	-17.2	B5
S3-hc=0.03m	Max	445.0	882.1	B1	212.9	429.8	B1	157.4	182.2	B2
	Min	-11.5	-32.5	B4	-8.6	-22.0	B5	-13.3	-63.1	
S4-L=2.00m	Max	1286.1	766.8	B5	700.7	399.6	B5	771.8	462.1	B5
	Min	-11.5	-3.8	B3	-13.5	-1.0		-1.9	-6.7	B2
S5-L=6.00m	Max	850.5	1001.3	B5	321.4	405.9	B5	265.8	331.0	B4
	Min	-10.6	-25.0		-26.9	-37.5	B1	-8.6	-14.4	B1

$\frac{1}{2}$ - mid-span; $\frac{1}{4}$ - quarter-span; lin - line load; 4P - 4-point load

Table 4.14 – Maximum stresses [MPa]

Floor specimen	Load case					
	$\frac{1}{2}$		$\frac{1}{4}$		lin/4P	
S1-BSp	6.84	B1	2.61	B2	8.60	B3 4P
S2-LWAC	10.50	B3	3.97	B5	3.45	B4
S3-hc=0.03m	7.40	B1	3.61	B1	1.58	B2
S4-L=2.00m	8.14	B5	4.44	B5	4.89	B5
S5-L=6.00m	9.18	B5	3.72	B5	2.96	B4

$\frac{1}{2}$ - mid-span; $\frac{1}{4}$ - quarter-span; lin - line load; 4P - 4-point load

As it was expected, generally, the extreme values of strain, maximum and minimum, are associated with the outer beams, B1 and B5, regardless of the load case. For point loads on S1 and S2 there is a trend to the maximum and minimum values to be associated with the same load case. For S4 almost all the extreme values are associated with the external beam B5. The same happens for S5, but with the exception associated with the mid-span load case. In this

case the minimum occurs for the opposite external beam, B1. In the case of S3, there is not a clear pattern.

As far as the strain magnitude is concerned, the values varied between $-63.1 \mu\epsilon$ (S3-hc=0.03m B2lin) and $1286.1 \mu\epsilon$ (S4-L=2.00m B5 ½), which correspond to stresses of -0.55 MPa and 8.14 MPa , respectively. Despite the minimum stress and strain correspond to the same specimen and loading, this do not apply for the maximum stress. The maximum stress happened for the S2-LWAC when loaded at mid-span of B3, taking the value of 10.50 MPa ($1066.4 \mu\epsilon$).

The mid-span load case tends to induce the greatest values of strains and stresses, in contrast to the line load case. The quarter-span loading led to lower values than those obtained for the mid-span load case. This is an expected behavior since the load applied at quarter-span is more likely to lead to greater strains at that section, while a point load at mid-span or a $lin/4P$ load tend to provoke greater strains at the mid-span section. In fact, the maximum values found for the point load cases seem to be related to each other. The maximum strains found when the load was applied at quarter-span were about 45 % of those found for the mid-span load case (varying between 37 % and 54 %). For the line load, the behavior is not that clear, in some cases the maximum value was the greatest for that specimen, as for S1, and in other cases they slightly exceeded the value found for the quarter-span loading, as for S4. For the remaining specimens the relation between the maximum values for the line load was about 29 % of those for the mid-span loading.

As Table B.10 supports, the values recorded for the pair of strain gauges at a beam section are not always similar. The specimen where the difference among the pairs ($S_i - S_{i+1}$, Fig. 4.27) are largest in average (among all the beams and several load cases) is S3. Nevertheless, the differences found for the pairs of strain gauges in specimen S5, among the various load cases, were the most uniform and the lowest, at the same time. Table 4.15 summarizes the mean differences, as well as the maximum and minimum differences associated with the various loading types.

Not similar strain values for the same beam section indicate different behavior at that section. This phenomenon could be associated with the material characteristics in the vicinity of the location where the strain gauges were glued. Specifically this is probably the effect of some timber defects, as resin bags or knots, or even patches or plugs to correct those. As far as possible those were avoided. It was also found that, the larger differences happened most of the times in the outer beams. This seems to be associated with the trend for the beam to suffer some lateral buckling. Since the beams were perched on the load cells, to approach the support conditions to simply supported, they were not restrained to twisting unless by the concrete slab to which they were connected. Nevertheless, as the measurement were

performed at the beam bottom face, the opposition to twisting provided by the concrete layer is less felt and more differences in the strain results were found.

Table 4.15 – Strain gauge pairs differences [$\mu\epsilon$]

Floor specimen	Extreme	Load case			Mean
		$\frac{1}{2}$	$\frac{1}{4}$	lin/4P	
S1-BSp	Max	309	109	342	19
	Min	-59	-20	-118	
S2-LWAC	Max	73	46	37	-13
	Min	-278	-120	-72	
S3-hc=0.03m	Max	250	120	77	-21
	Min	-437	-217	-75	
S4-L=2.00m	Max	519	301	310	18
	Min	-197	-71	-87	
S5-L=6.00m	Max	118	36	41	-4
	Min	-173	-102	-65	

$\frac{1}{2}$ - mid-span; $\frac{1}{4}$ - quarter-span; lin - line load; 4P - 4-point load

The distribution of strains among the five beams of each specimen follows essentially the same trend as found for the previous parameters, Fig. 4.51. The loaded beam is associated with the highest percentage, regardless the loading case (Table B.11). These percentages were obtained dividing the strain associated with a beam (using the sum of strains recorded with the pair of strain gauges in that beam) by the sum of strains for the same load case.

The spreading of strains varied between 6 % and 79 % for the five floor specimens. The percentages found for S1 varied between 26 % (B1 4P) and 79 % (B2 $\frac{1}{4}$). As previously noticed, the values found for S2 and for S3 are lower than the ones found for S1, 16 % (B5 $\frac{1}{2}$) - 59 % (B2 $\frac{1}{4}$), and 14 % (B5 $\frac{1}{2}$) - 69 % (B4 $\frac{1}{4}$), for S2 and S3 respectively. S4 presents the narrower strain spreading (6 % - B5 $\frac{1}{4}$, 40 % - B4 $\frac{1}{4}$), while S5 have the widest spreading for the all load cases (29 % - B5 $\frac{1}{2}$, 77 % - B3 $\frac{1}{4}$). Although in terms of distribution boundaries it seems to be slightly surpassed by S1, the average distribution for S5 is 56 %, against the 52 % found for S1.

The loading case that led to the widest spreading of strains seems to be the one on where the load was applied at quarter-span, Fig. B.91. When comparing the spreading behavior associated with this load case with the spreading behavior associated with the vertical displacement measured at mid-span for the load applied at quarter-span (*4.4.1 Vertical displacements*), results were in agreement, Fig. 4.51, Fig. B.52 and Fig. B.91, making this outcome less odd. Indeed, measuring the parameter, strains in this case, in a different location from that where the load was applied may imply that a certain amount of information can not

be assessed. The highest strains will be expected to arise in the section where the load is applied, nevertheless, without these values, the manner in which the strains spread throughout the floor could only be analyzed qualitatively, based on the measurements at the observed section.

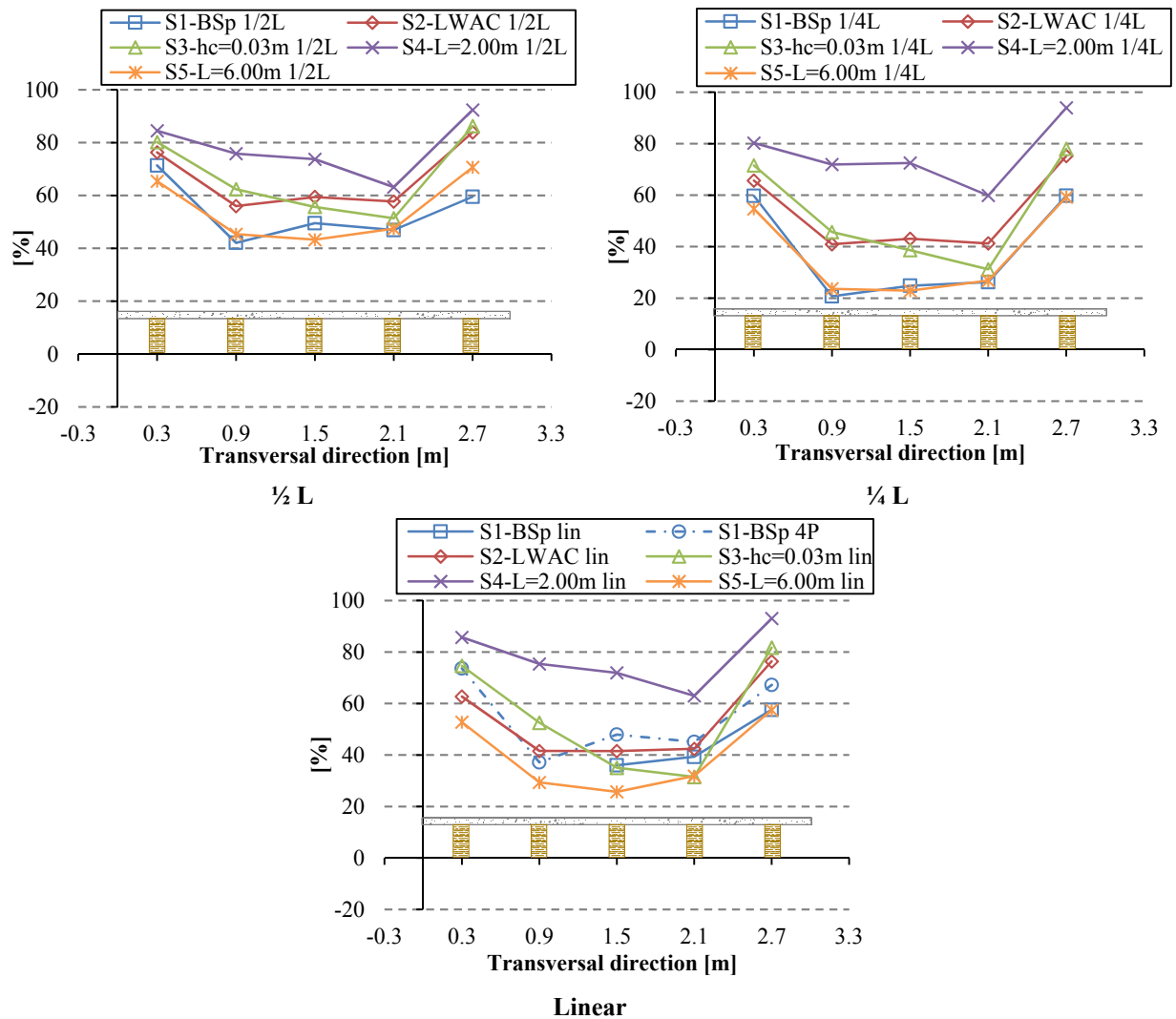


Fig. 4.51 – Strain distribution for the loaded beam, by load case

Moreover, contrary to the outcomes found in the previous sections, the loading at mid-span seem to lead to the lower spreading percentages than the remaining load cases. This can be consequence of the higher strain levels found for this load case, when compared with the remaining ones (Table 4.13). Given the nature of the loading actions, point vs. line (distributed) loads, the behavior in terms of strains is expected to have an irregular shape in

the case of the point loads. Also, the load level considered for the point loads in comparison with that defined for the line load cases, 40 % of the ultimate load for the point load cases vs. 20 % of the ultimate load for the line load ones, lead to higher strain levels and consequently to a higher percentage associated with the loaded beam. Together, these reasons justify the fact that strains associated with loading at mid-span were higher than those found for the line load cases. Furthermore, another contribution to explain the reason why a higher strain level was obtained associated with the loading at mid-span is that this one was also the observed section. Thus, since the point load at quarter-span was expected to produce higher strains at the location immediately below, it is likely that the strain recorded at mid-span do not led to comparable results. Therefore, quantitative conclusions may not be drawn relating point load cases, mid- and quarter-span.

4.4.6 Failure tests

After performing the load tests at service load levels, each of the specimens was loaded to failure. The specimens were loaded with a point load at mid-span of the central beam, in the same order as they were tested. In the cases where the integrity of the specimen was not implicated, other beams were loaded after the central one, Fig. 4.52 a) and c). This time, the specimens were placed over timber blocks, instead of the load cells, and no recording equipment was used but the pairs of strain gauges at the bottom mid-span section of the timber beams, Fig. 4.52.

In general, in the failure tests all the specimens tended to behave similarly. When the central beam is loaded till failure it tends to bend at the same time as its ends tend to uplift and to slide away from the concrete layer that shows some increase in the number and size of the cracks, becoming supported by a unique edge of the beam that contacts the blocks used as support. Also the farthest beams tend to uplift. This details can be clearly observed in Fig. 4.52 b), for the failure at the central beam of specimen S1.

The failure occurred first in the timber beams, followed in some cases by a punching shear failure in the concrete layer. Usually, the failures in the glulam beams started near knots or finger joints, in sections close to mid-span, Fig. 4.53.

Table 4.16 presents the loads and the strains recorded in the failure tests. Fig. 4.54 shows the load-stress curves obtained for the failure test at the central beam, B3, of each specimen.

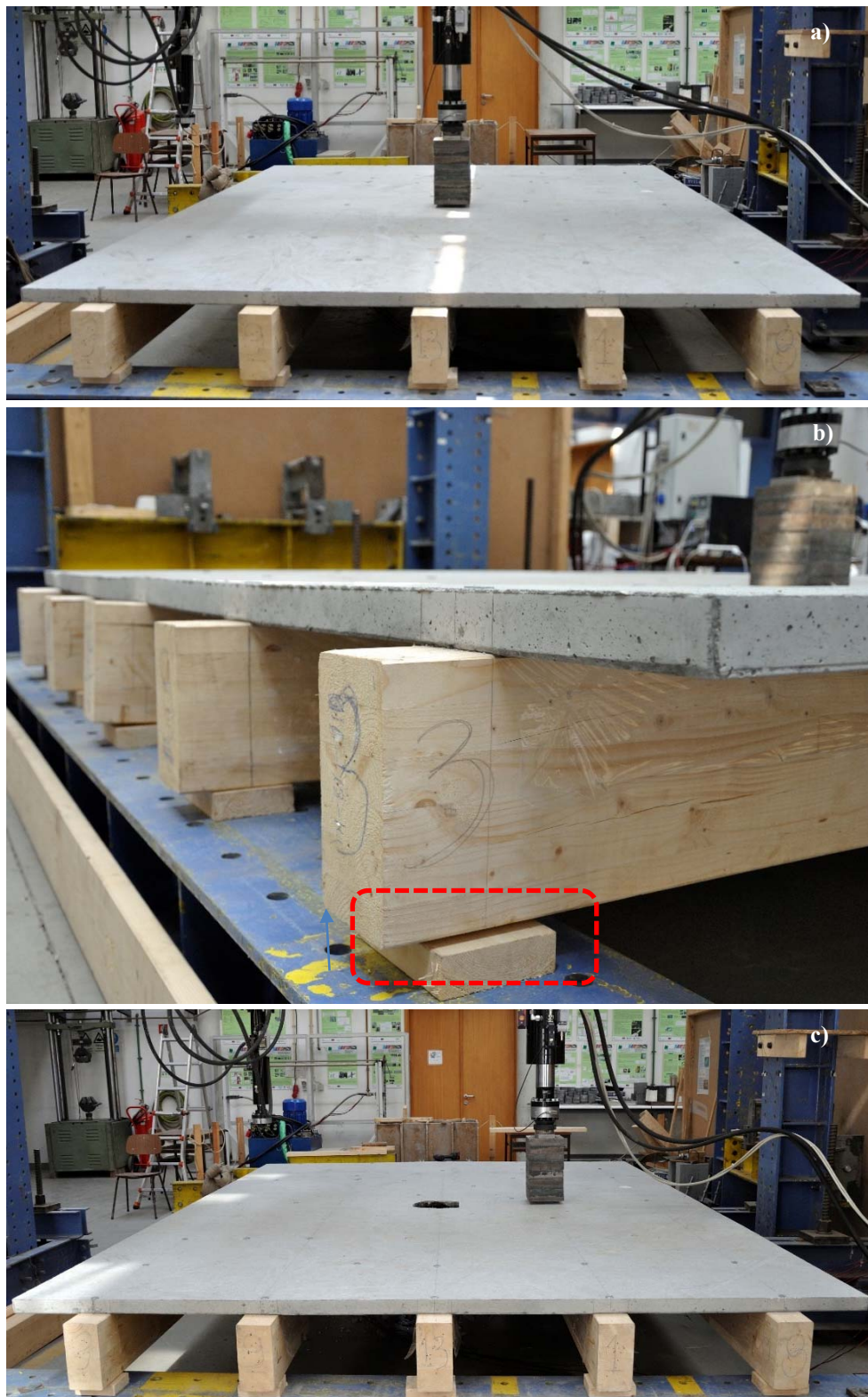


Fig. 4.52 – S1-BSp failure test: a) B3-GL13; b) B3-GL13 failure detail and c) B4-GL1

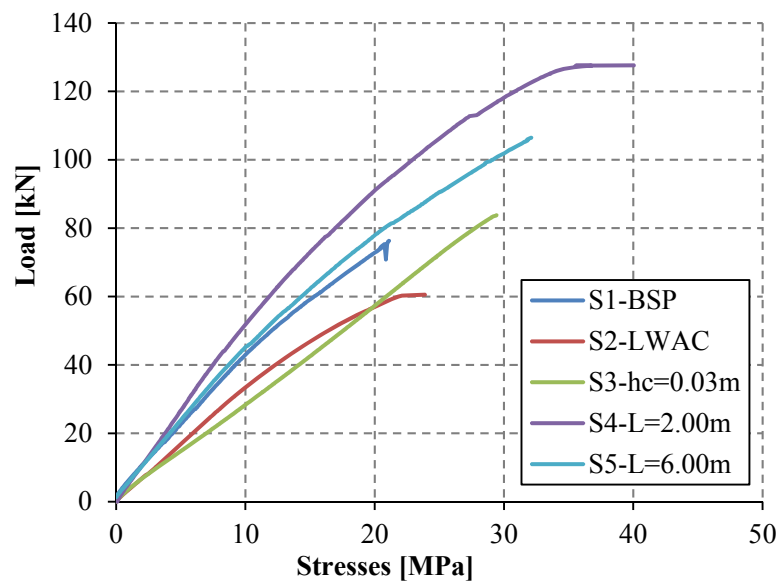


Fig. 4.53 – Failure sections

Table 4.16 – Loads and strains at failure

Floor specimen	Beam loaded	Failure load [kN]	Strain at the loaded beam			MOE [MPa]	Stress ^{a)} [MPa]
			S_i	S_{i+1}	Mean		
			[$\mu\epsilon$]				
S1-BSp	B3 ½	76.28	2269.6	2461.7	2365.65	8927.0	21.1
	B4 ½	91.02	4195.5	3825.4	4010.45	10164.8	40.8
S2-LWAC	B3 ½	60.54	2103.7	2749.5	2426.60	9846.0	23.9
S3-hc=0.03m	B3 ½	83.79	2590.7	2729.6	2660.15	11059.2	29.4
	B4 ½	72.12	1063.2	2997.2	2030.20	8981.4	18.0
	B2 ½	47.97	2284.1	2646.2	2465.15	8651.1	21.3
S4-L=2.00m	B3 ½	127.61	5311.3	5981.7	5646.50	7092.2	40.0
S5-L=6.00m	B3 ½	106.43	2911.7	3090.6	3001.15	10697.8	32.1
	B4 ½	86.43	3813.5	3167.7	3490.60	8931.4	31.2

a) Computed assuming a linear behavior until the failure.

**Fig. 4.54 – Load-stress curves for B3 at failure**

Considering only the tests where the load was applied in the central beam, the highest recorded failure load corresponds to specimen S4. This specimen is also associated with the highest stress level. This was an expected outcome since S4 was the specimen with shortest beams, turning it in a stiff structure when compared with those with a 4.00 m span. The lowest failure load refers to the central beam of specimen S2. The cause for this seems to be related to the existence of a knot near the timber section where the failure started. The presence of imperfections near the loaded section jeopardize the beam strength and therefore

the load level for which the failure occurs. Concerning the lowest stress it is associated with specimen S1. In this case the reason for this seems to be associated with the low MOE of the beam. When compared with the beams with similar strain levels, the lower MOE of this beam would imply a low maximum stress.

By its turn, concerning the whole tests, the failure strains varied between 1063.2 $\mu\epsilon$ and 5981.7 $\mu\epsilon$, found for B4 $\frac{1}{2}$ at S3 and B3 $\frac{1}{2}$ at S4, respectively. When considering only the central beam tests (when all the specimens were supported by five beams) the minimum strain at failure rose to 2103.7 $\mu\epsilon$. On average, the strain failure rounds 3120 $\mu\epsilon$. In terms of stresses, the average value at failure is about 30 MPa.

As well as it was found for several load tests, no similar strains were obtained for the pair of strain gauges of a section, for some of the failure tests. In fact, these results seem to support the causes to justify this behavior, already presented at the strain results section. The greatest difference found between the strains recorded by the pairs correspond to the loading B4 $\frac{1}{2}$ at S3 (1063.2 $\mu\epsilon$ and 2997.2 $\mu\epsilon$). After analyzing these results, the strain response of this specific beam was analyzed for the elastic load tests. As a consequence, a trend for the strains associated to this specific section was found. The reason for this can be found in Fig. 4.55. One of the strain gauges had to be glued a little over a knot, which led to the differences found in the strains measured by the two gauges at that section.



Fig. 4.55 – S3-hc=0.03m B4-GL5 failure

The previously presented results, displacements, reactions and strains, can be used for analyzing the way in which each composite floor behaved under concentrated loads. In spite of load distribution in the transversal direction being the essential focus of this study, it is a fact that all those parameters provide information on how the loads are distributed from the application point to the supports. This is also clear when the strains near the failure of the central beam are analyzed. Table 4.17 summarizes the strain distribution for the several failure test considering the loaded beam at the moment of failure and immediately after. For the same test in the upper line is the distribution at the failure (denoted by f) and in the line below the distribution in the moment following to failure (denoted by af). Marked in bold are the higher percentages for each situation.

Table 4.17 – Strain distribution at failure and immediately after [%]

Floor specimen	Beam loaded	Instant	Beam position				
			B1	B2	B3	B4	B5
MOE	[MPa]		7851.0	10248.8	8927.0	10164.8	8225.1
S1-BSp	B3 ½	f	4	14	60	18	4
		af	7	27	22	36	8
	B4 ½	f	1	5	0	73	21
		af	2	16	7	3	72
MOE	[MPa]		8312.8	9674.8	9846.0	9520.5	8331.4
S2-LWAC	B3 ½	f	1	16	71	13	0
		af	6	37	18	38	2
MOE	[MPa]		8387.8	8651.1	11059.2	8981.4	8571.3
S3-hc=0.03m	B3 ½	f	1	21	61	15	2
		af	3	50	3	39	5
	B4 ½	f	-1	10	5	64	23
		af	-8	70	31	-154	162
	B2 ½	f	17	77	4	0	1
		af	188	-166	46	13	19
MOE	[MPa]		6118.1	7959.9	7092.2	7467.2	6332.6
S4-L=2.00m	B3 ½	f	0	5	90	4	1
		af	8	55	0	34	3
MOE	[MPa]		9309.5	8643.4	10697.8	8931.4	9170.6
S5-L=6.00m	B3 ½	f	4	16	54	11	4
		af	14	35	-1	22	8
	B4 ½	f	1	6	6	62	24
		af	9	19	15	-6	62

f - failure; af - after failure

4.4.7 Parametric study of the tests

The results exposed in the previous sections clearly reveal that all the considered parameters affect the load distribution in the transversal direction of the composite floors in study. As it was expected, the loaded beam was the one with the greatest displacements and the one which receives the highest percentage of load. The way in which the load spreads to the remaining beams depends on the floor characteristics, being the span the aspect that most influences it.

Fig. 4.56 and Fig. 4.57 summarize the percentages of vertical displacement received by the loaded beam and the percentage of load received by the loaded beam, respectively, for the three loading cases, for each of the specimens. A similar trend among the results found for the various specimens can be seen despite the difference of magnitudes.

Distributions associated with displacements measured at mid- or quarter-span show the same trends and lead to identical conclusions. The influence of the span over the distribution is clear, with the graph limited above by the distributions of the shortest span specimen and below by the one with the longest span. Also the proximity between the distributions found for the *Base specimen*, S1, and the longest span specimen, S5, is highlighted, particularly when there is a point loading.

Concerning the distribution of support reactions, the specimen with the shortest span, S4, showed that except for the loaded beam, there is very little contribution of the remaining beams in receiving the applied load. A maximum load spreading of 27 % was found when the load was applied at the central beam mid-span, Fig. 4.42. This is owing to its limited capability for transversal load transfer. To transfer the load from the loaded point to the supports, deformation must occur. However, when the ability to deform is limited, due the higher stiffness of the structure or beam over which the load is applied, the supports associated with the loaded beam tend to “attract” a higher percentage of load, than a more flexible one. By opposition, the specimen with the longer span, S5, clearly shows a wider load spreading (66 % of maximum load spreading, found for B2 ½) and consequently, a higher effectiveness in distributing the load to the supports under each beam, Fig. 4.43. Its longer span turns it in to a more flexible specimen, which, for the same load level, undergoes a greater deflection. The greater deformation capacity increases the specimen’s ability to transfer the load, from the loaded beam to the remaining ones. This leads to a more uniform load distribution, and consequently to a structure where all the beams contribute in a more expressive way to support the applied load.

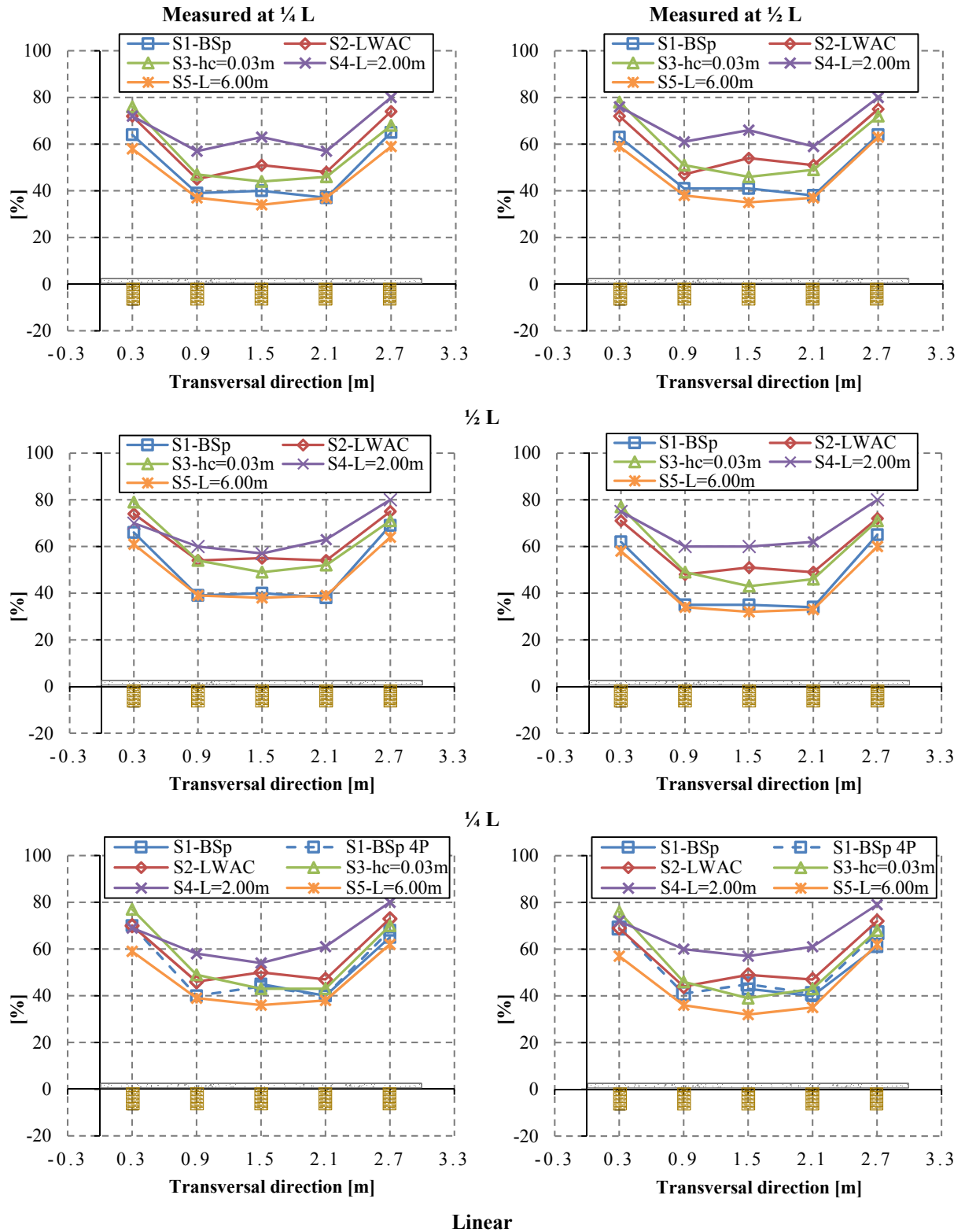


Fig. 4.56 – Distributions of vertical displacements for the loaded beam, by load case

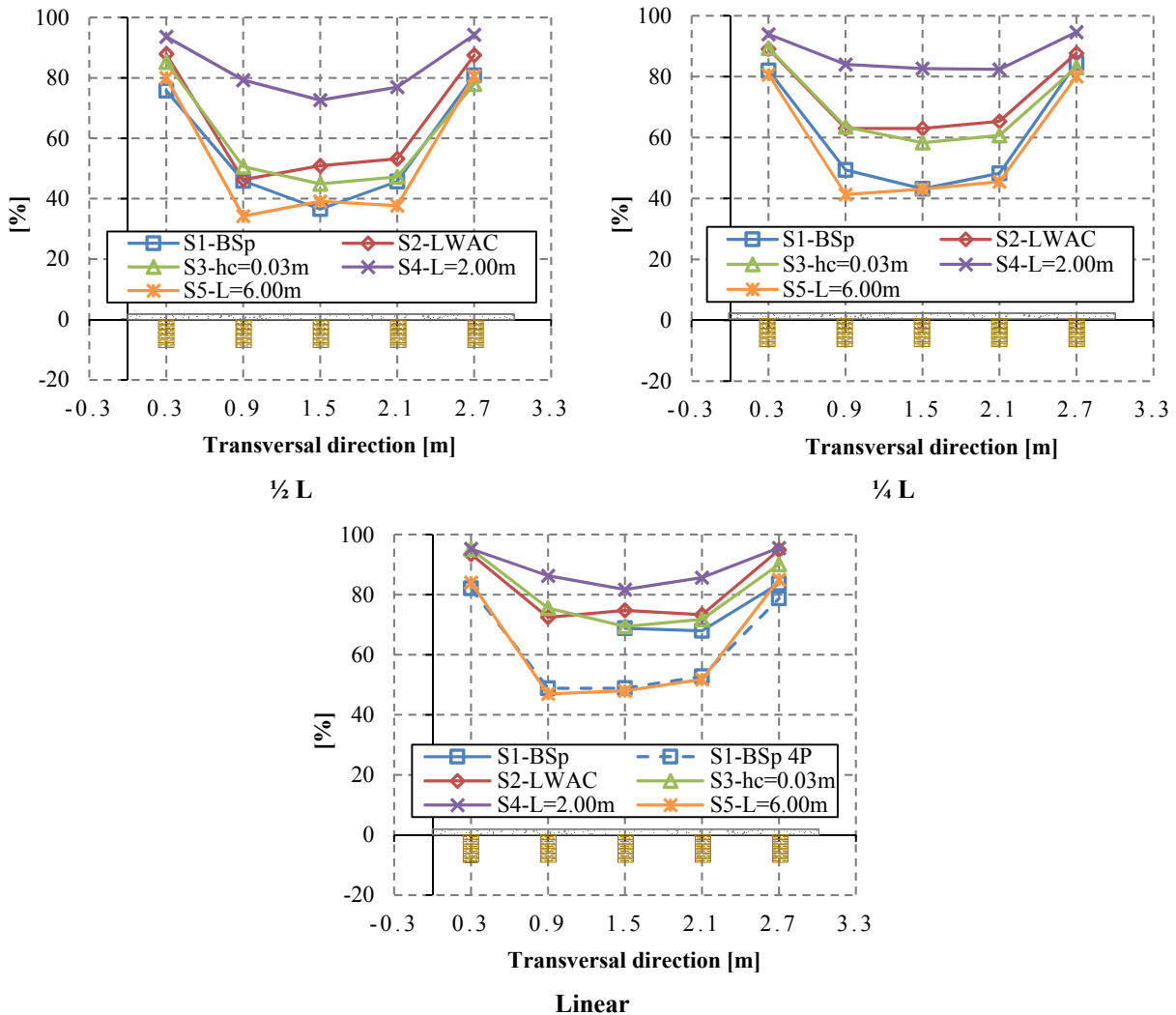


Fig. 4.57 – Distribution of support reactions for the loaded beam, by load case

The slab with the shortest span is the less favorable to load spreading while the one with the longest span is the most effective in terms of an even contribution of all transversal elements in resisting to concentrated loads. The use of a LWAC layer instead of a regular concrete, as well as a thinner concrete layer led to a less load spreading. Although with a similar spreading behavior, the loaded beams at S2 tend to attract more load than those of specimen S3.

With regard to the beams deflection, specifically to the percentages associated with the vertical displacement (vd) at the beam quarters, various deflection curves were drawn. Those corresponding to loading at the central beam, B3, for the five specimens are presented in Fig. 4.58. These percentages were obtained computing the relation between the beam deflection

and the maximum deflection for each load case, at that specific beam, $\frac{vd_i}{vd_{max}}$ with $i = \frac{1}{2} L$, $\frac{1}{4} L$ or $\frac{3}{4} L$, where vd_i is the vertical displacement at point i and vd_{max} is the maximum vertical displacement, both for the same load case.

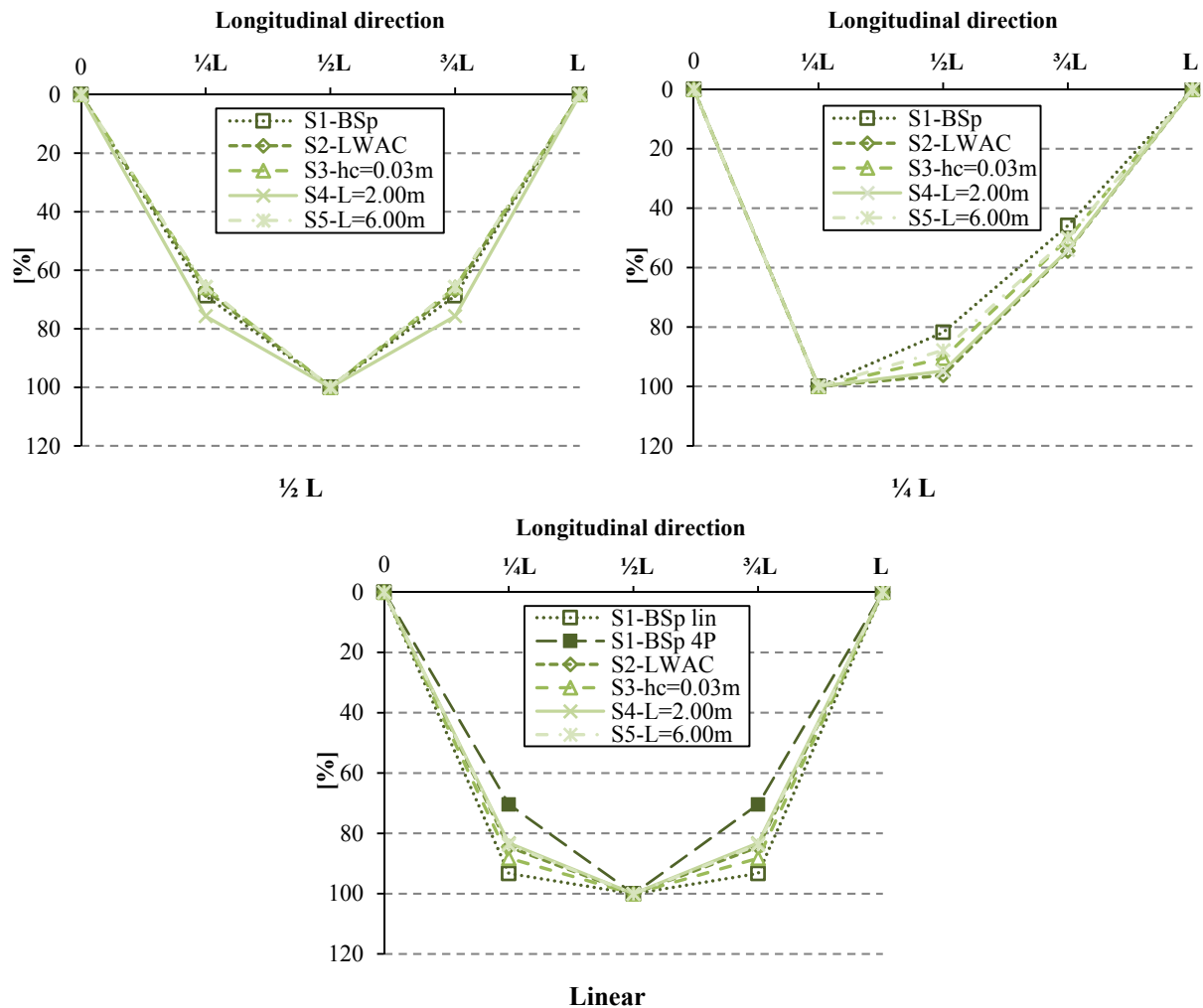


Fig. 4.58 – Distribution of deflections when the specimens were loaded at B3

These curves characterize the deflection shape associated with each load case and specimen. Concerning the symmetrical load cases, mid-span point load and line load, despite the symmetrical deflection, that was an assumption, it is possible to analyze the range in which vertical displacements at quarters of span vary. Thus, for the former case displacements at quarters seem to vary between 60 % and 80 % of the value recorded at mid-span. As for the line load case, the range of variation seems wider given the nature uniformly distributed of this load, with the vertical displacements at quarters varying between about 70 % and 90 % of

the displacement measured at mid-span. In both these load cases, the maximum vertical displacement was registered at mid-span, as for the point load applied at quarter-span, most of the times the maximum displacement was recorded at $\frac{1}{4} L$. For the last load case, displacements at three quarters-span were estimated with a magnitude varying between 40 % and 60 % of the maximum displacement, while displacements at mid-span showed to vary from about 80 % to 100 %. Table 4.18 summarizes these percentages, with the maximum displacement recorded in each load case and beam marked in bold.

Table 4.18 – Vertical displacement vs. maximum vertical displacement at the loaded beam

Specimen	Load case	Vertical displacement at $\frac{1}{2} L$					Vertical displacement at $\frac{1}{4} L$				
		[%]									
		Loaded beam					Loaded beam				
		B1	B2	B3	B4	B5	B1	B2	B3	B4	B5
S1	$\frac{1}{2} L$	100	100	100	100	100	71	68	69	68	72
	$\frac{1}{4} L$	94	83	82	87	93	100	100	100	100	100
	<i>lin</i>	-	-	100	100	100	-	-	93	82	89
	4P	100	100	100	100	100	72	71	70	69	73
S2	$\frac{1}{2} L$	100	100	100	100	100	69	67	67	64	67
	$\frac{1}{4} L$	100	91	96	97	100	100	100	100	100	96
	<i>lin</i>	100	100	100	100	100	85	81	84	78	89
S3	$\frac{1}{2} L$	100	100	100	100	100	68	63	66	65	68
	$\frac{1}{4} L$	100	92	90	92	100	99	100	100	100	100
	<i>lin</i>	100	100	100	100	100	84	88	88	80	94
S4	$\frac{1}{2} L$	100	100	100	100	100	75	77	76	76	74
	$\frac{1}{4} L$	92	90	95	87	94	100	100	100	100	100
	<i>lin</i>	100	100	100	100	100	81	84	83	91	81
S5	$\frac{1}{2} L$	100	100	100	100	100	70	66	66	68	66
	$\frac{1}{4} L$	99	88	88	90	100	100	100	100	100	98
	<i>lin</i>	100	100	100	100	100	86	84	84	84	79

Joining the percentages by loading case and measurement points, the distribution found for loaded beam, over the transversal direction, are presented in Fig. 4.59. These graphs highlight, not only the magnitude of displacement relatively to the maximum measured for a specific loaded beam and load case, but also the influence that analyzed parameters have in affecting those percentages. Looking at the graph associated with the point load at mid-span, the shortest span specimen (S4-L=2.00m) stands out as the specimen presenting the highest percentages. The lowest percentages, in turn, are shared between the longest span specimen (S5-L=6.00m) and the one with the thinnest concrete layer (S3-hc=0.03m). Concerning the loading at quarter-span, the percentages were generally higher for all the specimens, when

compared with the remaining load cases. For this loading case, almost all the lower percentages belong to the *Base specimen* (S1-BSp). About the linear load cases, the 4P load case stands out as the one associated with the lowest percentages. By its turn, the *lin* load cases showed relatively similar results for S1-BSp, S2-LWAC and S3-hc=0.03m, and between the specimens where the span was modified (S4-L=2.00m and S5-L=6.00m). Nevertheless, the behavior found for the last is not that close to the *Base specimen* (S1-BSp).

Although, it seems hard to relate the parameters and the manner in which the loaded beam deforms, an intricate relation exists between the percentages, the parameters, the beam position and the transversal “distribution” of the MOE of the timber beams. Fig. 4.60 evidences that relation. Thus, the extremity beams showed a trend to deform more, presenting consequently higher percentages of vertical displacement associated. Deflection on the inner beams tend to be distributed inversely to the beam MOE, as would be expected (although laterally joined through the concrete slab, the stiffer the beam the lower the deformation associated). Nevertheless, the degree this happens depends also on the effect of the changed parameter, and how it affects the stiffness of the specimen, and consequently the deformation associated with the loaded beam. The longer the span, the greater the ability to behave as a whole, distributing the load and its consequent deformation through the loaded beam and those adjacent, and the less the MOE of the timber beams will be felt in the portion associated to each beam. This become clear by analyzing the response for specimen S5-L=6.00m, Fig. 4.60. The similarity between the percentages associated with inner beams for each of the load cases stands out.

The effects that the analyzed parameters have in the design of the composite floors proved to be very important. The load distribution, evaluated through the analysis of the support reactions and the slab deflection, observed over each of the load locations, showed to strongly depend on the slab span. Parameters as the concrete thickness or strength also showed to have some influence, although in a more soft way, especially in the case of the strength.

4. EXPERIMENTAL ANALYSIS

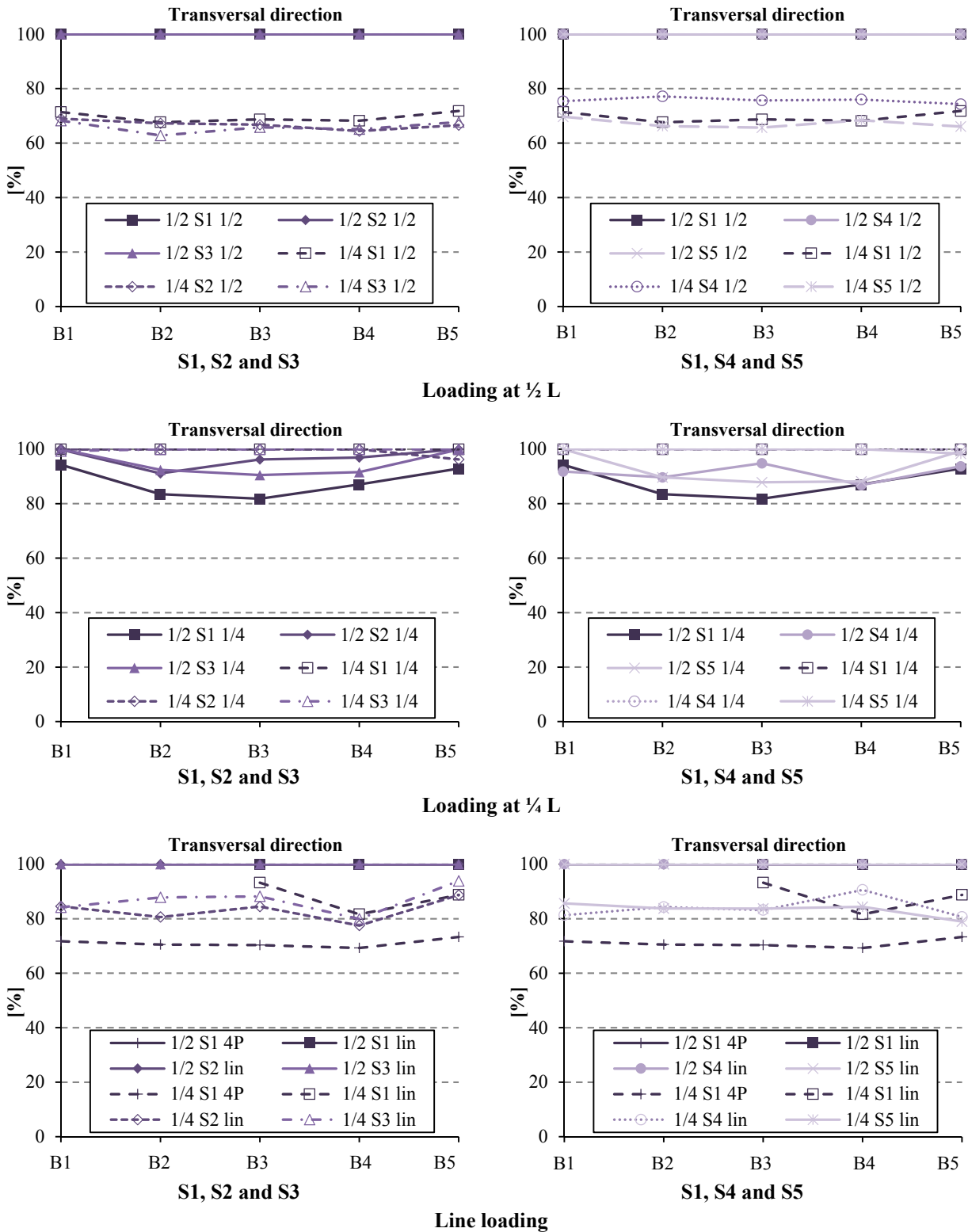


Fig. 4.59 – Transversal distribution of vertical displacements for the loaded beam

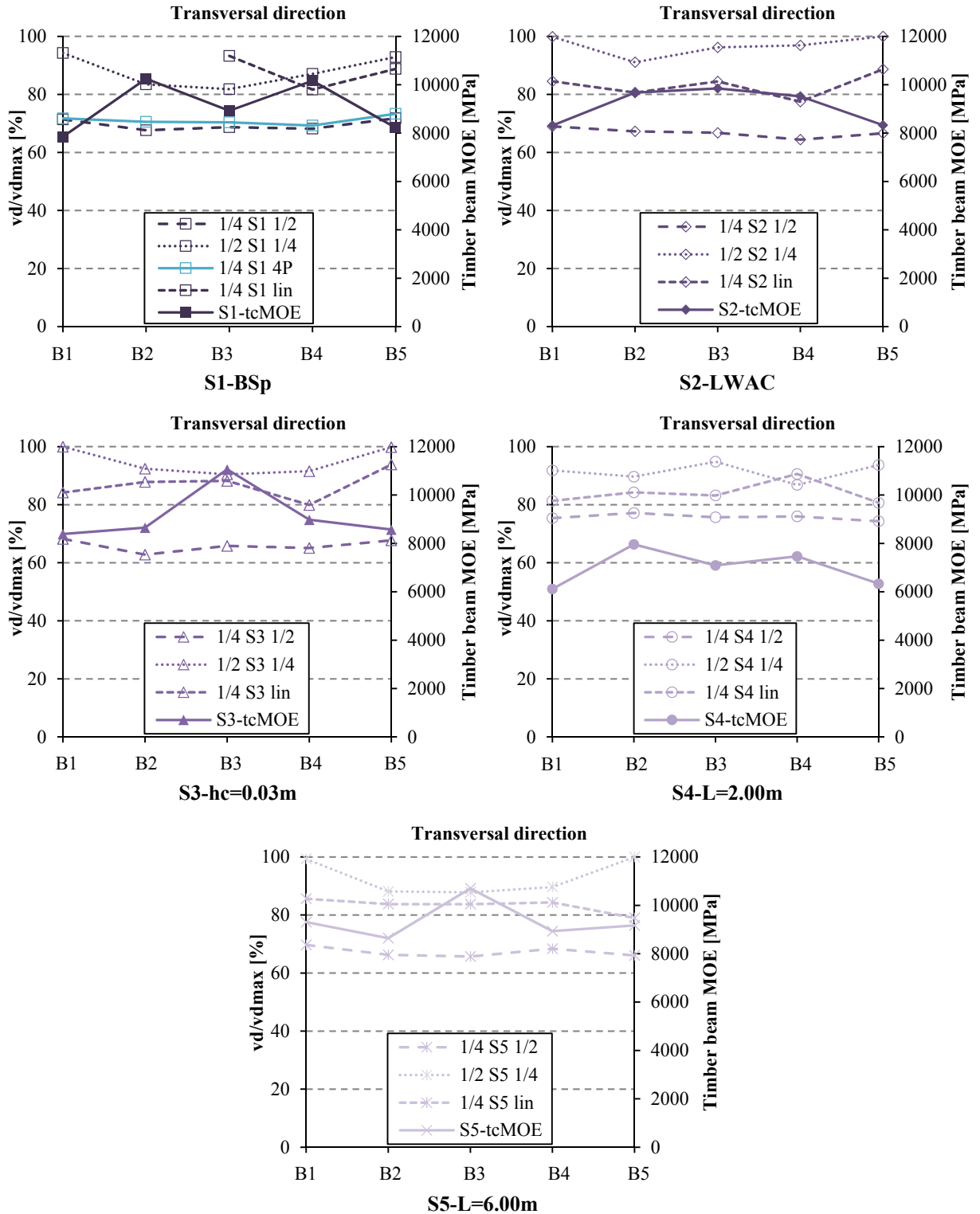


Fig. 4.60 – Transversal distribution of vertical displacements vs. timber beam MOE

4.5 Experimental vs. numerical results

As presented before, the current study intends to understand the distribution of load in the transversal direction. Aiming at attaining this goal it would be of great interest to utilize, in addition to the experimental tests, a numerical model capable of characterizing the behavior of the composite elements.

The Frame+Shell model, validated based on numerical models and experimental results (Monteiro *et al.* 2015), already proved its capabilities. Applied before to predict the ultimate load level for each beam, it was after used to model the experimental tests. It was composed by frame prismatic elements to represent the timber beams, and shell elements, to represent the concrete layer. Link elements were used to connect frame and shell elements, placed 0.20 m apart for specimen S3 and 0.10 m apart for the remaining. The geometrical properties were defined according to the real ones, Table 4.2. Regarding the material properties, a linear and isotropic material behavior was adopted, considering the data gathered in Table 4.4 and Table B.5. Also the connectors were defined using the linear properties listed in Table 4.6.

The frame elements were meshed with 0.10 m long elements, forty for S1-BSp to S3-hc=0.03m, twenty for S4-L=2.00m and sixty for S5-L=6.00m. As for the shell elements, a 0.10 m wide square mesh was defined, with the longitudinal direction matching the frame mesh. All the beams were considered to be simply supported. The loads were defined as point or line loads acting at the top surface of the shell element, considering the values listed at Table 4.7.

By performing an elastic linear analysis, the modeling of each specimen led to the vertical displacements at mid- and quarter-span, as well as the support reaction and the stress at mid-span associated with each beam, for the various load cases. Also the distributions in terms of displacements and reactions were computed.

The following sections present the comparison between experimental and numerical results for the mentioned parameters and the corresponding findings. The comprehensive results can be found in *APPENDIX B, B.3 - Results from the numerical analysis.*

4.5.1 Vertical displacements

The results, in terms of vertical displacements, are presented in *B.3.1 – Vertical displacements*. Fig. B.92 to Fig. B.116 summarize the vertical displacements numerically obtained for the five specimens and also the displacement percentage (Table B.13) received by each beam at every measuring location for the several loading cases. The numerical results designation is preceded by the tag “*Disp.*”, while the experimental ones are identified by the tag “*Exp*”. Follows the measuring location, $\frac{1}{4}$ for the quarter-span and $\frac{1}{2}$ for the mid-span. Also the loaded beam is identified, with the loading case ($\frac{1}{4}$, $\frac{1}{2}$ and *lin*).

As Fig. 4.61 shows for B3 and B4 in S1-BSp, in general numerical results showed to have the same trend as the experimental ones. Fig. 4.62 presents the vertical displacements obtained for the central beam in S3 and S2, the specimens to which the numerical values were farther and closer to the experimental ones, respectively.

The highest vertical displacement happened underneath the loaded beam, decreasing from this beam in both directions. Concerning the magnitude, mid-span load case showed to be the one leading to the highest vertical displacements for all the specimens that were modeled, and displacements at mid-span, except when the load was applied at quarter-span, showed to be higher than those obtained at quarter-span (ex.: Fig. 4.63 for B2-GL24 in S5). In terms of percentage distribution, and considering the loaded beam, similar values were found for the three loading cases (Table B.13).

Also, significant spreading of displacements between the five beams for the several load cases was found, varying between:

- 41 % (1/4 B1 1/4) and 72 % (1/2 B3 1/4) in S1;
- 43 % (1/4 B1 1/4) and 73 % (1/2 B3 1/4) in S2;
- 22 % (1/4 B5 1/4) and 56 % (1/2 B3 1/4) in S3;
- 20 % (1/4 B1 1/4) and 51 % (1/2 B3 1/4) in S4; and
- 46 % (1/4 B5 1/4) and 75 % (1/2 B3 1/4) in S5.

Thus, the maximum spreading was always associated with the vertical displacement measured at mid-span when the central beam was loaded at quarter-span. This was consequence of the increased capability of the central beam to spread the load to the adjacent ones. Together with the fact that, when the load was applied at quarter-span, the vertical displacement was higher than the one measured at mid-span. Concerning the minimum spreading, it is always associated with the loading at quarter-span and at the extremity beams, either B1 or B5.

4. EXPERIMENTAL ANALYSIS

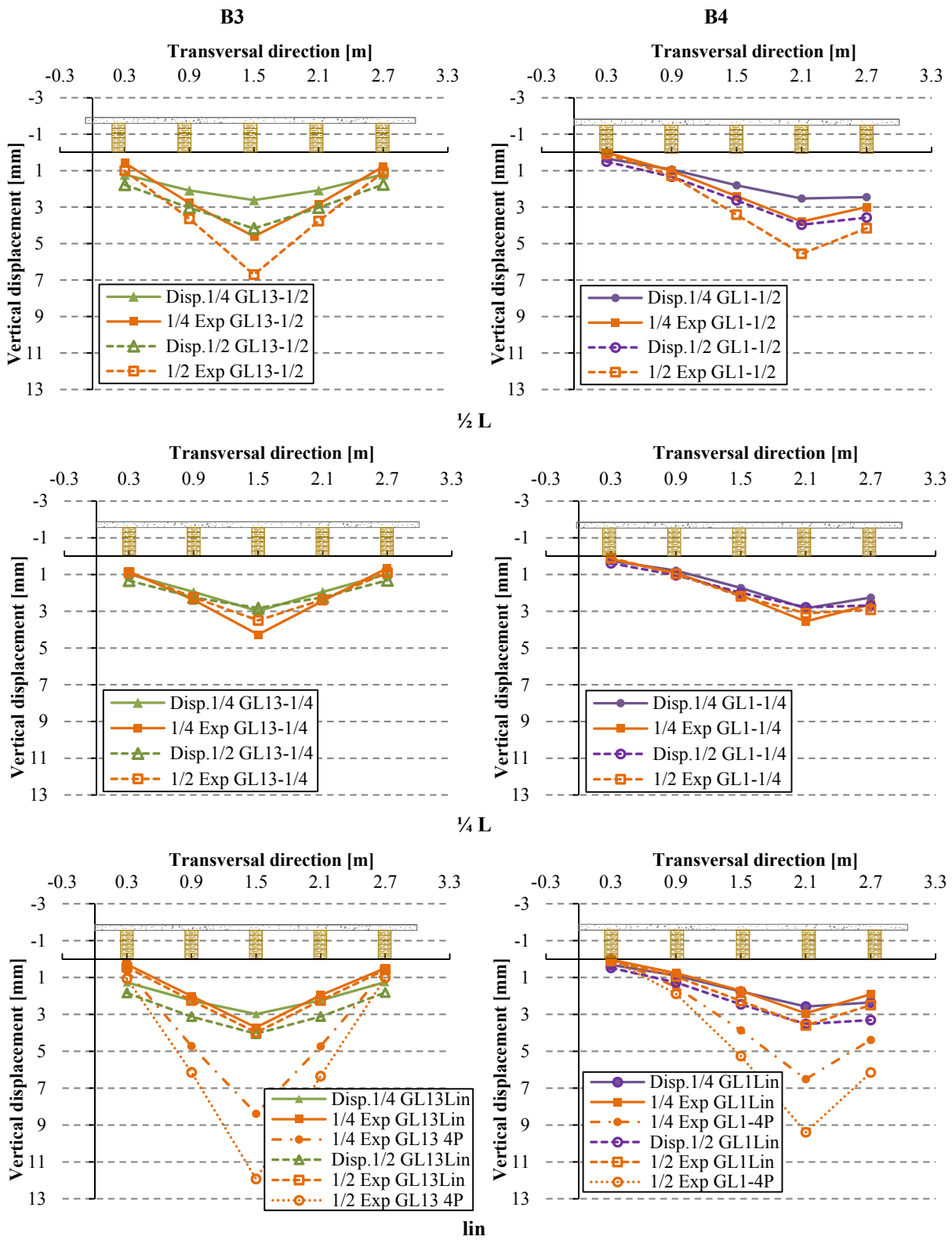


Fig. 4.61 – Experimental and numerical vertical displacements: S1 when loaded at B3 and B4

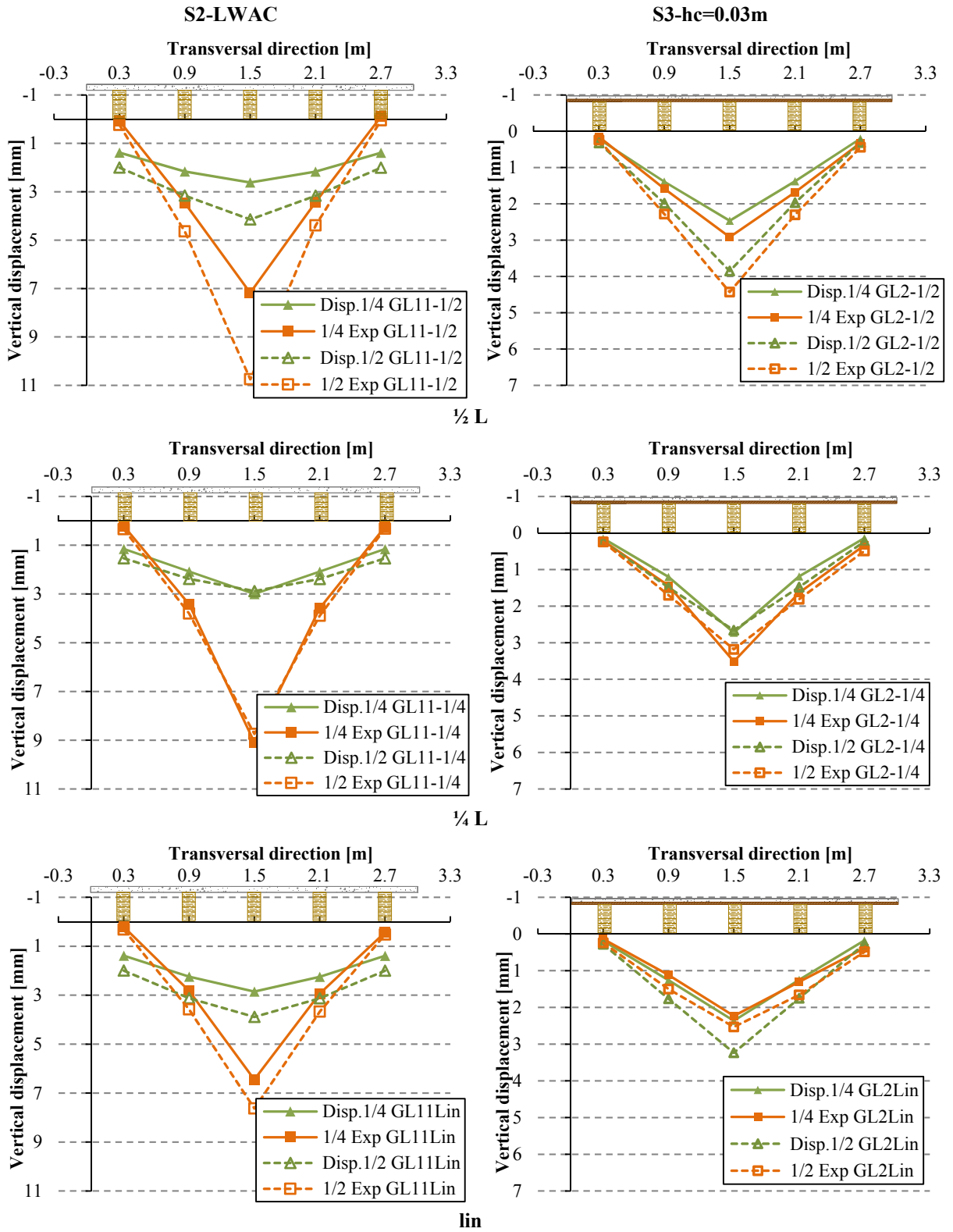


Fig. 4.62 – Experimental and numerical vertical displacements when loaded at B3: S2 and S3

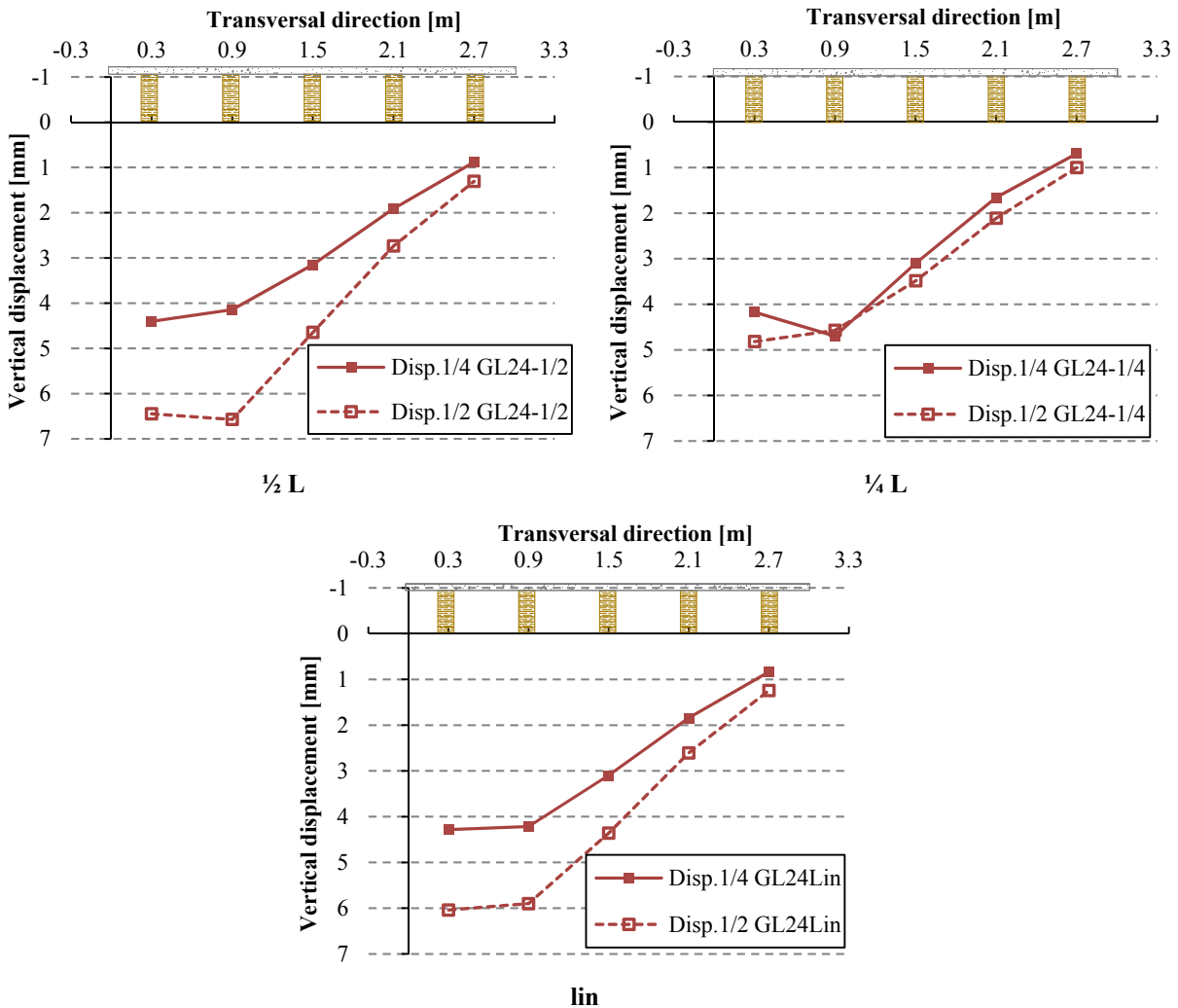


Fig. 4.63 – Numerical vertical displacements: S5 when loaded at B2

Fig. 4.64 shows the tridimensional deflection associated with the five specimens for the load applied at mid-span of the central beam, obtained with the numerical model. The trend of the vertical displacement to occur right below the point of application stands out, as well as the different behaviors of the various specimens for the same loading. Thus, S4-L=2.00m showed to be the specimen which concentrate the most the deflection under the load location. By opposition, S5-L=6.00m is the one which most spreads the deflection over the all slab. Also the specimen with a thinner concrete layer, S3-hc=0.03m, shows the same trend as the longest one, S5-L=6.00m. S1-BSp and S2-LWAC showed relatively close deformed shapes.

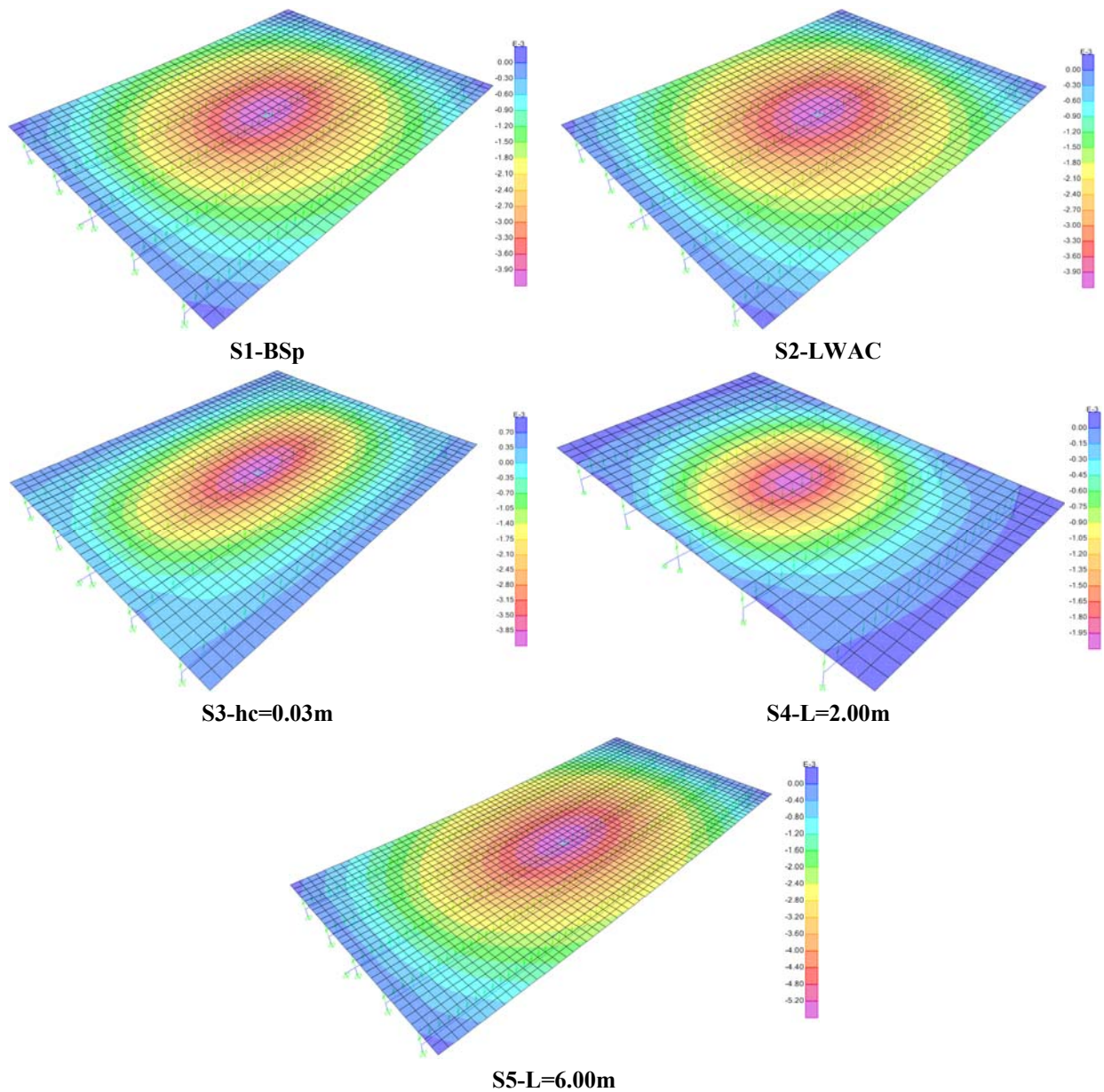


Fig. 4.64 – Numerical modeling deformed shape for the central beam loaded at mid-span

4.5.2 Support reactions

Concerning the support reactions, results are presented at Section *B.3.2 – Support reactions*, graphically in Fig. B.117 to Fig. B.141 and explicitly in Table B.15. Support reaction distribution, experimentally and numerically obtained, are presented using a symbology similar to the one adopted for the numerical vertical displacements.

Fig. 4.65 and Fig. 4.66 summarize the support reaction distribution, experimental and numerical, associated with S2 and S3 respectively, for the various load cases and loaded beams. Like it was found for the vertical displacements, numerically obtained support reactions showed to be very close to the experimental ones, for all the loading cases (Table B.16). This led to the characteristic behavior associated with each of the modeled specimens.

The loaded beam was the one with the highest percentage of the support reaction. The manner in which the remaining beams are requested depends on the specimen, more specifically in how each parameter affect its behavior. The extremity beams, contrarily to the central ones, are the ones associated with the higher percentages when loaded, which means that the spreading percentages to the other beams are the lowest ones. Significant spreading of support reactions was found, Table 4.19, with the percentages varying between:

- 65 % (B3 1/2) and 11 % (B5lin) in S1;
- 66 % (B3 1/2) and 11 % (B5lin) in S2;
- 50 % (B3 1/2) and 7 % (B5lin) in S3;
- 44 % (B3 1/2) and 5 % (B5lin) in S4; and
- 69 % (B2 1/2) and 15 % (B1 1/4) in S5.

There is a regularity in the beam *vs.* load case for the extreme spreading for all the specimens but S5-L=6.00m. Usually, the maximum spreading was associated with the central beam when loaded at mid-span, and the minimum spreading with B5 when the load was linear. As for the longest span specimen, the maximum spreading was associated to the mid-span loading in B2, as found experimentally, while the minimum occurred when B1 was loaded at quarter-span. By analyzing Table 4.19, the tendency that this specimen had to spread the load in a greater degree than the remaining is highlighted. Very similar spreading percentages were found for the three load cases and also among the extremity beams and among the three inner ones. For this specimen, B2 is the one supporting to the lowest share of load, above 30 %, and the extremity ones tend support about 80 % of the applied load. Once more, S4 and S5 seem to present the extreme values in terms of ability to spread the applied load to the beams other than the loaded one. S4 tends to concentrate the support reactions over the loaded beams, more obvious for the extremity ones, receiving above 90 % and the inner ones above 60 %. As well as the experimental results shown, also the numerical analysis led to the mid-span loading as the one providing the widest load spreading (39 % on average), by opposition to the line load case, associated with the lower load spreading (31 % on average).

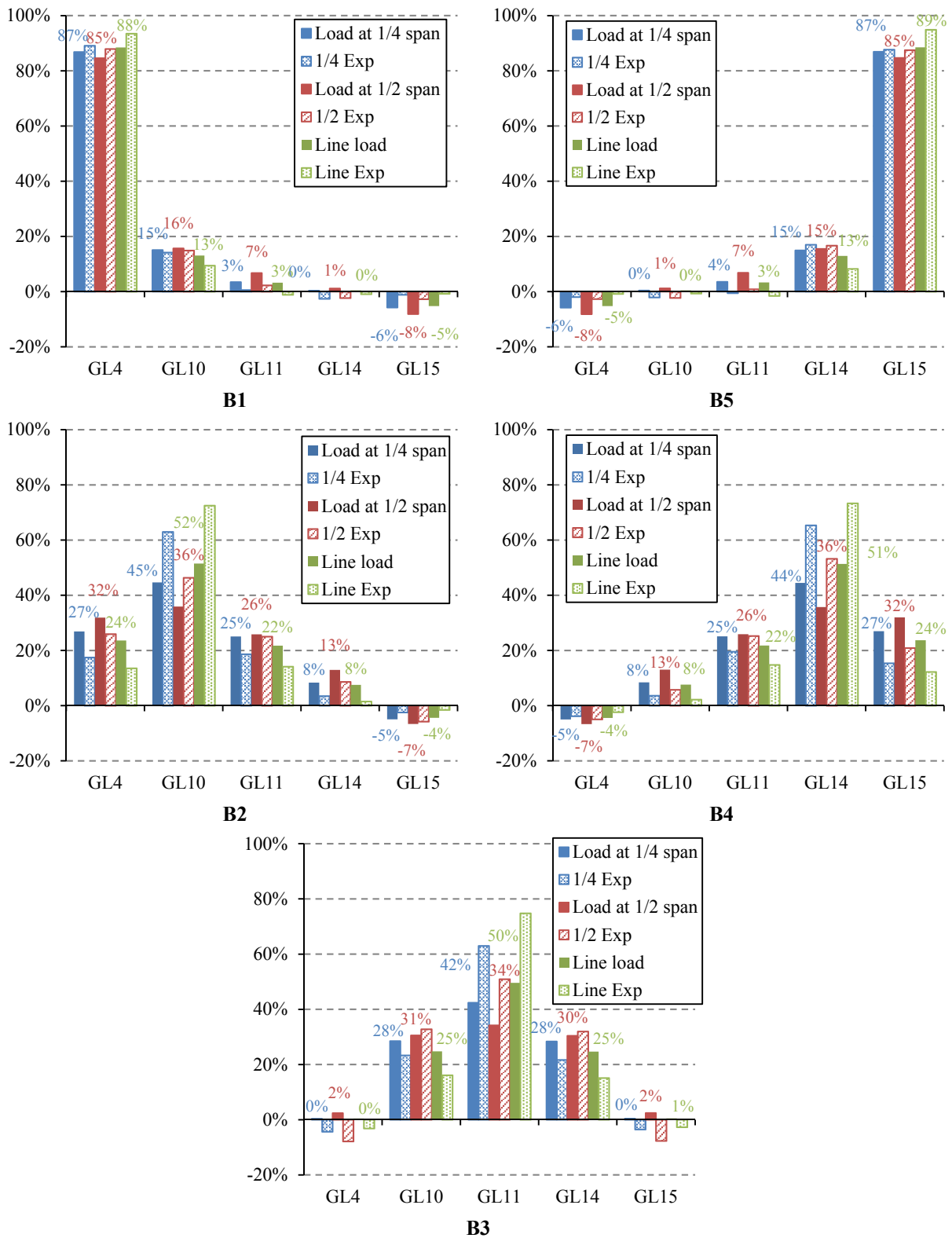


Fig. 4.65 – S2: experimental and numerical support reaction distribution

4. EXPERIMENTAL ANALYSIS

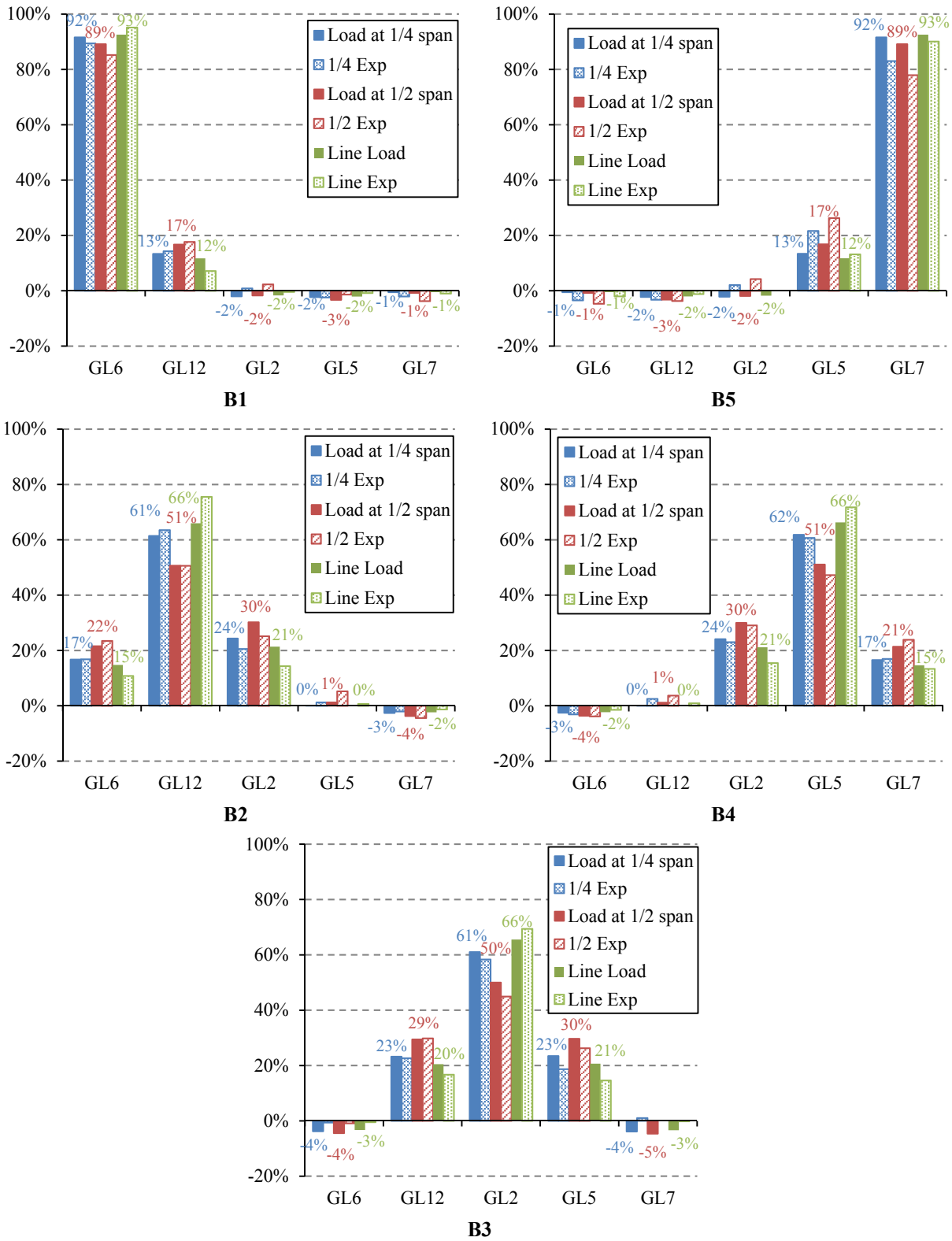


Fig. 4.66 – S3: experimental and numerical support reaction distribution

Table 4.19 – Numerical support reaction spreading summary [%]

Floor specimen	Extreme	Load case		
		$\frac{1}{2}$	$\frac{1}{4}$	<i>lin</i>
S1-BSp	max	65	56	49
	med	43	37	32
	min	15	12	11
S2-LWAC	max	66	58	50
	med	45	39	34
	min	15	13	11
S3- hc=0.03m	max	50	39	34
	med	34	27	23
	min	11	8	7
S4-L=2.00m	max	44	34	31
	med	27	21	19
	min	7	6	5
S5-L=6.00m	max	69	62	64
	med	48	43	45
	min	17	15	16
Average spreading		39	33	31

In terms of magnitude, as was found through the experimental results, the line load case is the one leading to the highest support reactions associated with the loaded beam, for all the modeled specimens, with the loading at the beam mid-span showing the opposite.

Once again, the effects that the parameters analyzed have in the mechanical behavior of these timber-concrete composite floors are highlighted through this numerical analysis, Fig. 4.67. By analyzing the graphs relating the percentages of support reaction associated with the loaded beam, it is clear the influence that the span has on the results. The distributions are limited above by the specimen with the shortest span and below by the specimen with the longest span.

Furthermore, the use of the developed model to predict the behavior of such structures is trusted with these results.

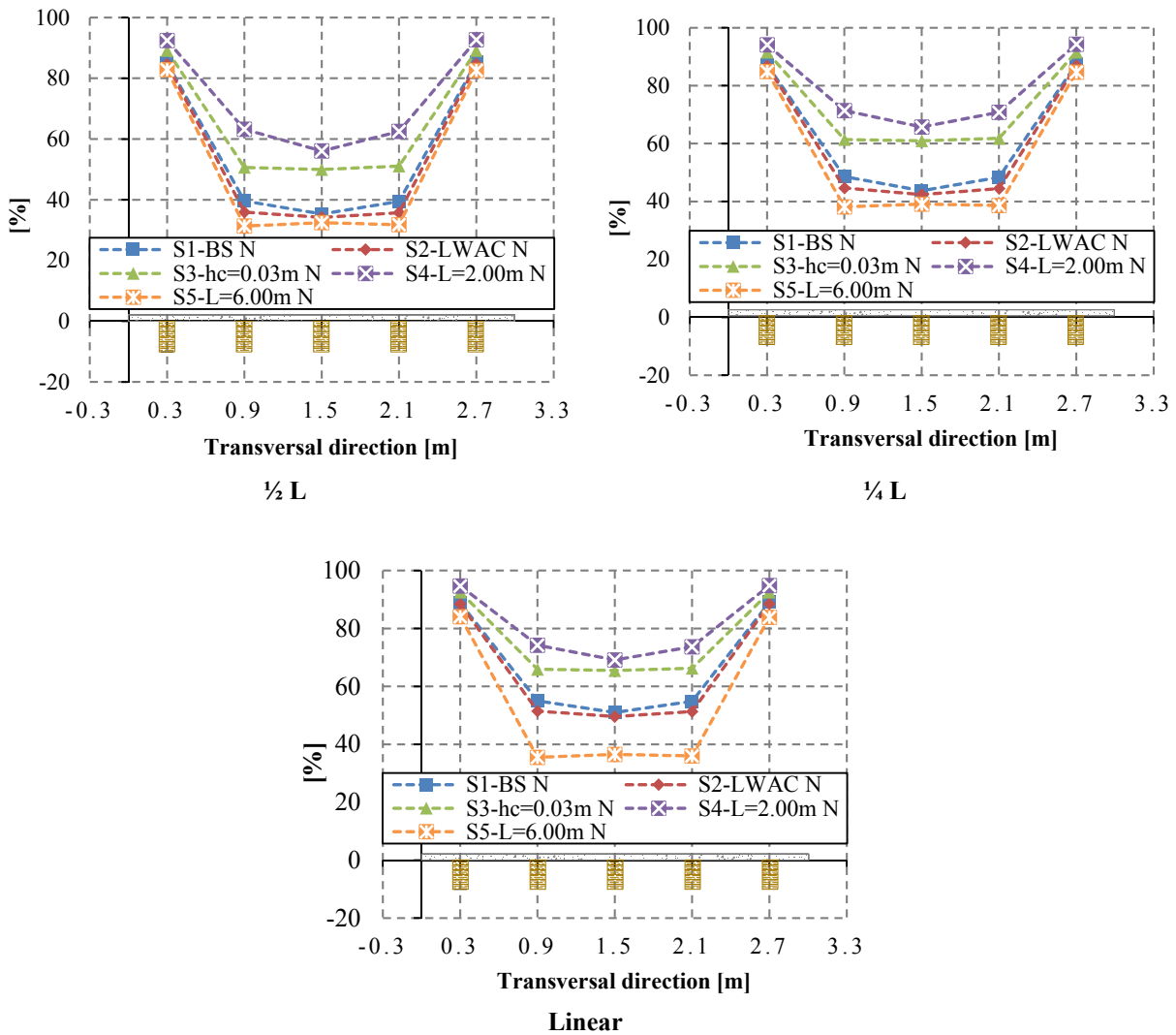


Fig. 4.67 – Numerical distribution of support reactions for the loaded beam, by load case

4.5.3 Stresses

Based on the experimental strain results the corresponding stresses were computed and compared with those from the numerical modeling. A linear behavior was assumed until failure, which as Fig. 4.54 shows is not far from the truth. Table B.16 summarizes the stresses computed based on the strains found for each loaded beam and the corresponding stresses numerically obtained. The cross-section of reference was considered that at mid-span of the loaded beam. Since the strains were measured at the bottom face of the timber beams that was

the face considered to perform the comparison. The strain values used to calculate the stresses correspond to the mean value of the two strain gauges.

Fig. 4.68 graphically depicts the gathered information for some of the loadings at mid-span, with the numerical results denoted with an “N”.

The numerical results show a clear trend to follow close the experimental ones. Considering the loaded beam, the stresses predicted numerically seemed to be closest to the experimental values when the load was applied at mid-span of B2, in specimen S3-hc=0.03m. The loading case for which the numerical stresses were further from the recorded ones were associated with the loading at mid-span of B1, for the specimen S2-LWAC. These findings are in accordance with those presented for the remaining quantities.

Concerning the failure tests, specifically the loading of the central beam, the results at Fig. 4.69 were obtained. As was found before, generally, the numerical stresses presented a tendency similar to the experimental ones. Indeed, for specimen S3-hc=0.03m a very close prediction was obtained for the stresses across the beams, with the experimental and the numerical stresses being almost coincident, Fig. 4.69. Even though, specimens as S2-LWAC and S4-L=2.00m did show some differences. This behavior follows the findings of the support reaction analysis, at the previous section, *i.e.* for the tests performed for a load level of 40 % of the ultimate load. Thus, when the load was applied at mid-span of the central beam of specimen S2-LWAC, the support reaction percentages found with the numerical predictions tended to be lower than those coming from the experimental results, see Fig. 4.65 (B3) and Fig. B.124. A similar trend was found when analyzing the support reaction distribution for B3 ½ of S4-L=2.00m, Fig. B.134. This tendency seems to increase around the failure load. Nevertheless, as the strain gauges were the only equipment applied at the specimen during the failure tests, this can not be confirmed.

4. EXPERIMENTAL ANALYSIS

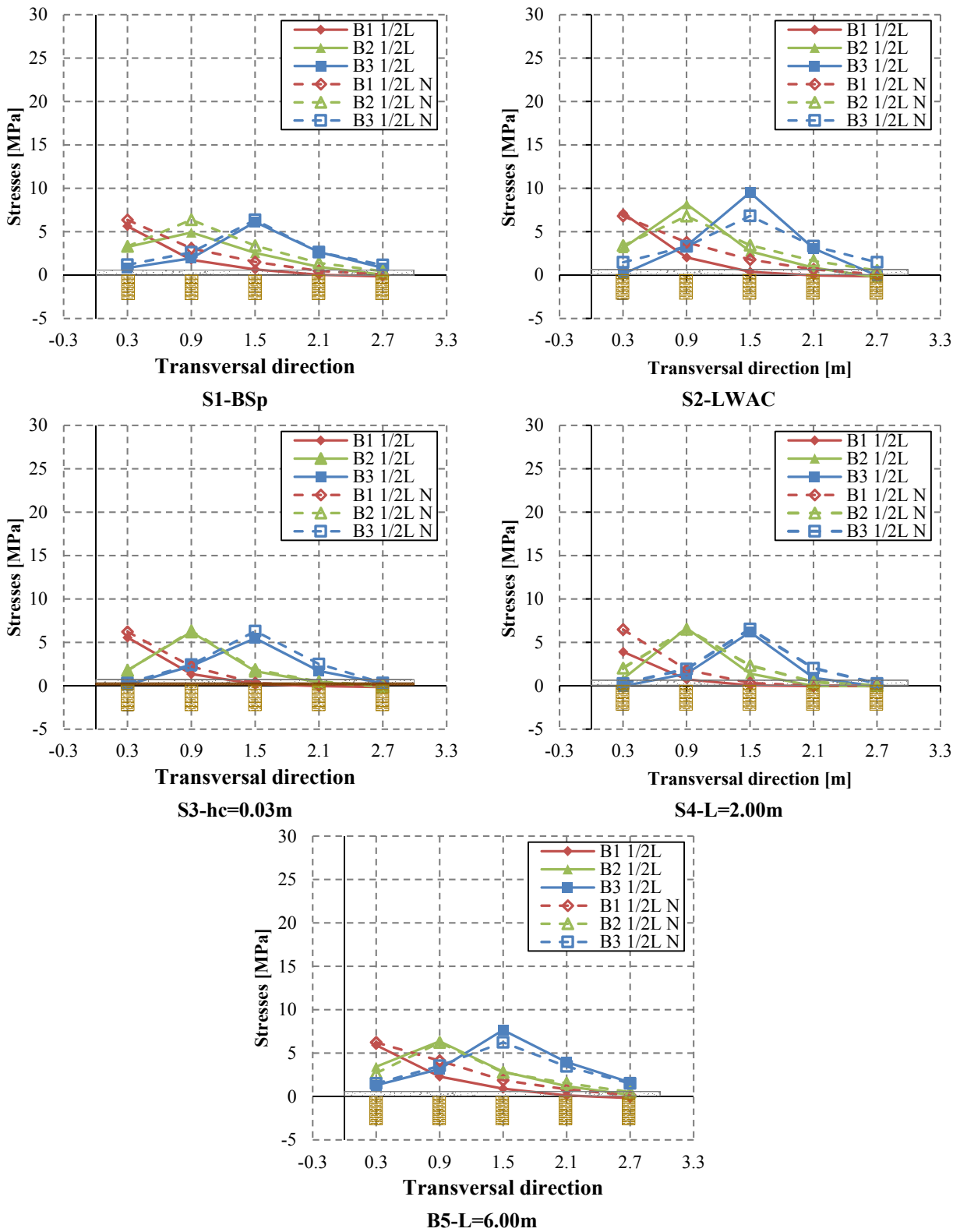


Fig. 4.68 – Stresses at each beam mid-span for load tests at B1 1/2 L, B2 1/2 L and B 3/2 L

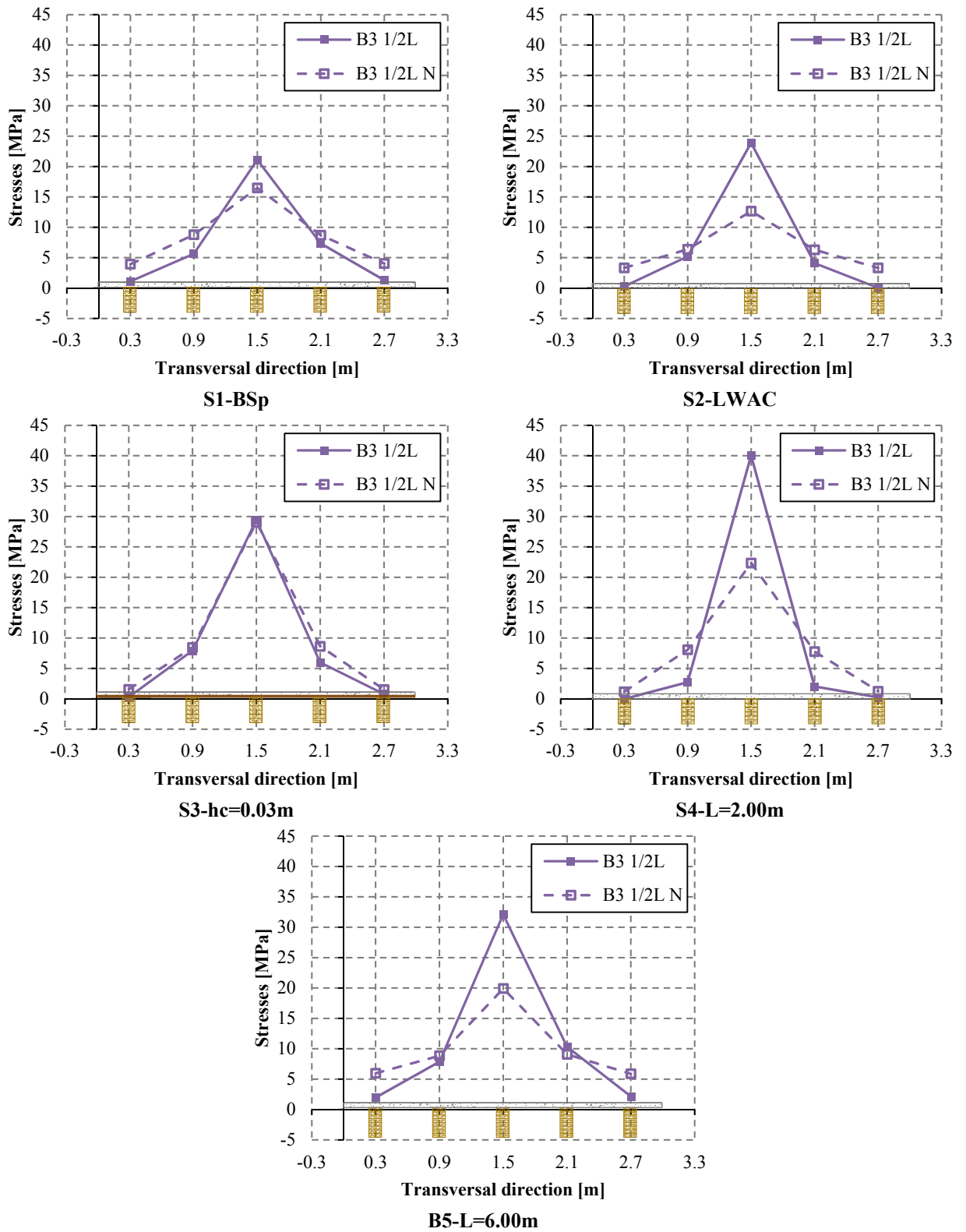


Fig. 4.69 – Stresses at each beam in failure test (loading at B3)

4.6 Summary

In general, the results clearly show the existence of transversal load distribution. Also, with no surprise it was found that the loaded beam tend to be the one that takes the greatest slice of load, as well as that with the highest vertical displacements, slip displacements and strains. The way in which the remaining beams participate in the distribution depends on the loaded beam position and on the specimen characteristics, with the span affecting it very strongly. Thus, in the shortest span specimen, S4, the only beams that seem to support the applied load are those to which the load is applied and in less extend those immediately adjacent. By opposition, in the longest span specimen, S5, a wider load spreading was found. This is valid not only for the support reaction distribution, but also for the various quantities that were analyzed.

A relatively similar trend was found for the results obtained for the three load cases, in all the specimens, whether for vertical displacements, Fig. 4.56, or support reactions, Fig. 4.57. As for the slip displacements and the uplift at the upper layer corners, relatively low magnitudes were found. For both, as for most of the quantities that were analyzed, the most even situation happened for the point load at mid-span. However, for strains an exception happened: the point load at quarter-span led to a wider spreading of strains, when compared to the remaining load cases.

Concerning the essential design quantities, as are the vertical displacement and support reactions, the numerical results showed the same trend as the experimental ones, and in some cases prove to be very close. This is the case of the specimen with the thinner concrete layer, S3. Between the three quantities numerically studied, the support reaction was identified as being the one that most closely matches the experimental findings. In terms of load spreading, for the loaded beam, the absolute mean differences between experimental and numerical results showed to be lower than (\pm) 10 %.

Also the stresses showed rather good agreement between experimental and numerical results, for the tests performed at the elastic range (load level around 40 % of the ultimate load), presenting similar trends when the load rises until the failure value.

All this supports the adequacy of the developed model to predict the load distribution of the timber-concrete floors that were considered. The use of numerical models is therefore, unquestionably, an important tool in the study of structural elements, provided it is capable of predicting the actual behavior of the modeled element. That was the case of the Frame+Shell model, previously validated, and used in this chapter.

5. SENSITIVITY ANALYSIS

5.1 Introduction

Although, some studies based on numerical modeling were found (Chiewanichakorn *et al.* 2004, Gara *et al.* 2009, Nie *et al.* 2008, Simon 2008), there are undeniable advantages that numerical models are accompanied by experimental tests. This is commonly accepted and the investigation presented in the previous chapters of this thesis do confirm this. With a validated model, it is possible to predict the actual behavior of the real floors, and also to study the effects of some parameters on their response (Oliveira 2002).

Thus, the already validated model is used to perform a parametric study. This numerical analysis aimed at evaluating the effects that a set of parameters have on the structure behavior when subjected to the loading conditions in study. Specifically, the transverse distribution of forces within the structures under concentrated loads is investigated. The set of parameters comprises the geometries, material properties, loads configurations and support conditions that are likely to be found in real structures. Questions as the degree in which the beams' cross-sections are used (if there is a oversizing or an undersizing of those sections when compared with the requirements specified in EC5 (EN1995 2004a)), showed to be of great importance in the behavior of timber-concrete floor systems, subjected to concentrated loads.

Based on the knowledge collected on the behavior of timber-concrete floor systems subjected to concentrated loads concerning the transversal distribution of load, a quick evaluation model to be applied together with the behavior models specified in applicable standards (EN1995 2004a) is proposed. The solutions presented intend to contribute to make the use of timber-concrete floors feasible in a wide set of situations, in bridges or building floors, either in rehabilitations or in new constructions.

5.2 Parametric study

With a validated numerical model it is possible to study the transversal load distribution for several conditions such as different connection stiffness, different span lengths or timber cross-sections, among others, by varying these characteristics at the composite floor simulation. As the results for the previous section showed, it is clear that the concentrated load is transversally distributed. Different slab configurations led to different degree of distribution of internal forces, but an important amount of distribution always took place.

Based on the explanation, a set of parameters aiming at analyzing the effects that they might have on the behavior of timber-concrete floor systems when subjected to concentrated loads was defined.


In a first phase, the main goal of the numerical study was to establish the experimental program. Therefore, a comprehensive group of parameters was gathered and, focusing in the actual characteristics of a timber-concrete composite floors, their boundaries were established. The set comprises the following:

- Span: 2.00 to 8.00 m;
- Width: 3.00 to 7.60 m, considering square and rectangular geometries for the floor;
- Beams spacing: 0.10 to 1.0 m, with the minor value intending to simulate a composite slab where the timber beams are juxtaposed (performed with rectangular section beams of 0.10 m width), creating a “timber slab”;
- Heights: of the concrete slab: 0.05 to 0.10 m; of the timber beams depending on the design requirements (EN1995 2004a), considering different cross-section shapes (rectangular, I-shape and round), with a minimum of 0.10 m; and of the timber interlayer: 0.00 to 0.02 m performed by timber floorboards, with the zero value simulating the inexistence of this layer;
- Concrete properties: Regular concrete (*RC*) C16/20 and C40/50; Light-weight aggregate concrete (*LWAC*) L16/18 and L35/38;
- Timber properties: Solid wood (Softwood - C14; Hardwood - D60); Glulam (GL24h and GL32h); Laminated veneer lumber (LVL) (Kerto-S, Kerto-Q); OSB + LVL; CLT;
- Material behavior: linear elastic (*LE*), elastic perfectly plastic (*EPP*);
- Connection: the connector spacing was assumed constant and equal to 0.10 m; for the stiffness (linear and non-linear behavior), aiming to cover a wide range of connections commonly used, a low (*lK*), a medium (*mK*) and a high stiffness connection (*hK*) were defined with slip modulus of 3000, 12000 and 100000 kN/m, respectively;
- Load type: point loads (*Pt*) at every beam mid-span and line loads (*Ln*) along each beam longitudinal axis, defined according to EC1 (EN1991 2001);
- Support conditions (*Sc*): simply supported (*Ss*) in two and in all ends (*Sae*); and fixed in two ends (*Fx*).

Since there were many variations in the parameters, the essential information is summarized in Table 5.1, and it complements the presented before. The values corresponding to the *base simulation* (*Bs*) are presented in bold. This modeling is the one to which the remaining were compared, serving as base modeling.

In a subsequent phase, the findings from the preliminary analysis led to a narrowing of field of the study to some parameters whose effects were more significant, as will be shown ahead.

Table 5.1 – First phase parameters

Parameter	Span	Width	Beam spacing	Height			Section	Concrete	Timber	Connection	Material behavior	Support conditions	Loading ^a	Imposed loads ^a
				Concrete layer	Interlayer	Beam								
	[m]	[m]	[m]	[m]										
Span	2.00 4.00 5.00 8.00													
Width		2.20 3.00 4.00 6.00 7.60												
Beam spacing			0.40 0.60 0.75											
Height				0.02 0.03 0.05 0.07 0.10	0.00 0.02	0.20								
Section														
Concrete							RC LWAC							
Timber								Solid Glulam LVL OSB+LVL CLT						
Connection									<i>lK</i> <i>mK</i> <i>hK</i>					
Material behavior										<i>LE</i> <i>EPP</i>				
Support conditions											<i>Ss</i> <i>Sae</i> <i>Fx</i>			
Loading ^a												<i>Pt</i> <i>Ln</i>		
Imposed loads ^a														A C4

^a – Defined according to (EN1991 2001)

The *Bs* modeling intends to characterize a square timber-concrete floor with 4.00 m side (as shown in Fig. 3.39). It is composed by seven C24 solid timber beams (according to (EN338 2003)) 0.60 m apart from each other with a rectangular (*Rt*) cross-section 0.10×0.20 m, and a C25/30 concrete layer 0.07 m thick. Between the timber beams and the concrete layer there is an interlayer 0.02 m thick, joined together by a connector system every 0.10 m. The connection stiffness was assumed to be 12000 kN/m. The beams are simply supported (*Ss*) in both ends. Concerning the loading, besides the self-weight (*sw*) of all the elements that compose the composite floor, two loads cases were considered to be acting uniformly distributed over the concrete upper surface. A point load of 9.0 kN acting vertically above each beam mid-span or a line load of 4.5 kN/m acting along each beam longitudinal axis. The concentrated loads were considered applied to all the beams, one at a time, and their values were set according to EC1 (EN1991 2001).

To perform this numerical analysis, the Frame+Shell was the chosen model, Fig. 5.1. The choice was made by weighing its ability to simulate the overall behavior of the composite floors in question, the simplicity of application and the time consumption when compared with the models presented before, as the Grid and the Solid models. Thus, based in the information gathered in Table 5.1 several modeling were performed.

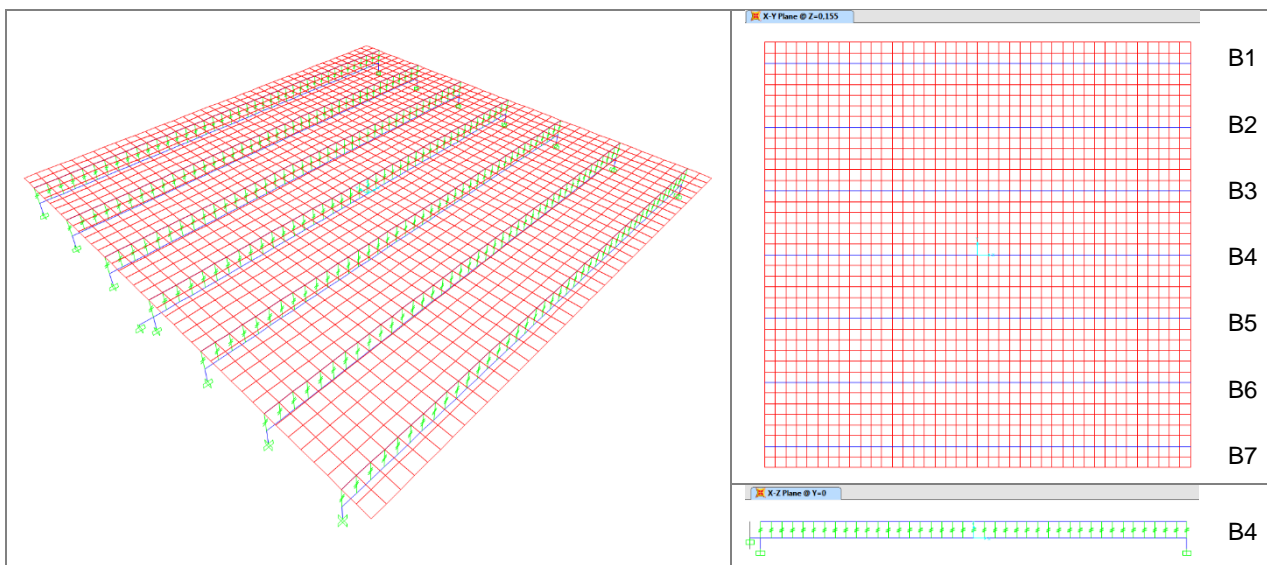


Fig. 5.1 – *Bs* modeling scheme

Table C.1 widely lists the modeling which were considered to perform the numerical analysis in the first phase, as well as their characteristics and denominations. Here, this information is summarized in Table 5.2, which gathers the *Bs* modeling characteristics, and in Table 5.3, which synthetizes the information about the remaining modeling relatively to *Bs*.

Table 5.2 – *Bs* modeling characteristics

Denomination	Span	Width	Interlayer	Connection stiffness	Beams			Concrete height	Timber	Concrete	Support conditions	Loads
					Spacing	Width	Section					
					L [m]	b_{slab} [m]	h_i [m]					
<i>Bs</i>	4.00	4.00	0.02	12000	0.60	0.10	R_t , 0.20	0.07	C24	C25/30	S_s	s_w , P_t , L_n

Table 5.3 – First phase modeling: description and variation

Denomination	Description	Variation
<i>Bs</i>	Base simulation	-
Bsi	<i>Bs</i> - interlayer	Interlayer, h_i
BsilA	<i>Bs</i> + Imposed load	Imposed load (l)
BsilC4	<i>Bs</i> + Imposed load	l + Beam height, h_t
Bs-lK	<i>Bs</i> + Low stiffness	Connection stiffness, K
Bs-hK	<i>Bs</i> + High stiffness	
Bs-fx	<i>Bs</i> + F_x	Support conditions (S_c)
Bs4sup	<i>Bs</i> + S_{ae}	
Bsjb01	<i>Bs</i> + $s_b = 0.00$	Juxtaposed beams, $s_b = 0.00$ m
Bsjb06	<i>Bs</i> + $s_b = 0.00 + b_t$	Juxtaposed beams + Beam width, b_t
Bsl2	<i>Bs</i> + $L = 2.00$	Span, L
Bsl5	<i>Bs</i> + $L = 5.00$	
Bsl8ht	<i>Bs</i> + $L = 8.00$	$L + h_t$
sb040	<i>Bs</i> + $s_b = 0.40$	Beam spacing, s_b
sb075	<i>Bs</i> + $s_b = 0.75$	
Bstc2	<i>Bs</i> + $h_c = 0.02$	Concrete height, h_c
Bstc3	<i>Bs</i> + $h_c = 0.03$	
Bstc5	<i>Bs</i> + $h_c = 0.05$	
Bstc10	<i>Bs</i> + $h_c = 0.10$	
3×4Bstc3	$b_{slab} = 3.00 + h_c = 0.03$	Width, $b_{slab} + h_c$
3×4Bstc5	$b_{slab} = 3.00 + h_c = 0.05$	
3×4Bstc7	$b_{slab} = 3.00 + h_c = 0.07$	b_{slab}
3×6Bstc5	$b_{slab} = 3.00 + L = 6.00 + h_c = 0.05$	$b_{slab} + L + h_c$
4×6Bstc5	<i>Bs</i> + $L = 6.00 + h_c = 0.05$	$L + h_c$

Table 5.3 – First phase modeling: description and variation (cont.)

Denomination	Description	Variation
Bsfi15	$B_s + \emptyset 15$	Round section beams
Bsfi25	$B_s + \emptyset 25$	
BsiOSB	$B_s + \text{OSB} + \text{LVL} + \text{I-shaped}$	Timber + I-shaped beams
BsiKertoS	$B_s + \text{LVL} + \text{I-shaped}$	
BsC16-20	$B_s + \text{C16/20}$	Concrete
BsC40-50	$B_s + \text{C40/50}$	
BsLC16-18	$B_s + \text{LC16/18}$	
BsLC35-38	$B_s + \text{LC35/38}$	
BsC14	$B_s + \text{C14}$	Timber
BsD60	$B_s + \text{D60}$	
BsGL24	$B_s + \text{GL24h}$	
BsGL32	$B_s + \text{GL32h}$	
BsKertoS	$B_s + \text{LVL}$	
BsCLT	$B_s + \text{CLTdeck}$	Timber + h_i
BsCLTfx	$B_s + \text{CLTdeck} + Fx$	Timber + $h_i + S_c$
BsCLT4s	$B_s + \text{CLTdeck} + Sae$	
BsCLT5	$B_s + \text{CLTdeck} + h_c = 0.05$	Timber + $h_i + h_c$
3BsCLT5	$B_s + \text{CLTdeck} + b_{slab} = 3.00 + h_c = 0.05$	Timber + $b_{slab} + h_i + h_c$
3BsCLT5_h12	$B_s + \text{CLTdeck} + b_{slab} = 3.00 + h_c = 0.05 + h_t = 0.120$	Timber + $b + h_i + h_c + h_t$
3BsCLT5_h9.9	$B_s + \text{CLTdeck} + b_{slab} = 3.00 + h_c = 0.05 + h_t = 0.099$	

Based on the B_s modeling, the remaining models were obtained by trying to vary only one parameter, as possible. However, there were modeling where more than one parameter was changed, either by design requirements or because it was found important to model a different geometry. This is the case, for example, of the $Bsl8ht$ modeling in which, beyond the span which was changed from 4.00 to 8.00 m, also the height of the timber beams had to be increased; or instead of a square plan floor it was intended to study a rectangular one by changing the slab width, with a different concrete thickness, $3 \times 4Bstc5$ ($b_{slab} = 3.00$ m; $h_c = 0.05$ m).

The modeling were created following the characteristics listed in Table 5.2 and the results associated with each one were compared and analyzed. As presented before, the analysis was focused on the vertical displacement (vd) at mid-span of the each beam, the support reactions (sr) in each beam, the longitudinal bending moment (bm) at mid-span cross section of each

beam and on the way in which they were “divided” by the several beams. To do so, each of the previous quantities was compared to the sum of the same quantity obtained for the overall beams at the same load case. Therefore, the vertical displacement at mid-span was compared to the sum of displacements at the same section of all the beams, the support reaction was compared to the sum of reactions, and the longitudinal bending moment at mid-span was compared with the sum of the moments at the same section considering all the beams.

Given the great quantity of data involved only some will be presented in this section. The exhaustive exposition is presented in the *APPENDIX C, C.1 Results from the primary numerical analysis*. By simplicity, only a summary of the results found when the central beam was loaded with a point load at mid-span is presented next. Fig. 5.2 shows the vertical displacement at the loaded beam mid-span compared with the sum of displacements in all the beams (see also Table C.2 to Table C.5, at *APPENDIX C*) for the various modeling. Since the point load was applied at the central beam, the percentages of displacements distributed symmetrically relatively to it, as it would be expected, with the loaded beam receiving the highest percentage. The relation between the support reaction associated to each beam and the sum of reactions in all beams, Fig. 5.3 (Table C.6 to Table C.9), and the relation between the longitudinal bending moment in the mid-span cross section of each beam and the sum of these in all the beams, Fig. 5.4 (Table C.10 to Table C.13), also behave in the same manner. Considering the line load case, when the load was uniformly distributed along the central beam length, a very similar behavior was found.

5. SENSITIVITY ANALYSIS

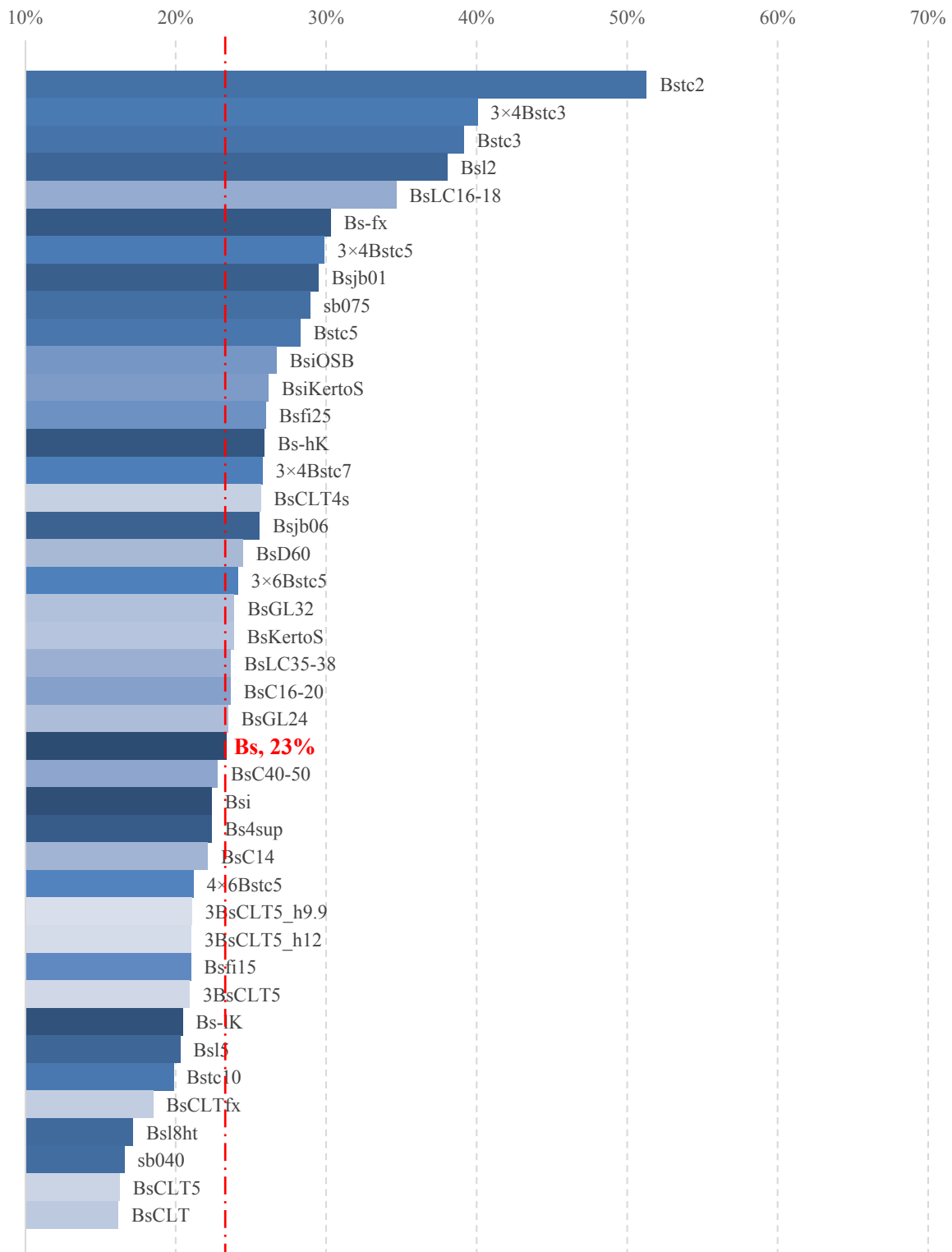


Fig. 5.2 – First phase analysis: vd received by the central beam when a point load acts over it

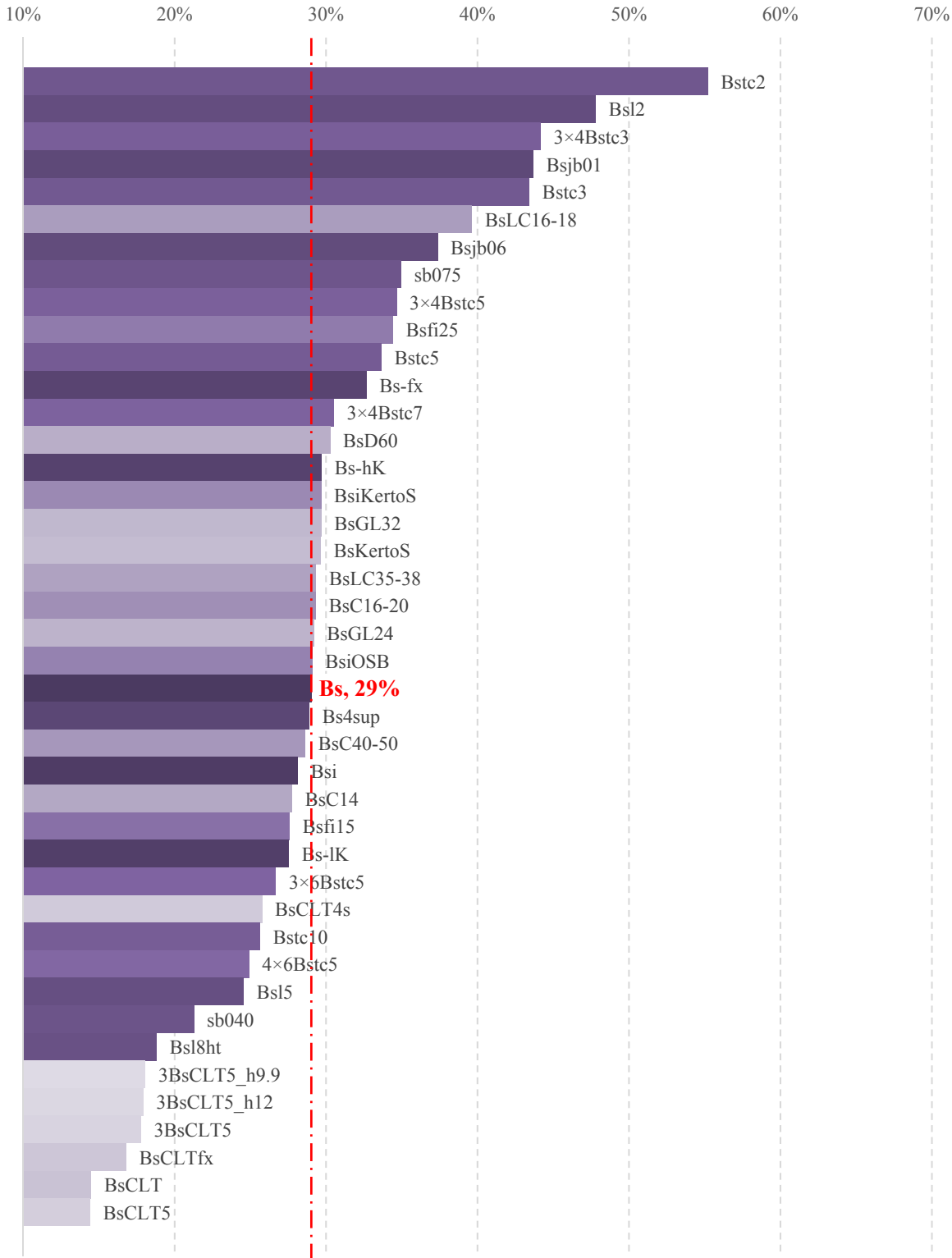


Fig. 5.3 – First phase analysis: *sr* received by the center beam when a point load acts over it

5. SENSITIVITY ANALYSIS

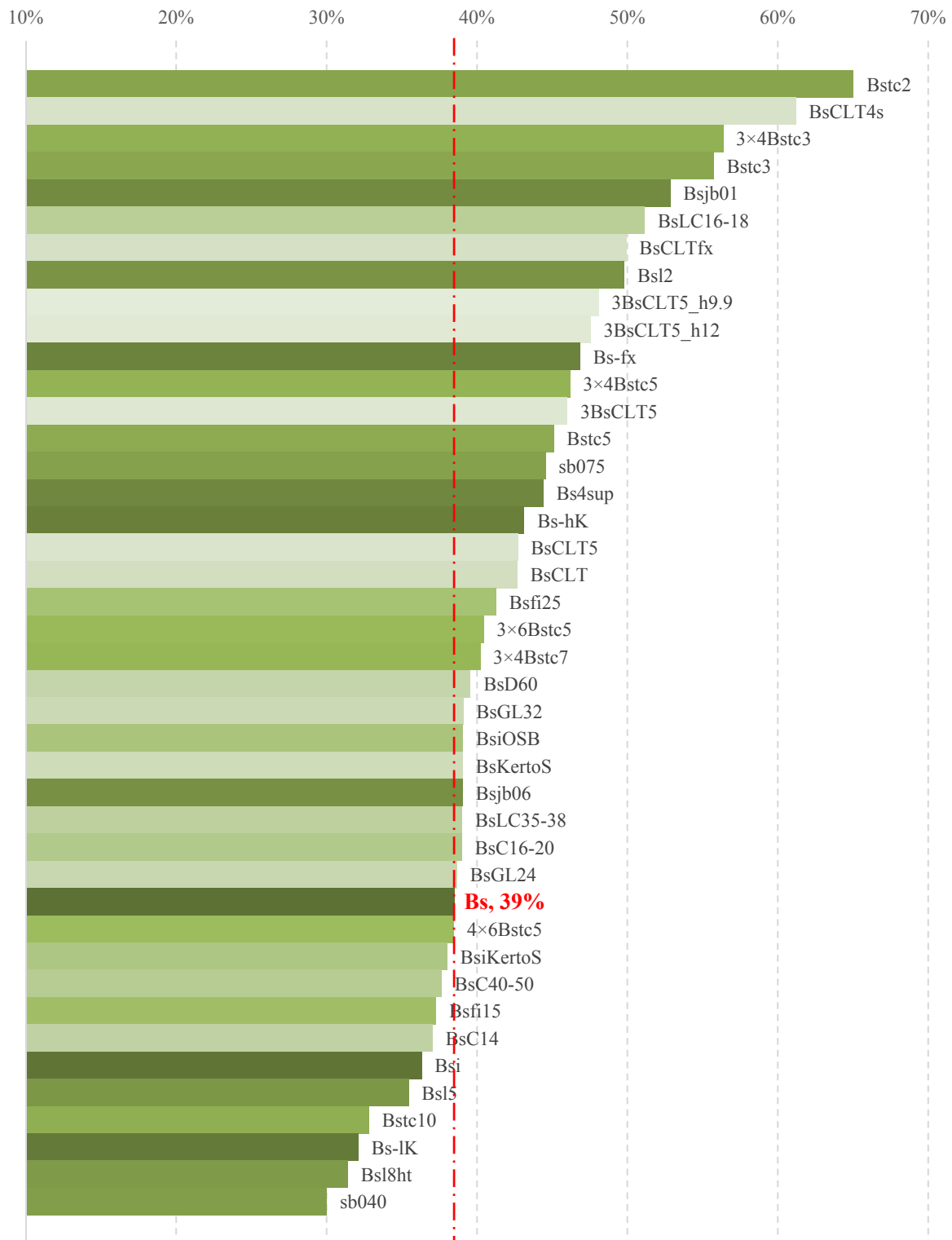
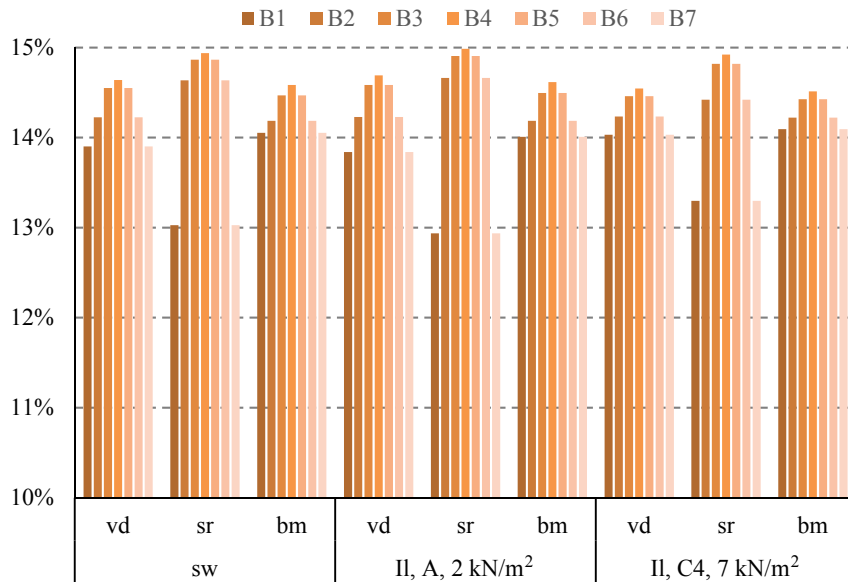


Fig. 5.4 – First phase analysis: *bm* associated with the center beam when a point load acts over it

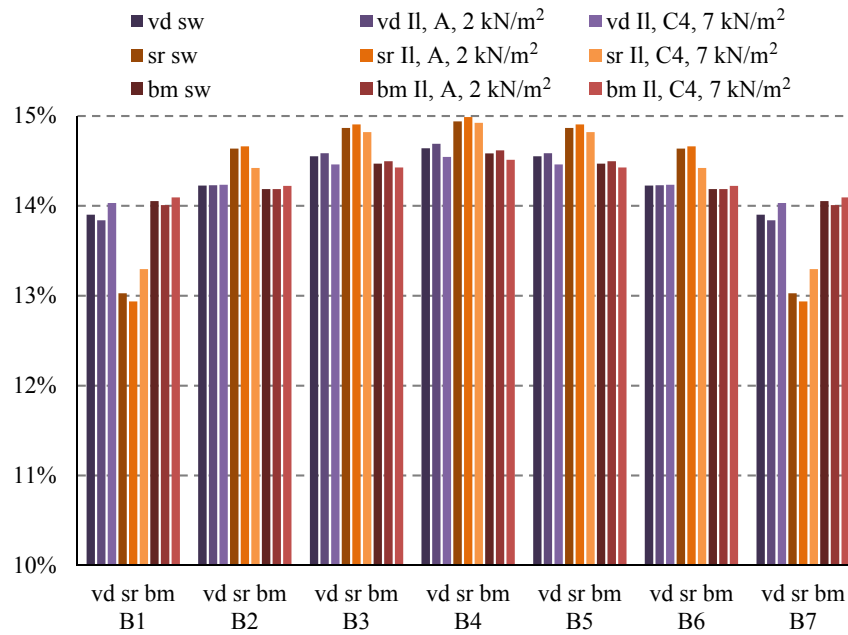
By comparing the results of the displacement distribution for the two load cases that were considered, Pt and Ln , when the central beam was loaded very similar values could be found, differing between about 0 to 2 %. Concerning the support reactions, although the results for the point and the line load cases had shown a similar trend, the last generally predicted higher percentages of load received for the loaded beam. This differences varied between 10 and 18 %, when the central beam was the loaded one. As for the results in terms of longitudinal bending moment, the tendency is the opposite. The mid-span cross section of the beams loaded with a line load were associated with a lower percentage of bending moment, when compared with those loaded with a point load. The differences found among these two load cases when the central beam was loaded, were greater for this quantity, varying between 14 and 32 %. This same tendency was verified for the cases where other beams were loaded (Table C.2 to Table C.13). In fact also the values for the variations are quite similar, with only the case where the extremity beam was loaded (B1) deviating slightly.

For the three quantities under consideration (vd , sr and bm), Fig. 5.5 (Table C.14) presents the percent distribution when only the self-weight or a uniformly distributed imposed load was considered to be acting over Bs . While Fig. 5.5 a) groups the results by loading, Fig. 5.5 b) groups them by beam. For the imposed loads, two different building categories were considered, defined according to (EN1991 2001), A and C4. As Fig. 5.5 shows, the percentages found for these load cases have almost no variation (≥ 13 %; ≤ 15 %), with each beam receiving about one seventh of the applied load. As it would be expected, the load cases under consideration, uniformly distributed over all the slab surface, show a nearly uniform distribution.

The distributions found for the quantities under consideration and the several load cases allowed identifying the parameters that most affect the transversal distribution of load in timber-concrete composite floor systems. This was achieved by comparing the percentage received by the loaded beam in the base modeling with those of the remaining modeling, and computing the corresponding deviation. Table 5.4 to Table 5.6 summarize the extreme deviations, maximum and minimum, for the various loading cases. Vertical displacements, support reactions and bending moments were considered separately. Deviations below 10 % were considered of minor relevance, and as a result, they were disregarded (on the tables they are identified by “-”). More information can be found in Section *C.1.5 Analysis of the parameters effects*.



a)



b)

Fig. 5.5 – First phase analysis: *vd*, *sr* and *bm* distributions for self-weight and imposed load cases; a) by load case; b) by beam

Table 5.4 – First phase: parameters with higher effect in the mid-span vertical displacement

Variation	Deviation [%]				Loaded beam				Maximum variation found between
	max		min		max		min		
	<i>Pt</i>	<i>Ln</i>	<i>Pt</i>	<i>Ln</i>	<i>Pt</i>	<i>Ln</i>	<i>Pt</i>	<i>Ln</i>	
Concrete thickness, h_c	31	31	25	25	B1	B2	$Bs + h_c = 0.02$ m and Bs ($h_c = 0.07$ m)		
	20	21	13	13			$Bs + h_c = 0.03$ m and Bs ($h_c = 0.07$ m)		
CLTdeck supports	18	26	-				$Bs + \text{CLTdeck}$ (Ss) and $Bs + \text{CLTdeck} + Sae$		
Span, L	18	19	12	12			$Bs + L = 2.00$ m and Bs ($L = 4.00$ m)		
Concrete	16	17	-				$Bs + \text{LC16/18}$ and Bs (C25/30)		
$L = 6.00$ m + $h_c = 0.05$ m	11	11	-				$Bs + h_c = 0.05$ m ($L = 4.00$ m) and $Bs + h_c = 0.05$ m + $L = 6.00$ m		
Support conditions	10	10	-				Bs (Ss) and $Bs + Fx$		

Table 5.5 – First phase: parameters with higher effect in the support reactions

Variation	Deviation [%]				Loaded beam				Maximum variation found between
	max		min		max		min		
	<i>Pt</i>	<i>Ln</i>	<i>Pt</i>	<i>Ln</i>	<i>Pt</i>	<i>Ln</i>	<i>Pt</i>	<i>Ln</i>	
Support conditions	75	37	-		B1	B4	B3	Bs (Ss) and $Bs + Sae$	
CLTdeck supports	70	22	-			B3	B2	$Bs + \text{CLTdeck}$ (Ss) and $Bs + \text{CLTdeck} + Sae$	
Concrete thickness, h_c	31	28	-		B2	B1		$Bs + h_c = 0.02$ m and Bs ($h_c = 0.07$ m)	
	18	18	-			$Bs + h_c = 0.03$ m and Bs ($h_c = 0.07$ m)			
CLTdeck vs. Juxtaposed beams	27	22	15	14	B1	B4	B2	Bs and $Bs + \text{CLTdeck}$	
Span, L	22	19	-		B2	B1		$Bs + L = 2.00$ m and Bs ($L = 4.00$ m)	
Concrete	14	14	-			$Bs + \text{LC16/18}$ and Bs (C25/30)			
$L = 6.00$ m + $h_c = 0.05$ m	11	11	-			$Bs + h_c = 0.05$ m ($L = 4.00$ m) and $Bs + h_c = 0.05$ m + $L = 6.00$ m			
Beam spacing, s_b	10	10	-			B1	B3	B2	B1

Table 5.6 – First phase: parameters with higher effect in the mid-span longitudinal bending moment

Variation	Deviation [%]				Loaded beam				Maximum variation found between	
	max		min		max		min			
	<i>Pt</i>	<i>Ln</i>	<i>Pt</i>	<i>Ln</i>	<i>Pt</i>	<i>Ln</i>	<i>Pt</i>	<i>Ln</i>		
Support conditions	-	36	-	-	B1		B3	B2	<i>Bs</i> (<i>Ss</i>) and <i>Bs</i> + <i>Sae</i>	
Concrete thickness, h_c	27	31	22	24	B4	B1	B2		<i>Bs</i> + $h_c = 0.02$ m and <i>Bs</i> ($h_c = 0.07$ m)	
	17	19	15	10					<i>Bs</i> + $h_c = 0.03$ m and <i>Bs</i> ($h_c = 0.07$ m)	
CLTdeck supports	23	15	-	-	B1		B4	B2	<i>Bs</i> + CLTdeck (<i>Ss</i>) and <i>Bs</i> + CLTdeck + <i>Sae</i>	
Span, <i>L</i>	13	18	-	10			B2		<i>Bs</i> + <i>L</i> = 2.00 m and <i>Bs</i> (<i>L</i> = 4.00 m)	
Concrete	14	16	11	-					<i>Bs</i> + LC16/18 and <i>Bs</i> (C25/30)	
CLTdeck vs. Juxtaposed beams	14	-	11	-	B4	B1	B2	<i>Bs</i> and <i>Bs</i> + Juxtaposed beams		
$L = 6.00$ m + $h_c = 0.05$ m	-	10	-	-	B1	B2		<i>Bs</i> + $h_c = 0.05$ m ($L = 4.00$ m) and <i>Bs</i> + $h_c = 0.05$ m + $L = 6.00$ m		

Almost all deviations were computed using the percentage associated to the loaded beam at the *Bs* modeling and the corresponding percentage obtained with the modeling associated to the parameter whose influence was intended to be studied. However, as the purpose was to analyze the influence of a single parameter each time, a different “comparing modeling” was chosen, as applicable. Thus, a modeling as close as possible to *Bs* and allowing, at the same time the intended analysis, was used. Example of this are the following:

- To evaluate the effect that support conditions might have in a composite floor with a lower deck of CLT, the comparison was made relatively to *BsCLT* modeling (simply supported in two opposite ends). For the comparison two CLT composite floors were considered: one with two opposite ends fixed and another with the four sides simply supported.
- The effect of the CLT thickness was also studied (“CLTdeck heights”). In this case, the comparison was performed between rectangular plan floors, with 3.00 m wide, and concrete layer 0.05 m thick. *3BsCLT5* was the “comparison modeling”, with CLT height equal to h_t in *Bs* modeling, 0.20 m.
- To analyze the combined influence of a 6.00 m span floor with a concrete layer 0.05 m thick and the floor width, “ $L = 6.00$ m + $h = 0.05$ m”, two “comparison modeling” were chosen: *Bstc5* and *3×4Bstc5*. The first, in all similar to *Bs* modeling but the concrete thickness (0.05 m instead of 0.07 m), and the second differing also on the width (3.00 m instead of 4.00 m). The first was used to compare with *4×6Bstc5* and the last with *3×6Bstc5*.

Fig. 5.6 summarizes the results of the first phase of the numerical study concerning the parameters that most affect timber-concrete composite floors subjected to concentrated loads, in terms of vertical displacements, support reactions and bending moments.

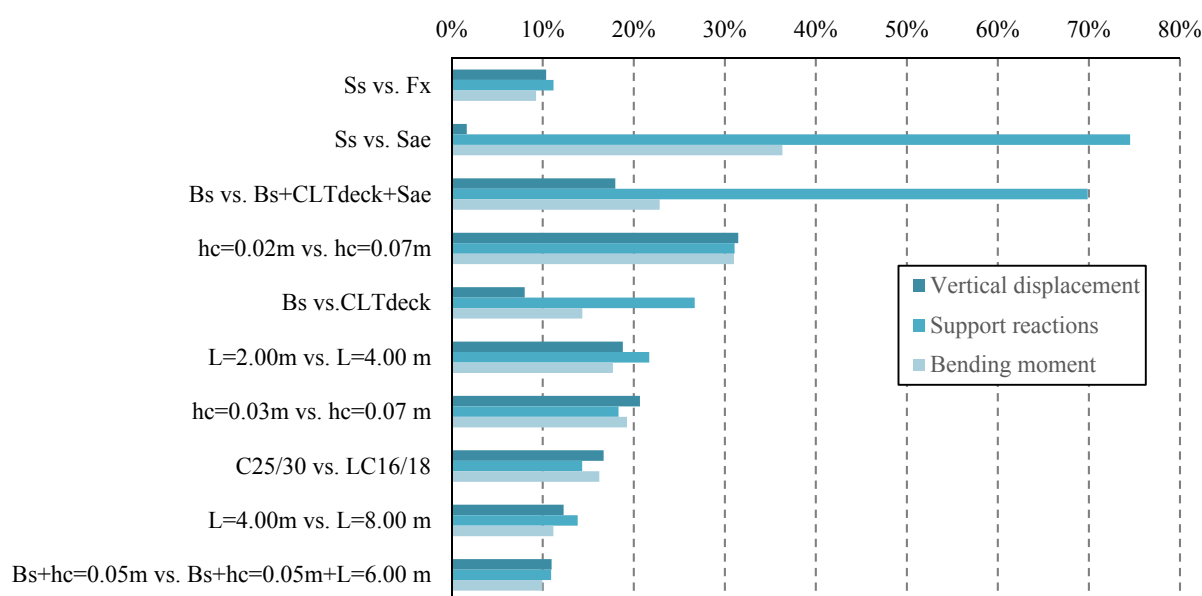


Fig. 5.6 – Parameters with higher effect in the studied quantities (maximum deviation percentages)

Support conditions stand out as one of the parameters with greatest influence in the behavior of such floors (2 - 75 %), followed by the concrete thickness (18 - 31 %), the use of a CLT deck (8 - 27 %) and the span length (11 - 22 %). Vertical displacement showed the most uniform behavior, with very similar deviations associated with point and line loads and always associated with the same loaded beam, B1. Support reactions and bending moment distributions are not that consistent but a trend is clear: the highest deviation was, most of the times, associated with the loading of the extreme beam B1. In the case of support reactions, highest deviations were associated with the point load cases, while for bending moments, as well as for vertical displacements, they were associated with the line load cases.

These conclusions led, not only to define the experimental program, as presented at 3.6 *Preliminary numerical analysis*, but also to provide the basis for new study lines. Based on the parameters that could have a wide range of variation, namely, span length and concrete thickness, several modeling were developed. Table 5.7 lists the modeling analyzed in the second phase, a broader exposition can be found in Table C.27.

Table 5.7 – Second phase modeling

Denomination	Description	Variation
Bstc12	$B_s + h_c = 0.12$	Concrete height, h_c
Bstc15	$B_s + h_c = 0.15$	
Bstc20	$B_s + h_c = 0.20$	
Bsl8un	$B_s + L = 8.00$	Span, L
Bsl12un	$B_s + L = 12.00$	
Bsl16un	$B_s + L = 16.00$	
L16ov	$B_s + L = 16.00 + h_i = 0.00 + b_t = 0.32 + h_t = 0.40 + s = 0.05 + \text{FE mesh}$	$L + h_i + b_t + h_t + s + \text{FE mesh}$
L12ov	$L16od + L = 12.00$	
L8ov	$L16od + L = 8.00$	
L4ov	$L16od + L = 4.00$	
L2ov	$L16od + L = 2.00$	
L16	$B_s + L = 16.00 + h_i = 0.00 + b_t = 0.24 + h_t = 0.36 + s = 0.05 + \text{FE mesh}$	$L + h_i + b_t + h_t + s + \text{FE mesh}$
L12	$B_s + L = 12.00 + h_i = 0.00 + b_t = 0.16 + h_t = 0.32 + s = 0.05 + \text{FE mesh}$	
L4	$B_s + h_i = 0.00 + h_c = 0.03$	$h_i + h_c$
L2	$B_s + L = 2.00 + h_i = 0.00 + b_t = 0.08 + h_t = 0.16 + h_c = 0.03$	$L + h_i + b_t + h_t + h_c$
L4un	$B_s + h_i = 0.00 + b_t = 0.05 + h_t = 0.15 + h_c = 0.03$	$h_i + b_t + h_t + h_c$
L2un	$L4un + L = 2.00$	$L + h_i + b_t + h_t + h_c$

Essentially, different concrete thicknesses and different spans were considered in the second phase of the parametric study. Nevertheless, concerning the modeling of different spans, also different design considerations were adopted. Based on the presented earlier, only one parameter was intended to be changed at a time. However, there were situations where it could not be accomplished. That was the case of *Bsl8ht* in the first phase, to which besides the span of 8.00 m (instead of 4.00 m, B_s), also a timber section with greater height was needed (0.25 m instead of 0.20 m, as in B_s). In the same manner, when the composited floors with spans longer than 8.00 m, as 12.00 m and 16.00 m, were designed, according to EC5 (EN1995 2004a), sections stiffer than those of B_s were required.

Thus, besides considering three new concrete thicknesses [0.12 m, 0.15 m, 0.20 m] and two new span lengths [12 m, 16 m], also different design assumptions were considered. In addition to those modeling guaranteeing the design requirements, [L2, L4, L12, L16], together with *Bsl8ht*, two other sets of span modeling were gathered, undersizing and oversizing of the structures relatively to the requirements of EC5 (EN1995 2004a). As for the undersized set, labeled as *un*, all the geometrical characteristics remained unchanged

relatively to B_s except for the span, regardless of the design requirements, [Bsl8un, Bsl12un, Bsl16un]. Later on, also the small span lengths were considered undersized [L2un, L4un], achieved by changing not only the timber cross-sections and the concrete thickness, but also removing the timber interlayer. Although, this sections do not guarantee the design code requirements, analyzing the consequences was considered theoretically relevant in an academic point of view. Concerning the oversized set, labeled as ov , the height of the timber beams and the connection stiffness were doubled, with $h_t = 0.40$ m instead of 0.20 m (B_s), and the spacing between connectors, s , decreasing from 0.10 m (B_s) to 0.05 m, keeping the connector stiffness unchanged, $K = 12000$ kN/m. Associated with the use of this connector spacing, also the FE mesh was adapted to the same dimension. These three sets of span modeling allowed comparing the consequences of different span lengths, at the same time that they enabled studying the effects that the use of “undersized” or “oversized” sections might cause in the transversal load distribution in such structures.

As in the previous analysis, vertical displacements at mid-span, support reactions and longitudinal bending moments at the mid-span cross-section and the manner in which they were distributed transversally over the composite floors were studied. Therefore, Fig. 5.7 to Fig. 5.9 expose the results for the percentage of vertical displacement associated with the loaded beam when it was loaded with a point load at mid-span.

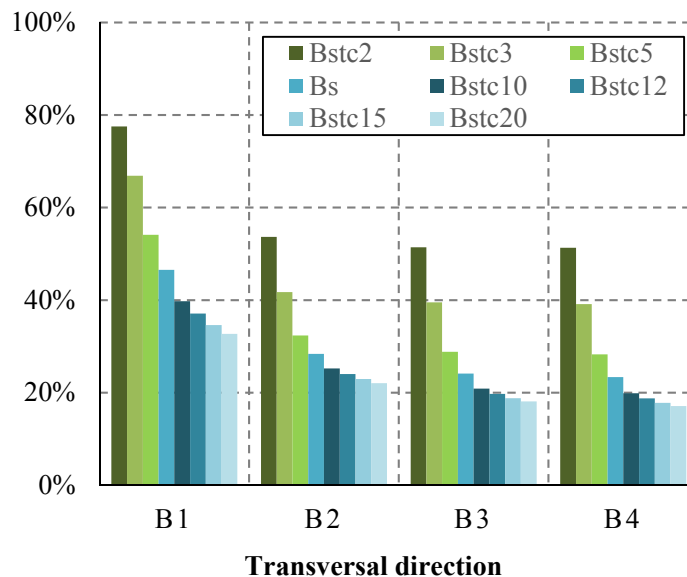


Fig. 5.7 – Distribution of vd for the point load case by concrete thickness

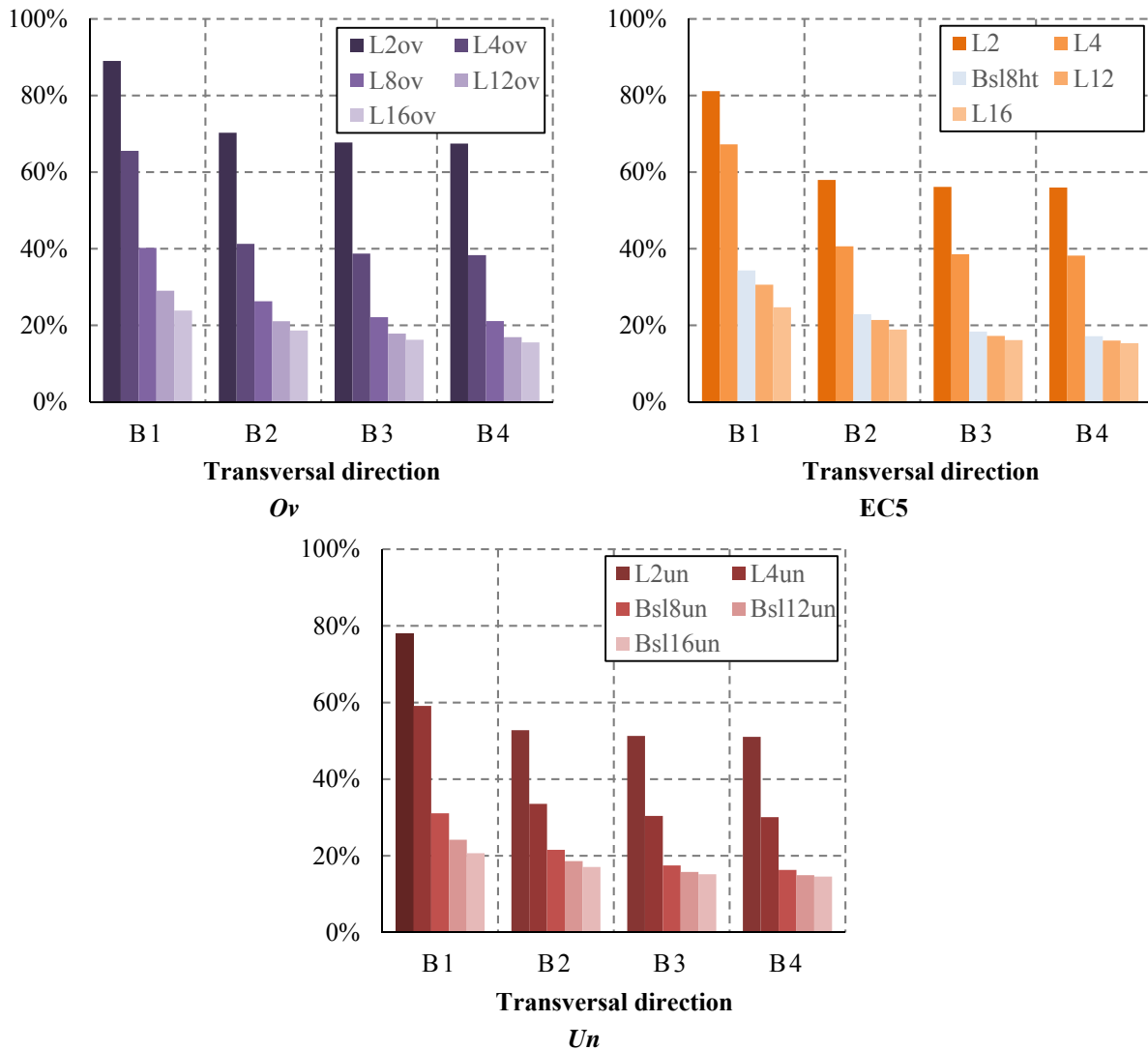


Fig. 5.8 – Distribution of v_d for the point load case by span

Fig. 5.7 is related with the several concrete thicknesses, whereas Fig. 5.8 refer to the various floor spans. Fig. 5.9 relates the percentage of vertical displacement with the span and design considerations, from the higher to the lower percentage, taking B4, the central beam as reference beam. In the same way, Fig. 5.10 to Fig. 5.12 gather the corresponding results in terms of support reactions, and Fig. 5.13 to Fig. 5.15 present them in terms of longitudinal bending moment. The results in which the following graphs were based are gathered in Section C.2 *Results from the second phase numerical analysis, Appendix C.*

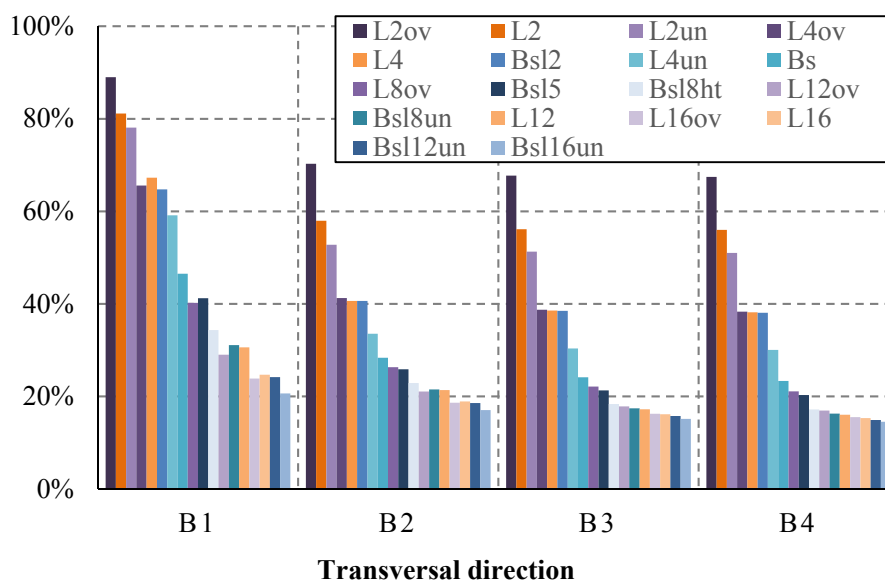


Fig. 5.9 – Second phase: distribution of vd by percentage at the loaded beam

The effect that the concrete thickness has on the manner in which the vertical displacements distribute in the transversal direction is clearly observed in Fig. 5.7, through the analysis of the percentage associated with the loaded beam. The highest influence was felt when the concrete height varied between 0.02 and 0.10 m, with emphasis on B1. For the extremity beam, 78 % of vd was received when $h_c = 0.02$ m, decreasing to 40 %, when $h_c = 0.10$ m. This means that, using a concrete layer five times thicker than one 0.02 m thick, almost 40 % of the vertical displacement will be distributed for the remaining beams, rather than being associated with the loaded one. Concerning the inner beams, this percentage decreases to about 30 %. Still, a significant percentage remains not associated with the loaded beam.

In line with the studies presented above in previous sections, the influence that the span length has is evident especially for the extremity beam, Fig. 5.8. For B1, the percentage of vd received changed about 65 % between spans of 2.00 and 16.00 m, when the sections were oversized. With undersized sections and with sections set “tight-fitting” to the EC5 (EN1995 2004a) requirements, this percentage was about 57 %. For the interior beams, these percentages decreased and were more significant between spans of 2.00 and 12.00 m, reaching 50 %, 35 % and 38 % for oversized, undersized and EC5 sections, respectively.

By analyzing the manner in which the percentages are associated with each beam, when loaded, for the various design considerations, a trend for the oversized sections to be associated with higher percentages was observed, Fig. 5.9. Thus, the smaller the span and the smaller “degree of oversizing”, the higher will be the percentage of vertical displacement that

would be no longer associated with the loaded beam, and consequently the transversal spreading.

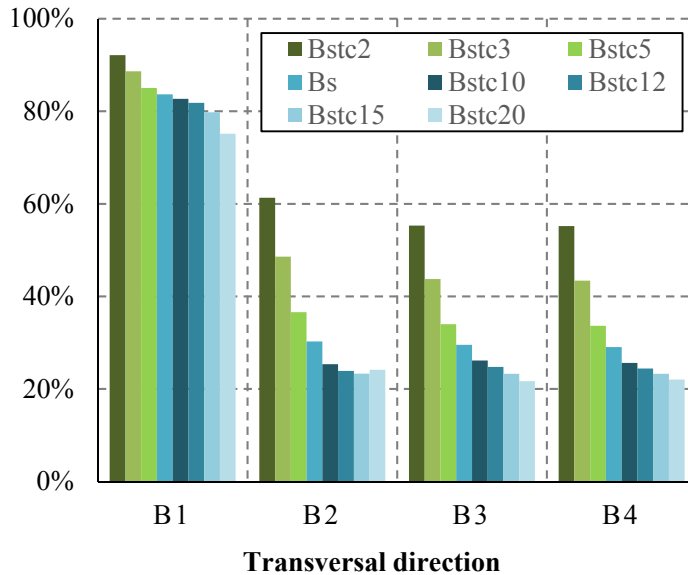


Fig. 5.10 – Distribution of *sr* for the point load case by concrete thickness

With respect to support reactions, despite the effect of the concrete thickness have in their transversal distribution, Fig. 5.10, the manner in which the various beams were affected is different from that found for *vd*. Once again the extremity beams show a different behavior when compared with the interior ones. However, in contrast to what was found for *vd*, for *sr* they are associated with the lowest influence of the concrete thickness. For B1, the thinnest concrete layer, $h_c = 0.02$ m, was associated with the highest percentage of *sr* received by this beam, 92 %, decreasing to 75 %, when for the thickest layer modeled, $h_c = 0.20$ m. This means that between the extreme thicknesses a 17 % gap of *sr* was found, with the largest difference taking place when the concrete height varied between 0.15 and 0.20 m. In turn, for the inner beams, the influence of this geometrical property seems to be similar to that found for *vd*, with higher differences found between $h_c = 0.02$ and 0.10 m. For B2 this difference is about 36 %, as for B3 and B4, is about 30 %.

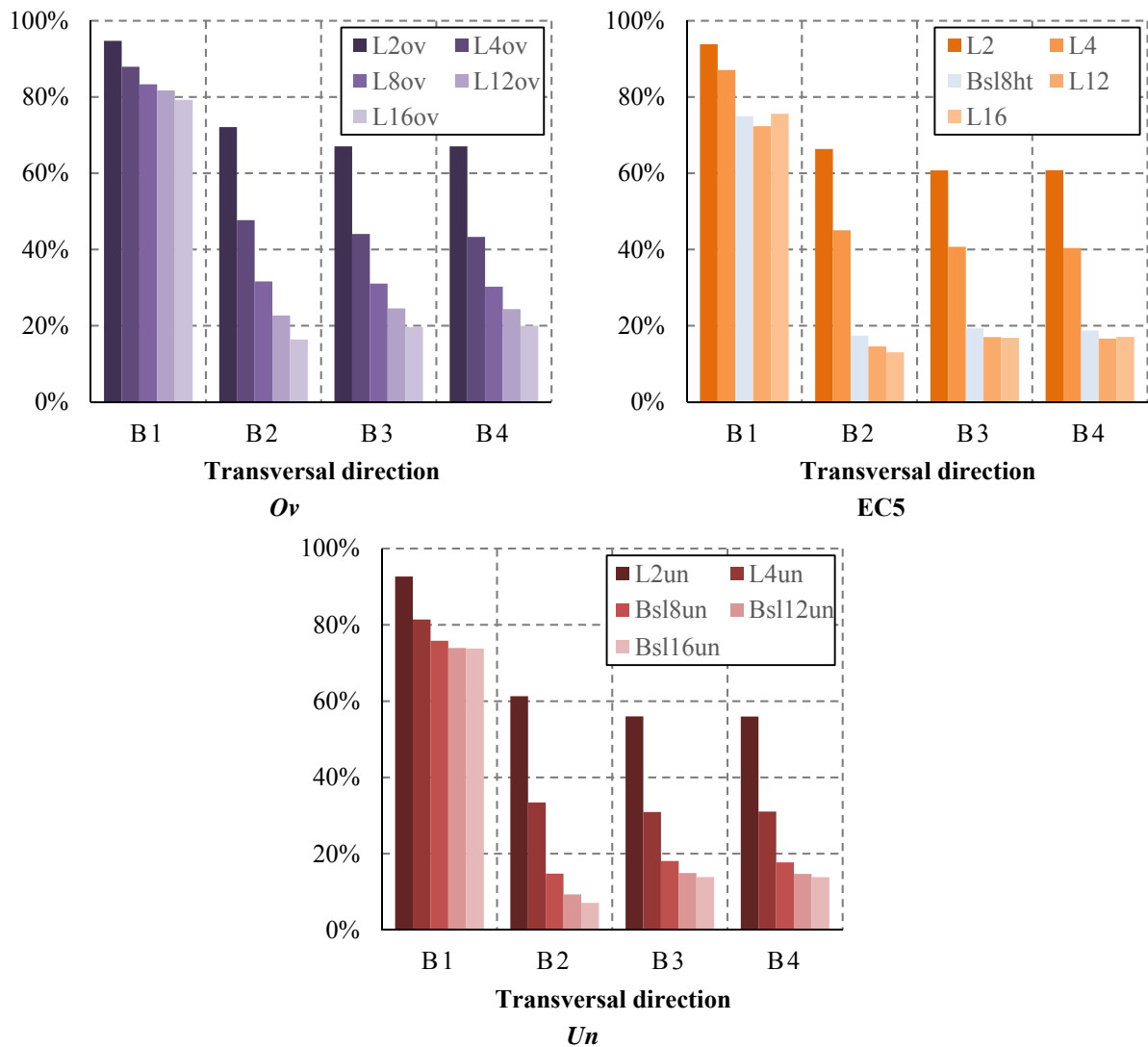


Fig. 5.11 – Distribution of sr for the point load case by span

Concerning the effect of the span in the distribution of sr , Fig. 5.11, a similar behavior was observed relatively to that found for the influence of the concrete height. Therefore, regardless of the design considerations, B1 stood out by being the less sensitive to the span variation, with a maximum difference of 15 %, found between $L = 2.00$ and 16.00 m with oversized sections. Conversely, B2 showed to be the most sensitive, with differences about 50 %, for the various sets, with a maximum of 56 %, found between $L = 2.00$ and 16.00m with oversized sections. The remaining beams showed very similar percentages when considering the same span boundaries, about 44 %. Nevertheless, analyzing the consequences of the span variation in the three design sets, the oversized sections showed to be associated with high percentages, and they remain significant between $L = 2.00$ and 16.00m, for the three

inner beams. For the undersized and the EC5 sections, differences in the sr distribution were essentially felt when the span changed between $L = 2.00$ and 8.00 m (40 %).

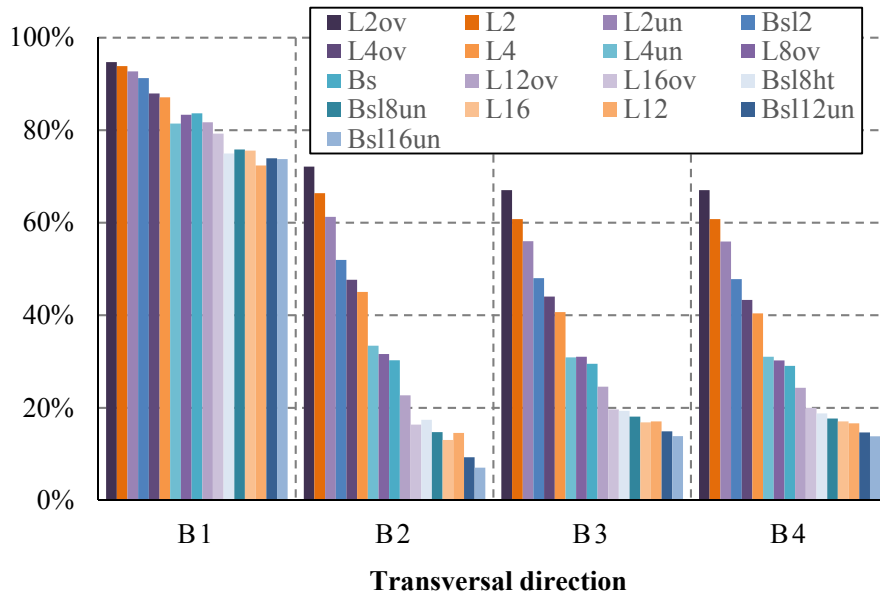


Fig. 5.12 – Second phase: distribution of sr by percentage at the loaded beam

Maintaining the span, a trend for the highest percentages, to be associated with the oversized sections whilst the lowest percentages were associated with the undersized ones can be observed in Fig. 5.12. Beam B2 emphasizes this behavior, with higher differences between $L2ov$ and $Bsl16un$ (45 %).

By analyzing the results associated with the longitudinal bending moments, a very similar behavior was found when comparing extremity and interior beams. Thus, considering the effect of the concrete thickness in the bending moment transversal distribution, Fig. 5.13 showed that the highest influence was felt between $h_c = 0.02$ and 0.12 m, differing about 34 %.

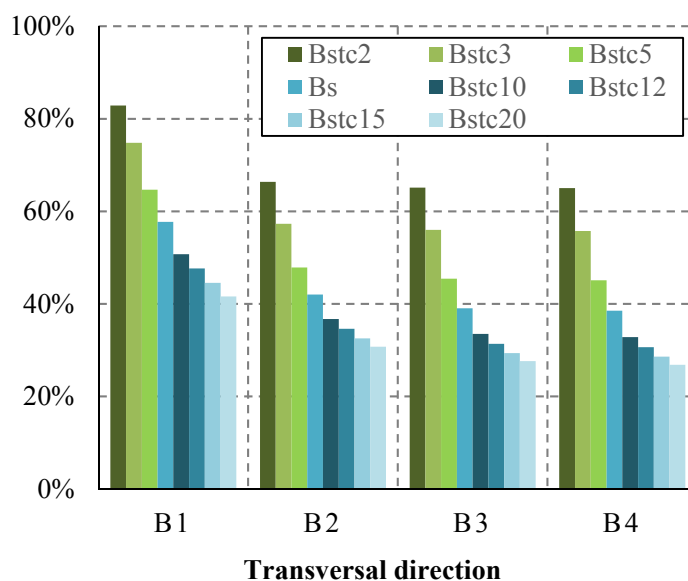


Fig. 5.13 – Distribution of bm for the point load case by concrete thickness

Concerning the influence of the span length, Fig. 5.14, the percentages of bm associated with B1 changed about 50 % between spans of 2.00 and 16.00 m, for the various design sets. For the interior beams, the design set began to show some influence in the differences. Hence, the difference between the percentages associated with $L = 2.00$ and 16.00 m, when the sections were oversized, was about 46 %. Between the spans of 2.00 and 12.00 m, this difference decreases to 42 %. In fact, the effect of the span length in the bm distribution is meaningful between $L = 2.00$ and 12.00 m, to which the undersized and EC5 sections presented differences of about 36 %.

As for the manner in which the percentages are associated with each loaded beam, concerning the various design considerations, Fig. 5.15, there is a tendency for the beams, mainly the interior ones, to behave very similarly. As in the case of the previous quantities, the oversized sections were associated with the higher percentages, followed by the EC5 and the undersized sections, in this order. A difference of 47 % was found among the percentages associated with $L2ov$ and $Bsl16un$, for the extremity beam, and about 36 % for the interior beams.

A similar tendency was found in the manner in which the concrete layer thickness and the floor span affected the transversal distribution of the three analyzed quantities. This conclusion was based on the differences found between the percentages received by the loaded beam with the various thicknesses. As exposed, these differences are associated to the existence of transversal spreading of the quantity in question, meaning that the considered

beam will receive a lower percentage of *vd*, *sr* or *bm*. In turn, this would affect the percentage received by the remaining beams.

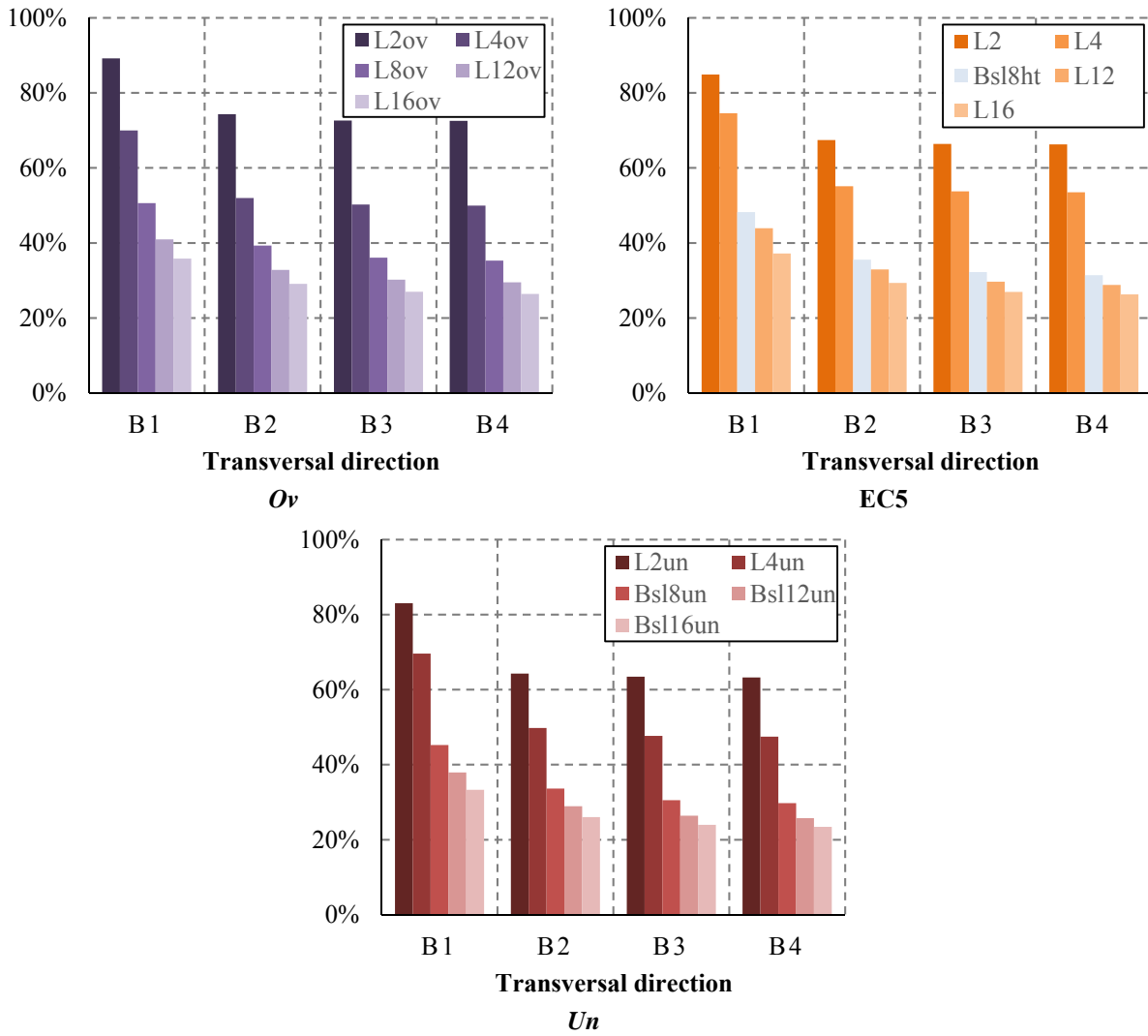


Fig. 5.14 – Distribution of *bm* for the point load case by span

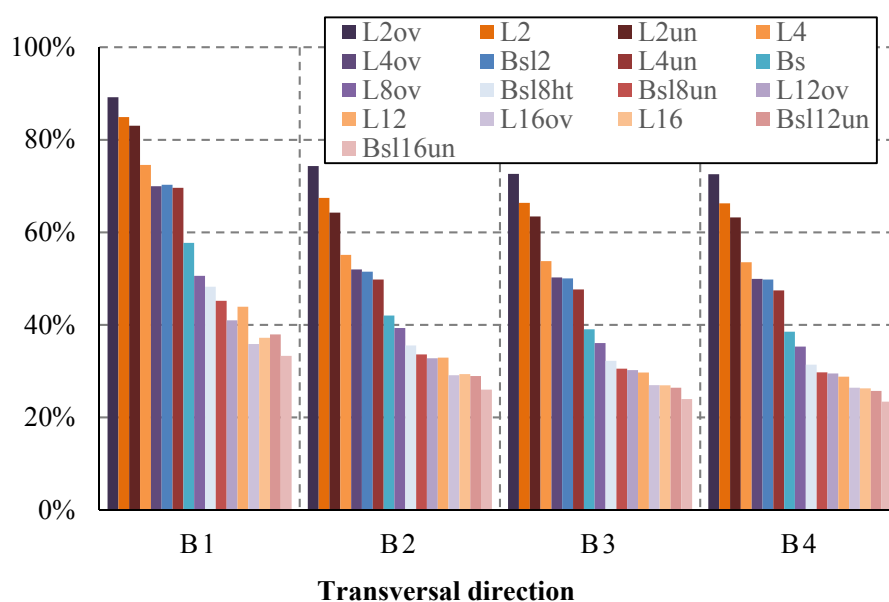


Fig. 5.15 – Second phase: distribution of bm by percentage at the loaded beam

In general, the highest differences found for the various quantities were observed between the heights of 0.02 and 0.10 m. Table 5.8 summarizes the differences found between those two thicknesses, for the vertical displacements, support reactions and longitudinal bending moment.

Table 5.8 – Transversal spreading [%] between the concrete height of 0.02 and 0.10 m

Beam location	Quantity		
	vd	sr	bm
B1	38	9	32
B2	28	36	30
B3	31	29	32
B4	31	30	32

The difference observed when the extremity beam was loaded, concerning sr , is the lowest, when compared with those associated with the other two quantities. This means that, for the thicknesses in the range between 0.02 and 0.10 m, B1 will always receive a similar amount of load. In fact, concerning sr , the highest difference, and consequently the spreading, only was noticed between 0.15 and 0.20 m (5 %, corresponding to 17 % when computed between $h_c = 0.02$ and 0.20 m), with a very small variation between 0.05 and 0.10 m (3 %), Fig. 5.10. In summary, B1 is the beam associated with the highest share of vd , sr and bm . This is also the beam for which it was observed the highest spreading of vd (38 %). When

concerning sr , B1 is almost unaffected by the change in the concrete height, from 0.02 to 0.10 m (9 %), with B2 standing out as the most affected (36 %). As for bm , all the beams showed very similar differences, about 30 %. In general, for B3 and B4, regardless of the quantity in question, very similar differences were found, also about 30 %.

In what concerns to the influence of the span length in the transversal distribution of vd , sr and bm , together with the design considerations (ov , un and EC5 section), the highest effect was felt between the spans of 2.00 and 12.00 m. Table 5.9 gathers the differences found among those extreme spans.

Table 5.9 – Transversal spreading [%] between the span length of 2.00 and 12.00 m

Beam location	Quantity								
	vd			sr			bm		
Sizing	ov	un	EC5	ov	un	EC5	ov	un	EC5
B1	60	54	51	13	19	21	48	45	41
B2	49	34	37	49	52	52	42	35	34
B3	50	36	39	43	41	44	42	37	37
B4	51	36	40	43	41	44	43	37	37

ov – section oversized; un – section undersized; EC5 - section “tight-fitting” to the EC5 (EN1995 2004a) requirements.

These results seem rather similar to those found for the concrete thickness, with the differences found for bm being more uniform among the four beams than for the other quantities. Also, there is a trend for the extremity beam to distinguish from the remaining, being associated with higher differences for vd and bm , and lower differences concerning sr , regardless of the design considerations. For the differences found for sr , B2 stands out as the beam associated with the highest percentages of spreading.

Analyzing the section sizing, although an oversized section may seem like “a safe choice”, from the outset, as the results for vd could suggest (a gain of 60 % of spreading for B1), those found for bm and, in a higher degree for sr , did not led to the same conclusion. In fact, mainly for B3 and B4 the values found for the differences are quite similar. Therefore, in addition to the economic issue, it seems to be no great advantage in oversizing the beams cross-sections, unless a serviceability issue may force it.

As for the undersized and the EC5 sections, relatively close differences were found, highlighting the fact that, there is no advantage in choosing cross-sections which do not ensure the design code requirements.

Thus, for the modeled structure, a spreading of, at least 21 % for B1 and 34 % for the interior beams, can be achieved between the spans of 2.00 and 12.00 m. This confirm, once

again, the advantage that could be taken in designing the timber-concrete composite floors in light of this conclusions.

5.3 Development of an expeditious tool

To know the percentage of load that will be associated with a specific beam in the design phase is an extremely interesting information, provided that it is obtained throughout simple rules. A fast and economical design can be achieved by taking advantage of the fact that the loaded beam does not receive the entire 100 % of the applied load.

Following the findings in the previous sections, namely the parameters that most affect the distribution of the various analyzed quantities and adding some complementary data, an equation to predict the percentage received by the loaded beam was developed.

Despite the intention in obtaining an equation capable to predict the percentage of each of the analyzed quantities, given its importance in the design process, the longitudinal bending moment was chosen for base the development of the equation. Given the proved relevance of parameters such as the span, the concrete thickness and the beam location in the transversal direction, these were the ones used to obtain the percentage prediction rule.

The consideration of the beam location intends to identify if the beam is an extremity one, a central or other. Therefore, a dimensionless parameter named “beam location”, b_l , was defined. It provides the transversal position of the beam in question, relatively to the longitudinal axis of the outermost beam (B1) for which $b_l = 0.00$. Taking into account that the central beam will be the innermost beam, for this beam $b_l = 1.00$. The intermediate beams will be associated with a beam location proportional to its number. Fig. 5.16 presents an identifying scheme of b_l .

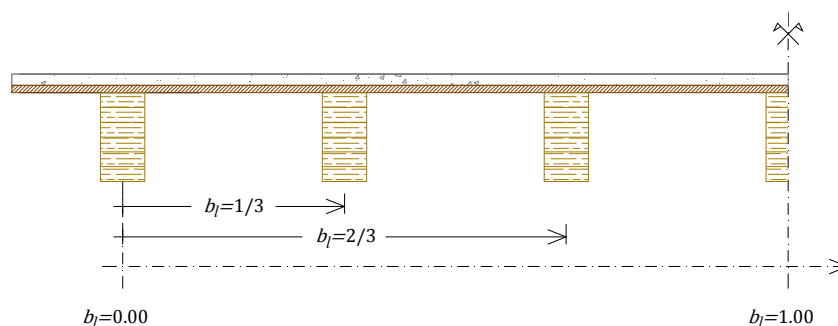


Fig. 5.16 – Beam location scheme

The results collected from the second phase parametric analysis, together with the first phase data concerning span and concrete thickness effects, for centered point and line loading, were added to those obtained with new modeling considering a decentered point load applied at quarter-span ($\frac{1}{4} L$), only for the Bs set (see *C.3.1 Longitudinal bending moment at the quarter-span section of each beam, Appendix C*). Table 5.10 gathers these results. Based on the distributions found for each of the influential parameters, by beam, by set and by loading, several distribution curves were created and approximated, each time. To do so, essentially polynomials were used. The next step was to create curves relating the parameters, in pairs, for the various sets and loadings and approximate them using the same technique. This procedure allowed understanding the progress of the curves when a specific parameter or combination of parameters were considered and the consequences in terms of approximation curve.

Table 5.10 – bm received by the beam when loaded at $\frac{1}{2} L$, lin and $\frac{1}{4} L$

Set	Beam	Modeling	Span (x_1)	Beam location (x_2)	Concrete thickness (x_3)	bm			
			L	b_l	h_c	Loading			
			[m]			$\frac{1}{2} L$	lin	$\frac{1}{4} L$	
						[%]			
Bs	B1	Bsl2	2.00	0.00	0.07	70	61	58	
		Bstc2	4.00		0.02	83	74	70	
		Bstc3			0.03	75	62	57	
		Bstc5			0.05	65	50	44	
		Bs			0.07	58	43	37	
		Bstc10			0.10	51	37	31	
		Bstc12			0.12	48	34	29	
		Bstc15			0.15	45	32	27	
		Bstc20			0.20	42	29	25	
		Bsl5			5.00	0.07	54	38	32
		Bsl8un			8.00		45	29	24
		Bsl12un	12.00		38		23	19	
		Bsl16un	16.00		33		19	17	
		Bs	B2		Bsl2	2.00	0.33	0.07	52
Bstc2	4.00			0.02	66	48		41	
Bstc3				0.03	57	36		27	
Bstc5				0.05	48	29		21	
Bs				0.07	42	26		20	
Bstc10				0.10	37	24		20	
Bstc12				0.12	35	23		19	
Bstc15				0.15	33	22		19	
Bstc20				0.20	31	21		18	

Table 5.10 – bm received by the beam when loaded at $\frac{1}{2} L$, lin and $\frac{1}{4} L$ (cont.)

Set	Beam	Modeling	Span	Beam	Concrete	bm		
			(x_1)	location (x_2)	thickness (x_3)	Loading		
			L	b_l	h_c	$\frac{1}{2} L$	lin	$\frac{1}{4} L$
			[m]			[%]		
Bs	B2	Bsl5	5.00	0.33	0.07	39	24	20
		Bsl8un	8.00			34	20	18
		Bsl12un	12.00			29	18	17
		Bsl16un	16.00			26	17	16
Bs	B3	Bsl2	2.00	0.67	0.07	50	34	28
		Bstc2	4.00		0.02	65	46	39
		Bstc3			0.03	56	34	25
		Bstc5			0.05	45	25	16
		Bs			0.07	39	21	15
		Bstc10	0.10		34	19	14	
		Bstc12	0.12		31	18	14	
		Bstc15	0.15		29	17	14	
		Bstc20	0.20		28	17	14	
		Bsl5	5.00		0.07	36	19	14
		Bsl8un	8.00			31	16	14
		Bsl12un	12.00			26	15	14
		Bsl16un	16.00			24	15	14
		Bs	B4		Bsl2	2.00	1.00	0.07
Bstc2	4.00			0.02	65	46		38
Bstc3				0.03	56	34		24
Bstc5				0.05	45	24		16
Bs				0.07	39	21		14
Bstc10	0.10			33	18	13		
Bstc12	0.12			31	17	13		
Bstc15	0.15			29	16	13		
Bstc20	4.00			0.20	27	16		13
Bsl5	5.00			0.07	35	18		12
Bsl8un	8.00				30	15		12
Bsl12un	12.00				26	14		13
Bsl16un	16.00				23	14		14
Un	B1			L2un	2.00	0.00		0.03
		L4un	4.00	70	56		-	
		Bsl8un	8.00	0.07	45		29	24
		Bsl12un	12.00		38		23	19
		Bsl16un	16.00		33		19	17
Un	B2	L2un	2.00	0.33	0.03	64	49	-
		L4un	4.00			50	31	-

Table 5.10 – bm received by the beam when loaded at $\frac{1}{2} L$, lin and $\frac{1}{4} L$ (cont.)

Set	Beam	Modeling	Span	Beam	Concrete	bm		
			(x_1)	location (x_2)	thickness (x_3)	Loading		
			L	b_l	h_c	$\frac{1}{2} L$	lin	$\frac{1}{4} L$
[m]						[%]		
Un	B2	Bsl8un	8.00	0.33	0.07	34	20	18
		Bsl12un	12.00			29	18	17
		Bsl16un	16.00			26	17	16
Un	B3	L2un	2.00	0.67	0.03	63	47	-
		L4un	4.00			48	27	-
		Bsl8un	8.00		0.07	31	16	14
		Bsl12un	12.00			26	15	14
		Bsl16un	16.00			24	15	14
Un	B4	L2un	2.00	1.00	0.03	63	47	-
		L4un	4.00			47	27	-
		Bsl8un	8.00		0.07	30	15	12
		Bsl12un	12.00			26	14	13
		Bsl16un	16.00			23	14	14
EC5	B1	L2	2.00	0.00	0.03	85	79	-
		L4	4.00			75	64	
		Bsl8ht	8.00		0.07	48	32	
		L12	12.00			44	29	
		L16	16.00			37	23	
EC5	B2	L2	2.00	0.33	0.03	67	54	
		L4	4.00			55	36	
		Bsl8ht	8.00		0.07	36	22	
		L12	12.00			33	20	
		L16	16.00			29	18	
EC5	B3	L2	2.00	0.67	0.03	66	52	
		L4	4.00			54	34	
		Bsl8ht	8.00		0.07	32	17	
		L12	12.00			30	16	
		L16	16.00			27	15	
EC5	B4	L2	2.00	1.00	0.03	66	52	
		L4	4.00			54	34	
		Bsl8ht	8.00		0.07	31	16	
		L12	12.00			29	15	
		L16	16.00			26	15	
Ov	B1	L2ov	2.00	0.00	0.07	89	86	-
		L4ov	4.00			70	60	
		L8ov	8.00			51	35	

Table 5.10 – bm received by the beam when loaded at $\frac{1}{2} L$, lin and $\frac{1}{4} L$ (cont.)

Set	Beam	Modeling	Span (x_1)	Beam location (x_2)	Concrete thickness (x_3)	bm		
			L	b_l	h_c	Loading		
			[m]			$\frac{1}{2} L$	lin	$\frac{1}{4} L$
O_v	B1	L12ov	12.00	0.00	0.07	41	26	-
		L16ov	16.00			36	22	
O_v	B2	L2ov	2.00	0.33	0.07	74	64	
		L4ov	4.00			52	36	
		L8ov	8.00			39	24	
		L12ov	12.00			33	20	
		L16ov	16.00			29	18	
O_v	B3	L2ov	2.00	0.67	0.07	73	61	
		L4ov	4.00			50	33	
		L8ov	8.00			36	19	
		L12ov	12.00			30	16	
		L16ov	16.00			27	15	
O_v	B4	L2ov	2.00	1.00	0.07	73	61	
		L4ov	4.00			50	33	
		L8ov	8.00			35	18	
		L12ov	12.00			30	15	
		L16ov	16.00			26	15	

Finally, the curves were created joining all the parameters, namely their variation and the corresponding percentages of bm . These curves were considered “continuous”, gathering the results for B1 to B4, and were presented for each loading by span and set, Fig. 5.17, with the data grouped by set of modeling considering all the related ones.

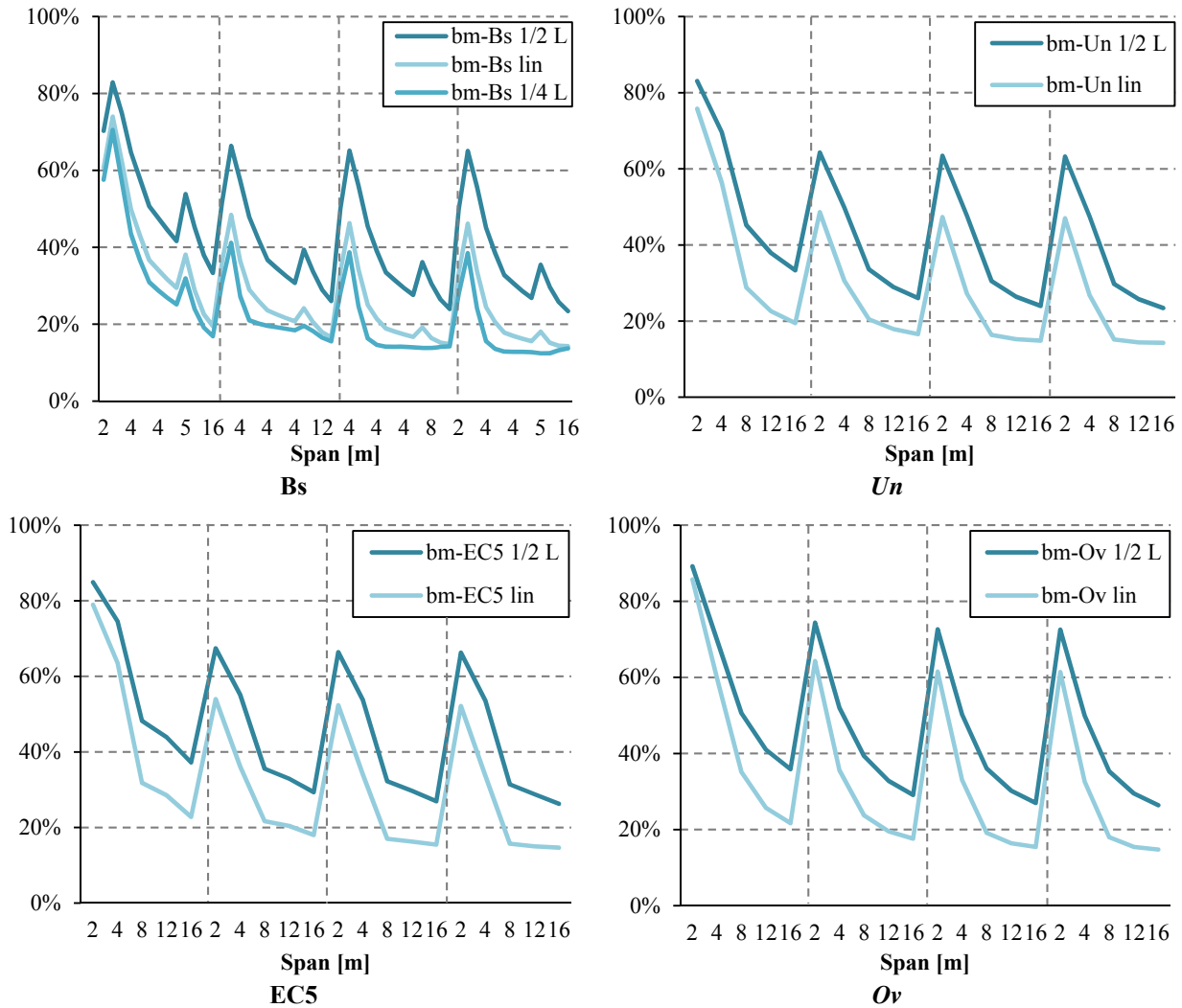


Fig. 5.17 – Parameter variation curves for the various sets

Based in these curves and considering as variables for the sought equation:

- x_1 the span length;
- x_2 the beam location;
- x_3 the concrete thickness;

various polynomial equations were used to approximate the concerned curves. Starting from the simplest polynomials, *i.e.*, first degree polynomials until the fourth degree, simple and with crossed terms, all were tried in the approximation process. The following equations, (24) to (29) express the form of each of the polynomials that were used.

First degree polynomial, simple:

$$z = a_0 + a_1 \cdot x_1 + a_2 \cdot x_2 + a_3 \cdot x_3 \quad (24)$$

First degree polynomial, crossed terms:

$$z = a_0 + a_1 \cdot x_1 + a_2 \cdot x_2 + a_3 \cdot x_3 + a_4 \cdot x_1 \cdot x_2 + a_5 \cdot x_1 \cdot x_3 + a_6 \cdot x_2 \cdot x_3 \quad (25)$$

Second degree polynomial, simple:

$$z = a_0 + a_1 \cdot x_1 + a_2 \cdot x_2 + a_3 \cdot x_3 + a_4 \cdot x_1^2 + a_5 \cdot x_2^2 + a_6 \cdot x_3^2 \quad (26)$$

Second degree polynomial, crossed terms:

$$z = a_0 + a_1 \cdot x_1 + a_2 \cdot x_2 + a_3 \cdot x_3 + a_4 \cdot x_1 \cdot x_2 + a_5 \cdot x_1 \cdot x_3 + a_6 \cdot x_2 \cdot x_3 + a_7 \cdot x_1^2 + a_8 \cdot x_2^2 + a_9 \cdot x_3^2 \quad (27)$$

Third degree polynomial, simple:

$$z = a_0 + a_1 \cdot x_1 + a_2 \cdot x_2 + a_3 \cdot x_3 + a_4 \cdot x_1^2 + a_5 \cdot x_2^2 + a_6 \cdot x_3^2 + a_7 \cdot x_1^3 + a_8 \cdot x_2^3 + a_9 \cdot x_3^3 \quad (28)$$

Fourth degree polynomial, simple:

$$z = a_0 + a_1 \cdot x_1 + a_2 \cdot x_2 + a_3 \cdot x_3 + a_4 \cdot x_1^2 + a_5 \cdot x_2^2 + a_6 \cdot x_3^2 + a_7 \cdot x_1^3 + a_8 \cdot x_2^3 + a_9 \cdot x_3^3 + a_{10} \cdot x_1^4 + a_{11} \cdot x_2^4 + a_{12} \cdot x_3^4 \quad (29)$$

For each of the polynomials, a set of coefficients $\{a_0, a_1, a_2, \dots, a_{11}, a_{12}\}$, depending on the polynomial degree, was obtained attempting to adjust each of the parameter variation curves. This was attained by minimizing the sum of the squared differences between the numerical and the polynomial predictions. Table 5.11 shows the coefficients that were obtained for the various sets and loading cases. A wide exposition can be found in the *C.3.2 Adjustment of bm distribution through polynomial equations, Appendix C*, with the corresponding curves. Also the determination coefficient, R^2 , is presented. This coefficient provides a measure of the “approximation degree” between the polynomial equation and the data which is to be approximated, *i.e.* it denotes the strength of the approximation. The determination coefficient ranges between 0 (weakest approximation) and 1 (strongest approximation), and it is given by:

$$R^2 = \frac{\sum(z_i - \bar{Z})^2}{\sum(Z_i - \bar{Z})^2} \quad (30)$$

where: R is the correlation coefficient;

z_i is the value given by the polynomial fit for the i point;

\bar{Z} is the average of the values to approximation;
 Z_i is the value to approximate for the i point.

Table 5.11 – Polynomial coefficients to approximate the parameter variation curves

Set	Loading	Polynomial													R ²			
		Degree	Coefficients															
			a ₀	a ₁	a ₂	a ₃	a ₄	a ₅	a ₆	a ₇	a ₈	a ₉	a ₁₀	a ₁₁		a ₁₂		
Bs	½ L	1 st , s	0.8	0.0	-0.2	-1.9											0.80	
		1 st , c	0.7	0.0	-0.2	-0.1	0.0	-0.5	0.2								0.81	
		2 nd , s	1.1	0.0	-0.5	-5.5	0.0	0.3	16.7								0.97	
		2 nd , c	0.7	0.0	-0.5	-0.3	0.0	-1.3	0.2	0.0	0.3	16.7					0.98	
		3 rd , s	1.2	-0.1	-0.7	-9.1	0.0	0.9	56.4	0.0	-0.4	-121					0.99	
		4 th , s	1.3	-0.1	-0.6	-13.0	0.0	0.5	129	0.0	0.2	-621	0.0	-0.3	1143		0.99	
	lin	1 st , s	0.6	0.0	-0.2	-1.5											0.70	
		1 st , c	0.5	0.0	-0.3	-0.1	0.0	-0.5	0.7								0.73	
		2 nd , s	0.9	-0.1	-0.5	-5.0	0.0	0.3	16.0								0.90	
		2 nd , c	0.6	0.0	-0.6	-0.3	0.0	-1.3	0.7	0.0	0.3	16.0					0.93	
		3 rd , s	1.1	-0.1	-0.7	-9.9	0.0	0.9	70.6	0.0	-0.4	-166					0.93	
		4 th , s	1.4	-0.2	-0.6	-18.3	0.0	0.5	226	0.0	0.2	-1239	0.0	-0.3	2459		0.94	
	¼ L	1 st , s	0.5	0.0	-0.2	-1.2											0.61	
		1 st , c	0.5	0.0	-0.4	-0.1	0.0	-0.4	1.0								0.67	
		2 nd , s	0.8	0.0	-0.5	-4.4	0.0	0.3	14.8								0.81	
		2 nd , c	0.5	0.0	-0.7	-0.3	0.0	-1.2	1.0	0.0	0.3	14.8					0.87	
		3 rd , s	1.1	-0.1	-0.6	-9.9	0.0	0.8	76.0	0.0	-0.3	-186					0.87	
		4 th , s	1.4	-0.3	-0.6	-21.5	0.0	0.5	288	0.0	0.2	-1645	0.0	-0.3	3334		0.89	
	Un	½ L	1 st , s	1.3	-0.1	-0.2	-10.5											0.83
			1 st , c	1.3	-0.1	-0.2	-10.5	0.0	1.6	0.6								0.95
			2 nd , s	0.9	-0.1	-0.4	0.0	0.0	0.3	0.0								0.97
			2 nd , c	1.2	-0.1	-0.5	-8.5	0.0	1.3	0.6	0.0	0.3	-0.9					0.99
			3 rd , s	1.0	-0.1	-0.7	-0.7	0.0	0.9	-0.1	0.0	-0.4	0.0					0.99
			4 th , s	1.0	-0.1	-0.6	0.1	0.0	0.5	0.0	0.0	0.2	0.0	0.0	-0.3	0.0		0.99
lin		1 st , s	0.7	0.0	-0.2	-4.4											0.77	
		1 st , c	1.3	-0.2	-0.4	-13.7	0.0	2.3	2.4								0.93	
		2 nd , s	0.8	-0.1	-0.5	1.9	0.0	0.3	0.2								0.90	
		2 nd , c	1.3	-0.2	-0.7	-12.2	0.0	2.1	2.4	0.0	0.3	-1.2					0.96	
		3 rd , s	0.9	-0.2	-0.7	0.8	0.0	0.9	0.1	0.0	-0.4	0.0					0.93	
		4 th , s	1.0	-0.2	-0.6	0.1	0.0	0.5	0.0	0.0	0.2	0.0	0.0	-0.3	0.0		0.93	
EC5	½ L	1 st , s	1.2	-0.1	-0.2	-9.7											0.77	
		1 st , c	1.2	-0.1	-0.2	-9.7	0.0	1.3	-0.2								0.96	
		2 nd , s	1.0	-0.1	-0.5	-1.9	0.0	0.3	-0.2								0.98	
		2 nd , c	1.3	-0.1	-0.5	-10.5	0.0	1.4	-0.2	0.0	0.3	-1.1					0.99	
		3 rd , s	1.1	-0.2	-0.6	0.1	0.0	0.8	0.0	0.0	-0.3	0.0					0.99	
		4 th , s	0.9	0.0	-0.6	0.1	0.0	0.5	0.0	0.0	0.2	0.0	0.0	-0.3	0.0		0.99	

Table 5.11 – Polynomial coefficients to approximate the parameter variation curves (cont.)

Set	Loading	Polynomial														R ²	
		Degree	Coefficients														
			a ₀	a ₁	a ₂	a ₃	a ₄	a ₅	a ₆	a ₇	a ₈	a ₉	a ₁₀	a ₁₁	a ₁₂		
EC5	<i>lin</i>	1 st , s	0.8	0.0	-0.2	-5.5											0.84
		1 st , c	1.3	-0.2	-0.3	-13.6	0.0	2.1	1.5								0.94
		2 nd , s	0.9	-0.1	-0.5	-0.1	0.0	0.3	0.0								0.93
		2 nd , c	1.4	-0.2	-0.7	-14.3	0.0	2.2	1.5	0.0	0.3	-1.4					0.97
		3 rd , s	1.2	-0.2	-0.6	0.1	0.0	0.8	0.0	0.0	-0.4	0.0					0.96
		4 th , s	0.9	-0.1	-0.7	0.1	0.0	0.6	0.0	0.0	0.2	0.0	0.0	-0.3	0.0		0.96
Ov	$\frac{1}{2}$ L	1 st , s	0.8	0.0	-0.2	0.1											0.40
		1 st , c	0.8	0.0	-0.2	0.1	0.0	0.0	0.0								0.83
		2 nd , s	1.0	-0.1	-0.4	0.1	0.0	0.3	0.0								0.96
		2 nd , c	1.0	-0.1	-0.4	0.1	0.0	0.0	0.0	0.0	0.3	0.0					0.97
		3 rd , s	1.1	-0.2	-0.6	0.1	0.0	0.8	0.0	0.0	-0.3	0.0					0.99
		4 th , s	1.3	-0.3	-0.5	0.1	0.0	0.4	0.0	0.0	0.2	0.0	0.0	-0.3	0.0		0.99
	<i>lin</i>	1 st , s	0.7	0.0	-0.2	0.0											0.73
		1 st , c	0.7	0.0	-0.3	0.1	0.0	0.0	0.0								0.75
		2 nd , s	0.9	-0.1	-0.5	0.1	0.0	0.3	0.0								0.93
		2 nd , c	1.0	-0.1	-0.6	0.1	0.0	0.0	0.0	0.0	0.3	0.0					0.94
		3 rd , s	1.2	-0.2	-0.6	0.1	0.0	0.8	0.0	0.0	-0.4	0.0					0.97
		4 th , s	1.3	-0.4	-0.6	0.1	0.1	0.5	0.0	0.0	0.2	0.0	0.0	-0.3	0.0		0.97

s - simple; c - with crossed terms

Aiming to obtain a single polynomial capable to predict the behavior of the composite floors under study when a concentrated load is acting, the polynomial coefficients had to be analyzed in order to find similarities. Thus, since for the Bs set those results were available for three different loadings, they were compared against each other, $\frac{1}{2}$ L vs. *lin*, $\frac{1}{4}$ L vs. $\frac{1}{2}$ L and $\frac{1}{4}$ vs. *lin*. Table 5.12 summarizes the results.

In general, all the tested polynomial curves present relatively similar coefficients. This comes from the ratios comparing the three loadings, Table 5.12, which differ on average 12 % from each other. From this analysis it was also observed a tendency for the second degree polynomial, simple, to present very similar coefficients for the analyzed loading, as the values in bold prove, by their proximity to 1.00. Therefore, this was the chosen polynomial to approximate the parameter variation curves, Fig. 5.18, and consequently the percentage of *vd*, *sr*, or *bm* received by the loaded beam.

Table 5.12 – Comparison between coefficients of the polynomial fit for Bs

Ratio	Polynomial														
	Degree	Relation between coefficients													Average
		a ₀	a ₁	a ₂	a ₃	a ₄	a ₅	a ₆	a ₇	a ₈	a ₉	a ₁₀	a ₁₁	a ₁₂	
½ L vs. lin	1 st , s	1.33	1.24	0.88	1.28										1.18
	1 st , c	1.25	1.43	0.64	1.00	0.43	1.08	0.26							0.87
	2 nd , s	1.20	0.95	0.93	1.12	0.82	0.96	1.04							1.00
	2 nd , c	1.18	1.43	0.80	1.04	0.43	1.06	0.26	0.82	0.96	1.04				0.90
	3 rd , s	1.09	0.76	0.99	0.92	0.65	1.07	0.80	0.61	1.12	0.73				0.87
	4 th , s	0.98	0.66	0.98	0.71	0.57	1.08	0.57	0.54	0.95	0.50	0.53	1.06	0.46	0.74
¼ L vs. ½ L	1 st , s	0.64	0.61	1.15	0.64										0.76
	1 st , c	0.71	0.75	1.79	0.97	2.88	0.87	5.49							1.92
	2 nd , s	0.73	0.97	1.05	0.80	1.21	1.00	0.88							0.95
	2 nd , c	0.76	0.61	1.33	0.90	2.88	0.88	5.49	1.21	1.00	0.88				1.59
	3 rd , s	0.88	1.51	0.96	1.09	1.96	0.85	1.35	2.20	0.78	1.53				1.31
	4 th , s	1.08	2.03	0.98	1.65	2.62	0.87	2.23	2.90	0.92	2.65	3.05	0.83	2.92	1.90
¼ L vs. lin	1 st , s	0.84	0.76	1.01	0.82										0.86
	1 st , c	0.89	1.07	1.15	0.96	1.24	0.94	1.41							1.09
	2 nd , s	0.88	0.92	0.98	0.89	0.99	0.97	0.92							0.94
	2 nd , c	0.91	0.87	1.06	0.93	1.24	0.93	1.41	0.99	0.97	0.92				1.02
	3 rd , s	0.96	1.15	0.95	1.01	1.27	0.91	1.08	1.34	0.87	1.12				1.07
	4 th , s	1.06	1.34	0.96	1.18	1.49	0.93	1.28	1.56	0.87	1.33	1.60	0.87	1.36	1.22

s - simple; c - with crossed terms

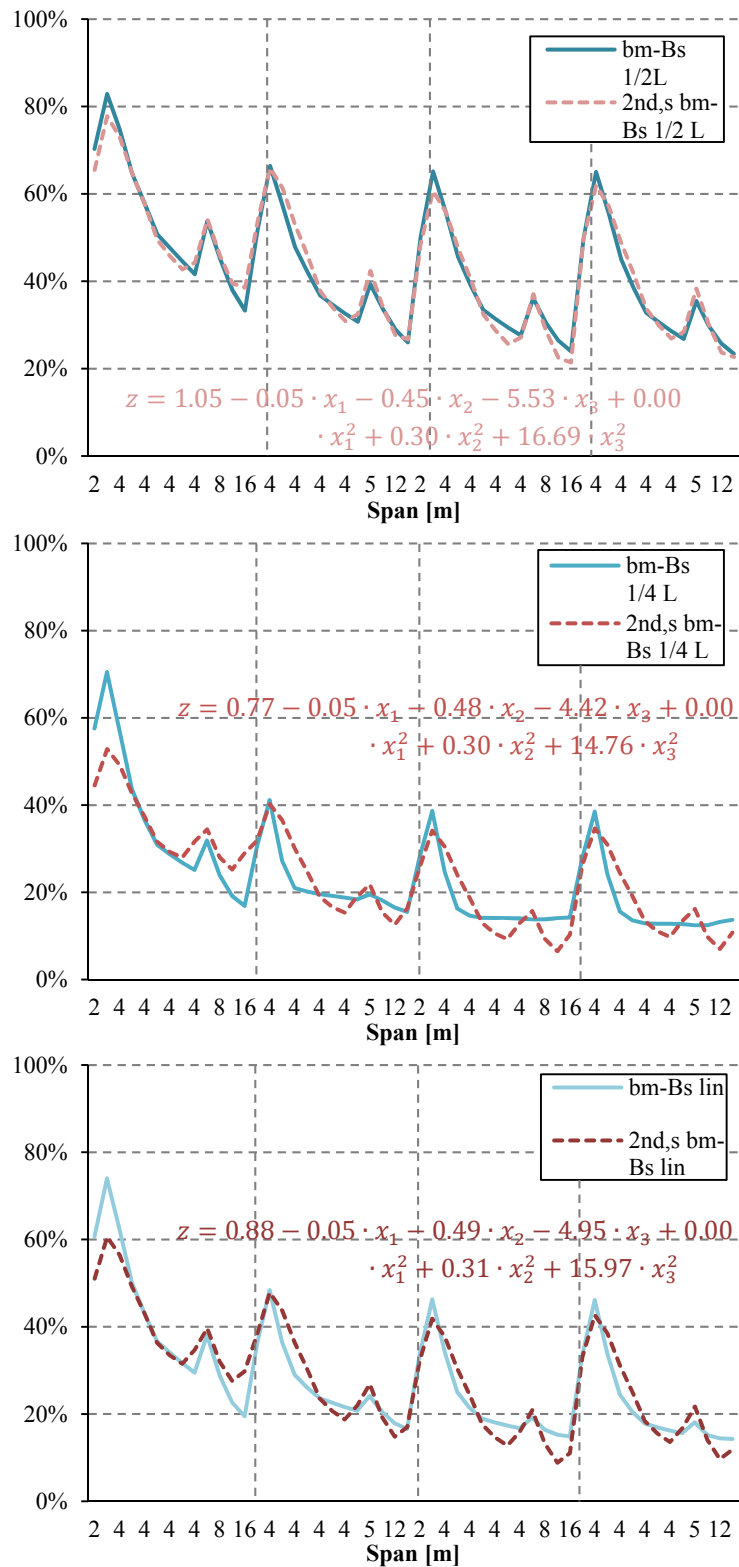


Fig. 5.18 – Bs set parameter variation curves and 2nd degree polynomial fit for 1/2 L, 1/4 L and lin

To define the searched polynomial, the coefficients were obtained by computing the average between those found for the three loading cases. As the equation in question intends to determine the percentage received by the loaded beam, Pr was the designation chosen for the polynomial. Fig. 5.19 shows the course of Pr , as function of the floor span, together with the Bs curves. As can be observed there are some difference between the polynomial prediction and the numerical one, with Pr tending to be closer to the *lin* load case curve than to the other load cases. Table 5.13 gathers the percentages found numerically and with Pr , as well as the associated differences.

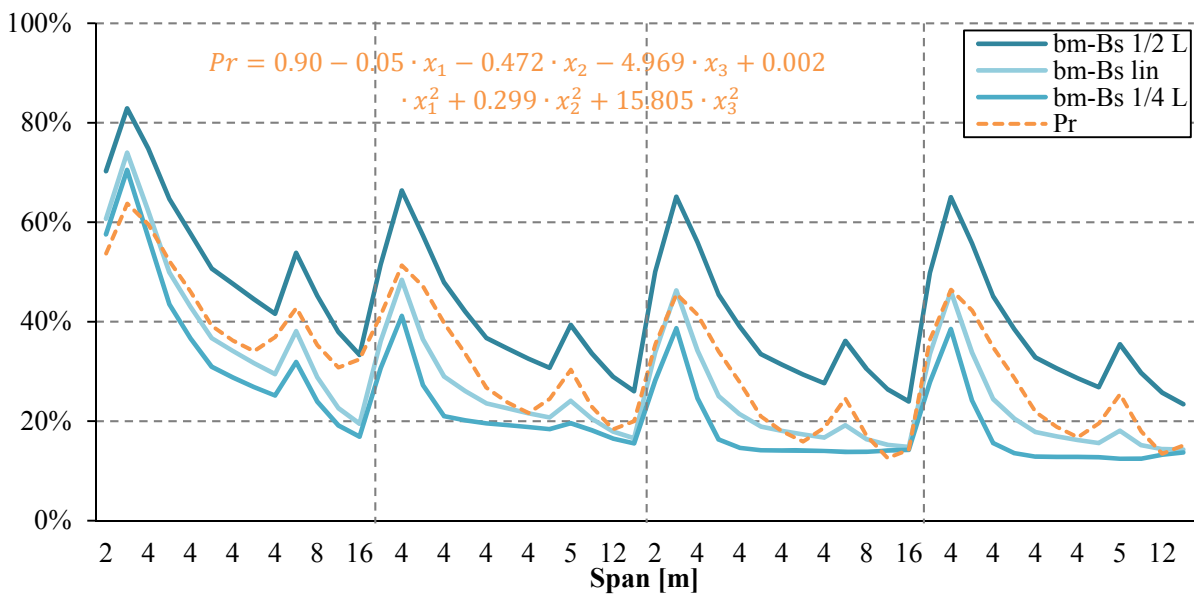


Fig. 5.19 – Bs set parameter variation curves and Pr polynomial

In general, Pr tends to underestimate the percentages associated with the point load at mid-span, presenting an opposite trend concerning the remaining load cases. Despite the fact that for both point loadings, the maximum difference found was $\pm 20\%$, essentially associated with small concrete thicknesses, the average differences were about -11% and $+8\%$, for $\frac{1}{2}L$ and $\frac{1}{4}L$ respectively. For the *lin* loading, as could be expected from Fig. 5.19, the differences are smaller than the previous ranging between -10% and $+15\%$, with an average difference of $+4\%$.

Table 5.13 – *bm* percentages predicted for Bs: numerical vs. *Pr* polynomial

Beam	Modeling	x_1	x_2	x_3	<i>bm</i>			Differences				
					Numerical		<i>Pr</i>	<i>Pr</i> vs. $\frac{1}{2}$ L	<i>Pr</i> vs. <i>lin</i>	<i>Pr</i> vs. $\frac{1}{4}$ L		
		Loading		$\frac{1}{2}$ L	<i>lin</i>	$\frac{1}{4}$ L						
		<i>L</i>	<i>b_l</i>	<i>h_c</i>	$\frac{1}{2}$ L	<i>lin</i>	$\frac{1}{4}$ L	$\frac{1}{2}$ L	<i>lin</i>	$\frac{1}{4}$ L		
[m]				[%]								
B1	Bsl2	2.00	4.00	0.00	0.07	70	61	58	54	-17	-7	-4
	Bstc2	4.00			0.02	83	74	70	64	-19	-10	-7
	Bstc3				0.03	75	62	57	60	-15	-3	3
	Bstc5				0.05	65	50	44	52	-12	2	9
	Bs				0.07	58	43	37	46	-12	3	10
	Bstc10				0.10	51	37	31	39	-11	3	8
	Bstc12				0.12	48	34	29	36	-11	2	8
	Bstc15				0.15	45	32	27	34	-10	3	7
	Bstc20				0.20	42	29	25	37	-5	8	12
	Bsl5				5.00	0.07	54	38	32	43	-11	5
	Bsl8un	8.00			45		29	24	36	-9	7	12
	Bsl12un	12.00			38		23	19	32	-6	9	13
	Bsl16un	16.00			33		19	17	34	1	15	17
B2	Bsl2	2.00	4.00	0.33	0.07	52	36	31	41	-10	5	11
	Bstc2	4.00			0.02	66	48	41	51	-15	3	10
	Bstc3				0.03	57	36	27	47	-10	11	20
	Bstc5				0.05	48	29	21	40	-8	11	19
	Bs				0.07	42	26	20	34	-8	8	14
	Bstc10				0.10	37	24	20	27	-10	3	7
	Bstc12				0.12	35	23	19	24	-11	1	5
	Bstc15				0.15	33	22	19	22	-11	0	3
	Bstc20				0.20	31	21	18	25	-6	4	6
	Bsl5				5.00	0.07	39	24	20	31	-9	6
	Bsl8un	8.00			34		20	18	23	-10	3	5
	Bsl12un	12.00			29		18	17	19	-10	1	3
	Bsl16un	16.00			26		17	16	22	-4	5	6
B3	Bsl2	2.00	4.00	0.67	0.07	50	34	28	36	-14	2	7
	Bstc2	4.00			0.02	65	46	39	46	-19	-1	7
	Bstc3				0.03	56	34	25	42	-14	7	17
	Bstc5				0.05	45	25	16	34	-11	9	18
	Bs				0.07	39	21	15	28	-11	7	13
	Bstc10				0.10	34	19	14	21	-12	2	7
	Bstc12				0.12	31	18	14	18	-13	0	4
	Bstc15				0.15	29	17	14	16	-13	-1	2
	Bstc20				0.20	28	17	14	19	-9	2	5
	Bsl5				5.00	0.07	36	19	14	25	-11	6
Bsl8un	8.00	31	16	14	18		-13	1	4			

Table 5.13 – *bm* percentages predicted for Bs: numerical vs. *Pr* polynomial (cont.)

Beam	Modeling	x_1	x_2	x_3	<i>bm</i>			Differences				
					Numerical		<i>Pr</i>	<i>Pr</i> vs. ½ L	<i>Pr</i> vs. <i>lin</i>	<i>Pr</i> vs. ¼ L		
		Loading		½ L	<i>lin</i>	¼ L						
		<i>L</i>	<i>b_l</i>	<i>h_c</i>	½ L	<i>lin</i>	¼ L	½ L	<i>lin</i>	¼ L		
[m]				[%]								
B3	Bsl12un	12.00	0.67	0.07	26	15	14	14	-13	-2	-1	
	Bsl16un	16.00			24	15	14	16	-8	1	2	
B4	Bsl2	2.00	4.00	1.00	0.07	50	33	28	36	-13	3	9
	Bstc2				0.02	65	46	38	47	-18	0	8
	Bstc3				0.03	56	34	24	42	-13	9	18
	Bstc5				0.05	45	24	16	35	-10	11	19
	Bs				0.07	39	21	14	29	-10	8	15
	Bstc10				0.10	33	18	13	22	-11	4	9
	Bstc12				0.12	31	17	13	19	-12	2	6
	Bstc15				0.15	29	16	13	17	-12	1	4
	Bstc20				0.20	27	16	13	20	-7	4	7
	Bsl5				5.00	0.07	35	18	12	26	-10	8
	Bsl8un		8.00	30	15		12	18	-11	3	6	
	Bsl12un	12.00	26	14	13		14	-11	0	1		
	Bsl16un	16.00	23	14	14		17	-7	3	3		

Aiming at confirming the adequacy of *Pr* for any configuration of timber-concrete composite floors, also the remaining sets were compared with its predictions, Table 5.14 and Fig. 5.20. The differences between numerical and polynomial predictions, for *Un* and EC5 sets, tended to be very similar to those found for Bs. In fact, extreme differences, maximum and minimum, decreased, whereas the average differences were rather similar: - 9 % (*Un*) and - 12 % (EC5) for ½ L; + 5 % (*Un*) and + 2 % (EC5) for *lin*; + 6 % (*Un*) for ¼ L.

Table 5.14 – *bm* percentages predicted for *Un*, EC5 and *Ov*: numerical vs. *Pr* polynomial

Set	Beam	Modeling	x_1	x_2	x_3	<i>bm</i>				Differences		
			<i>L</i>	<i>b_l</i>	<i>h_c</i>	Numerical			<i>Pr</i>	<i>Pr</i>	<i>Pr</i>	<i>Pr</i>
						Loading				vs.	vs.	vs.
						$\frac{1}{2}$ L	<i>lin</i>	$\frac{1}{4}$ L		$\frac{1}{2}$ L	<i>lin</i>	$\frac{1}{4}$ L
[m]					[%]							
<i>Un</i>	B1	L2un	2.00	0.00	0.03	83	76	-	67	-16	-8	-
		L4un	4.00			70	56	-	60	-10	3	-
		Bsl8un	8.00		0.07	45	29	24	36	-9	7	12
		Bsl12un	12.00			38	23	19	32	-6	9	13
		Bsl16un	16.00			33	19	17	34	1	15	17
<i>Un</i>	B2	L2un	2.00	0.33	0.03	64	49	-	55	-9	6	-
		L4un	4.00			50	31	-	47	-2	17	-
		Bsl8un	8.00		0.07	34	20	18	23	-10	3	5
		Bsl12un	12.00			29	18	17	19	-10	1	3
		Bsl16un	16.00			26	17	16	22	-4	5	6
<i>Un</i>	B3	L2un	2.00	0.67	0.03	63	47	-	49	-14	2	-
		L4un	4.00			48	27	-	42	-6	14	-
		Bsl8un	8.00		0.07	31	16	14	18	-13	1	4
		Bsl12un	12.00			26	15	14	14	-13	-2	-1
		Bsl16un	16.00			24	15	14	16	-8	1	2
<i>Un</i>	B4	L2un	2.00	1.00	0.03	63	47	-	50	-13	3	-
		L4un	4.00			47	27	-	42	-5	16	-
		Bsl8un	8.00		0.07	30	15	12	18	-11	3	6
		Bsl12un	12.00			26	14	13	14	-11	0	1
		Bsl16un	16.00			23	14	14	17	-7	3	3
EC5	B1	L2	2.00	0.00	0.03	85	79	-	67	-18	-12	-
		L4	4.00			75	64		60	-15	-4	
		Bsl8ht	8.00		0.07	48	32		36	-12	4	
		L12	12.00			44	29		32	-12	3	
		L16	16.00			37	23		34	-3	11	
EC5	B2	L2	2.00	0.33	0.03	67	54	-	55	-13	1	-
		L4	4.00			55	36		47	-8	11	
		Bsl8ht	8.00		0.07	36	22		23	-12	2	
		L12	12.00			33	20		19	-14	-1	
		L16	16.00			29	18		22	-8	4	
EC5	B3	L2	2.00	0.67	0.03	66	52	-	49	-17	-3	-
		L4	4.00			54	34		42	-12	7	
		Bsl8ht	8.00		0.07	32	17		18	-15	1	
		L12	12.00			30	16		14	-16	-3	
		L16	16.00			27	15		16	-11	1	

Table 5.14 – *bm* percentages predicted for *Un*, EC5 and *Ov*: numerical vs. *Pr* polynomial

Set	Beam	Modeling	x_1	x_2	x_3	bm			Differences			
			<i>L</i>	<i>b_t</i>	<i>h_c</i>	Numerical		<i>Pr</i>	<i>Pr</i> vs. $\frac{1}{2}$ L	<i>Pr</i> vs. <i>lin</i>	<i>Pr</i> vs. $\frac{1}{4}$ L	
						$\frac{1}{2}$ L	<i>lin</i>					$\frac{1}{4}$ L
			[m]					[%]				
EC5	B4	L2	2.00	1.00	0.03	66	52	-	50	-16	-2	-
		L4	4.00			54	34		42	-11	9	
		Bsl8ht	8.00		31	16	18		-13	3		
		L12	12.00	29	15	14	-14		-1			
		L16	16.00	26	15	17	-9		2			
<i>Ov</i>	B1	L2ov	2.00	0.00	0.07	89	86	-	54	-35	-32	-
		L4ov	4.00			70	60		46	-24	-14	
		L8ov	8.00			51	35		36	-15	1	
		L12ov	12.00			41	26		32	-9	6	
		L16ov	16.00			36	22		34	-2	12	
<i>Ov</i>	B2	L2ov	2.00	0.33	0.07	74	64	-	41	-33	-23	-
		L4ov	4.00			52	36		34	-18	-2	
		L8ov	8.00			39	24		23	-16	0	
		L12ov	12.00			33	20		19	-13	0	
		L16ov	16.00			29	18		22	-7	4	
<i>Ov</i>	B3	L2ov	2.00	0.67	0.07	73	61	-	36	-37	-26	-
		L4ov	4.00			50	33		28	-22	-5	
		L8ov	8.00			36	19		18	-18	-2	
		L12ov	12.00			30	16		14	-17	-3	
		L16ov	16.00			27	15		16	-11	1	
<i>Ov</i>	B4	L2ov	2.00	1.00	0.07	73	61	-	36	-36	-25	-
		L4ov	4.00			50	33		29	-21	-4	
		L8ov	8.00			35	18		18	-17	0	
		L12ov	12.00			30	15		14	-15	-1	
		L16ov	16.00			26	15		17	-10	2	

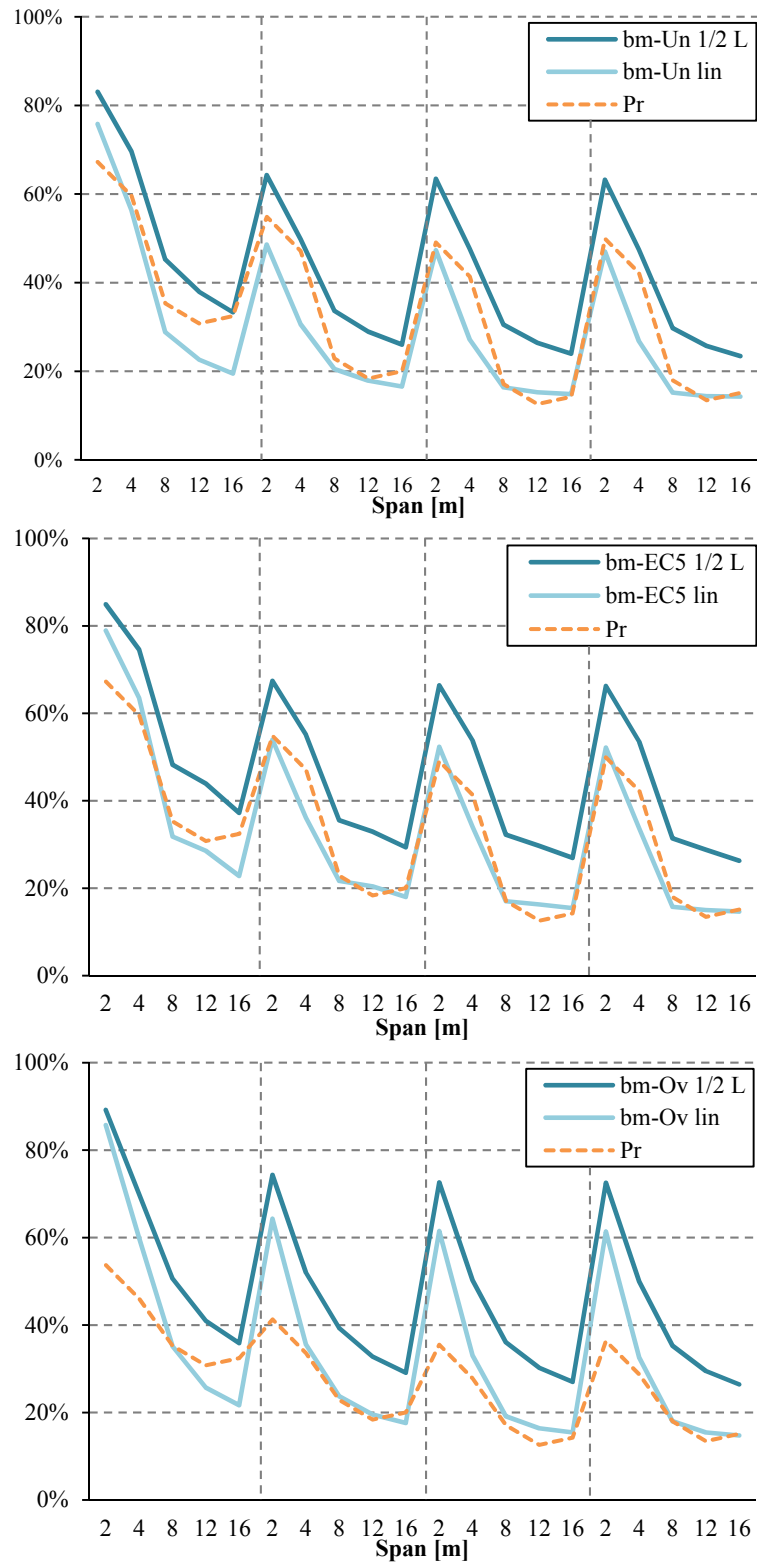


Fig. 5.20 – Un, EC5 and Ov parameter variation curves and Pr polynomial

Concerning the O_v set, P_r predictions tended to deviate from the numerical ones, underestimating them. The differences ranged from - 37 % to - 2 % approximately, with an average of - 19 % for $\frac{1}{2} L$ and - 32 % and + 12 %, with an average of - 5 % for lin .

Through the presented in the previous section, oversized sections tended to concentrate over the loaded beam a higher percentage, when compared with each of the other design sets. Indeed, the P_r polynomial was obtained essentially based on designs, where a higher percentage of the sections was really effective. Hence, the differences found between O_v set and P_r are somehow expected, given the modeling basis of the polynomial fit. Following the presented before about the inadequacy of using oversized sections in the design of the studied structural elements, the fact that P_r does not predict with such accuracy the behavior of this particular set is not relevant.

In addition, a different composite floor was designed according to EC5 (EN1995 2004a, EN1995 2004b), for the loads required by EC1 (EN1991 2001). It corresponds to a 4.00 m wide bridge deck with 20.00 m span. A C30/37 concrete slab 0.20 m thick and seven GL24h timber beams, whose characteristics are presented in Fig. 5.21, composed the floor. The connection system was assumed to be composed by “X” steel connectors and notches. The material properties considered are summarized in Table 3.2. Three loadings were considered: $\frac{1}{2} L$ and $\frac{1}{4} L$, using value recommended by EC1(EN1991 2001); and lin , producing the same bending moment at mid-span as $\frac{1}{2} L$.

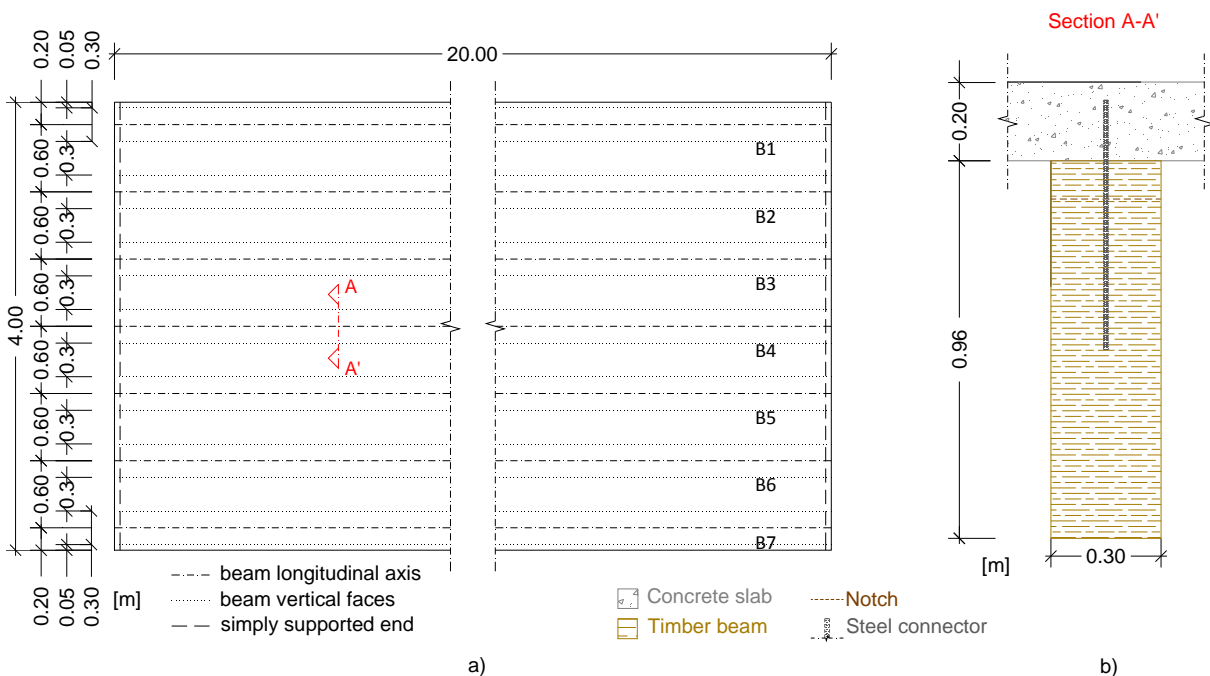
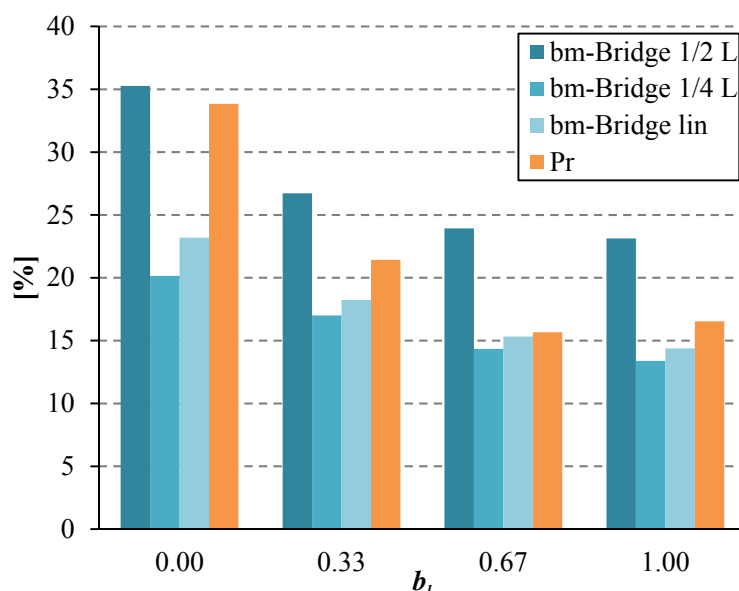


Fig. 5.21 – Bridge geometrical characteristics: a) plan view; b) cross section

Table 5.15 – Bridge material properties

Timber beams		Concrete slab		Connection system	
GL24h		C30/37		“X” steel connector + notches	
MOE	Density	MOE	Mean compressive strength	Shear stiffness	Spacing
$E_{m,g}$	ρ	E_c	f_{cm}	K	s
[MPa]	[kg/m ³]	[MPa]	[MPa]	[kN/m]	[m]
11500	385	33000	38	120000	0.10

This example was modeled using the Frame+Shell model and the results were gathered, for the percentage of bm received by the loaded beam in Fig. 5.22. This figure also represents the prediction obtained with Pr .

Fig. 5.22 – Distribution of bm for $\frac{1}{2}$ L, $\frac{1}{4}$ L and lin loadings in the bridge example

As can be observed, the Pr prediction was relatively similar to the numerical ones. Presenting a clear tendency to approximate to bm at B1 when loaded at mid-span, whereas for the remaining beams this trend does not happen, with Pr being closer to the numerical prediction associated with $\frac{1}{4}$ L and lin . The absolute differences showed to range between -8 ($\frac{1}{2}$ L, B3) and +14 % (lin , B1), while the partial average differences among each loading case ranged between -5 ($\frac{1}{2}$ L) and 6 % (lin), Table 5.16.

Despite the differences found it was considered that the Pr polynomial led to a good prediction of the percentage of bm received by the loaded beams.

Table 5.16 – Numerical vs. Pr polynomial predictions for bm : bridge example

bm				Differences		
Numerical			Pr	Pr	Pr	Pr
Loading				vs.	vs.	vs.
$\frac{1}{2} L$	lin	$\frac{1}{4} L$		$\frac{1}{2} L$	lin	$\frac{1}{4} L$
[%]						
35	23	20	34	-1	11	14
27	18	17	21	-5	3	4
24	15	14	16	-8	0	1
23	14	13	17	-7	2	3
Average			Partial	-5	4	6
			Global	1		

Aiming at evaluating its adequacy to predict the percentage of vd and sr associated to the loaded beams, the results obtained with Pr were compared with the experimental ones for S1 to S5, Fig. 5.23 and Fig. 5.24. Both vertical displacements, at mid- and quarter-span, $vd \frac{1}{2} L$ and $vd \frac{1}{4} L$ respectively, were considered. Table C.48 to Table C.50, in Section C.3.3 *Comparison between experimental and polynomial predictions for S1 to S5*, gather the experimental and the Pr percentages as well as the comparison between the two, through the absolute difference among them. Table 5.17 summarizes the average differences.

Concerning the vertical displacements, either mid- or quarter-span, Pr showed a close approximation to the experimental results, Fig. 5.23, following the progress of the curves. This is more evident for the odd specimens, S1-BSp, S3-hc=0.03m and S5-L=6.00m, with differences ranging between - 10 and - 4 % for $vd \frac{1}{2} L$, and between - 12 and - 6 % for $vd \frac{1}{4} L$, Table 5.17. When considering the even specimens, S2-LWAC and S4-L=2.00m, this closeness tended to decrease, with the differences ranging from - 18 to - 14 % for $vd \frac{1}{2} L$, and between - 20 and - 14 % for $vd \frac{1}{4} L$.

As for the distribution of support reactions, despite presenting a similar progress, the Pr prediction tended to deviate more from the experimental results, Fig. 5.24. In fact, the differences found, Table 5.17, confirmed these findings with differences relatively higher for this quantity, varying among - 39 and - 11 %.

Therefore, in order to make the Pr polynomial suitable to predict the percentages associated with the loaded beams when considering the bending moment, the vertical displacement and the support reaction, an extra coefficient by which Pr should be multiplied was defined: cf_i with $i = \{bm, vd, sr\}$. Thus, instead of using Pr , $cf_i \cdot Pr$ was used.

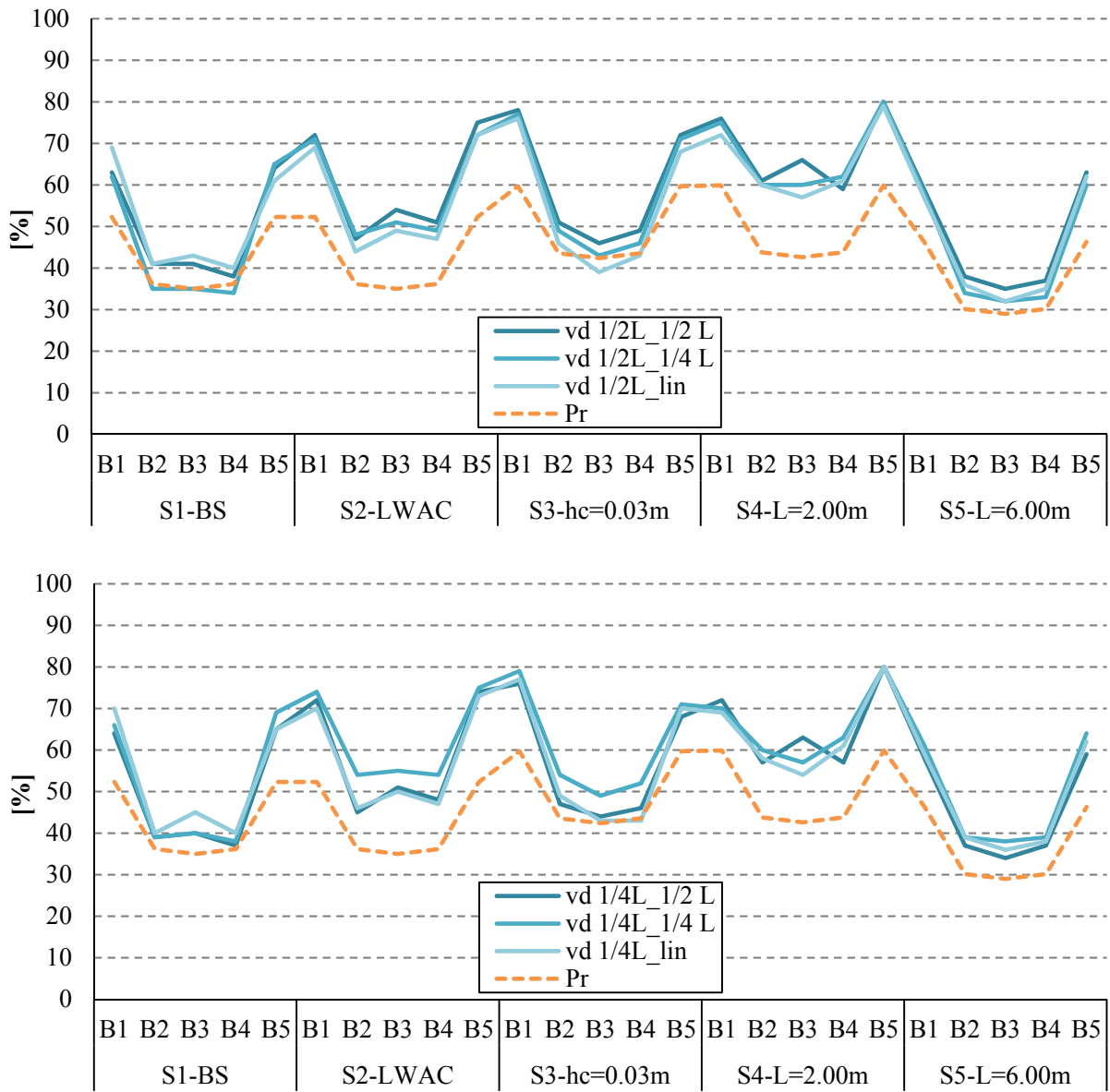


Fig. 5.23 – Experimental $vd \frac{1}{2}L$ and $vd \frac{1}{4}L$ vs. Pr distribution for S1 to S5

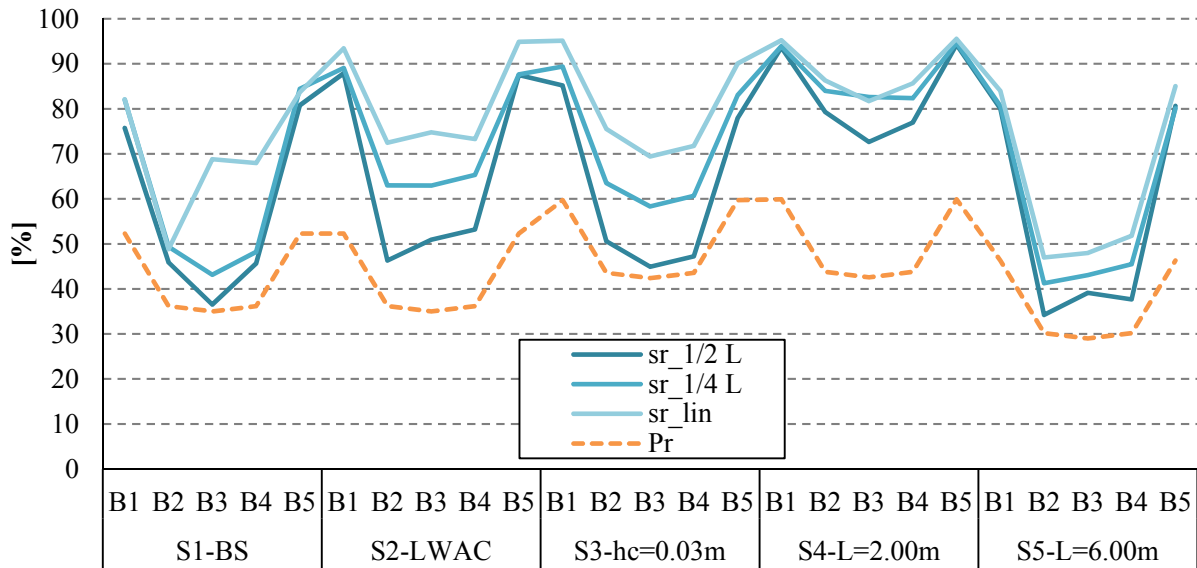


Fig. 5.24 – Distribution of *sr* for S1 to S5 when loaded with ½ L, ¼ L and *lin*

Table 5.17 – Average partial differences: experimental vs. *Pr* for S1 to S5

Specimen	Average partial differences								
	<i>vd</i> ½ L			<i>vd</i> ¼ L			<i>sr</i>		
	<i>Pr</i>	<i>Pr</i>	<i>Pr</i>	<i>Pr</i>	<i>Pr</i>	<i>Pr</i>	<i>Pr</i>	<i>Pr</i>	<i>Pr</i>
	vs.	vs.	vs.	vs.	vs.	vs.	vs.	vs.	vs.
	½ L	¼ L	<i>lin</i>	½ L	¼ L	<i>lin</i>	½ L	¼ L	<i>lin</i>
[%]									
S1	-7	-4	-8	-7	-8	-10	-15	-19	-28
S2	-17	-16	-14	-16	-20	-15	-23	-31	-39
S3	-9	-7	-5	-6	-11	-7	-11	-21	-31
S4	-18	-17	-16	-16	-16	-14	-33	-38	-39
S5	-10	-7	-8	-9	-12	-10	-18	-22	-27

For the bending moment, based on the previous analysis, this coefficient was kept equal to the unity, $cf_{bm} \cdot Pr = 1.00 \cdot Pr = Pr$. Nevertheless, when concerning the vertical displacements and the support reactions distribution the unity is not an adequate value. By using a similar procedure to those which led to define the coefficients a_i associated to Pr , both coefficients, cf_{vd} and cf_{sr} , were obtained by minimizing the squared difference between prediction and experimental results, Table 5.18.

By using the cf_i coefficients, a clearly closer prediction was found with the polynomial approximation as Fig. 5.25, Fig. 5.26 and Table 5.19 confirm. In Section C.3.3, Appendix C, a detailed exposition can be found, with experimental and polynomial percentages, as well as

the corresponding differences obtained for the several specimens and load cases (Table C.51 to Table C.53).

Table 5.18 – cf_i coefficients

Quantity	Coefficients	
Bending moment	cf_{bm}	1.00
Vertical displacement	cf_{vd}	1.25
Support reaction	cf_{sr}	1.60

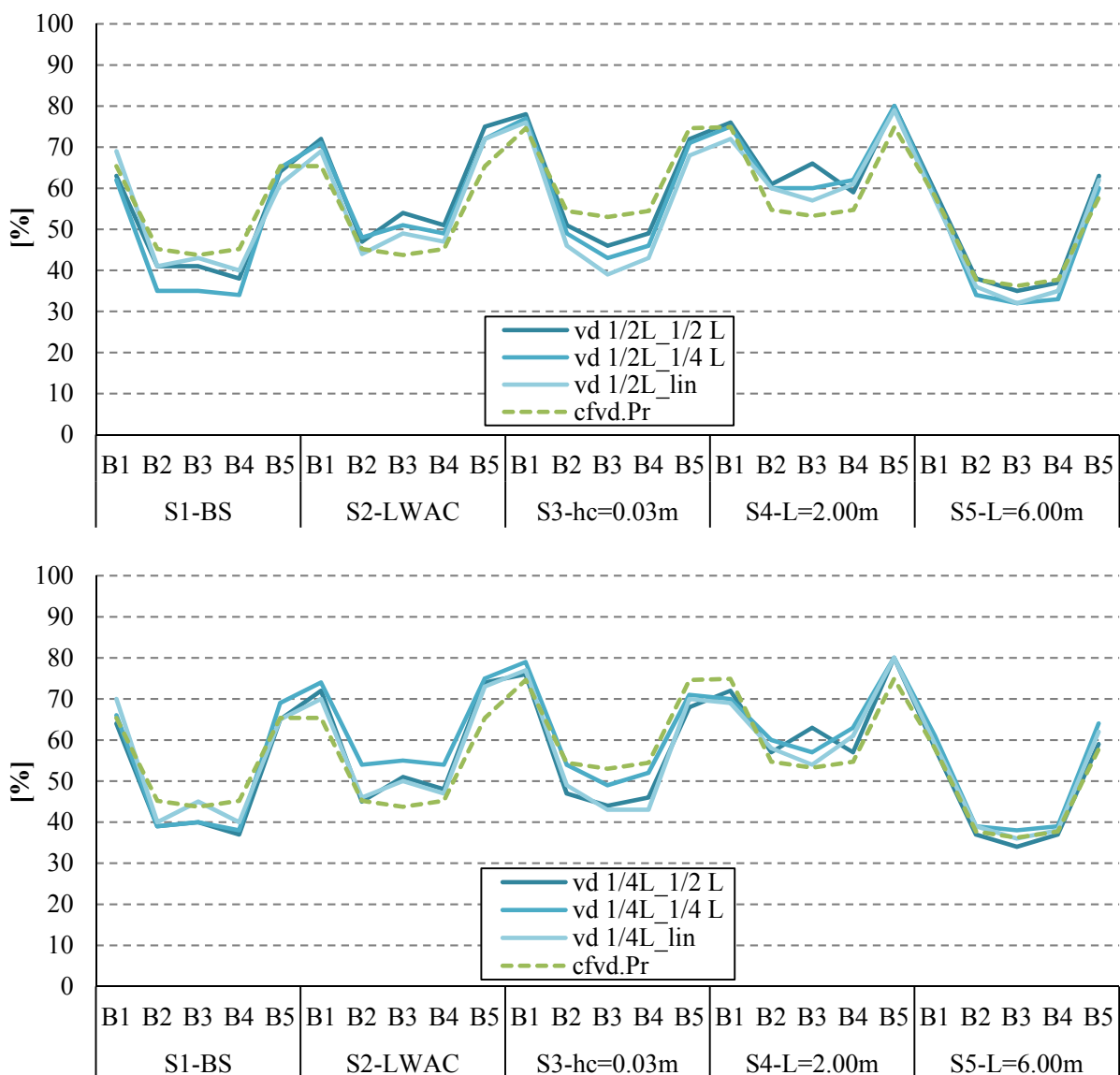


Fig. 5.25 – Experimental $vd \frac{1}{2} L$ and $vd \frac{1}{4} L$ vs. $cf_{vd} \cdot Pr$ distribution for S1 to S5

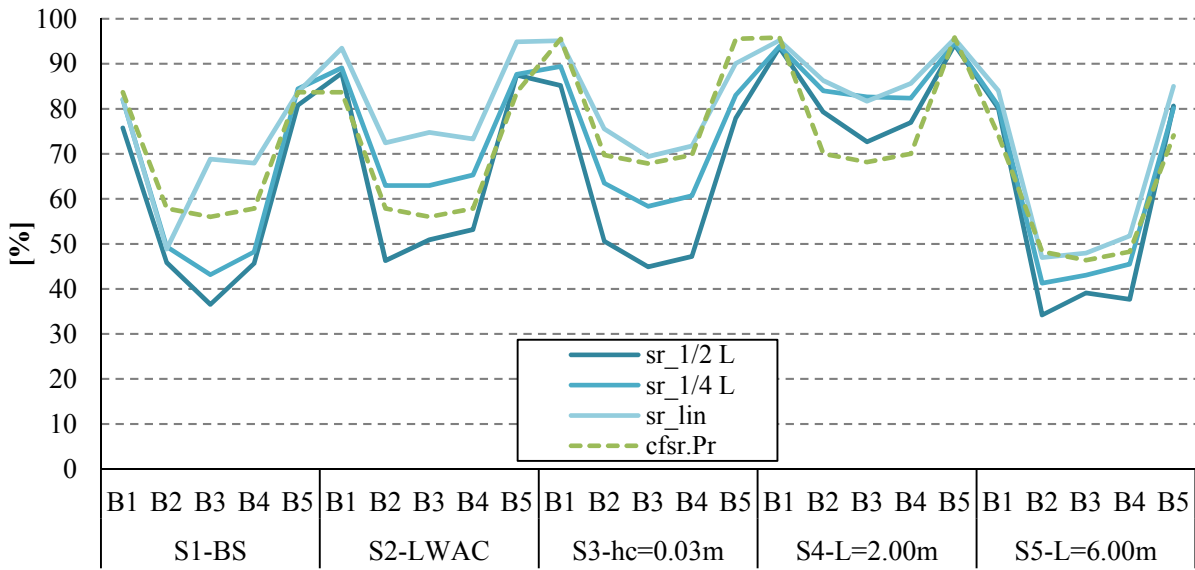


Fig. 5.26 – Experimental sr vs. $cf_{sr} \cdot Pr$ distribution for S1 to S5

Table 5.19 – Average partial differences: experimental vs. $cf_i \cdot Pr$ for S1 to S5

Specimen	Average partial differences								
	$vd \frac{1}{2} L$			$vd \frac{1}{4} L$			sr		
	$cf_{vd} \cdot Pr$	$cf_{vd} \cdot Pr$	$cf_{vd} \cdot Pr$	$cf_{vd} \cdot Pr$	$cf_{vd} \cdot Pr$	$cf_{vd} \cdot Pr$	$cf_{sr} \cdot Pr$	$cf_{sr} \cdot Pr$	$cf_{sr} \cdot Pr$
	vs.	vs.	vs.	vs.	vs.	vs.	vs.	vs.	vs.
	$\frac{1}{2} L$	$\frac{1}{4} L$	lin	$\frac{1}{2} L$	$\frac{1}{4} L$	lin	$\frac{1}{2} L$	$\frac{1}{4} L$	lin
[%]									
S1	4	7	2	4	3	1	11	6	-2
S2	-7	-5	-3	-5	-9	-4	3	-6	-14
S3	3	5	8	6	1	6	19	9	-1
S4	-6	-5	-3	-3	-4	-2	-3	-8	-9
S5	-1	2	1	0	-3	-1	4	0	-5

The $cf_i \cdot Pr$ fit led to the decrease of the absolute differences, especially when concerning the support reactions. The extreme values varied from - 7 and 8 % for $vd \frac{1}{2} L$, - 9 and 6 % for $vd \frac{1}{4} L$, and from - 14 and 19 % for sr , Table 5.19.

With the final polynomial approximation defined, Equation (31), and since the results from the preliminary test were also available, experimental and $cf_i \cdot Pr$ fit percentages were compared (see Section C.3.4 Comparison between experimental and polynomial predictions for CSGL and CSTL, Appendix C). Fig. 5.27, Fig. 5.28 and Table 5.20 summarize the results found.

$$cf_i \cdot Pr = cf_i \cdot (0.90 - 0.05 \cdot L - 0.472 \cdot b_l - 4.969 \cdot h_c + 0.002 \cdot L^2 + 0.299 \cdot b_l^2 + 15.805 \cdot h_c^2) \quad (31)$$

where: cf_i is the quantity coefficient: cf_{bm} for longitudinal bending moment, cf_{vd} for vertical displacement, and cf_{sr} for support reactions, and takes the values in Table 5.18;
 L is the span length;
 b_l is the beam location; and
 h_c is the concrete thickness.

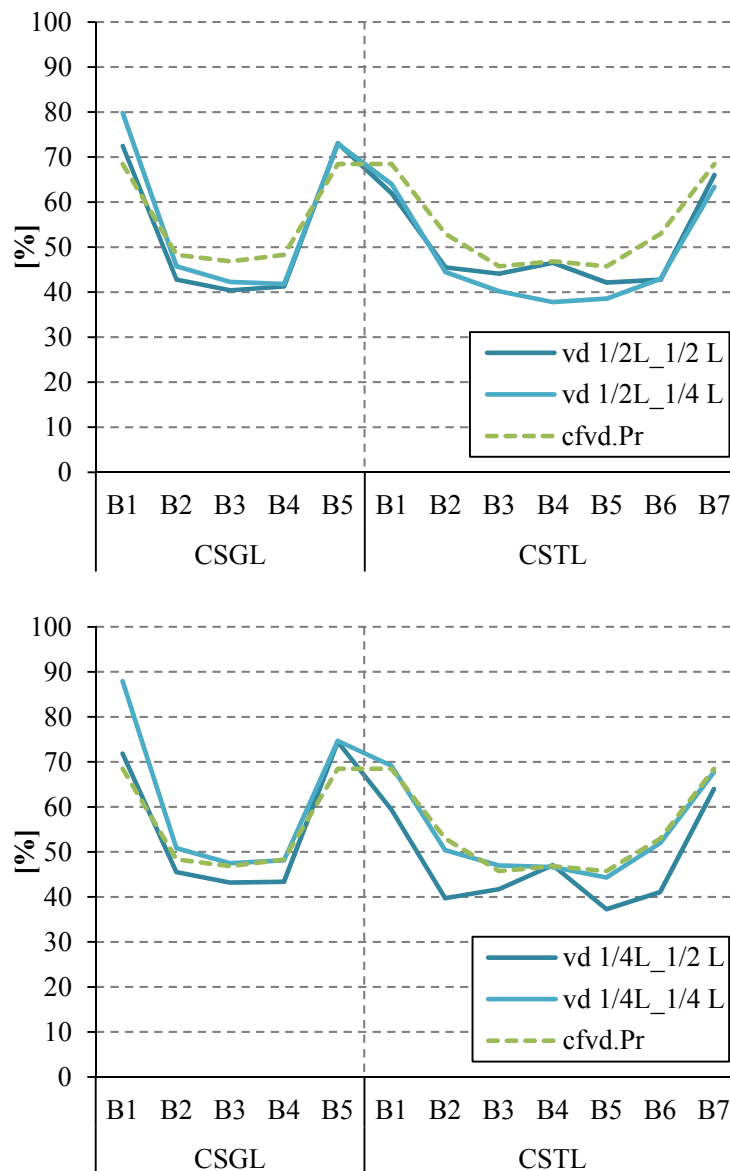


Fig. 5.27 – Experimental $vd \frac{1}{2} L$ and $vd \frac{1}{4} L$ vs. $cf_{vd} \cdot Pr$ distribution for CSGL and CSTL

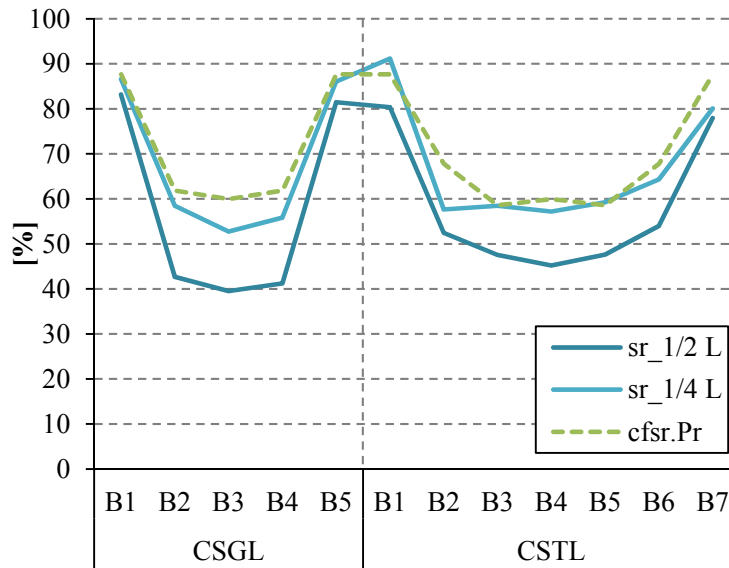


Fig. 5.28 – Experimental sr vs. $cf_{sr} \cdot Pr$ distribution for CSGL and CSTL

Table 5.20 – Average partial differences: experimental vs. $cf_i \cdot Pr$ for CSGL and CSTL

Specimen	Average partial differences					
	$vd \frac{1}{2} L$		$vd \frac{1}{4} L$		sr	
	$cf_{vd} \cdot Pr$	$cf_{vd} \cdot Pr$	$cf_{vd} \cdot Pr$	$cf_{vd} \cdot Pr$	$cf_{sr} \cdot Pr$	$cf_{sr} \cdot Pr$
	vs.	vs.	vs.	vs.	vs.	vs.
	$\frac{1}{2} L$	$\frac{1}{4} L$	$\frac{1}{2} L$	$\frac{1}{4} L$	$\frac{1}{2} L$	$\frac{1}{4} L$
[%]						
CSGL	2	0	0	-6	14	4
CSTL	5	7	7	1	12	3

For these specimens, even a closer approximation was found with the $cf_i \cdot Pr$ polynomial. As found for specimens S1 to S5, the vertical displacements were closely approximated, when compared with the support reactions. However, for the CSGL and CSTL specimens, the average absolute differences managed to be lower than those obtained for S1 to S5.

5.4 Summary

Given its capability to predict the actual behavior of the modeled elements, the Frame+Shell model was used in this chapter. With such a model, several modeling were performed aiming at finding the parameters that can affect the most the load distribution in

timber-concrete floors, when concerning the transversal direction. By defining a base simulation and changing, whenever possible, only one parameter at a time on each modeling, the most influential parameters were found. Thus, parameters as:

- the concrete type;
- the thickness of the concrete layer;
- the span length;
- the load type: point or line load; among the point load, its location: at mid- or quarter-span;
- the loaded beam, *i.e.*, its location transversally;

showed to be the ones which most affect the analyzed quantities, namely, vertical displacements, support reactions and longitudinal bending moments. This information besides serving as a support to define the experimental program, allowed deepening the effects that some of the parameters showed to have. The concrete thickness, the span and the specific effect of the “degree of oversizing” were object of study. This analysis revealed the negative effect that the use of an oversized timber section has in the distribution of the analyzed quantities, by comparison with one “tight-fitting” to the EC5 (EN1995 2004a) requirements. The oversized sections tended to concentrate a higher quantity over the loaded beam, hindering the participation of the remaining beams over the action in question which could make the structural element more efficient. Hence, an anti-economic solution, from the outset, becomes even less attractive, since the potential benefit which could be drawn of the larger sections turns out to be detrimental.

Aiming at obtaining a simplified rule capable to predict the distribution of a specific quantity that a concentrated load can induce on a timber-concrete composite floor, an equation was developed. Based on the data collected from the parametric study and analyzing the distribution of bm for several modeling, a polynomial fit was achieved. Also the vertical displacements and support reactions collected on the experimental tests performed were used to obtain an adequate equation. A good approximation was attained by using a second order polynomial, with the span length, the beam location and the concrete thickness as variables to establish the sought expression.

6. SUMMARY AND CONCLUSIONS

6.1 Summary

Several studies on the distribution of concentrated loads on slabs made from different material types, combined together or standing alone are available in bibliography. However for timber-concrete composite systems such type of studies were not found. Even so, for specific situations where an effective load distribution system can be guaranteed, the existing standard rules (EN1995 2004a) imply an increase of the timber strength properties. These rules naturally reflect the lack of knowledge on the topic and a more optimized procedure could be adopted if specific studies would be carried out to improve the knowledge on the behavior of the composite timber-concrete structures. The present investigation intends to fulfill this goal and, consequently more optimized structures can be designed with more information on the actual behavior of such structures. To accomplish this, numerical work was developed together with experimental tests on real scale specimens. A sensitivity analysis was also performed.

To obtain a numerical model that would be adequate to predict the load distribution in the studied floors three numerical models, Grid, Frame+Shell and Solid models, were developed and their results compared to each other. Also an analytical model, the Guyon-Massonnet Method (Bareš and Massonnet 1966), also known as Distribution Coefficients Method, was considered in the numerical model validation. To complete the validation two composite floors were tested with point loads applied consecutively at mid- and quarter-span. From this analysis, given its ability to simulate the behavior of the structural elements subjected to the loads in study and its computational characteristics (simplicity of application *vs.* time consumption), the Frame+Shell model was chosen to perform the study.

After the model validation, a preliminary parametric study was performed to identify the parameters that most affected the transversal distribution of internal forces for the composite floors. This information was the basis to define the experimental program. Five real-scale floor specimens were build and tested.

In order to analyze the effect that each of the parameters might have on the transversal distribution of load, one of the specimens was considered as the *Base specimen* and its results served as a basis for comparison with the remaining ones. The remaining specimens were designed so that a parameter was changed each time, relatively to the *Base specimen*. Hence, the studied parameters were: the concrete type by means of a light-weight aggregate concrete;

the concrete thickness by using a thinner layer; and the span, a small ($L = 2.00$ m) and a long one ($L = 6.00$ m). The five specimens were tested with point loads, at mid- and quarter-span of each beam and with line loads along the longitudinal axis of one beam each time.

The sensitivity analysis was performed in order to improve the knowledge on the distribution of concentrated loads. This focused mainly in the parameters that had showed great influence over the composite floor behavior together with some design considerations, as is the “oversizing degree” of the timber section. The effect that an oversized timber cross-section has, when compared to the requirements of the EC5 (EN1995 2004a) is also an important aspect. Moreover, the numerical results served as a basis for the development of a simplified rule to predict the load distribution on this type of composite floors.

6.2 Conclusions

The present research, carried out to understand how timber-concrete composite floors subjected to concentrated loads distribute the load in the direction perpendicular to the beams longitudinal axis, clearly showed that the transversal distribution of load in such composite structures when subjected to concentrated load might be significant. Indeed, for a floor with medium span as the *Base specimen*, the spreading in terms of support reactions ranged from 16 % (border beam loaded at quarter-span) and 63 % (central beam loaded at mid-span). Generally, regardless of the quantity in study (vertical displacement, support reaction...) or the analysis type, the loaded beam is the one having the highest share of displacements, reactions or strains. The way in which the remaining beams participate in the distribution depends on several parameters which are investigated here.

From the experimental tests, the results showed a relatively similar trend for the three load cases, point load at mid- or quarter-span and line load. Even so, the type of load proved to be a parameter that has a significant influence on the behavior of timber-concrete floors. When the load was applied at mid-span of a border beam in the *Base specimen*, at least 19 % of the load applied above this beam was redistributed for the adjacent beams. This percentage increased as the load was applied to a beam closer to the center of the slab. When the load was applied at mid-span of the central beam over 60 % of it was found to be redistributed for the adjacent beams. This means that less than 40 % of the applied load was received by the beam immediately below. Hence, also the loaded beam position showed to be a parameter that has a great influence on the load distribution.

When the load was applied at quarter-span there was a tendency for the loaded beam to support a higher load percentage than that found for the mid-span loading cases. Consequently, the load distribution shows to be more effective as the load was applied further away from the supports.

The four other tested specimens, obtained by changing the concrete type, the concrete thickness and the span, relatively to the *Base specimen*, revealed that also the structural bending stiffness affected the load distribution. For the shortest span specimen ($L = 2.00$ m) the only beams that seemed to support the applied load were those to which the load is applied and those immediately adjacent to them. By opposition, for the longest span specimen ($L = 6.00$ m) a wider load spreading was found. In percent terms:

- the shortest span specimen was the one with the lower load spreading, varying between 4 % (border beam loaded with a line load) and 27 % (central beam loaded at mid-span);
- by its turn, the longest span specimen presented the highest percentage of load spreading which varied between 15 % (border beam loaded with a line load) and 66 % (intermediate beam loaded at mid-span).

For the specimen composed by LWAC and the specimen with a thinner concrete layer ($h_c = 0.03$ m) relatively close spreading behavior was found. However, when compared with the values found for the *Base specimen*, the spreading percentages tended to decrease:

- 5 % (border beam loaded with a line load) and 54 % (intermediate beam loaded at mid-span) for LWAC specimen; and
- 5 % (border beam loaded with a line load) and 55 % (central beam loaded at mid-span) for the thinner concrete layer specimen.

Hence, significant load spreading was observed as for the *Base specimen* as for the longest span specimen, still when comparing the global behavior of these two specimens the latter denoted a better ability to mobilize all the beams of the slab. This is true for all the load cases, but becomes clearer for the point load applied at mid-span. This clearly shows the important effect that the span has on the distribution of a concentrated load across the composite floors under consideration, being the parameter that most affects.

Also between the specimen composed by LWAC and the specimen with a thinner concrete layer, despite the proximity of the spreading limits, the global behavior showed some differences. The first denotes a slight trend to concentrate the load over the loaded beam when compared with the second, which tended to distribute more the load to the remaining beams.

Concerning the various specimens and loadings, an average spreading of 30 % was found. Among the three load cases, the one providing the widest load spreading was the point load at the mid-span (36 % on average), in contrast with the line load case, showing the lowest load spreading (24 % on average). On the other hand, concerning the percentage of load received by the loaded beam, the trend for the various load types is very similar, the differences being at the level of redistribution.

These findings are rather in line with those observed for the vertical displacements. In terms of distribution, the loaded beam, regardless of the load type, receives the higher percentage, decreasing from this beam to the farthest away beams. When the load was

symmetrically applied (point load at mid-span or line load) the vertical displacements showed to be higher at mid-span than at quarter-span. When the load was decentered (point load at quarter-span) mid- and quarter-span displacements were very close to each other. For the beams loaded at quarter-span, displacement immediately below the load tends to be higher than at mid-span. For the remaining beams, this does not apply. The use of light-weight concrete, as well as adopting the thinnest concrete layer, led to a minor “displacement distribution”, with the displacement occurring essentially over the loaded beam and in its vicinity. Also a shorter span ($L = 2.00$ m) led to a minor “displacement distribution”, while the opposite occurs when a longer span ($L = 6.00$ m) was used.

Concerning the slip displacements and the uplift at the upper layer corners, relatively low magnitudes were found. For both, as for most of the quantities that were analyzed, the widest spreading happened associated with the point load at mid-span. However, when considering the strains an exception happened, with the point load at quarter-span leading to a wider spreading of strains, when compared to the remaining load cases.

With regard to the use of numerical models to study the behavior of a structural element, it must be guaranteed that the model chosen to develop the study is capable of simulate the behavior in question. Hence, a validation process was undertaken. This process included comparing results from experimental preliminary tests with those from analytical and numerical models. Several modeling tasks were performed, including those corresponding to the preliminary tests' floors, using the analytical and the three numerical models. The results associated substantiated the choice of the most adequate model to perform the numerical analysis, confirming its ability to model the phenomena under consideration. The evaluation of vertical displacements, support reactions and longitudinal bending moments for the various composite floors under the action of point loads at mid- and quarter-span was the basis for the choice. Thus, in a compromise between adequate prediction of the actual behavior and computational cost, the Frame+Shell model was chosen. Despite the simplified consideration of the material characteristics, namely through the definition of isotropic materials with an elastic behavior, this model showed to be a powerful tool. The numerical results showed to follow the same trend as the experimental ones, either for vertical displacement or for support reactions. The specimen with a thin concrete layer showed to be the one for which the numerical prediction was closer to the experimental results, while for LWAC specimen the opposite was found. This happened for both vertical displacements and support reactions. Nevertheless, the absolute mean differences in distribution were lower than (\pm) 10 %. This supports the adequacy of the developed model to predict the load distribution of the timber-concrete floors.

In addition to providing a simple rule for the prediction of the actual behavior of the composite floors, the Frame+Shell model was also used for a parametric study, identifying the

effect that chosen parameters might have on the main goal of this investigation. With the characteristics from the commonly used floors systems in mind, a set of parameters was established to perform the study. Taking the *Base simulation* as the reference simulation, to which the remaining would be compared, the various simulations of the composite floor were obtained by varying the intended characteristics. Different span lengths, timber cross-sections, material properties, connection stiffnesses and concentrated loads, among others, were modeled. By analyzing the transversal load distribution for the several slab configurations led to find different degree of distribution of internal forces, highlighting the parameters that most affected that distribution. Thus, the parameters that showed to affect the distribution of load in the transversal direction were:

- the span;
- the concrete height;
- the concrete type;
- the support conditions; or
- the use of a CLT deck under the concrete layer instead of timber beams;

with the first two affecting it most significantly. With this information, the influence of the span and the thickness of the concrete layer was detailed through specific numerical modeling, from which the great influence of the span stood out. Furthermore, also the effect of some design considerations, as is the “degree of oversizing” the timber section was studied. The use of oversized sections, relatively to the requirements of EC5 (EN1995 2004a) showed to be detrimental because of their tendency to concentrate a higher percentage of load over the loaded beam. This, besides being uneconomical by the excessive size of the timber cross-sections, does not take advantage of the existence of the remaining beams of the slab, and therefore it should be avoided.

Aiming at obtaining a simplified rule to predict the percentage of load that will be associated with a specific beam in the design phase, an equation was developed. Following the findings in the previous sections, namely the parameters that most affect the distribution of the various quantities analyzed, through the percentage received by the loaded beam, and the main conclusions associated, a polynomial expression was chosen and their coefficients obtained by approximating the parameter variation curves. The proposed rule showed to be capable to adequately predict the transversal distribution of bending moments at the loading section, vertical displacement and support reactions based on the span length, the beam location and the concrete thickness. By comparing the percentages computed with this equation and those experimentally obtained only occasionally exceed the absolute value of 10 %. This is also true when concerning the percentages achieved based on numerically modeling.

Predicting the percentage of any of those quantities makes it a useful tool to apply in design. This can lead to a more efficient structural element, taking advantage of the economy that can be reached optimizing the cross-sections for the loads. At the same time, it can contribute to make the use of timber-concrete floors feasible in wider set of situations, in bridges or building floors, either in rehabilitation works or new constructions.

6.3 Recommendations for future work

Hardly a doctoral research results in a finished work, and normally it opens doors to subsequent investigations. This one is no exception.

Some of the parameters which showed to affect the load distribution could not be experimentally tested. Following the findings from the parametric study, the use of a CLT deck instead of timber beams, the floor support conditions, specifically the simple support on all the ends, and the use of oversized sections should be experimentally studied. The effect of other parameters can also be analyzed, completing the parametric study: the use of prefabricated concrete slabs or the existence of continuity over the supports on timber-concrete composite floors systems, are some of them.

Also the simplified prediction of the load distribution through a polynomial fit can be improved. The use of test specimens associated with parameters different from those already tested, as the ones suggested before, will produce data which complement the existent one and at the same time prove the adequacy of the proposed equation. The search for an even simpler expression is also a possible future development.

Thus, the knowledge on the behavior of timber-concrete floor systems subjected to concentrated loads, concerning the transversal distribution of load, can contribute to the establishment of more reliable rules, aiming at obtaining optimized structural solutions for the given conditions.

7. REFERENCES

- Adekola, A. O. (1968). "Effective widths of composite beams of steel and concrete". *The structural engineer* Vol. 46, 9, pp. 285-289.
- Adekola, A. O. (1974a). "The dependence of shear lag on partial interaction in composite beams". *International Journal of Solids and Structures* Vol. 10, 4, pp. 389-400.
- Adekola, A. O. (1974b). "On shear lag effects in orthotropic composite beams". *International Journal of Solids and Structures* Vol. 10, pp. 735-754.
- Amadio, C., Fedrigo, C., Fragiaco, M. and Macorini, L. (2004). "Experimental evaluation of effective width in steel-concrete composite beams". *Journal of Constructional Steel Research* Vol. 60, 2, pp. 199-220.
- Ansourian, P. (1975). "An application of the method of finite elements to the analysis of composite floor systems". *Proceedings of the Institute of Civil Engineering (ICE)* Vol. 59, Part 2, pp. 669-726.
- Araujo, M. C. (2009). "Slab-on-Girder Prestressed Concrete Bridges: Linear and Nonlinear Finite Element Analysis and Experimental Load Tests". *Dorctoral Thesis, Graduate Faculty of the Louisiana State University and Agricultural and Mechanical College*.
- Bareš, R. and Massonnet, C. (1966). "Le calcul des grillages de poutres et dalles orthotropes selon la méthode Guyon-Massonet-Bares"
- Bathon, L. A., Bletz, O. and Bahmer, R. (2006). "Retrofit of Timber Bridges - A System Approach Using Prefabricated Wood-Concrete-Composite Element". 9th WCTE, Portland, USA.
- Blass, H. J. (1995). "STEP lecture B16". STEP1 Basis of design, material properties, structural components and joints. H. J. Blass, P. Aune, B. S. Choet al. First Edition, Centrum Hout, Almere, The Netherlands.
- Calgaro, J.-A. and Virlogeux, M. (1988). "Projet et Construction des Ponts: Analyse structurale des tabliers de ponts". *Presses de l'école nationale des ponts et chaussées Paris*.
- Castro, J. M., Elghazouli, A. Y. and Izzuddin, B. A. (2007). "Assessment of effective slab widths in composite beams". *Journal of Constructional Steel Research* Vol. 63, 10, pp. 1317-1327.
- Ceccotti, A. (2002). "Composite concrete-timber structures". *Progress in Structural Engineering Materials* Vol. 4, 3, pp. 264-275.
- Chasten, C., Lu, L.-W. and Driscoll, G. (1992). "Prying and Shear in End-Plate Connection Design". *Journal of Structural Engineering-asce* Vol. 118, 5, pp. 1295-1311.
- Chen, Y. (1995a). "Refined and simplified methods of lateral load distribution for bridges with unequally spaced girders: I. Theory". *Computers and Structures* Vol. 55, 1, pp. 1-15.

- Chen, Y. (1995b). "Refined and simplified methods of lateral load distribution for bridges with unequally spaced girders: II. Applications". *Computers and Structures* Vol. 55, 1, pp. 17-32.
- Chiewanichakorn, M., Aref, A. J., Chen, A. S. and Ahn, I.-S. (2004). "Effective flange width definition for steel-concrete composite bridge girder". *Journal of Structural Engineering ASCE* Vol. 130, 12, pp. 2016-2031.
- Chiewanichakorn, M., Aref, A. J., Chen, S. S., Ahn, I.-S. and Carpenter, J. A. (2005). "Effective flange width of composite girders in negative moment region". *Journal of the Transportation Research Board* Vol., pp. 203-216.
- Clayton, S. and Stephens, S. F. (2010). "Feasibility study for a repetitive member factor for cold-formed steel framing systems". *20th International Specialty Conference on Cold-Formed Steel Structures - Recent Research and Developments in Cold-Formed Steel Design and Construction*, St. Louis, MO, USA.
- Cosenza, E. and Zandonini, R. (1999). "Composite Construction". *Structural Engineering Handbook*.
- Cramer, S. M. and Drozdek, J. (2000). "Load-sharing in metal-plate connected wood truss assemblies". *World Conference on Timber Engineering*, Vancouver, BC, Canada.
- Cramer, S. M., Drozdek, J. M. and Wolfe, R. W. (2000). "Load sharing effects in light-frame wood-truss assemblies". *Journal of Structural Engineering ASCE* Vol. 126, 12, pp. 1388–1394.
- CSI, Basic Analysis Reference Manual - 9.0 ed. (2004). SAP2000 - CSI, Berkeley, California.
- Dahl, K., Bovim, N. I. and Malo, K. A. (2006). "Evaluation of stress laminated bridge decks based on full scale tests". *9th WCTE*, Portland, USA.
- Daniels, B. J. (1990). "Comportment et capacite portante des dalles mixtes-Modelization matematicque et etude experimentale". *Dorctoral Thesis*, École Polytechnique Fédérale de Lausanne,
- Daniels, B. J. and Crisinel, M. (1993). "Composite slab behavior and strength analysis. Part II: Comparisons with test results and parametric analysis". *Journal of Structural Engineering ASCE* Vol. 119, 1, pp. 36-49.
- Deam, B. L., Fragiaco, M. and Buchanan, A. H. (2008). "Connections for Composite Concrete Slab and LVL Flooring Systems". *Materials and Structures/Matériaux et Constructions* Vol. 41, 3, pp. 495-507.
- Dias, A. M. P. G. (2005). "Mechanical behaviour of timber-concrete joints". *PhD Thesis*, Technische Universiteit Delft, Delft.
- Dias, A. M. P. G. (2010). "Non linear modelling of timber-concrete composite structures". *11th WCTE*, Riva del Garda, Trentino, Italy.
- Dias, A. M. P. G. (2012). "Analysis of the Nonlinear Behavior of Timber-Concrete Connections". *Journal of Structural Engineering ASCE* Vol. 138, 9, pp. 1128-1137.
- Dias, A. M. P. G., Cruz, H. M. P., Lopes, S. M. R. and Kuilen, J. W. v. d. (2010). "Stiffness of dowel-type fasteners in timber-concrete joints". *Proceedings of the Institution of Civil Engineers (ICE) - Structures and Buildings* Vol. 163, 4, pp. 257 –266.
- Dias, A. M. P. G., Ferreira, M. C. P., Jorge, L. F. C. and Martins, H. M. G. (2011). "Timber-concrete practical applications - bridge case study". *Proceedings of the Institution of Civil Engineers-Structures and Buildings* Vol. 164, pp. 130-140.

-
- Dias, A. M. P. G., Kuilen, J. W. G. V. d., Lopes, S. M. R. and Cruz, H. M. P. (2007a). "A non linear 3D FEM model to simulate timber-concrete joints". *Advances in Engineering Software* Vol. 38, 8-9, pp. 522-530.
- Dias, A. M. P. G., Lopes, S. M. R., Kuilen, J. W. G. V. d. and Cruz, H. M. P. (2007b). "Load-Carrying Capacity of Timber–Concrete Joints with Dowel Type Fasteners". *Journal of Structural Engineering ASCE* Vol. 133, 5, pp. 720-727.
- Dias, A. M. P. G. and Martins, C. E. J. (2012). "Mechanical performance of a new, more environmentally friendly, timber-concrete connection". 12th WCTE, Auckland, New Zeland.
- Dias, A. M. P. G., Monteiro, S. R. S. and Martins, C. E. J. (2013). "Reinforcement of timber floors- transversal load distribution on timber-concrete systems". *Advanced Materials Research* Vol. 778 pp. 657-664.
- Domingues, J. C. M. (2012). "Uso de soluções mistas madeira-betão leve para reabilitação e reforço de pavimento". Master thesis, University of Coimbra, Coimbra.
- E397 LNEC (1993). "Betões - Determinação do módulo de elasticidade em compressão". LNEC, Portugal.
- El-Lobody, E. A. E.-F. M. (2002). "Finite element modelling of shear connection for steel-concrete composite girders". PhD, University of Leeds,
- EN 338 CEN (2003). "Structural timber - Strength classes". CEN, Brussels.
- EN 408 CEN (2010). "Timber structures - Structural timber and glued laminated timber - Determination of some physical and mechanical properties". CEN, Brussels.
- EN 1991 CEN (2001). "Eurocode 1: Actions on structures - Part 1-1: General actions - Densities, self-weight, imposed loads for buildings; Part 2: Traffic loads on bridges". CEN, Brussels.
- EN 1992 CEN (2004). "Eurocode 2: Design of concrete structures - Part 1-1: General rules and rules for buildings; Part 2: Concrete bridges; Design and detailing rules". CEN, Brussels.
- EN 1993 CEN (2005). "Eurocode 3: Design of steel structures - Part 1-1: General structural rules". CEN, Brussels.
- EN 1993 CEN (2006). "Eurocode 3: Design of steel structures - Part 1-5: Plated structural elements". CEN, Brussels.
- EN 1994 CEN (2004). "Eurocode 4: Design of composite steel and concrete structures - Part 1-1: General rules and rules for buildings". CEN, Brussels.
- EN 1994 CEN (2008). "Eurocode 4: Design of composite steel and concrete structures - Part 2: Rules for bridges". CEN, Brussels.
- EN 1995 CEN (2004a). "Eurocode 5: Design of timber structures - Part 1-1: General - Common rules and rules for buildings". CEN, Brussels.
- EN 1995 CEN (2004b). "Eurocode 5: Design of timber structures - Part 2: Bridges". CEN, Brussels.
- EN 26891 CEN (1991). "Timber Structures – Joints made with mechanical fasteners – General principles for the determination of strength and deformation characteristics (ISO 6891:1983) - EN 26891". Brussels.
- Etournaud, P. J.-F. (1998). "Load tests of composite wood-concrete decking under point loads". Master's thesis, Colorado State University, Fort Collins, Colorado.
-

7. REFERENCES

- Evans, H. R. and Wright, H. D. (1988). "Steel-concrete composite flooring deck structures". Steel-concrete composite structures: stability and strength. N. R., Elsevier Applied Science.
- Fernández-Cabo, J. L., Fernández-Lavandera, J. and Ávila-Jalvo, J. M. (2008). "Wood-Concrete and Wood-Wood Mixed Beams: Rational Basis for Selecting Connections". Journal of Structural Engineering ASCE Vol. 134, 3, pp. 440-447.
- Fragiacomo, M., Amadio, C. and Macorini, L. (2007). "Short- and Long-Term Performance of the "Tecnaria" Stud Connector for Timber-Concrete Composite Beams". Materials and Structures Vol. 40, 10, pp. 1013-1026.
- Fragiacomo, M., Gutkowski, R. M., Balogh, J. and Fast, R. S. (2006). "Long-Term Behaviour of Wood-Concrete Composite Beams with Notched Connection Detail". 9th WCTE, Portland, USA.
- Gara, F., Leoni, G. and Dezi, L. (2009). "A beam finite element including shear lag effect for the time-dependent analysis of steel-concrete composite decks". Engineering Structures Vol. 31, 8, pp. 1888-1902.
- Girhammar, U. A. and Gopu, V. K. A. (1991). "Analysis of P- Δ effect in composite concrete/timber beams columns". Proceedings of the Institute of Civil Engineers, part 2.
- Godycki, T., Pawlica, J. and Kleszczewski, J. (1984). "Verbunddecke aus Holzrippen und Betonplatte". Bauingenieur Vol. 59, 12, pp. 477-483.
- Gutkowski, R., Balogh, J., Natterer, J., Brown, K., Koike, E. and Etournaud, P. (2000). "Laboratory Tests of Composite Wood-Concrete Beam and Floor Specimens". 6th WCTE, Whistler, British Columbia, Canada.
- Gutkowski, R., Balogh, J. and To, L. G. (2010). "Finite-element modeling of short-term field response of composite wood-concrete floors/decks". Journal of Structural Engineering ASCE Vol. 136, 6, pp. 707-714.
- Harris, D. K. (2010). "Assessment of flexural lateral load distribution methodologies for stringer bridges". Engineering Structures Vol. 32, 11, pp. 3443-3451.
- Ilharco, T. (2008). "Pavimentos de madeira em edifícios antigos. Diagnóstico e intervenção estrutural". Master's Thesis, University of Porto, OPorto.
- Johnson, R. P. (1994). "Simply-supported Composite Slabs and Beams". Composite Structures Of Steel And Concrete. C. S. R. a. D. Organisation. Oxford, Blackwell Scientific Publications, pp. 210.
- Kearley, V. C. and Carruthers, J. F. S. (1991). "Assesment of the distribution and effects of concentrated loads applied to wood-based sheet materials".
- Kuhlmann, U. and Michelfelder, B. (2004). "Grooves as Shear Connectors in Timber-Concrete Composite Structures". 8th WCTE, Lahti, Finland.
- Lind, N. C., Ravindra, M. K. and Schorn, G. (1976). "Empirical effective width formula". Journal of the Structural Division Vol. 102, 9, pp. 1741-1757.
- Linden, M. v. d. (1999). "Timber Concrete Composite Floor Systems". Doctoral Thesis, Technical University of Delft, Delft.
- Lopes, S., Jorge, L. and Cruz, H. (2012). "Evaluation of non-linear behavior of timber-concrete composite structures using FE model". Materials and Structures Vol., pp.

-
- Lukaszewska, E., Fragiaco, M. and Johnsson, H. (2010). "Laboratory Tests and Numerical Analyses of Prefabricated Timber-Concrete Composite Floors". *Journal of Structural Engineering ASCE* Vol. 136, 1, pp. 46-55.
- Lukaszewska, E., Johnsson, H. and Stehn, L. (2006). "Connections for Prefabricated Timber-Concrete Composite Systems". 9th WCTE, Portland, USA.
- Luttrell, C. B. (1995). "Transverse distribution of non-uniform loads on composite slabs". Master's Thesis, West Virginia University, Morgantown, West Virginia.
- Macorini, L., Fragiaco, M., Amadio, C. and Izzuddin, B. A. (2006). "Long-term analysis of steel-concrete beams: FE modelling for effective width evaluation". *Engineering Structures* Vol. 28, 8, pp. 1110-1121.
- Martins, C. E. J., Dias, A. M. P. G. C., R. J. T. and Santos, P. G. G. (2015). "Environmentally friendly high performance timber-concrete panel". *Construction and Building Materials* Vol., pp.
- Mettern, C. (2003). "Structural timber-concrete composites—Advantages of a little known innovation". *The Structural Engineer* Vol. 81, 4, pp. 17-19.
- Miotto, J. L. (2009). "Estruturas mistas de madeira-concreto: avaliação das vigas de madeira laminada colada reforçadas com fibra de vidro". Doctoral Thesis, Universidade de São Paulo, São Carlos.
- Monteiro, S., Dias, A. and Negrão, J. (2010). "Experimental and Numerical Evaluation of Notched Timber-Concrete Joints Mechanical Behavior". 11th WCTE, Riva del Garda, Trentino, Italy.
- Monteiro, S. R., Dias, A. M. and Negrão, J. H. (2011). "Avaliação experimental e numérica do comportamento mecânico de ligações mistas madeira-betão realizadas através de entalhes colados.". CIMAD 11 - 1º Congresso Ibero-LatinoAmericano da Madeira na Construção, Coimbra, PORTUGAL.
- Monteiro, S. R. S. (2008). "Avaliação Experimental e Numérica do Comportamento Mecânico de Ligações Madeira-Betão Entalhadas". Master's Thesis, University of Coimbra, Coimbra.
- Monteiro, S. R. S., Dias, A. M. P. G. and Lopes, S. M. R. (2015). "Bi-dimensional numerical modeling of timber-concrete slab-type structures". *Materials and Structures* Vol. 48, 10, pp. 3391-3406.
- Moraes, V. M. d. (2007). "Ponte mista madeira-concreto em vigas treliçadas de madeira". Master's Thesis, Universidade Estadual Paulista "Júlio de Mesquita Filho", Ilha Solteira.
- Moreira, L. F. N. (2001). "Dimensionamento à flexão de vigas mistas madeira/concreto". Master's Thesis, Universidade Federal de Minas Gerais, Belo Horizonte.
- Mtenga, P. V., Cramer, S. M., Peyrot, A. H. and Wolfe, R. W. (1995). "System factors for light-frame wood truss assemblies". *Journal of Structural Engineering ASCE* Vol. 121, 2, pp. 290-300.
- Mullenex, D. L. (1993). "The effects of rust and concentrated loads on composite slabs". Master's Thesis, West Virginia University, Morgantown, West Virginia.
- Natterer, J. and Hoefl, M. (1987). "Zum Tragverhalten von Holz-Beton Verbundkonstruktionen". Lausanne.
-

- Nie, J.-G., Tian, C.-Y. and Cai, C. S. (2008). "Effective width of steel-concrete composite beam at ultimate strength state". *Engineering Structures* Vol. 30, 5, pp. 1396-1407.
- NP-EN1194 CEN (2002). "Estruturas de madeira. Madeira lamelada-colada. - Classes de resistência e determinação dos valores característicos". IPQ, Portugal.
- NP-EN12390 CEN (2012). "Ensaio do betão endurecido - IPQ, Portugal.
- NTC (2002). "Nordic Timber Council (2002). "Nordic Timber Bridges. A presentation of timber bridges from Finland, Sweden, Norway and Estonia"". Nordic Industrial Fund, Palm & Co. Stockholm.
- Oliveira, A. L. C. (2002). "Contribuição para a análise de vigas mistas de madeira laminada colada e concreto (MLC/concreto)". Master's Thesis, Universidade Federal de Minas Gerais, Belo Horizonte.
- Oudjene, M., Meghlat, E. M., Ait-Aider, H. and Batoz, J. L. (2013). "Non-linear finite element modelling of the structural behaviour of screwed timber-to-concrete composite connections". *Composite Structures* Vol. 102, pp. 20-28.
- Ozelton, E. C. and Baird, J. A. (2006). "Concentrated Loadings". *Timber Designers' Manual*, Blackwell Science Ltd., pp. 50-63.
- Pennings, K. R., Frank, K. H., Wood, S. L., Yura, J. A. and Jirsa, J. O. (2000). "Lateral load distribution on transverse floor beams in steel plate girder bridges". Austin.
- Piazza, M. and Ballerini, M. (2000). "Experimental and Numerical Results on Timber-Concrete Composite Floors with Different Connection Systems". 6th WCTE, Whistler, British Columbia, Canada.
- Piazza, M. and Turrini, G. (1983). "Il comportamento statico della struttura mista legno-calcestruzzo". *Recuperare* Vol. 6, pp. 214-225.
- Porter, M. L. and Ekberg-Jr., C. E. (1977). "Behavior of Steel-Deck-Reinforced Slabs". *Journal of the Structural Division* Vol. 103, 3, pp. 663-677.
- Poštulka, J. (1997). "Holz-Beton-Verbunddecken, 36 Jahre Erfahrung". *Bautechnik* Vol. 74, 7, pp. 478-480.
- RILEM (1992). "RILEM TC 111 CST (1992) "Behavior of Timber-Concrete Load-Bearing Structures"". *Proceedings of ACMAR-Ravenna International Symposium*, Department of Civil Engineering, University of Florence, Italy.
- Roeder, C. W. (1981). "Point loads on composite deck-reinforced slabs". *Journal of the Structural Division (DEC)* Vol. 107, ST12, pp. 2421-2429.
- Samartin, A. and Martinez, J. (1974). "Reparto transversal de la en tableros sobrecarga de puentes". *Revista Hormigón y Acero* Vol., 113, pp.
- Sedlacek, G. and Bild, S. (1993). "A simplified method for the determination of the effective width due to shear lag effects". *Journal of Constructional Steel Research* Vol. 24, 3, pp. 155-182.
- Segundinho, P. G. d. A. (2005). "Análise teórico-experimental de um tabuleiro misto madeira-concreto composto por vigas circulares". Master's thesis, Universidade Estadual de São Paulo - UNESP, Ilha Solteira, São Paulo, Brasil.
- Sieffert, Y. (2004). "L'entretoisement des ponts mixtes multipoutres ferroviaires Analyse numérique et expérimentale". L'INSTITUT NATIONAL DES SCIENCES APPLIQUEES DE LYON,

-
- Simon, A. (2008). "Analyse zum Trag- und Verformungsverhalten von Straßenbrücken in Holz-Beton-Verbundbauweise". Doctoral Thesis, University of Bauhaus ,Weimar, Weimar.
- Simulea, Abaqus 6.11 Documentation collection - (2011). AbaqusCAE - Simulea, .
- Smilovic, M., Cubela, D., Radnic, J. and Harapin, A. (2013). "Experimental testing of wood-concrete and steel-concrete composite elements in comparison with numerical testing". *Materialwissenschaft und Werkstofftechnik* Vol. 44, 6, pp. 562-570.
- Souza, C. R. d. (2004). "Utilização de estruturas mistas na recuperação da capacidade de carga das pontes de madeira do Estado de Mato Grosso do Sul". Master's Thesis, Faculdade de Engenharia de Ilha Solteira, Universidade Estadual Paulista (UNESP), Ilha Solteira, São Paulo, Brasil.
- STEP1 (1995). "Timber Engineering STEP 1" First Edition, Centrum Hout, Almere, The Netherlands.
- Stojić, D. and Cvetković, R. (2001). "Analysis of composite timber-concrete structures according to the limit states". *Facta Universitatis, Series: Architecture and Civil Engineering* Vol. 2, 3, pp. 169 - 184.
- Thomas, W. H. (2000). "Shear and flexural deflection equations for OSB floor decking under point load", Whistler, British Columbia, Canada.
- Thomas, W. H. (2003). "Models for concentrated load performance assessment of isotropic wood sheathing". *Journal of Structural Engineering ASCE* Vol. 129, 8, pp. 1080-1086.
- Thomas, W. H. (2004a). "Modelling the influence of boundary conditions on the concentrated load performance of oriented strand board floor decking". *Holz Roh Werkst* Vol. 62, pp. 44-49.
- Thomas, W. H. (2004b). "Test-piece size uniformly distributed and concentrated load performance assessment of wood floor panel". *Materials and Structures* Vol. 37, 274, pp. 732-739.
- Timmermann, K. and Meierhofer, U. A. (1993). "Holz/Beton-Verbundkonstruktionen. Untersuchungen und Entwicklungen zum mechanischen Verbund von Holz und Beton". Swiss.
- Tucker, B. J. and Fridley, K. J. (1999). "Concentrated load design procedures for wood-joint floor systems". *Journal of Structural Engineering ASCE* Vol. 125, 7, pp. 706-712.
- Vallenilla, C. R. and Bjorhovde, R. (1985). "Effective width criteria for composite beams". *Engineering Journal (American Institute of Steel Construction)* Vol. Fourth Quarter, pp. 169-175.
- Vicente, R. d. S. (2008). "Estratégias e metodologias para intervenções de reabilitação urbana Avaliação da vulnerabilidade e do risco sísmico do edificado da Baixa de Coimbra". Doctoral Thesis, Universidade de Aveiro, Aveiro.
- Werner, H. (1992). "Holz-Beton-Verbunddecken mit einer neuartigen Fugenausbildung". *Bauen mit Holz* Vol. 94, 4, pp.
- Yeoh, D., Fragiaco, M., Aldi, P., Mazzilli, M. and Kuhlmann, U. (2008). "Performance of Notched Coach Screw Connection for Timber-Concrete Composite Floor System". 10th WCTE, Miyazaki, Japan.
- Yttrup, P. J. (1996). "Concrete Enhanced Timber". International Wood Engineering Conference, New Orleans.
-

7. REFERENCES

APPENDICES

APPENDICES INDEX

APPENDICES LIST OF FIGURES	269
APPENDICES LIST OF TABLES	281
APPENDIX A	285
A.1 Results from the preliminary experimental tests	287
A.1.1 Support reactions	287
A.1.2 Vertical displacements when the beams are loaded at mid-span	293
A.1.3 Vertical displacements when the beams are loaded at quarter-span	299
A.2 Results from the theoretical analysis	307
A.2.1 Vertical displacements at each beam mid-span	307
A.2.2 Vertical displacements at each beam quarter-span	312
A.2.3 Support reactions for loading at mid-span	316
A.2.4 Support reactions for loading at quarter-span	321
A.2.5 Longitudinal bending moment at the mid-span section	325
A.2.6 Longitudinal bending moment at the quarter-span section	330
APPENDIX B	335
B.1 Materials characteristics	337
B.1.1 Concrete	337
B.1.2 Timber	340
B.2 Results from the experimental analysis	343
B.2.1 Vertical displacements	344
B.2.2 Support reactions	403
B.2.3 Slip displacements	428
B.2.4 Uplift displacements	431
B.2.5 Strains	432

B.3 Results from the numerical prediction analysis	438
B.3.1 Vertical displacements.....	438
B.3.2 Support reactions	470
B.3.3 Stresses	487
APPENDIX C	489
C.1 First phase numerical analysis	491
C.1.1 Vertical displacement at each beam mid-span.....	496
C.1.2 Support reactions at each beam.....	501
C.2.1 Longitudinal bending moment at the mid-span section of each beam.....	506
C.1.4 Self-weight and imposed loads	511
C.1.5 Analysis of the parameters effects	511
C.2 Second phase numerical analysis.....	524
C.2.1 Vertical displacement at each beam mid-span.....	526
C.2.2 Support reactions at each beam.....	529
C.2.3 Longitudinal bending moment at the mid-span section of each beam.....	532
C.3 Results from the development of an expeditious tool.....	536
C.3.1 Longitudinal bending moment at the quarter-span section of each beam.....	536
C.3.2 Adjustment of <i>bm</i> distribution through polynomial equations	539
C.3.3 Comparison between experimental and polynomial predictions for S1 to S5...	557
C.3.4 Comparison between experimental and polynomial predictions for CSGL and CSTL	563

APPENDICES LIST OF FIGURES

Fig. A.1 – CSGL: support reactions when loaded at $\frac{1}{2}$ span and at $\frac{1}{4}$ span of B1 beam	287
Fig. A.2 – CSGL: support reactions when loaded at $\frac{1}{2}$ span and at $\frac{1}{4}$ span of B2 beam	288
Fig. A.3 – CSGL: support reactions when loaded at $\frac{1}{2}$ span and at $\frac{1}{4}$ span of B3 beam	288
Fig. A.4 – CSGL: support reactions when loaded at $\frac{1}{2}$ span and at $\frac{1}{4}$ span of B4 beam	289
Fig. A.5 – CSGL: support reactions when loaded at $\frac{1}{2}$ span and at $\frac{1}{4}$ span of B5 beam	289
Fig. A.6 – CSTL: support reactions when loaded at $\frac{1}{2}$ span and at $\frac{1}{4}$ span of B1 beam	290
Fig. A.7 – CSTL: support reactions when loaded at $\frac{1}{2}$ span and at $\frac{1}{4}$ span of B2 beam	290
Fig. A.8 – CSTL: support reactions when loaded at $\frac{1}{2}$ span and at $\frac{1}{4}$ span of B3 beam	291
Fig. A.9 – CSTL: support reactions when loaded at $\frac{1}{2}$ span and at $\frac{1}{4}$ span of B4 beam	291
Fig. A.10 – CSTL: support reactions when loaded at $\frac{1}{2}$ span and at $\frac{1}{4}$ span of B5 beam	292
Fig. A.11 – CSTL: support reactions when loaded at $\frac{1}{2}$ span and at $\frac{1}{4}$ span of B6 beam	292
Fig. A.12 – CSTL: support reactions when loaded at $\frac{1}{2}$ span and at $\frac{1}{4}$ span of B7 beam	293
Fig. A.13 – CSGL: vertical displacement at $\frac{1}{2}$ and $\frac{1}{4}$ span when loaded at $\frac{1}{2}$ span of B1 beam	293
Fig. A.14 – CSGL: vertical displacement at $\frac{1}{2}$ and $\frac{1}{4}$ span when loaded at $\frac{1}{2}$ span of B2 beam	294
Fig. A.15 – CSGL: vertical displacement at $\frac{1}{2}$ and $\frac{1}{4}$ span when loaded at $\frac{1}{2}$ span of B3 beam	294
Fig. A.16 – CSGL: vertical displacement at $\frac{1}{2}$ and $\frac{1}{4}$ span when loaded at $\frac{1}{2}$ span of B4 beam	295
Fig. A.17 – CSGL: vertical displacement at $\frac{1}{2}$ and $\frac{1}{4}$ span when loaded at $\frac{1}{2}$ span of B5 beam	295
Fig. A.18 – CSTL: vertical displacement at $\frac{1}{2}$ and $\frac{1}{4}$ span when loaded at $\frac{1}{2}$ span of B1 beam	296
Fig. A.19 – CSTL: vertical displacement at $\frac{1}{2}$ and $\frac{1}{4}$ span when loaded at $\frac{1}{2}$ span of B2 beam	296
Fig. A.20 – CSTL: vertical displacement at $\frac{1}{2}$ and $\frac{1}{4}$ span when loaded at $\frac{1}{2}$ span of B3 beam	297

Fig. A.21 – CSTL: vertical displacement at $\frac{1}{2}$ and $\frac{1}{4}$ span when loaded at $\frac{1}{2}$ span of B4 beam	297
Fig. A.22 – CSTL: vertical displacement at $\frac{1}{2}$ and $\frac{1}{4}$ span when loaded at $\frac{1}{2}$ span of B5 beam	298
Fig. A.23 – CSTL: vertical displacement at $\frac{1}{2}$ and $\frac{1}{4}$ span when loaded at $\frac{1}{2}$ span of B6 beam	298
Fig. A.24 – CSTL: vertical displacement at $\frac{1}{2}$ and $\frac{1}{4}$ span when loaded at $\frac{1}{2}$ span of B7 beam	299
Fig. A.25 – CSGL: vertical displacement at $\frac{1}{2}$ and $\frac{1}{4}$ span when loaded at $\frac{1}{4}$ span of B1 beam	299
Fig. A.26 – CSGL: vertical displacement at $\frac{1}{2}$ and $\frac{1}{4}$ span when loaded at $\frac{1}{4}$ span of B2 beam	300
Fig. A.27 – CSGL: vertical displacement at $\frac{1}{2}$ and $\frac{1}{4}$ span when loaded at $\frac{1}{4}$ span of B3 beam	300
Fig. A.28 – CSGL: vertical displacement at $\frac{1}{2}$ and $\frac{1}{4}$ span when loaded at $\frac{1}{4}$ span of B4 beam	301
Fig. A.29 – CSGL: vertical displacement at $\frac{1}{2}$ and $\frac{1}{4}$ span when loaded at $\frac{1}{4}$ span of B5 beam	301
Fig. A.30 – CSTL: vertical displacement at $\frac{1}{2}$ and $\frac{1}{4}$ span when loaded at $\frac{1}{4}$ span of B1 beam	302
Fig. A.31 – CSTL: vertical displacement at $\frac{1}{2}$ and $\frac{1}{4}$ span when loaded at $\frac{1}{4}$ span of B2 beam	302
Fig. A.32 – CSTL: vertical displacement at $\frac{1}{2}$ and $\frac{1}{4}$ span when loaded at $\frac{1}{4}$ span of B3 beam	303
Fig. A.33 – CSTL: vertical displacement at $\frac{1}{2}$ and $\frac{1}{4}$ span when loaded at $\frac{1}{4}$ span of B4 beam	303
Fig. A.34 – CSTL: vertical displacement at $\frac{1}{2}$ and $\frac{1}{4}$ span when loaded at $\frac{1}{4}$ span of B5 beam	304
Fig. A.35 – CSTL: vertical displacement at $\frac{1}{2}$ and $\frac{1}{4}$ span when loaded at $\frac{1}{4}$ span of B6 beam	304
Fig. A.36 – CSTL: vertical displacement at $\frac{1}{2}$ and $\frac{1}{4}$ span when loaded at $\frac{1}{4}$ span of B7 beam	305
Fig. A.37 – CSGL: vertical displacement at each beam mid-span	307

Fig. A.38 – CSGLi: vertical displacement at each beam mid-span.....	308
Fig. A.39 – CSGLnla: vertical displacement at each beam mid-span.....	308
Fig. A.40 – CSGL-lK: vertical displacement at each beam mid-span	309
Fig. A.41 – CSGL-mK: vertical displacement at each beam mid-span	309
Fig. A.42 – CSGL-hK: vertical displacement at mid-span.....	310
Fig. A.43 – CSGLsb: vertical displacement at each beam mid-span	310
Fig. A.44 – CSGLjb: vertical displacement at each beam mid-span.....	311
Fig. A.45 – CSGLl: vertical displacement at each beam mid-span.....	311
Fig. A.46 – CSGL: vertical displacement at each beam quarter-span.....	312
Fig. A.47 – CSGLi: vertical displacement at each beam quarter-span.....	312
Fig. A.48 – CSGLnla: vertical displacement at each beam quarter-span.....	313
Fig. A.49 – CSGL-lK: vertical displacement at each beam quarter-span	313
Fig. A.50 – CSGL-mK: vertical displacement at each beam quarter-span	314
Fig. A.51 – CSGL-hK: vertical displacement at quarter-span	314
Fig. A.52 – CSGLsb: vertical displacement at each beam quarter-span.....	315
Fig. A.53 – CSGLjb: vertical displacement at each beam quarter-span.....	315
Fig. A.54 – CSGLl: vertical displacement at each beam quarter-span.....	316
Fig. A.55 – CSGL: support reactions for a centered load	316
Fig. A.56 – CSGLi: support reactions for a centered load	317
Fig. A.57 – CSGLnla: support reactions for a centered load	317
Fig. A.58 – CSGL-lK: support reactions for a centered load.....	318
Fig. A.59 – CSGL-mK: support reactions for a centered load.....	318
Fig. A.60 – CSGL-hK: support reactions for a centered load	319
Fig. A.61 – CSGLsb: support reactions for a centered load.....	319
Fig. A.62 – CSGLjb: support reactions for a centered load	320
Fig. A.63 – CSGLl: support reactions for a centered load	320
Fig. A.64 – CSGL: support reactions for a decentered load.....	321
Fig. A.65 – CSGLi: support reactions for a decentered load	321
Fig. A.66 – CSGLnla: support reactions for a decentered load.....	322

Fig. A.67 – CSGL-IK: support reactions for a decentered load.....	322
Fig. A.68 – CSGL-mK: support reactions for a decentered load.....	323
Fig. A.69 – CSGL-hK: support reactions for a decentered load.....	323
Fig. A.70 – CSGLsb: support reactions for a decentered load	324
Fig. A.71 – CSGLjb: support reactions for a decentered load.....	324
Fig. A.72 – CSGLl: support reactions for a decentered load.....	325
Fig. A.73 – CSGL: longitudinal bending moment at the mid-span section.....	325
Fig. A.74 – CSGLi: longitudinal bending moment at the mid-span section.....	326
Fig. A.75 – CSGLnla: longitudinal bending moment at the mid-span section.....	326
Fig. A.76 – CSGL-IK: longitudinal bending moment at the mid-span section	327
Fig. A.77 – CSGL-mK: longitudinal bending moment at the mid-span section	327
Fig. A.78 – CSGL-hK: longitudinal bending moment at the mid-span section.....	328
Fig. A.79 – CSGLsb: longitudinal bending moment at the mid-span section	328
Fig. A.80 – CSGLjb: longitudinal bending moment at the mid-span section.....	329
Fig. A.81 – CSGLl: longitudinal bending moment at the mid-span section.....	329
Fig. A.82 – CSGL: longitudinal bending moment at the quarter-span section.....	330
Fig. A.83 – CSGLi: longitudinal bending moment at the quarter-span section.....	330
Fig. A.84 – CSGLnla: longitudinal bending moment at the quarter-span section.....	331
Fig. A.85 – CSGL-IK: longitudinal bending moment at the quarter-span section	331
Fig. A.86 – CSGL-mK: longitudinal bending moment at the quarter-span section	332
Fig. A.87 – CSGL-hK: longitudinal bending moment at the quarter-span section	332
Fig. A.88 – CSGLsb: longitudinal bending moment at the quarter-span section	333
Fig. A.89 – CSGLjb: longitudinal bending moment at the quarter-span section.....	333
Fig. A.90 – CSGLl: longitudinal bending moment at the quarter-span section.....	334
Fig. B.1 – S1-BSp: vertical displacements when loaded at B1-GL3.....	344
Fig. B.2 – S1-BSp: vertical displacements when loaded at B2-GL9	345
Fig. B.3 – S1-BSp: vertical displacements when loaded at B3-GL13.....	346
Fig. B.4 – S1-BSp: vertical displacements when loaded at B4-GL1	347
Fig. B.5 – S1-BSp: vertical displacements when loaded at B5-GL8.....	348

Fig. B.6 – S2-LWAC: vertical displacements when loaded at B1-GL4.....	349
Fig. B.7 – S2-LWAC: vertical displacements when loaded at B2-GL10.....	350
Fig. B.8 – S2-LWAC: vertical displacements when loaded at B3-GL11.....	351
Fig. B.9 – S2-LWAC: vertical displacements when loaded at B4-GL14.....	352
Fig. B.10 – S2-LWAC: vertical displacements when loaded at B5-GL15.....	353
Fig. B.11 – S3-hc=0.03m: vertical displacements when loaded at B1-GL6.....	354
Fig. B.12 – S3-hc=0.03m: vertical displacements when loaded at B2-GL12.....	355
Fig. B.13 – S3-hc=0.03m: vertical displacements when loaded at B3-GL2.....	356
Fig. B.14 – S3-hc=0.03m: vertical displacements when loaded at B4-GL5.....	357
Fig. B.15 – S3-hc=0.03m: vertical displacements when loaded at B5-GL7.....	358
Fig. B.16 – S4-L=2.00m: vertical displacements when loaded at B1-GL17.....	359
Fig. B.17 – S4-L=2.00m: vertical displacements when loaded at B2-GL20.....	360
Fig. B.18 – S4-L=2.00m: vertical displacements when loaded at B3-GL19.....	361
Fig. B.19 – S4-L=2.00m: vertical displacements when loaded at B4-GL18.....	362
Fig. B.20 – S4-L=2.00m: vertical displacements when loaded at B5-GL16.....	363
Fig. B.21 – S5-L=6.00m: vertical displacements when loaded at B1-GL23.....	364
Fig. B.22 – S5-L=6.00m: vertical displacements when loaded at B2-GL24.....	365
Fig. B.23 – S5-L=6.00m: vertical displacements when loaded at B3-GL22.....	366
Fig. B.24 – S5-L=6.00m: vertical displacements when loaded at B4-GL25.....	367
Fig. B.25 – S5-L=6.00m: vertical displacements when loaded at B5-GL21.....	368
Fig. B.26 – Vertical displacement relatively to the higher displacement for each beam in S1-BSp considering 4P loading.....	373
Fig. B.27 – Vertical displacement relatively to the higher displacement for each beam in S1-BSp disregarding 4P loading.....	374
Fig. B.28 – Vertical displacement relatively to the higher displacement for each beam in S2-LWAC.....	375
Fig. B.29 – Vertical displacement relatively to the higher displacement for each beam in S3-hc=0.03m.....	376
Fig. B.30 – Vertical displacement relatively to the higher displacement for each beam in S4-L=2.00m.....	377

Fig. B.31 – Vertical displacement relatively to the higher displacement for each beam in S5-L=6.00m.....	378
Fig. B.32 – Slab deflections: B1 ½	380
Fig. B.33 – Slab deflections: B2 ½	381
Fig. B.34 – Slab deflections: B3 ½	382
Fig. B.35 – Slab deflections: B4 ½	383
Fig. B.36 – Slab deflections: B5 ½	384
Fig. B.37 – Slab deflections: B1 ¼	385
Fig. B.38 – Slab deflections: B2 ¼	386
Fig. B.39 – Slab deflections: B3 ¼	387
Fig. B.40 – Slab deflections: B4 ¼	388
Fig. B.41 – Slab deflections: B5 ¼	389
Fig. B.42 – Slab deflections: linear loading at B1	390
Fig. B.43 – Slab deflections: linear loading at B2	391
Fig. B.44 – Slab deflections: linear loading at B3	392
Fig. B.45 – Slab deflections: linear loading at B4	393
Fig. B.46 – Slab deflections: linear loading at B5	394
Fig. B.47 – Beams deflection in S1-BSp	396
Fig. B.48 – Beams deflection in S2-LWAC	397
Fig. B.49 – Beams deflection in S3-hc=0.03m.....	398
Fig. B.50 – Beams deflection in S4-L=2.00m	399
Fig. B.51 – Beams deflection in S5-L=6.00m	400
Fig. B.52 – Vertical displacements at ¼ L distribution for the loaded beam	401
Fig. B.53 – Vertical displacements at ½ L distribution for the loaded beam	402
Fig. B.54 – S1-BSp: distribution of support reactions when loaded at B1-GL3	403
Fig. B.55 – S1-BSp: distribution of support reactions when loaded at B2-GL9	403
Fig. B.56 – S1-BSp: distribution of support reactions when loaded at B3-GL13	404
Fig. B.57 – S1-BSp: distribution of support reactions when loaded at B4-GL1	404
Fig. B.58 – S1-BSp: distribution of support reactions when loaded at B5-GL8	405
Fig. B.59 – S2-LWAC: distribution of support reactions when loaded at B1-GL4	405

Fig. B.60 – S2-LWAC: distribution of support reactions when loaded at B2-GL10.....	406
Fig. B.61 – S2-LWAC: distribution of support reactions when loaded at B3-GL11.....	406
Fig. B.62 – S2-LWAC: distribution of support reactions when loaded at B4-GL14.....	407
Fig. B.63 – S2-LWAC: distribution of support reactions when loaded at B5-GL15.....	407
Fig. B.64 – S3-hc=0.03m: distribution of support reactions when loaded at B1-GL6.....	408
Fig. B.65 – S3-hc=0.03m: distribution of support reactions when loaded at B2-GL12.....	408
Fig. B.66 – S3-hc=0.03m: distribution of support reactions when loaded at B3-GL2.....	409
Fig. B.67 – S3-hc=0.03m: distribution of support reactions when loaded at B4-GL5.....	409
Fig. B.68 – S3-hc=0.03m: distribution of support reactions when loaded at B5-GL7.....	410
Fig. B.69 – S4-L=2.00m: distribution of support reactions when loaded at B1-GL17.....	410
Fig. B.70 – S4-L=2.00m: distribution of support reactions when loaded at B2-GL20.....	411
Fig. B.71 – S4-L=2.00m: distribution of support reactions when loaded at B3-GL19.....	411
Fig. B.72 – S4-L=2.00m: distribution of support reactions when loaded at B4-GL18.....	412
Fig. B.73 – S4-L=2.00m: distribution of support reactions when loaded at B5-GL16.....	412
Fig. B.74 – S5-L=6.00m: distribution of support reactions when loaded at B1-GL23.....	413
Fig. B.75 – S5-L=6.00m: distribution of support reactions when loaded at B2-GL24.....	413
Fig. B.76 – S5-L=6.00m: distribution of support reactions when loaded at B3-GL22.....	414
Fig. B.77 – S5-L=6.00m: distribution of support reactions when loaded at B4-GL25.....	414
Fig. B.78 – S5-L=6.00m: distribution of support reactions when loaded at B5-GL21.....	415
Fig. B.79 – Support reaction distribution for $\frac{1}{2}$ L loading.....	416
Fig. B.80 – Support reaction distribution for $\frac{1}{4}$ L loading.....	417
Fig. B.81 – Support reaction distribution for line loading.....	418
Fig. B.82 – Support reaction distribution for $\frac{1}{2}$ L loading: S2 vs S1.....	419
Fig. B.83 – Support reaction distribution for $\frac{1}{4}$ L loading: S2 vs S1.....	420
Fig. B.84 – Support reaction distribution for line loading: S2-LWAC vs S1-BSp.....	421
Fig. B.85 – Support reaction distribution for $\frac{1}{2}$ L loading: S3-hc=0.03m vs S1-BSp.....	422
Fig. B.86 – Support reaction distribution for $\frac{1}{4}$ L loading: S3-hc=0.03m vs S1-BSp.....	423
Fig. B.87 – Support reaction distribution for line loading: S3-hc=0.03m vs S1-BSp.....	424
Fig. B.88 – Support reaction distribution for $\frac{1}{2}$ L: S4-L=2.00m, S5-L=6.00m and S1-BSp.....	425

Fig. B.89 – Support reaction distribution for $\frac{1}{4}$ L loading: S4-L=2.00m, S5-L=6.00m and S1-BSp.....	426
Fig. B.90 – Support reaction distribution for line loading: S4-L=2.00m, S5-L=6.00m and S1-BSp.....	427
Fig. B.91 – Strain distribution for the loaded beam.....	437
Fig. B.92 – S1-BSp: experimental and numerical vertical displacements when loaded at B1-GL3	439
Fig. B.93 – S1-BSp: experimental and numerical vertical displacements when loaded at B2-GL9	440
Fig. B.94 – S1-BSp: experimental and numerical vertical displacements when loaded at B3-GL13	441
Fig. B.95 – S1-BSp: experimental and numerical vertical displacements when loaded at B4-GL1	442
Fig. B.96 – S1-BSp: experimental and numerical vertical displacements when loaded at B5-GL8	443
Fig. B.97 – S2-LWAC: experimental and numerical vertical displacements when loaded at B1-GL4	444
Fig. B.98 – S2-LWAC: experimental and numerical vertical displacements when loaded at B2-GL10	445
Fig. B.99 – S2-LWAC: experimental and numerical vertical displacements when loaded at B3-GL11	446
Fig. B.100 – S2-LWAC: experimental and numerical vertical displacements when loaded at B4-GL14	447
Fig. B.101 – S2-LWAC: experimental and numerical vertical displacements when loaded at B5-GL15	448
Fig. B.102 – S3-hc=0.03m: experimental and numerical vertical displacements when loaded at B1-GL6	449
Fig. B.103 – S3-hc=0.03m: experimental and numerical vertical displacements when loaded at B2-GL12	450
Fig. B.104 – S3-hc=0.03m: experimental and numerical vertical displacements when loaded at B3-GL2	451
Fig. B.105 – S3-hc=0.03m: experimental and numerical vertical displacements when loaded at B4-GL5	452

Fig. B.106 – S3-hc=0.03m: experimental and numerical vertical displacements when loaded at B5-GL7.....	453
Fig. B.107 – S4-L=2.00m: experimental and numerical vertical displacements when loaded at B1-GL17.....	454
Fig. B.108 – S4-L=2.00m: experimental and numerical vertical displacements when loaded at B2-GL20.....	455
Fig. B.109 – S4-L=2.00m: experimental and numerical vertical displacements when loaded at B3-GL19.....	456
Fig. B.110 – S4-L=2.00m: experimental and numerical vertical displacements when loaded at B4-GL18.....	457
Fig. B.111 – S4-L=2.00m: experimental and numerical vertical displacements when loaded at B5-GL16.....	458
Fig. B.112 – S5-L=6.00m: experimental and numerical vertical displacements when loaded at B1-GL23.....	459
Fig. B.113 – S5-L=6.00m: experimental and numerical vertical displacements when loaded at B2-GL24.....	460
Fig. B.114 – S5-L=6.00m: experimental and numerical vertical displacements when loaded at B3-GL22.....	461
Fig. B.115 – S5-L=6.00m: experimental and numerical vertical displacements when loaded at B4-GL25.....	462
Fig. B.116 – S5-L=6.00m: experimental and numerical vertical displacements when loaded at B5-GL21.....	463
Fig. B.117 – S1-BSp: experimental and numerical distribution of support reactions when loaded at B1-GL3.....	470
Fig. B.118 – S1-BSp: experimental and numerical distribution of support reactions when loaded at B2-GL9.....	471
Fig. B.119 – S1-BSp: experimental and numerical distribution of support reactions when loaded at B3-GL13.....	471
Fig. B.120 – S1-BSp: experimental and numerical distribution of support reactions when loaded at B4-GL1.....	472
Fig. B.121 – S1-BSp: experimental and numerical distribution of support reactions when loaded at B5-GL8.....	472

Fig. B.122 – S2-LWAC: experimental and numerical distribution of support reactions when loaded at B1-GL4.....	473
Fig. B.123 – S2-LWAC: experimental and numerical distribution of support reactions when loaded at B2-GL10.....	473
Fig. B.124 – S2-LWAC: experimental and numerical distribution of support reactions when loaded at B3-GL11.....	474
Fig. B.125 – S2-LWAC: experimental and numerical distribution of support reactions when loaded at B4-GL14.....	474
Fig. B.126 – S2-LWAC: experimental and numerical distribution of support reactions when loaded at B5-GL15.....	475
Fig. B.127 – S3-hc=0.03m: experimental and numerical distribution of support reactions when loaded at B1-GL6.....	475
Fig. B.128 – S3-hc=0.03m: experimental and numerical distribution of support reactions when loaded at B2-GL12.....	476
Fig. B.129 – S3-hc=0.03m: experimental and numerical distribution of support reactions when loaded at B3-GL2.....	476
Fig. B.130 – S3-hc=0.03m: experimental and numerical distribution of support reactions when loaded at B4-GL5.....	477
Fig. B.131 – S3-hc=0.03m: experimental and numerical distribution of support reactions when loaded at B5-GL7.....	477
Fig. B.132 – S4-L=2.00m: experimental and numerical distribution of support reactions when loaded at B1-GL17.....	478
Fig. B.133 – S4-L=2.00m: experimental and numerical distribution of support reactions when loaded at B2-GL20.....	478
Fig. B.134 – S4-L=2.00m: experimental and numerical distribution of support reactions when loaded at B3-GL19.....	479
Fig. B.135 – S4-L=2.00m: experimental and numerical distribution of support reactions when loaded at B4-GL18.....	479
Fig. B.136 – S4-L=2.00m: experimental and numerical distribution of support reactions when loaded at B5-GL16.....	480
Fig. B.137 – S5-L=6.00m: experimental and numerical distribution of support reactions when loaded at B1-GL23.....	480

Fig. B.138 – S5-L=6.00m: experimental and numerical distribution of support reactions when loaded at B2-GL24	481
Fig. B.139 – S5-L=6.00m: experimental and numerical distribution of support reactions when loaded at B3-GL22	481
Fig. B.140 – S5-L=6.00m: experimental and numerical distribution of support reactions when loaded at B4-GL25	482
Fig. B.141 – S5-L=6.00m: experimental and numerical distribution of support reactions when loaded at B5-GL21	482
Fig. C.1 – <i>bm</i> distribution for $\frac{1}{2}$ L loading vs. 1 st degree polynomial, simple	539
Fig. C.2 – <i>bm</i> distribution for <i>lin</i> loading vs. 1 st degree polynomial, simple	540
Fig. C.3 – <i>bm</i> distribution for $\frac{1}{4}$ L loading vs. 1 st degree polynomial, simple	541
Fig. C.4 – <i>bm</i> distribution for $\frac{1}{2}$ L loading vs. 1 st degree polynomial, crossed terms	542
Fig. C.5 – <i>bm</i> distribution for <i>lin</i> loading vs. 1 st degree polynomial, crossed terms	543
Fig. C.6 – <i>bm</i> distribution for $\frac{1}{4}$ L loading vs. 1 st degree polynomial, crossed terms	544
Fig. C.7 – <i>bm</i> distribution for $\frac{1}{2}$ L loading vs. 2 nd degree polynomial, simple	545
Fig. C.8 – <i>bm</i> distribution for <i>lin</i> loading vs. 2 nd degree polynomial, simple	546
Fig. C.9 – <i>bm</i> distribution for $\frac{1}{4}$ L loading vs. 2 nd degree polynomial, simple	547
Fig. C.10 – <i>bm</i> distribution for $\frac{1}{2}$ L loading vs. 2 nd degree polynomial, crossed terms	548
Fig. C.11 – <i>bm</i> distribution for <i>lin</i> loading vs. 2 nd degree polynomial, crossed terms	549
Fig. C.12 – <i>bm</i> distribution for $\frac{1}{4}$ L loading vs. 2 nd degree polynomial, crossed terms	550
Fig. C.13 – <i>bm</i> distribution for $\frac{1}{2}$ L loading vs. 3 rd degree polynomial, simple	551
Fig. C.14 – <i>bm</i> distribution for <i>lin</i> loading vs. 3 rd degree polynomial, simple	552
Fig. C.15 – <i>bm</i> distribution for $\frac{1}{4}$ L loading vs. 3 rd degree polynomial, simple	553
Fig. C.16 – <i>bm</i> distribution for $\frac{1}{2}$ L loading vs. 4 th degree polynomial, simple	554
Fig. C.17 – <i>bm</i> distribution for <i>lin</i> loading vs. 4 th degree polynomial, simple	555
Fig. C.18 – <i>bm</i> distribution for $\frac{1}{4}$ L loading vs. 4 th degree polynomial, simple	556

APPENDICES LIST OF TABLES

Table B.1 – Material properties of the concrete poured into S1 specimen	337
Table B.2 – Material properties of the concrete poured into S2 specimen	338
Table B.3 – Material properties of the concrete poured into S3 and S4 specimens.....	338
Table B.4 – Material properties of the concrete poured into S5 specimen	339
Table B.5 – Material properties and span dimensions of the timber beams.....	340
Table B.6 – Cross sectional dimensions of the beams	341
Table B.7 – Vertical displacements distribution [%]	370
Table B.8 – Experimental slip displacements [mm]	428
Table B.9 – Experimental uplift displacements [mm].....	431
Table B.10 – Experimental strains [$\mu\epsilon$].....	432
Table B.11 – Strain distribution [%]	435
Table B.12 – Numerical distribution of vertical displacements [%]	464
Table B.13 – Difference between experimental and numerical distribution of vertical displacements [%]	467
Table B.14 – Experimental and numerical support reaction distribution [%].....	483
Table B.15 – Difference between experimental and numerical support reaction distribution [%]	485
Table B.16 – Stresses comparison [MPa].....	487
Table C.1 – First phase modeling.....	491
Table C.2 – Vertical displacements at $\frac{1}{2} L$, when the load is applied at B1 $\frac{1}{2} L$ [%].....	497
Table C.3 – Vertical displacements at $\frac{1}{2} L$, when the load is applied at B2 $\frac{1}{2} L$ [%].....	498
Table C.4 – Vertical displacements at $\frac{1}{2} L$, when the load is applied at B3* $\frac{1}{2} L$ [%].....	499
Table C.5 – Vertical displacements at $\frac{1}{2} L$, when the load is applied at B4* $\frac{1}{2} L$ [%].....	500
Table C.6 – Support reactions at each beam, when the load is applied at B1 $\frac{1}{2} L$ [%].....	502
Table C.7 – Support reactions at each beam, when the load is applied at B2 $\frac{1}{2} L$ [%].....	503
Table C.8 – Support reactions at each beam, when the load is applied at B3* $\frac{1}{2} L$ [%].....	504
Table C.9 – Support reactions at each beam, when the load is applied at B4* $\frac{1}{2} L$ [%].....	505

Table C.10 – Longitudinal bending moment at $\frac{1}{2} L$, when the load is applied at B1 $\frac{1}{2} L$ [%]	507
Table C.11 – Longitudinal bending moment at $\frac{1}{2} L$, when the load is applied at B2 $\frac{1}{2} L$ [%]	508
Table C.12 – Longitudinal bending moment at $\frac{1}{2} L$, when the load is applied at B3* $\frac{1}{2} L$ [%]	509
Table C.13 – Longitudinal bending moment at $\frac{1}{2} L$, when the load is applied at B4* $\frac{1}{2} L$ [%]	510
Table C.14 – Self-weight and imposed load cases.....	511
Table C.15 – Deviation between <i>Bs</i> and the remaining modeling considering the vertical displacement, when B1 is loaded [%].....	512
Table C.16 – Deviation between <i>Bs</i> and the remaining modeling considering the vertical displacement, when B2 is loaded [%].....	513
Table C.17 – Deviation between <i>Bs</i> and the remaining modeling considering the vertical displacement when B3 is loaded [%].....	514
Table C.18 – Deviation between the <i>Bs</i> and the remaining modeling considering the vertical displacement when the central beam is loaded [%].....	515
Table C.19 – Deviation between the <i>Bs</i> and the remaining modeling considering the support reactions when B1 is loaded [%].....	516
Table C.20 – Deviation between the <i>Bs</i> and the remaining modeling considering the support reactions when B2 is loaded [%].....	517
Table C.21 – Deviation between the <i>Bs</i> and the remaining modeling considering the support reactions when B3 is loaded [%].....	518
Table C.22 – Deviation between the <i>Bs</i> and the remaining modeling considering the support reactions when the central beam is loaded [%].....	519
Table C.23 – Deviation between the <i>Bs</i> and the remaining modeling considering the bending moment when B1 is loaded [%].....	520
Table C.24 – Deviation between the <i>Bs</i> and the remaining modeling considering the bending moment when B2 is loaded [%].....	521
Table C.25 – Deviation between the <i>Bs</i> and the remaining modeling considering the bending moment when B3 is loaded [%].....	522
Table C.26 – Deviation between the <i>Bs</i> and the remaining modeling considering the bending moment when the central beam is loaded [%].....	523

Table C.27 – Second phase modeling	524
Table C.28 – vd $\frac{1}{2}$ L when the load is applied at B1 $\frac{1}{2}$ L [%]	526
Table C.29 – vd $\frac{1}{2}$ L when the load is applied at B2 $\frac{1}{2}$ L [%]	527
Table C.30 – vd $\frac{1}{2}$ L when the load is applied at B3 $\frac{1}{2}$ L [%]	527
Table C.31 – vd $\frac{1}{2}$ L when the load is applied at B4 $\frac{1}{2}$ L [%]	528
Table C.32 – vd $\frac{1}{2}$ L received by the loaded beam [%]	528
Table C.33 – sr when the load is applied at B1 $\frac{1}{2}$ L [%]	529
Table C.34 – sr when the load is applied at B2 $\frac{1}{2}$ L [%]	530
Table C.35 – sr when the load is applied at B3 $\frac{1}{2}$ L [%]	530
Table C.36 – sr when the load is applied at B4 $\frac{1}{2}$ L [%]	531
Table C.37 – sr received by the loaded beam [%].....	531
Table C.38 – bm when the load is applied at B1 $\frac{1}{2}$ L [%].....	532
Table C.39 – bm when the load is applied at B2 $\frac{1}{2}$ L [%].....	533
Table C.40 – bm when the load is applied at B3 $\frac{1}{2}$ L [%].....	533
Table C.41 – bm when the load is applied at B4 $\frac{1}{2}$ L [%].....	534
Table C.42 – bm received by the loaded beam [%].....	534
Table C.43 – Numerical analysis: bm , when the load is applied at B1 $\frac{1}{4}$ L [%].....	536
Table C.44 – Numerical analysis: bm , when the load is applied at B2 $\frac{1}{4}$ L [%].....	537
Table C.45 – Numerical analysis: bm , when the load is applied at B3 $\frac{1}{4}$ L [%].....	537
Table C.46 – Numerical analysis: bm , when the load is applied at B4 $\frac{1}{4}$ L [%].....	538
Table C.47 – bm received by the loaded beam [%].....	538
Table C.48 – Experimental vs. Pr polynomial predictions for vd $\frac{1}{2}$ L: S1 to S5.....	557
Table C.49 – Experimental vs. Pr polynomial predictions for vd $\frac{1}{4}$ L: S1 to S5.....	558
Table C.50 – Experimental vs. Pr polynomial predictions for sr : S1 to S5.....	559
Table C.51 – Experimental vs. $cfvd \cdot Pr$ predictions for vd at $\frac{1}{2}$ L: S1 to S5	560
Table C.52 – Experimental vs. $cfvd \cdot Pr$ predictions for vd $\frac{1}{4}$ L: S1 to S5	561
Table C.53 – Experimental vs. $cf sr \cdot Pr$ predictions for sr : S1 to S5	562
Table C.54 – Experimental vs. Pr polynomial predictions for vd $\frac{1}{2}$ L: CSGL and CSTL.....	563
Table C.55 – Experimental vs. Pr polynomial predictions for vd $\frac{1}{4}$ L: CSGL and CSTL.....	563

Table C.56 – Experimental vs. Pr polynomial predictions for sr : CSGL and CSTL	564
Table C.57 – Average partial differences: experimental vs. Pr for CSGL and CSTL.....	564
Table C.58 – Experimental vs. $cfvd \cdot Pr$ predictions for vd at $\frac{1}{2} L$: CSGL and CSTL.....	565
Table C.59 – Experimental vs. $cfvd \cdot Pr$ predictions for vd at $\frac{1}{4} L$: CSGL and CSTL.....	565
Table C.60 – Experimental vs. $cfsr \cdot Pr$ predictions for sr : CSGL and CSTL	566

APPENDIX A

A.1 Results from the preliminary experimental tests

The following figures present the results in terms of support reactions and vertical displacements when the beams are loaded at mid- and at quarter-span for the preliminary experimental tests presented at 3.2 *Preliminary experimental tests*. The symbology is the same as used in the same section.

A.1.1 Support reactions

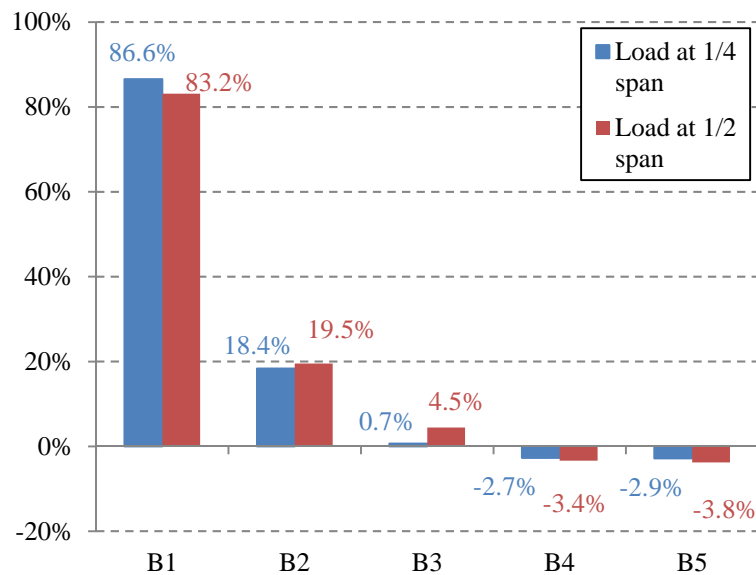


Fig. A.1 – CSGL: support reactions when loaded at $\frac{1}{2}$ span and at $\frac{1}{4}$ span of B1 beam

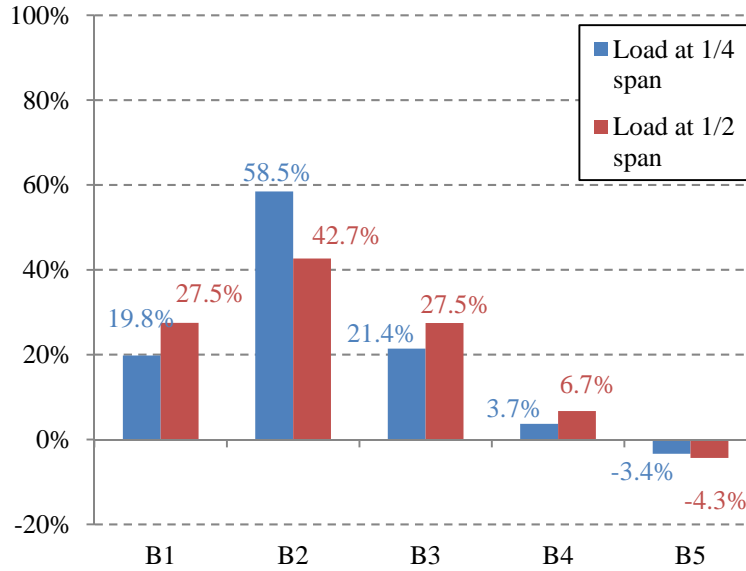


Fig. A.2 – CSGL: support reactions when loaded at 1/2 span and at 1/4 span of B2 beam

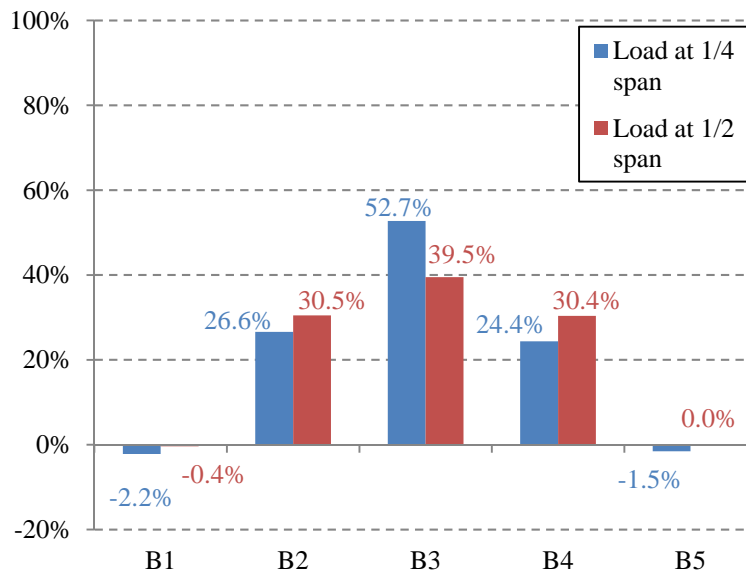


Fig. A.3 – CSGL: support reactions when loaded at 1/2 span and at 1/4 span of B3 beam

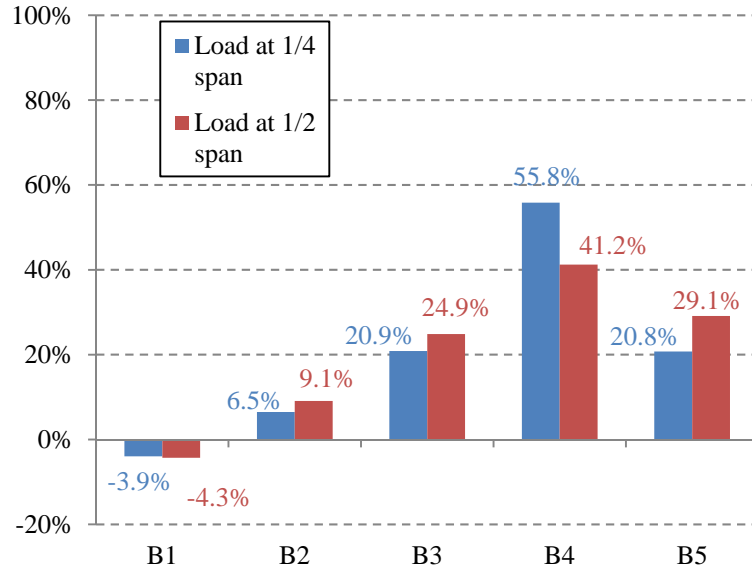


Fig. A.4 – CSGL: support reactions when loaded at 1/2 span and at 1/4 span of B4 beam

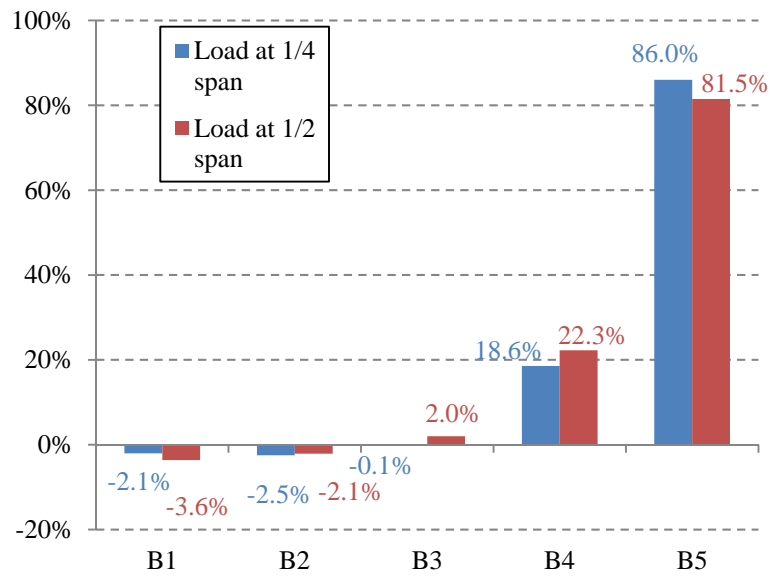


Fig. A.5 – CSGL: support reactions when loaded at 1/2 span and at 1/4 span of B5 beam

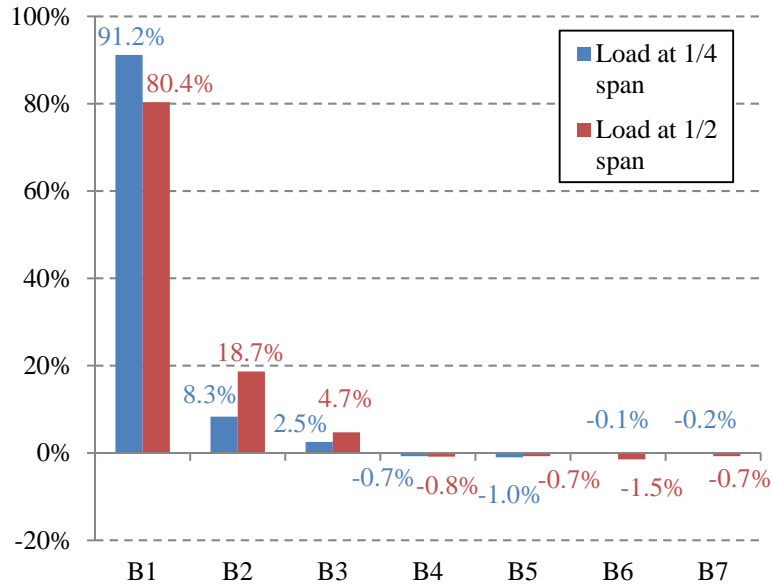


Fig. A.6 – CSTL: support reactions when loaded at 1/2 span and at 1/4 span of B1 beam

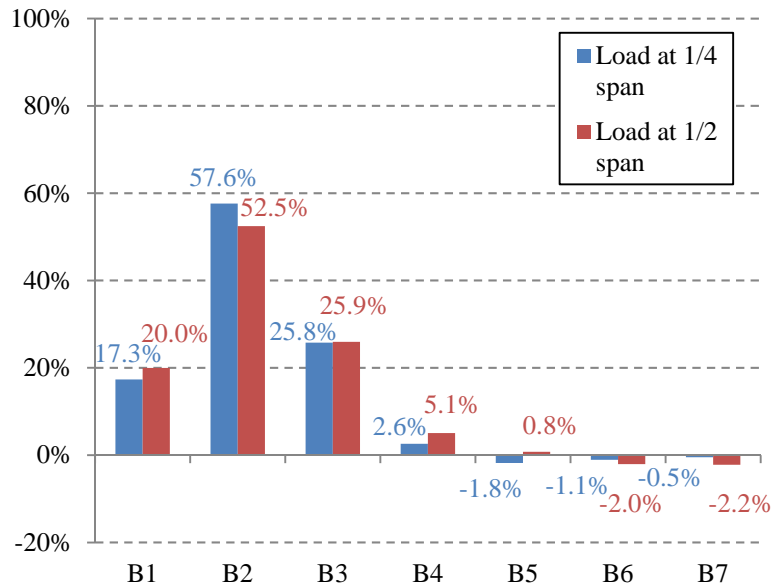


Fig. A.7 – CSTL: support reactions when loaded at 1/2 span and at 1/4 span of B2 beam

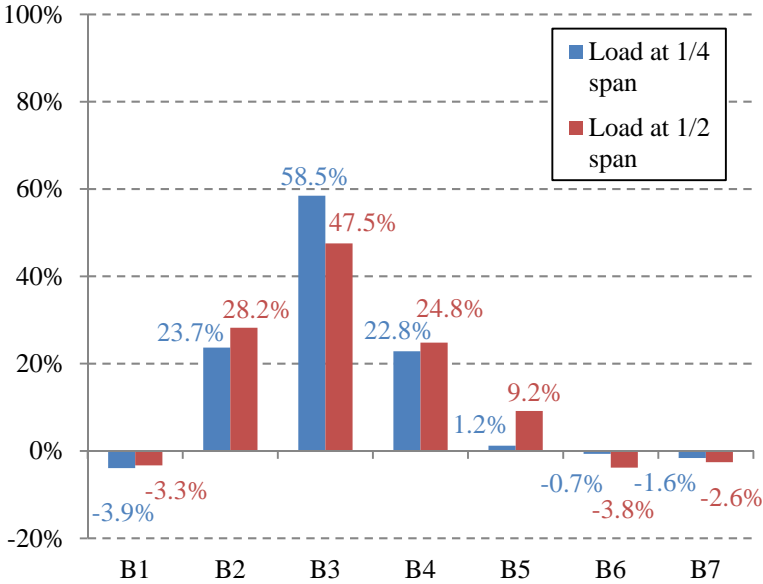


Fig. A.8 – CSTL: support reactions when loaded at 1/2 span and at 1/4 span of B3 beam

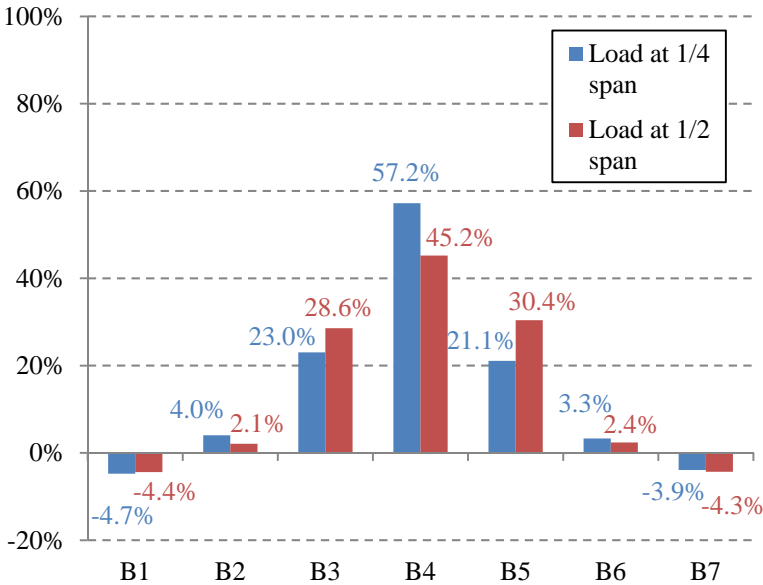


Fig. A.9 – CSTL: support reactions when loaded at 1/2 span and at 1/4 span of B4 beam

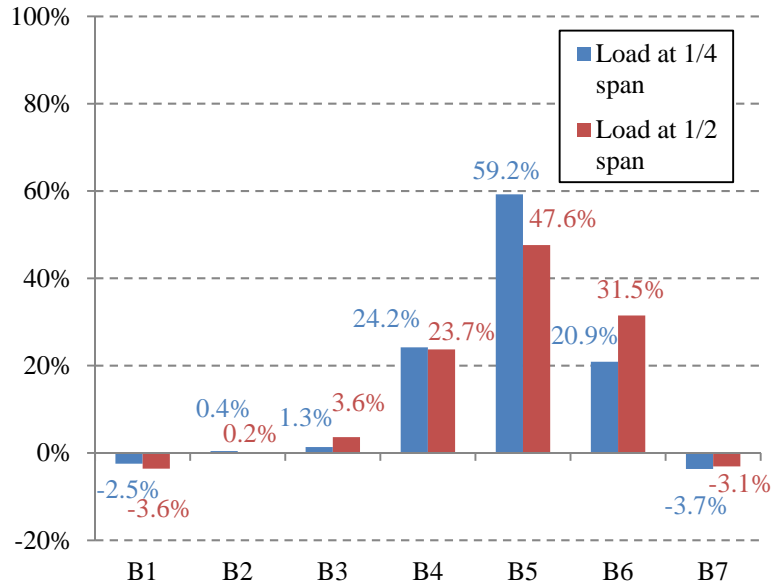


Fig. A.10 – CSTL: support reactions when loaded at 1/2 span and at 1/4 span of B5 beam

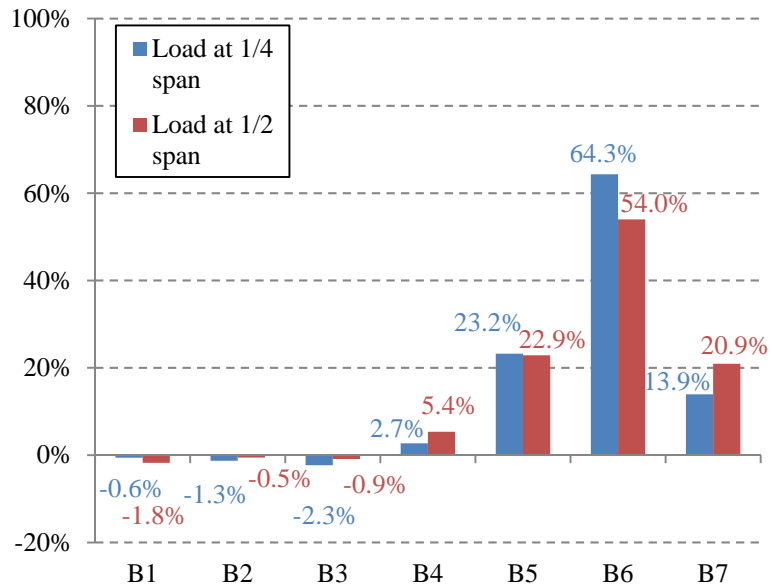


Fig. A.11 – CSTL: support reactions when loaded at 1/2 span and at 1/4 span of B6 beam

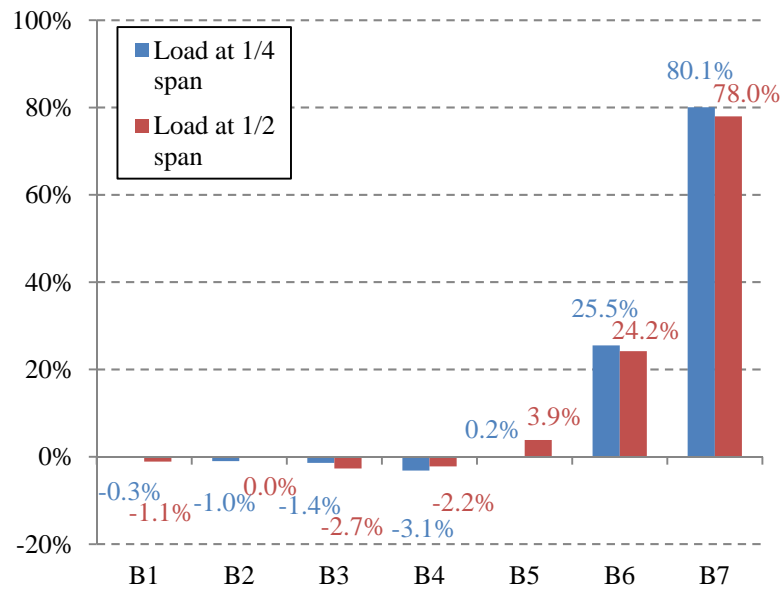


Fig. A.12 – CSTL: support reactions when loaded at 1/2 span and at 1/4 span of B7 beam

A.1.2 Vertical displacements when the beams are loaded at mid-span

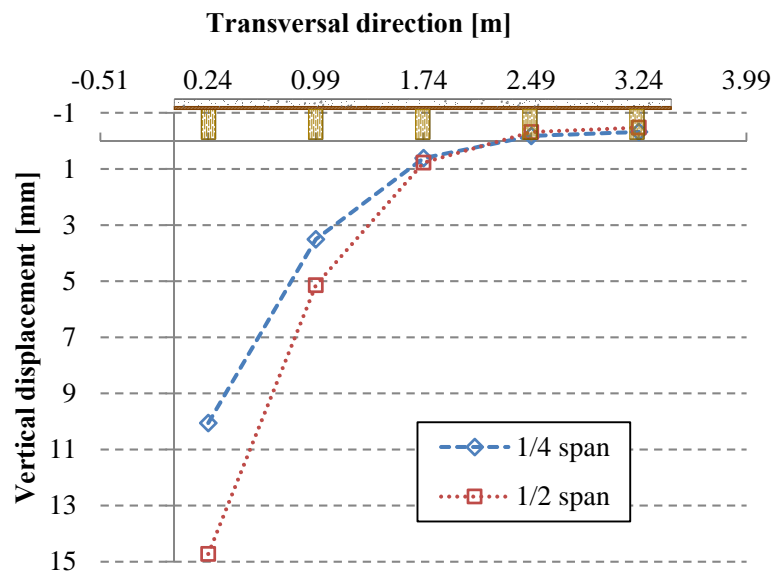


Fig. A.13 – CSGL: vertical displacement at 1/2 and 1/4 span when loaded at 1/2 span of B1 beam

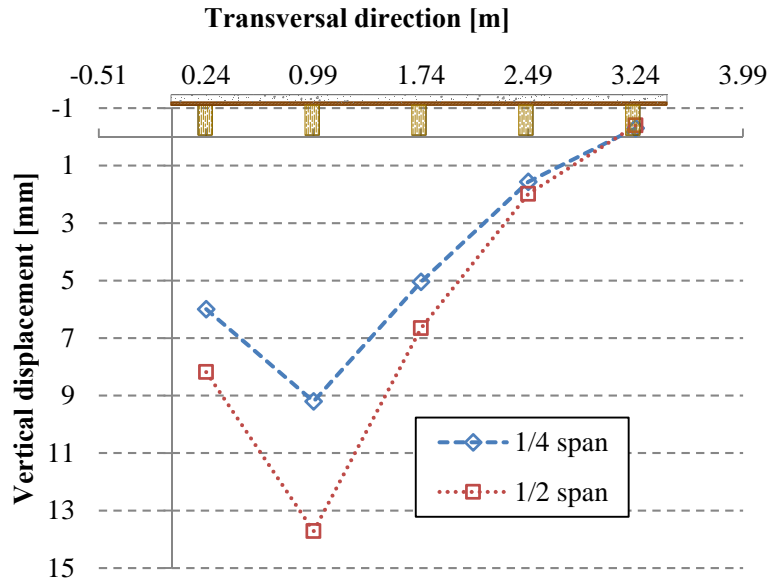


Fig. A.14 – CSDL: vertical displacement at 1/2 and 1/4 span when loaded at 1/2 span of B2 beam

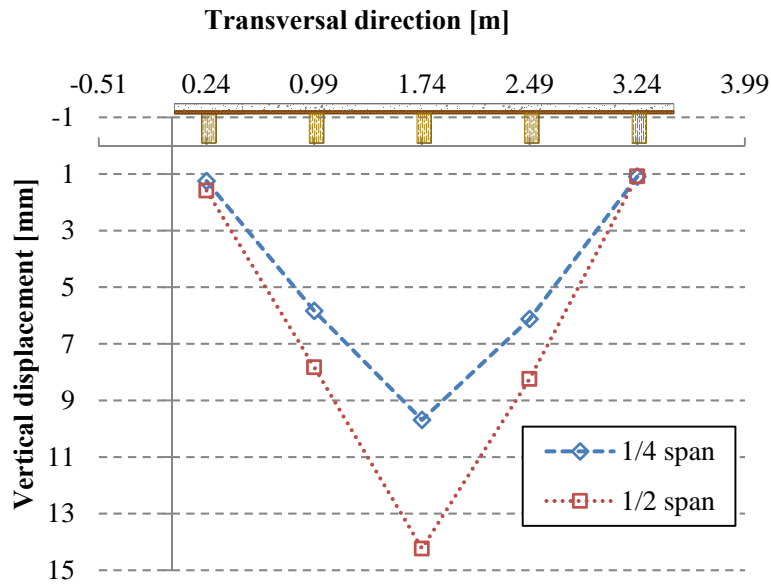


Fig. A.15 – CSDL: vertical displacement at 1/2 and 1/4 span when loaded at 1/2 span of B3 beam

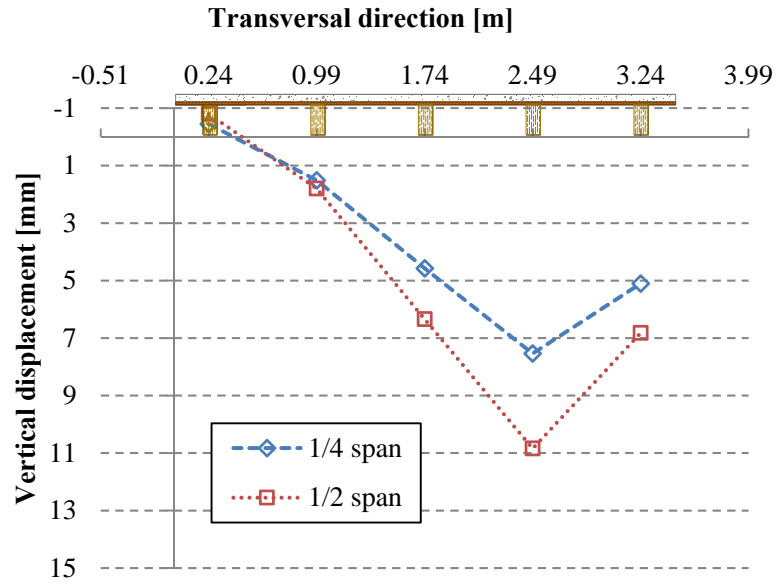


Fig. A.16 – CSGL: vertical displacement at 1/2 and 1/4 span when loaded at 1/2 span of B4 beam

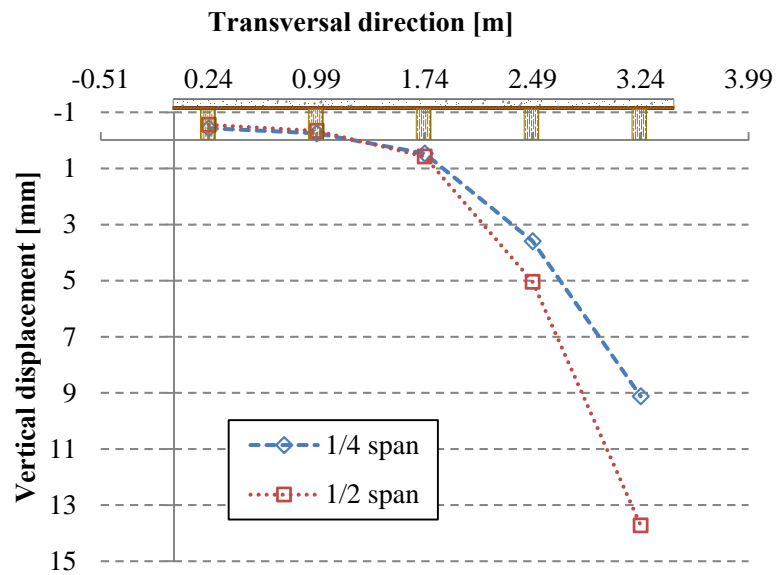


Fig. A.17 – CSGL: vertical displacement at 1/2 and 1/4 span when loaded at 1/2 span of B5 beam

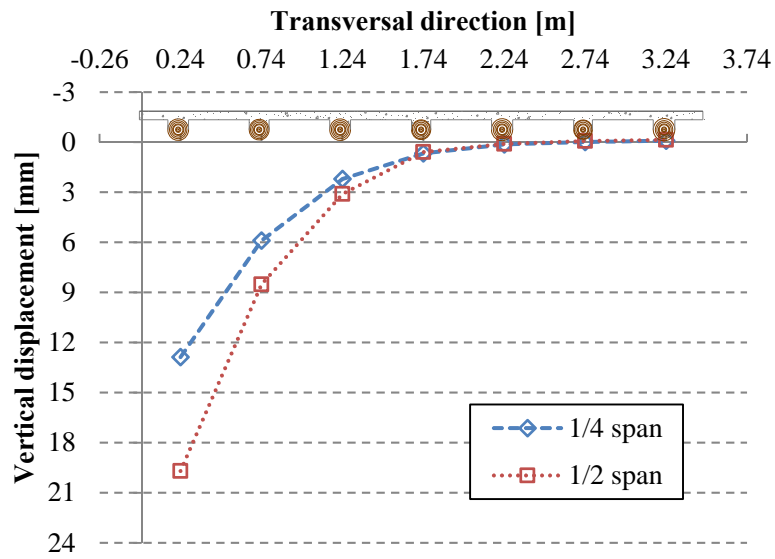


Fig. A.18 – CSTL: vertical displacement at 1/2 and 1/4 span when loaded at 1/2 span of B1 beam

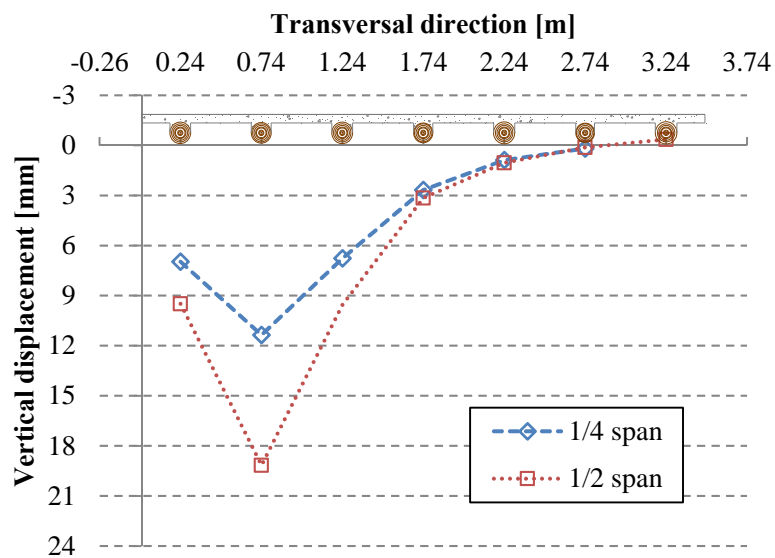


Fig. A.19 – CSTL: vertical displacement at 1/2 and 1/4 span when loaded at 1/2 span of B2 beam

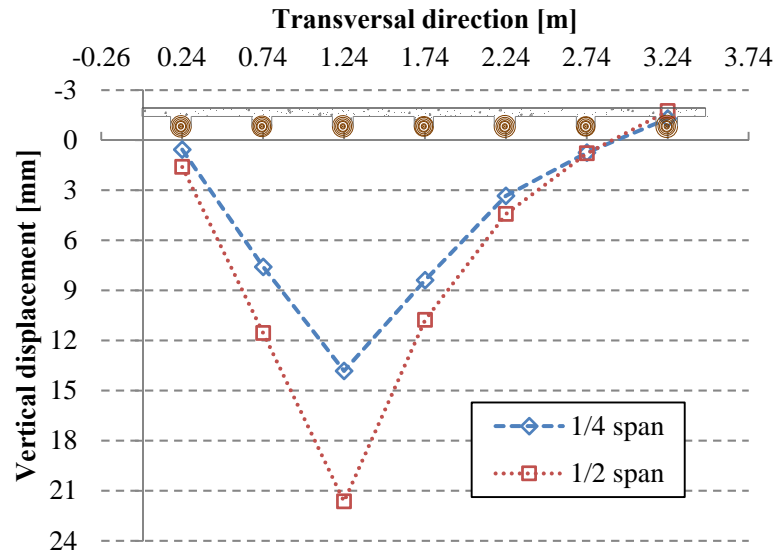


Fig. A.20 – CSTL: vertical displacement at 1/2 and 1/4 span when loaded at 1/2 span of B3 beam

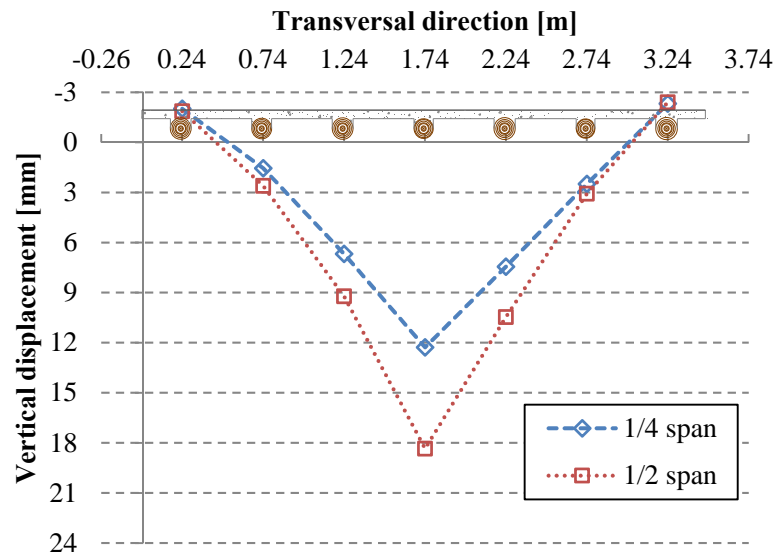


Fig. A.21 – CSTL: vertical displacement at 1/2 and 1/4 span when loaded at 1/2 span of B4 beam

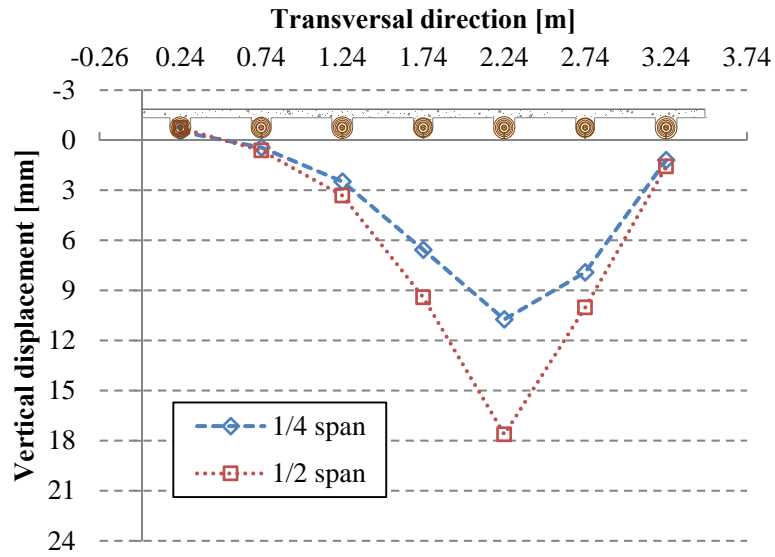


Fig. A.22 – CSTL: vertical displacement at 1/2 and 1/4 span when loaded at 1/2 span of B5 beam

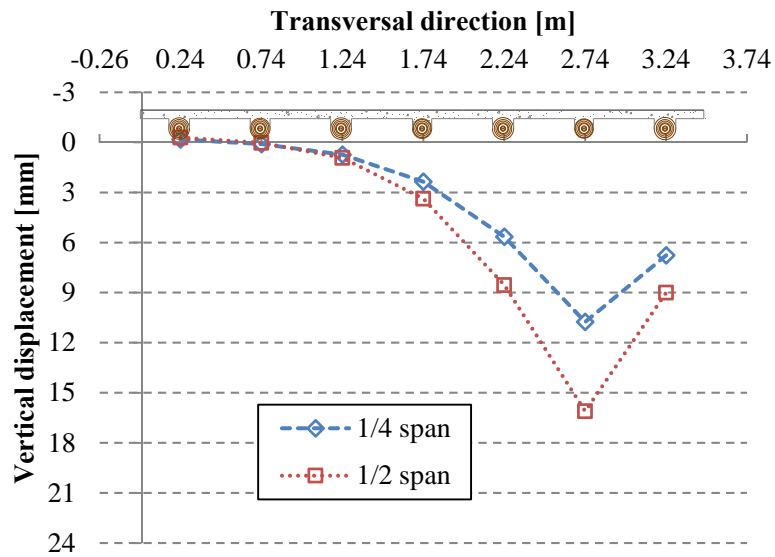


Fig. A.23 – CSTL: vertical displacement at 1/2 and 1/4 span when loaded at 1/2 span of B6 beam

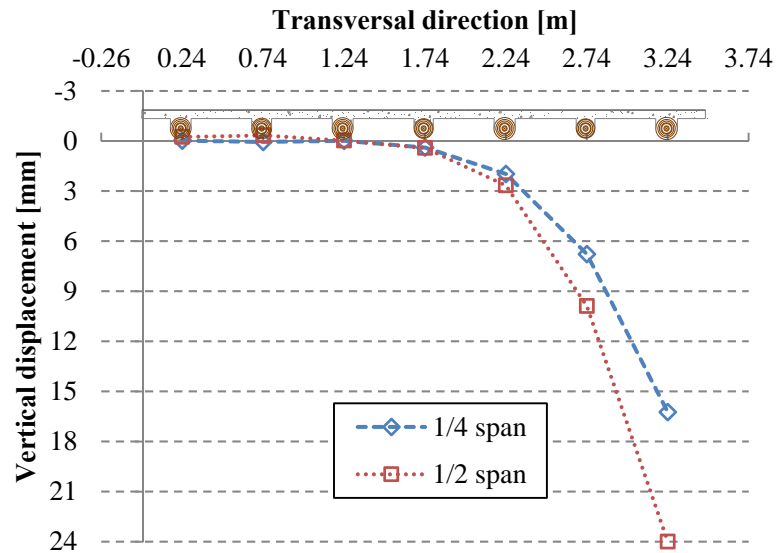


Fig. A.24 – CSTL: vertical displacement at 1/2 and 1/4 span when loaded at 1/2 span of B7 beam

A.1.3 Vertical displacements when the beams are loaded at quarter-span

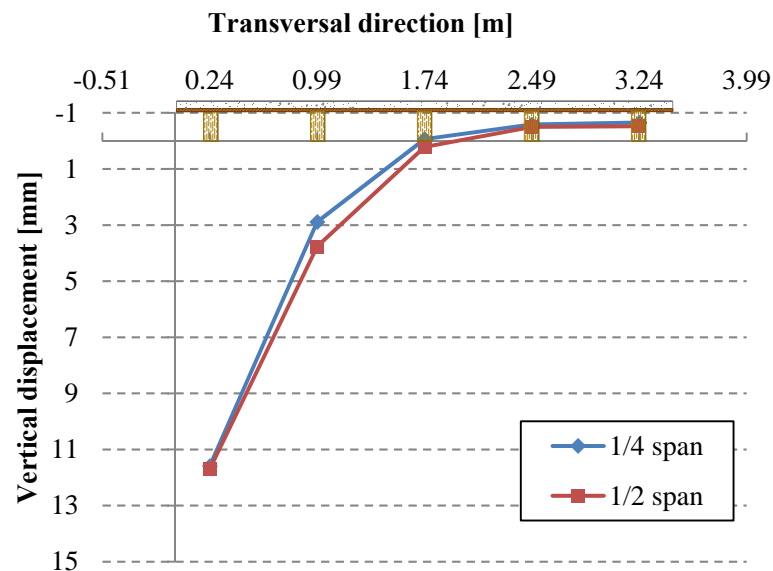


Fig. A.25 – CSGL: vertical displacement at 1/2 and 1/4 span when loaded at 1/4 span of B1 beam

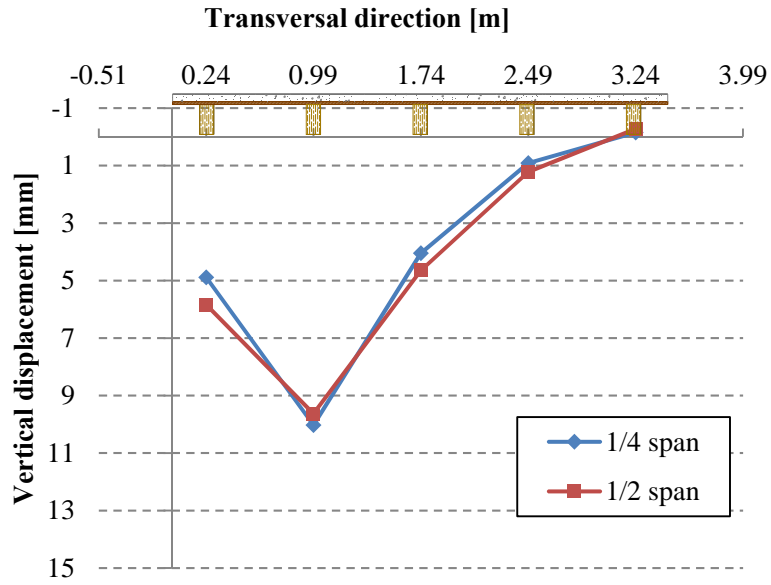


Fig. A.26 – CSDL: vertical displacement at 1/2 and 1/4 span when loaded at 1/4 span of B2 beam

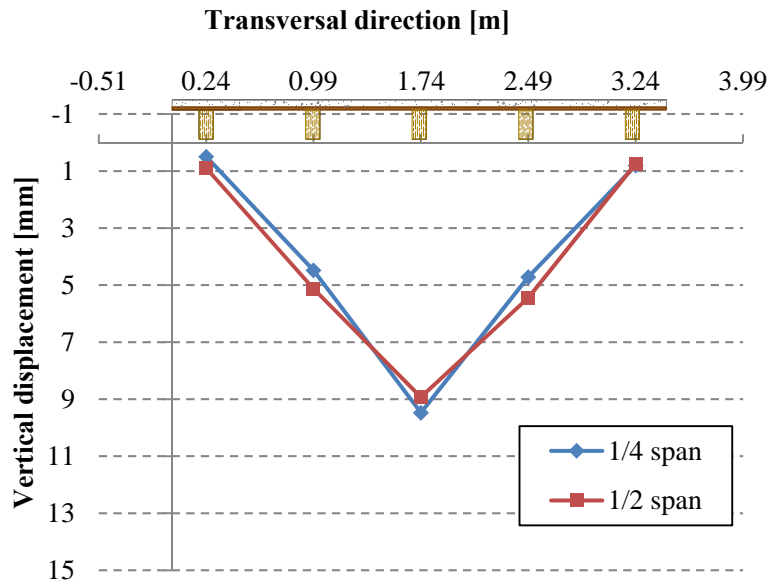


Fig. A.27 – CSDL: vertical displacement at 1/2 and 1/4 span when loaded at 1/4 span of B3 beam

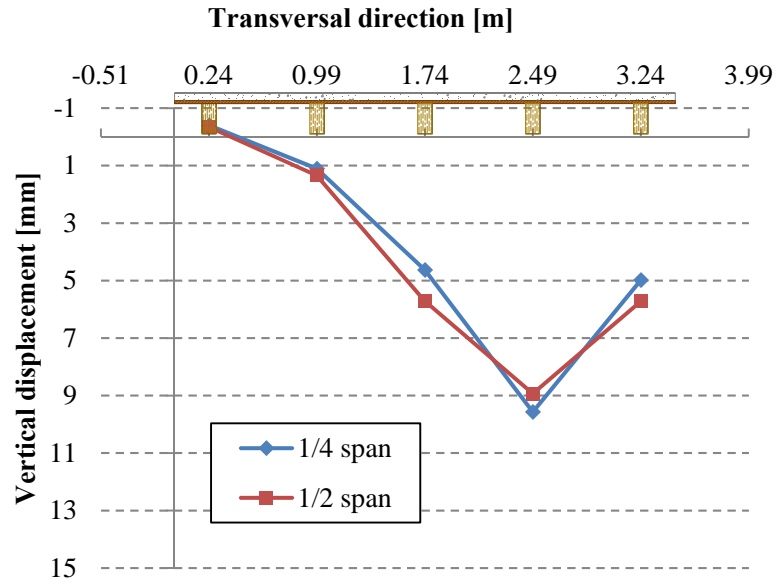


Fig. A.28 – CSDL: vertical displacement at 1/2 and 1/4 span when loaded at 1/4 span of B4 beam

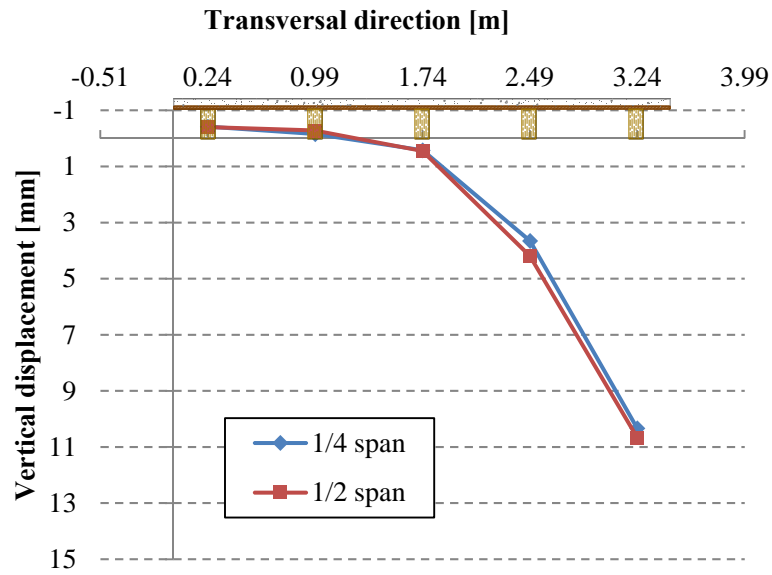


Fig. A.29 – CSDL: vertical displacement at 1/2 and 1/4 span when loaded at 1/4 span of B5 beam

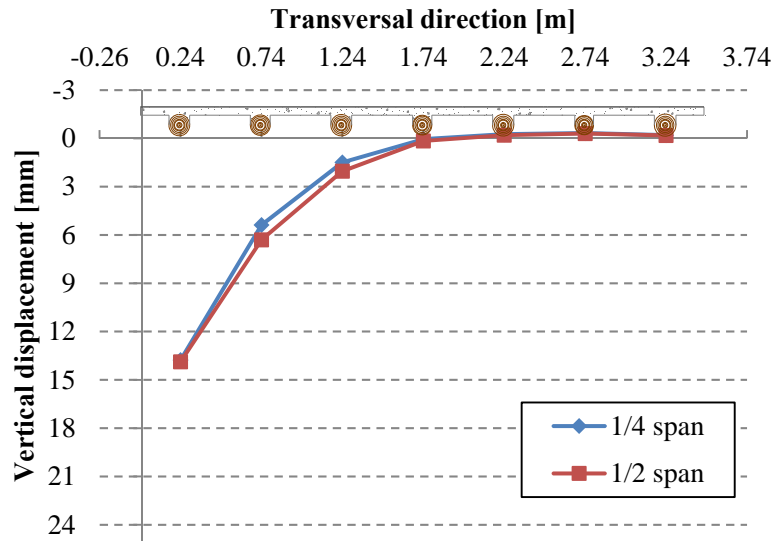


Fig. A.30 – CSTL: vertical displacement at 1/2 and 1/4 span when loaded at 1/4 span of B1 beam

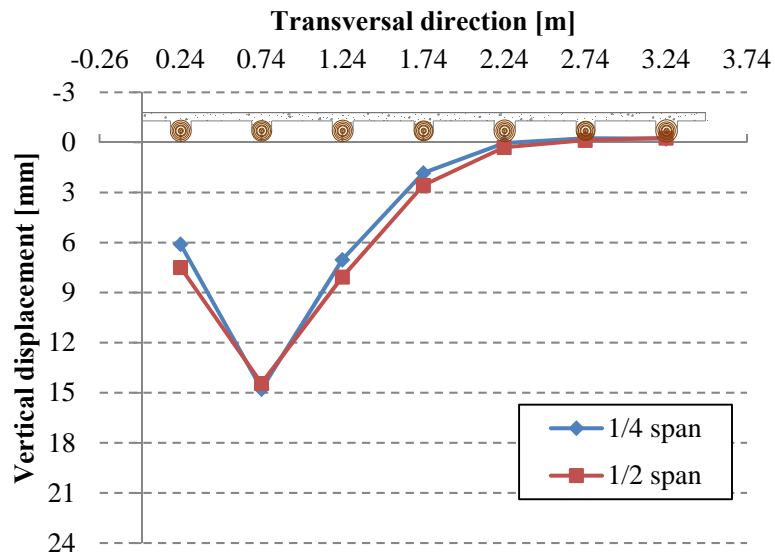


Fig. A.31 – CSTL: vertical displacement at 1/2 and 1/4 span when loaded at 1/4 span of B2 beam

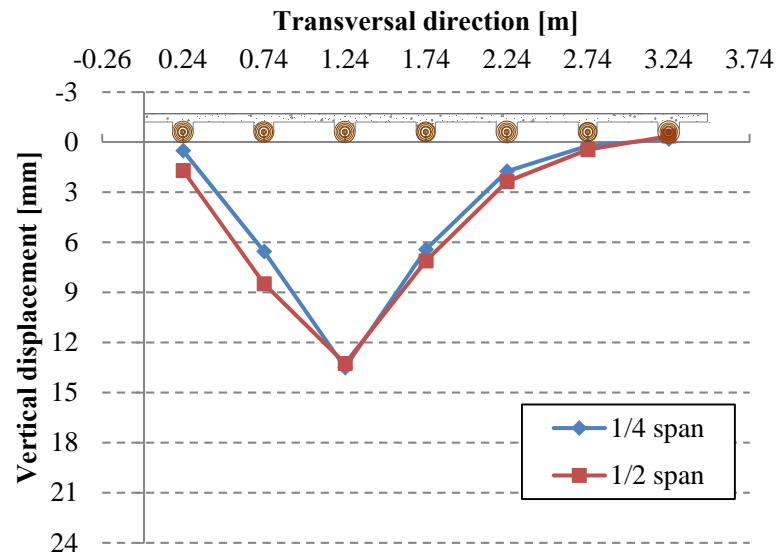


Fig. A.32 – CSTL: vertical displacement at $\frac{1}{2}$ and $\frac{1}{4}$ span when loaded at $\frac{1}{4}$ span of B3 beam

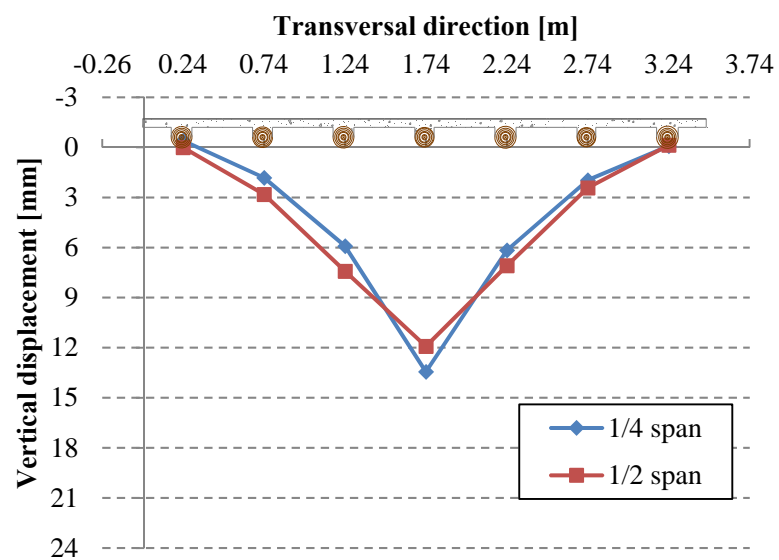


Fig. A.33 – CSTL: vertical displacement at $\frac{1}{2}$ and $\frac{1}{4}$ span when loaded at $\frac{1}{4}$ span of B4 beam

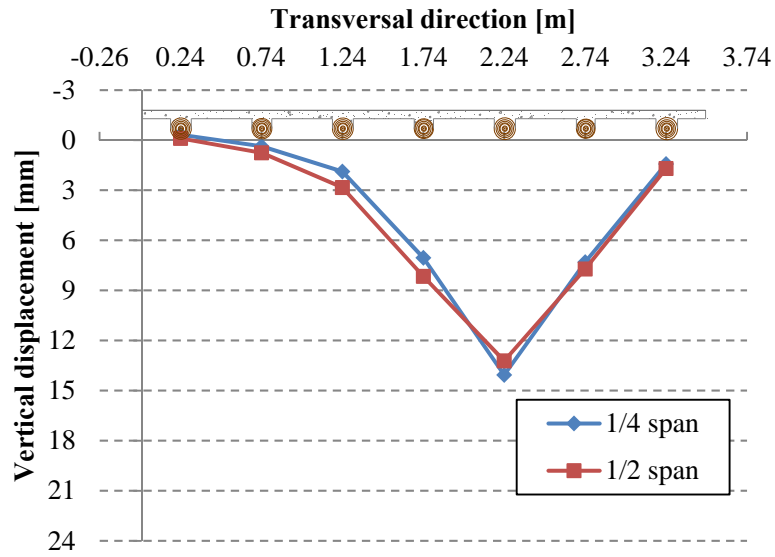


Fig. A.34 – CSTL: vertical displacement at 1/2 and 1/4 span when loaded at 1/4 span of B5 beam

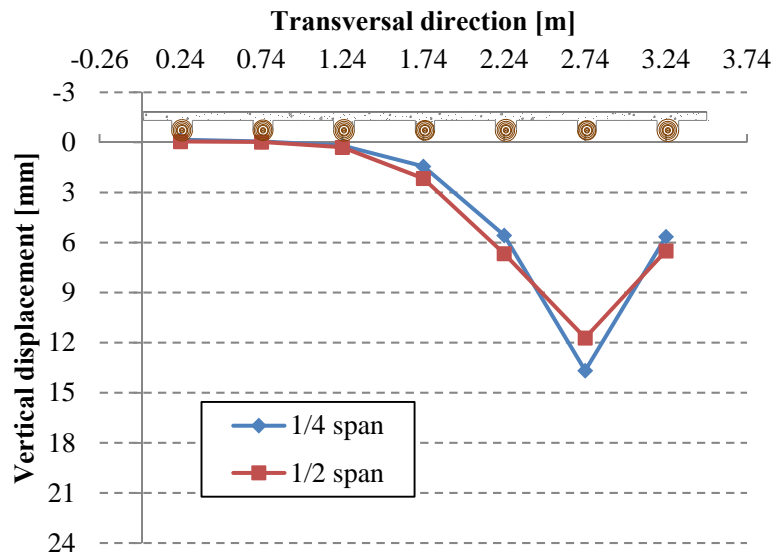


Fig. A.35 – CSTL: vertical displacement at 1/2 and 1/4 span when loaded at 1/4 span of B6 beam

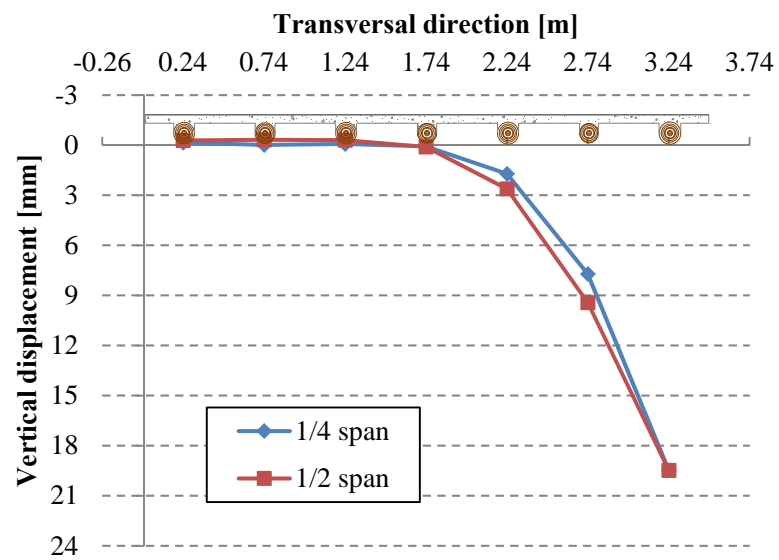


Fig. A.36 – CSTL: vertical displacement at $\frac{1}{2}$ and $\frac{1}{4}$ span when loaded at $\frac{1}{4}$ span of B7 beam

A.2 Results from the theoretical analysis

The following figures present the results in terms of vertical displacements at each beam mid-span, support reactions and longitudinal bending moment at the mid-span section for the theoretical analysis presented in 3.5 *Numerical model validation*, more specifically in the section 3.5.2 *Modeling analysis*.

The symbology is the same defined in the chapter, as well as the designation for each modeling.

A.2.1 Vertical displacements at each beam mid-span

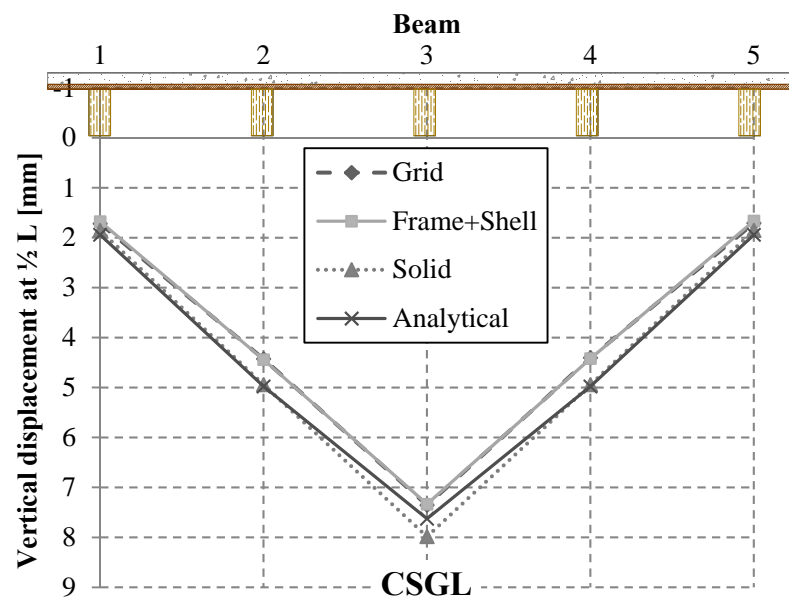


Fig. A.37 – CSGL: vertical displacement at each beam mid-span

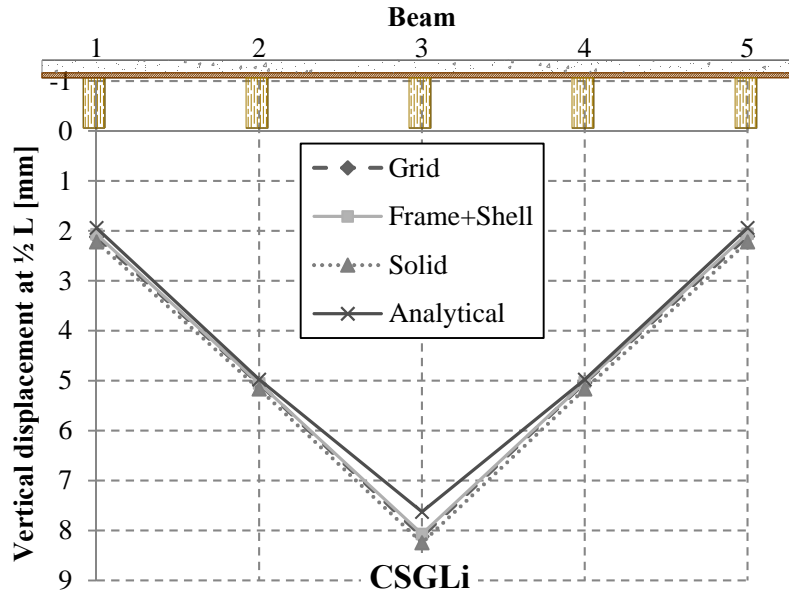


Fig. A.38 – CSGLi: vertical displacement at each beam mid-span

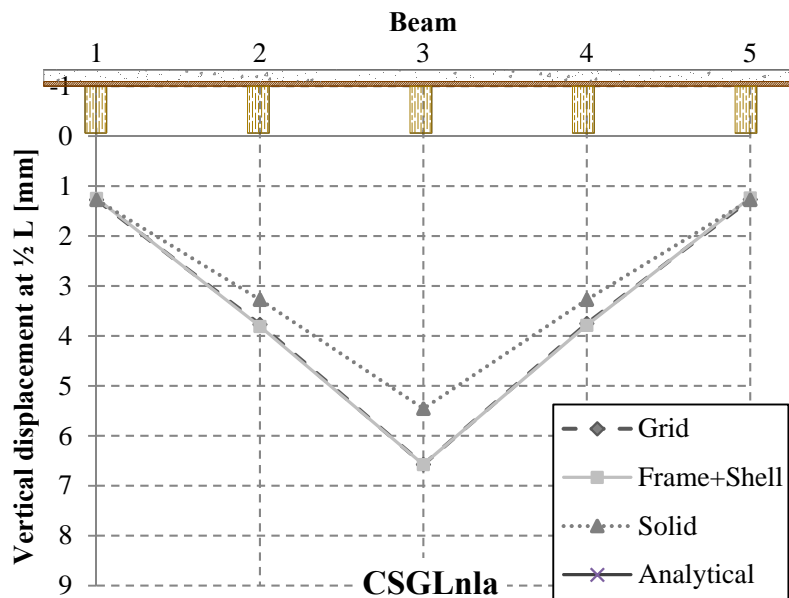


Fig. A.39 – CSGLnla: vertical displacement at each beam mid-span

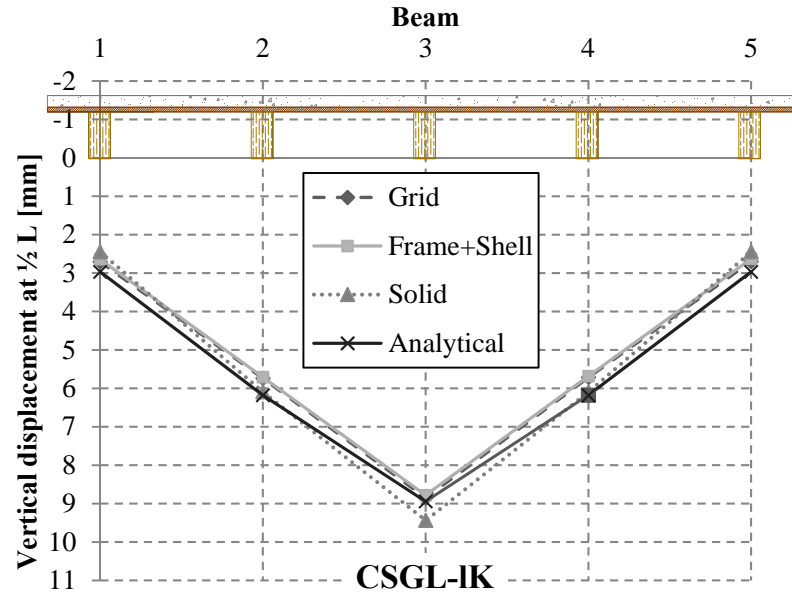


Fig. A.40 – CSGL-1K: vertical displacement at each beam mid-span

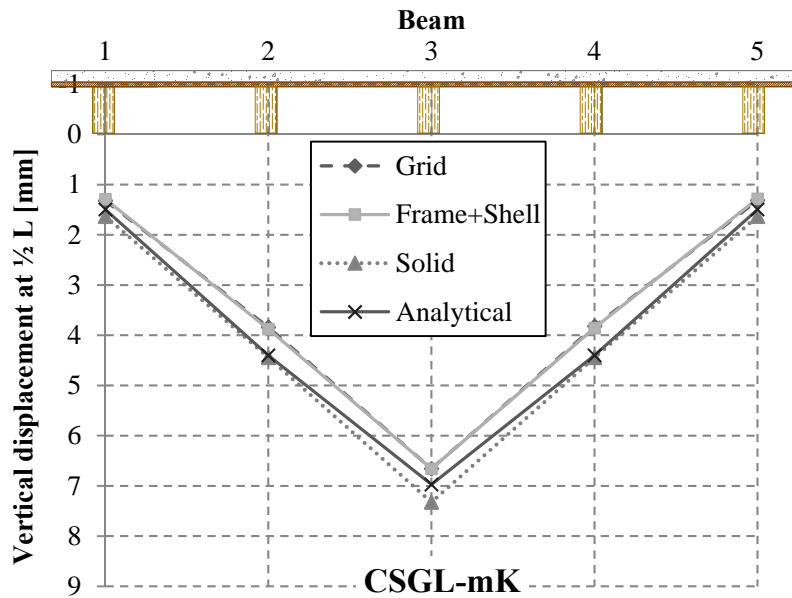


Fig. A.41 – CSGL-mK: vertical displacement at each beam mid-span

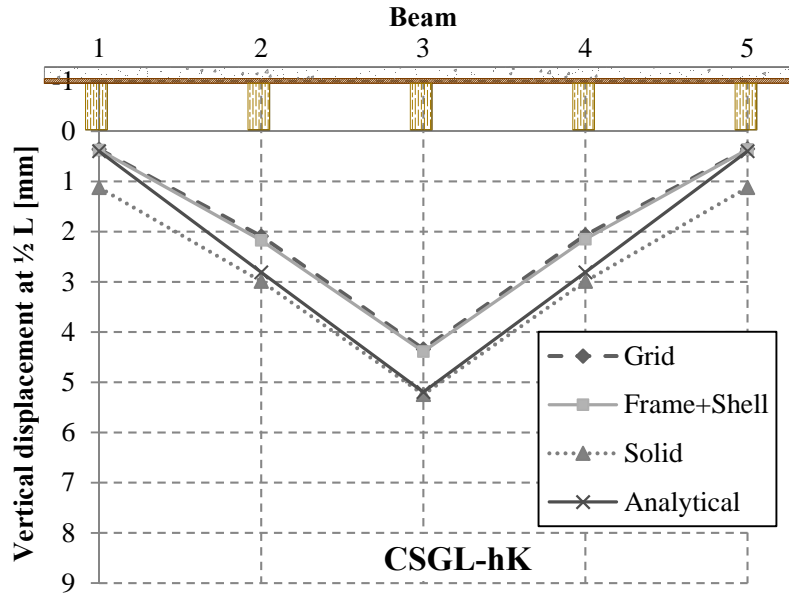


Fig. A.42 – CSGL-hK: vertical displacement at mid-span

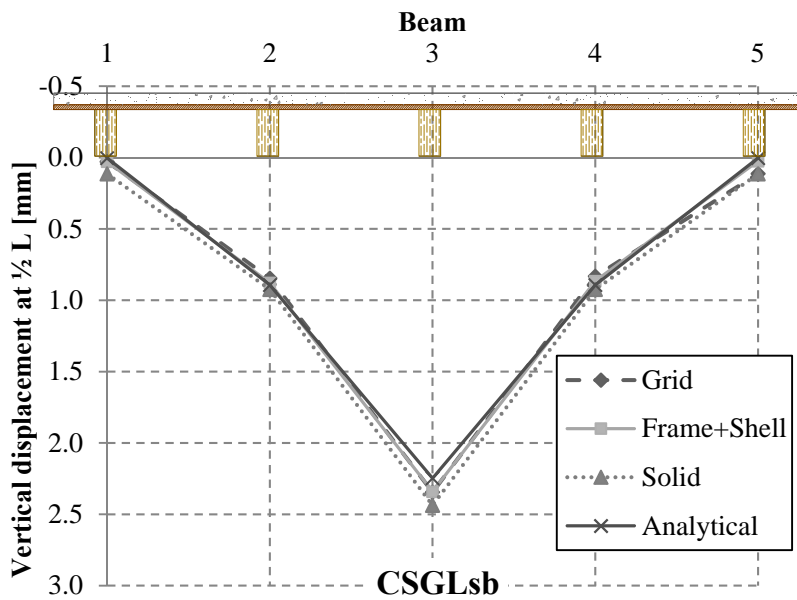


Fig. A.43 – CSGLsb: vertical displacement at each beam mid-span

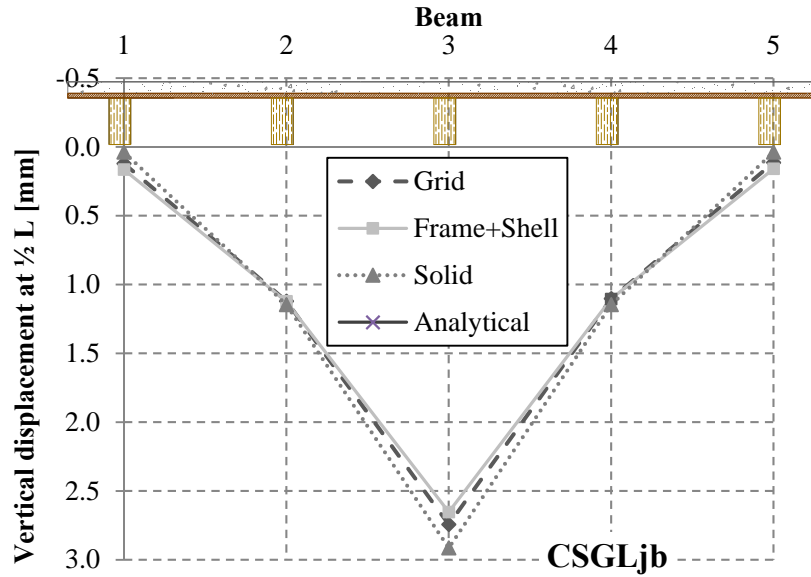


Fig. A.44 – CSDLjb: vertical displacement at each beam mid-span

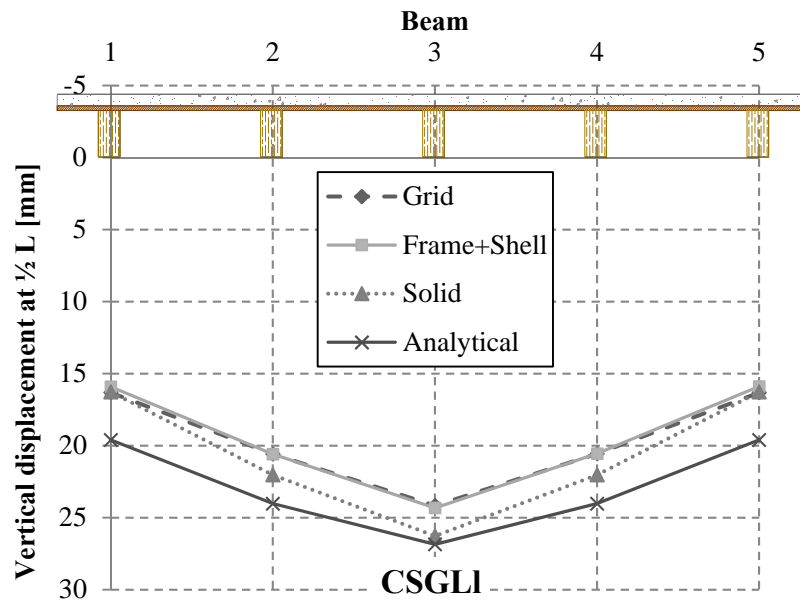


Fig. A.45 – CSDLl: vertical displacement at each beam mid-span

A.2.2 Vertical displacements at each beam quarter-span

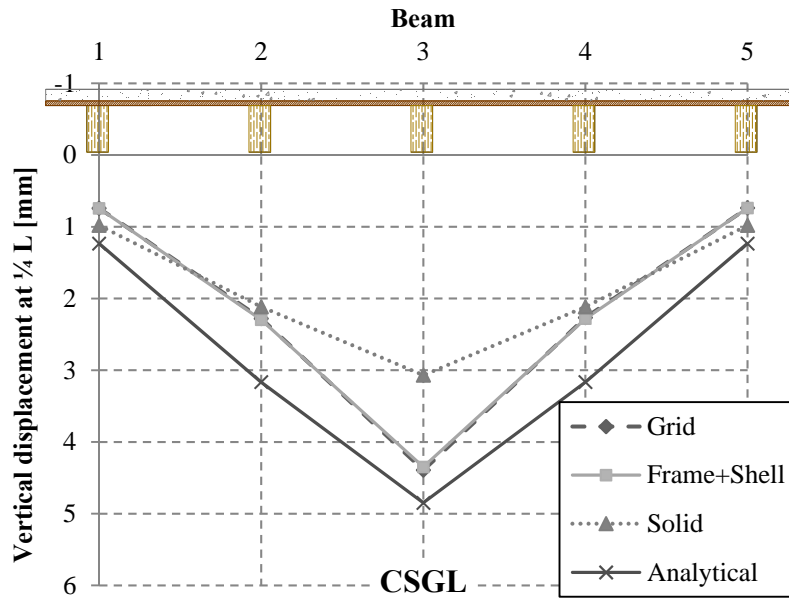


Fig. A.46 – CSGL: vertical displacement at each beam quarter-span

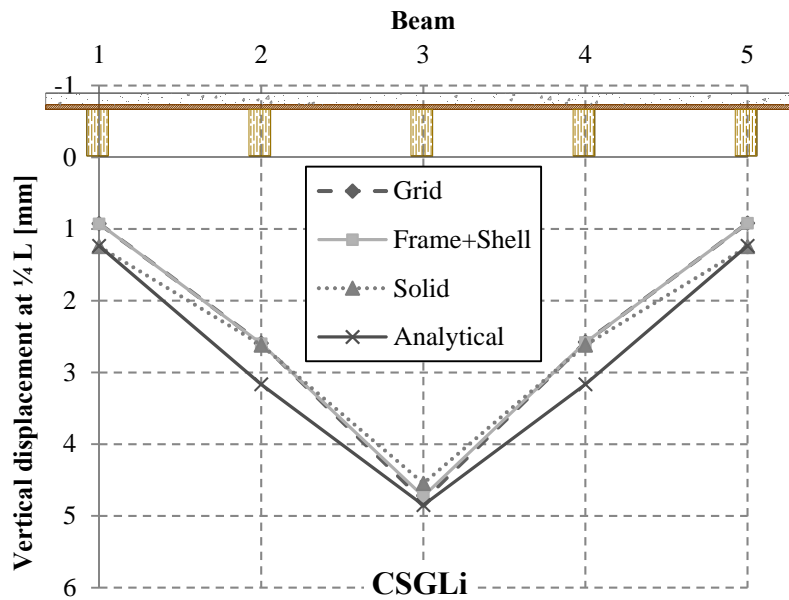


Fig. A.47 – CSGLi: vertical displacement at each beam quarter-span

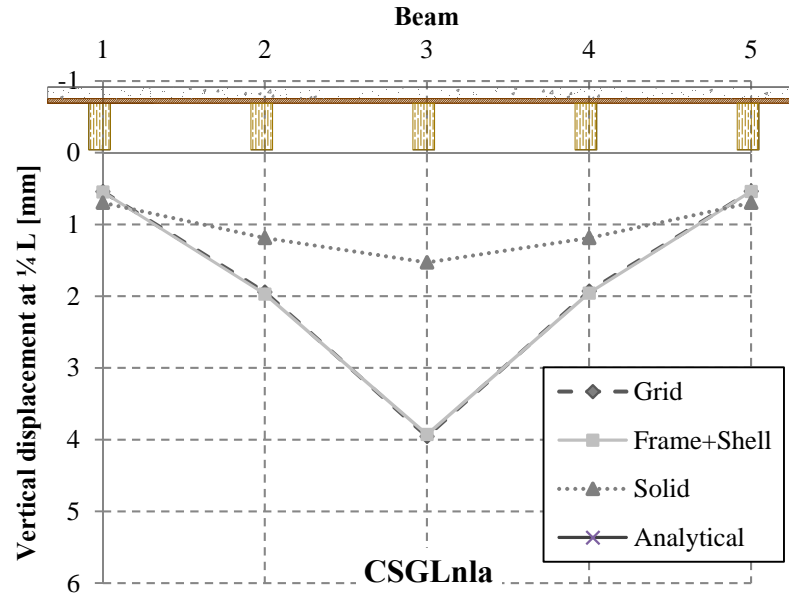


Fig. A.48 – CSGLn1a: vertical displacement at each beam quarter-span

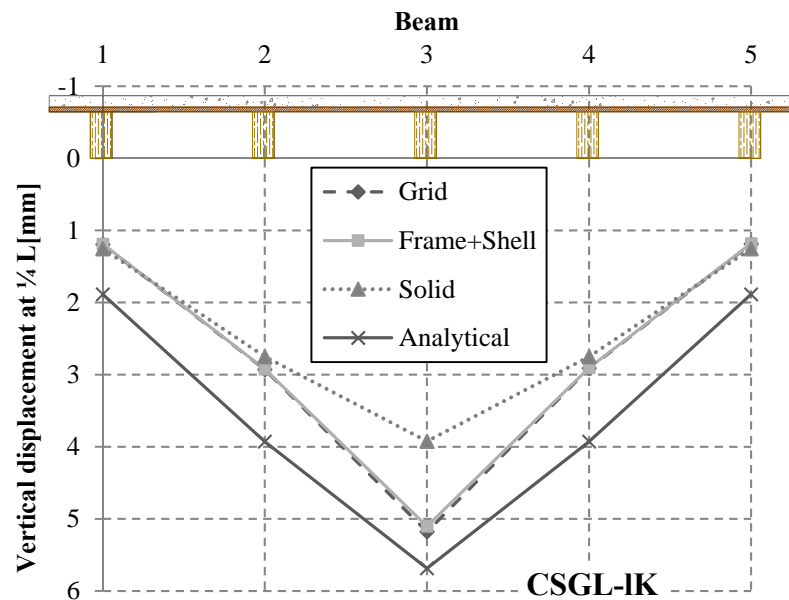


Fig. A.49 – CSGL-1K: vertical displacement at each beam quarter-span

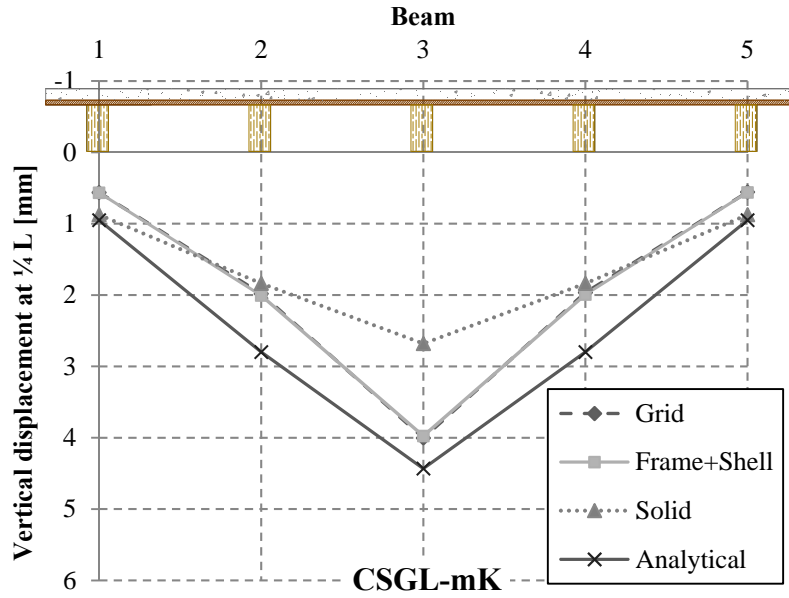


Fig. A.50 – CSGL-mK: vertical displacement at each beam quarter-span

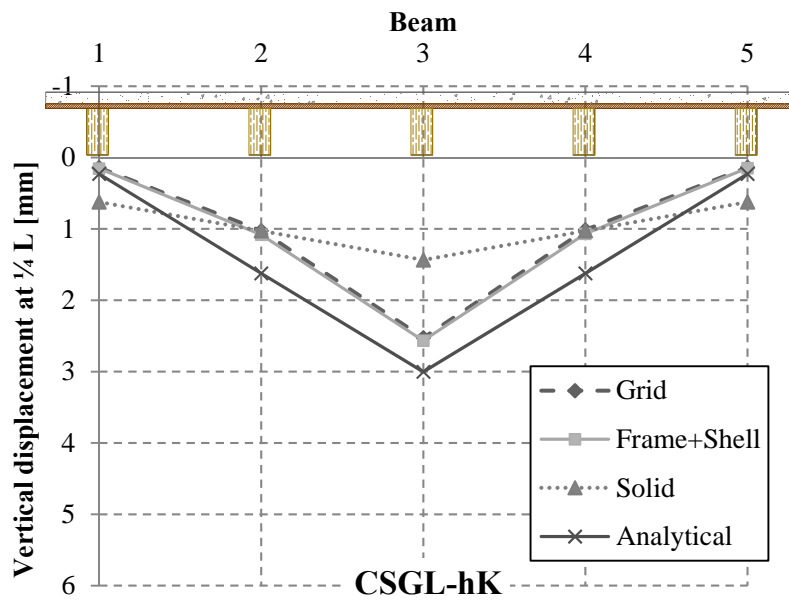


Fig. A.51 – CSGL-hK: vertical displacement at quarter-span

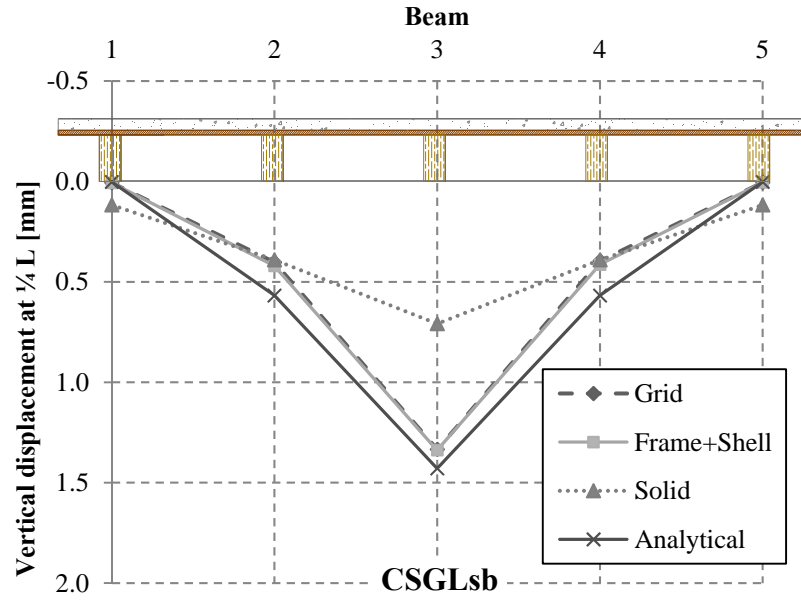


Fig. A.52 – CSGLsb: vertical displacement at each beam quarter-span

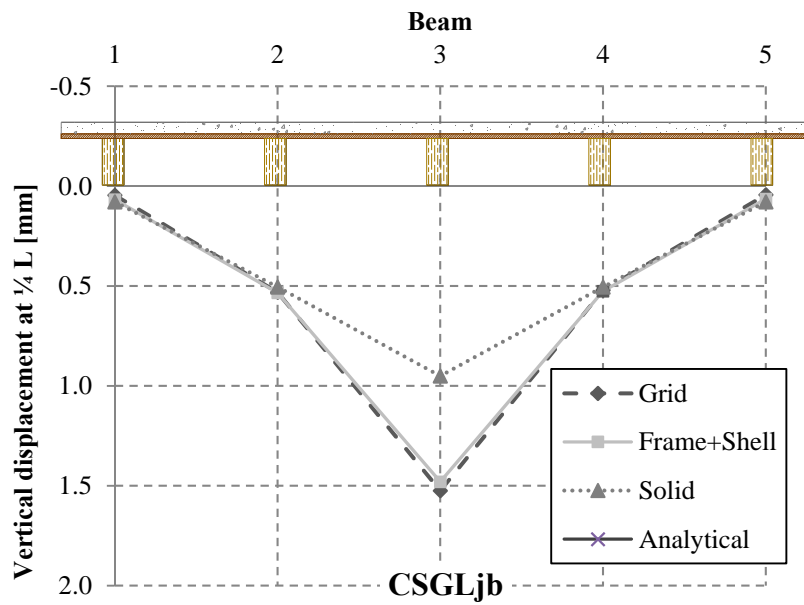


Fig. A.53 – CSGLjb: vertical displacement at each beam quarter-span

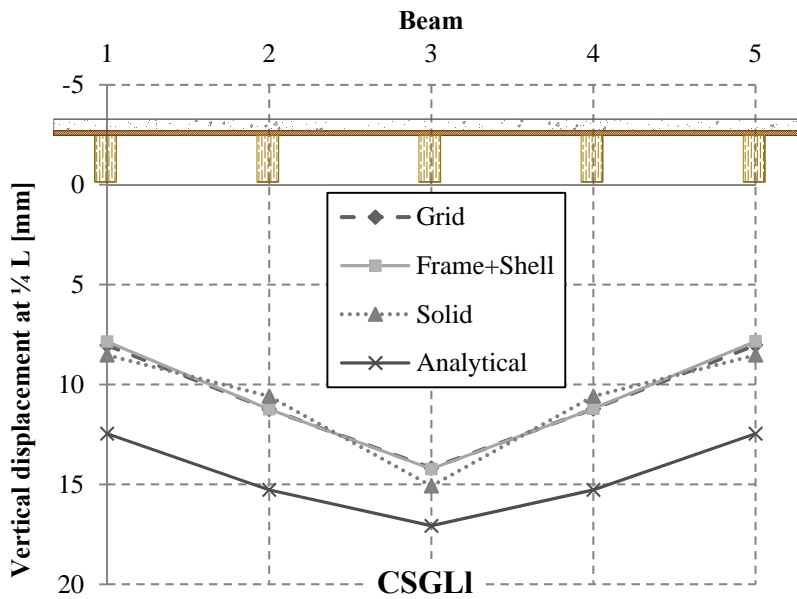


Fig. A.54 – CSGL: vertical displacement at each beam quarter-span

A.2.3 Support reactions for loading at mid-span

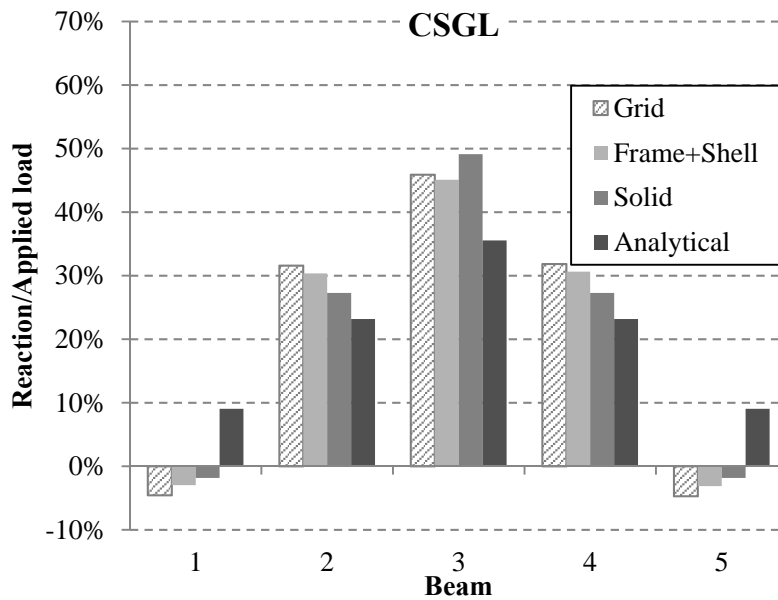


Fig. A.55 – CSGL: support reactions for a centered load

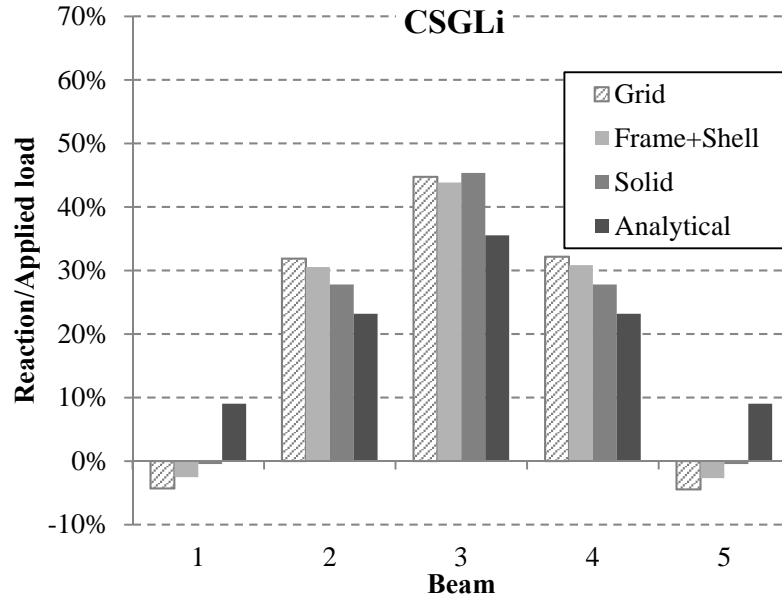


Fig. A.56 – CSGLi: support reactions for a centered load

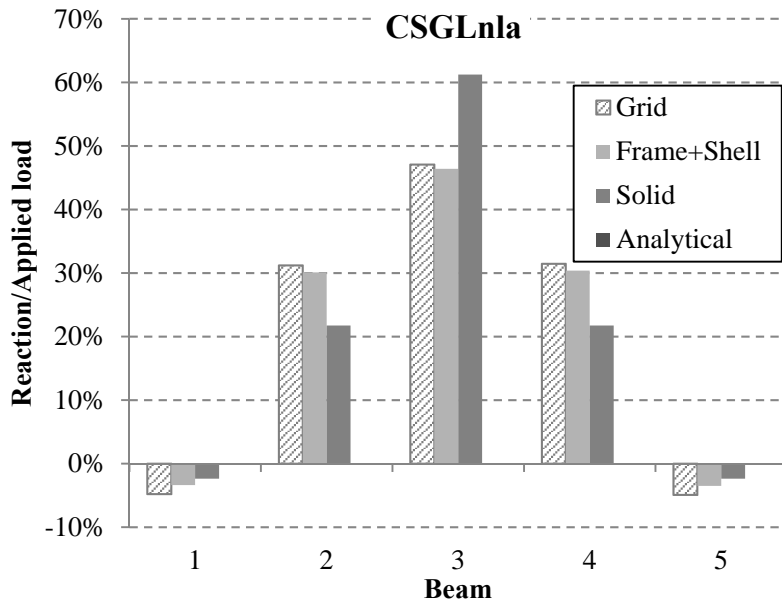


Fig. A.57 – CSGLnla: support reactions for a centered load

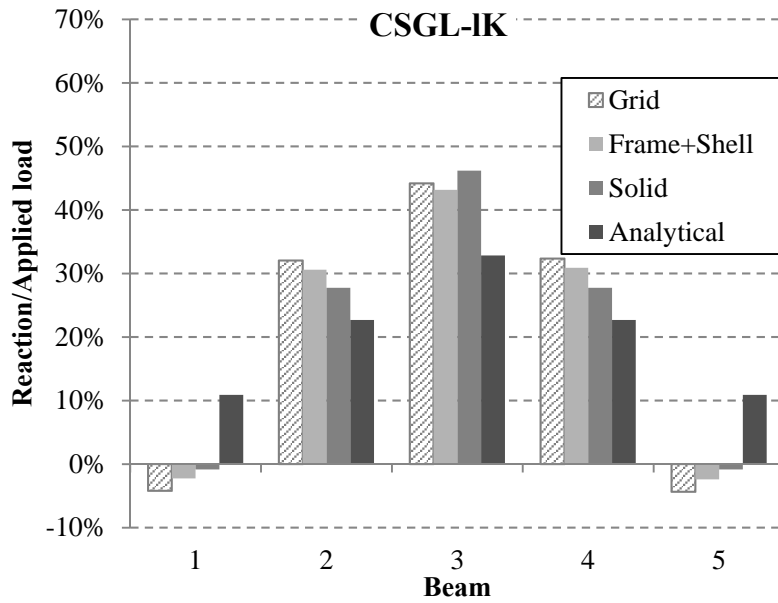


Fig. A.58 – CSGL-1K: support reactions for a centered load

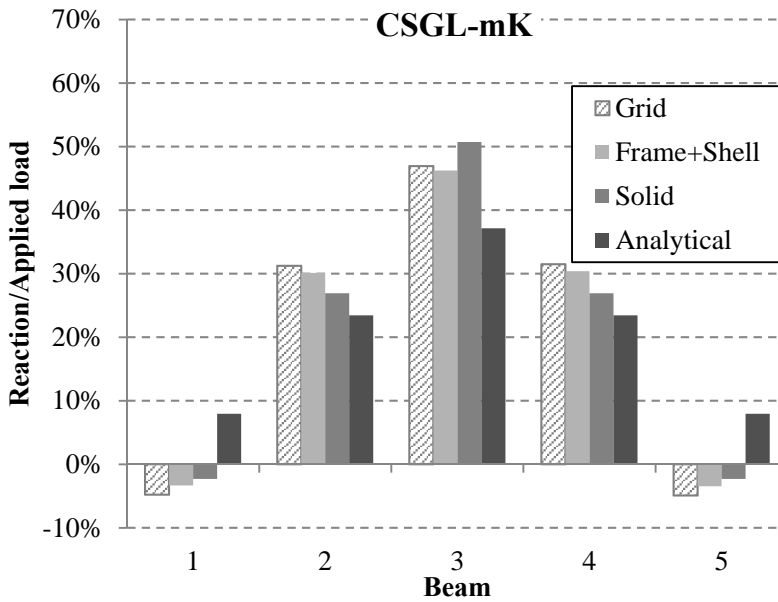


Fig. A.59 – CSGL-mK: support reactions for a centered load

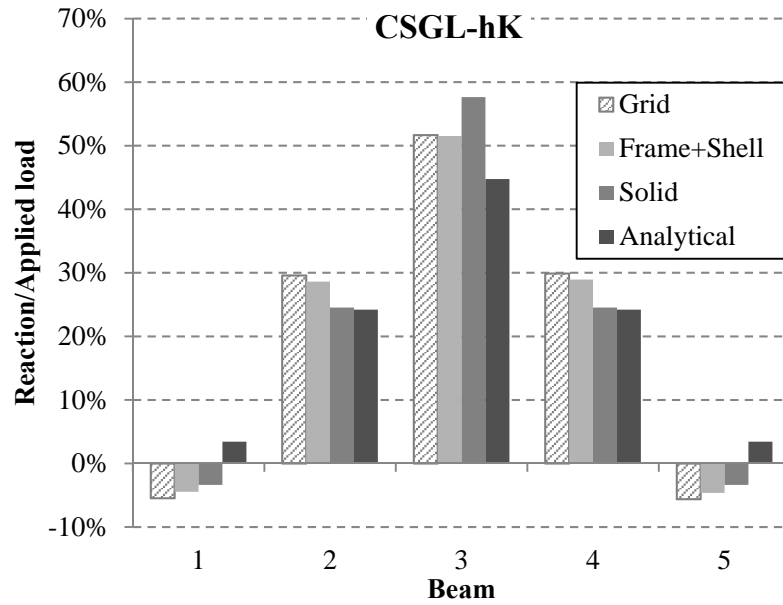


Fig. A.60 – CSGL-hK: support reactions for a centered load

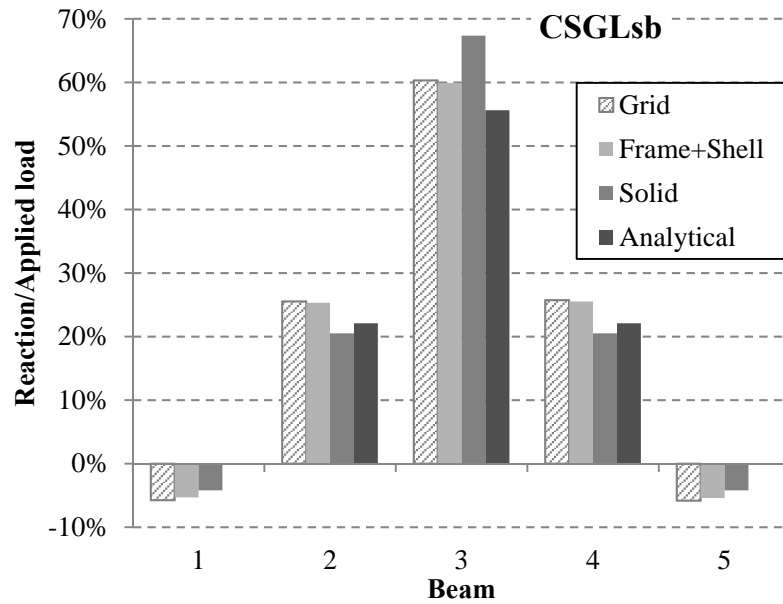


Fig. A.61 – CSGLsb: support reactions for a centered load

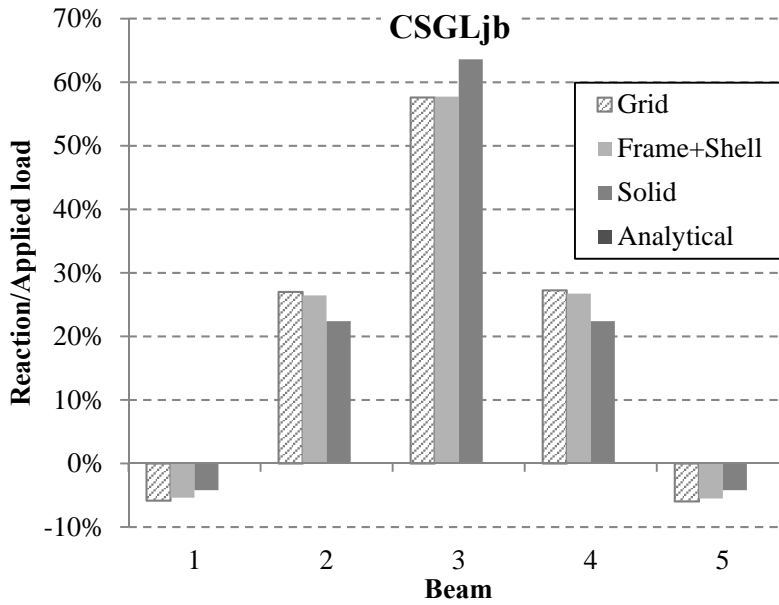


Fig. A.62 – CSGLjb: support reactions for a centered load

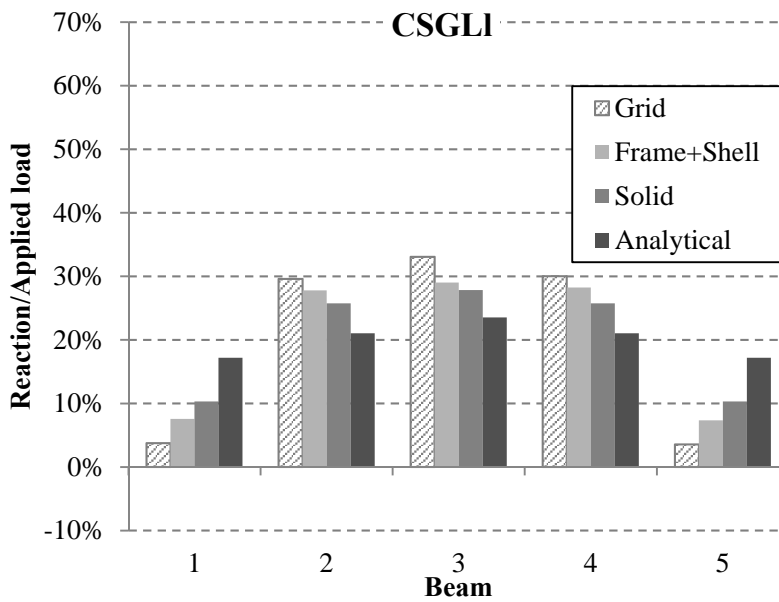


Fig. A.63 – CSGLI: support reactions for a centered load

A.2.4 Support reactions for loading at quarter-span

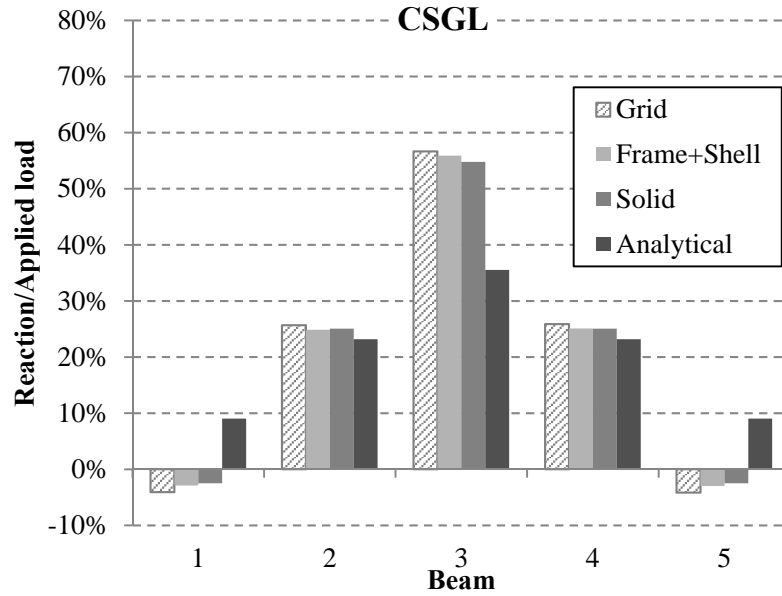


Fig. A.64 – CSGL: support reactions for a decentered load

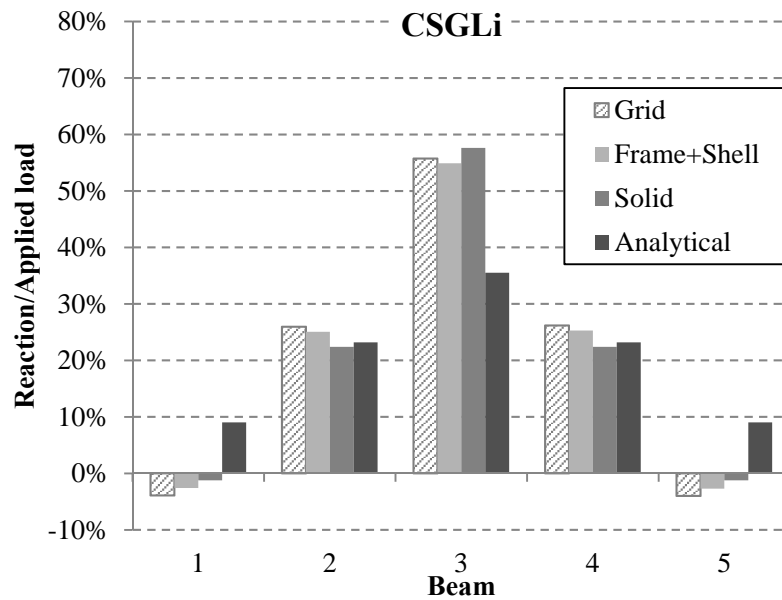


Fig. A.65 – CSGLi: support reactions for a decentered load

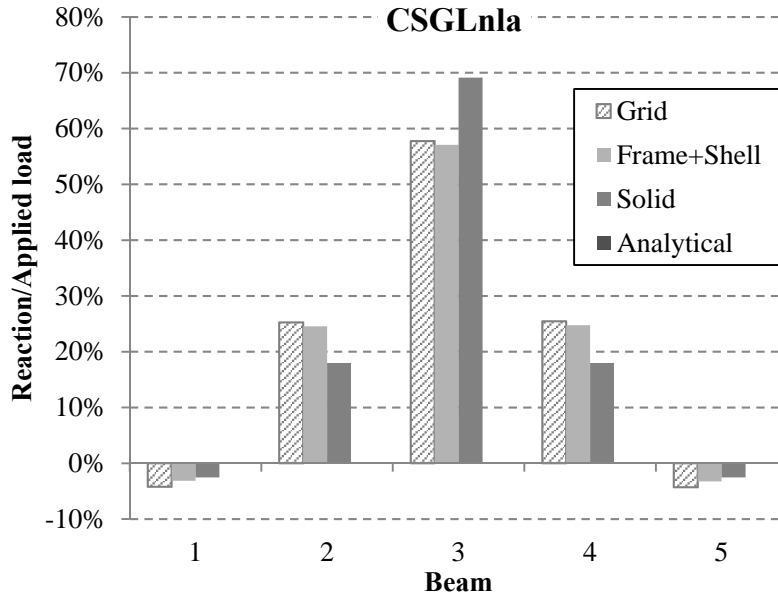


Fig. A.66 – CSGLnla: support reactions for a decentered load

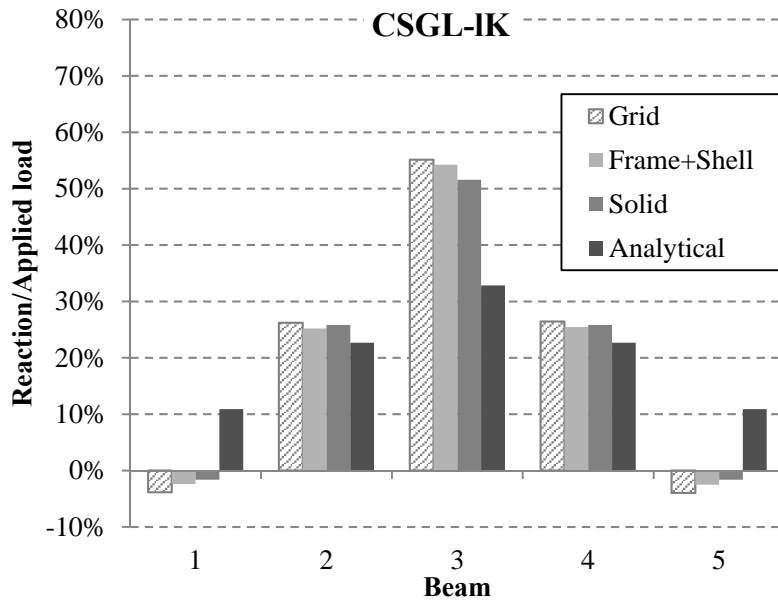


Fig. A.67 – CSGL-1K: support reactions for a decentered load

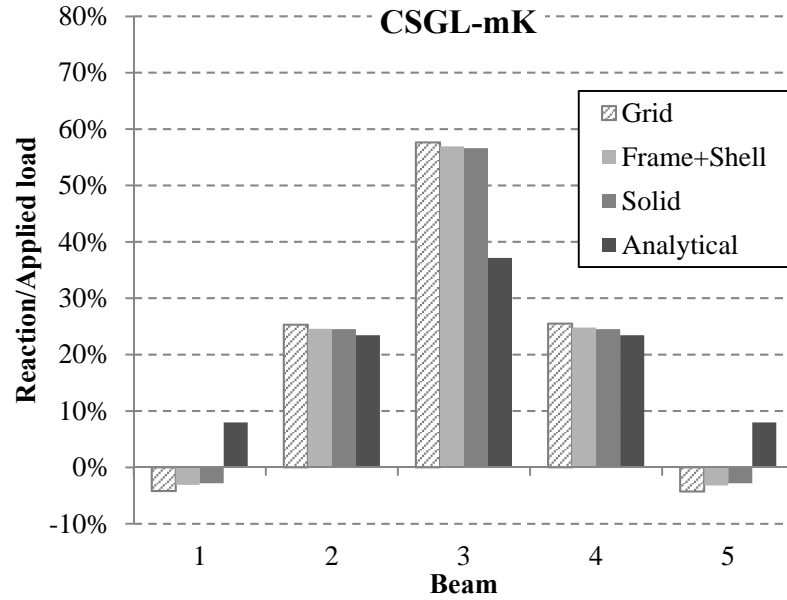


Fig. A.68 – CSGL-mK: support reactions for a decentered load

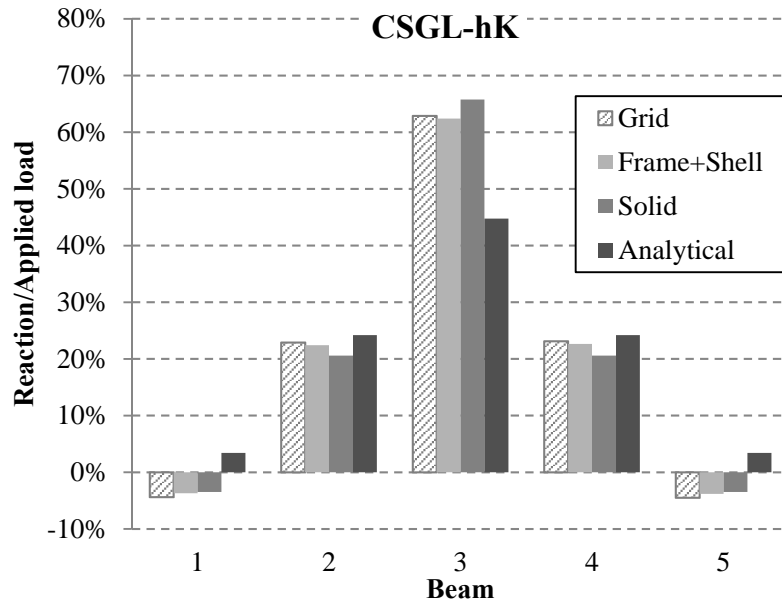


Fig. A.69 – CSGL-hK: support reactions for a decentered load

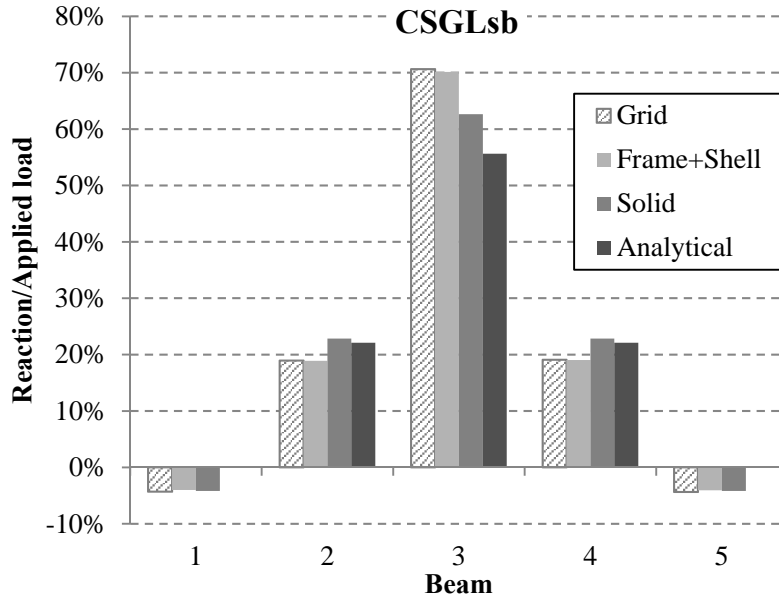


Fig. A.70 – CSGLsb: support reactions for a decentered load

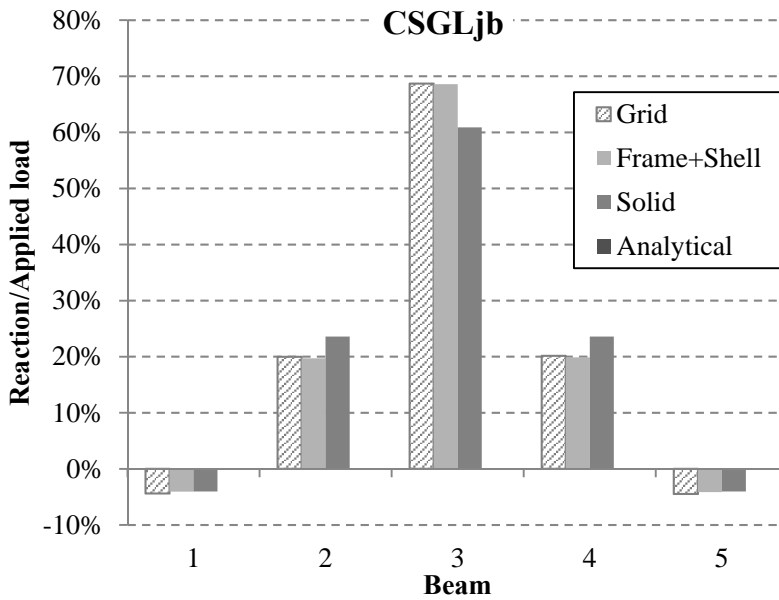


Fig. A.71 – CSGLjb: support reactions for a decentered load

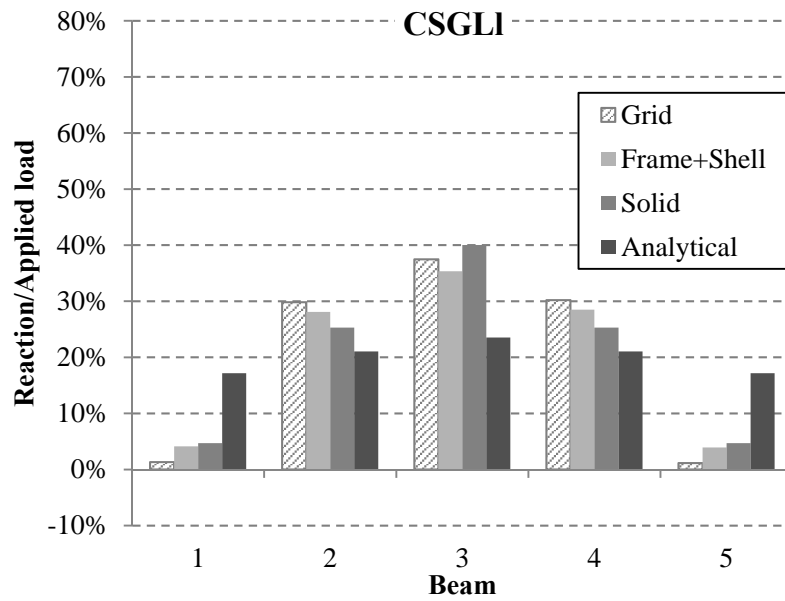


Fig. A.72 – CSGLI: support reactions for a decentered load

A.2.5 Longitudinal bending moment at the mid-span section

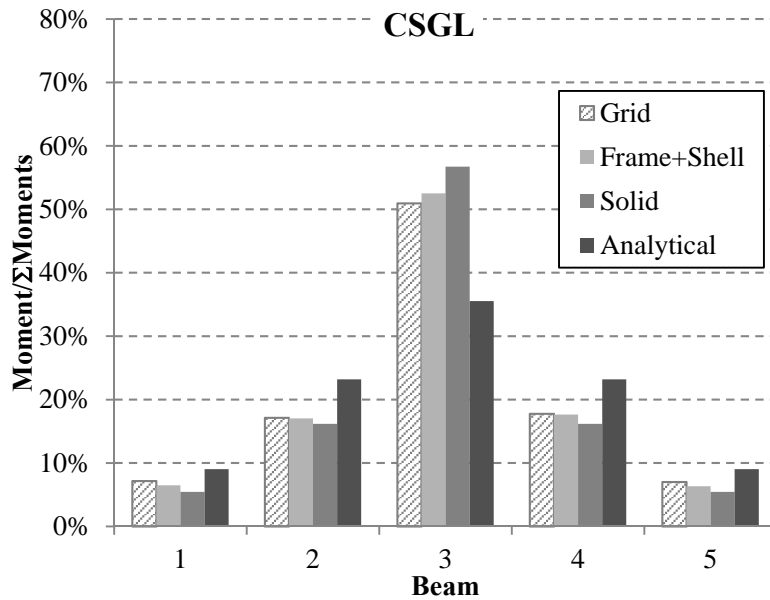


Fig. A.73 – CSGL: longitudinal bending moment at the mid-span section

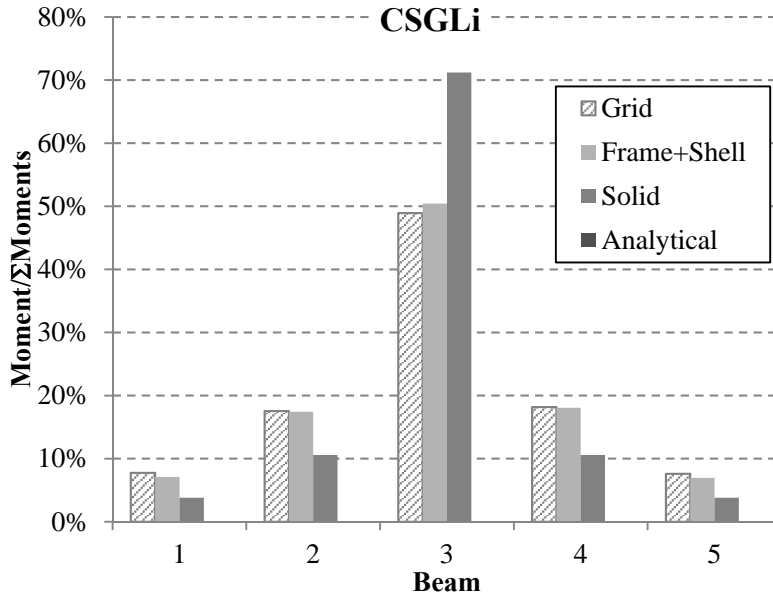


Fig. A.74 – CSGLi: longitudinal bending moment at the mid-span section

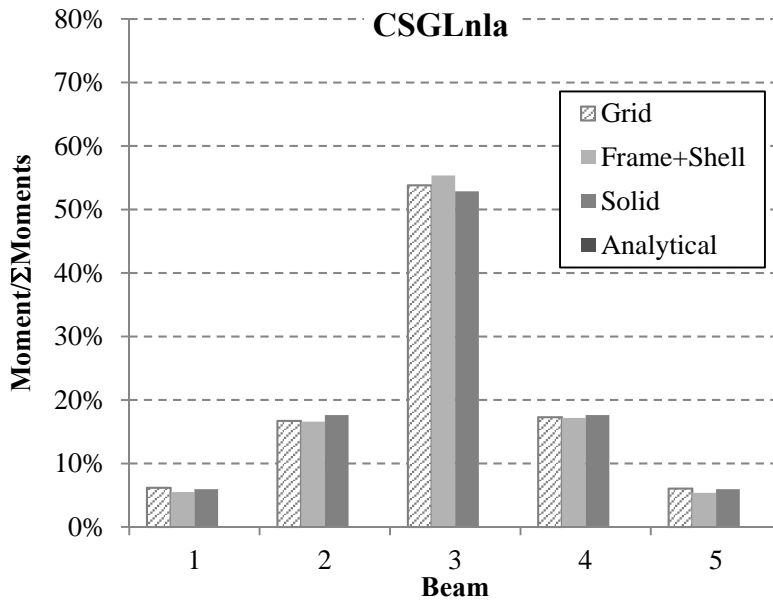


Fig. A.75 – CSGLnla: longitudinal bending moment at the mid-span section

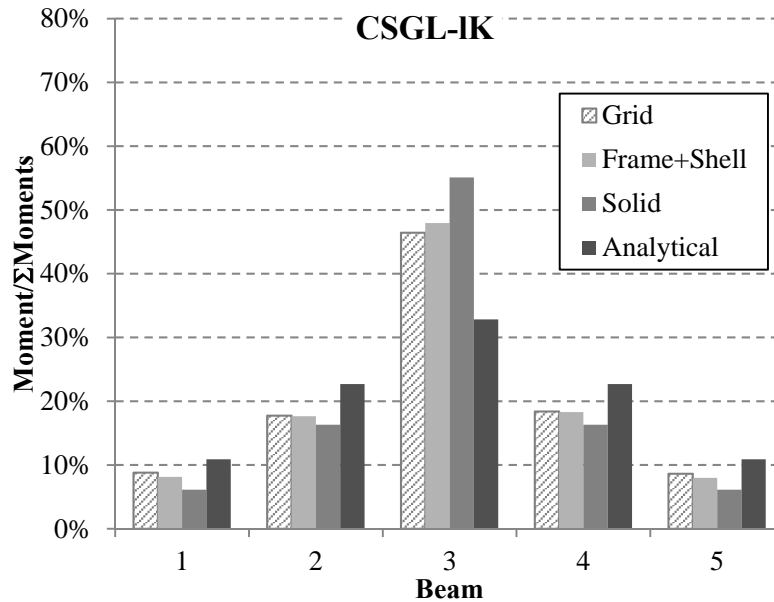


Fig. A.76 – CSGL-1K: longitudinal bending moment at the mid-span section

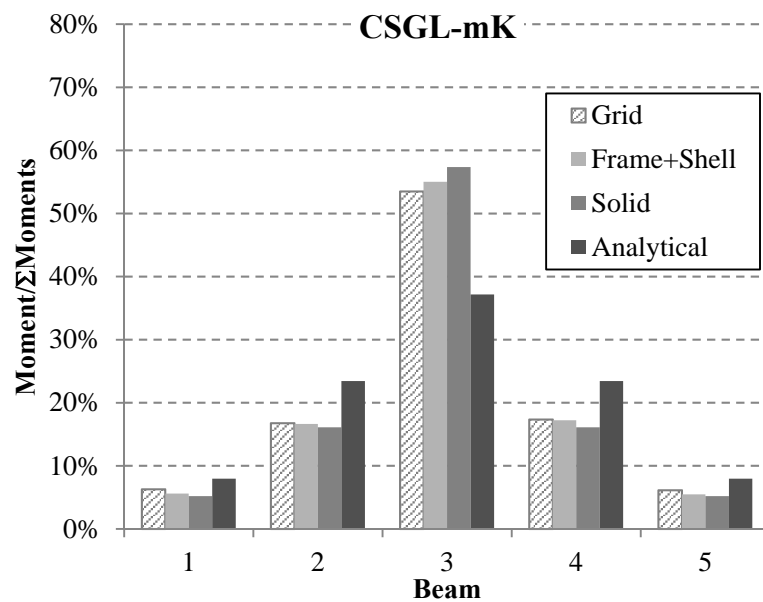


Fig. A.77 – CSGL-mK: longitudinal bending moment at the mid-span section

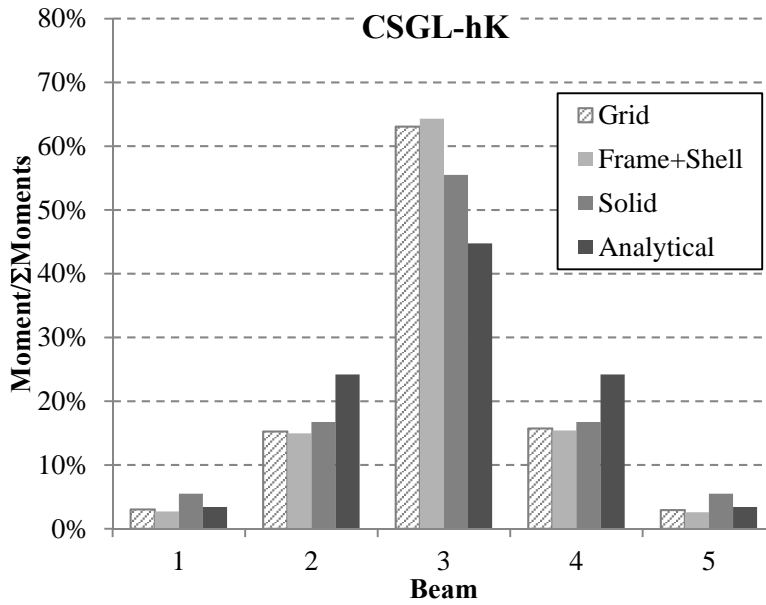


Fig. A.78 – CSGL-hK: longitudinal bending moment at the mid-span section

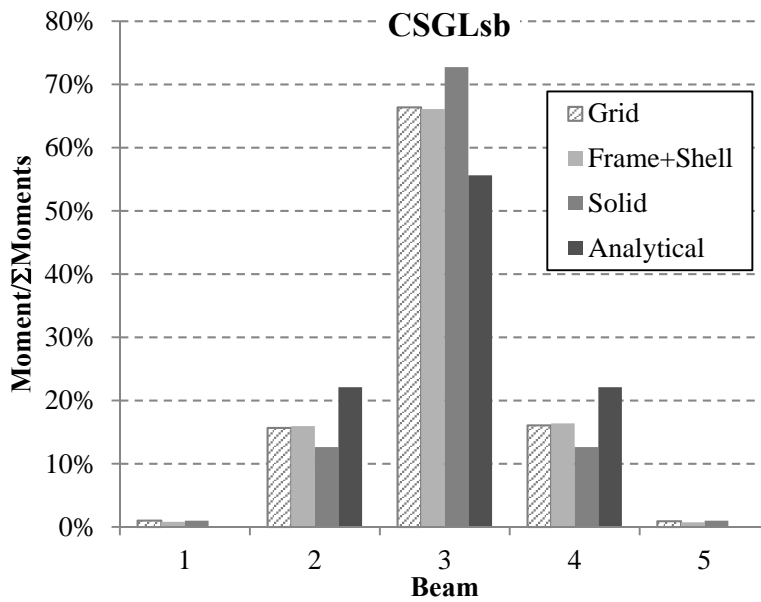


Fig. A.79 – CSGLsb: longitudinal bending moment at the mid-span section

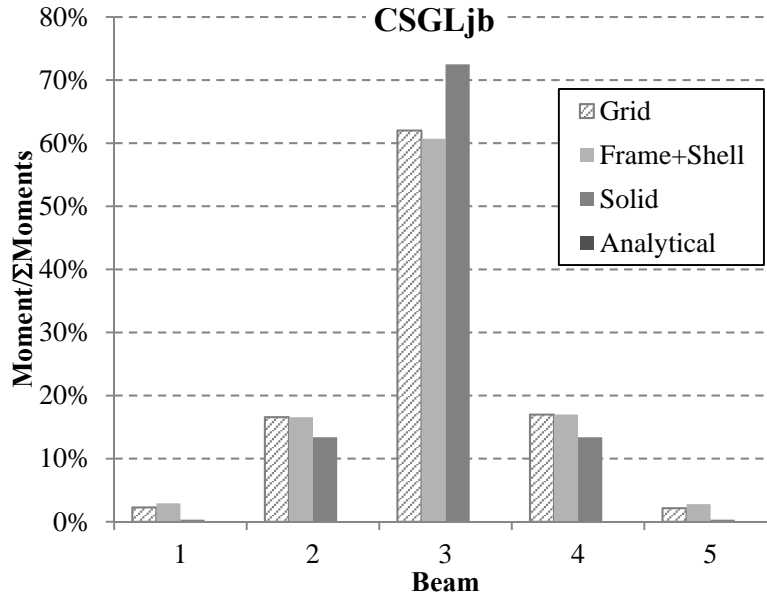


Fig. A.80 – CSGLjb: longitudinal bending moment at the mid-span section

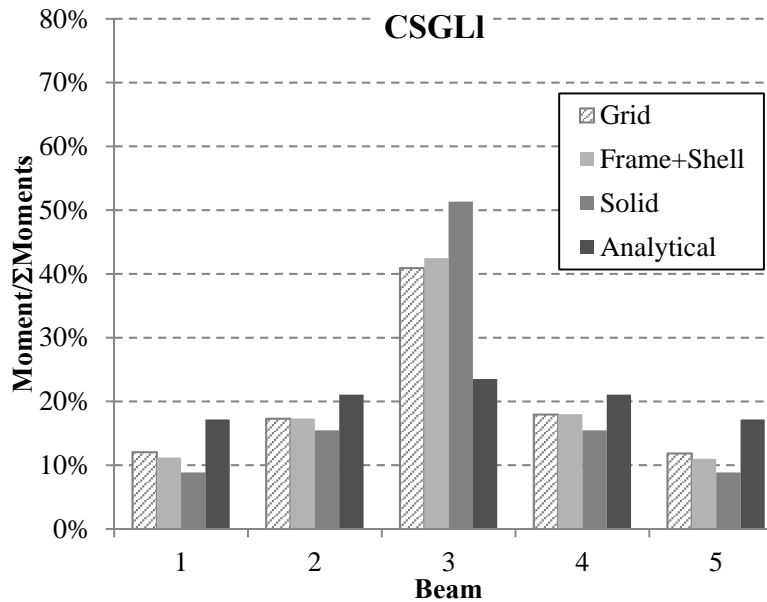


Fig. A.81 – CSGLI: longitudinal bending moment at the mid-span section

A.2.6 Longitudinal bending moment at the quarter-span section

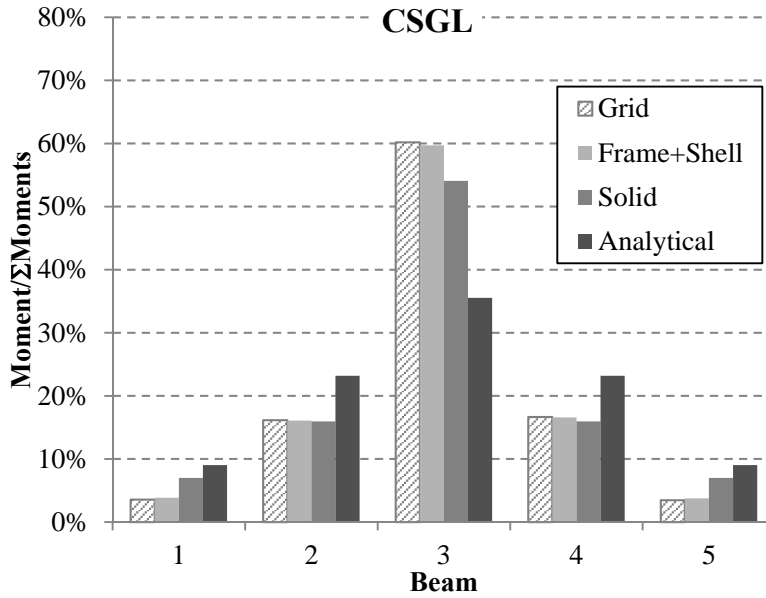


Fig. A.82 – CSGL: longitudinal bending moment at the quarter-span section

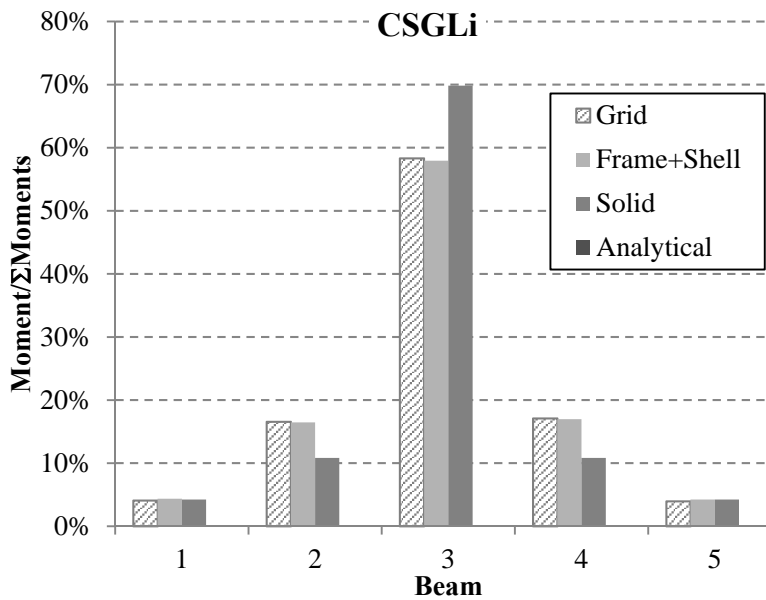


Fig. A.83 – CSGLi: longitudinal bending moment at the quarter-span section

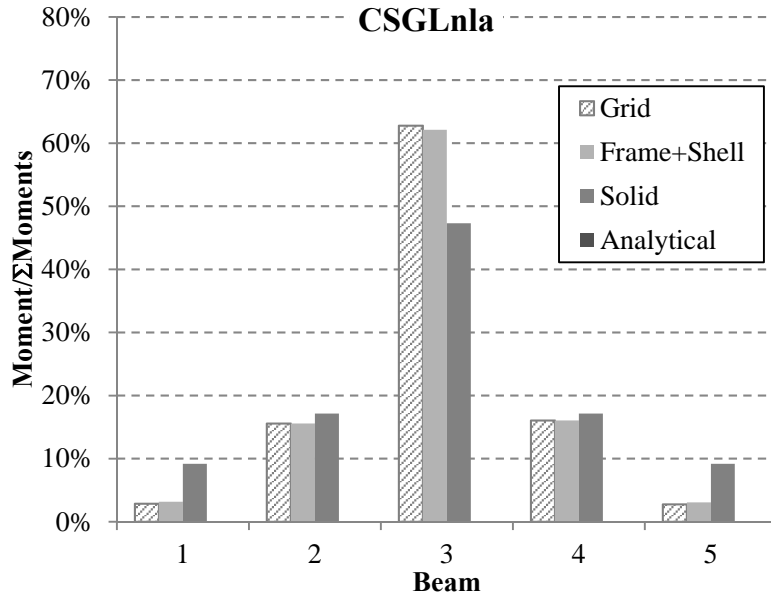


Fig. A.84 – CSGLn1a: longitudinal bending moment at the quarter-span section

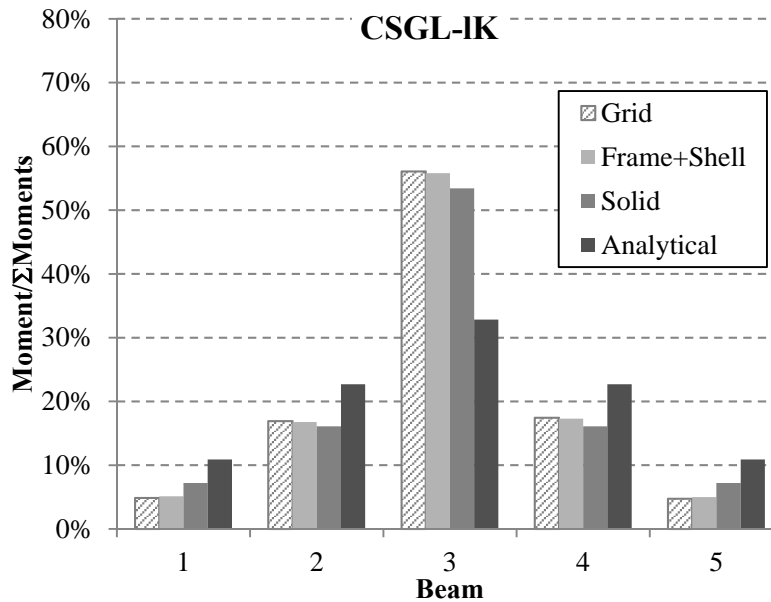


Fig. A.85 – CSGL-1K: longitudinal bending moment at the quarter-span section

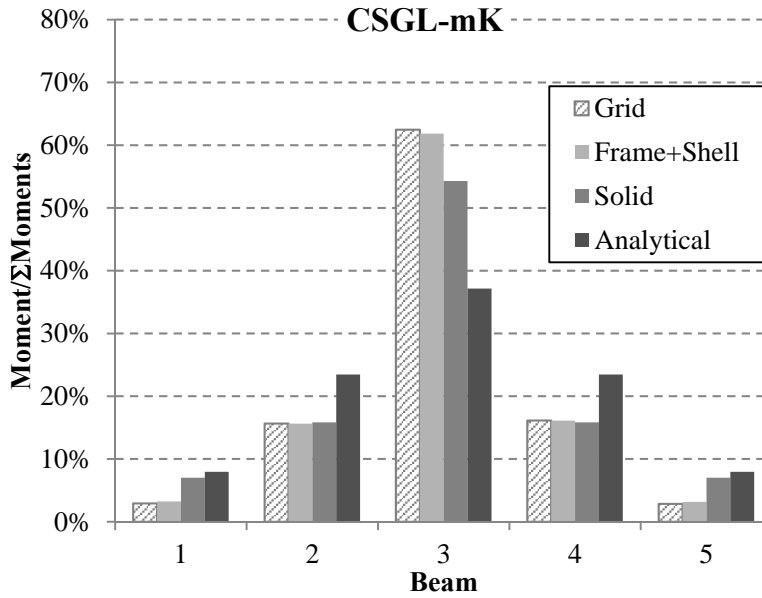


Fig. A.86 – CSGL-mK: longitudinal bending moment at the quarter-span section

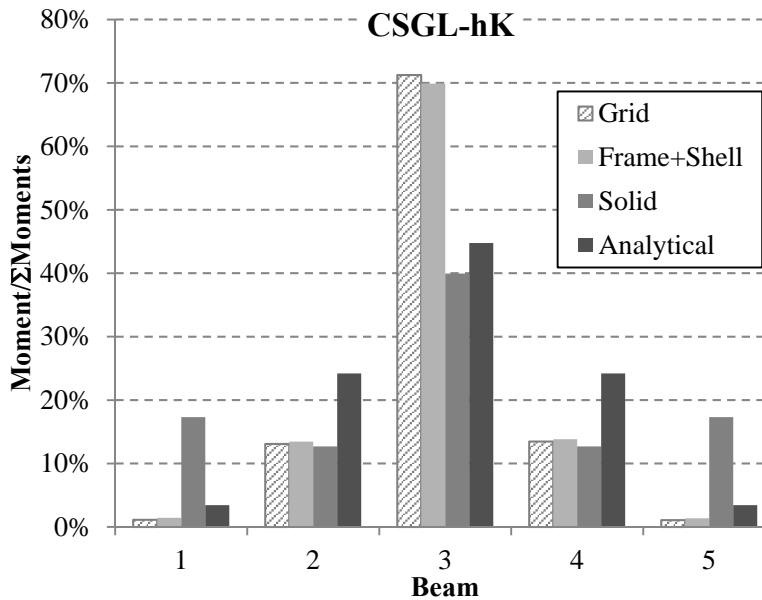


Fig. A.87 – CSGL-hK: longitudinal bending moment at the quarter-span section

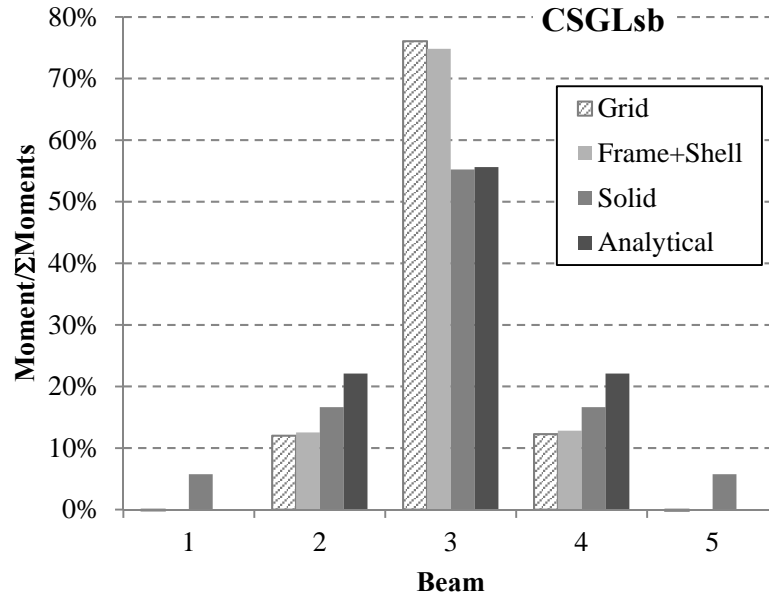


Fig. A.88 – CSGLsb: longitudinal bending moment at the quarter-span section

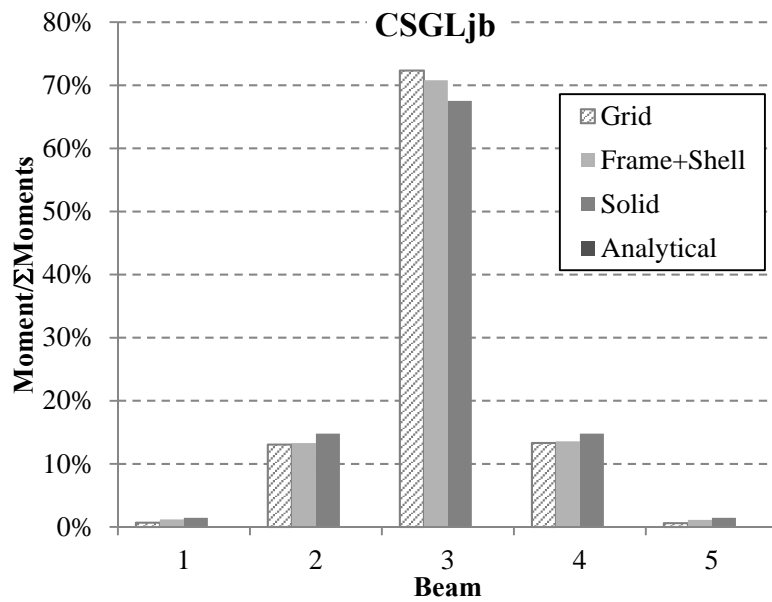


Fig. A.89 – CSGLjb: longitudinal bending moment at the quarter-span section

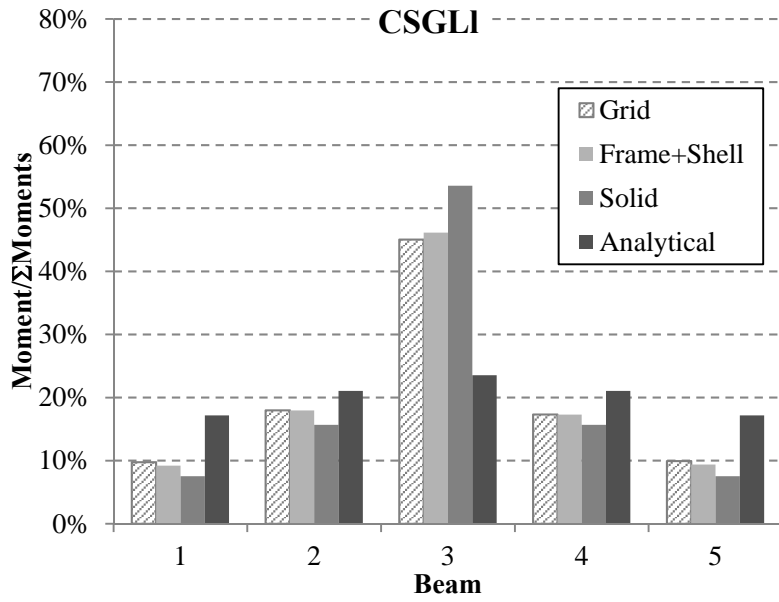


Fig. A.90 – CSGLI: longitudinal bending moment at the quarter-span section

APPENDIX B

B.1 Materials characteristics

This section presents the results of the measurements and tests to characterize the materials to be used to assemble the five experimental specimens together with their geometrical characteristics.

B.1.1 Concrete

The properties listed in this section were obtained for several ages, before and after the loading tests, as possible. Nevertheless, the ultimate stress and load were computed considering the age closer to the loading test. Exception was made in the case of S2, where the two dates before the loading tests, 28 and 40 days, were used. The age for which those quantities were computed is explained at each of the following tables.

Table B.1 – Material properties of the concrete poured into S1 specimen

Age [days]	Cube n.º	Mass	Density	Specific weight	Ultimate stress	Ultimate load
		m [kg]	ρ [kg/m ³]	γ [kN/m ³]	$f_{c,cube,max}$ [MPa]	F_{max} [kN]
7	13	7.75	2296.30	22.52	12.1576	273.50
	14	7.85	2325.93	22.81	12.1576	273.50
	15	7.80	2311.11	22.66	12.2773	276.20
14	1	7.80	2311.11	22.66	13.9799	314.50
	2	7.70	2281.48	22.37	14.0331	315.70
	3	7.65	2266.67	22.23	13.0089	292.70
21	10	7.98	2362.96	23.17	17.8373	401.30
	11	7.85	2325.93	22.81	18.0568	406.30
	12	7.85	2325.93	22.81	16.4606	370.40
30	4	7.80	2311.11	22.66	16.9993	382.50
	5	8.00	2370.37	23.25	18.9680	426.80
	7	7.80	2311.11	22.66	19.0943	429.60
	6	7.80	2311.11	22.66	17.3651	390.70
	8	7.80	2311.11	22.66	17.8174	400.90
	9	7.90	2340.74	22.95	18.6421	419.40
Mean		7.82	2317.53	22.73	18.15 ^{a)}	408.32 ^{a)}
Minimum		7.65	2266.67	22.23	17.00 ^{a)}	382.50 ^{a)}
Maximum		8.00	2370.37	23.25	19.09 ^{a)}	429.60 ^{a)}

^{a)} - These quantities were computed considering the age of 30 days.

Table B.2 – Material properties of the concrete poured into S2 specimen

Age	Cube n.º	Mass	Density	Specific weight	Ultimate stress	Ultimate load
		m	ρ	γ	$f_{c,cube,max}$	F_{max}
[days]		[kg]	[kg/m ³]	[kN/m ³]	[MPa]	[kN]
7	1	6.15	1822.22	17.87	9.37093	210.80
	2	6.05	1792.59	17.58	7.47546	168.20
	3	6.20	1837.04	18.02	6.37000	-
14	4	6.20	1837.04	18.02	8.37331	188.40
	5	6.00	1777.78	17.43	10.97380	246.90
	6	6.20	1837.04	18.02	8.83886	198.90
28	10	6.05	1792.59	17.58	12.29060	276.50
	11	6.00	1777.78	17.43	11.71200	263.50
	12	6.03	1785.19	17.51	11.69200	263.10
40	13	6.00	1777.78	17.43	12.99560	292.40
	14	6.00	1777.78	17.43	13.46110	302.90
	16	5.90	1748.15	17.14	12.60320	283.60
Mean		6.00	1776.54	17.42	12.46 ^{a)}	280.33 ^{a)}
Minimum		5.90	1748.15	17.14	7.67 ^{a)}	172.50 ^{a)}
Maximum		6.18	1829.63	17.94	13.46 ^{a)}	302.90 ^{a)}

^{a)} - These quantities were computed considering the age of 28 and 40 days.

Table B.3 – Material properties of the concrete poured into S3 and S4 specimens

Age	Cube n.º	Mass	Density	Specific weight	Ultimate stress	Ultimate load
		m	ρ	γ	$f_{c,cube,max}$	F_{max}
[days]		[kg]	[kg/m ³]	[kN/m ³]	[MPa]	[kN]
7	1	7.80	2311.11	22.66	12.4170	279.40
	2	7.80	2311.11	22.66	12.0977	272.20
	3	7.80	2311.11	22.66	12.7628	287.20
33	13	7.64	2264.59	22.21	16.1000	362.90
	14	7.73	2288.89	22.45	16.8000	377.60
	15	7.68	2276.15	22.32	15.7000	352.50
50	10	7.60	2251.85	22.08	17.7974	400.40
	11	7.60	2251.85	22.08	17.8839	402.40
	12	7.70	2281.48	22.37	17.7442	399.20
Mean		7.77	2302.22	22.58	16.20 ^{a)}	364.33 ^{a)}
Minimum		7.60	2251.85	22.08	15.70 ^{a)}	352.50 ^{a)}
Maximum		7.99	2367.41	23.22	16.80 ^{a)}	377.60 ^{a)}

^{a)} - These quantities were computed considering the age of 33 days.

Table B.4 – Material properties of the concrete poured into S5 specimen

Age [days]	Cube n.º	Mass	Density	Specific weight	Ultimate stress	Ultimate load
		m [kg]	ρ [kg/m ³]	γ [kN/m ³]	$f_{c,cube,max}$ [MPa]	F_{max} [kN]
7	1	7.92	2346.67	23.01	13.7000	308.50
	2	7.99	2367.41	23.22	13.6000	306.90
	3	7.96	2358.52	23.13	14.1000	317.10
29	4	7.70	2281.48	22.37	23.2112	522.30
	5	7.70	2281.48	22.37	21.1095	475.00
	6	7.70	2281.48	22.37	22.8853	514.90
36	7	7.80	2311.11	22.66	24.7674	557.30
	8	7.80	2311.11	22.66	24.8539	559.20
	9	7.75	2296.30	22.52	23.9494	538.90
Mean		7.81	2315.06	22.70	22.40 ^{a)}	504.07 ^{a)}
Minimum		7.70	2281.48	22.37	21.11 ^{a)}	475.00 ^{a)}
Maximum		7.99	2367.41	23.22	23.21 ^{a)}	522.30 ^{a)}

^{a)} - These quantities were computed considering the age of 29 days.

B.1.2 Timber

The following tables summarize the dimensions measured in the twenty five glulam beams and also those resulting from the tests performed according to (EN408 2010) to obtain the global MOE.

Table B.5 – Material properties and span dimensions of the timber beams

Beam designation	Global MOE ^a	Mass	Density	Specific weight	Dimensions			
					Length			
					Upper face		Bottom face	Mean span
					Top	Mid-span		
$E_{m,g}$	m	ρ	γ	[mm]				
[MPa]	[kg]	[kg/m ³]	[kN/m ³]	[mm]				
GL1	10164.8	54.150	444.7540	4.3615	4211	-	4214	4212.5
GL2	11059.2	53.100	436.0252	4.2759	4212	-	4215	4213.5
GL3	7851.0	53.150	435.7219	4.2730	4216	-	4220	4218.0
GL4	8312.8	53.850	441.5749	4.3304	4217	-	4218	4217.5
GL5	8981.4	54.500	446.4024	4.3777	4220	-	4219	4219.5
GL6	8387.8	52.050	426.4662	4.1822	4215	-	4215	4215.0
GL7	8571.3	51.350	420.1916	4.1207	4218	-	4216	4217.0
GL8	8225.1	50.900	416.7579	4.0870	4219	-	4217	4218.0
GL9	10248.8	57.200	469.6486	4.6057	4216	-	4219	4217.5
GL10	9674.8	54.350	444.8962	4.3629	4221	-	4218	4219.5
GL11	9846.0	56.000	458.4196	4.4956	4219	-	4217	4218.0
GL12	8651.1	51.700	422.9058	4.1473	4219	-	4218	4218.5
GL13	8927.0	53.650	439.5275	4.3103	4218	-	4217	4217.5
GL14	9520.5	54.850	449.7235	4.4103	4218	-	4217.5	4217.8
GL15	8331.4	52.850	432.9418	4.2457	4218	-	4221	4219.5
GL16	6332.6	29.700	462.2580	4.5332	2220	-	2221	2220.3
GL17	6118.1	27.900	434.2158	4.2582	2223	-	2220	2221.3
GL18	7467.2	29.200	457.8249	4.4897	2220	-	2218	2219.0
GL19	7092.2	30.500	475.3704	4.6618	2220	-	2223	2221.5
GL20	7959.9	29.950	467.2553	4.5822	2221	-	2220	2220.5
GL21	9170.6	104.000	435.3721	4.2695	6220	6219	6220	6219.7
GL22	10697.8	107.600	452.2636	4.4352	6222	6224	6222	6222.7
GL23	9309.5	104.550	438.0210	4.2955	6214	6216	6216	6215.2
GL24	8643.4	101.000	422.1475	4.1399	6221	6225	6221	6222.3
GL25	8931.4	102.950	428.3738	4.2009	6217	6216	6222	6218.3

^a according to (EN408 2010)

Table B.6 – Cross sectional dimensions of the beams

Beam designation	Dimensions										
	Cross section										
	Width ($b_{t,i}$)						Height ($h_{t,i}$)			Mean values	
	Section 1	Section 2	Section 3	Section 1	Section 2	Section 3	b_t	h_t			
	[mm]										
GL1	120.43	120.69	120.46	120.45	120.38	120.66	240.00	239.00	240.50	120.51	239.83
GL2	120.42	120.32	120.37	120.50	120.26	120.70	240.00	240.00	240.00	120.43	240.00
GL3	120.70	120.32	120.38	120.42	120.26	120.40	240.00	240.50	240.00	120.41	240.17
GL4	120.39	120.62	120.35	120.50	120.58	120.44	240.00	240.00	240.00	120.48	240.00
GL5	120.59	120.83	120.67	120.39	120.37	120.30	239.65	240.55	240.00	120.53	240.07
GL6	120.46	120.53	120.72	120.58	120.87	120.74	240.00	240.00	240.00	120.65	240.00
GL7	120.67	120.48	120.51	120.58	120.56	120.58	240.00	240.30	240.80	120.56	240.37
GL8	120.61	120.50	120.56	120.47	120.63	120.86	240.00	240.35	239.90	120.61	240.08
GL9	120.64	120.52	120.46	120.71	120.67	120.66	238.50	240.00	239.80	120.61	239.43
GL10	120.39	120.65	120.54	120.42	120.55	120.80	240.00	240.50	239.95	120.56	240.15
GL11	120.62	120.48	120.50	120.51	120.50	120.82	240.15	240.70	239.75	120.57	240.20
GL12	120.42	120.63	120.60	120.62	120.81	120.60	240.00	240.50	240.30	120.61	240.27
GL13	120.72	120.74	120.59	120.37	120.59	120.54	240.00	240.00	240.00	120.59	240.00
GL14	120.59	120.33	120.30	120.53	120.84	120.33	240.00	240.00	240.00	120.49	240.00
GL15	120.64	120.65	120.56	120.46	120.39	120.56	240.00	240.00	240.00	120.54	240.00
GL16	120.37	120.64	120.74	120.35	120.28	120.37	239.90	240.30	240.50	120.46	240.23
GL17	120.47	120.60	120.44	120.55	120.42	120.39	240.30	240.00	240.00	120.48	240.10
GL18	120.52	120.41	120.41	120.46	120.53	120.30	239.05	238.60	238.30	120.44	238.65
GL19	120.22	120.59	120.25	120.32	120.28	120.28	240.00	240.00	240.10	120.32	240.03
GL20	120.26	120.31	120.29	120.48	120.37	120.40	240.00	240.10	239.45	120.35	239.85
GL21	120.00	120.00	120.00	120.00	120.00	119.00	320.50	321.00	320.00	119.83	320.50
GL22	118.00	119.50	120.00	120.50	120.00	120.00	320.50	320.00	318.00	119.67	319.50
GL23	120.00	120.00	120.00	120.00	119.95	120.50	320.00	320.50	319.00	120.08	319.83
GL24	120.50	120.50	120.00	120.00	120.00	119.95	320.00	320.00	320.00	120.16	320.00
GL25	121.00	120.95	121.00	120.00	120.95	120.00	320.00	320.00	321.00	120.65	320.33

B.2 Results from the experimental analysis

The following sections present the results obtained during the experimental tests in terms of vertical displacements, support reactions, slip and uplift displacements and strains. Measurements of vertical displacements were taken at mid- and at quarter-span of each beam. Slip between each timber beam and concrete layer was recorded at each beam top, as for the uplift displacement, they were obtained for each corner of the concrete layer. Concerning the support reactions they are presented for each beam by summing the loads supported in each beam end when they were loaded at mid- and at quarter-span with a point load and with a line load along each beam at a time. Further information is presented at *4.3 Test setup*. The symbology is the same used at that same section.

B.2.1 Vertical displacements

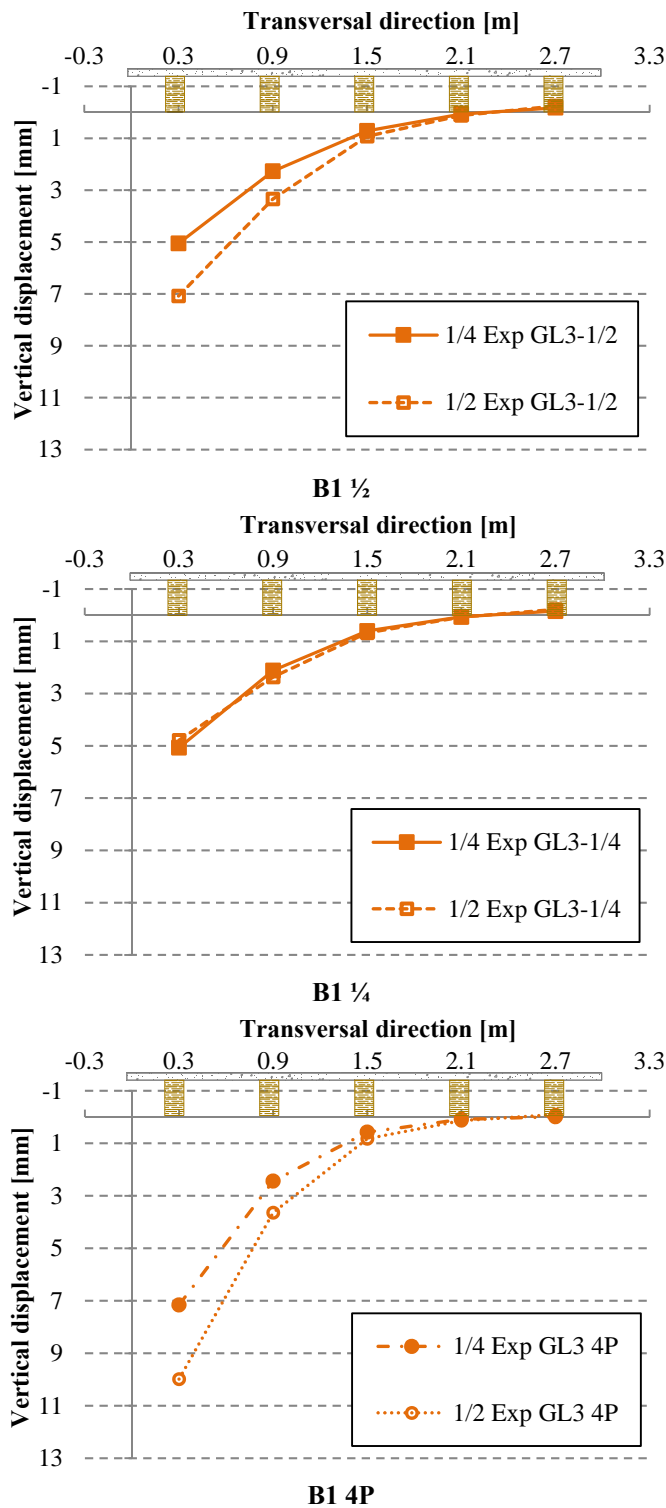


Fig. B.1 – S1-BSp: vertical displacements when loaded at B1-GL3

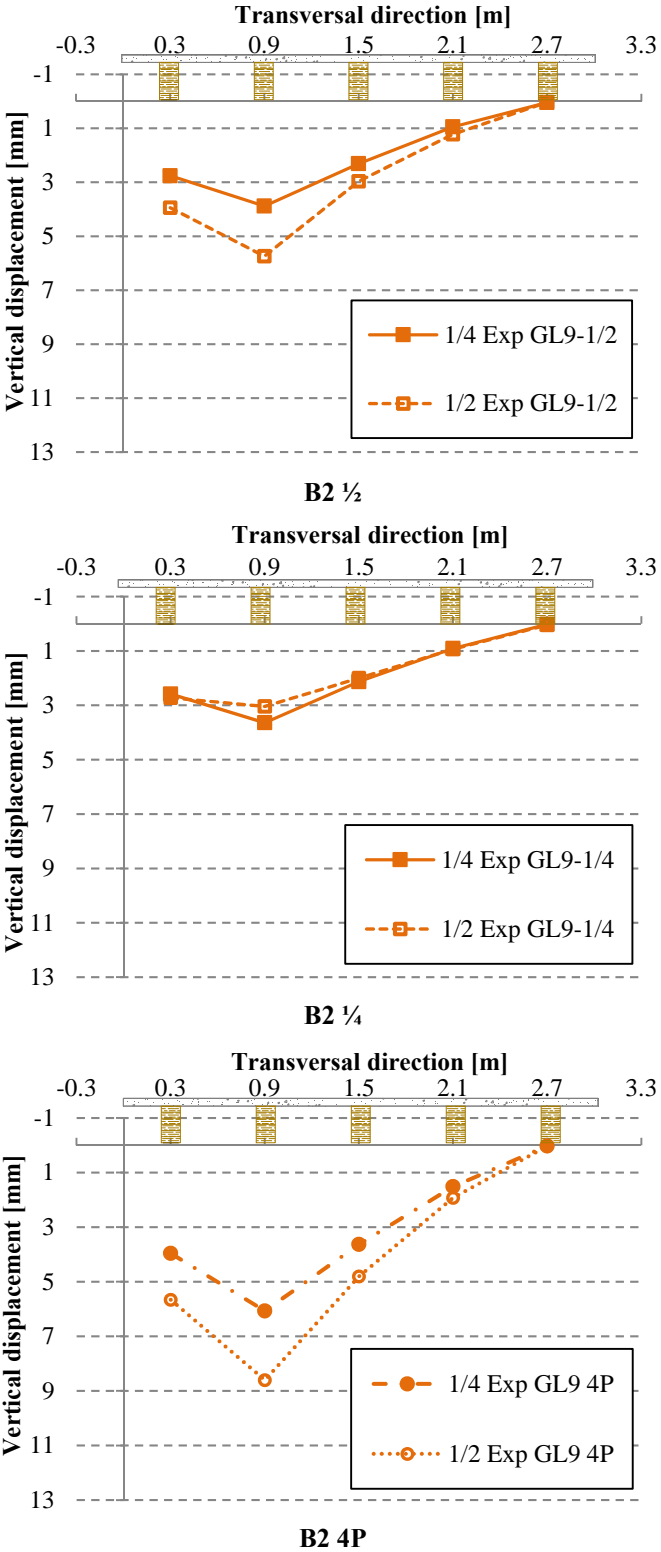


Fig. B.2 – S1-BSp: vertical displacements when loaded at B2-GL9

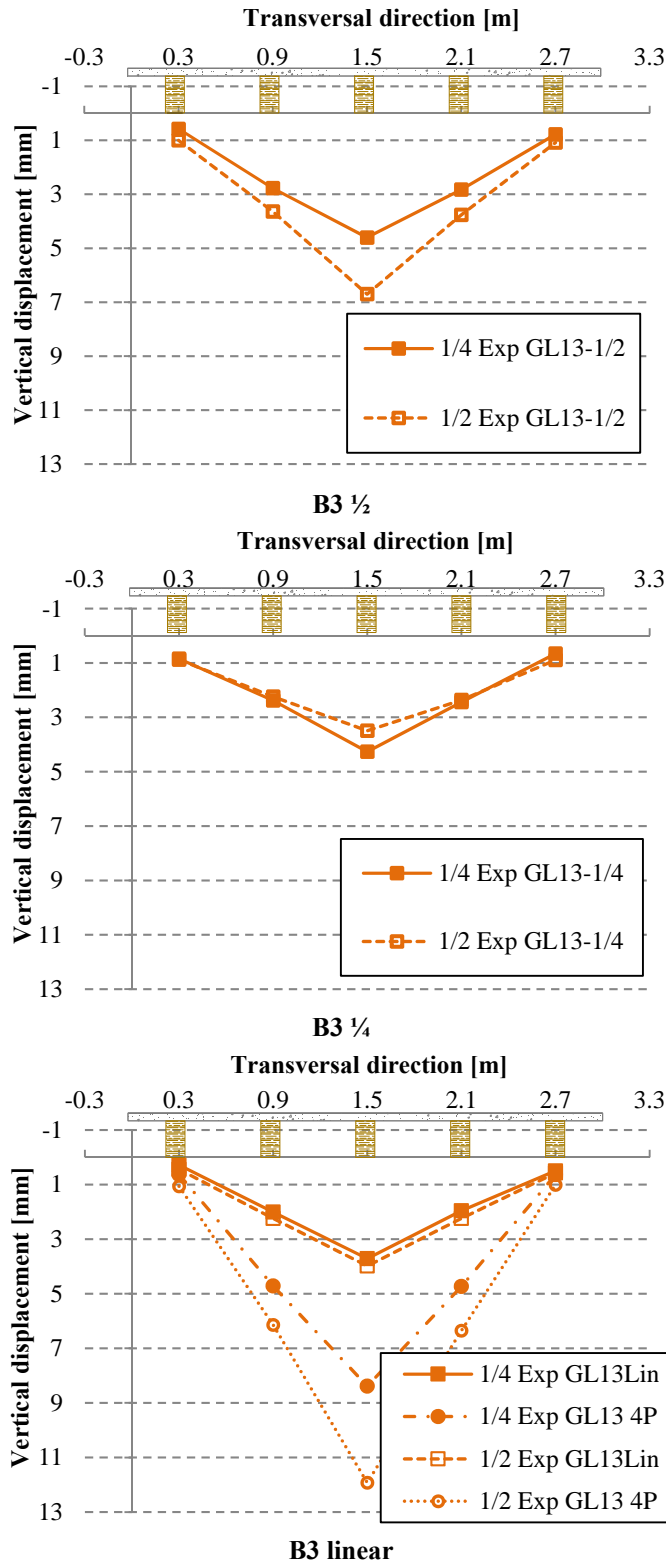


Fig. B.3 – S1-BSp: vertical displacements when loaded at B3-GL13

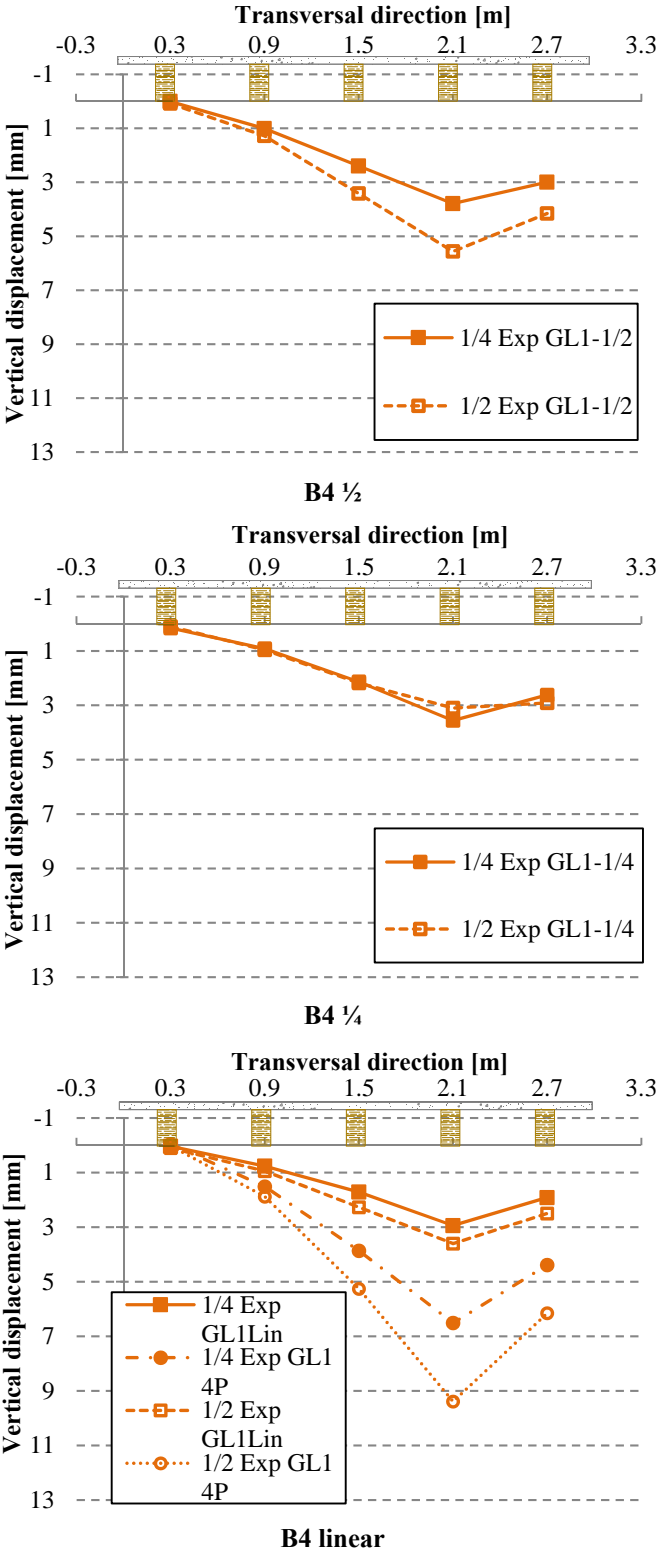


Fig. B.4 – S1-BSp: vertical displacements when loaded at B4-GL1

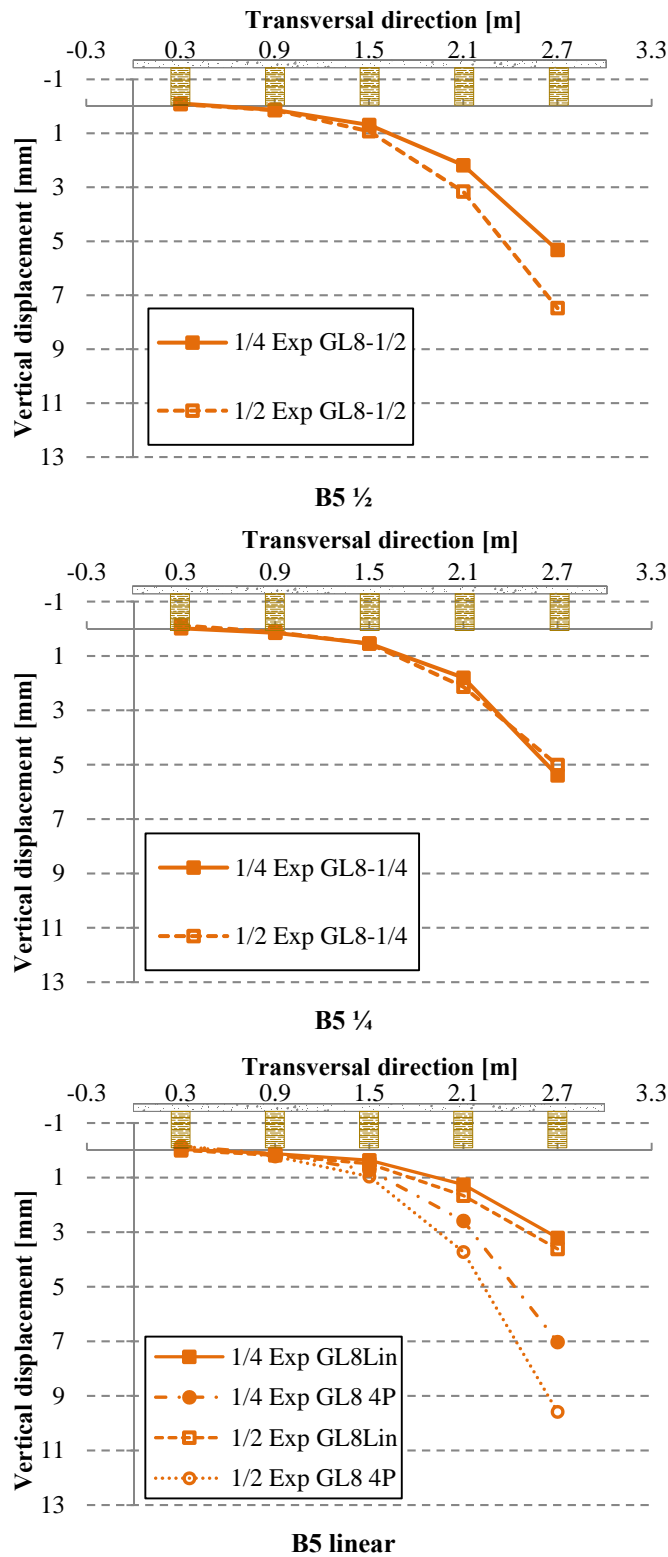


Fig. B.5 – S1-BSp: vertical displacements when loaded at B5-GL8

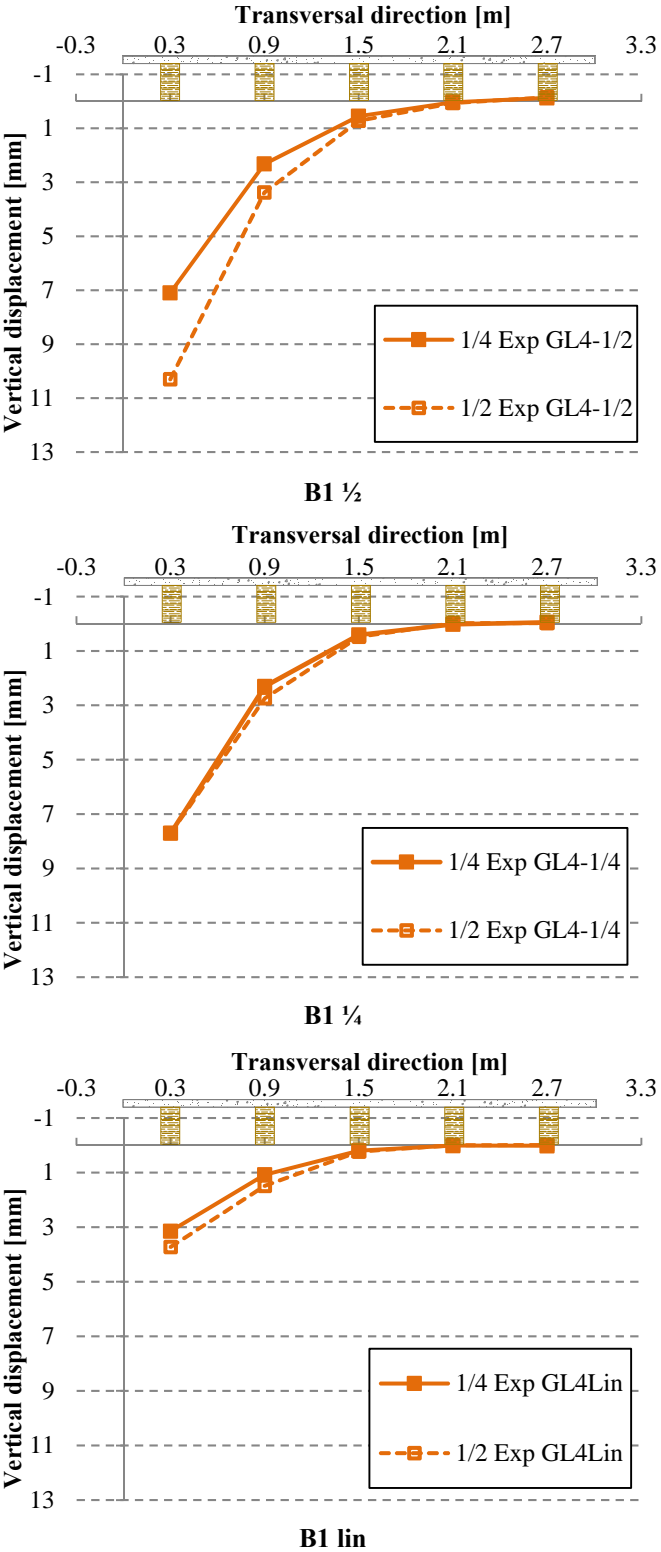


Fig. B.6 – S2-LWAC: vertical displacements when loaded at B1-GL4

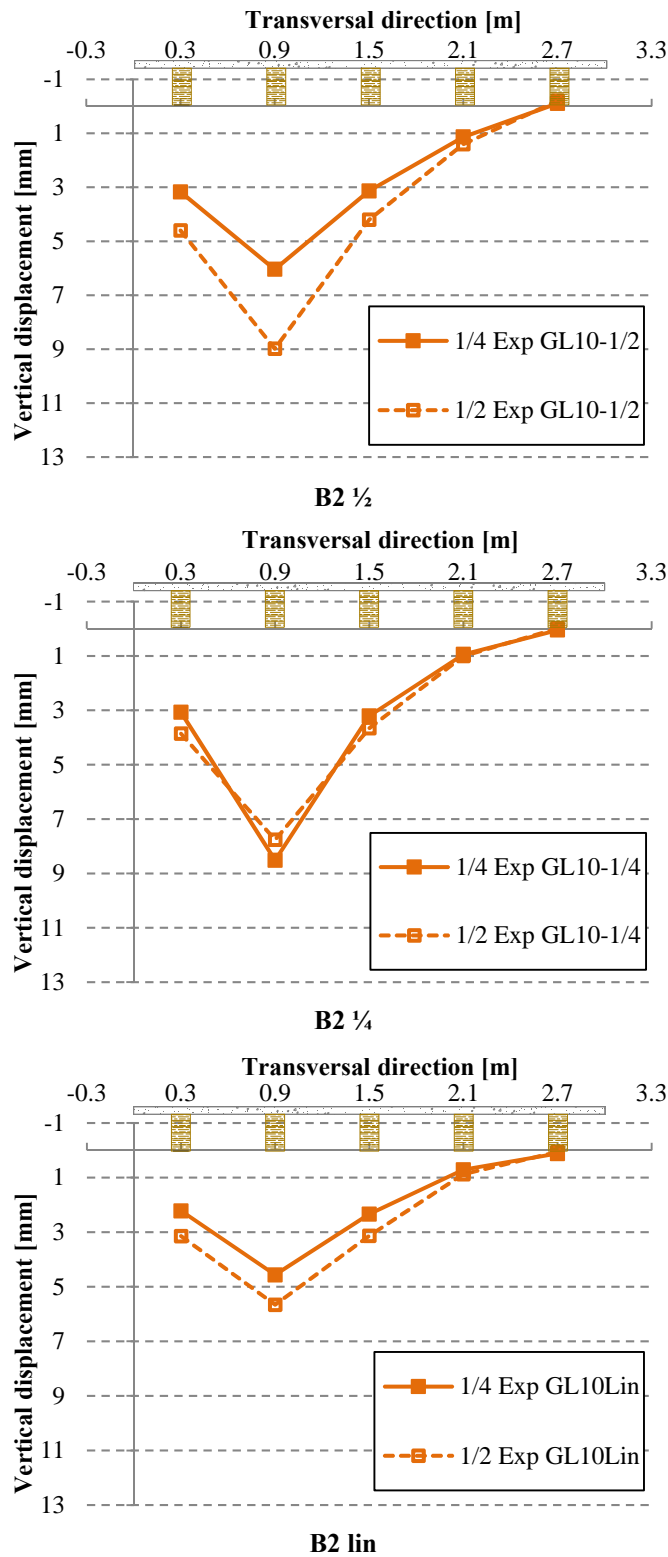


Fig. B.7 – S2-LWAC: vertical displacements when loaded at B2-GL10

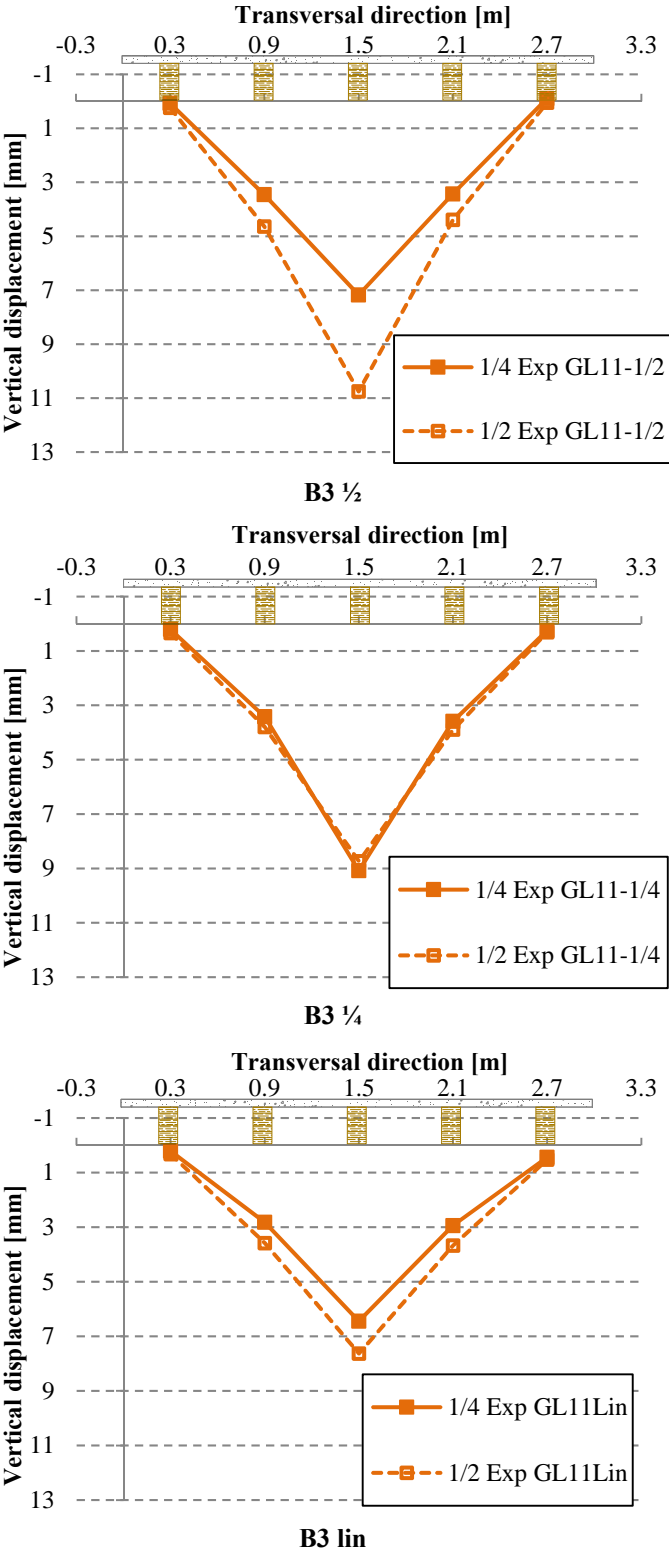


Fig. B.8 – S2-LWAC: vertical displacements when loaded at B3-GL11

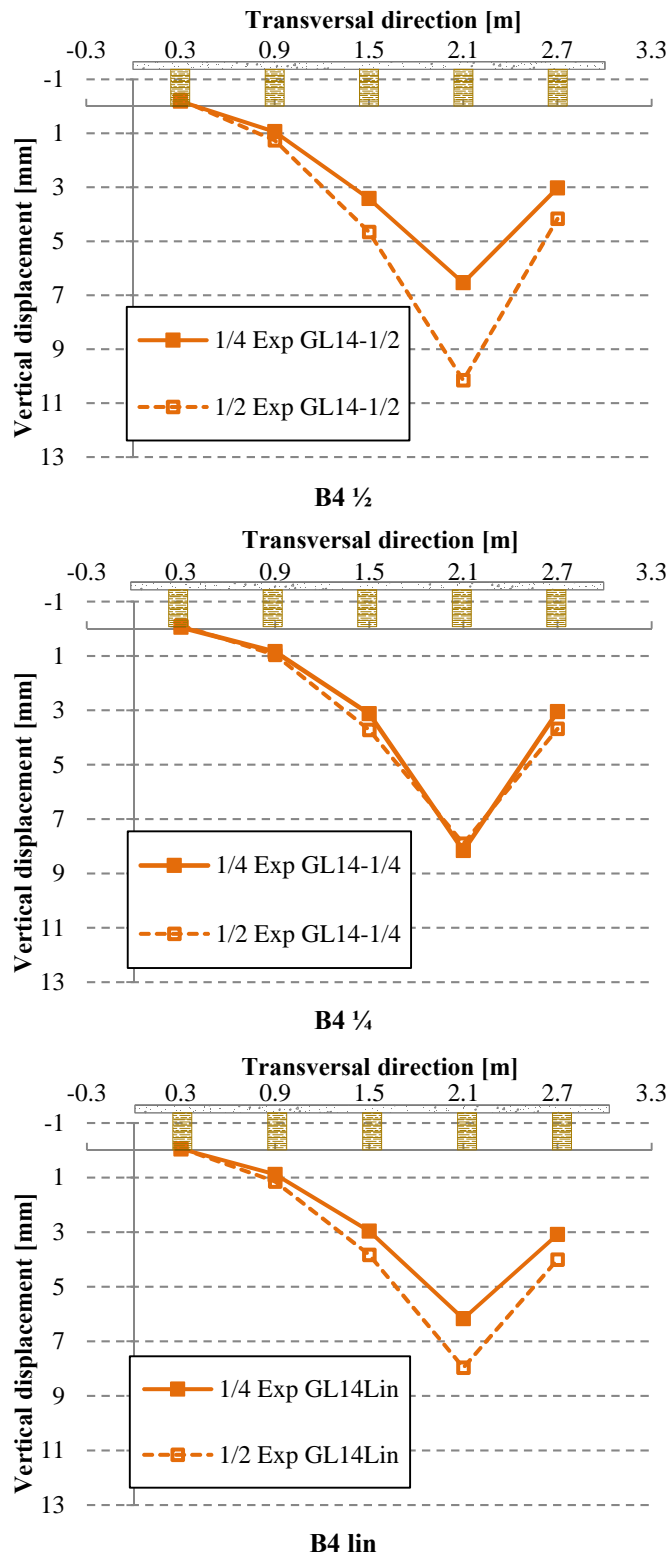


Fig. B.9 – S2-LWAC: vertical displacements when loaded at B4-GL14

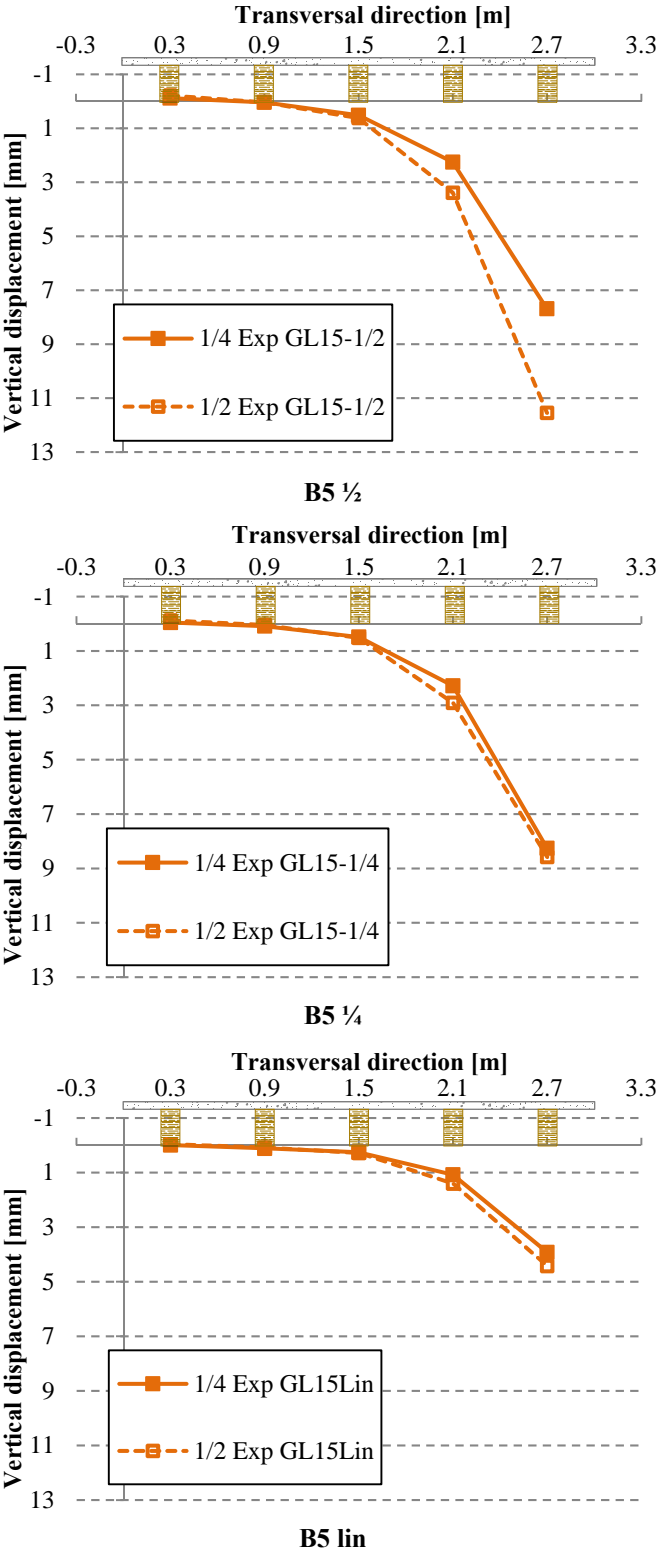


Fig. B.10 – S2-LWAC: vertical displacements when loaded at B5-GL15

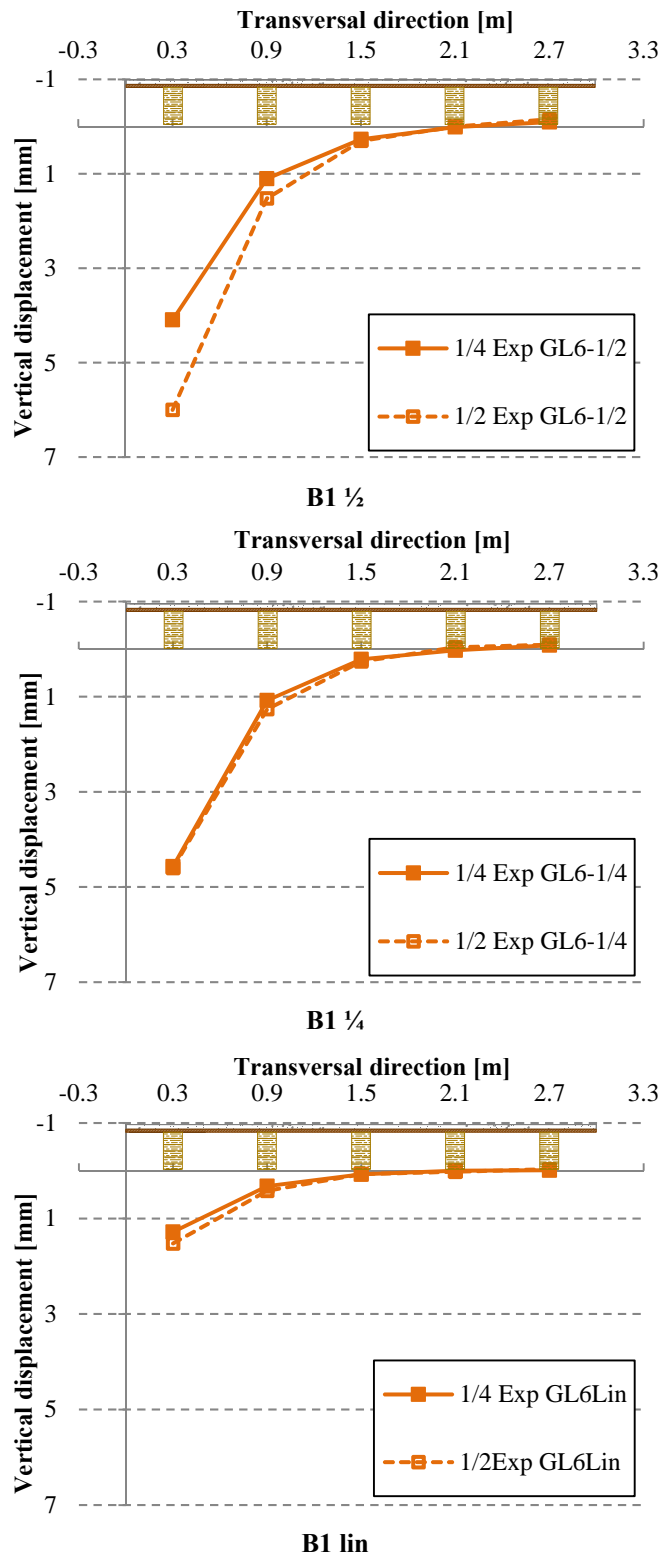


Fig. B.11 – S3-hc=0.03m: vertical displacements when loaded at B1-GL6

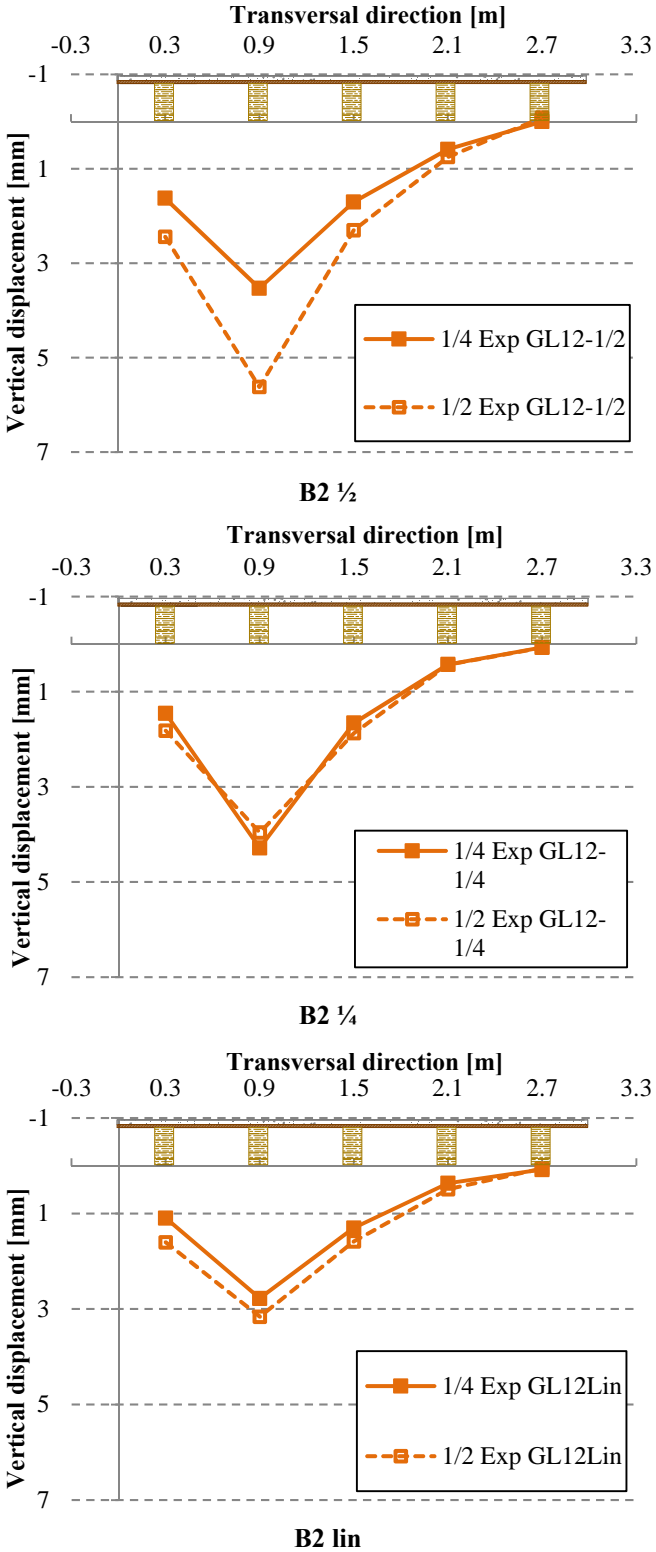


Fig. B.12 – S3-hc=0.03m: vertical displacements when loaded at B2-GL12

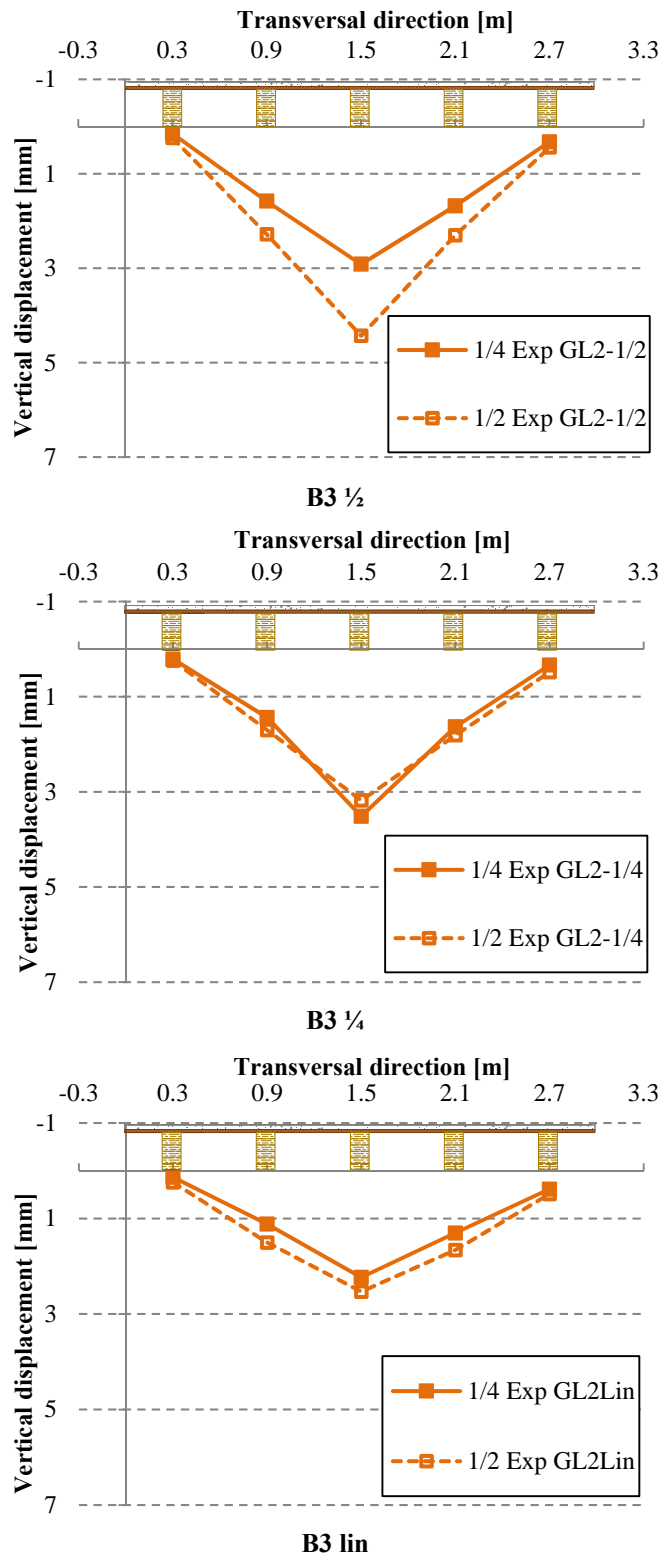


Fig. B.13 – S3-hc=0.03m: vertical displacements when loaded at B3-GL2

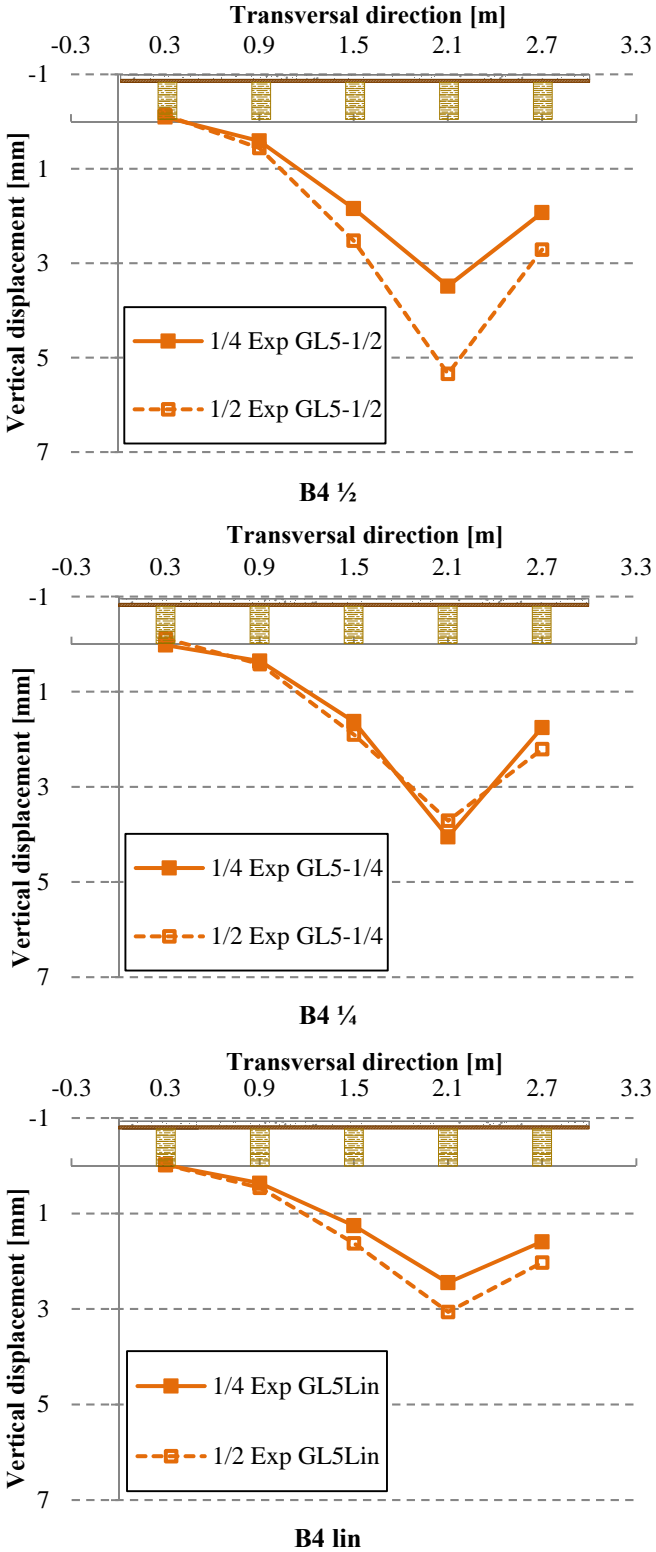


Fig. B.14 – S3-hc=0.03m: vertical displacements when loaded at B4-GL5

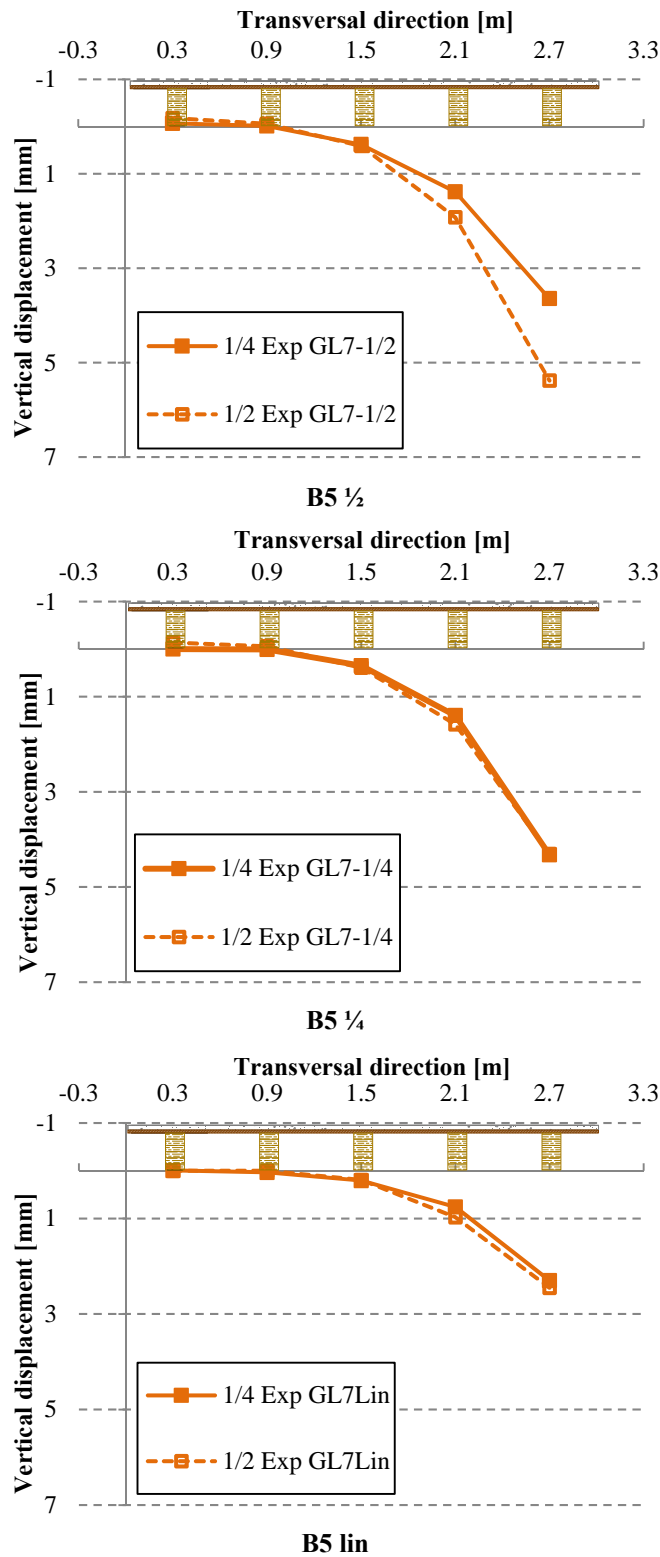


Fig. B.15 – S3-hc=0.03m: vertical displacements when loaded at B5-GL7

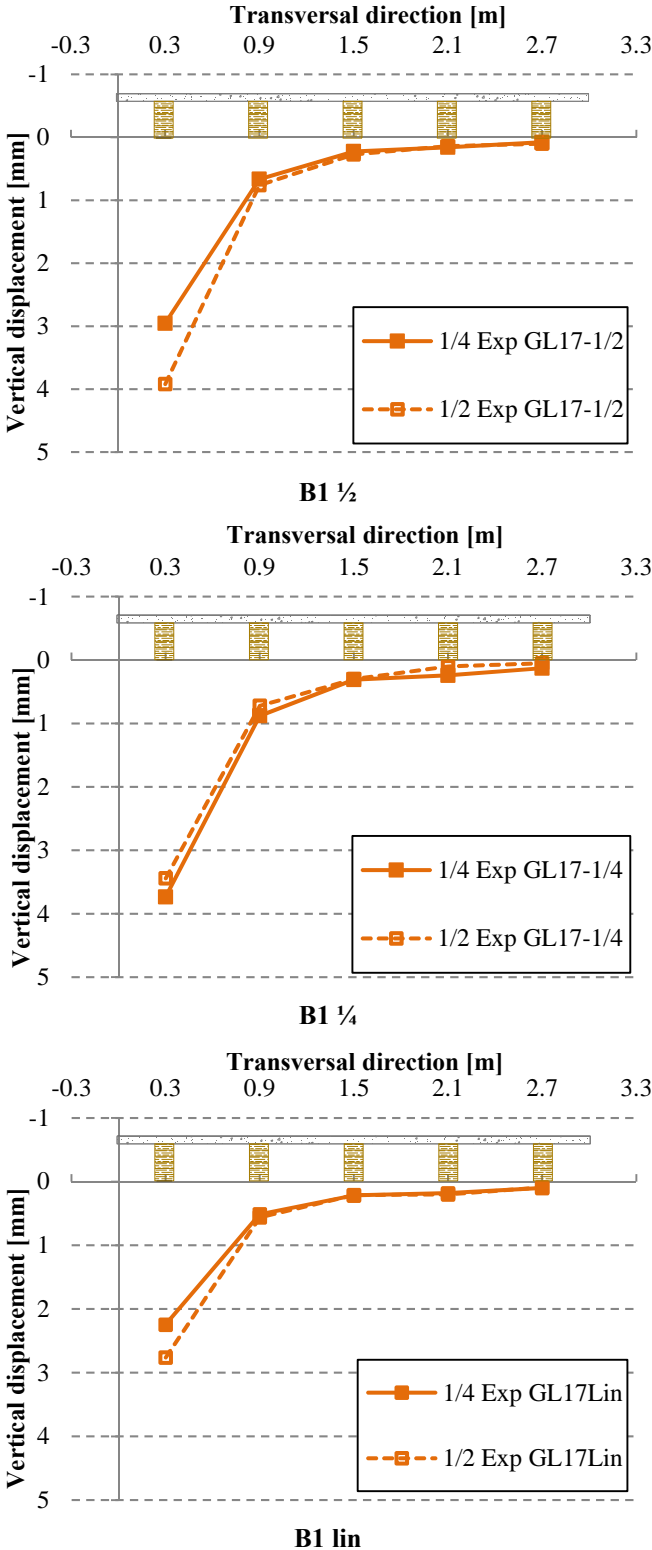


Fig. B.16 – S4-L=2.00m: vertical displacements when loaded at B1-GL17

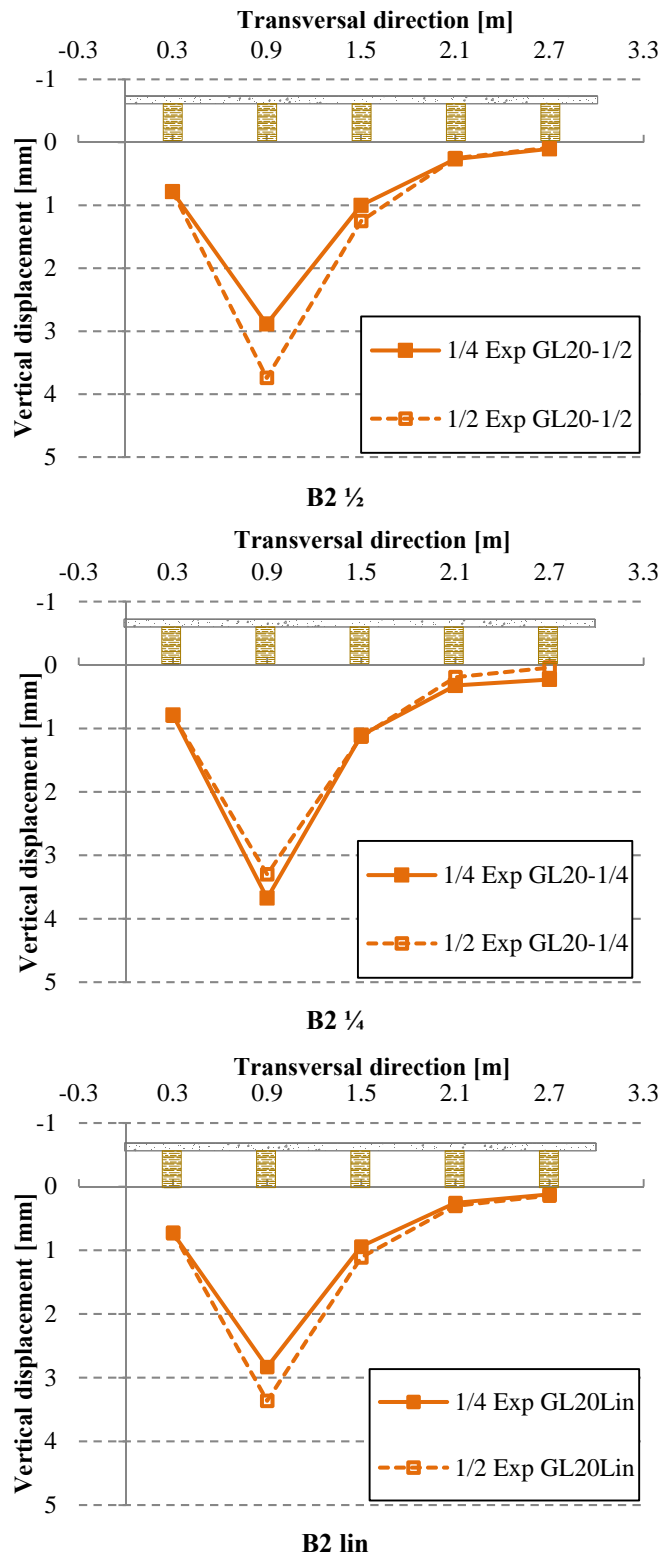


Fig. B.17 – S4-L=2.00m: vertical displacements when loaded at B2-GL20

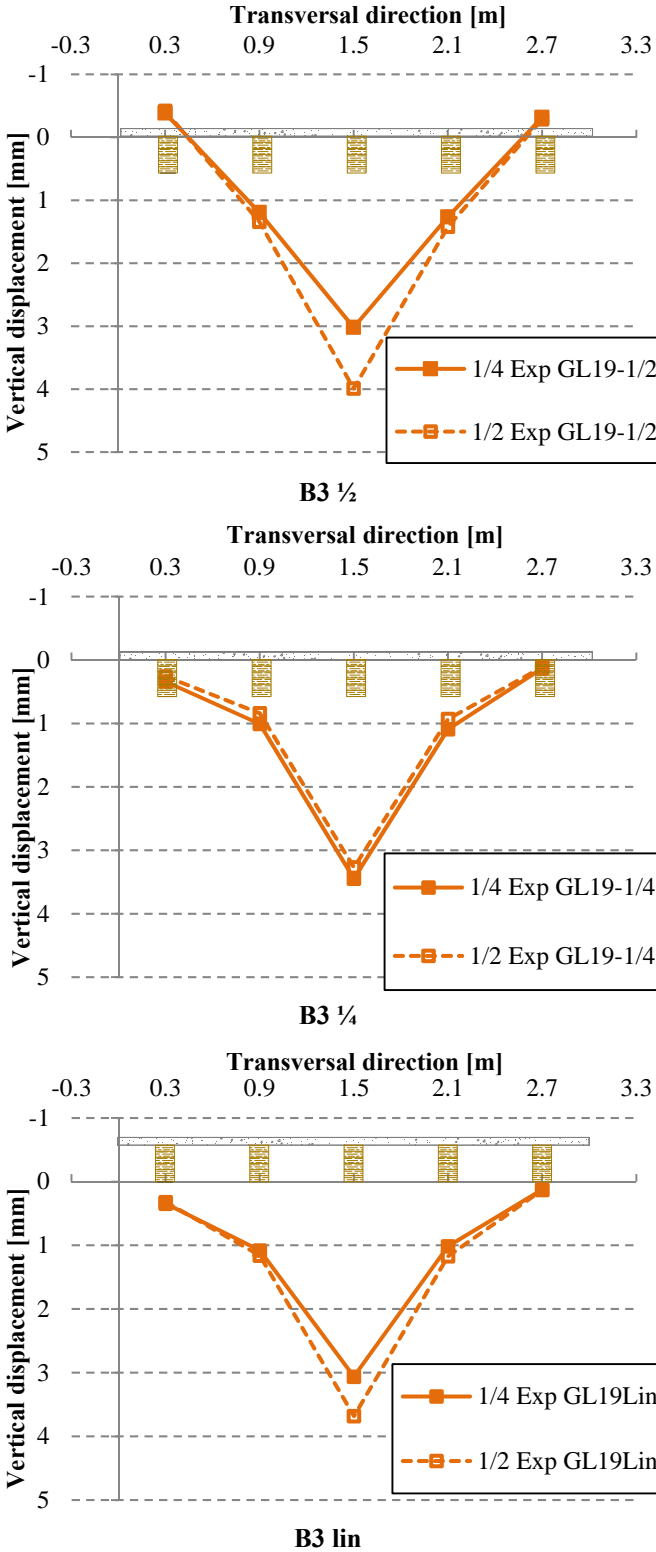


Fig. B.18 – S4-L=2.00m: vertical displacements when loaded at B3-GL19

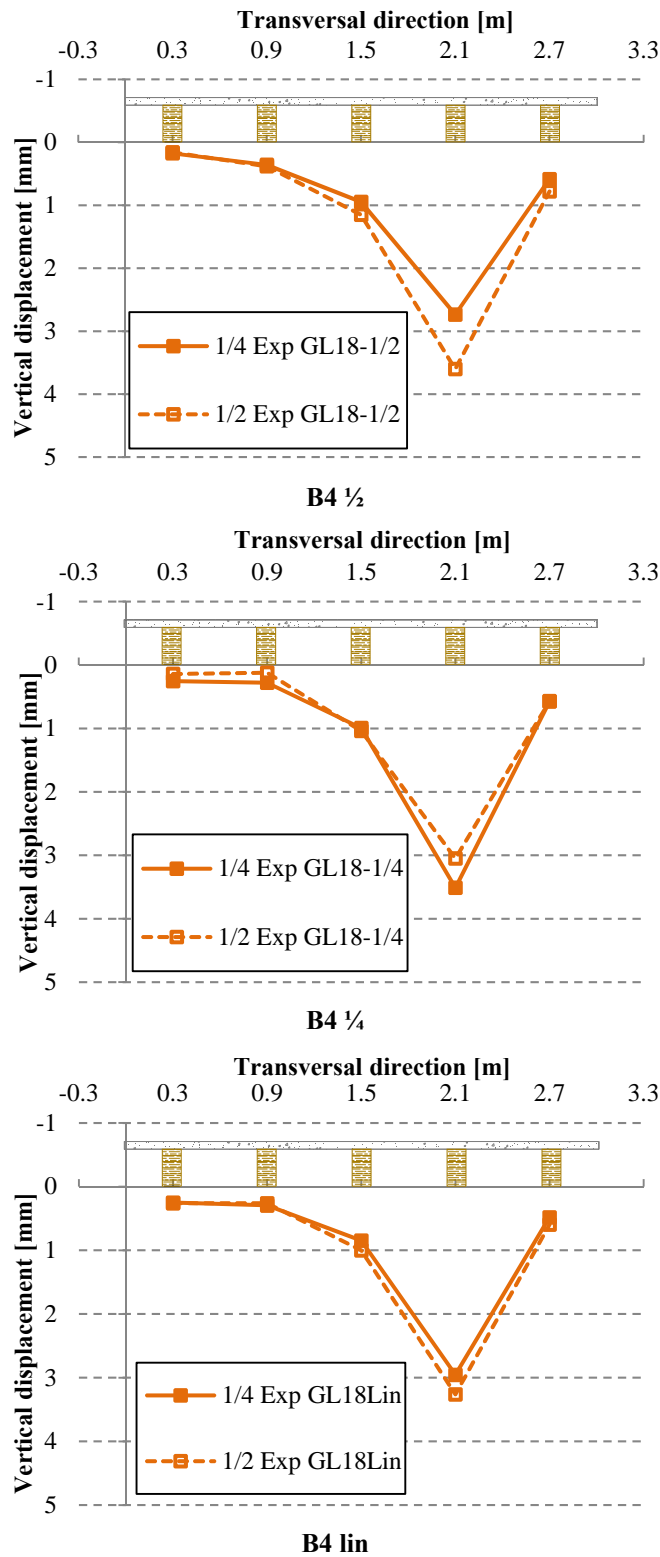


Fig. B.19 – S4-L=2.00m: vertical displacements when loaded at B4-GL18

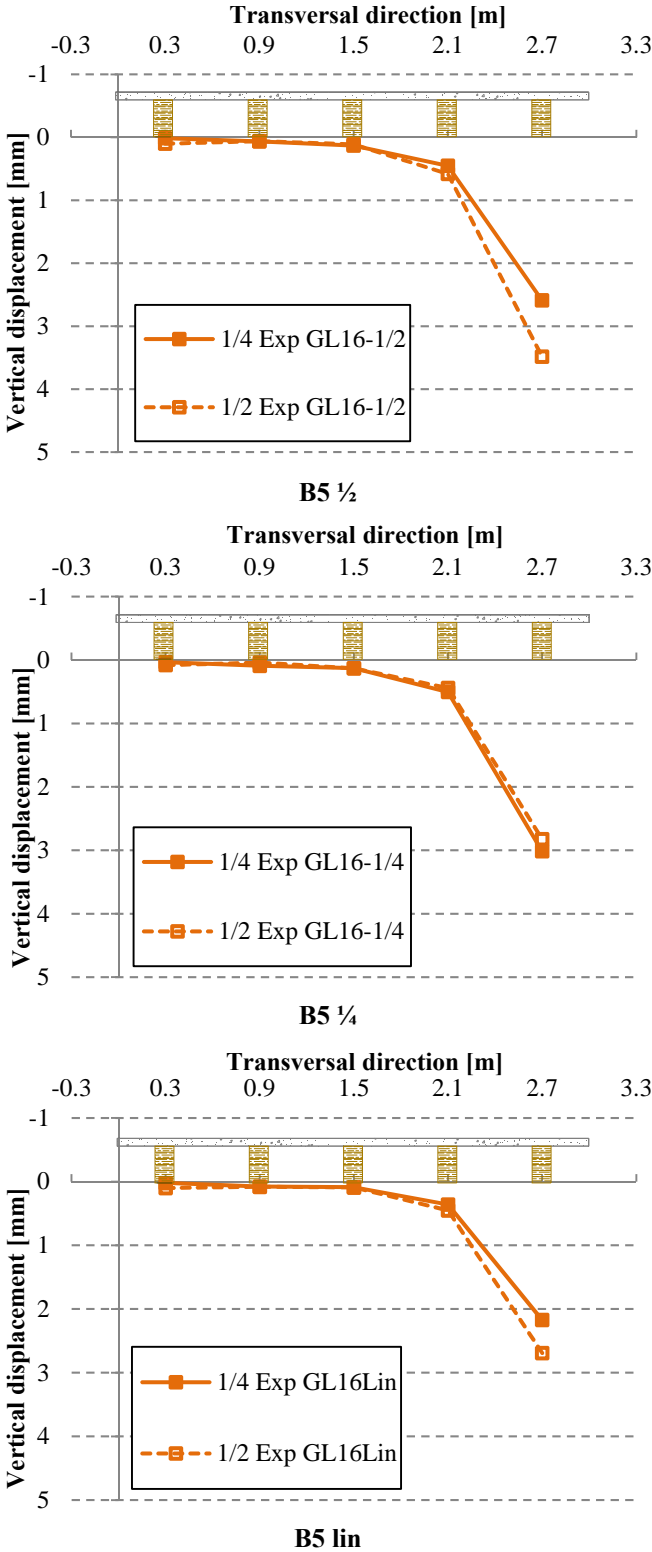


Fig. B.20 – S4-L=2.00m: vertical displacements when loaded at B5-GL16

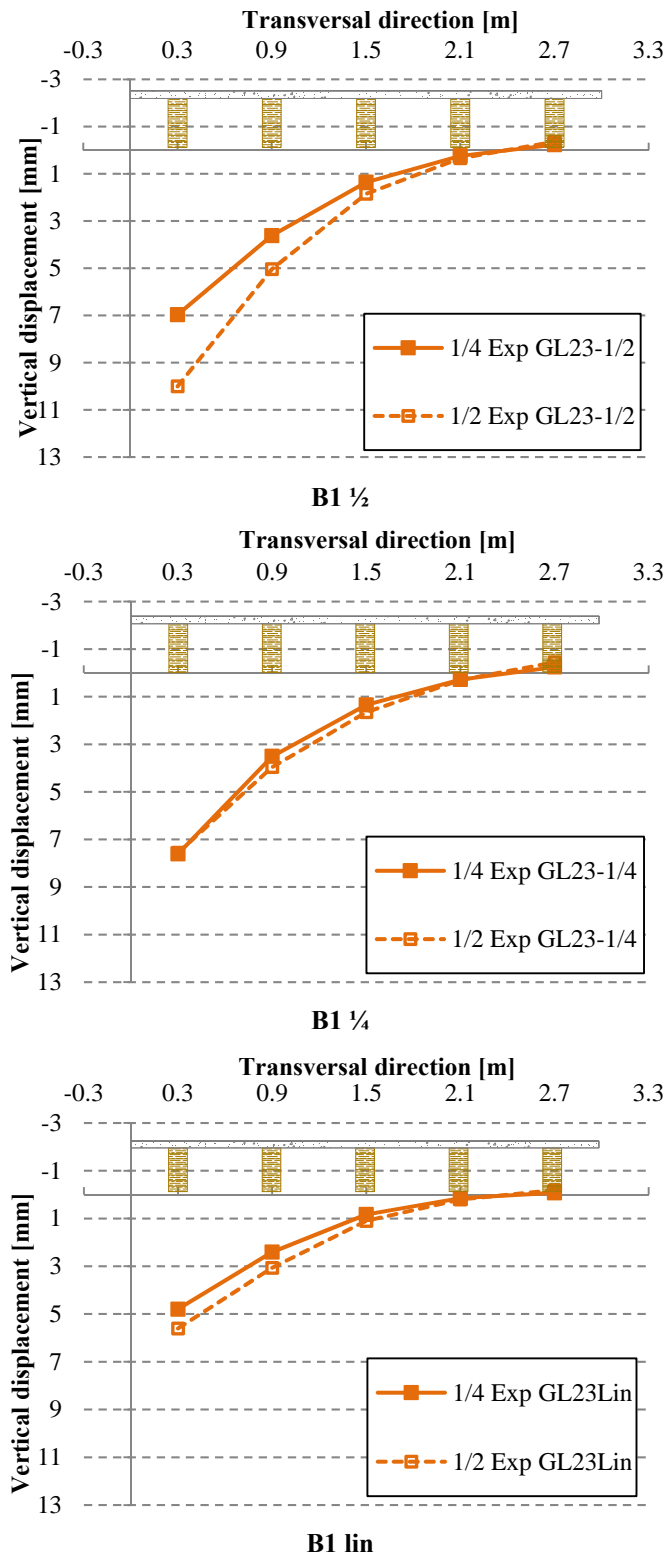


Fig. B.21 – S5-L=6.00m: vertical displacements when loaded at B1-GL23

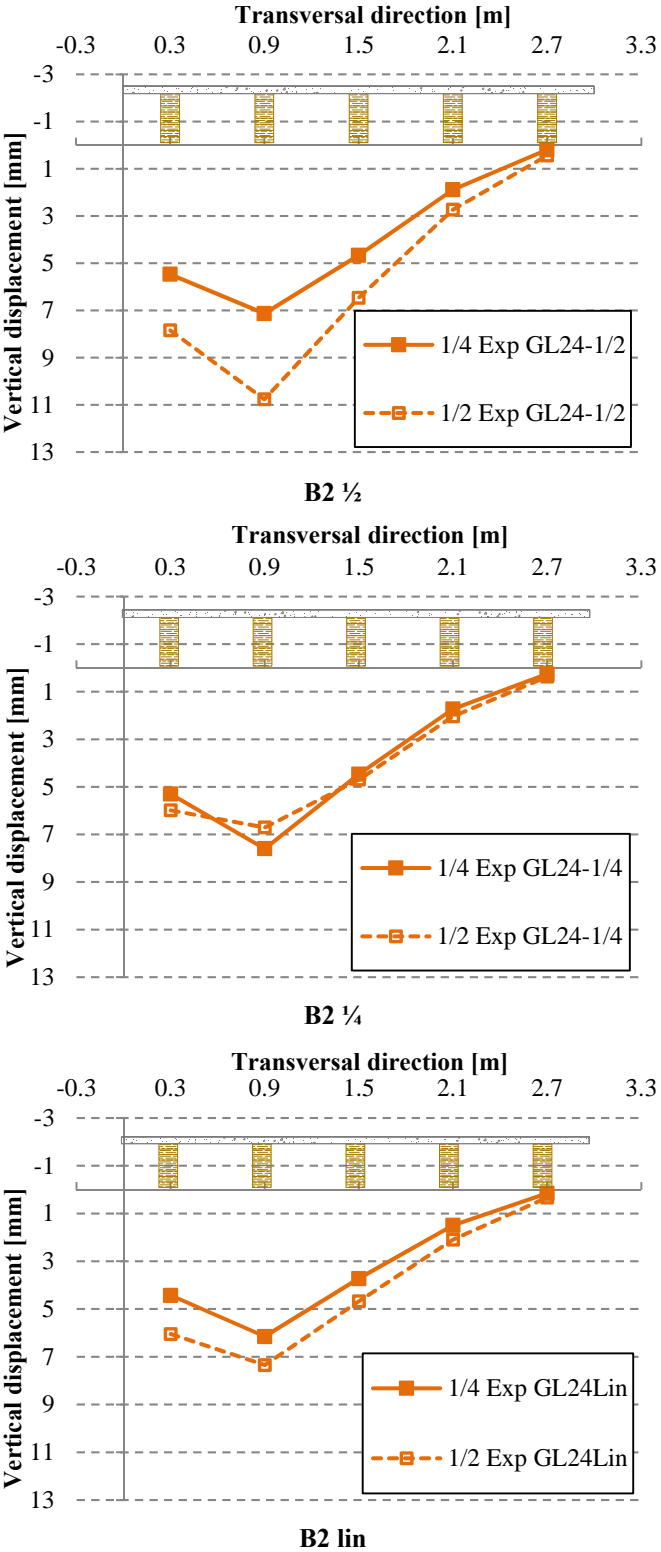


Fig. B.22 – S5-L=6.00m: vertical displacements when loaded at B2-GL24

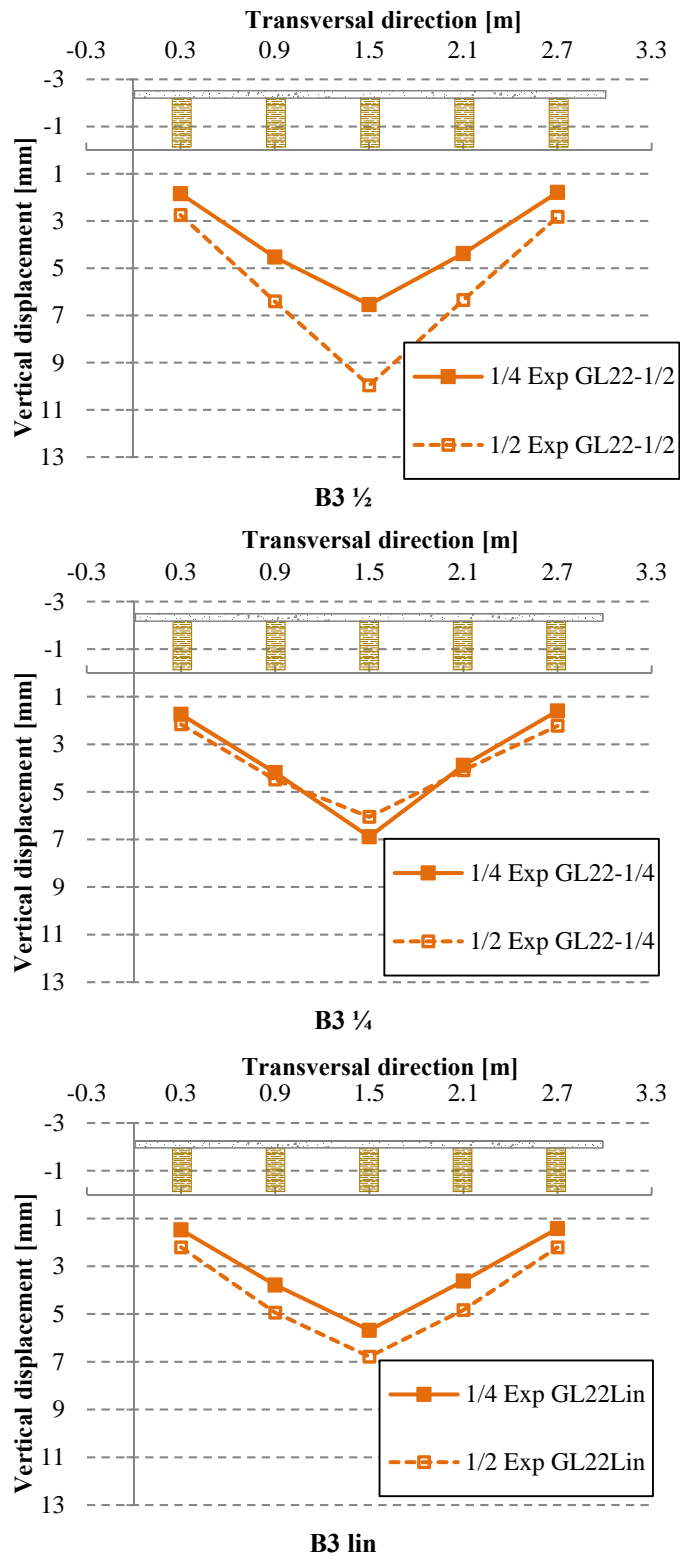


Fig. B.23 – S5-L=6.00m: vertical displacements when loaded at B3-GL22

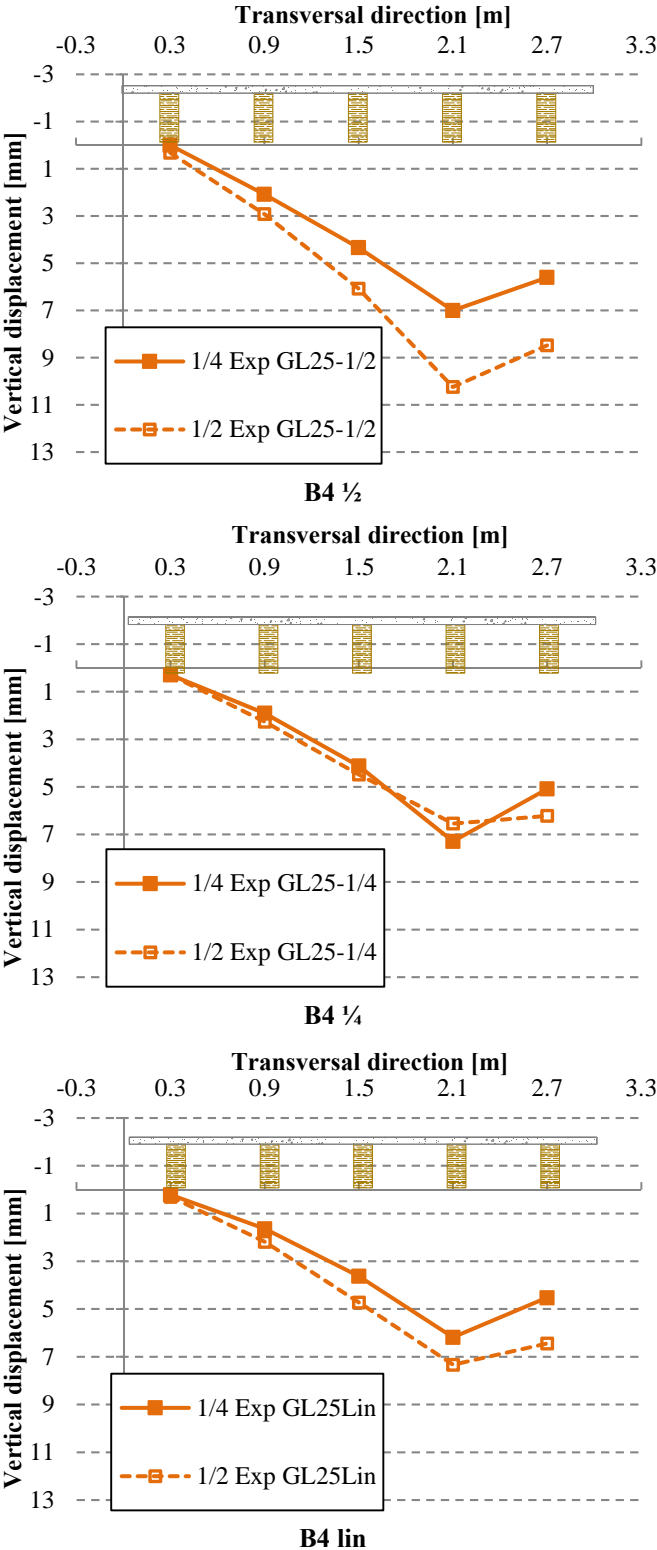


Fig. B.24 – S5-L=6.00m: vertical displacements when loaded at B4-GL25

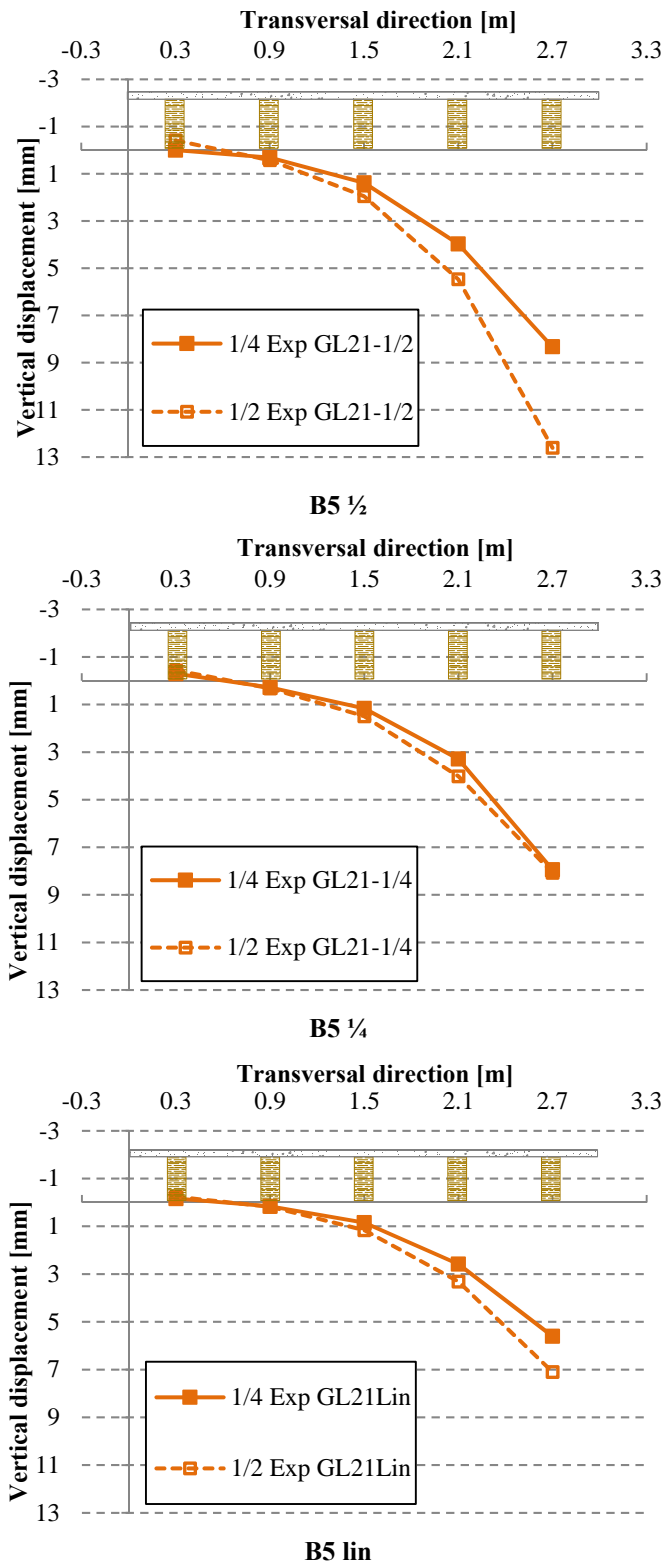


Fig. B.25 – S5-L=6.00m: vertical displacements when loaded at B5-GL21

Table B.7 summarizes the distribution of vertical displacements for the several load cases at mid- and quarter-span along the transversal direction. These percentages were obtained by comparing the displacement in question with the sum of displacements for the same load case at the same location in all the beams.

Table B.7 – Vertical displacements distribution [%]

Floor specimen	Load case	Measuring location	Beam position					Floor specimen	Load case	Measuring location	Beam position				
			B1	B2	B3	B4	B5				B1	B2	B3	B4	B5
S1-BSp	B1 ½	¼	64	29	9	1	-2	S4- L=2.00m	B1 ½	¼	72	16	6	4	2
		½	63	30	8	1	-2			½	76	15	5	3	2
	B2 ½	¼	28	39	23	10	0		B2 ½	¼	16	57	20	5	2
		½	28	41	21	9	0			½	13	61	20	4	1
	B3 ½	¼	5	24	40	24	7		B3 ½	¼	-8	25	63	26	-7
		½	6	22	41	23	7			½	-7	22	66	23	-5
	B4 ½	¼	0	10	23	37	29		B4 ½	¼	4	7	20	57	12
		½	1	9	24	38	29			½	3	6	19	59	13
	B5 ½	¼	-1	2	8	27	65		B5 ½	¼	0	2	4	14	80
		½	-1	1	8	27	64			½	2	1	3	13	80
	B1 ¼	¼	66	27	8	1	-2		B1 ¼	¼	70	17	6	5	2
		½	62	31	9	1	-3			½	75	16	7	2	1
	B2 ¼	¼	28	39	23	10	0		B2 ¼	¼	13	60	18	5	4
		½	31	35	23	11	0			½	15	60	21	3	1
	B3 ¼	¼	8	22	40	23	6		B3 ¼	¼	6	17	57	18	2
		½	9	23	35	24	9			½	5	16	60	17	2
	B4 ¼	¼	2	10	23	38	28		B4 ¼	¼	5	5	18	63	10
		½	1	10	24	34	31			½	3	2	21	62	12
	B5 ¼	¼	0	2	7	23	69		B5 ¼	¼	1	2	3	13	80
		½	-2	2	7	28	65			½	2	1	4	13	80
	B1 4P	¼	70	24	6	1	0		B1lin	¼	69	16	7	6	3
		½	69	25	6	1	-1			½	72	15	5	5	2
	B2 4P	¼	26	40	24	10	0		B2lin	¼	15	58	19	5	2
		½	27	41	23	9	0			½	13	60	20	5	2
	B3lin	¼	3	24	45	23	5		B3lin	¼	6	19	54	18	2
		½	4	23	43	24	6			½	5	18	57	18	2
	B3 4P	¼	3	25	44	25	3		B4lin	¼	5	6	18	61	10
		½	4	23	45	24	4			½	5	5	19	61	11
	B4lin	¼	0	10	23	40	26		B5lin	¼	1	3	3	13	80
		½	0	10	23	40	26			½	3	2	3	13	79
	B4 4P	¼	0	9	24	40	27		B5 4P	¼	-2	1	7	25	68
		½	0	8	23	41	27			½	-1	2	7	26	67
B5lin	¼	-1	3	7	26	65									
	½	0	3	8	28	61									

Table B.7 – Vertical displacements distribution [%] (cont.)

Floor specimen	Load case	Measuring location	Beam position					Floor specimen	Load case	Measuring location	Beam position				
			B1	B2	B3	B4	B5				B1	B2	B3	B4	B5
S2-LWAC	B1 ½	¼	72	23	6	0	-1	S5- L=6.00m	B1 ½	¼	58	30	11	2	-2
		½	72	24	5	0	-1			½	59	30	11	2	-2
	B2 ½	¼	24	45	23	9	-1		B2 ½	¼	28	37	24	10	1
		½	24	47	22	7	-1			½	28	38	23	10	2
	B3 ½	¼	1	25	51	24	-1		B3 ½	¼	10	24	34	23	9
		½	1	23	54	22	0			½	10	23	35	22	10
	B4 ½	¼	-1	7	25	48	22		B4 ½	¼	0	11	23	37	29
		½	-1	6	23	51	21			½	1	10	22	37	30
	B5 ½	¼	-1	0	5	22	74		B5 ½	¼	0	2	10	28	59
		½	-1	0	4	22	75			½	-2	2	10	27	63
	B1 ¼	¼	74	22	4	0	0		B1 ¼	¼	61	28	11	2	-2
		½	71	25	4	0	0			½	58	30	13	2	-3
	B2 ¼	¼	19	54	20	6	0		B2 ¼	¼	27	39	23	9	1
		½	24	48	23	6	0			½	30	34	24	10	2
	B3 ¼	¼	1	21	55	22	2		B3 ¼	¼	10	23	38	21	9
		½	2	22	51	23	2			½	11	24	32	22	12
	B4 ¼	¼	0	6	21	54	20		B4 ¼	¼	2	10	22	39	27
		½	-1	6	23	49	23			½	2	11	23	33	31
	B5 ¼	¼	0	1	4	21	75		B5 ¼	¼	-2	2	9	27	64
		½	-1	0	4	24	72			½	-3	2	11	30	60
	B1lin	¼	70	24	4	0	0		B1lin	¼	59	30	10	2	-1
		½	69	27	4	0	0			½	57	31	11	2	-2
	B2lin	¼	22	46	23	7	1		B2lin	¼	28	39	23	9	1
		½	24	44	24	7	0			½	30	36	23	10	2
	B3lin	¼	2	22	50	23	3		B3lin	¼	9	24	36	23	9
		½	2	23	49	23	3			½	11	24	32	23	11
	B4lin	¼	0	7	23	47	24		B4lin	¼	1	10	22	38	28
		½	0	7	23	47	24			½	1	10	23	35	31
B5lin	¼	0	2	5	20	73	B5lin	¼	-2	2	9	29	62		
	½	-1	1	5	23	72		½	-2	2	10	29	62		
S3- hc=0.03m	B1 ½	¼	76	21	5	0	-2		B1 ½	¼	76	21	5	0	-2
		½	78	20	4	0	-2			½	78	20	4	0	-2
	B2 ½	¼	22	47	23	8	0		B2 ½	¼	22	47	23	8	0
		½	22	51	21	7	-1			½	22	51	21	7	-1
	B3 ½	¼	2	24	44	25	5		B3 ½	¼	2	24	44	25	5
		½	2	24	46	24	5			½	2	24	46	24	5

Table B.7 – Vertical displacements distribution [%] (cont.)

Floor specimen	Load case	Measuring location	Beam position					Floor specimen	Load case	Measuring location	Beam position																										
			B1	B2	B3	B4	B5				B1	B2	B3	B4	B5																						
S3- hc=0.03m	B4 ½	¼	-1	5	24	46	25																														
		½	-1	5	23	49	25																														
	B5 ½	¼	-1	0	7	26	68																														
		½	-2	-1	5	26	72																														
	B1 ¼	¼	79	19	4	0	-1																														
		½	77	21	4	-1	-2																														
	B2 ¼	¼	18	54	21	5	1																														
		½	22	49	23	5	1																														
	B3 ¼	¼	3	20	49	23	5																														
		½	3	23	43	24	7																														
	B4 ¼	¼	0	5	21	52	22																														
		½	-1	5	23	46	27																														
	B5 ¼	¼	0	0	6	23	71																														
		½	-2	-1	6	26	71																														
	B1lin	¼	77	19	4	0	-1																														
		½	76	21	4	1	-2																														
	B2lin	¼	19	49	23	7	1																														
		½	23	46	23	7	1																														
	B3lin	¼	3	22	43	25	7																														
		½	4	23	39	26	8																														
B4lin	¼	0	6	22	43	28																															
	½	0	6	23	43	28																															
B5lin	¼	0	1	6	23	70																															
	½	0	0	5	27	68																															

½ - mid-span; ¼ - quarter-span; lin - line load; 4P - 4-point load

Fig. B.26 to Fig. B.31 present the vertical displacement distribution relatively to the highest displacement recorded for each beam, in each specimen. The percentage associated with each beam, regardless of the load case, was computed dividing the vertical displacement associated with the beam in question for the various load cases by the highest displacement recorded for the loaded beam. Thus, for the case of S1 when B1 is loaded, all displacements were divided by the displacement measured at B1 mid-span when the point load is acting on that location (since that was the highest recorded).

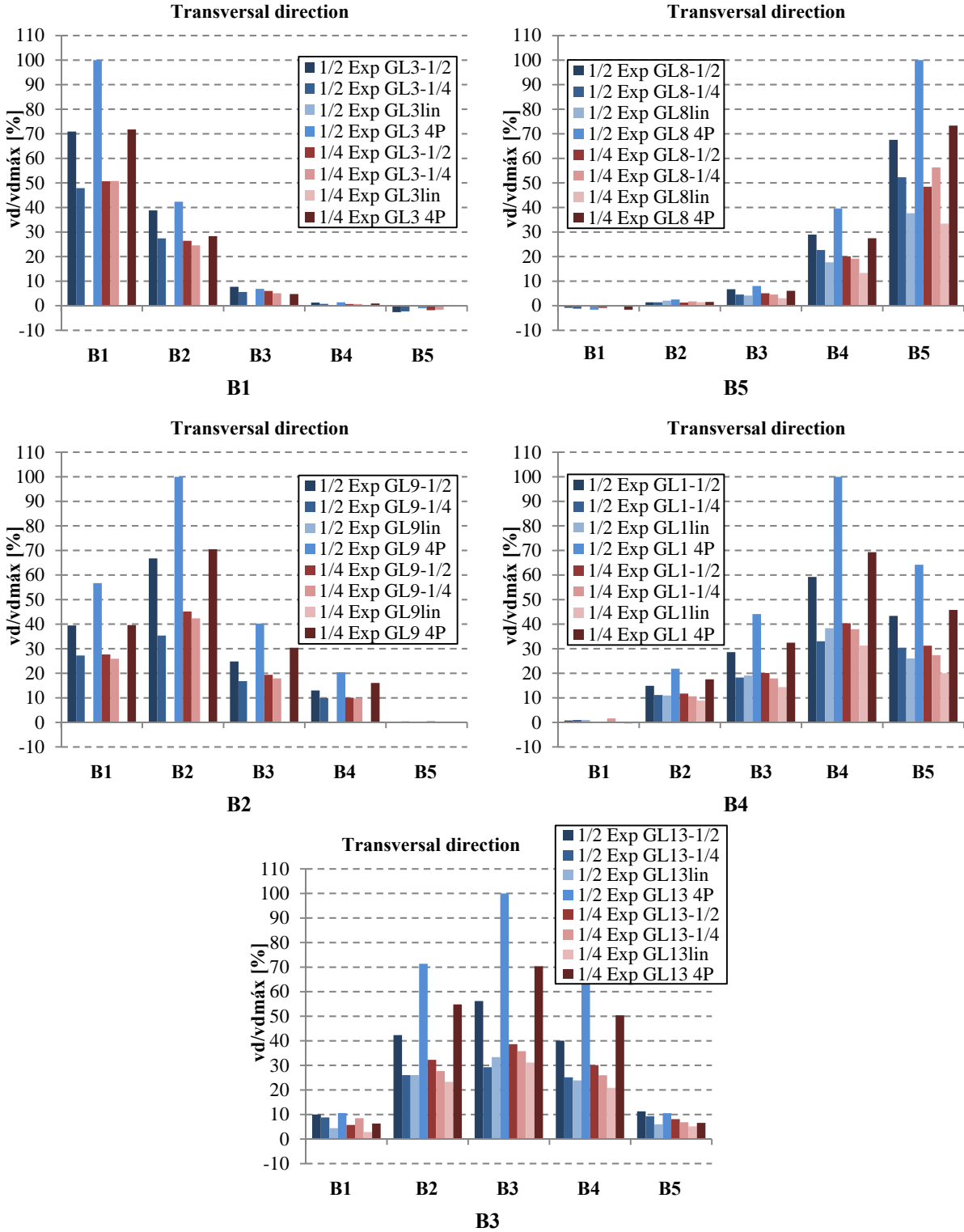


Fig. B.26 – Vertical displacement relatively to the higher displacement for each beam in S1-BSp considering 4P loading

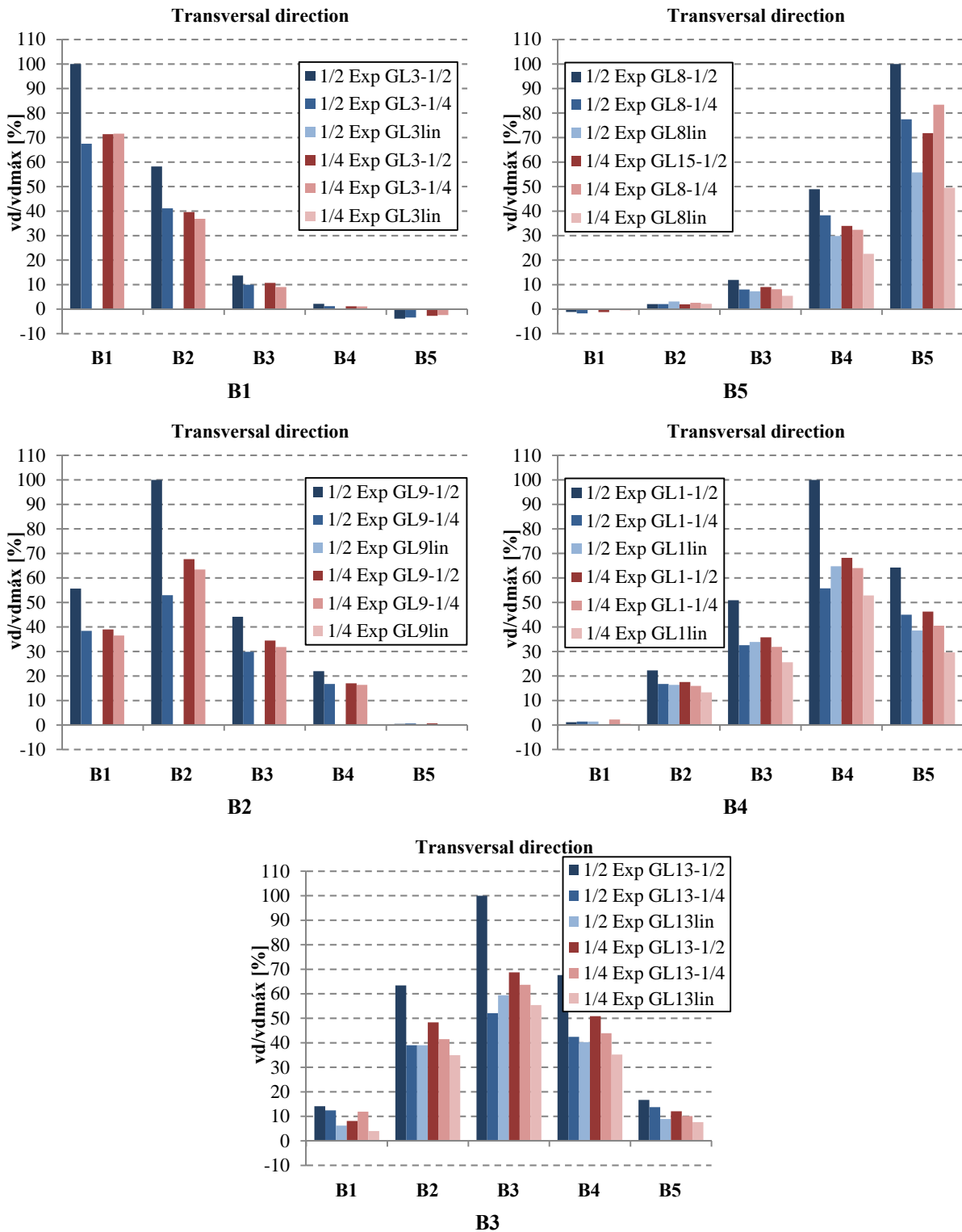


Fig. B.27 – Vertical displacement relatively to the higher displacement for each beam in S1-BSp disregarding 4P loading

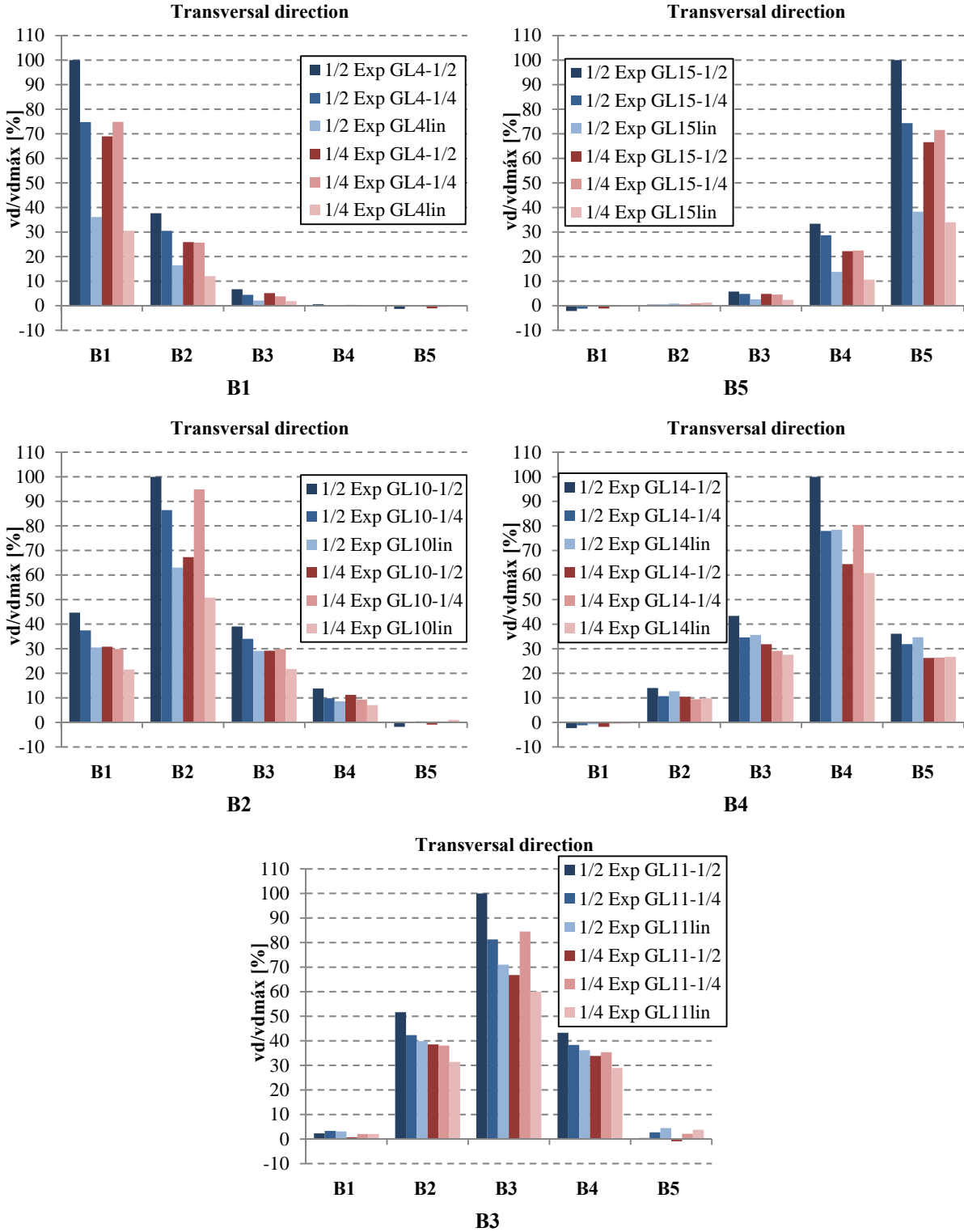


Fig. B.28 – Vertical displacement relatively to the higher displacement for each beam in S2-LWAC

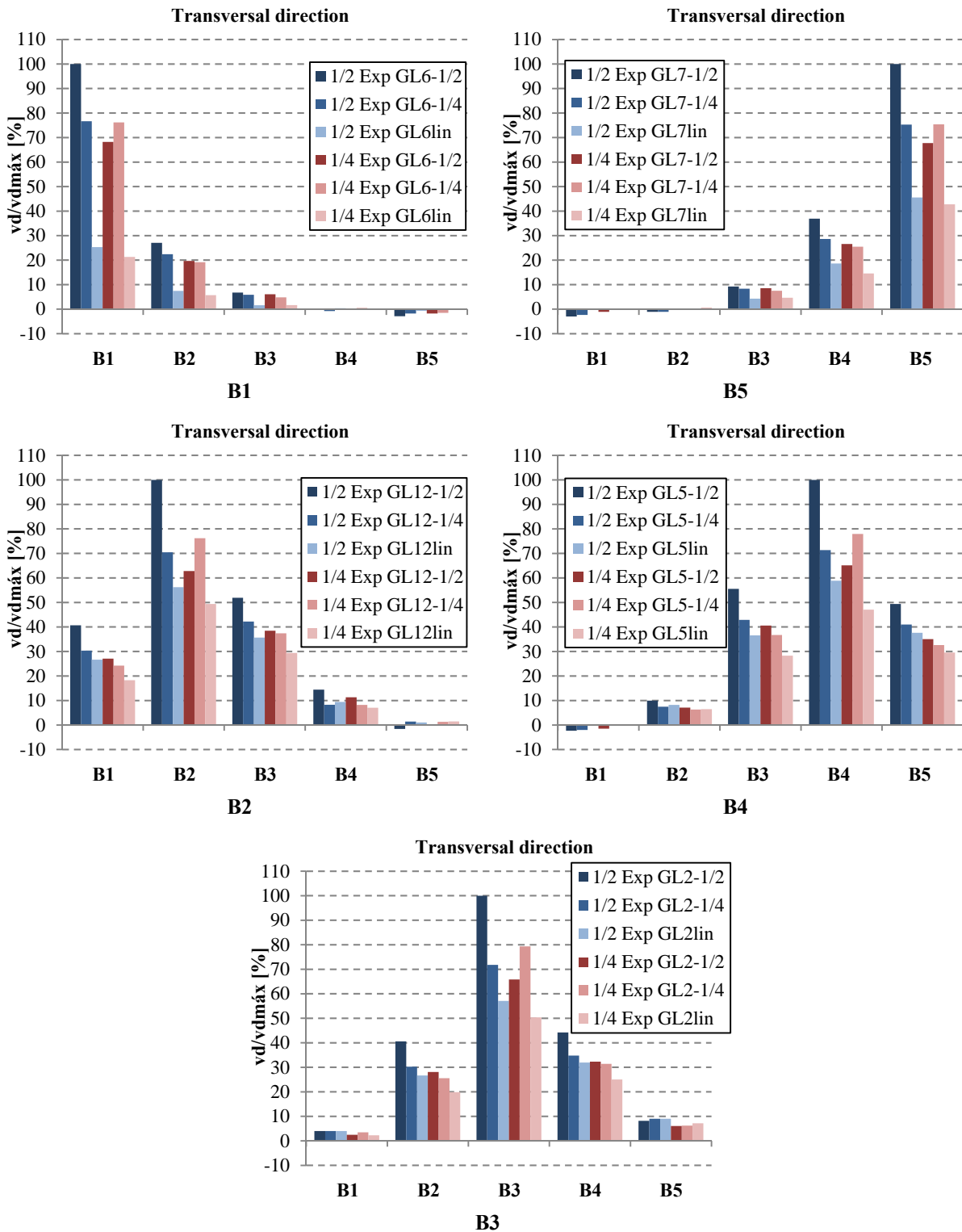


Fig. B.29 – Vertical displacement relatively to the higher displacement for each beam in S3-hc=0.03m

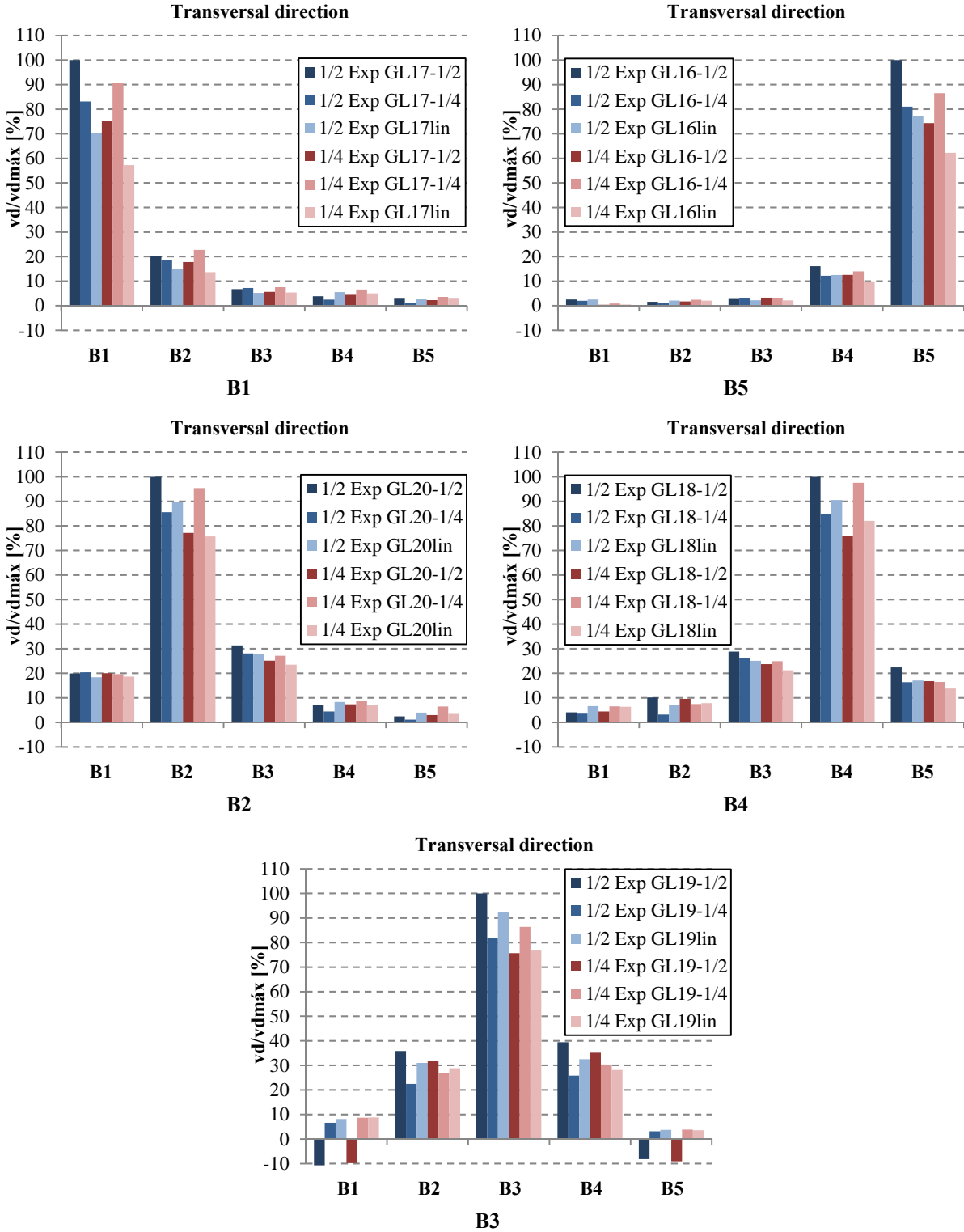


Fig. B.30 – Vertical displacement relatively to the higher displacement for each beam in S4-L=2.00m

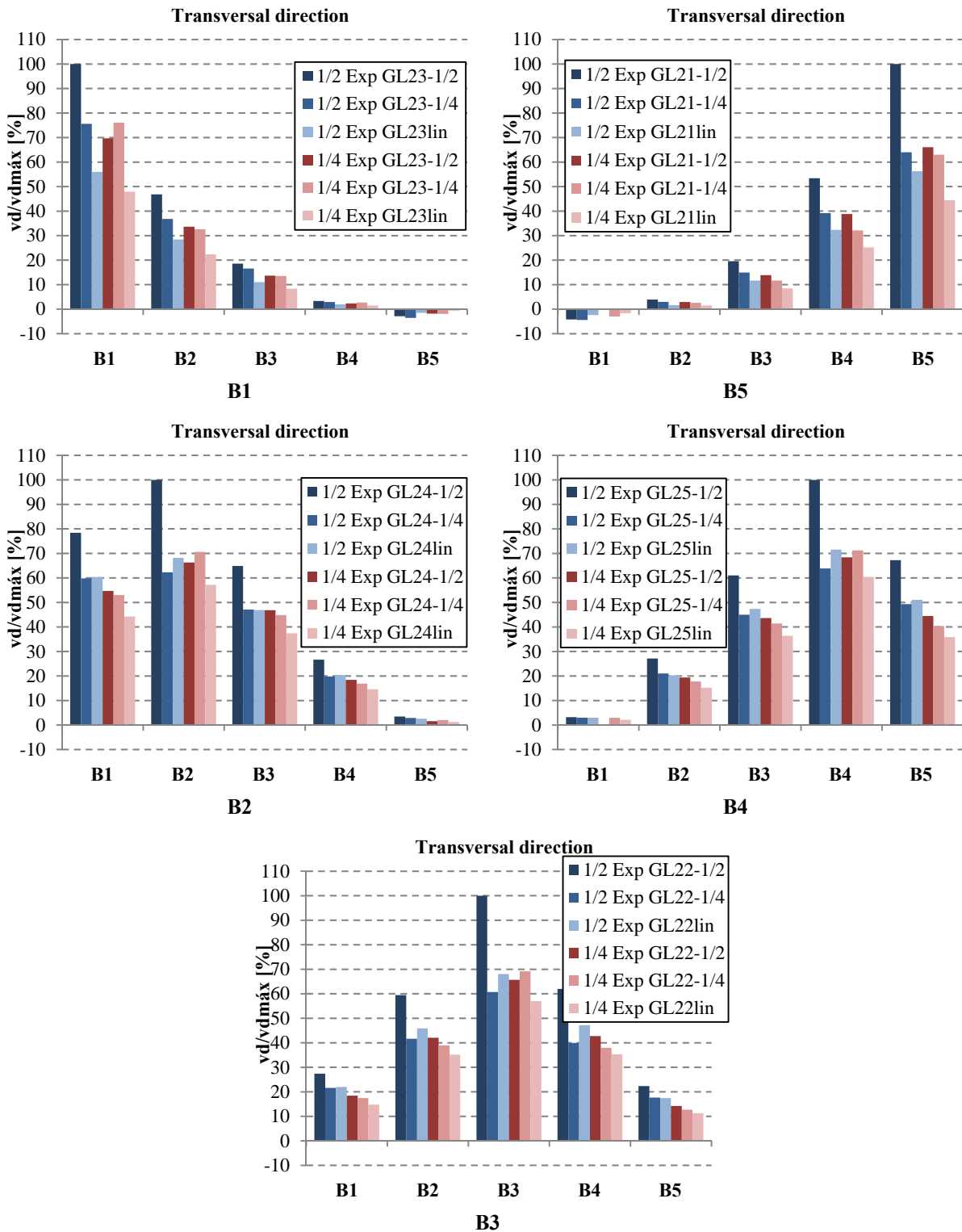


Fig. B.31 – Vertical displacement relatively to the higher displacement for each beam in S5-L=6.00m

The tridimensional deflection of the five specimens was obtained by joining the data of vertical displacements read at mid- and quarter-span. In the case of the symmetric load cases, the assumption of symmetric deflection relatively to the mean mid-span was adopted and vertical displacement at three quarters-span taken as the same as it was read at quarter-span. Fig. B.32 to Fig. B.46 summarize the graphs for all the specimens by load case and loaded beam.

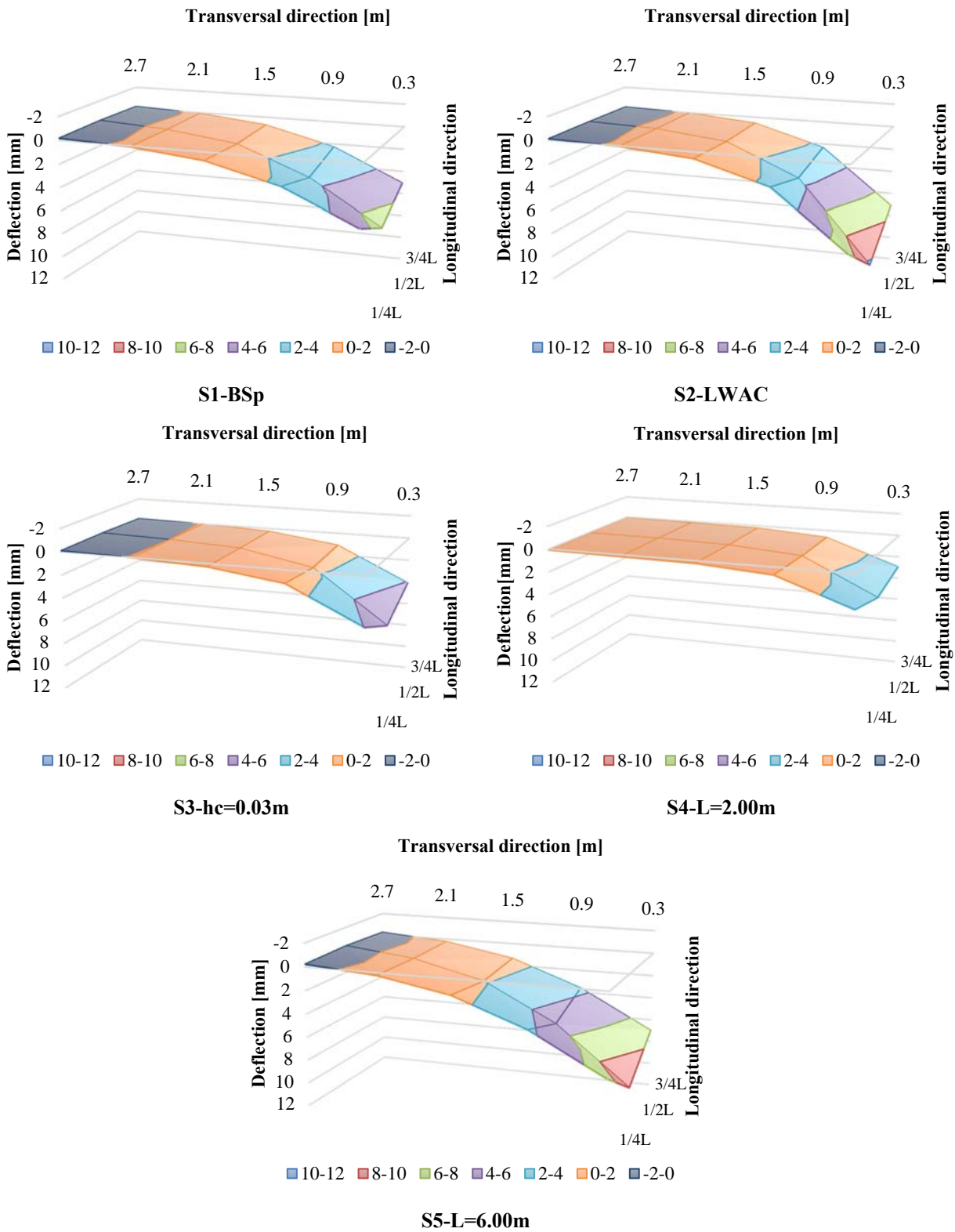


Fig. B.32 – Slab deflections: B1 ½

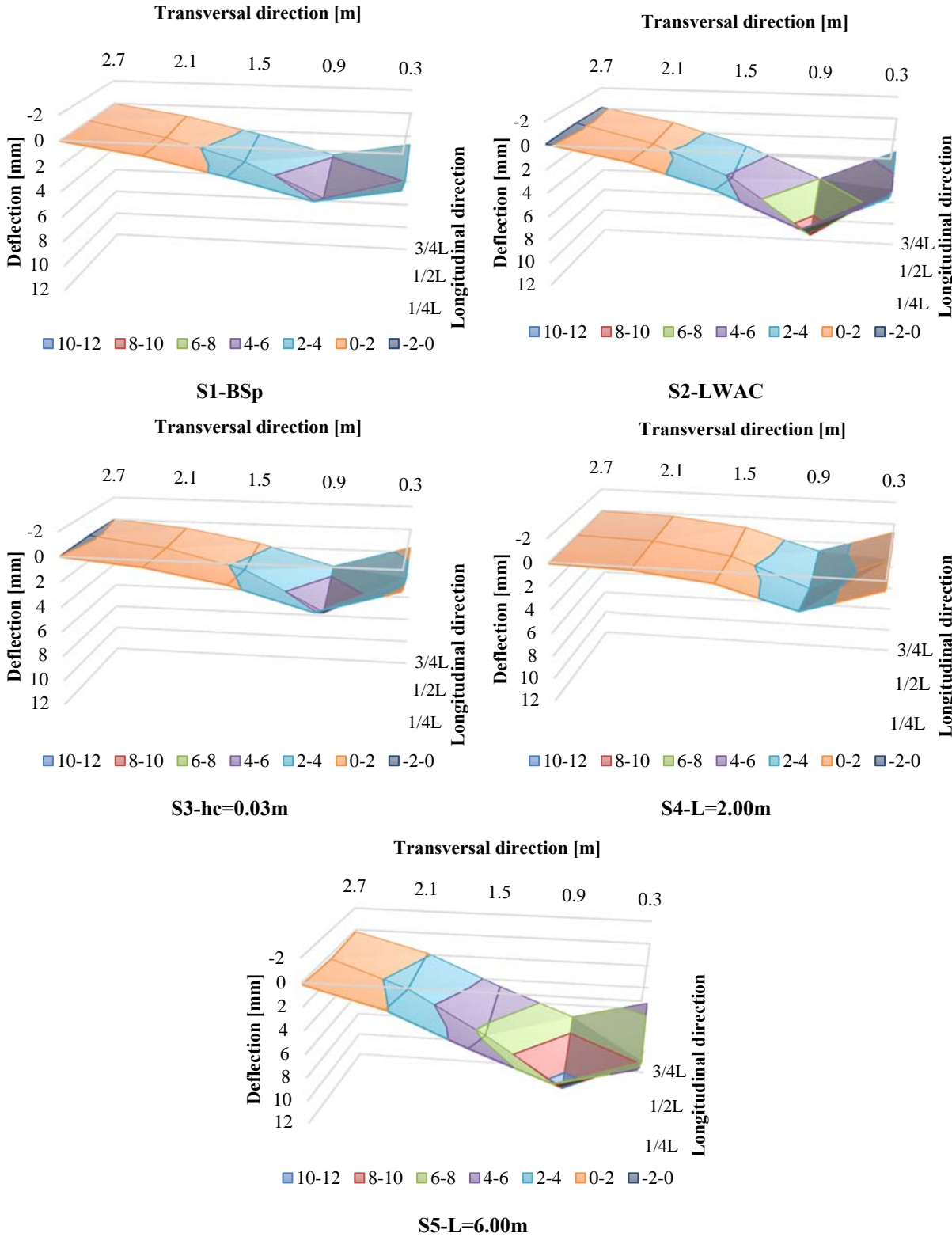


Fig. B.33 – Slab deflections: B2 ½

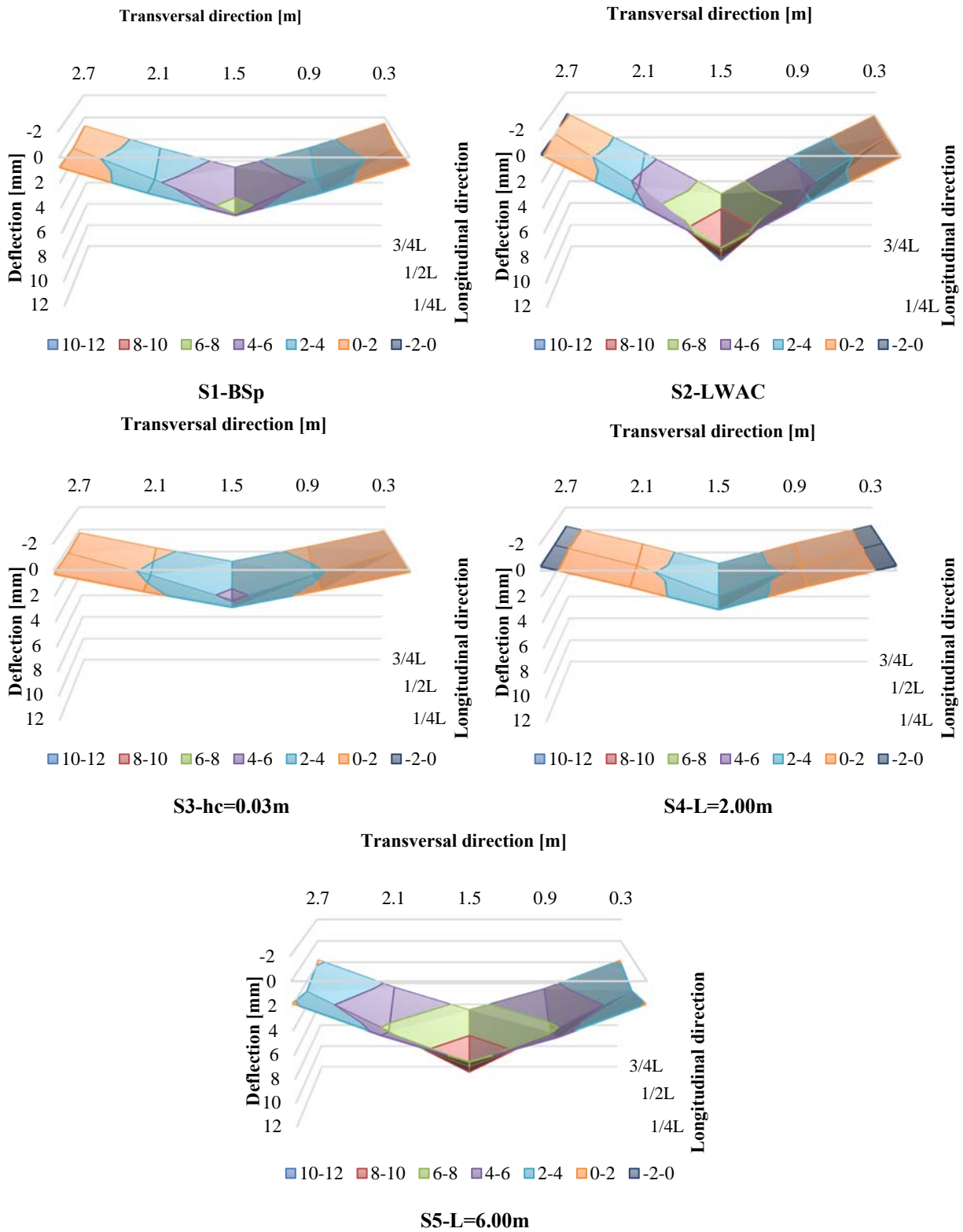


Fig. B.34 – Slab deflections: B3 ½

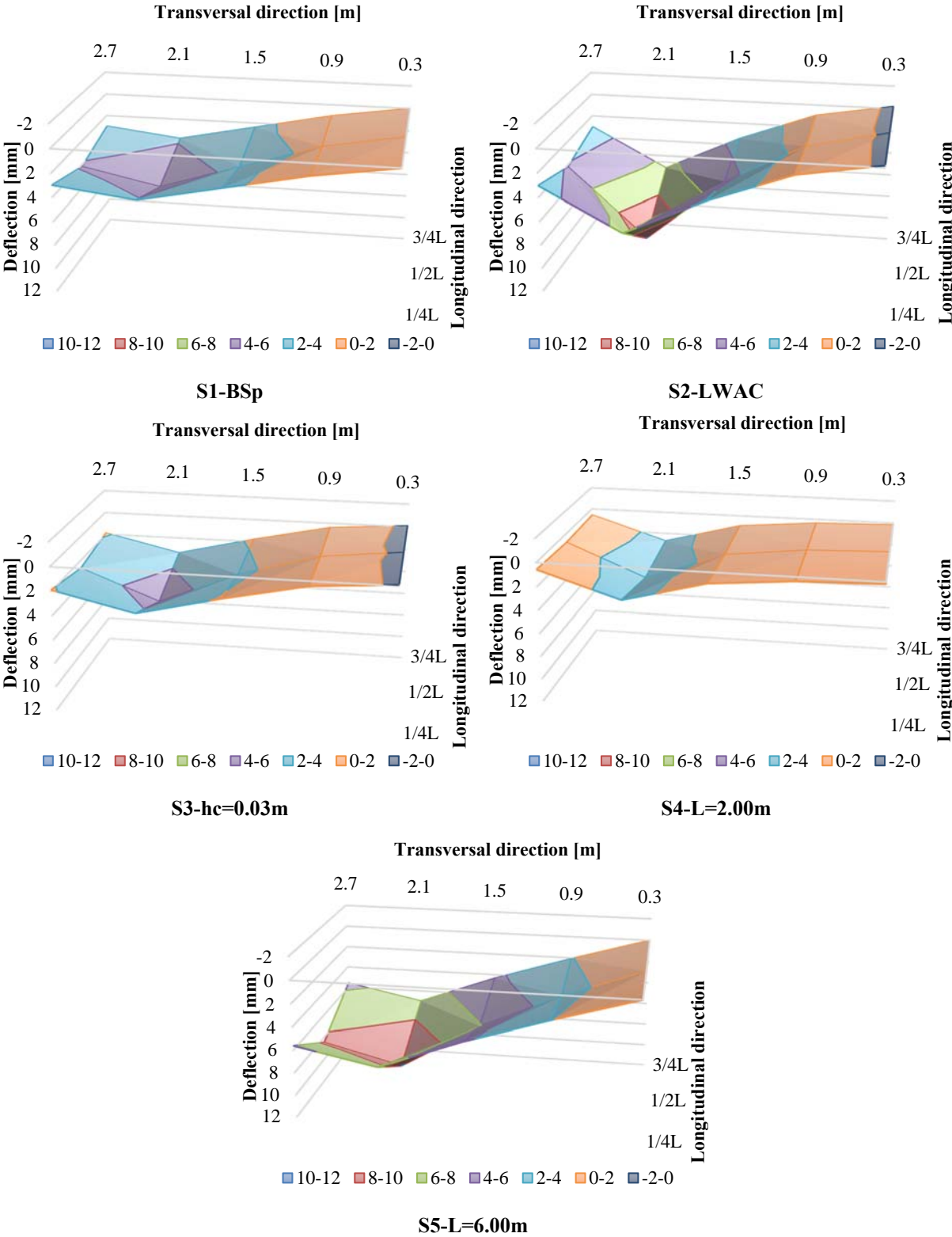


Fig. B.35 – Slab deflections: B4 ½

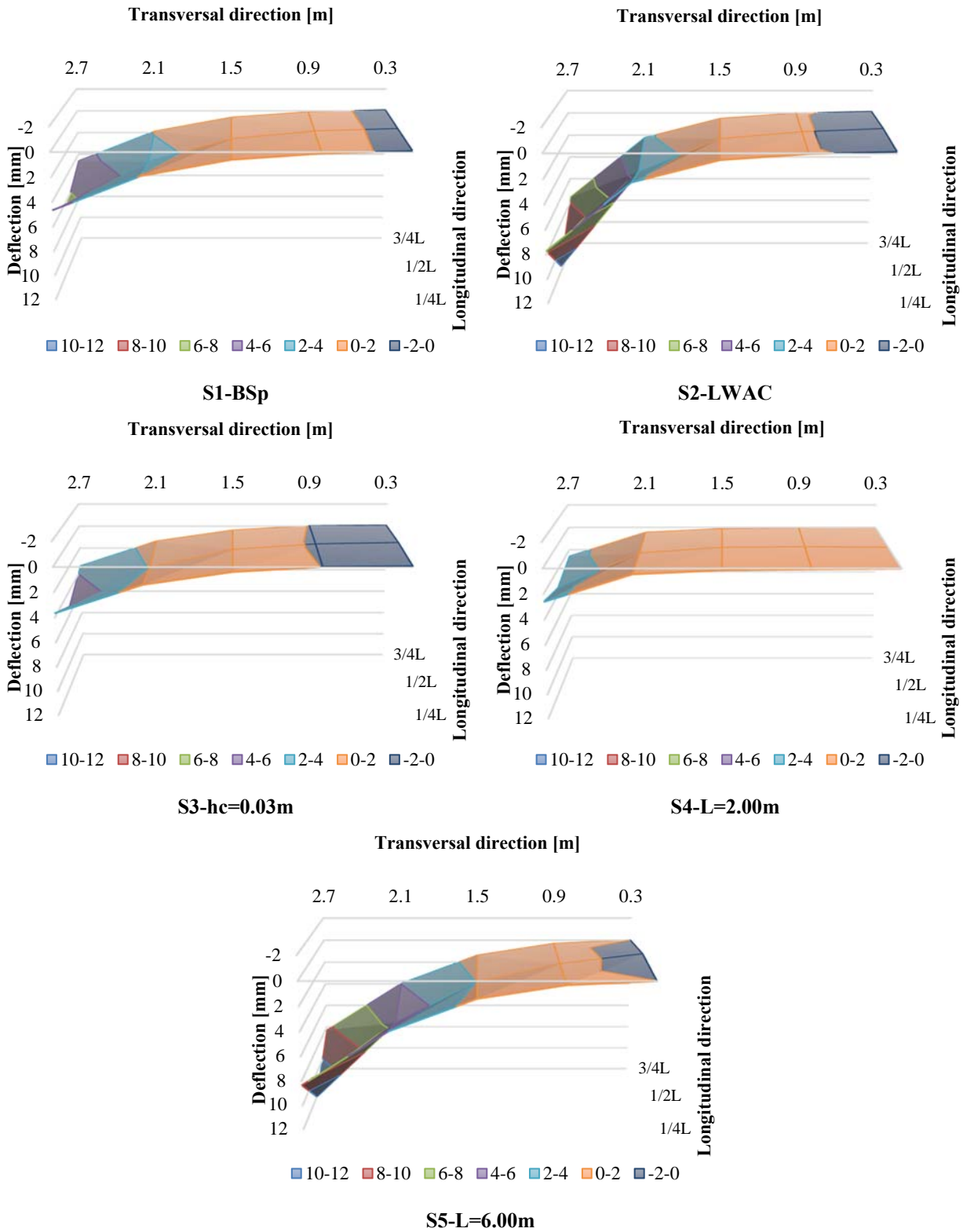


Fig. B.36 – Slab deflections: B5 ½

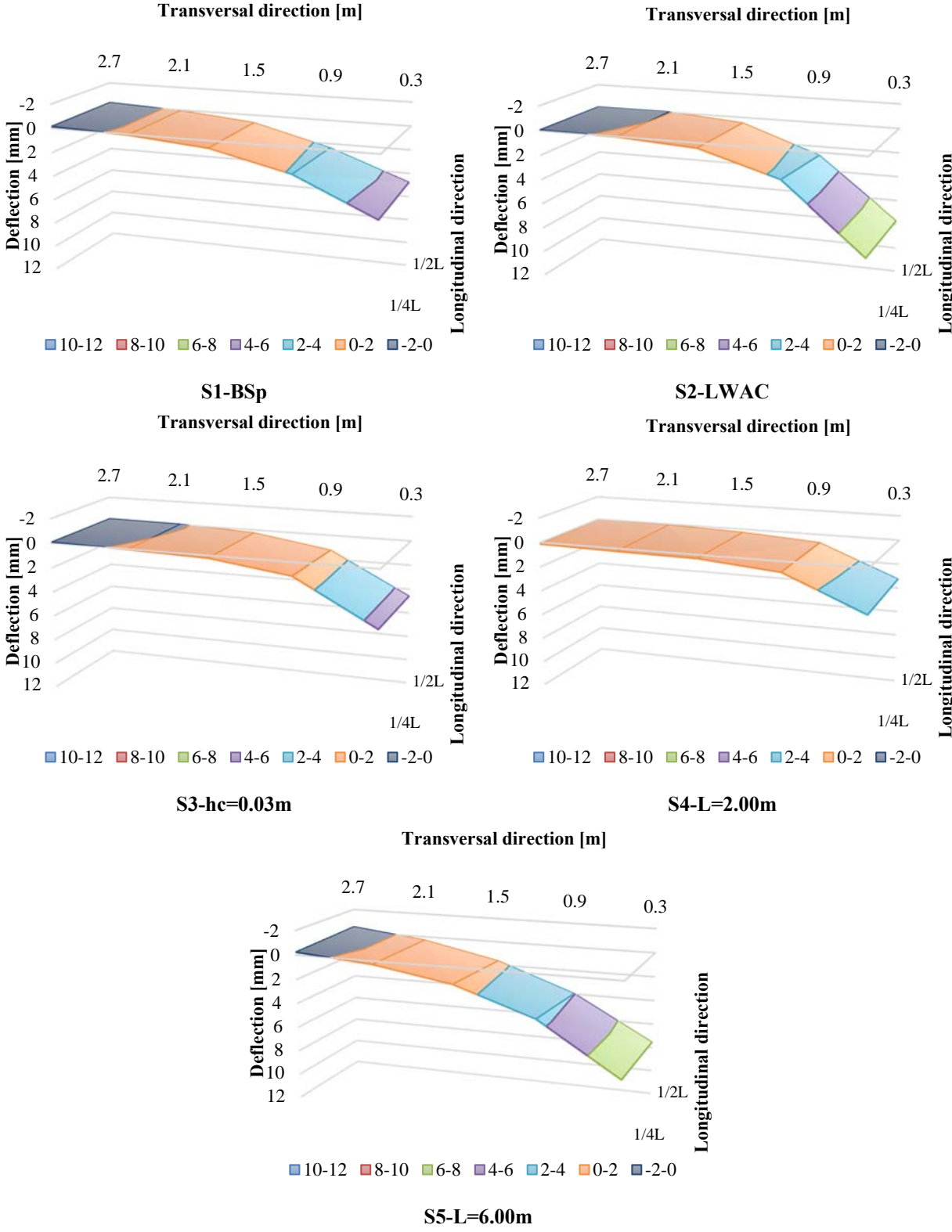


Fig. B.37 – Slab deflections: B1 ¼

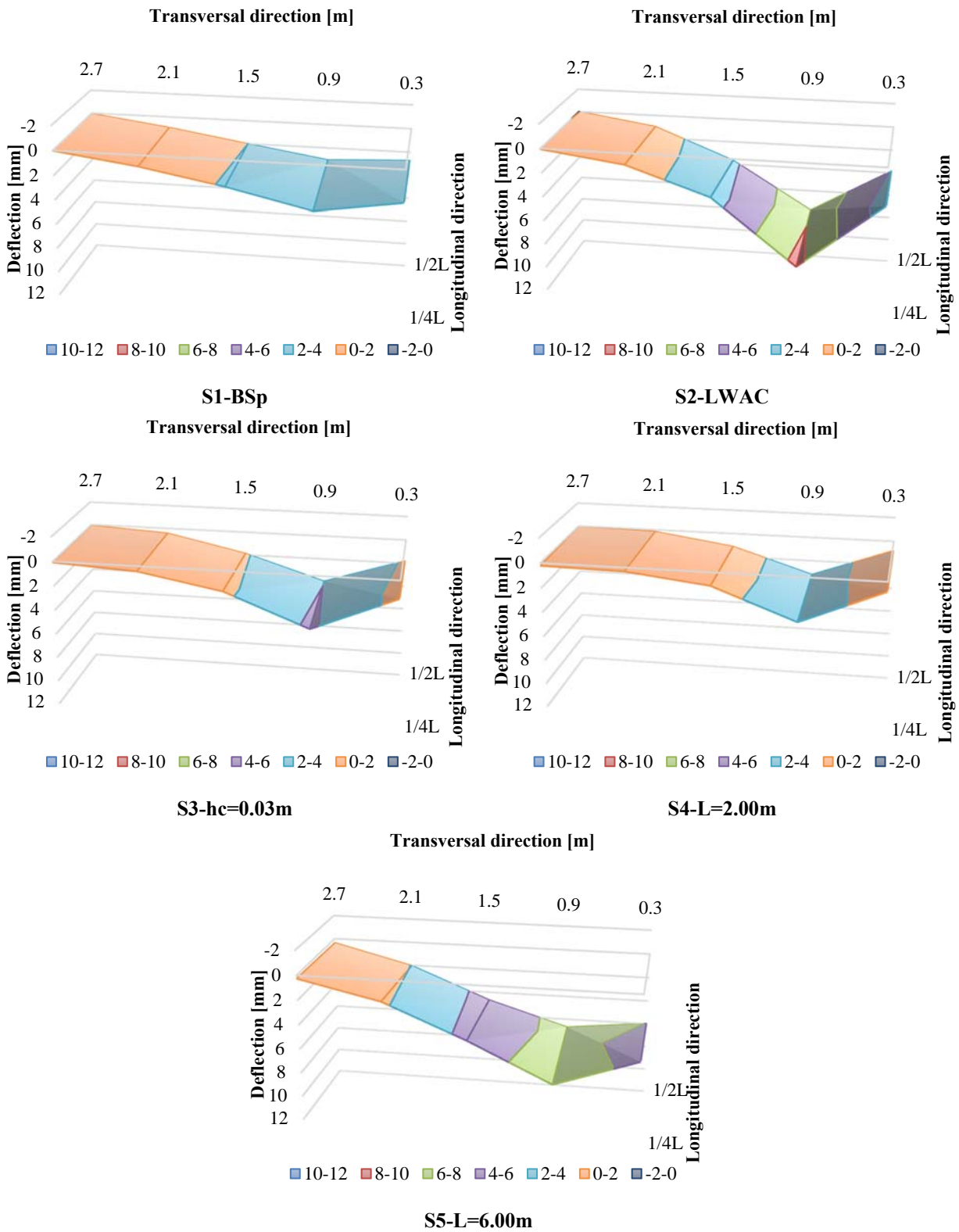


Fig. B.38 – Slab deflections: B2 ¼

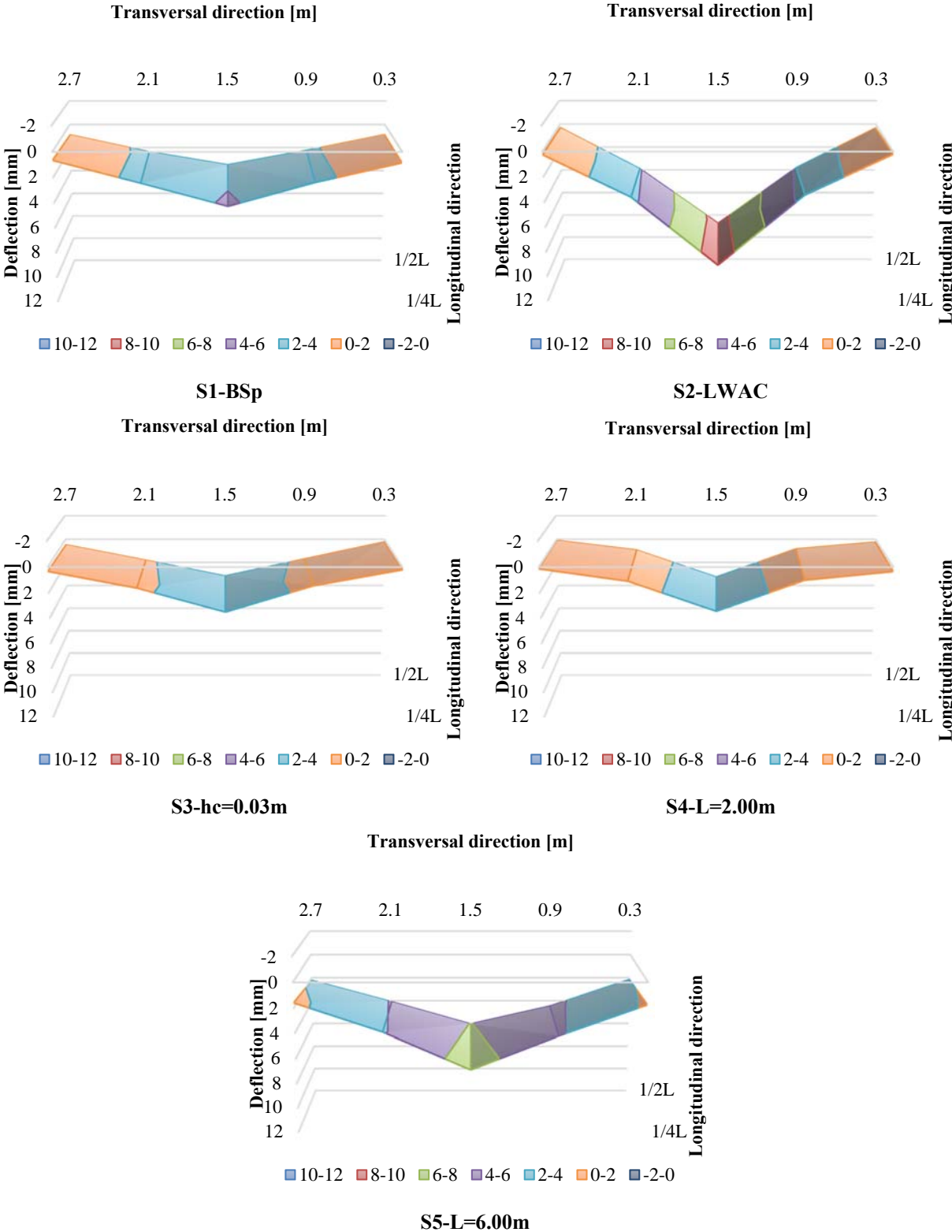


Fig. B.39 – Slab deflections: B3 ¼

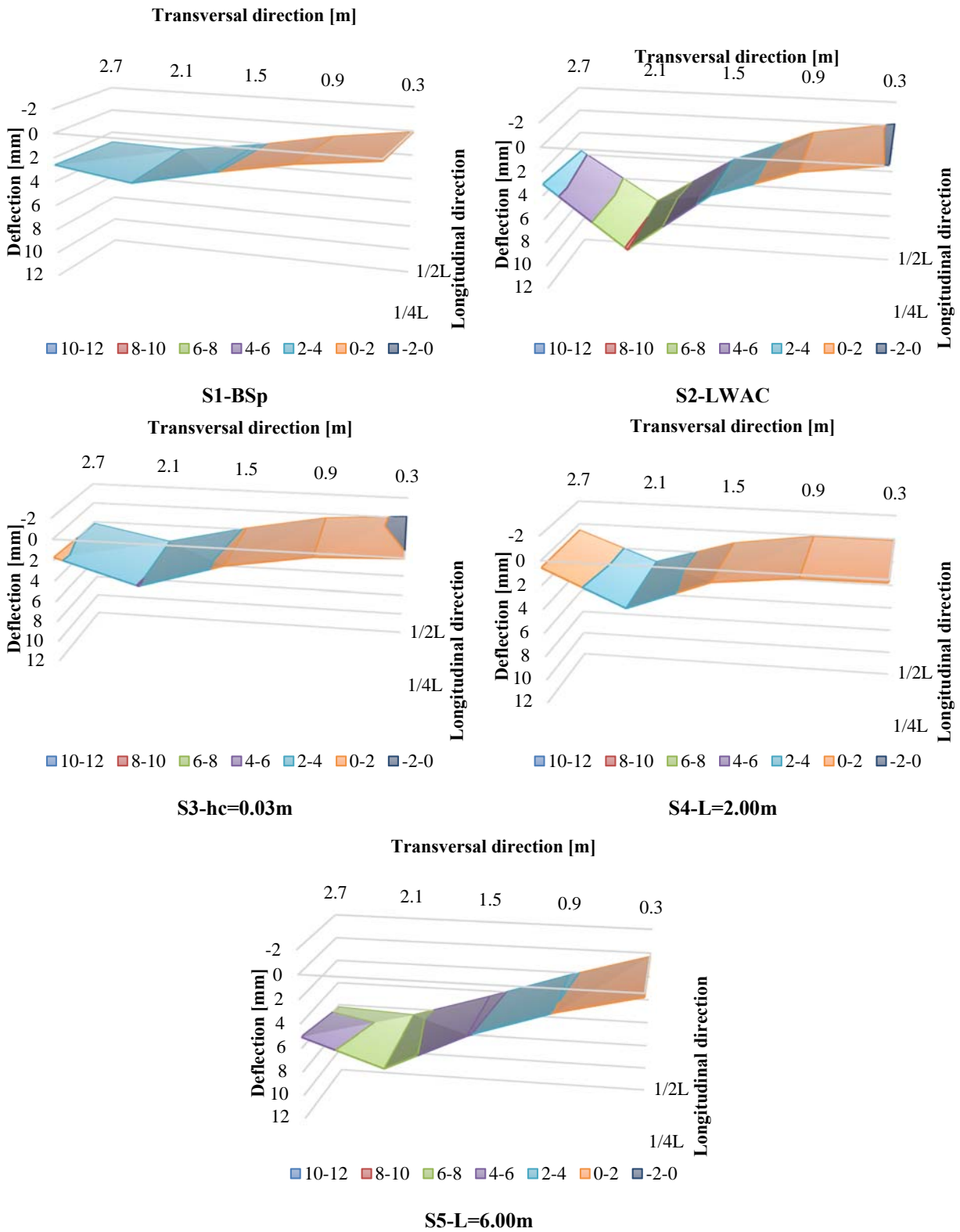


Fig. B.40 – Slab deflections: B4 ¼

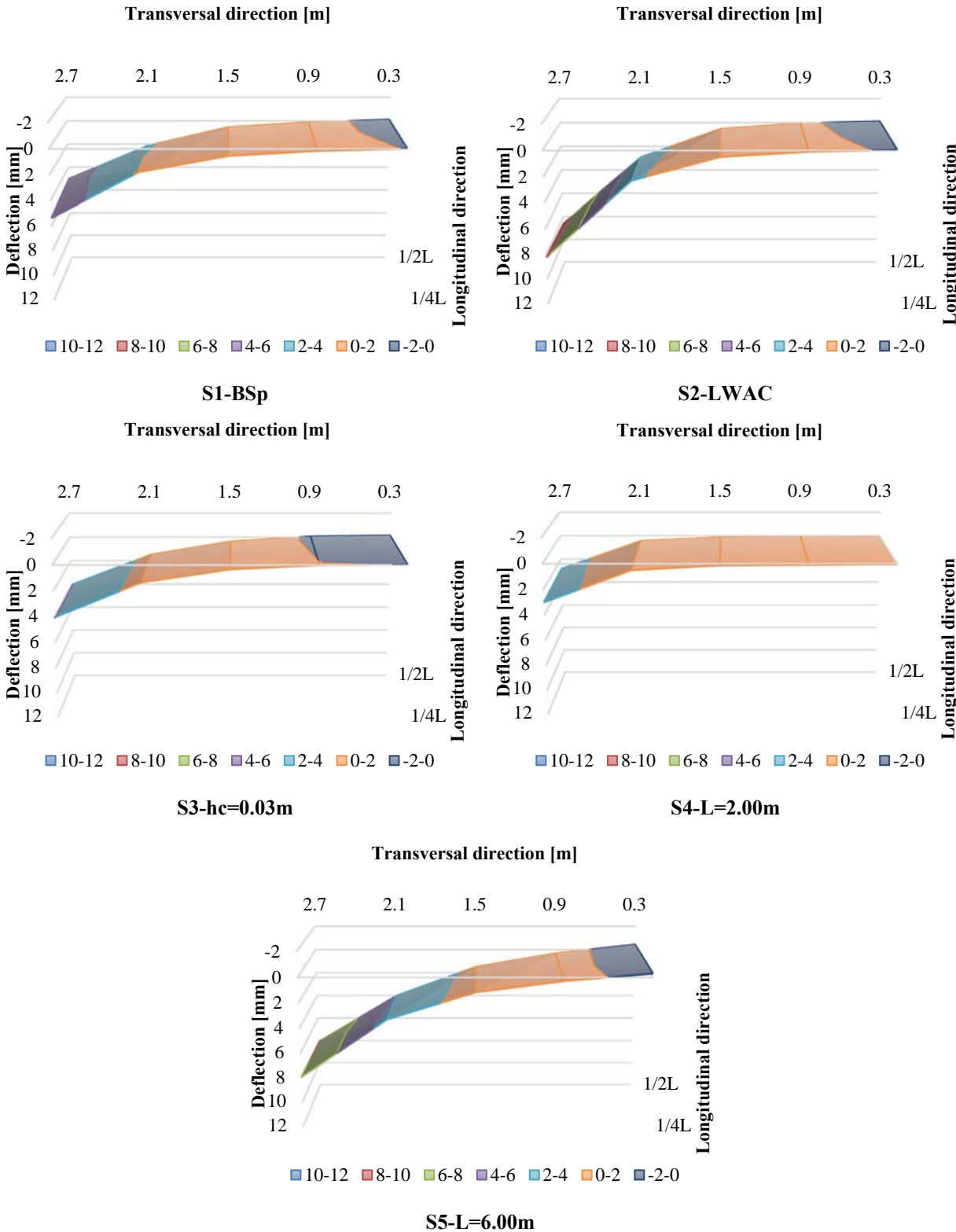


Fig. B.41 – Slab deflections: B5 ¼

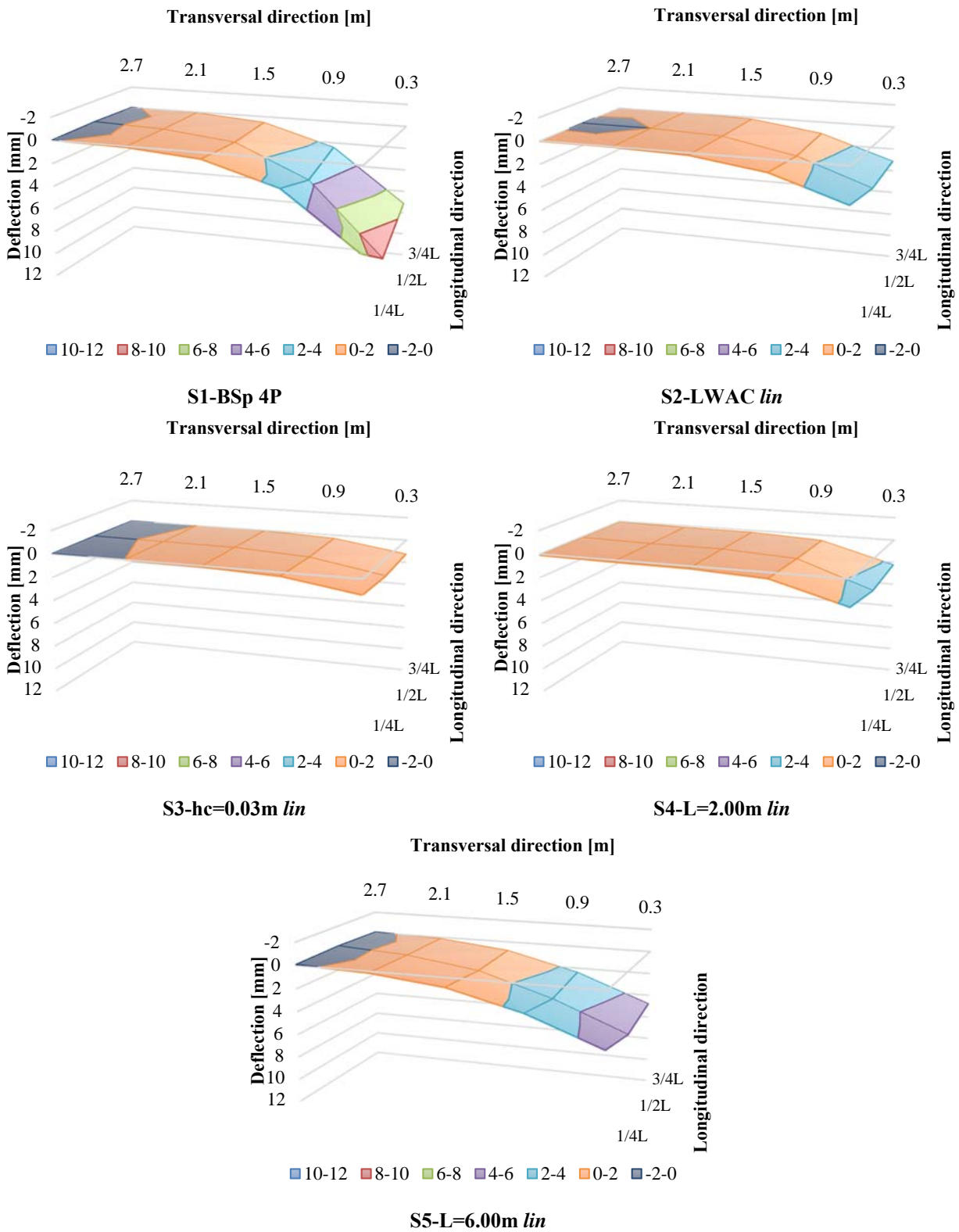


Fig. B.42 – Slab deflections: linear loading at B1

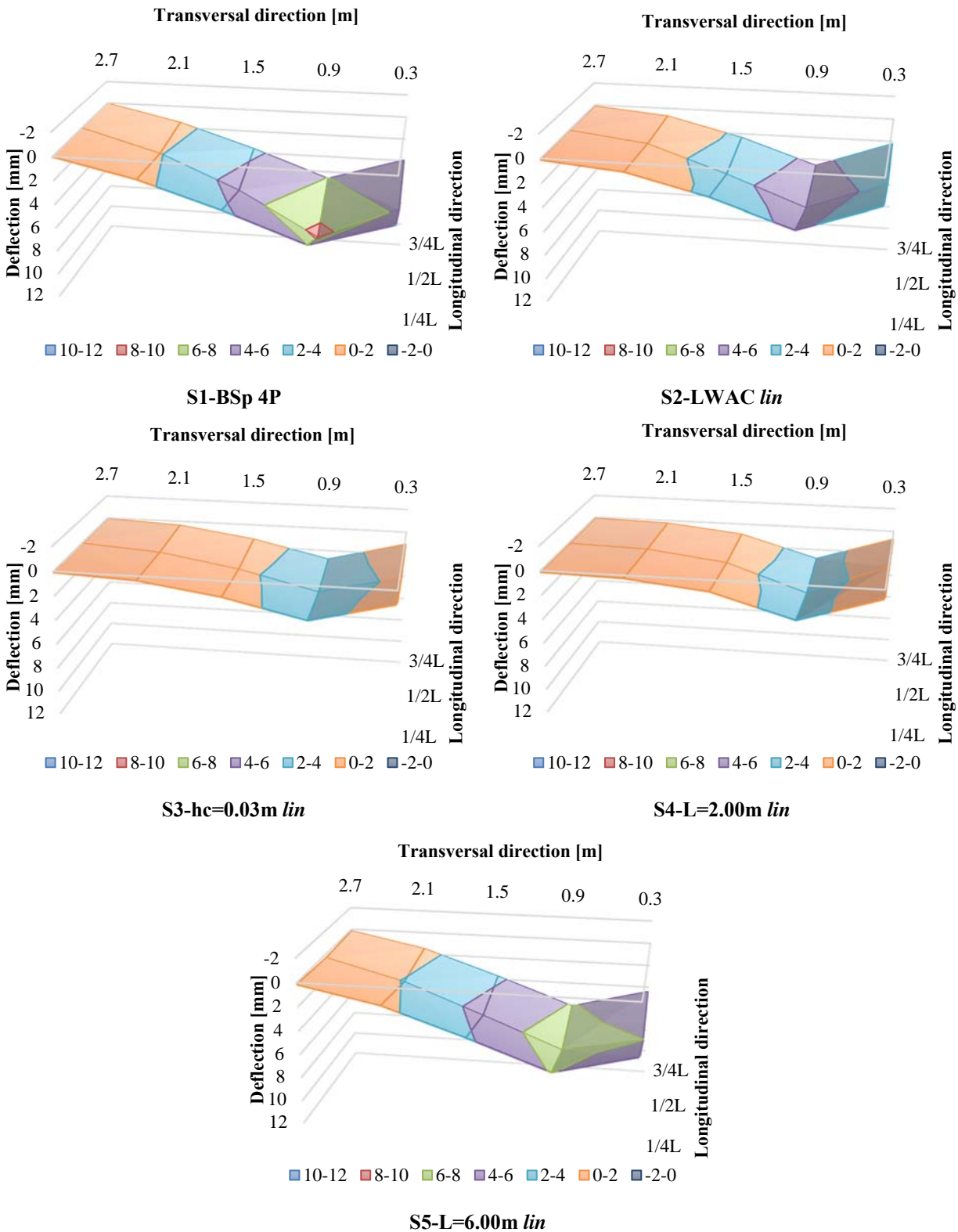


Fig. B.43 – Slab deflections: linear loading at B2

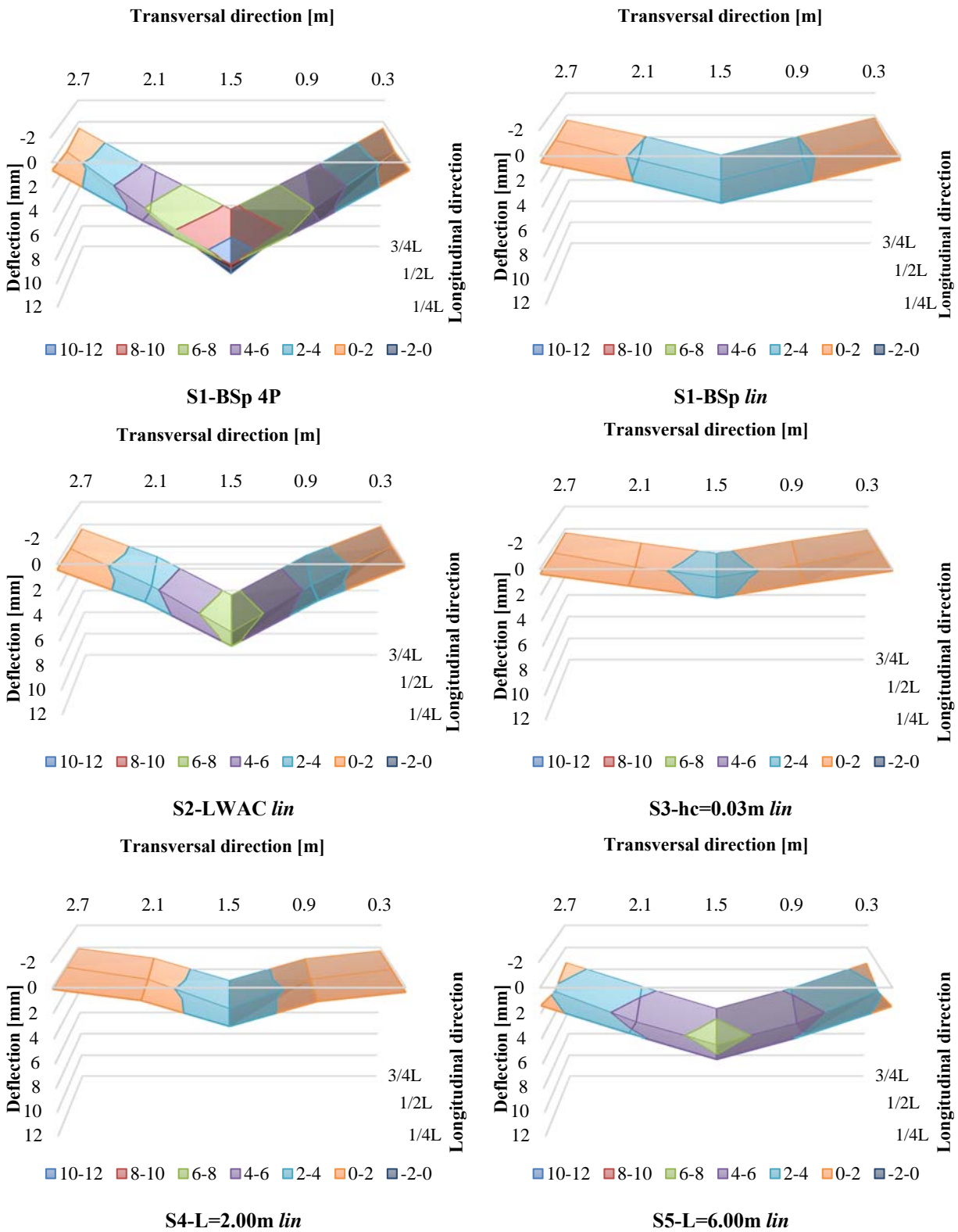


Fig. B.44 – Slab deflections: linear loading at B3

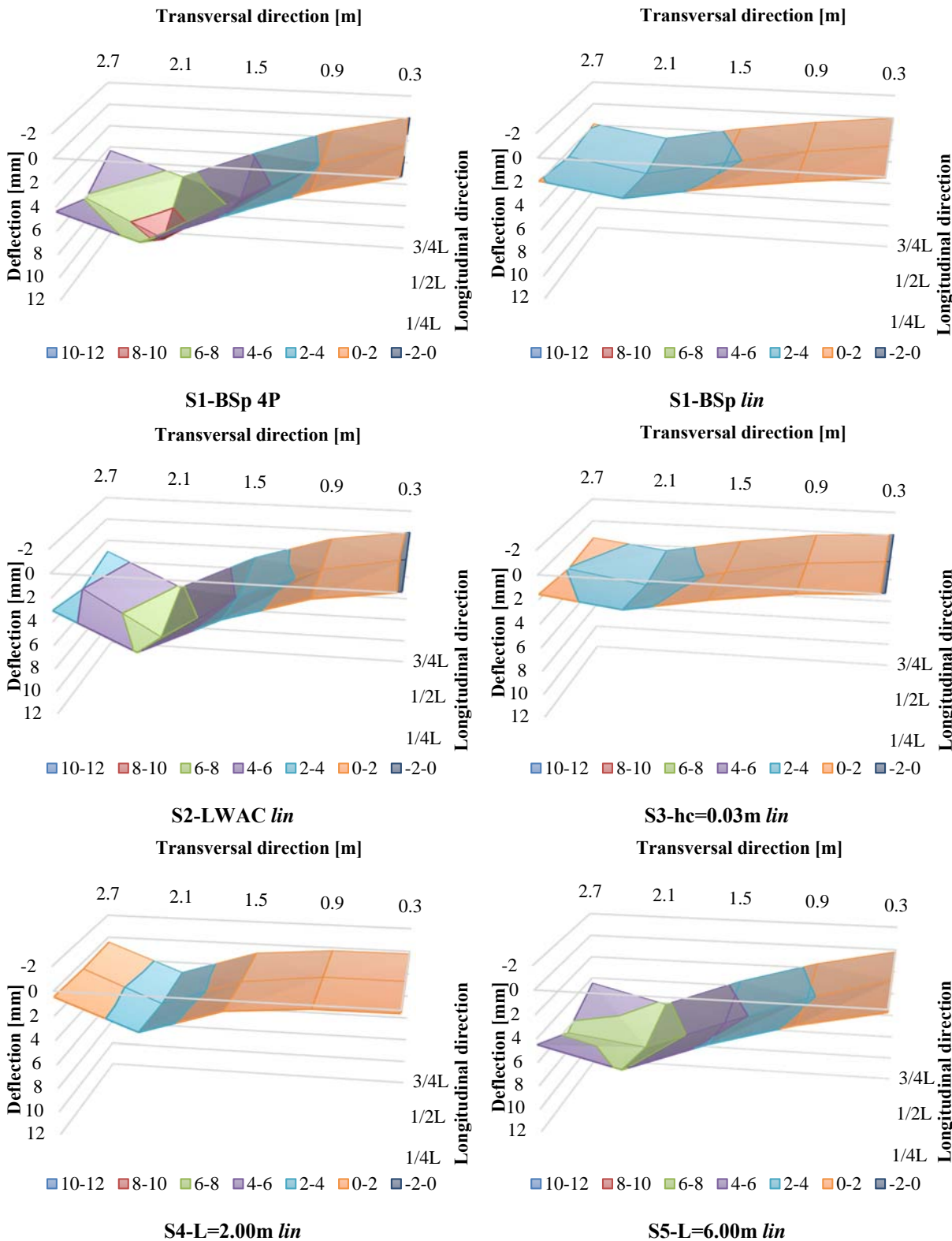


Fig. B.45 – Slab deflections: linear loading at B4

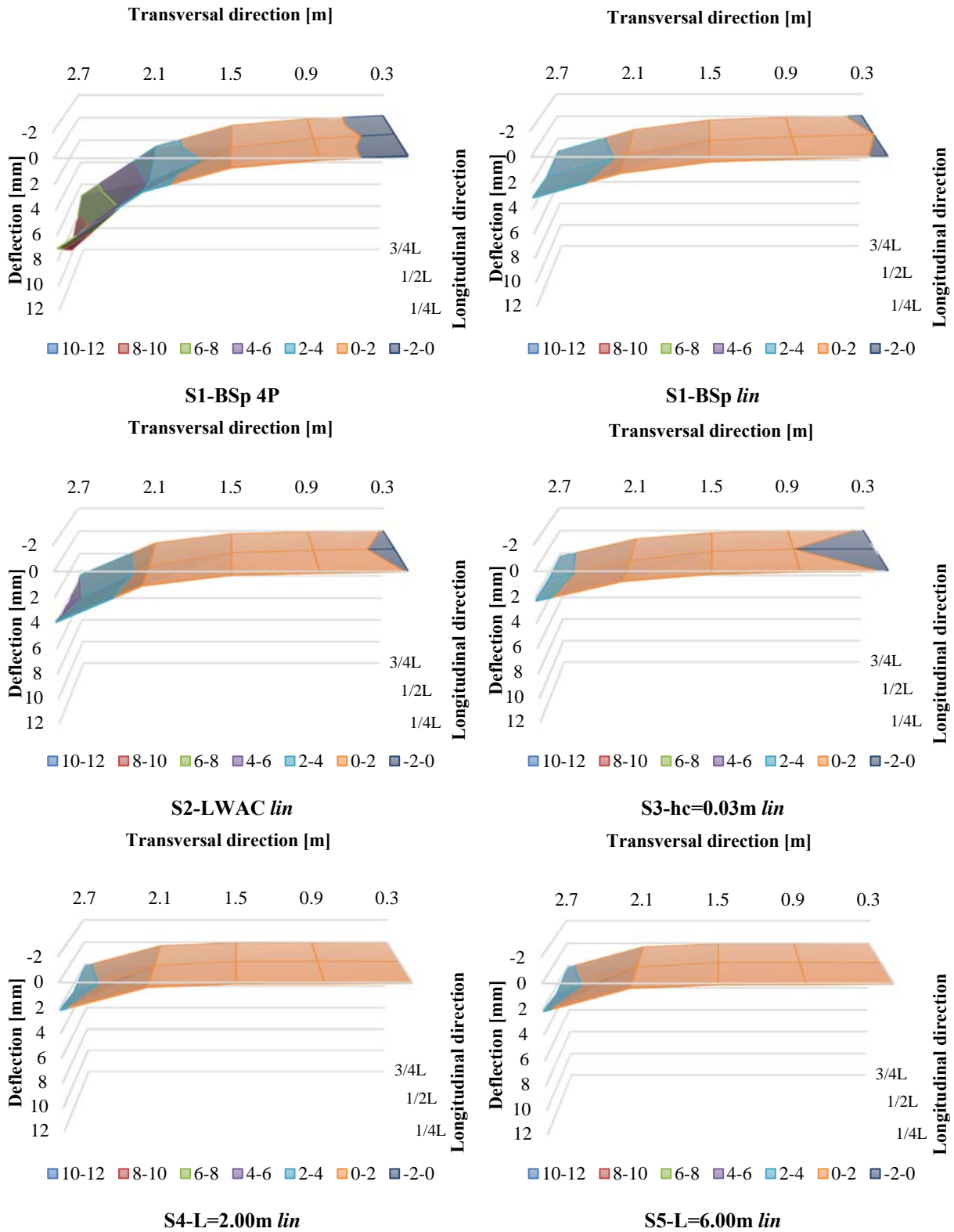


Fig. B.46 – Slab deflections: linear loading at B5

Concerning the beams longitudinal direction, Fig. B.47 to Fig. B.51 show the deflections of each beam for the various loading cases. The beams that were placed symmetrically with respect to the central beam are presented side-by-side (B1-B5 and B2-B4).

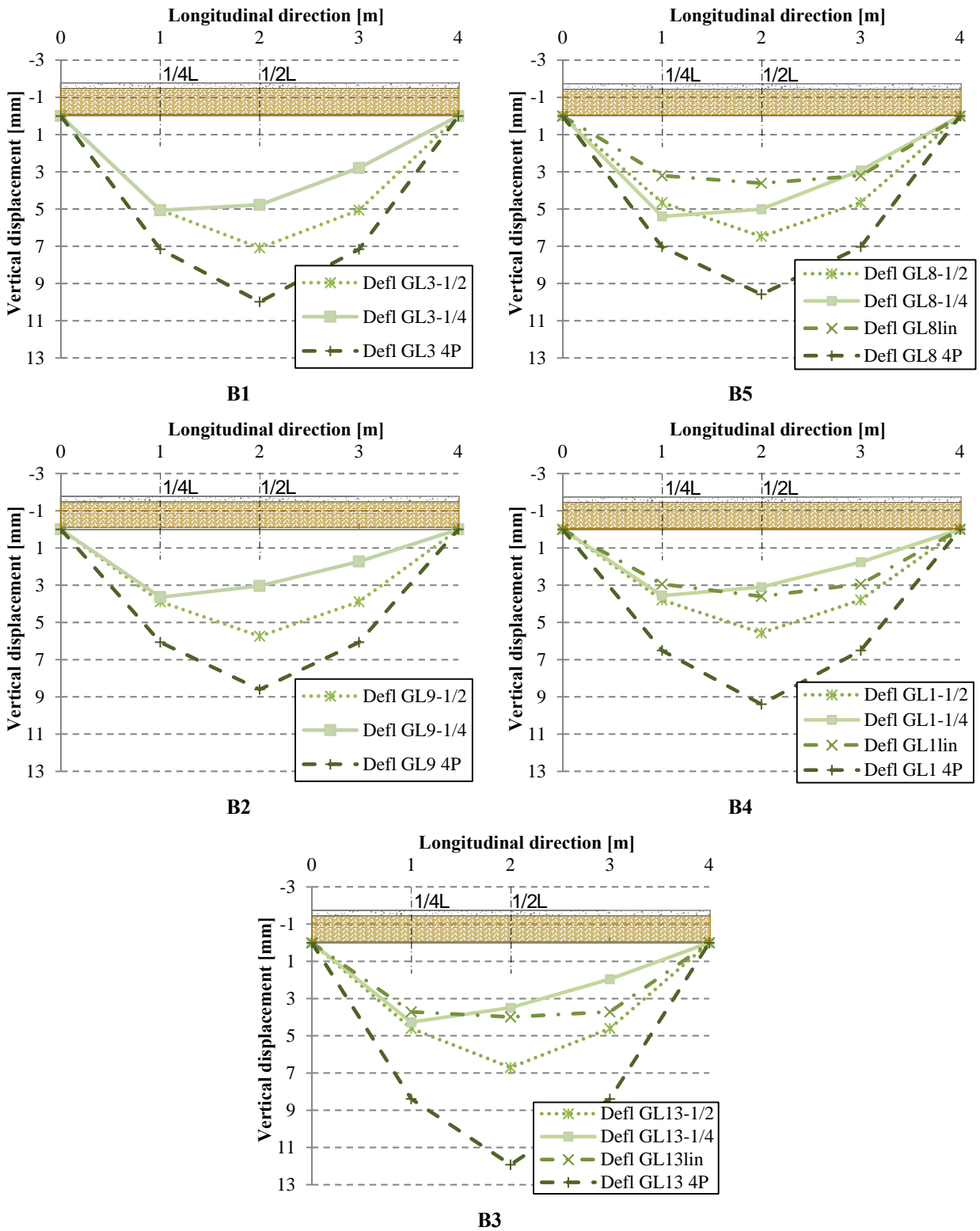


Fig. B.47 – Beams deflection in S1-BSp

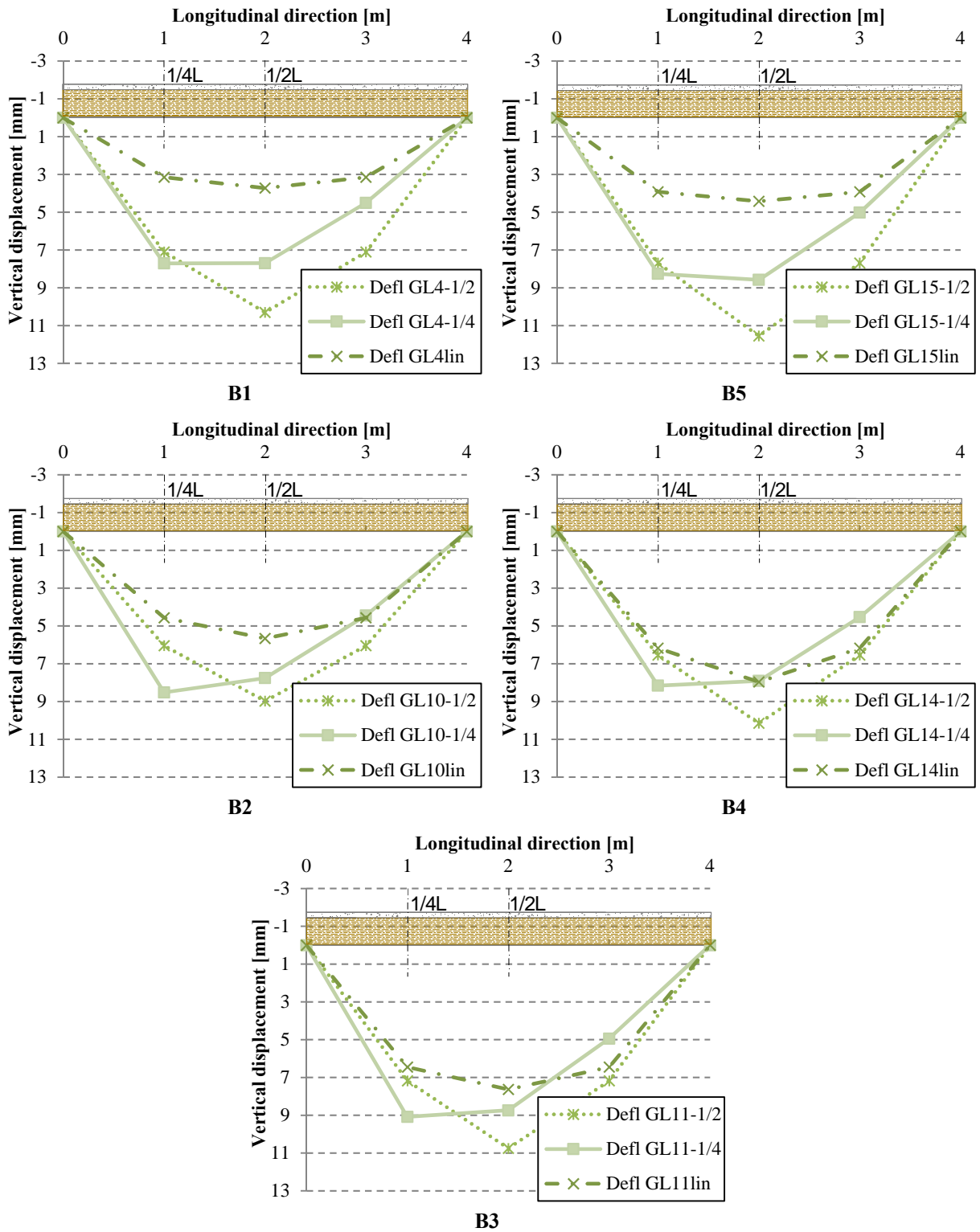


Fig. B.48 – Beams deflection in S2-LWAC

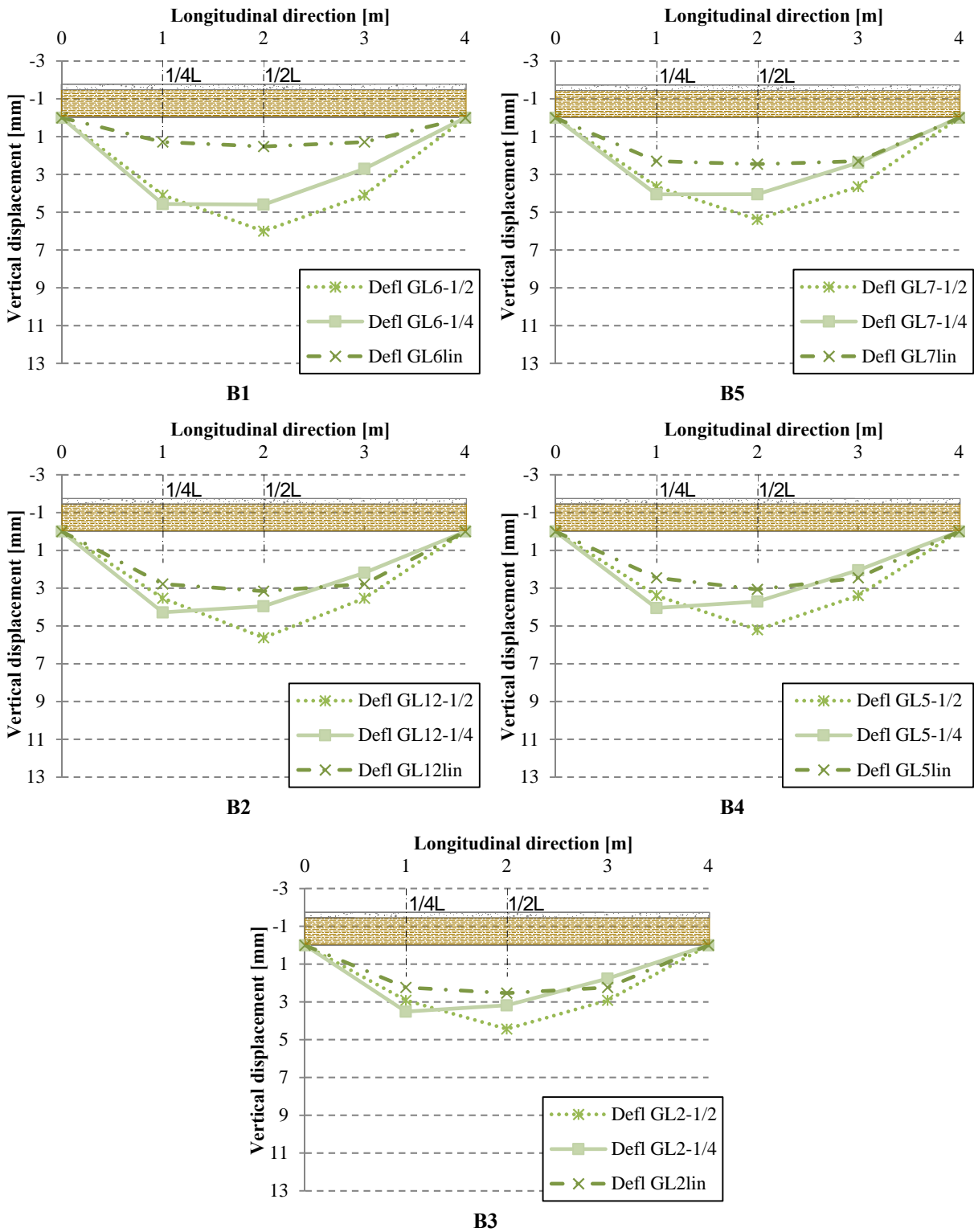


Fig. B.49 – Beams deflection in S3-hc=0.03m

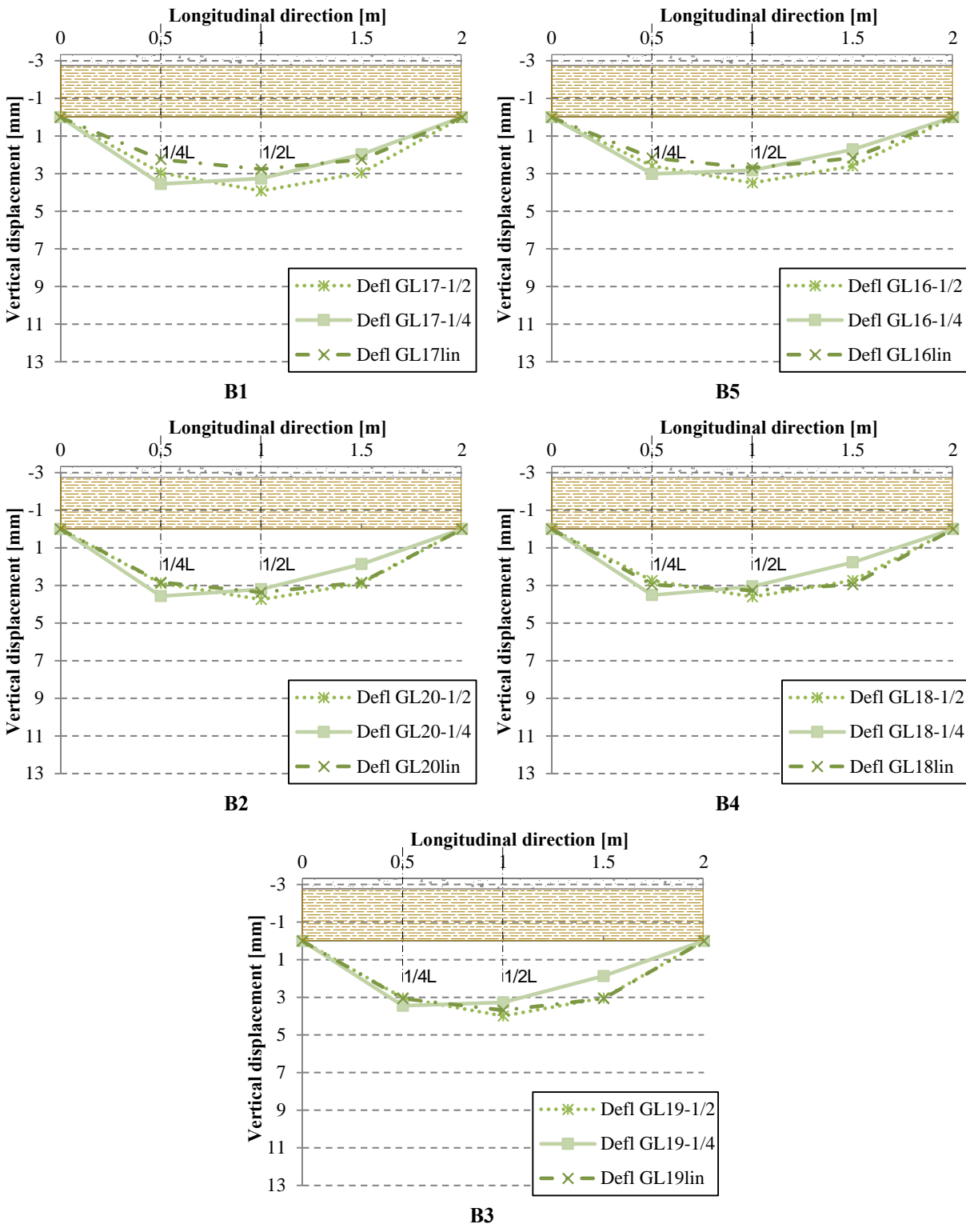


Fig. B.50 – Beams deflection in S4-L=2.00m

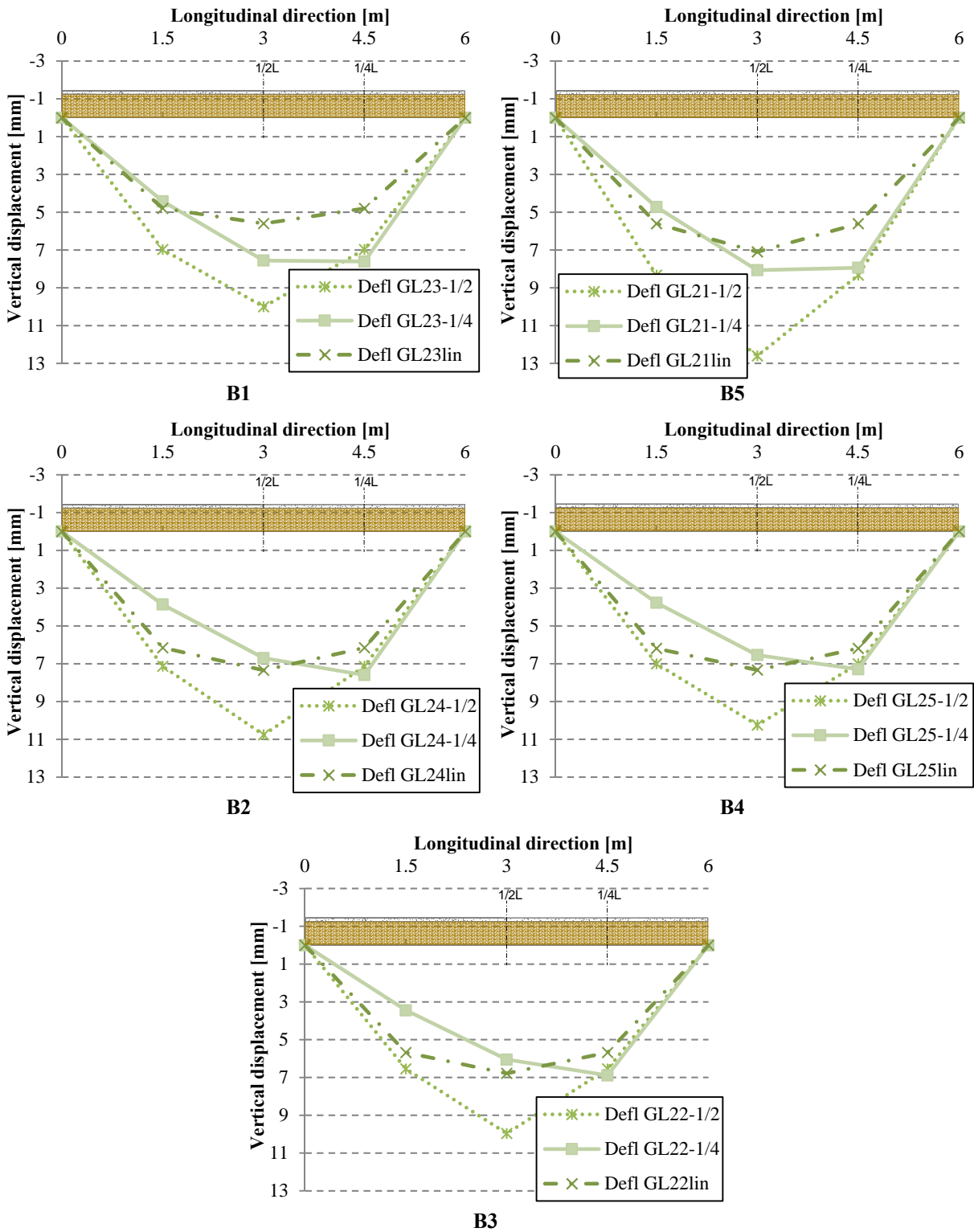


Fig. B.51 – Beams deflection in S5-L=6.00m

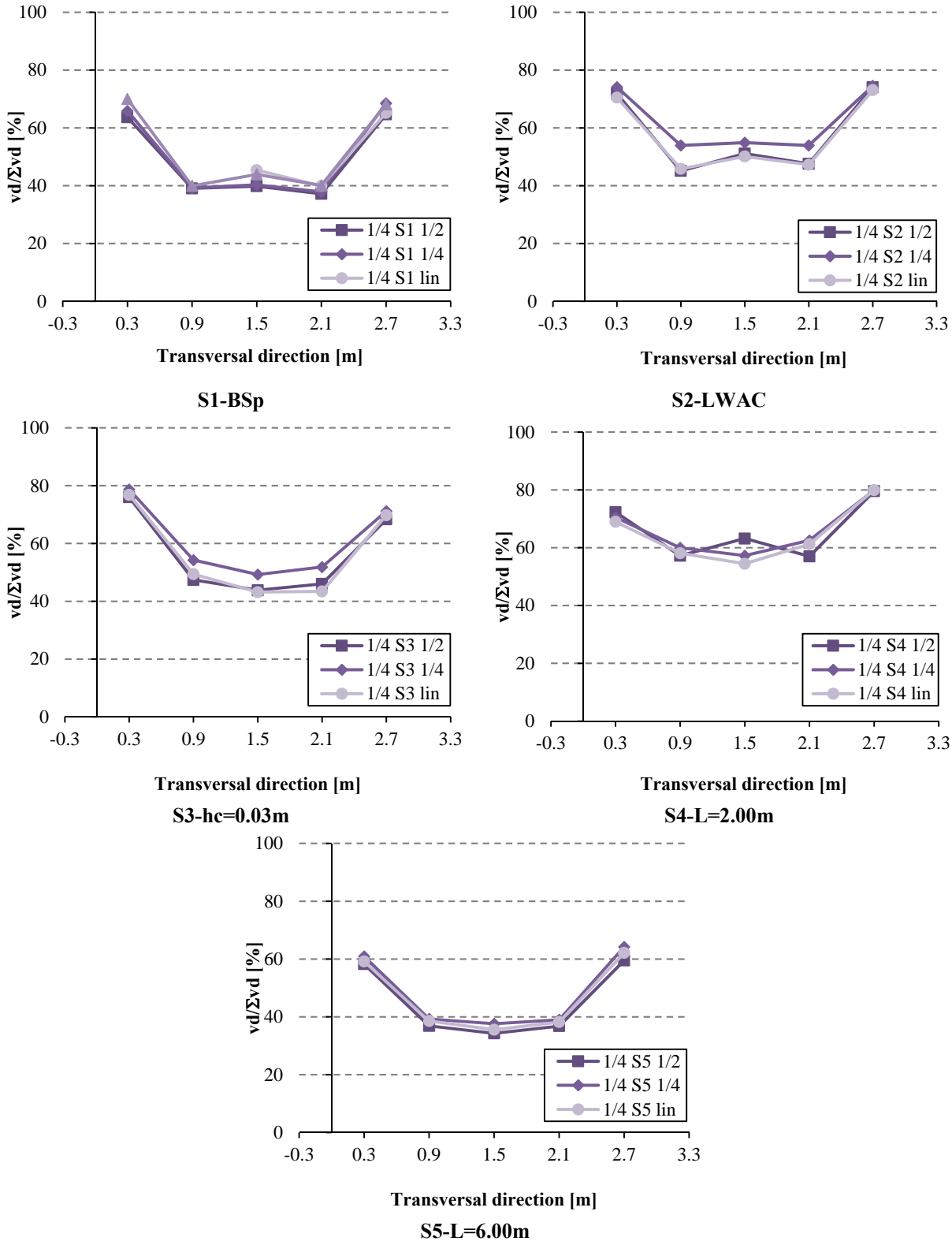


Fig. B.52 – Vertical displacements at 1/4 L distribution for the loaded beam

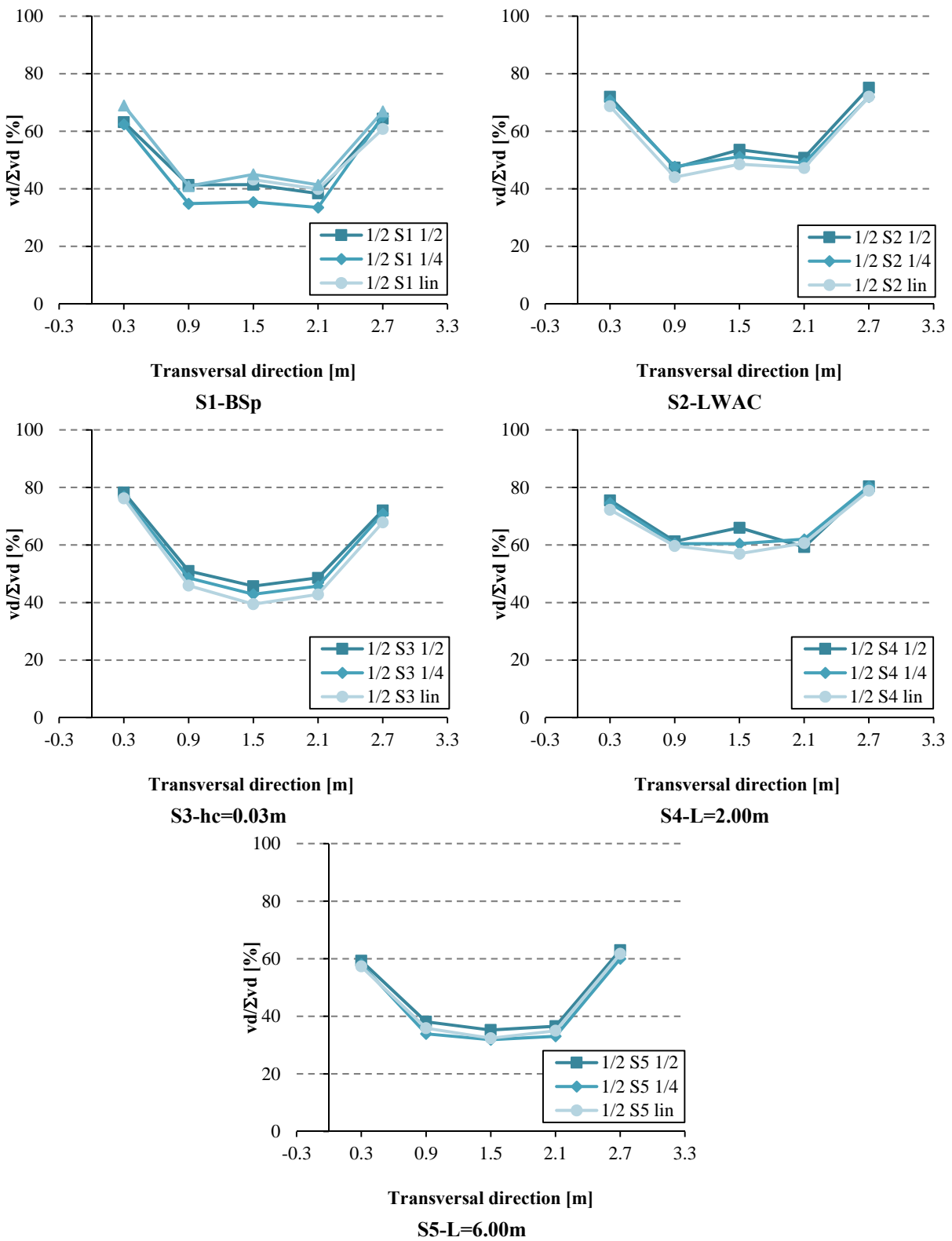


Fig. B.53 – Vertical displacements at $1/2$ L distribution for the loaded beam

B.2.2 Support reactions

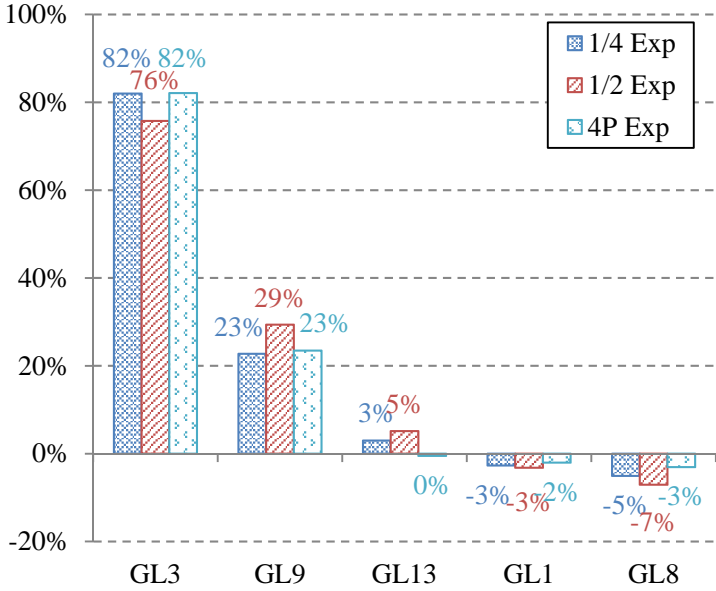


Fig. B.54 – S1-BSp: distribution of support reactions when loaded at B1-GL3

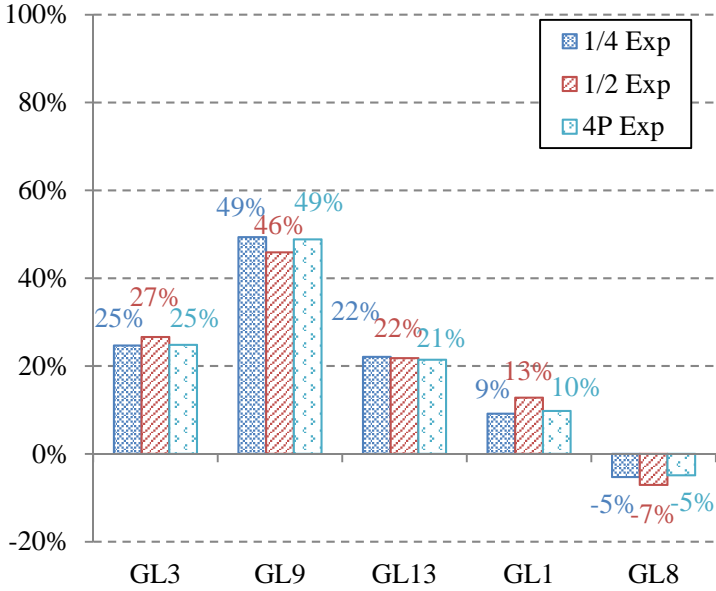


Fig. B.55 – S1-BSp: distribution of support reactions when loaded at B2-GL9

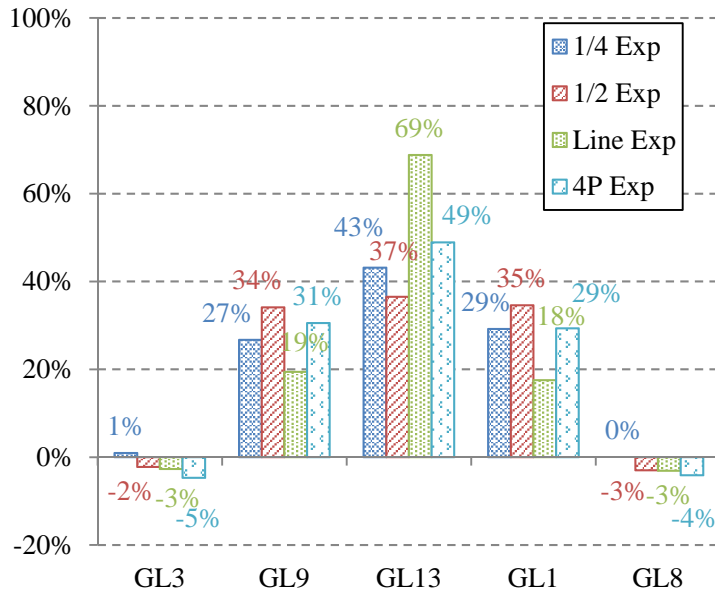


Fig. B.56 – S1-BSp: distribution of support reactions when loaded at B3-GL13

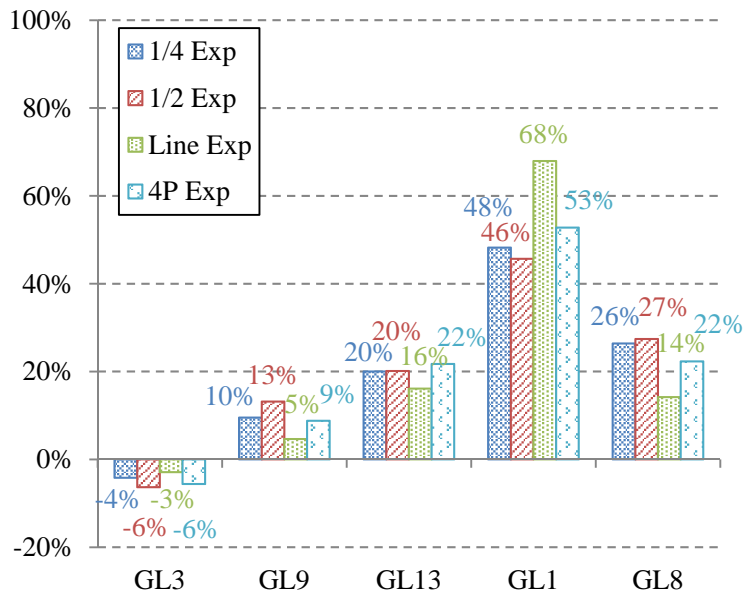


Fig. B.57 – S1-BSp: distribution of support reactions when loaded at B4-GL1

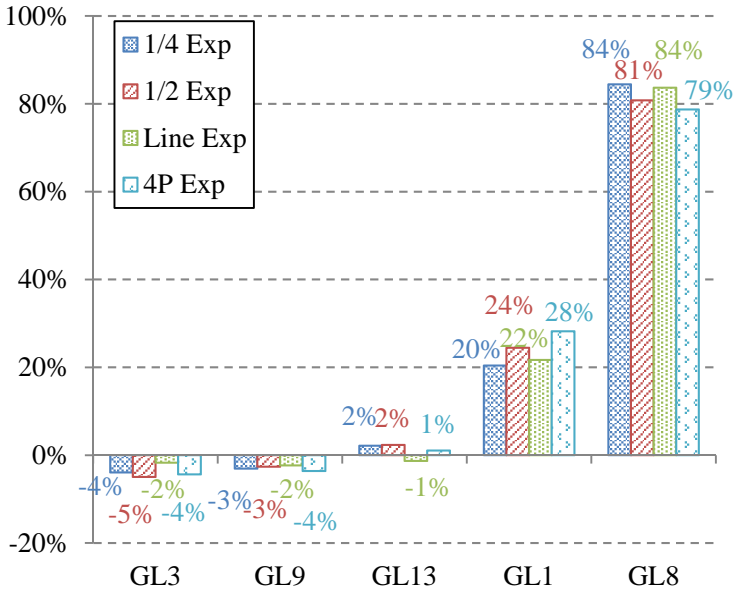


Fig. B.58 – S1-BSp: distribution of support reactions when loaded at B5-GL8

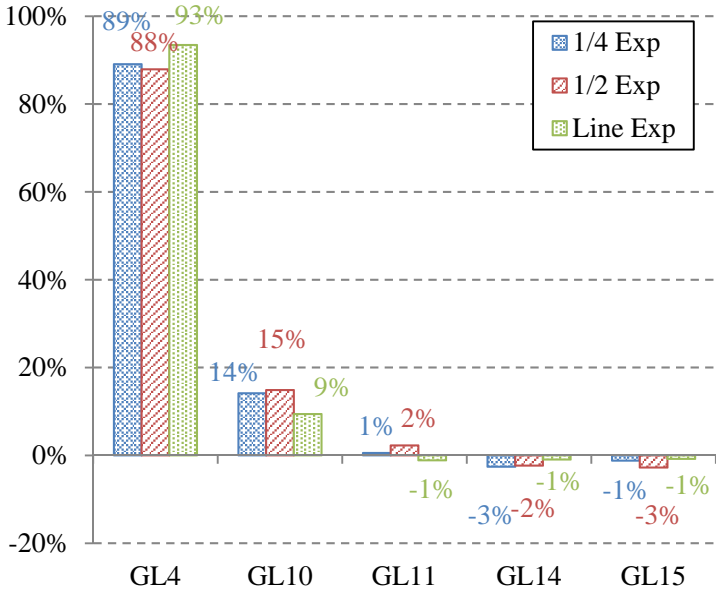


Fig. B.59 – S2-LWAC: distribution of support reactions when loaded at B1-GL4

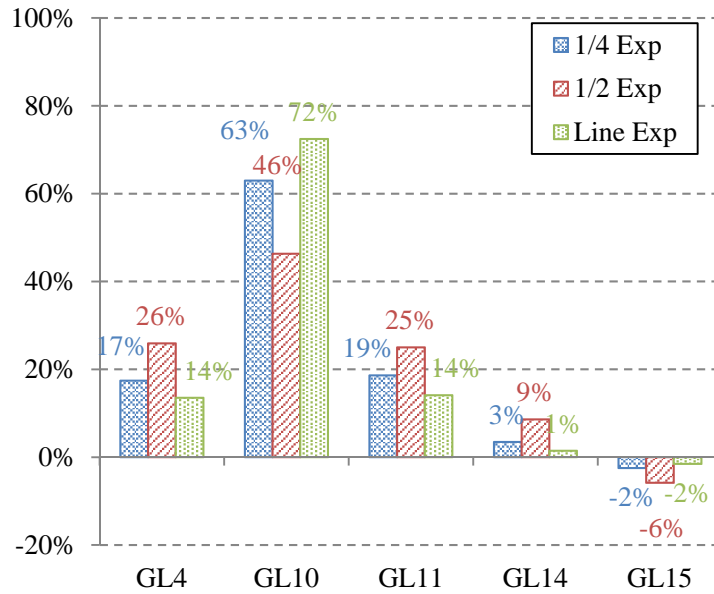


Fig. B.60 – S2-LWAC: distribution of support reactions when loaded at B2-GL10

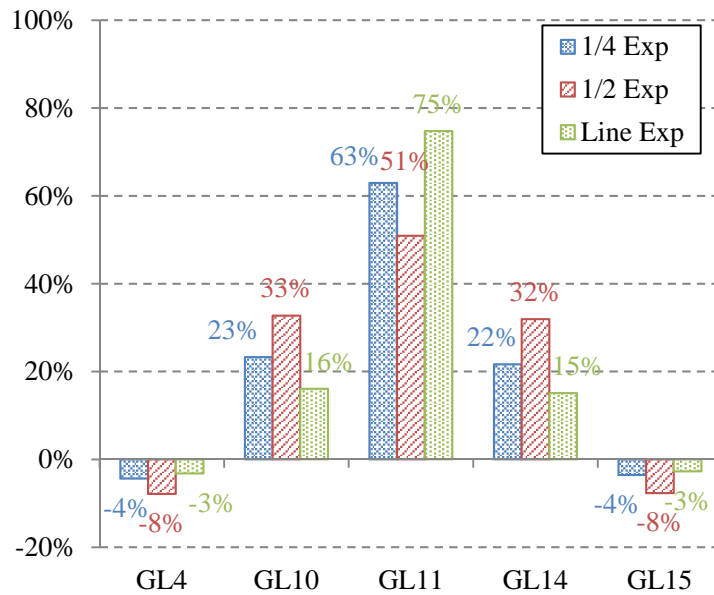


Fig. B.61 – S2-LWAC: distribution of support reactions when loaded at B3-GL11

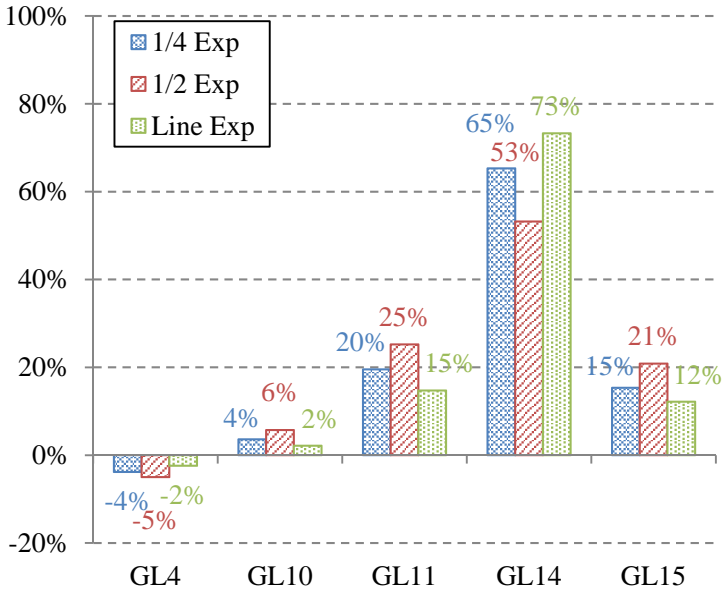


Fig. B.62 – S2-LWAC: distribution of support reactions when loaded at B4-GL14

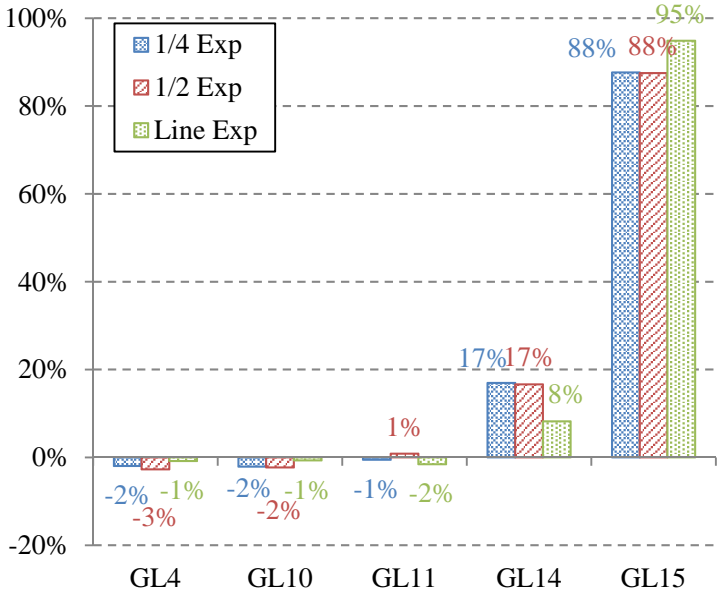


Fig. B.63 – S2-LWAC: distribution of support reactions when loaded at B5-GL15

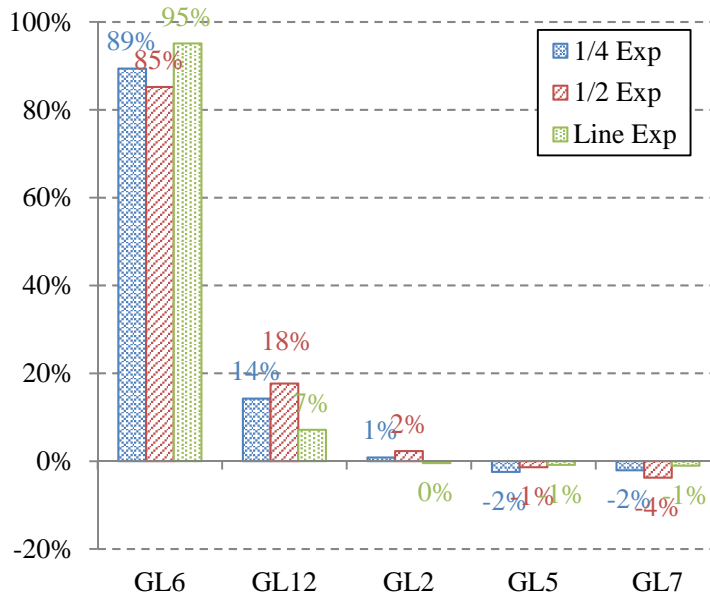


Fig. B.64 – S3-hc=0.03m: distribution of support reactions when loaded at B1-GL6

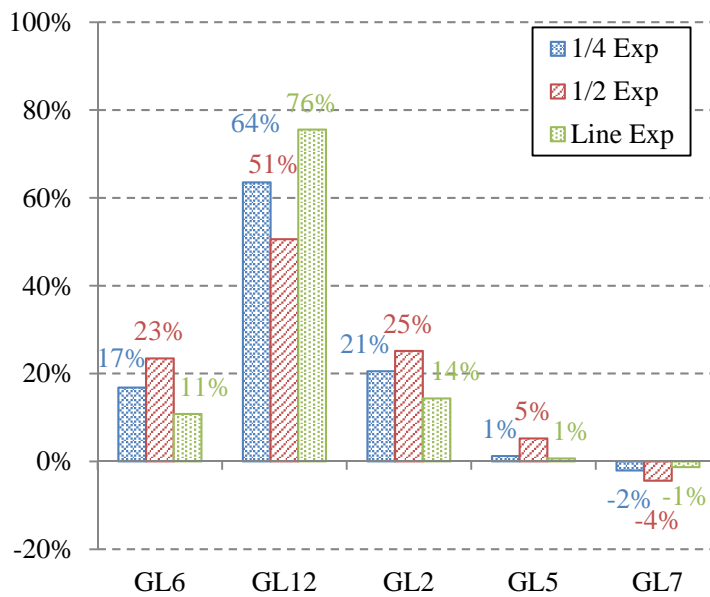


Fig. B.65 – S3-hc=0.03m: distribution of support reactions when loaded at B2-GL12

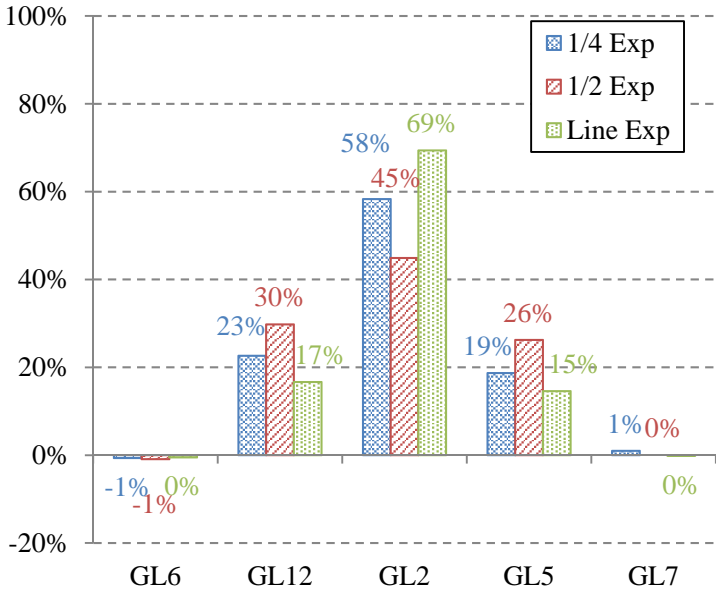


Fig. B.66 – S3-hc=0.03m: distribution of support reactions when loaded at B3-GL2

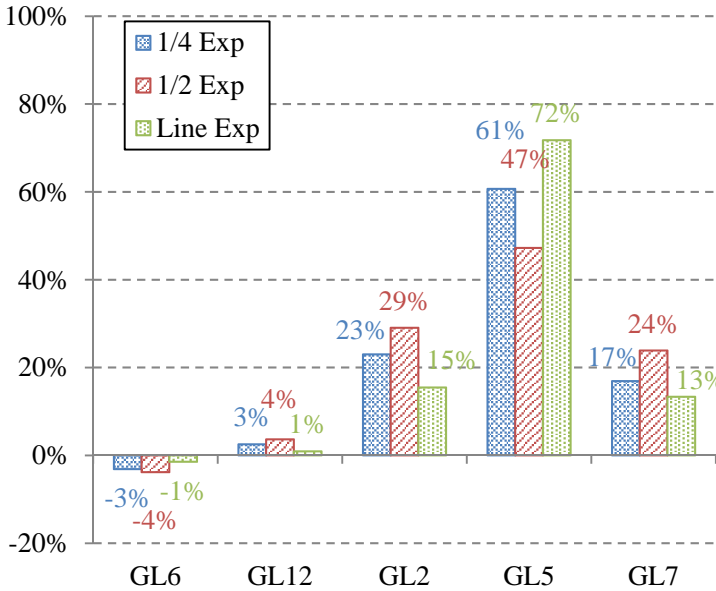


Fig. B.67 – S3-hc=0.03m: distribution of support reactions when loaded at B4-GL5

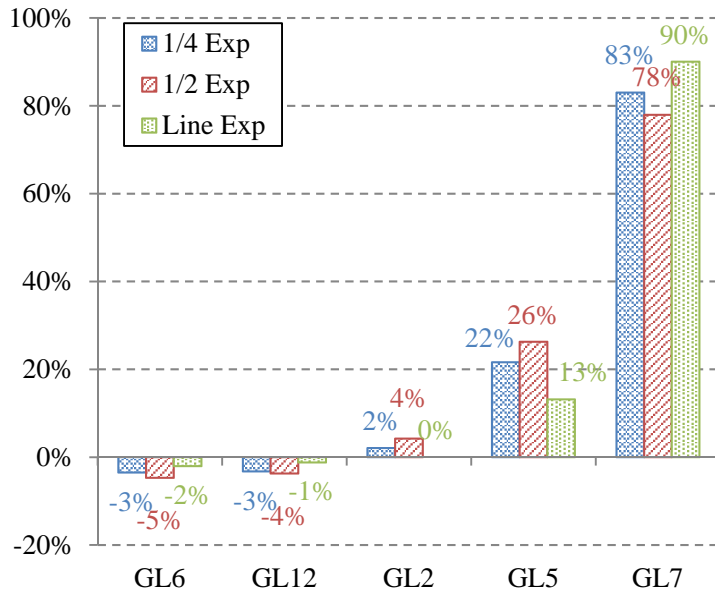


Fig. B.68 – S3-hc=0.03m: distribution of support reactions when loaded at B5-GL7

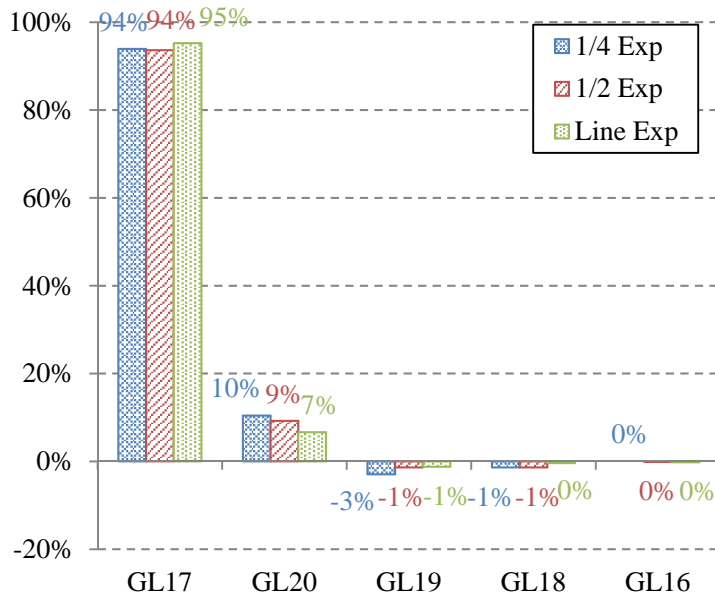


Fig. B.69 – S4-L=2.00m: distribution of support reactions when loaded at B1-GL17

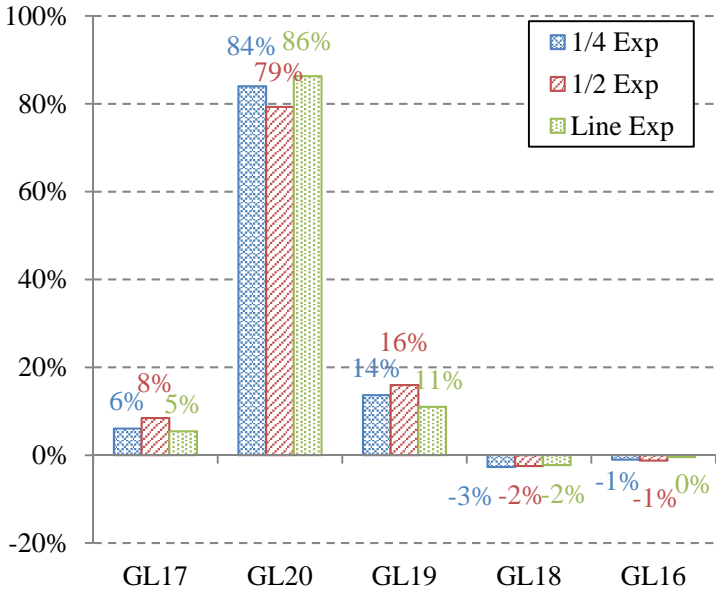


Fig. B.70 – S4-L=2.00m: distribution of support reactions when loaded at B2-GL20

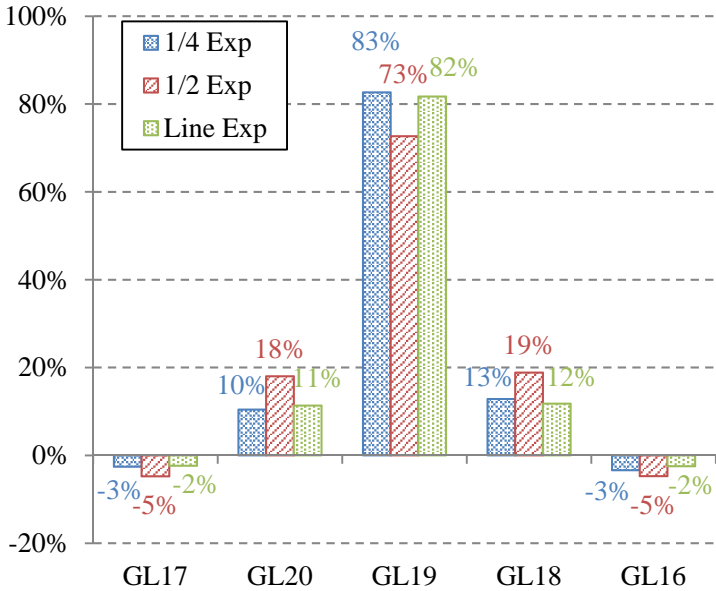


Fig. B.71 – S4-L=2.00m: distribution of support reactions when loaded at B3-GL19

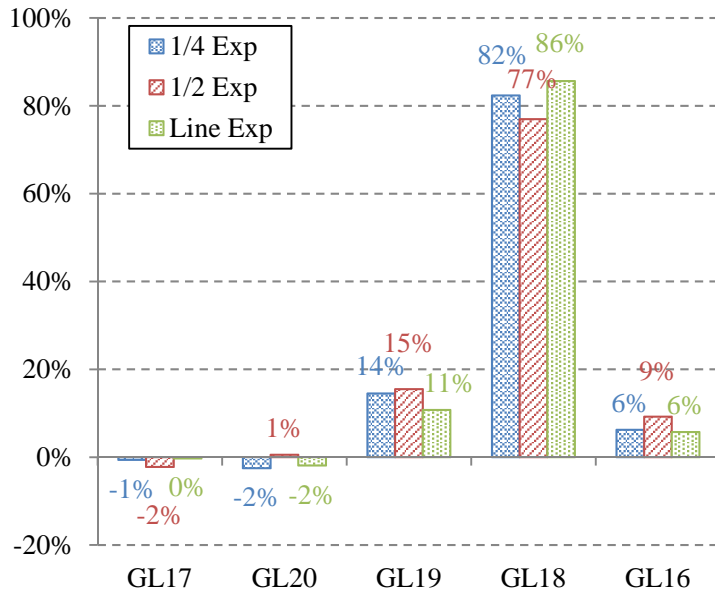


Fig. B.72 – S4-L=2.00m: distribution of support reactions when loaded at B4-GL18

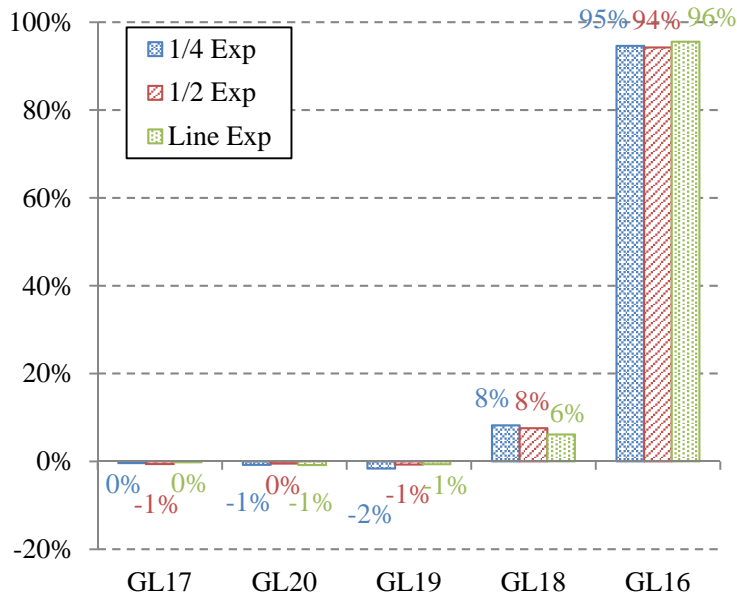


Fig. B.73 – S4-L=2.00m: distribution of support reactions when loaded at B5-GL16

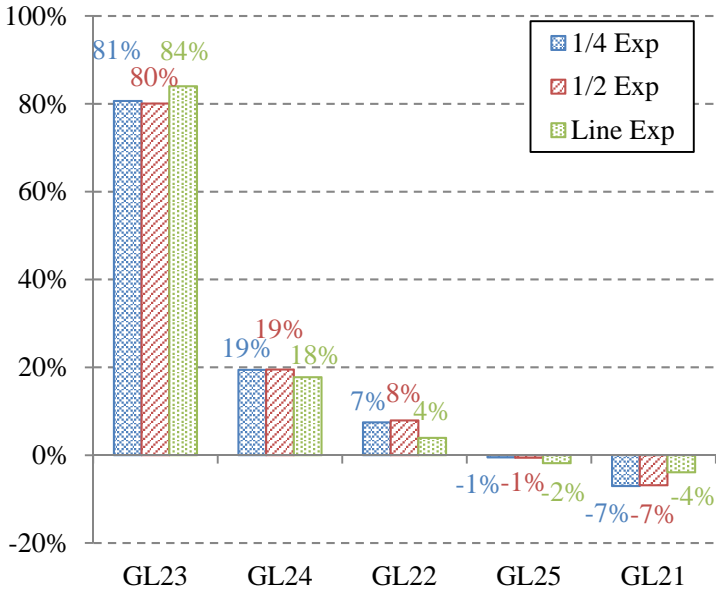


Fig. B.74 – S5-L=6.00m: distribution of support reactions when loaded at B1-GL23

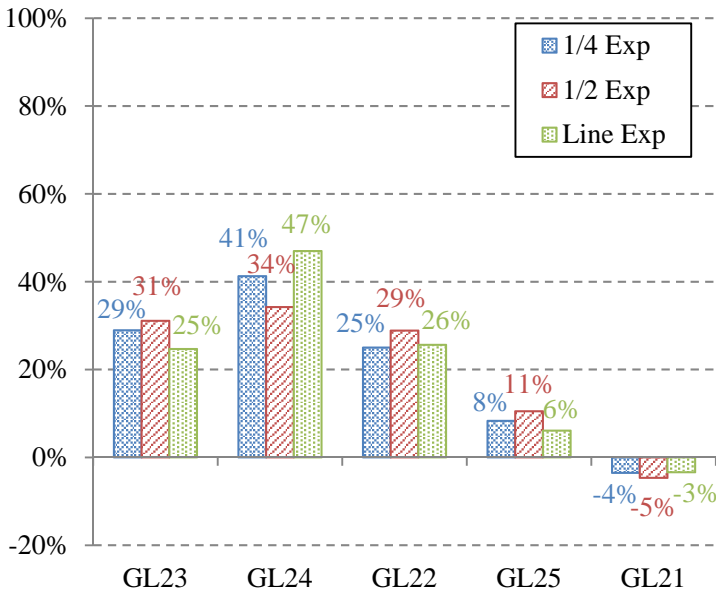


Fig. B.75 – S5-L=6.00m: distribution of support reactions when loaded at B2-GL24

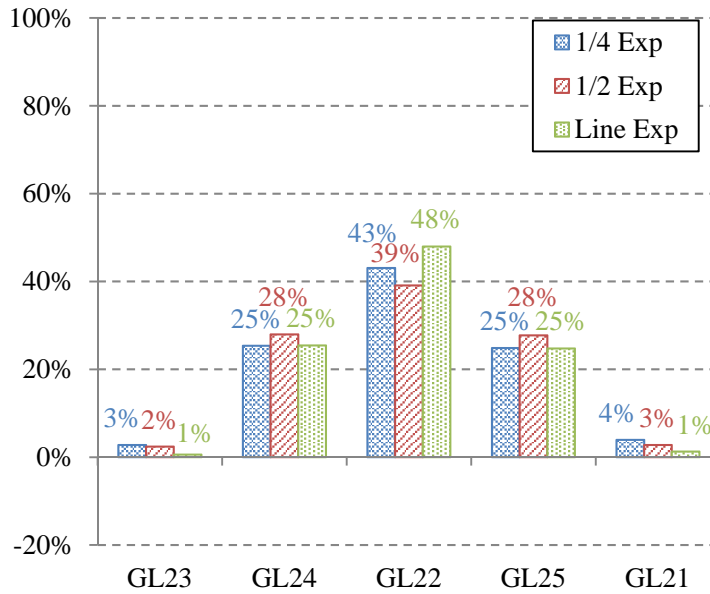


Fig. B.76 – S5-L=6.00m: distribution of support reactions when loaded at B3-GL22

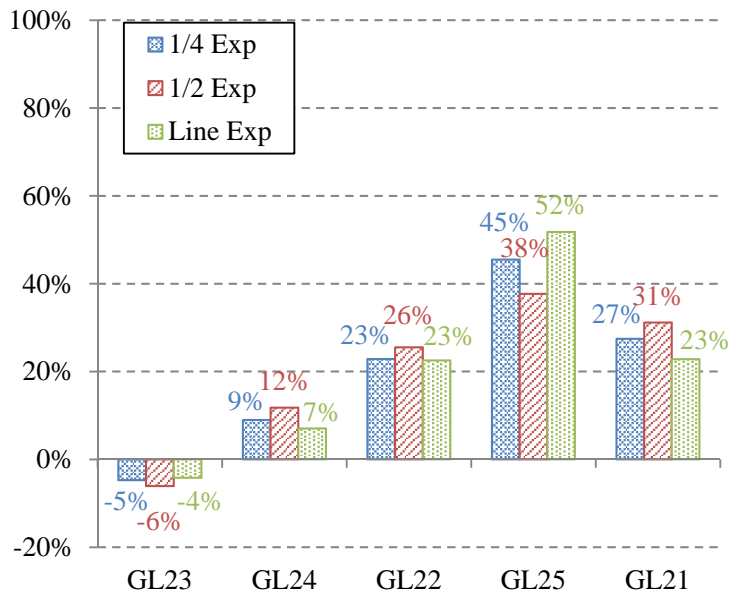


Fig. B.77 – S5-L=6.00m: distribution of support reactions when loaded at B4-GL25

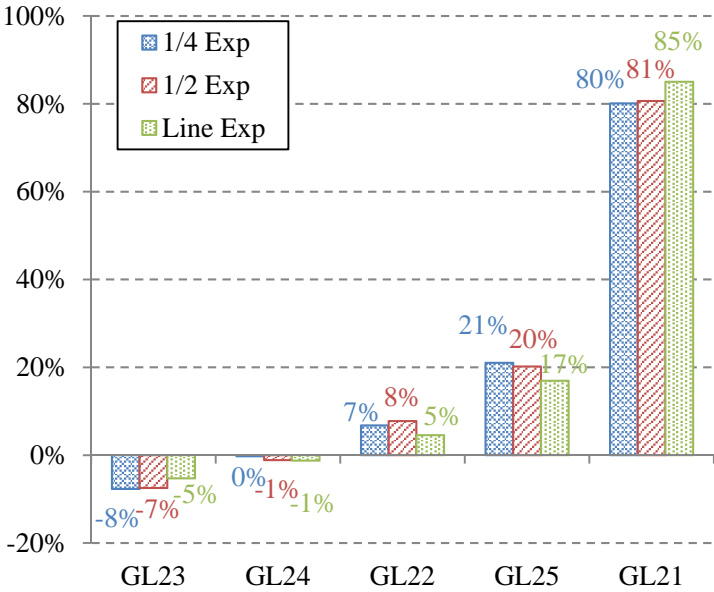


Fig. B.78 – S5-L=6.00m: distribution of support reactions when loaded at B5-GL21

Fig. B.79 to Fig. B.81 show the load distribution found for the five specimens by load type.

Fig. B.82 to Fig. B.90 summarize the comparison between the support reaction distributions associated with the Base Specimen for the various load cases and the changed parameters, concrete strength, concrete thickness and beam span.

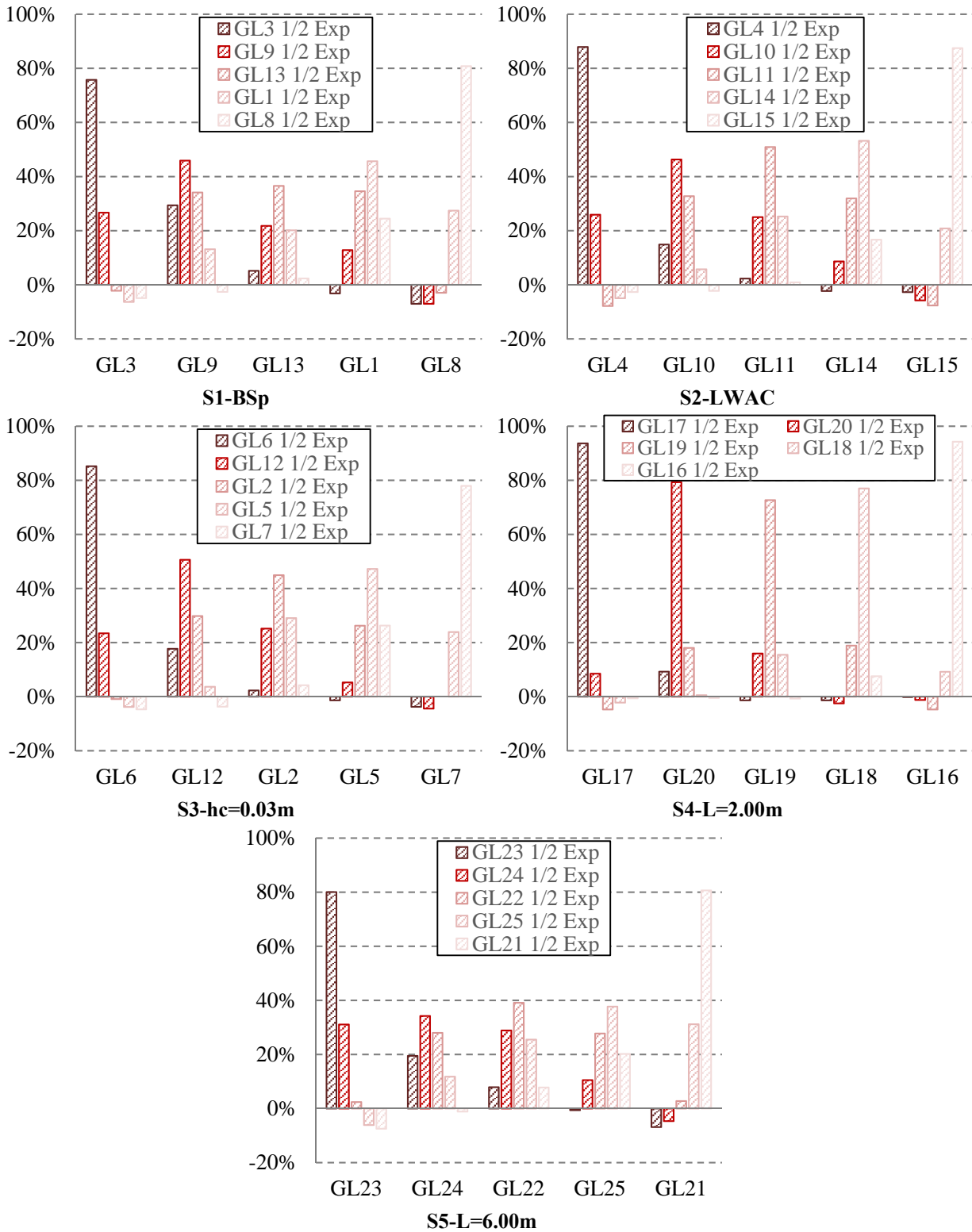


Fig. B.79 – Support reaction distribution for 1/2 L loading

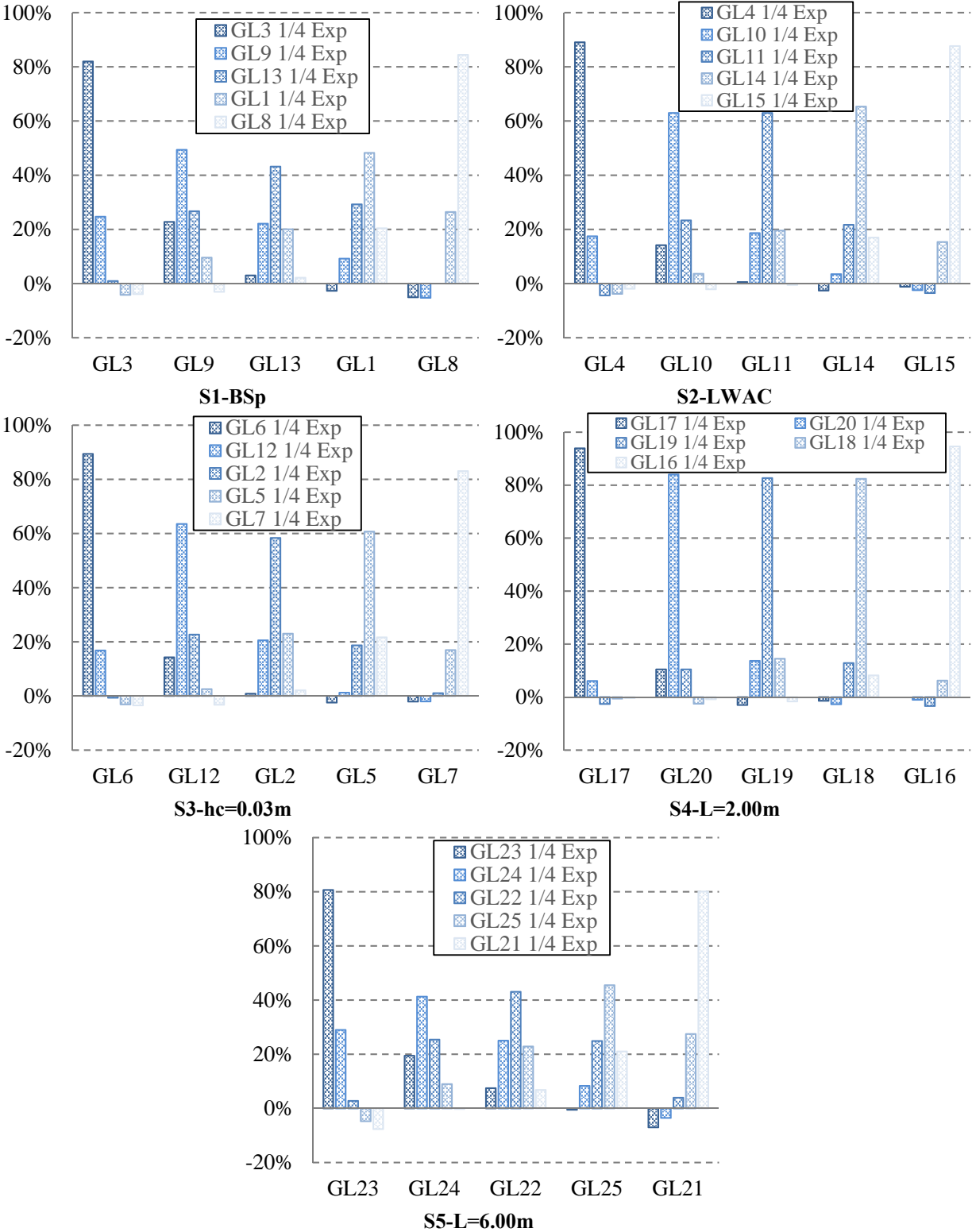


Fig. B.80 – Support reaction distribution for 1/4 L loading

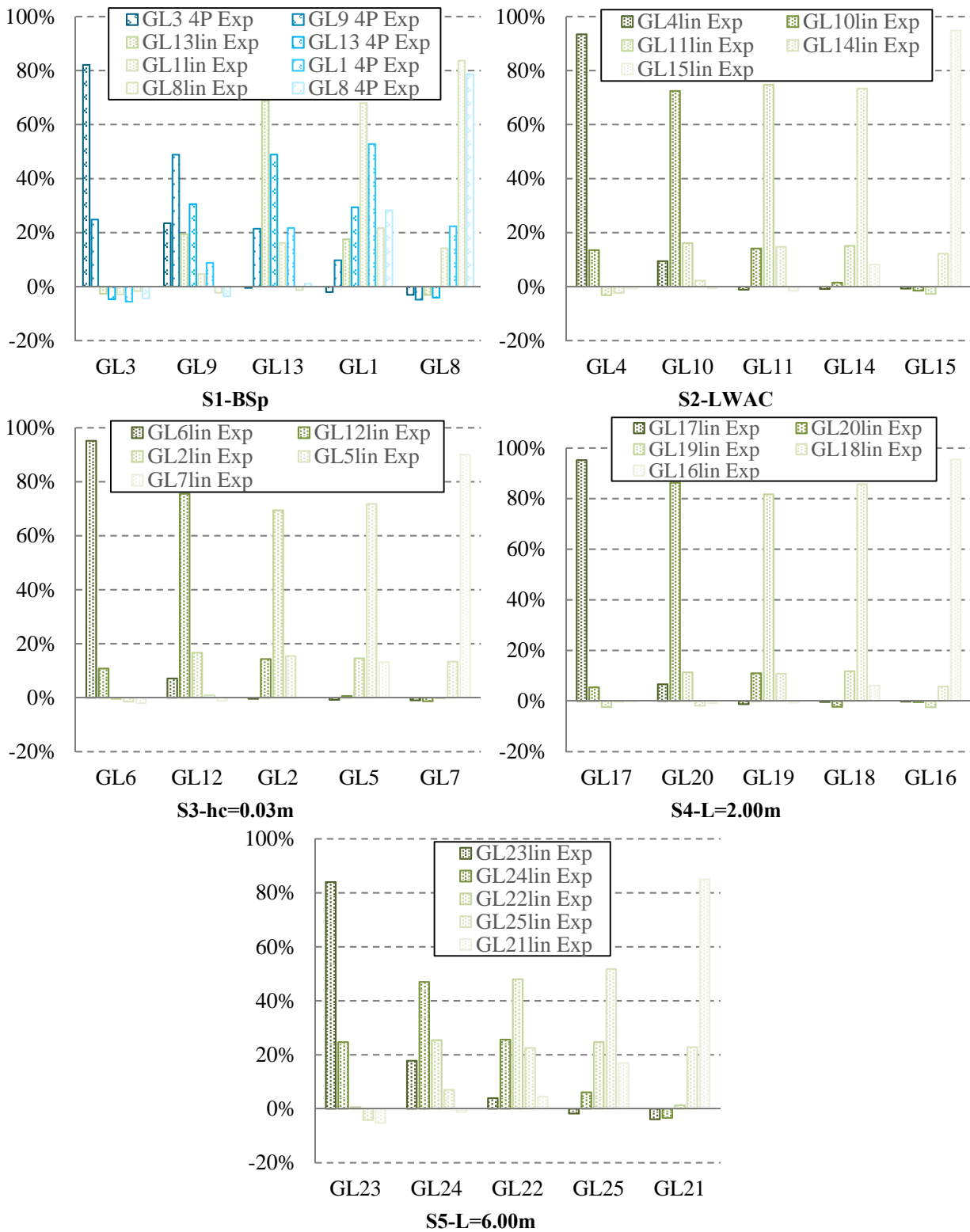


Fig. B.81 – Support reaction distribution for line loading

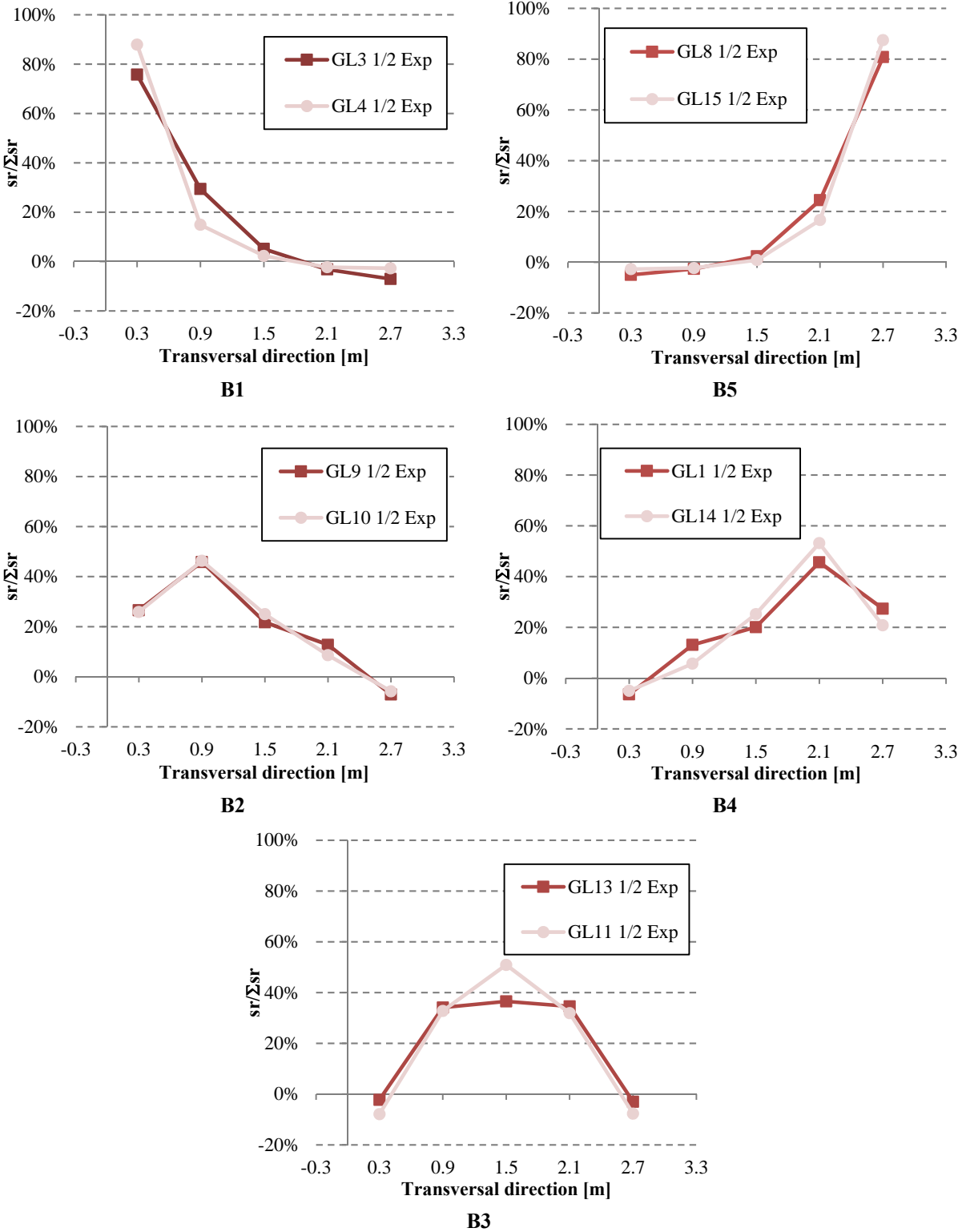


Fig. B.82 – Support reaction distribution for 1/2 L loading: S2 vs S1

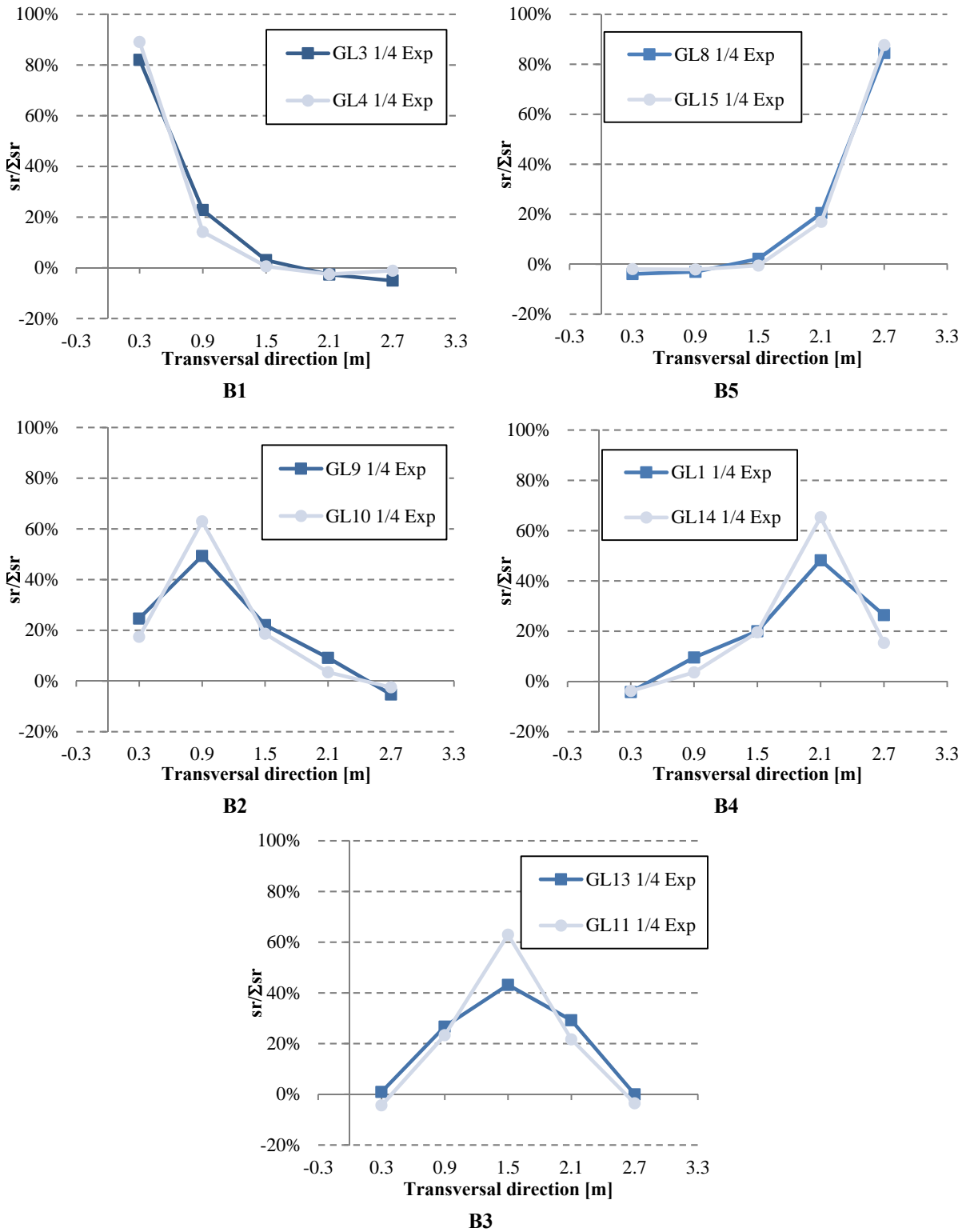


Fig. B.83 – Support reaction distribution for 1/4 L loading: S2 vs S1

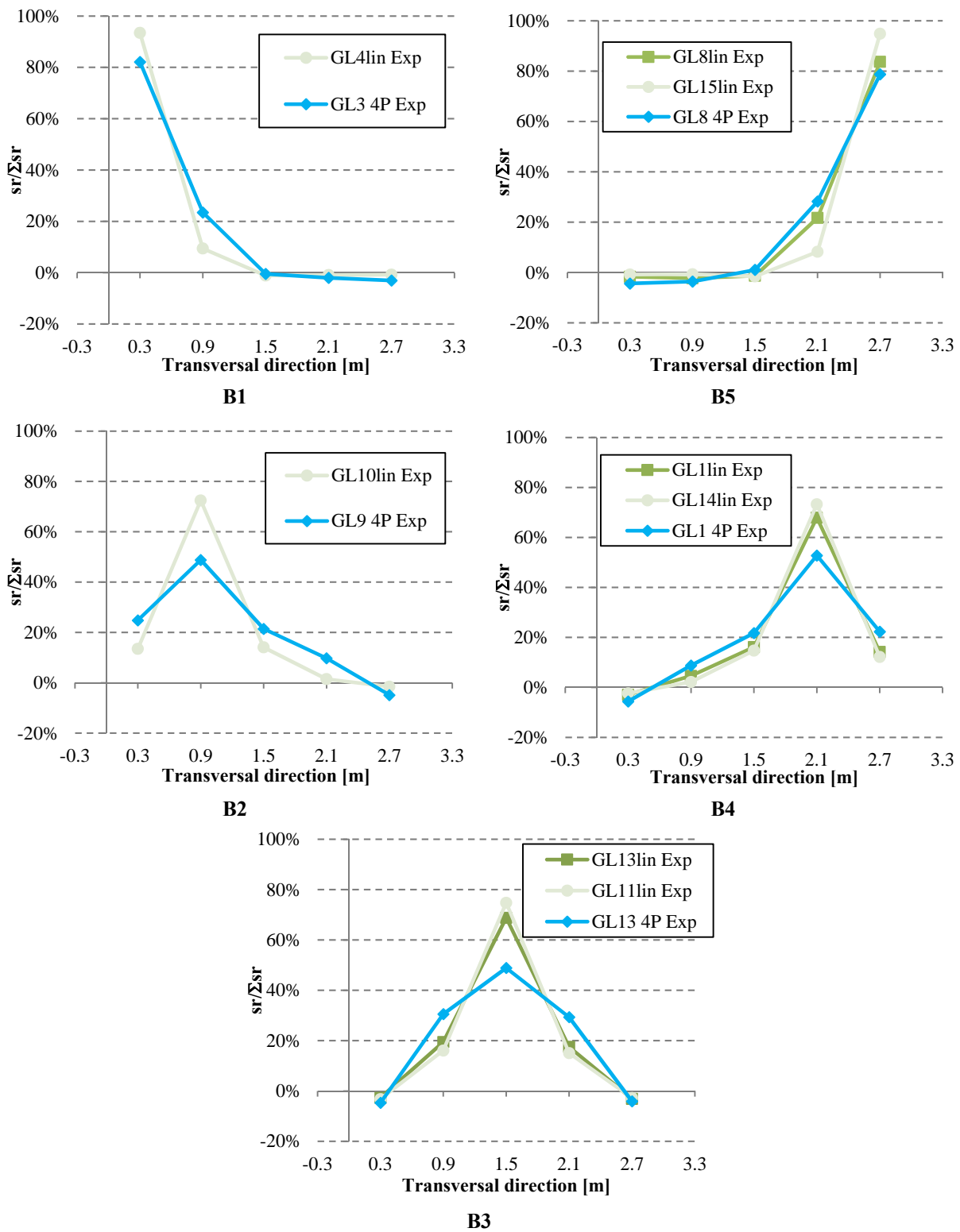


Fig. B.84 – Support reaction distribution for line loading: S2-LWAC vs S1-BSp

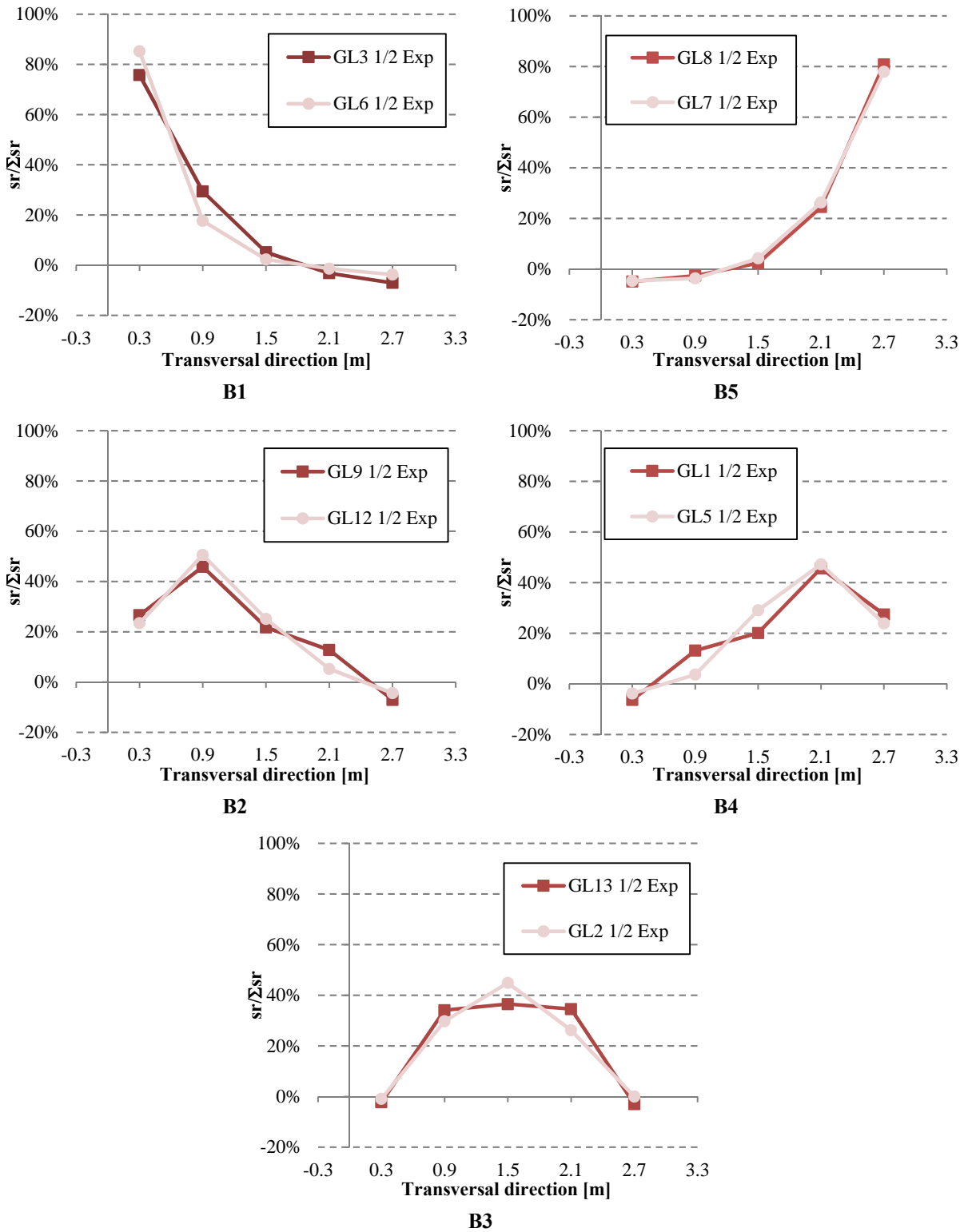


Fig. B.85 – Support reaction distribution for 1/2 L loading: S3-hc=0.03m vs S1-BSp

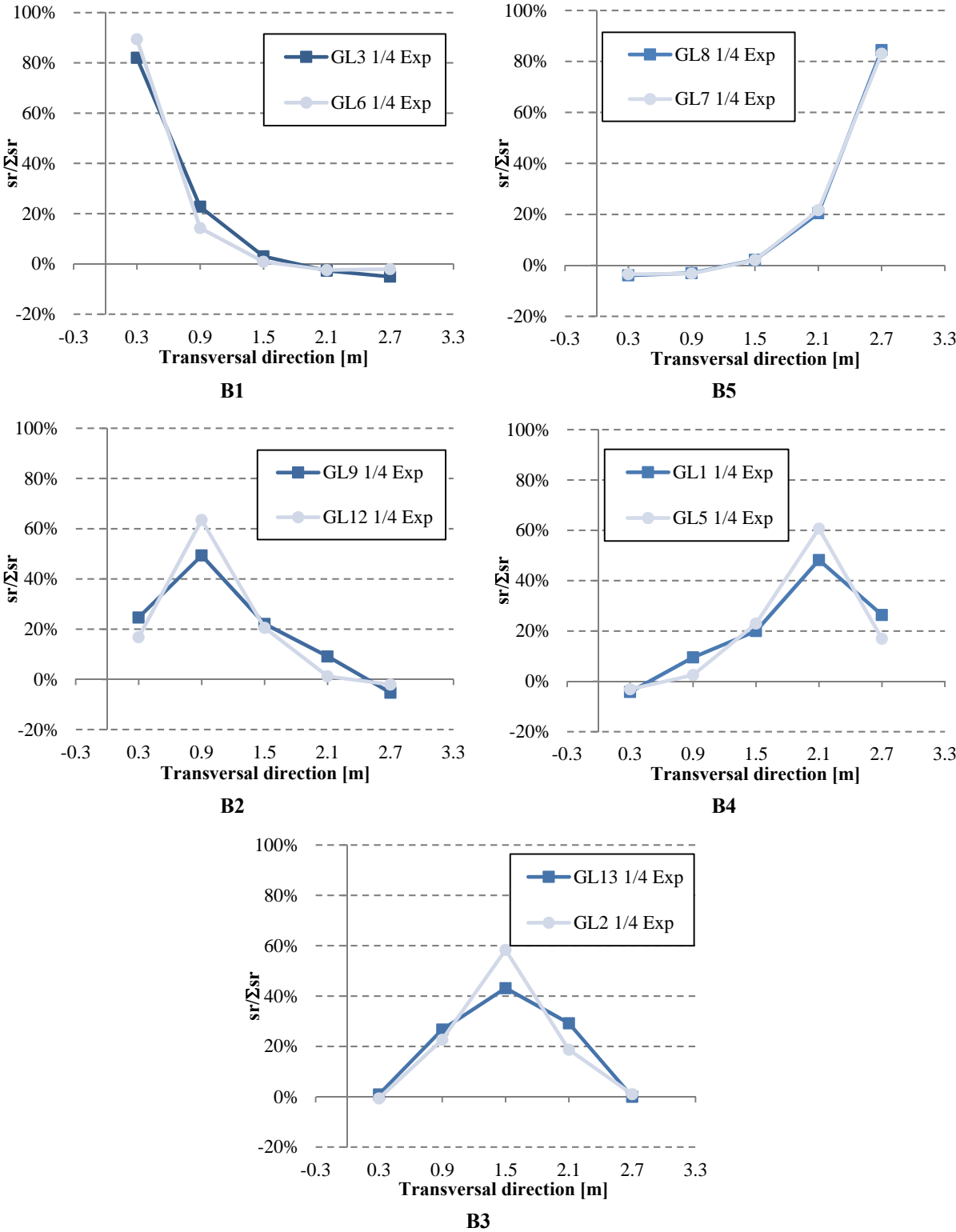


Fig. B.86 – Support reaction distribution for 1/4 L loading: S3-hc=0.03m vs S1-BSp

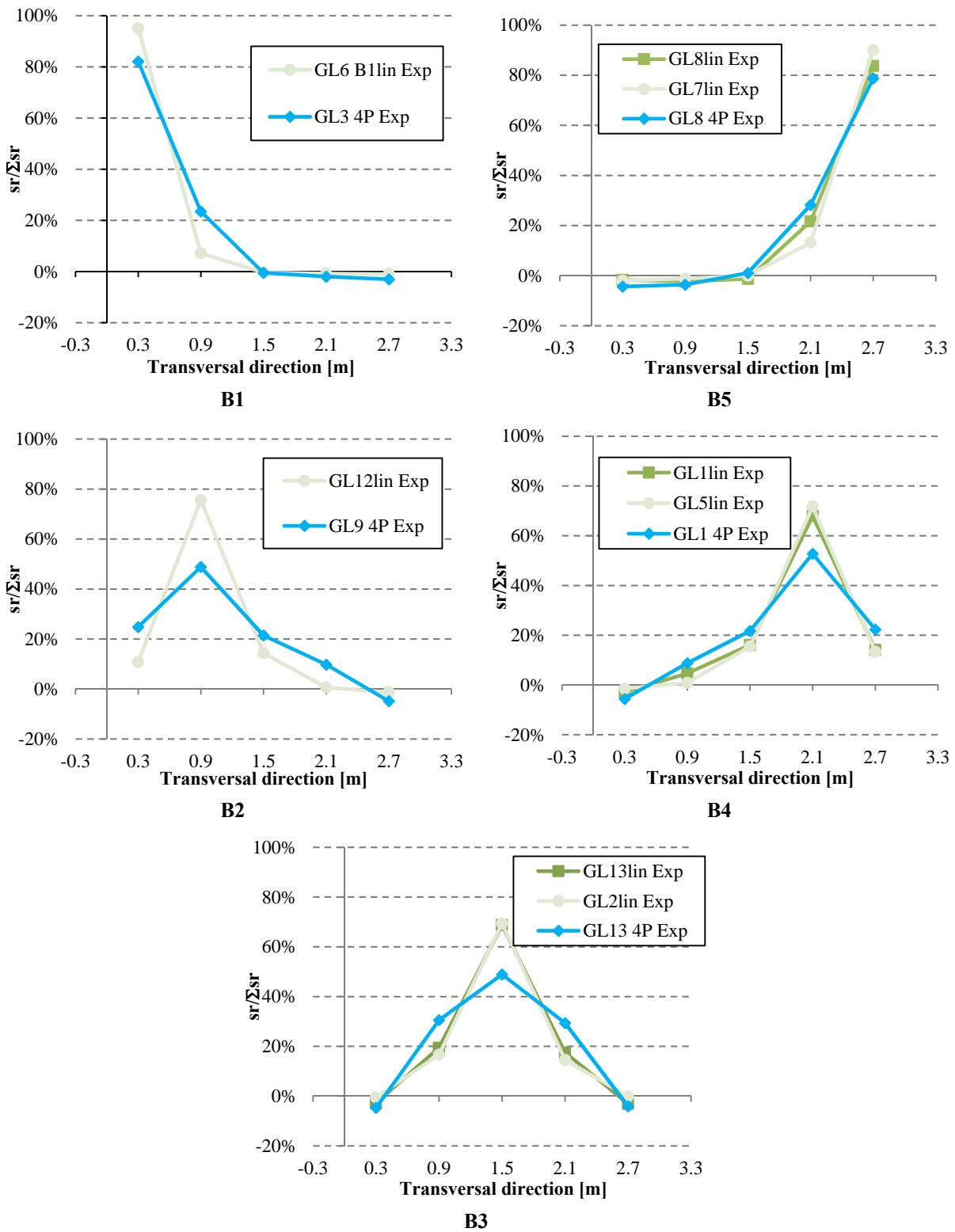


Fig. B.87 – Support reaction distribution for line loading: S3-hc=0.03m vs S1-BSp

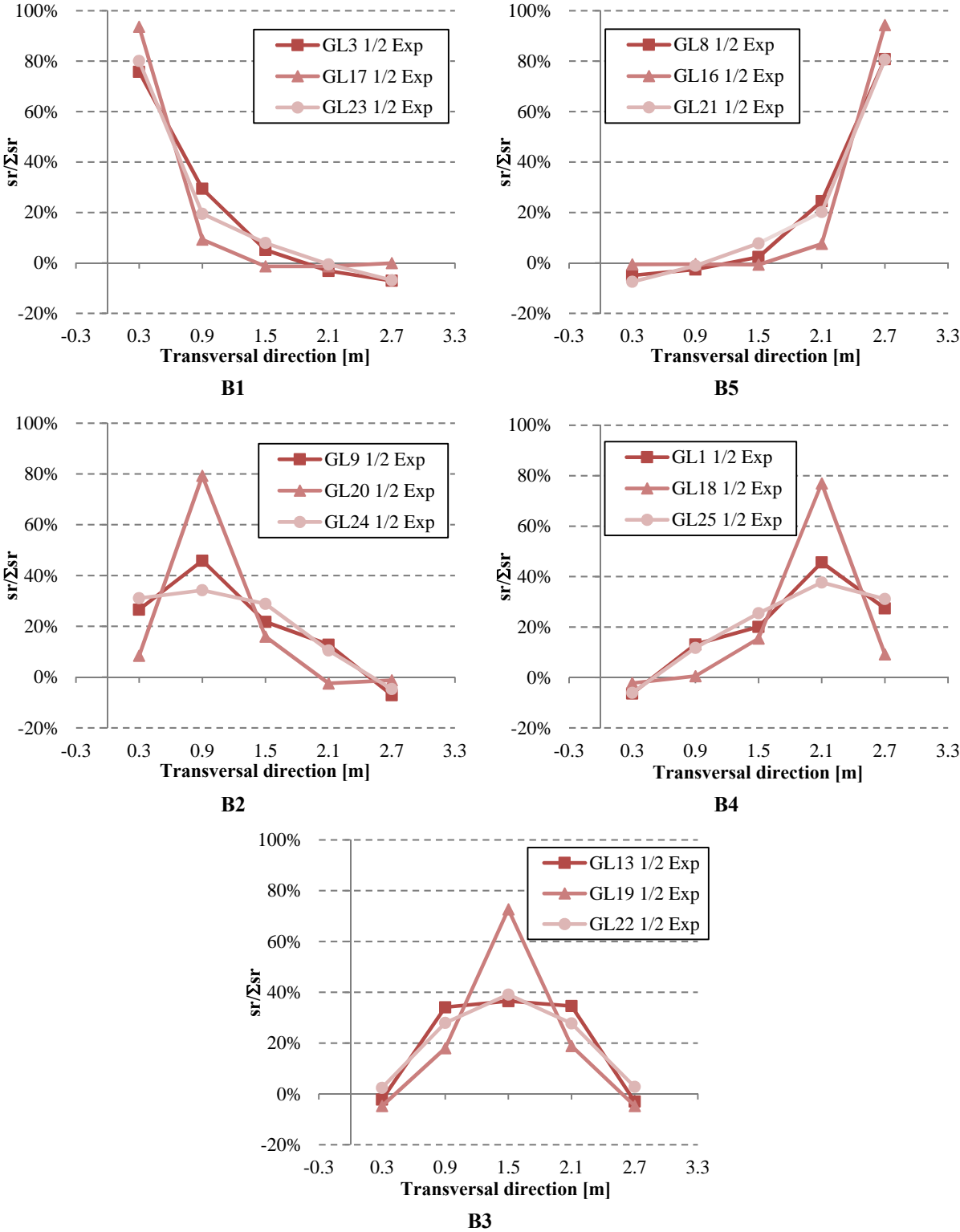


Fig. B.88 – Support reaction distribution for 1/2 L: S4-L=2.00m, S5-L=6.00m and S1-BSp

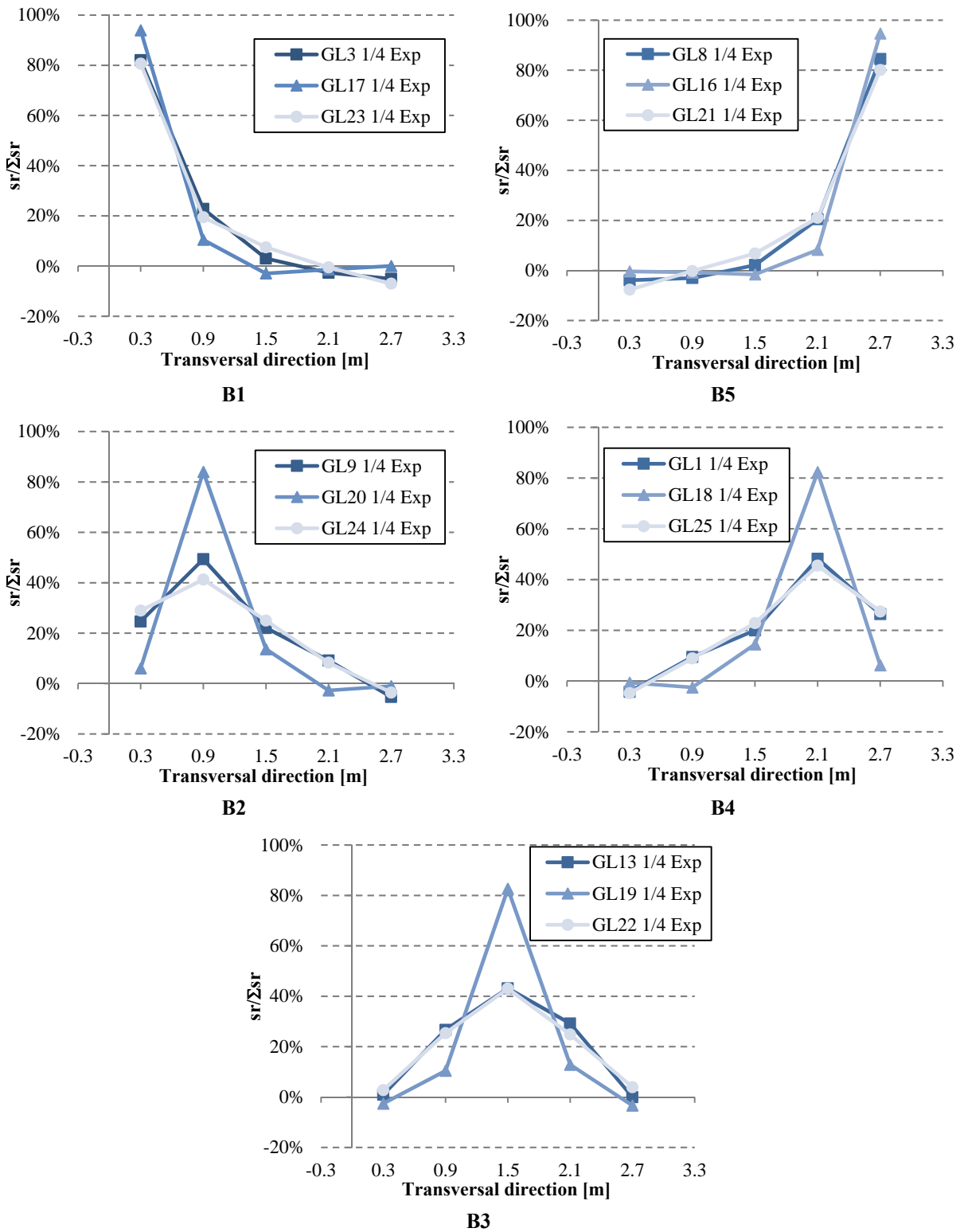


Fig. B.89 – Support reaction distribution for 1/4 L loading: S4-L=2.00m, S5-L=6.00m and S1-BSp

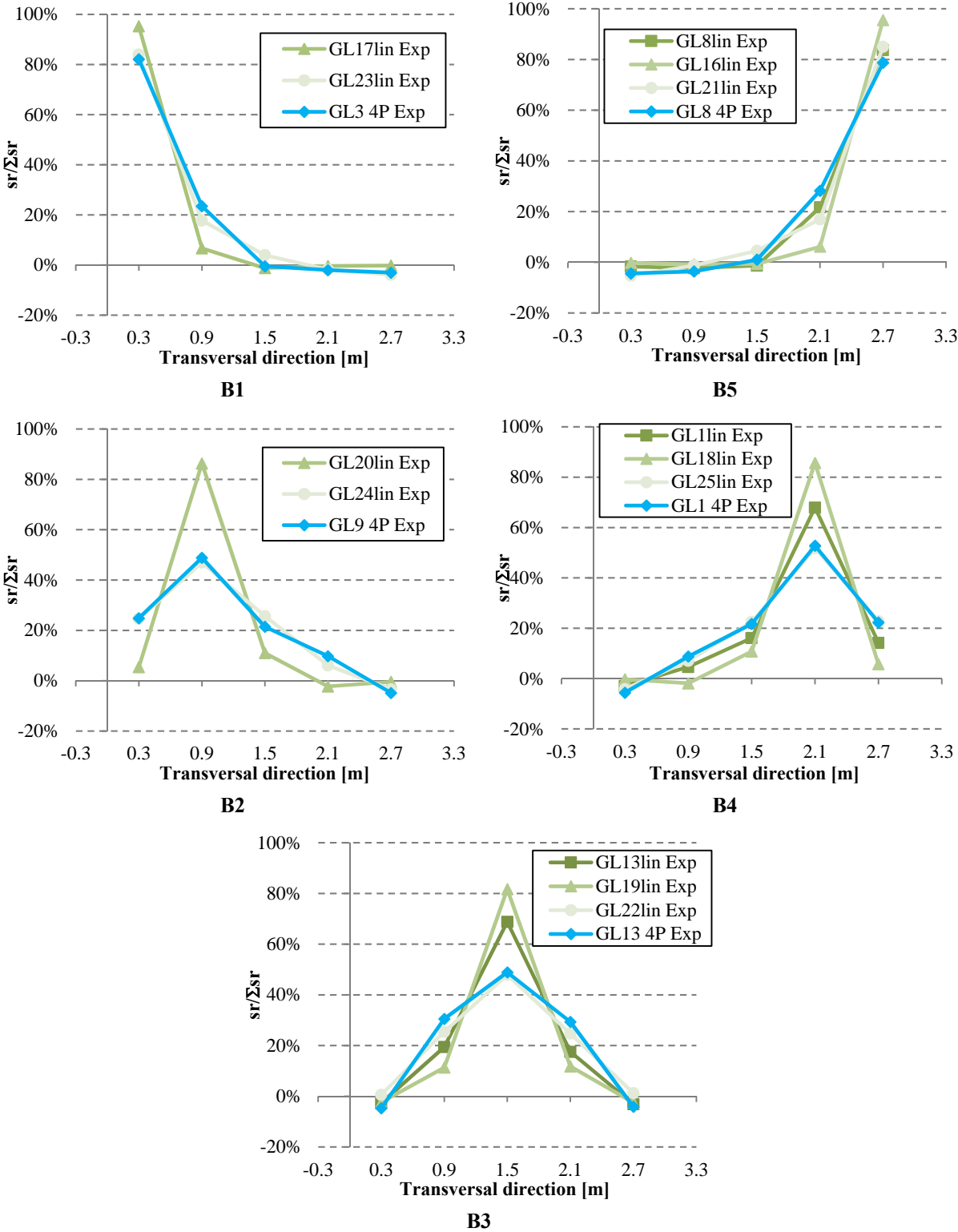


Fig. B.90 – Support reaction distribution for line loading: S4-L=2.00m, S5-L=6.00m and S1-BSp

B.2.3 Slip displacements

Table B.8 – Experimental slip displacements [mm]

Floor specimen	Load case	Displacement transducer location									
		SD1	SD2	SD3	SD4	SD5	SD6	SD7	SD8	SD9	SD10
S1-BSp	B1 ½	-0.507	-0.206	-0.020	0.000	0.009	-0.440	-0.176	-0.004	0.000	0.010
	B2 ½	-0.241	-0.376	-0.196	-0.018	0.006	-0.272	-0.304	-0.108	-0.020	0.004
	B3 ½	-0.013	-0.236	-0.466	-0.226	-0.029	-0.022	-0.278	-0.288	-0.156	-0.022
	B4 ½	0.013	-0.040	-0.210	-0.386	-0.273	0.010	-0.074	-0.192	-0.224	-0.250
	B5 ½	0.005	0.004	-0.022	-0.168	-0.569	0.000	0.000	-0.004	-0.160	-0.466
	B1 ¼	-0.507	-0.182	-0.010	0.000	0.011	-0.202	-0.080	0.000	0.000	0.012
	B2 ¼	-0.197	-0.352	-0.154	-0.020	0.007	-0.108	-0.076	-0.022	0.000	0.002
	B3 ¼	-0.032	-0.202	-0.424	-0.174	-0.015	-0.018	-0.088	-0.040	-0.030	-0.018
	B4 ¼	0.004	-0.040	-0.212	-0.360	-0.218	0.000	-0.032	-0.042	-0.046	-0.114
	B5 ¼	0.004	0.004	-0.014	-0.148	-0.606	0.000	0.000	0.002	-0.054	-0.198
	B1 4P	-0.717	-0.230	0.000	0.003	0.002	-0.836	-0.282	-0.006	0.012	0.002
	B2 4P	-0.350	-0.580	-0.316	-0.158	0.000	-0.404	-0.646	-0.366	-0.024	0.028
	B3lin	0.007	-0.134	-0.360	-0.124	0.000	0.008	-0.134	-0.278	-0.070	0.010
	B3 4P	-0.031	-0.394	-0.916	-0.798	-0.004	-0.012	-0.474	-0.948	-0.322	-0.008
	B4lin	0.004	-0.014	-0.108	-0.310	-0.161	0.008	-0.036	-0.120	-0.278	-0.184
	B4 4P	0.018	-0.036	-0.332	-1.39	-0.229	0.012	-0.152	-0.422	-0.626	-0.524
	B5lin	0.003	0.004	0.000	-0.162	-0.167	0.002	0.006	0.000	-0.086	-0.270
	B5 4P	0.010	0.008	-0.024	-0.362	-0.478	0.010	0.000	-0.020	-0.188	-0.692
S2-LWAC	B1 ½	-0.558	-0.184	-0.012	-0.002	0.003	-0.670	-0.216	0.000	0.008	0.000
	B2 ½	-0.042	-0.536	-0.252	-0.064	0.017	-0.294	-0.530	-0.280	-0.064	0.016
	B3 ½	0.004	-0.220	-0.664	-0.186	0.020	0.014	-0.252	-0.644	-0.238	0.028
	B4 ½	0.062	-0.024	-0.282	-0.574	-0.208	0.028	-0.048	-0.288	-0.722	-0.162
	B5 ½	0.005	0.010	0.000	-0.166	-0.772	0.004	0.004	-0.004	-0.248	-0.768
	B1 ¼	-0.892	-0.206	0.000	0.004	-0.001	-0.414	-0.150	0.000	0.012	0.006
	B2 ¼	-0.283	-1.046	-0.334	-0.032	0.011	-0.240	-0.358	-0.200	-0.052	0.016
	B3 ¼	0.146	-0.292	-1.200	-0.342	0.010	0.002	-0.224	-0.434	-0.270	0.014
	B4 ¼	0.006	-0.016	-0.250	-0.924	-0.330	0.012	-0.036	-0.194	-0.480	-0.196
	B5 ¼	0.026	0.012	0.004	-0.200	-1.017	0.002	0.006	-0.002	-0.186	-0.500
	B1lin	-0.366	-0.086	0.000	0.002	0.004	-0.322	-0.098	0.002	0.006	0.002
	B2lin	-0.233	-0.550	-0.230	-0.018	0.009	-0.262	-0.446	-0.212	-0.028	0.010
	B3lin	0.001	-0.264	-0.722	-0.262	0.002	0.010	-0.250	-0.612	-0.286	0.022
	B4lin	-0.002	-0.012	-0.278	-0.704	-0.313	0.016	-0.036	-0.228	-0.738	-0.258
	B5lin	-0.003	0.002	0.006	-0.069	-0.484	0.002	0.004	0.008	-0.114	1.628 ⁱ

Table B.8 – Experimental slip displacements [mm] (cont.)

Floor specimen	Load case	Displacement transducer location									
		SD1	SD2	SD3	SD4	SD5	SD6	SD7	SD8	SD9	SD10
S3-hc=0.03m	B1 ½	-0.317	-0.074	0.000	0.000	0.002	-0.334	-0.080	0.000	0.000	0.002
	B2 ½	-0.128	-0.276	-0.110	-0.022	0.002	-0.152	-0.294	-0.134	-0.016	0.006
	B3 ½	-0.011	-0.096	-0.200	-0.120	-0.011	-0.012	-0.120	-0.244	-0.124	-0.008
	B4 ½	0.004	-0.018	-0.104	-0.290	-0.144	0.006	-0.030	-0.154	-0.148	-0.160
	B5 ½	-0.001	0.004	-0.014	-0.136	-0.262	0.002	-0.002	-0.006	-0.122	-0.334
	B1 ¼	-0.473	-0.086	0.000	0.004	0.004	-0.210	-0.050	0.000	0.000	0.004
	B2 ¼	-0.125	-0.446	-0.128	-0.012	-0.001	-0.124	-0.172	-0.076	-0.004	-0.002
	B3 ¼	-0.008	-0.104	-0.302	-0.184	-0.017	-0.010	-0.092	-0.114	-0.050	-0.006
	B4 ¼	0.004	-0.002	-0.080	-0.416	-0.198	0.002	-0.020	-0.088	-0.148	-0.104
	B5 ¼	0.000	-0.002	-0.008	-0.120	-0.379	0.002	-0.002	-0.010	-0.088	-0.216
	B1lin	-0.148	-0.016	0.006	0.002	0.006	-0.138	-0.020	0.002	0.000	0.000
	B2lin	-0.108	-0.282	-0.080	0.000	0.003	-0.108	-0.256	-0.084	-0.006	0.002
	B3lin	-0.005	-0.086	-0.188	-0.138	-0.017	-0.006	-0.094	-0.220	-0.094	-0.010
	B4lin	0.002	-0.008	-0.068	-0.216	-0.159	0.004	-0.016	-0.094	-0.290	-0.142
	B5lin	-0.004	0.000	-0.008	-0.060	-0.216	0.000	0.000	0.000	-0.054	-0.134
S4-L=2.00m	B1 ½	-0.536	-0.068	0.000	0.002	0.000	-0.460	-0.040	0.000	0.000	0.000
	B2 ½	-0.072	-0.378	-0.106	0.002	0.003	-0.058	-0.420	-0.042	0.000	0.002
	B3 ½	0.008	-0.106	-0.488	-0.134	0.015	0.008	-0.098	-0.350	-0.096	0.010
	B4 ½	0.001	-0.006	-0.098	-0.428	-0.053	0.004	-0.008	-0.052	-0.400	-0.070
	B5 ½	0.000	0.000	-0.002	-0.056	-0.405	0.000	-0.002	0.002	-0.040	-0.480
	B1 ¼	-0.554	-0.074	0.008	0.004	0.000	-0.336	-0.016	0.000	0.002	0.000
	B2 ¼	-0.032	-0.390	-0.082	0.008	0.002	-0.036	-0.322	-0.016	0.004	0.002
	B3 ¼	0.004	-0.044	-0.546	-0.084	0.012	0.006	-0.060	-0.268	-0.056	0.002
	B4 ¼	0.000	0.006	-0.092	-0.452	-0.026	0.002	0.002	-0.018	-0.282	-0.032
	B5 ¼	0.001	0.000	0.008	-0.050	-0.402	0.002	0.000	0.014	-0.032	-0.370
	B1lin	-0.335	-0.032	0.004	0.000	-0.004	-0.318	-0.012	0.006	0.000	0.000
	B2lin	-0.040	-0.334	-0.070	0.000	-0.001	-0.038	-0.344	-0.036	0.004	0.000
	B3lin	0.000	-0.070	-0.538	-0.086	0.005	0.000	-0.070	-0.300	-0.078	0.002
	B4lin	0.000	0.006	-0.068	-0.392	-0.033	0.002	0.004	-0.022	-0.342	-0.046
	B5lin	0.002	0.004	0.002	-0.026	-0.325	0.000	-0.004	0.000	-0.034	-0.386
S5-L=6.00m	B1 ½	-0.448	-0.264	-0.056	0.000	0.016	-0.620	-0.300	-0.028	0.000	0.008
	B2 ½	-0.383	-0.430	-0.342	-0.110	-0.001	-0.500	-0.568	-0.338	-0.082	0.000
	B3 ½	-0.144	-0.324	-0.440	-0.294	-0.144	-0.130	-0.372	-0.518	-0.324	-0.104
	B4 ½	0.001	-0.132	-0.316	-0.360	-0.446	0.000	-0.112	-0.316	-0.500	-0.474
	B5 ½	0.008	0.000	-0.034	-0.240	-0.631	0.000	-0.004	-0.040	-0.280	-0.702

Table B.8 – Experimental slip displacements [mm] (cont.)

Floor specimen	Load case	Displacement transducer location									
		SD1	SD2	SD3	SD4	SD5	SD6	SD7	SD8	SD9	SD10
S5-L=6.00m	B1 ¼	-0.240	-0.150	-0.044	0.000	0.021	-0.668	-0.306	-0.022	0.002	0.012
	B2 ¼	-0.235	-0.168	-0.148	-0.066	-0.001	-0.418	-0.694	-0.350	-0.054	0.002
	B3 ¼	-0.100	-0.140	-0.144	-0.116	-0.109	-0.068	-0.380	-0.600	-0.298	-0.084
	B4 ¼	0.001	-0.060	-0.140	-0.130	-0.276	0.006	-0.110	-0.300	-0.592	-0.412
	B5 ¼	0.021	0.000	-0.046	-0.112	-0.290	0.016	0.000	-0.016	-0.254	-0.766
	B1lin	-0.349	-0.204	-0.028	0.002	0.005	-0.490	-0.212	0.004	0.000	0.000
	B2lin	-0.360	-0.466	-0.314	-0.070	0.000	-0.440	-0.586	-0.292	-0.052	0.002
	B3lin	-0.111	-0.298	-0.472	-0.274	-0.101	-0.098	-0.334	-0.524	-0.278	-0.082
	B4lin	0.005	-0.090	-0.288	-0.430	-0.432	0.000	-0.066	-0.308	-0.500	-0.400
	B5lin	0.003	0.000	-0.016	-0.162	-0.513	0.008	0.002	-0.004	-0.184	-0.556

½ - mid-span; ¼ - quarter-span; lin - line load; 4P - 4-point load

ⁱ This value has no sense for the actual behavior of the slab when subjected to a vertical load, with the sense of gravity. When such a load acts over a composite beam the vertical displacement tends to be from top down and the concrete layer and the timber beam tend to slip relative to one another, Fig. N.1. This trend is counteracted by the connection between timber and concrete.

Therefore, is clear that the slip measured relatively to the beam end, placing the displacement transducer as Fig. 4.21 a) shows, must tend to be negative. Contrary to the values recorded for SD10 transducer when the slab was loaded with a line load over B5. After analyzing all the results, behaviors of the remaining beams and of the other specimens, photos of the specific test and laboratory notebook no explanation was found to justify this values, unless a fault in reading associated to the equipment. Thus, it was chosen to ignore the values recorded with SD10 in S2 B5lin test.

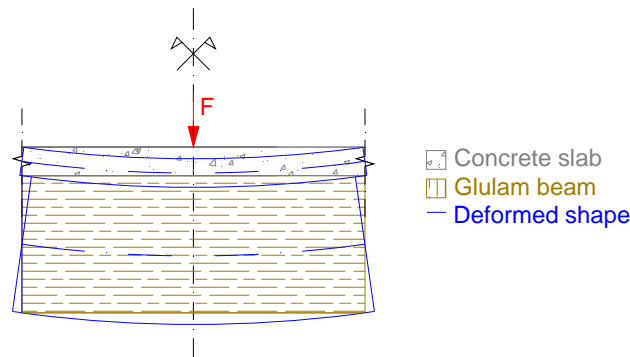


Fig. N.1 –Behavior of a composite beam in bending

B.2.4 Uplift displacements

Table B.9 – Experimental uplift displacements [mm]

Floor specimen	Load case	Displacement transducer position				Floor specimen	Load case	Displacement transducer position			
		UP1	UP 2	UP 3	UP 4			UP1	UP 2	UP 3	UP 4
S1-BSp	B1 ½	-1.515	0.285	-1.186	0.144	S4- L=2.00m	B1 ½	-2.130	0.089	-2.042	-0.001
	B2 ½	0.044	0.344	-0.131	0.256		B2 ½	0.836	0.069	0.953	-0.001
	B3 ½	0.649	0.415	0.377	0.339		B3 ½	1.185	1.004	1.327	0.985
	B4 ½	0.344	-0.408	0.260	-0.447		B4 ½	0.039	0.803	0.019	0.719
	B5 ½	0.044	-2.165	0.144	-0.772		B5 ½	0.004	-1.912	0.007	-1.773
	B1 ¼	-1.716	0.112	-0.672	0.133		B1 ¼	-2.497	0.033	-1.328	0.042
	B2 ¼	-0.074	0.207	-0.198	0.172		B2 ¼	1.068	-0.158	0.924	0.020
	B3 ¼	0.283	0.208	0.112	0.144		B3 ¼	-0.020	0.276	0.186	0.251
	B4 ¼	0.150	-0.468	0.201	-0.312		B4 ¼	-0.157	0.998	0.003	0.756
	B5 ¼	0.048	-2.390	0.142	-0.867		B5 ¼	-0.006	-2.297	0.021	-1.278
	B1 4P	-2.607	0.197	-3.074	0.056		B1lin	-2.112	0.090	-1.997	0.016
	B2 4P	0.237	0.665	-0.089	0.506		B2lin	0.825	0.092	0.924	0.007
	B3lin	0.504	0.402	0.390	0.219		B3lin	0.055	0.181	0.151	0.224
	B3 4P	1.333	1.504	1.753	1.392		B4lin	-0.061	0.922	-0.033	0.908
	B4lin	0.193	-0.010	-0.004	-0.152		B5lin	0.021	-1.849	0.018	-1.689
	B4 4P	0.632	0.212	0.606	0.060						
	B5lin	0.023	-1.770	-0.073	-1.421						
	B5 4P	0.109	-2.835	0.173	-2.695						
S2-LWAC	B1 ½	-2.186	0.148	-1.702	0.098	S5- L=6.00m	B1 ½	-1.197	0.147	-1.198	0.113
	B2 ½	0.060	0.349	0.109	0.281		B2 ½	-0.423	0.260	-0.241	0.234
	B3 ½	0.753	1.048	0.858	0.755		B3 ½	0.247	0.130	0.269	0.279
	B4 ½	0.278	0.452	0.264	0.538		B4 ½	0.378	-0.594	0.272	-0.194
	B5 ½	0.087	-2.591	0.060	-2.552		B5 ½	0.209	-1.574	0.134	-1.529
	B1 ¼	-2.604	0.059	-1.040	0.042		B1 ¼	-0.679	0.262	-1.945	0.094
	B2 ¼	1.221	0.106	0.109	0.244		B2 ¼	-0.433	0.253	-0.187	0.112
	B3 ¼	0.625	0.790	0.425	0.657		B3 ¼	-0.031	-0.046	0.268	0.208
	B4 ¼	0.154	1.368	0.160	0.373		B4 ¼	0.196	-0.539	0.239	-0.180
	B5 ¼	0.060	-3.100	0.045	-1.555		B5 ¼	0.188	-0.778	0.158	-2.218
	B1lin	-1.718	0.072	-1.546	0.014		B1lin	-1.001	0.086	-1.055	0.054
	B2lin	0.608	0.236	0.402	0.138		B2lin	-0.113	0.204	-0.032	0.146
	B3lin	0.693	0.797	0.782	0.598		B3lin	0.251	0.123	0.235	0.214
	B4lin	0.254	0.794	0.228	0.864		B4lin	0.296	-0.275	0.197	0.049
	B5lin	0.061	-2.008	0.068	-1.973		B5lin	0.116	-1.346	0.069	-1.253

Table B.9 – Experimental uplift displacements [mm] (cont.)

Floor specimen	Load case	Displacement transducer position				Floor specimen	Load case	Displacement transducer position			
		UP1	UP 2	UP 3	UP 4			UP1	UP 2	UP 3	UP 4
S3- hc=0.03m	B1 ½	-1.309	0.004	-1.386	0.009						
	B2 ½	0.042	0.004	-0.071	0.015						
	B3 ½	0.172	0.120	0.210	0.121						
	B4 ½	0.114	-0.026	0.130	-0.178						
	B5 ½	0.053	-0.803	0.034	-0.975						
	B1 ¼	-1.848	0.011	-0.791	0.011						
	B2 ¼	0.338	-0.050	-0.088	-0.020						
	B3 ¼	0.096	0.052	0.076	0.027						
	B4 ¼	0.000	0.133	0.026	-0.184						
	B5 ¼	0.010	-1.092	0.036	-0.655						
	B1lin	-0.914	0.033	-1.114	-0.045						
	B2lin	0.250	-0.041	0.143	-0.065						
	B3lin	0.090	0.017	0.107	0.001						
	B4lin	0.057	0.022	0.060	0.010						
	B5lin	0.042	-0.780	0.010	-0.925						

B.2.5 Strains**Table B.10 – Experimental strains [µε]**

Floor specimen	Load case	Beam position									
		B1		B2		B3		B4		B5	
S1-BSp	B1 ½	871.7	563.0	204.0	241.0	70.0	95.6	1.0	5.8	-24.0	-17.2
	B2 ½	395.5	236.4	455.1	502.4	220.7	274.4	88.2	94.9	0.0	7.7
	B3 ½	119.7	65.1	224.2	207.4	654.7	713.5	292.3	299.3	90.2	97.6
	B4 ½	12.4	3.8	71.8	62.4	244.7	255.2	616.4	560.3	355.0	327.2
	B5 ½	-11.5	-9.6	6.7	6.7	30.7	33.5	162.0	132.4	285.0	230.5
	B1 ¼	319.8	210.6	128.4	142.1	53.7	68.8	-1.9	1.9	-20.1	-15.3
	B2 ¼	254.6	160.8	107.3	108.5	125.7	145.3	71.9	72.9	-4.8	1.0
	B3 ¼	107.2	62.2	114.9	113.3	142.0	144.3	162.9	154.4	76.7	75.5
	B4 ¼	15.3	7.7	57.5	55.7	128.6	133.8	156.2	134.3	226.4	193.2
	B5 ¼	-12.4	-9.6	7.7	7.7	33.6	36.3	175.4	142.9	313.8	253.5
	B1 4P	958.0	615.7	195.4	244.9	57.6	79.3	4.8	6.7	-14.4	-11.5
	B2 4P	541.0	326.4	513.6	551.4	294.6	367.1	123.6	132.3	-1.0	13.4
	B3lin	50.7	27.7	90.0	81.6	155.4	162.5	120.7	118.0	35.5	40.2

Table B.10 – Experimental strains [$\mu\epsilon$] (cont.)

Floor specimen	Load case	Beam position									
		B1		B2		B3		B4		B5	
S1-BSp	B3 4P	158.9	87.1	345.9	316.9	845.8	963.3	417.9	436.5	95.0	104.3
	B4lin	4.8	1.9	39.3	34.6	115.1	124.3	217.5	193.7	165.0	149.2
	B4 4P	8.6	1.9	94.8	81.6	345.4	357.5	778.6	690.9	464.6	431.6
	B5lin	-7.7	-4.8	0.0	-1.9	30.7	31.5	110.2	88.2	184.3	150.2
	B5 4P	-17.2	-12.4	1.0	-1.0	76.7	80.3	338.3	259.0	813.3	676.7
S2-LWAC	B1 ½	717.3	995.1	246.6	239.7	36.3	54.6	-4.8	-3.8	-19.1	-18.2
	B2 ½	295.2	347.8	881.8	809.3	237.1	328.7	81.4	92.8	-28.6	-24.9
	B3 ½	19.2	7.7	376.6	305.6	865.7	1066.4	289.4	332.1	-11.4	0.0
	B4 ½	-13.4	-29.7	84.1	60.1	253.4	304.7	930.1	885.0	324.4	346.9
	B5 ½	-16.3	-31.6	-8.6	-6.7	7.6	33.5	237.7	208.7	1122.9	1086.4
	B1 ¼	304.8	424.5	176.8	174.7	25.8	37.4	-6.7	-6.7	-10.5	-9.6
	B2 ¼	199.4	249.1	325.0	325.7	182.6	240.5	42.2	53.6	-14.3	-14.4
	B3 ¼	31.6	26.8	245.6	199.6	326.0	399.6	200.3	214.4	15.3	25.9
	B4 ¼	-7.7	-18.2	64.0	45.8	173.0	204.1	323.9	319.7	226.1	229.0
	B5 ¼	-12.5	-24.9	-5.7	-6.7	3.8	23.9	164.8	159.8	476.2	439.9
	B1lin	115.0	155.2	78.4	76.4	8.6	15.3	-4.8	-3.8	-4.8	-4.8
	B2lin	156.2	189.7	262.0	254.1	139.6	189.7	36.4	42.1	-11.4	-17.2
	B3lin	24.9	24.9	198.8	161.4	247.7	319.2	167.7	184.7	15.3	20.1
	B4lin	-9.6	-15.3	65.0	49.6	179.7	214.6	361.4	362.9	246.2	253.0
	B5lin	-5.7	-9.6	-5.7	-6.7	-2.9	6.7	65.2	68.9	186.1	170.6
S3-hc=0.03m	B1 ½	445.0	882.1	130.5	191.8	20.1	28.7	-3.8	-3.8	-21.0	-14.4
	B2 ½	151.5	261.3	662.5	770.3	181.0	207.0	28.8	65.0	-20.0	-9.6
	B3 ½	6.7	13.4	193.8	216.6	485.7	506.0	95.0	213.2	27.6	23.9
	B4 ½	-11.5	-32.5	34.5	35.3	191.6	182.0	279.2	591.1	253.7	171.3
	B5 ½	-13.4	-21.1	-6.7	-15.3	27.8	28.7	47.0	130.0	679.3	429.8
	B1 ¼	212.9	429.8	108.4	140.2	15.3	22.0	-3.8	-6.7	-12.4	-7.7
	B2 ¼	102.6	177.1	236.1	252.8	130.3	142.8	10.6	30.6	-8.6	-3.8
	B3 ¼	13.4	20.1	124.7	143.1	176.2	166.7	59.5	126.2	32.4	24.9
	B4 ¼	-5.8	-15.3	28.8	30.5	128.3	121.7	83.5	182.6	175.5	123.5
	B5 ¼	-8.6	-22.0	-9.6	-9.5	22.0	21.1	49.9	94.6	304.2	184.7
	B1lin	50.8	104.3	29.7	40.1	0.0	7.7	-4.8	-7.6	-5.7	-6.7
	B2lin	75.7	127.3	157.4	182.2	75.7	98.7	-4.8	10.5	-13.3	-63.1
	B3lin	11.5	15.3	96.0	105.9	111.1	114.0	39.3	98.5	29.6	21.1
	B4lin	-6.7	-14.4	22.1	21.9	91.9	90.1	65.2	140.6	145.0	97.6
	B5lin	-7.7	-9.6	-2.9	-8.6	3.8	9.6	21.1	44.9	151.6	74.7

Table B.10 – Experimental strains [$\mu\epsilon$] (cont.)

Floor specimen	Load case	Beam position									
		B1		B2		B3		B4		B5	
S4-L=2.00m	B1 ½	542.3	738.9	138.1	101.7	7.7	6.7	-6.6	-6.7	1.0	-6.7
	B2 ½	97.8	100.8	957.1	711.2	161.5	190.1	-3.8	-1.9	-4.8	-7.7
	B3 ½	-2.9	-8.6	237.9	153.5	852.4	890.7	73.9	182.5	-11.5	-3.8
	B4 ½	-5.8	-3.8	29.7	19.2	199.0	181.5	608.2	652.4	170.5	145.0
	B5 ½	-1.9	1.0	-1.0	2.9	5.8	7.7	74.8	79.7	1286.1	766.8
	B1 ¼	336.8	408.2	116.1	81.5	1.9	0.0	-4.7	-6.7	-1.0	-3.8
	B2 ¼	63.3	59.5	536.4	380.9	116.3	135.4	-6.6	-2.9	-4.8	-1.9
	B3 ¼	-1.9	-4.8	114.1	67.1	436.6	466.8	70.9	99.9	-1.0	-1.9
	B4 ¼	-1.9	-6.7	-1.0	-5.8	141.3	127.7	331.7	324.7	104.4	81.6
	B5 ¼	-2.9	-7.7	-3.8	-4.8	-13.5	-1.0	51.9	52.8	700.7	399.6
	B1lin	259.1	345.8	63.3	46.0	1.9	-1.0	-2.8	-3.8	0.0	-2.9
	B2lin	64.3	59.5	601.7	452.9	112.5	129.6	-6.6	-6.7	-1.9	-6.7
	B3lin	-1.0	-1.9	168.8	99.8	614.7	644.6	87.7	129.6	1.0	7.7
	B4lin	-1.0	1.9	1.9	3.8	128.8	113.3	380.1	381.3	102.5	96.0
	B5lin	-1.9	0.0	-3.8	-1.9	-2.9	1.0	49.0	52.8	771.8	462.1
S5-L=6.00m	B1 ½	621.7	648.0	247.4	244.7	88.6	103.8	9.6	16.3	-18.2	-20.2
	B2 ½	405.4	386.4	795.3	677.6	304.4	359.5	131.7	144.2	14.4	28.8
	B3 ½	129.7	113.4	330.8	260.0	692.8	738.4	369.2	370.1	124.7	178.9
	B4 ½	25.0	16.3	143.8	110.3	315.9	304.7	936.0	831.8	435.6	608.9
	B5 ½	-10.6	-25.0	21.1	12.5	73.2	86.5	328.8	282.6	850.5	1001.3
	B1 ¼	255.5	262.4	167.8	153.5	68.4	79.8	9.6	14.4	-26.9	-37.5
	B2 ¼	254.5	254.7	188.9	169.8	173.3	197.0	123.0	124.0	9.6	23.1
	B3 ¼	108.5	98.0	173.5	157.4	165.6	190.3	217.2	201.8	101.7	141.4
	B4 ¼	14.4	7.7	99.7	79.6	168.5	180.7	238.4	208.6	284.0	385.7
	B5 ¼	-25.0	-31.7	12.5	10.6	67.4	65.3	218.2	182.6	321.4	405.9
	B1lin	174.8	182.6	117.0	107.5	49.1	59.6	2.9	6.7	-8.6	-14.4
	B2lin	205.6	214.4	231.1	190.0	164.7	191.2	101.9	104.8	12.5	18.3
	B3lin	101.8	88.4	181.2	148.7	193.6	209.5	215.3	200.9	92.1	135.6
	B4lin	17.3	9.6	102.6	77.7	164.7	182.6	289.4	249.0	265.8	331.0
	B5lin	-4.8	-10.6	10.5	6.7	44.3	54.8	164.4	149.9	261.0	300.2

½ - mid-span; ¼ - quarter-span; lin - line load; 4P - 4-point load

Table B.11 – Strain distribution [%]

Floor specimen	Load case	Beam position					Floor specimen	Load case	Beam position				
		B1	B2	B3	B4	B5			B1	B2	B3	B4	B5
S1-BSp	B1 ½	71	22	8	0	-2	S4-L=2.00m	B1 ½	84	16	1	-1	0
	B2 ½	28	42	22	8	0		B2 ½	9	76	16	0	-1
	B3 ½	7	16	50	21	7		B3 ½	0	17	74	11	-1
	B4 ½	1	5	20	47	27		B4 ½	0	2	19	63	16
	B5 ½	-2	2	7	34	59		B5 ½	0	0	1	7	92
	B1 ¼	60	30	14	0	-4		B1 ¼	80	21	0	-1	-1
	B2 ¼	40	21	26	14	0		B2 ¼	10	72	20	-1	-1
	B3 ¼	15	20	25	28	13		B3 ¼	-1	15	73	14	0
	B4 ¼	2	10	24	26	38		B4 ¼	-1	-1	25	60	17
	B5 ¼	-2	2	7	34	60		B5 ¼	-1	-1	-1	9	94
	B1 4P	74	21	6	1	-1		B1lin	86	15	0	-1	0
	B2 4P	30	37	23	9	0		B2lin	9	75	17	-1	-1
	B3lin	9	19	36	27	9		B3lin	0	15	72	12	0
	B3 4P	7	18	48	23	5		B4lin	0	0	20	63	16
	B4lin	1	7	23	39	30		B5lin	0	0	0	8	93
	B4 4P	0	5	22	45	28							
	B5lin	-2	0	11	34	58							
	B5 4P	-1	0	7	27	67							
S2-LWAC	B1 ½	76	22	4	0	-2	S5-L=6.00m	B1 ½	65	25	10	1	-2
	B2 ½	21	56	19	6	-2		B2 ½	24	45	20	8	1
	B3 ½	1	21	59	19	0		B3 ½	7	18	43	22	9
	B4 ½	-1	5	18	58	21		B4 ½	1	7	17	47	28
	B5 ½	-2	-1	2	17	84		B5 ½	-1	1	6	23	71
	B1 ¼	66	32	6	-1	-2		B1 ¼	55	34	16	3	-7
	B2 ¼	28	41	27	6	-2		B2 ¼	34	24	24	16	2
	B3 ¼	3	26	43	25	2		B3 ¼	13	21	23	27	16
	B4 ¼	-2	7	24	41	29		B4 ¼	1	11	21	27	40
	B5 ¼	-3	-1	2	27	75		B5 ¼	-5	2	11	33	59
	B1lin	63	36	6	-2	-2		B1lin	53	33	16	1	-3
	B2lin	28	42	27	6	-2		B2lin	29	29	25	14	2
	B3lin	4	26	42	26	3		B3lin	12	21	26	27	15
	B4lin	-1	7	23	42	29		B4lin	2	11	21	32	35
B5lin	-3	-3	1	29	76	B5lin	-2	2	10	32	57		
S3-hc=0.03m	B1 ½	80	19	3	0	-2							
	B2 ½	18	62	17	4	-1							
	B3 ½	1	23	56	17	3							
	B4 ½	-3	4	22	51	25							
	B5 ½	-3	-2	4	14	86							

Table B.11 – Strain distribution [%] (cont.)

Floor specimen	Load case	Beam position					Floor specimen	Load case	Beam position				
		B1	B2	B3	B4	B5			B1	B2	B3	B4	B5
S3-hc=0.03m	B1 ¼	72	28	4	-1	-2							
	B2 ¼	26	46	26	4	-1							
	B3 ¼	4	30	39	21	6							
	B4 ¼	-2	7	29	31	35							
	B5 ¼	-5	-3	7	23	78							
	B1lin	75	34	4	-6	-6							
	B2lin	31	53	27	1	-12							
	B3lin	4	31	35	21	8							
	B4lin	-3	7	28	32	37							
	B5lin	-6	-4	5	24	82							

½ - mid-span; ¼ - quarter-span; lin - line load; 4P - 4-point load

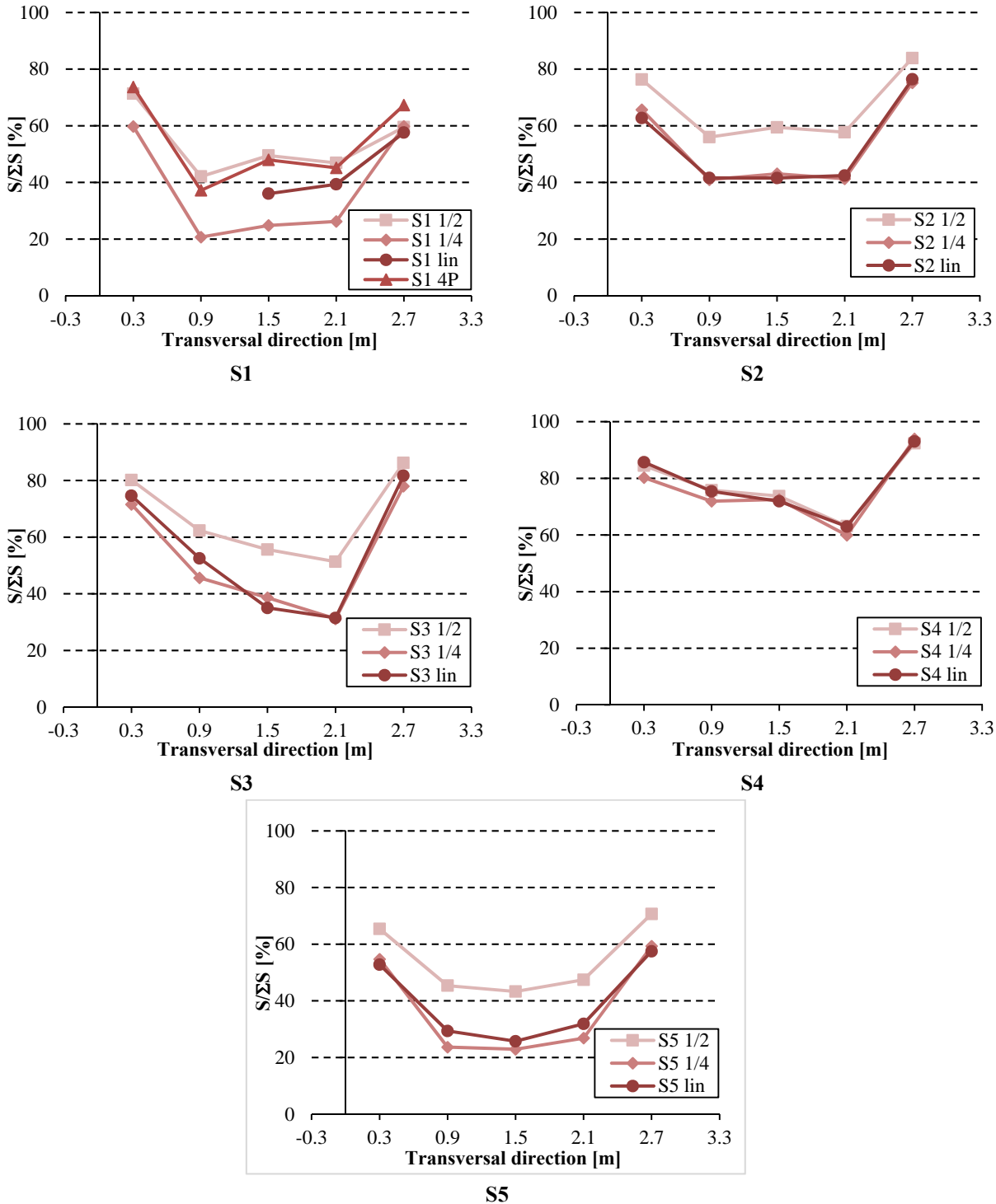


Fig. B.91 – Strain distribution for the loaded beam

B.3 Results from the numerical prediction analysis

The following figures present the results obtained with the numerical model in terms of vertical displacements and support reactions together with the experimental ones. Also the distributions, in terms of displacements and reactions, were computed and presented. For each load case and every measuring location, the displacement associated with a beam was divided by the sum of displacements in the five beams, for the same location and load case. A similar procedure was adopted to compute the support reaction distribution.

The symbology is the same used at the *4.5 Experimental vs. numerical results*.

B.3.1 Vertical displacements

Fig. B.92 to Fig. B.116 summarize the vertical displacements numerically obtained (left) for the five specimens and also the displacement distribution (right), received by each beam at every measuring location for the several loading cases. Table B.12 gathers the numerical distribution of vertical displacements and Table B.13 the differences found between experimental and numerical results.

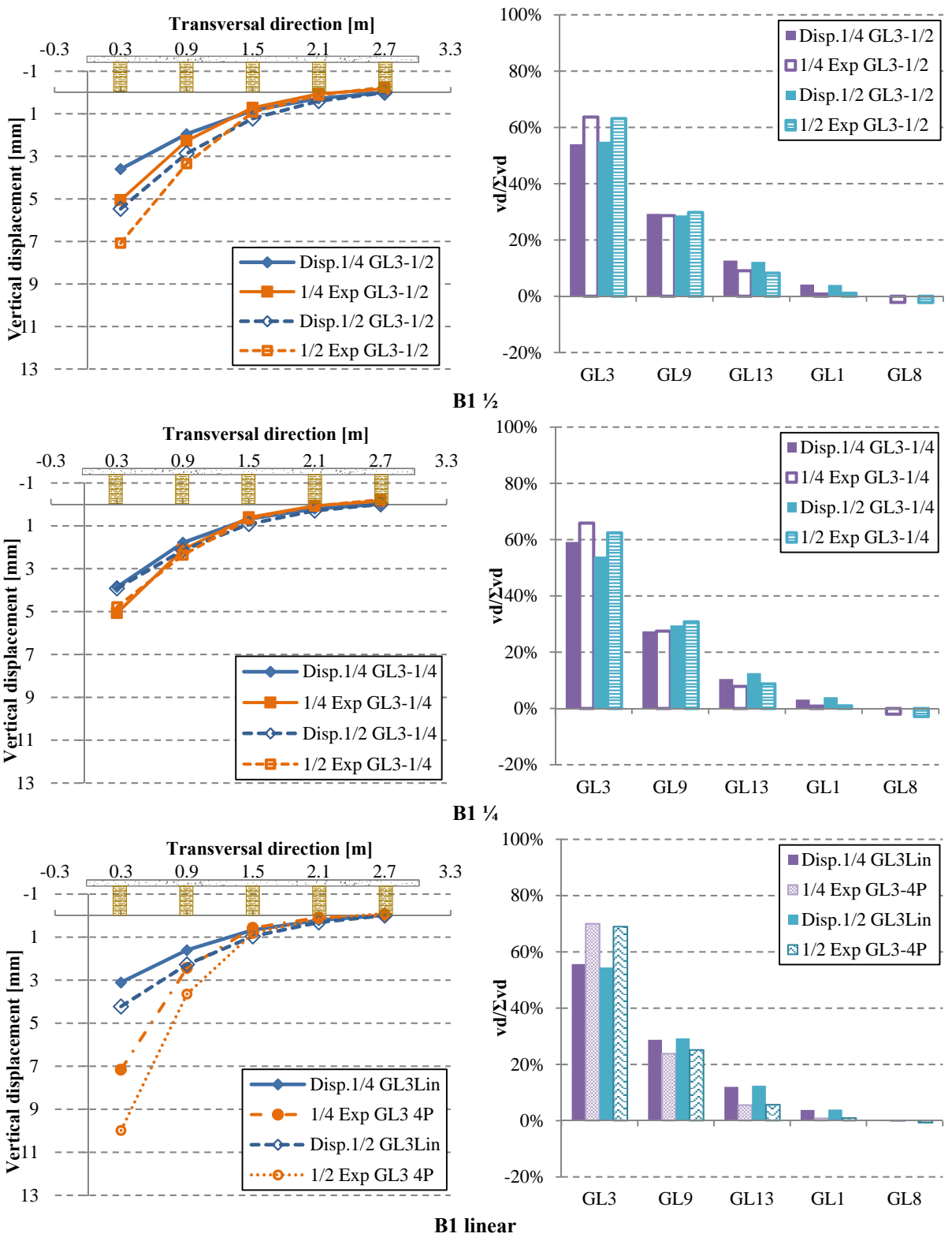


Fig. B.92 – S1-BSp: experimental and numerical vertical displacements when loaded at B1-GL3

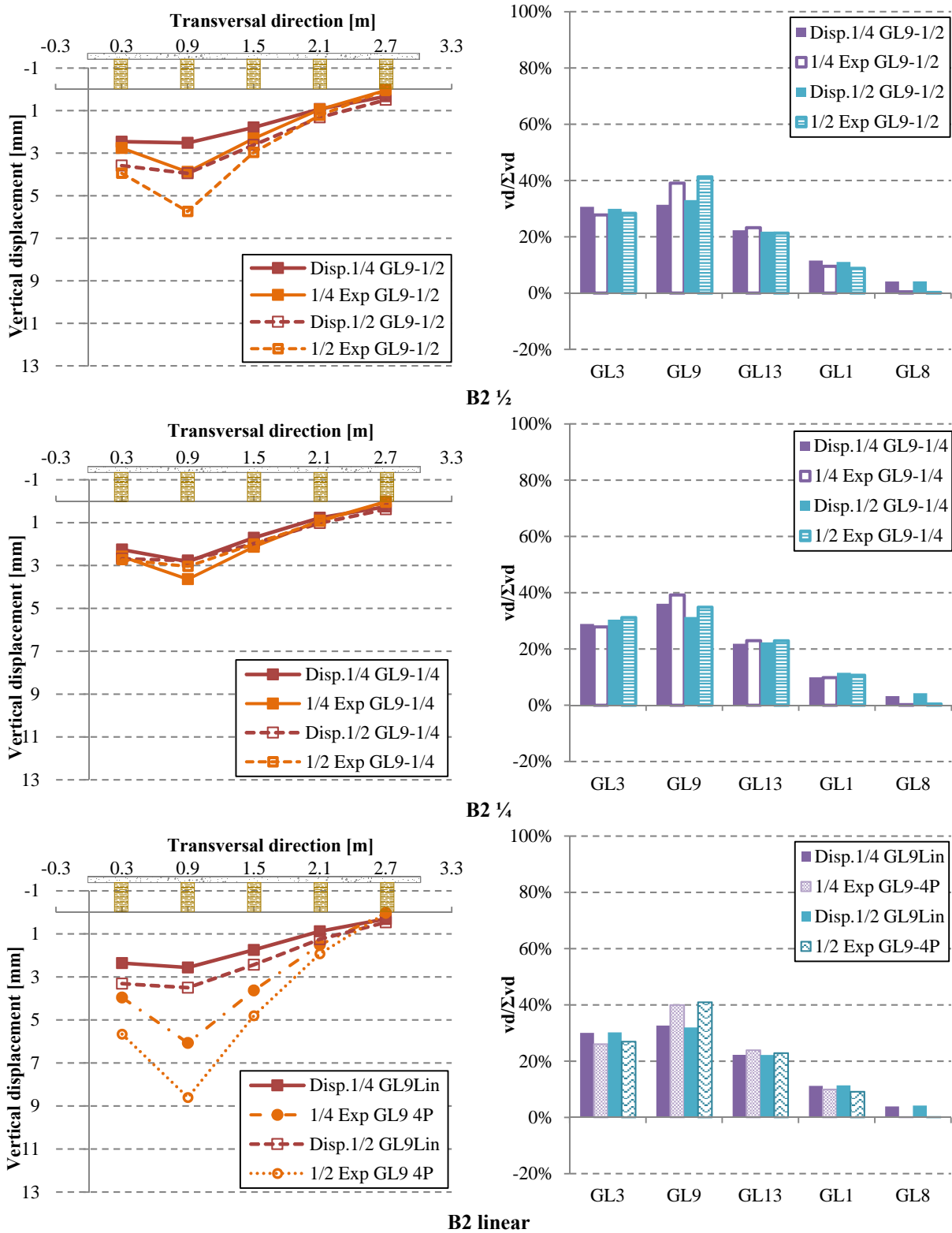


Fig. B.93 – S1-BSp: experimental and numerical vertical displacements when loaded at B2-GL9

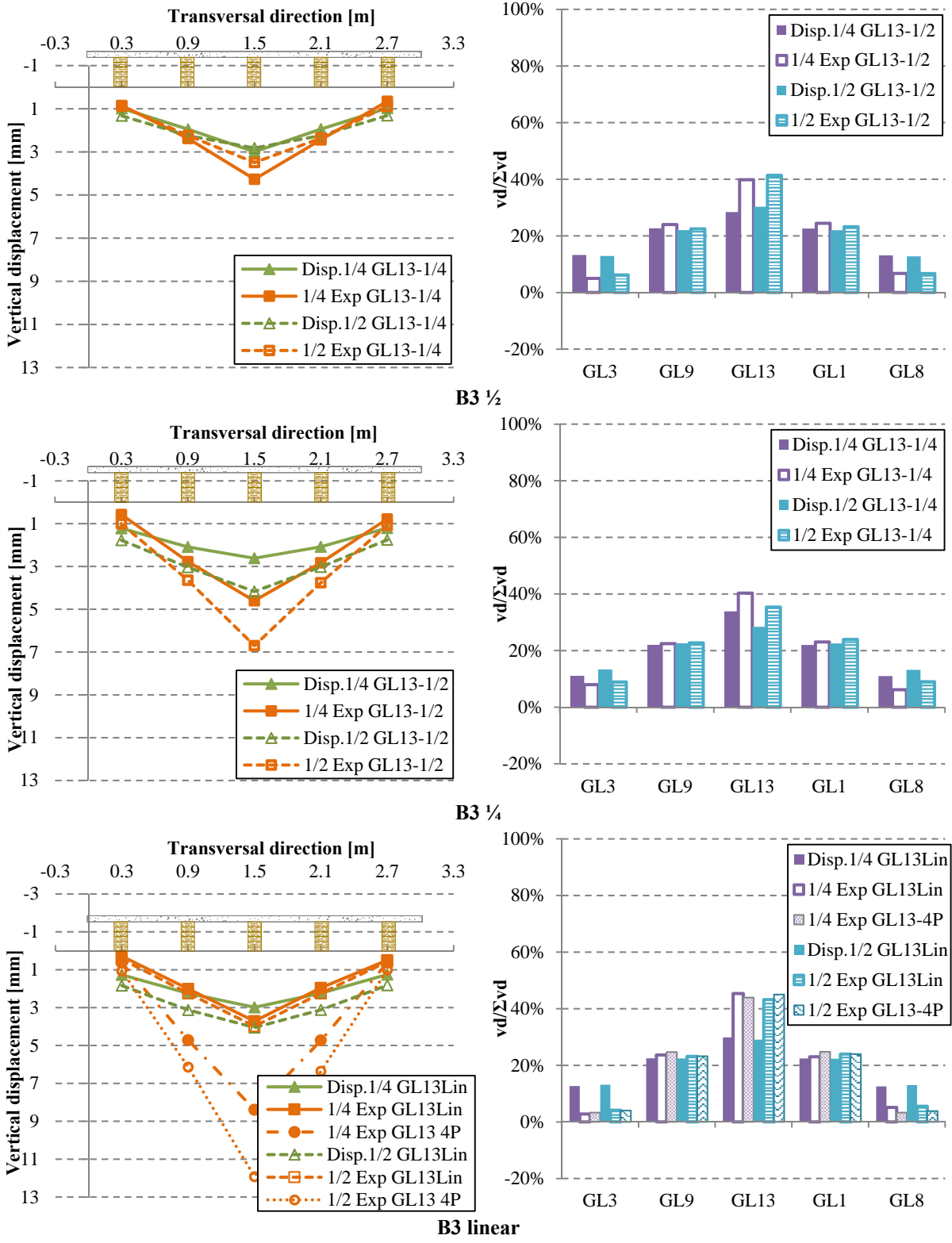


Fig. B.94 – S1-BSp: experimental and numerical vertical displacements when loaded at B3-GL13

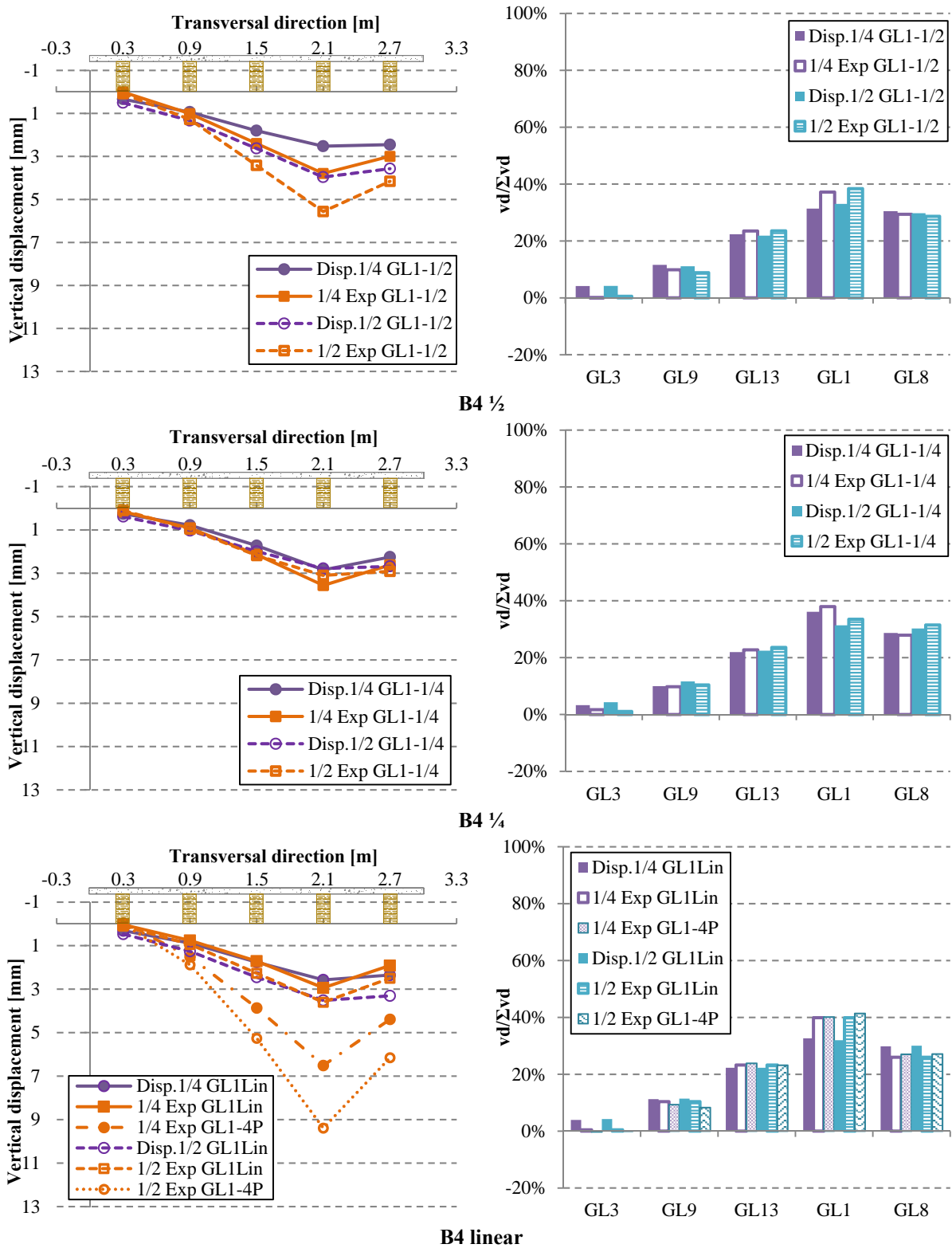


Fig. B.95 – S1-BSp: experimental and numerical vertical displacements when loaded at B4-GL1

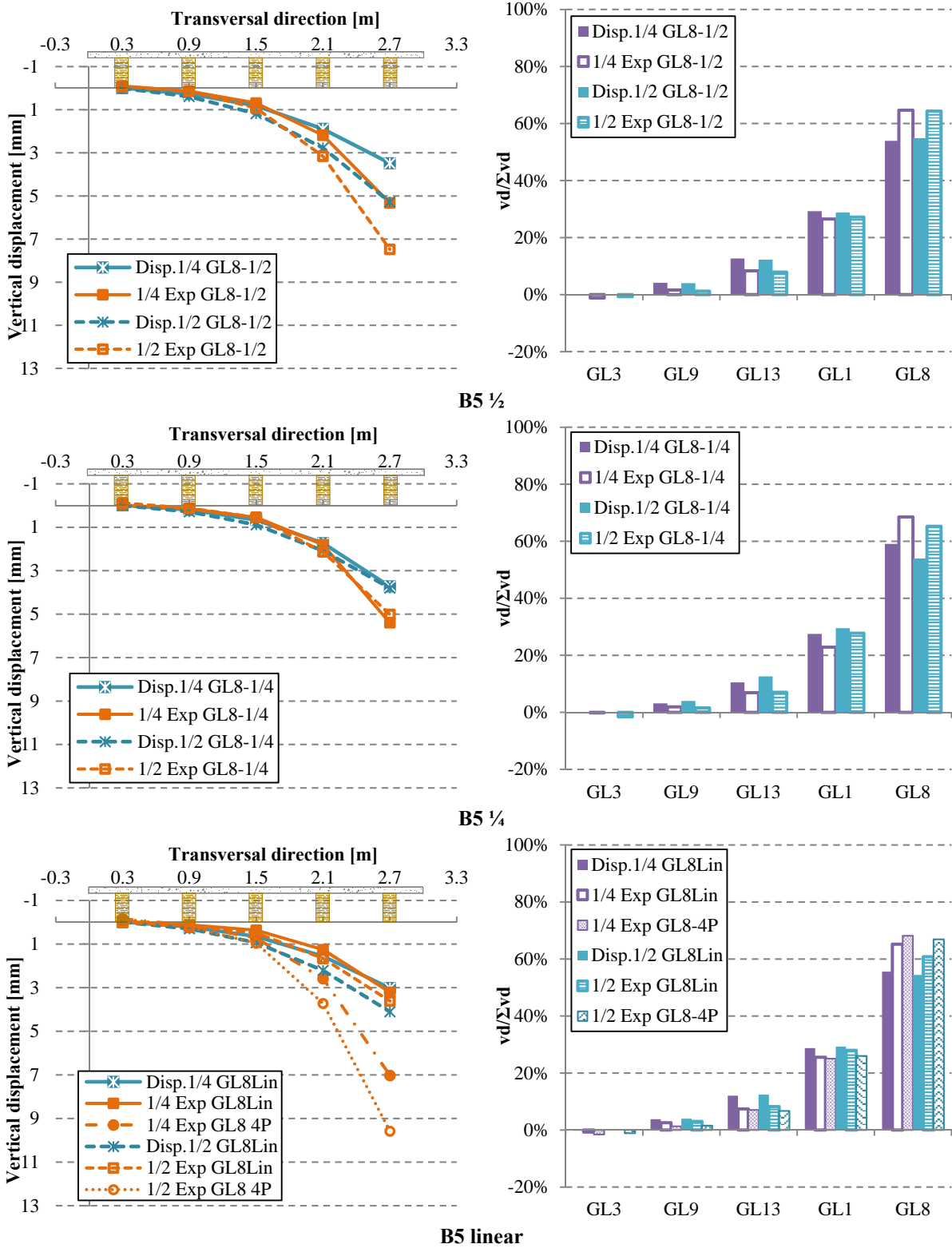


Fig. B.96 – S1-BSp: experimental and numerical vertical displacements when loaded at B5-GL8

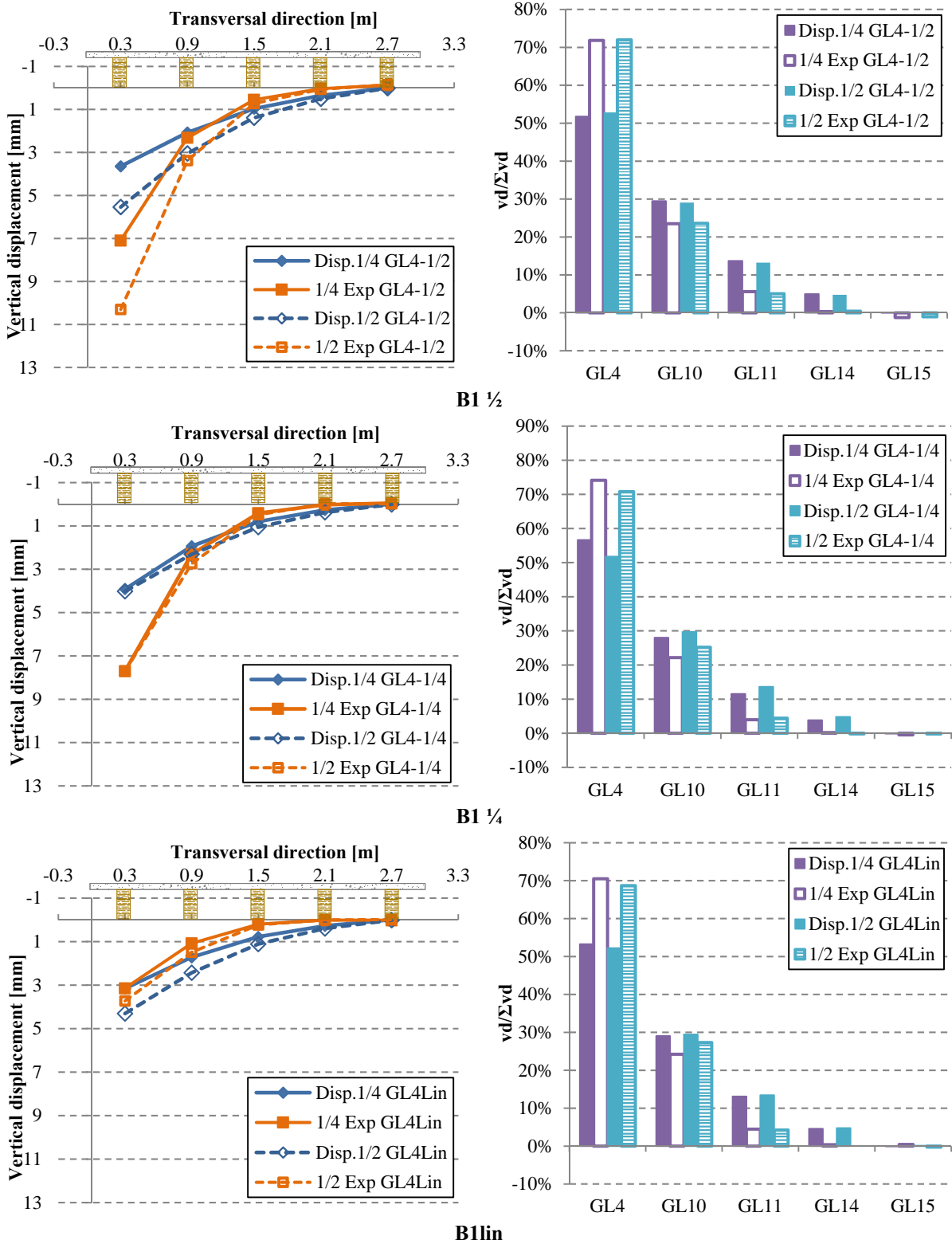


Fig. B.97 – S2-LWAC: experimental and numerical vertical displacements when loaded at B1-GL4

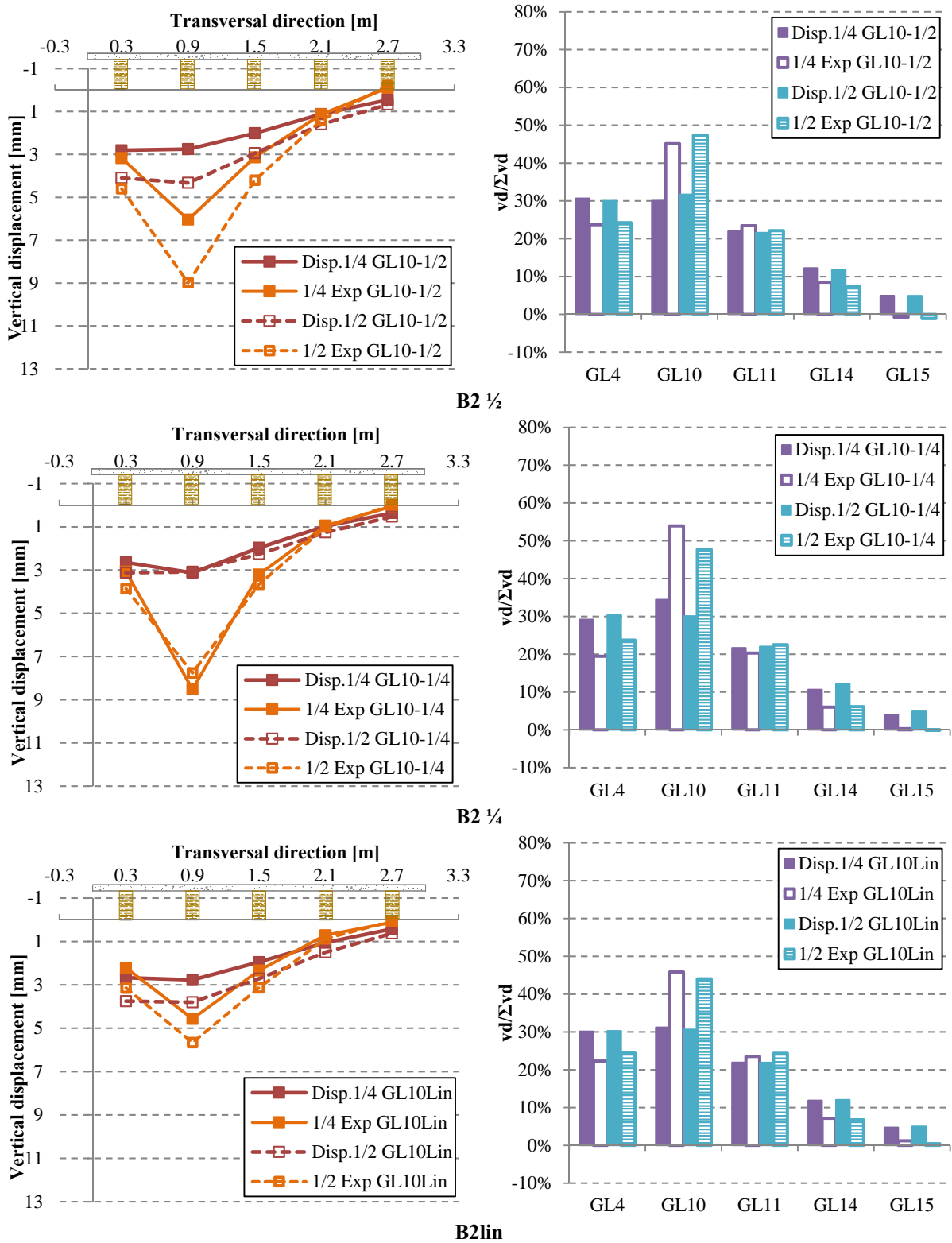


Fig. B.98 – S2-LWAC: experimental and numerical vertical displacements when loaded at B2-GL10

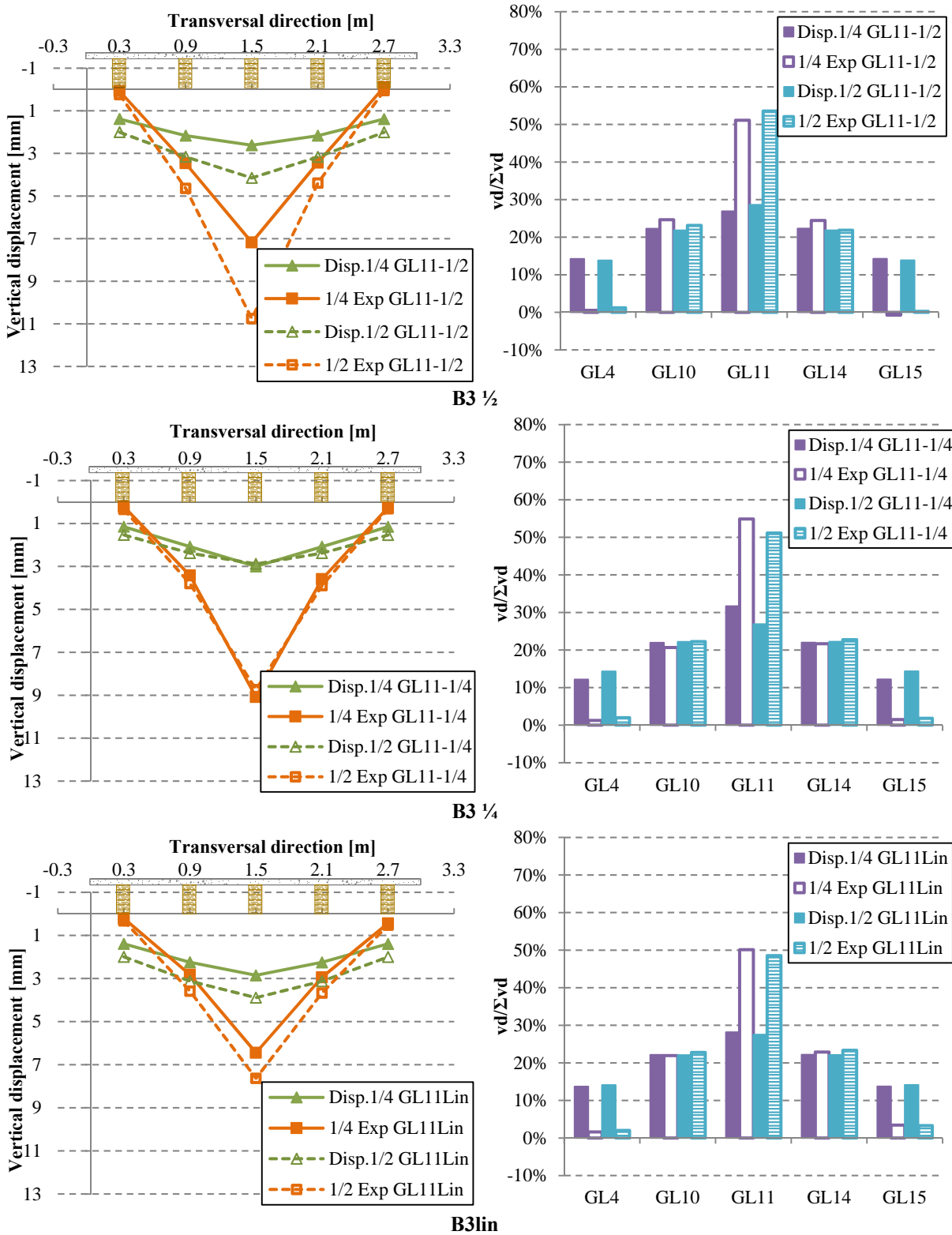
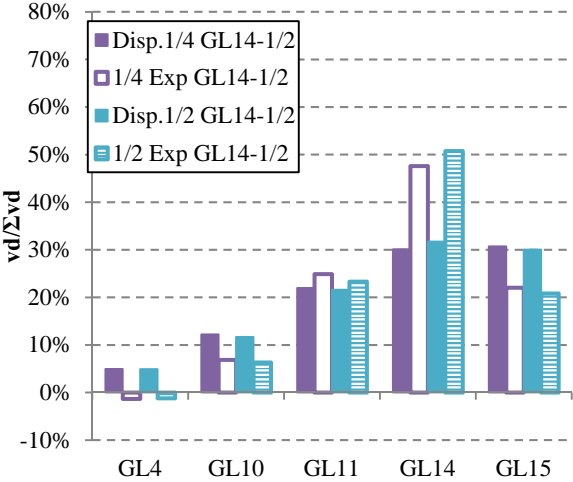
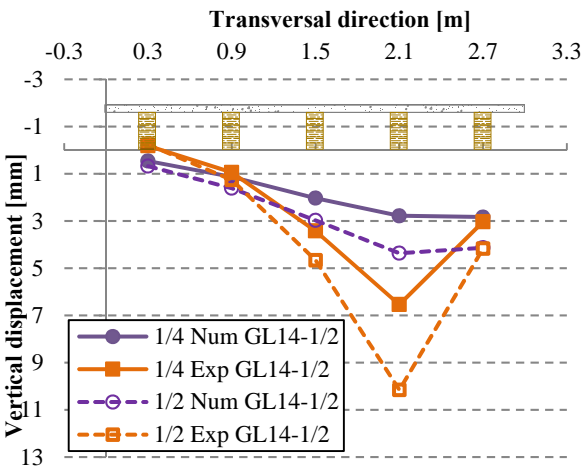
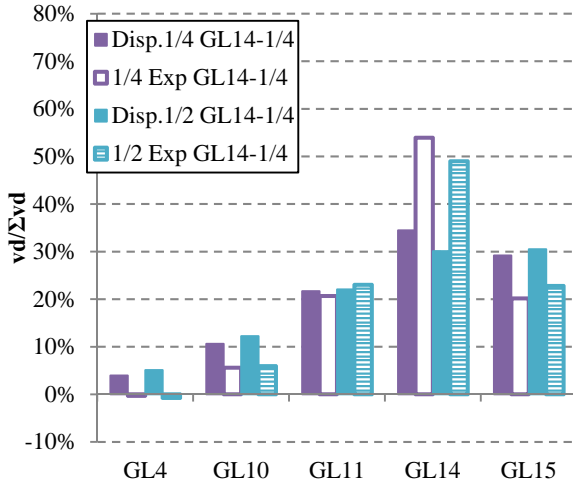
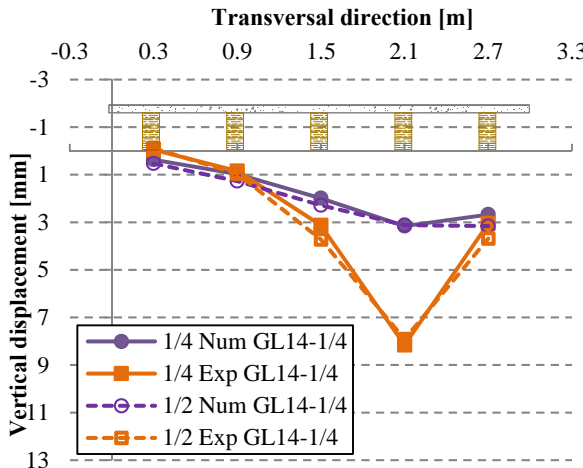


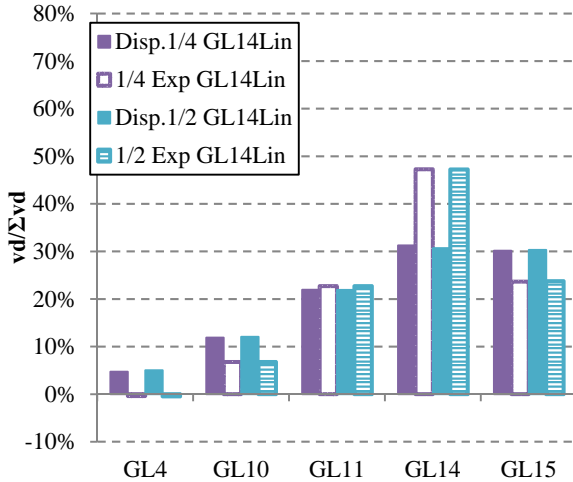
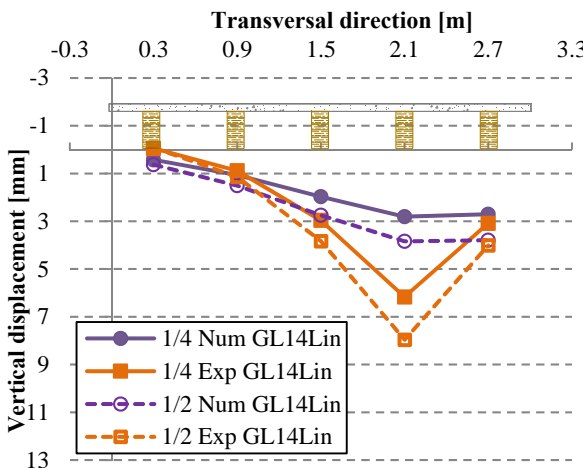
Fig. B.99 – S2-LWAC: experimental and numerical vertical displacements when loaded at B3-GL11



B4 1/2



B4 1/4



B4lin

Fig. B.100 – S2-LWAC: experimental and numerical vertical displacements when loaded at B4-GL14

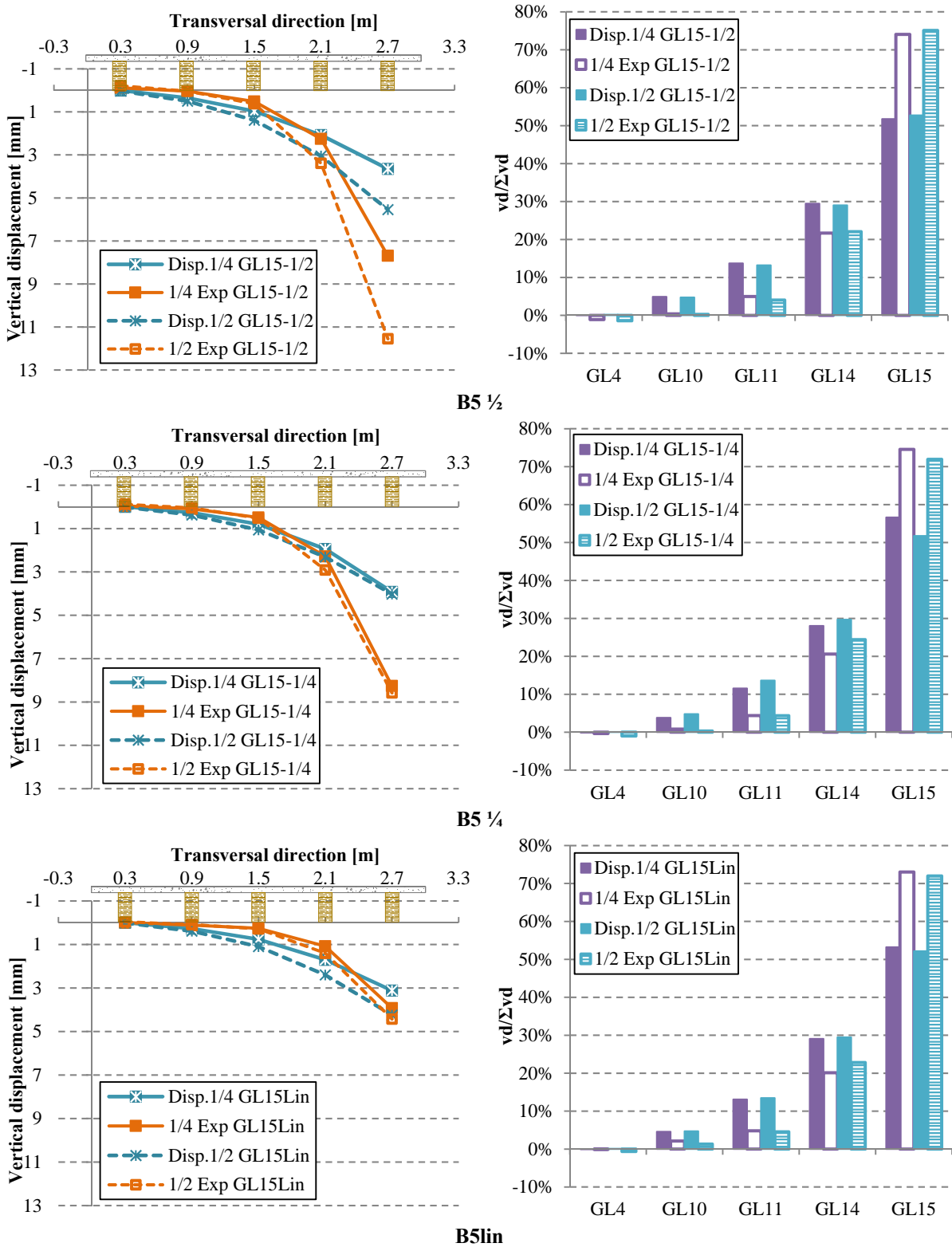


Fig. B.101 – S2-LWAC: experimental and numerical vertical displacements when loaded at B5-GL15

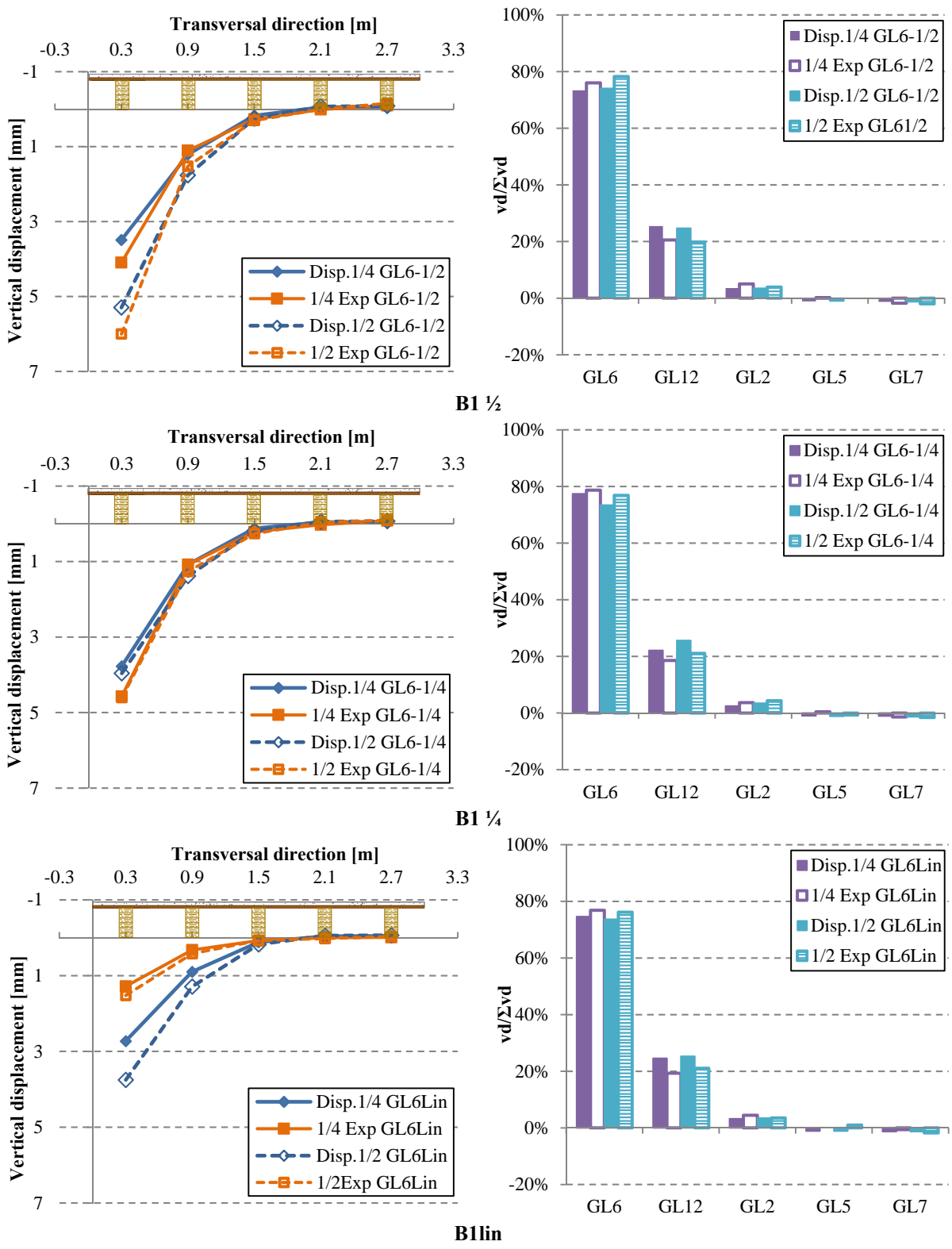


Fig. B.102 – S3-hc=0.03m: experimental and numerical vertical displacements when loaded at B1-GL6

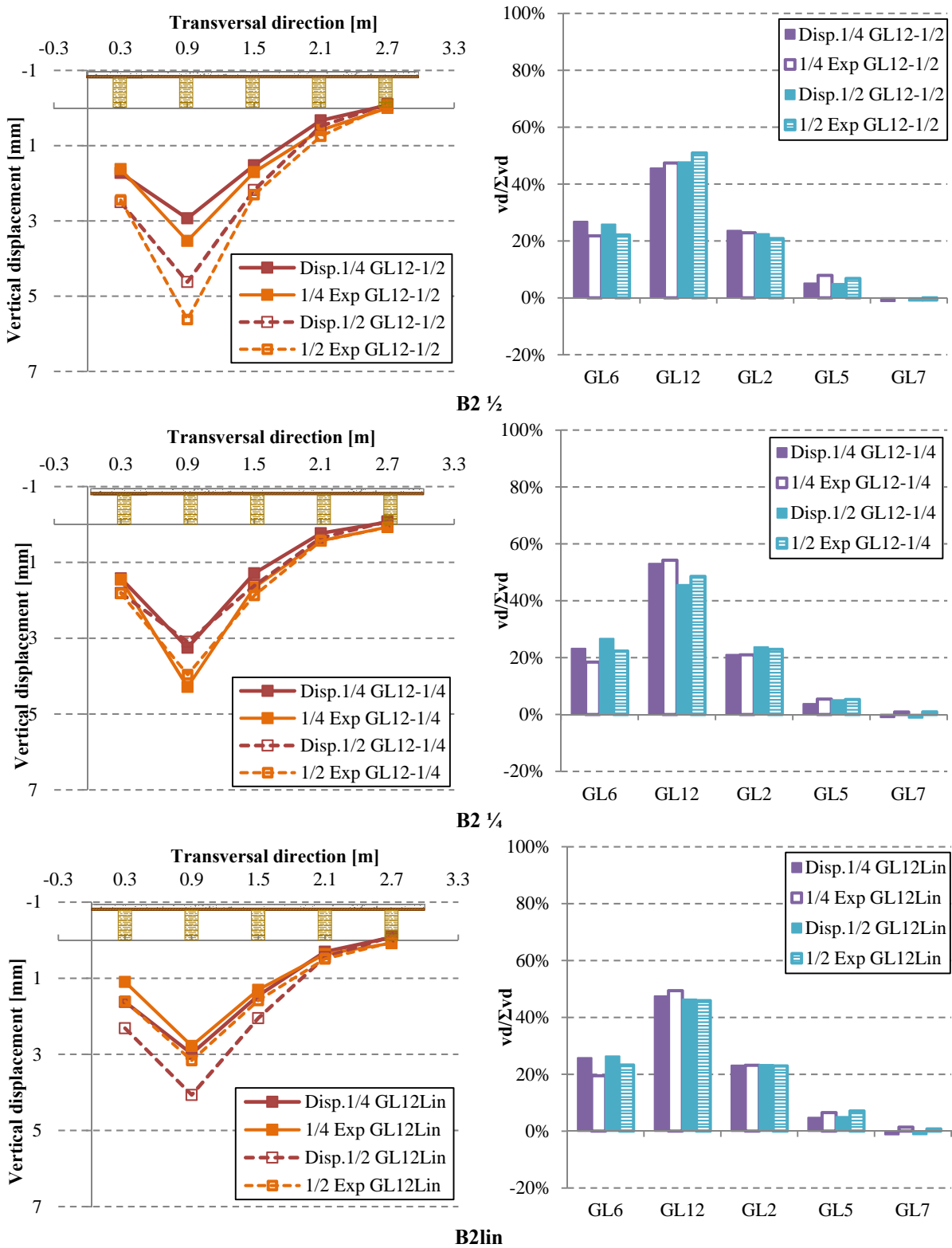


Fig. B.103 – S3-hc=0.03m: experimental and numerical vertical displacements when loaded at B2-GL12

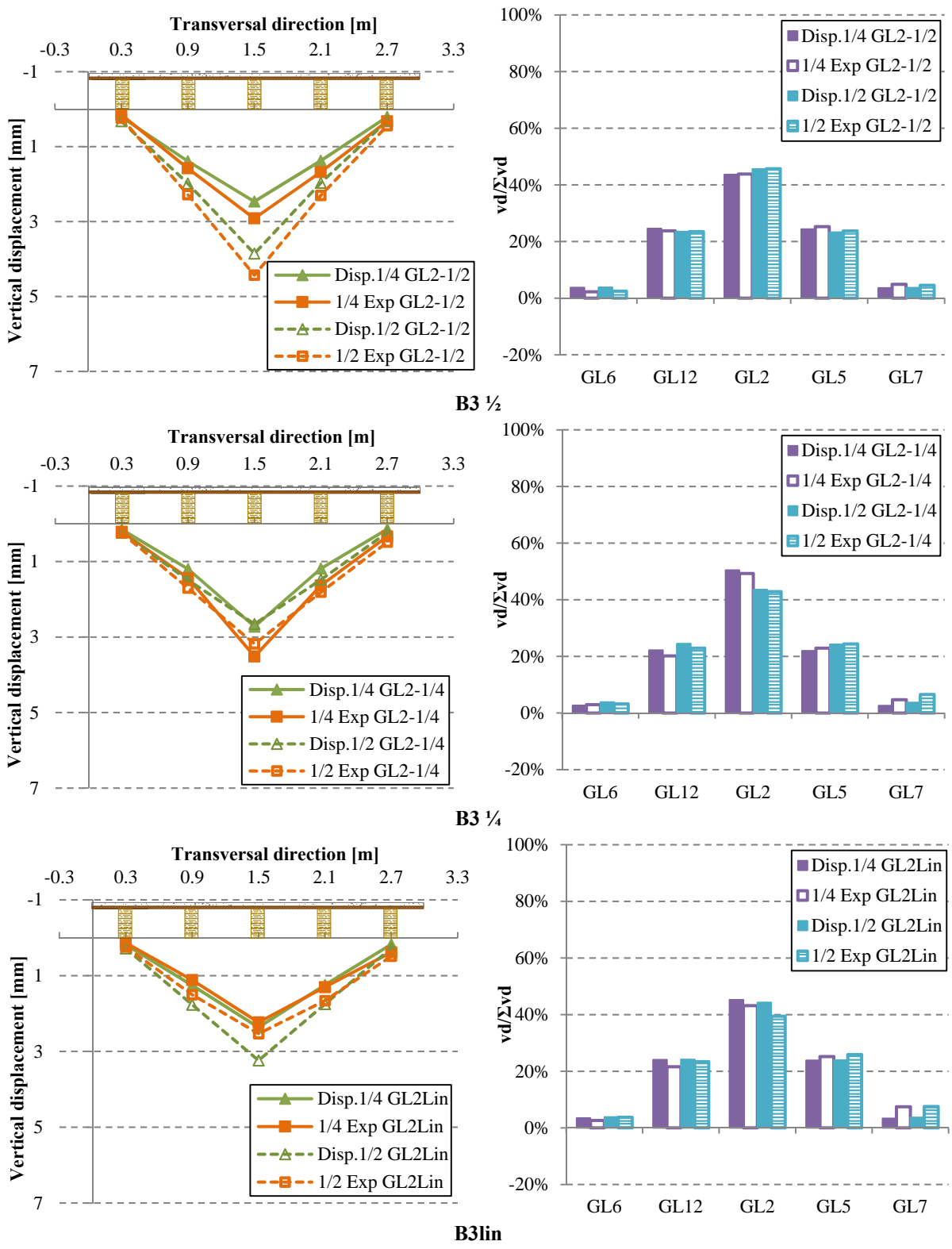


Fig. B.104 – S3-hc=0.03m: experimental and numerical vertical displacements when loaded at B3-GL2

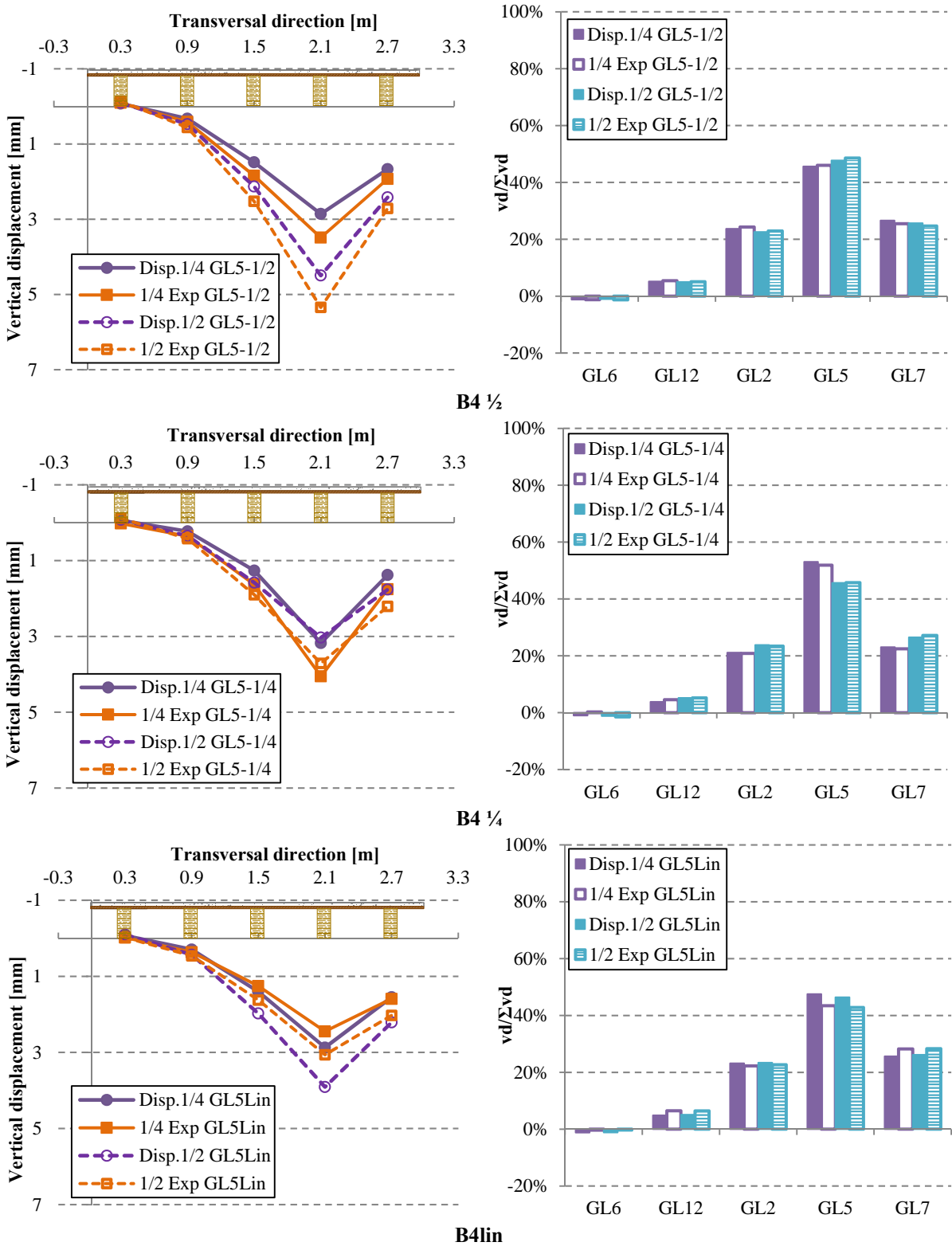


Fig. B.105 – S3-hc=0.03m: experimental and numerical vertical displacements when loaded at B4-GL5

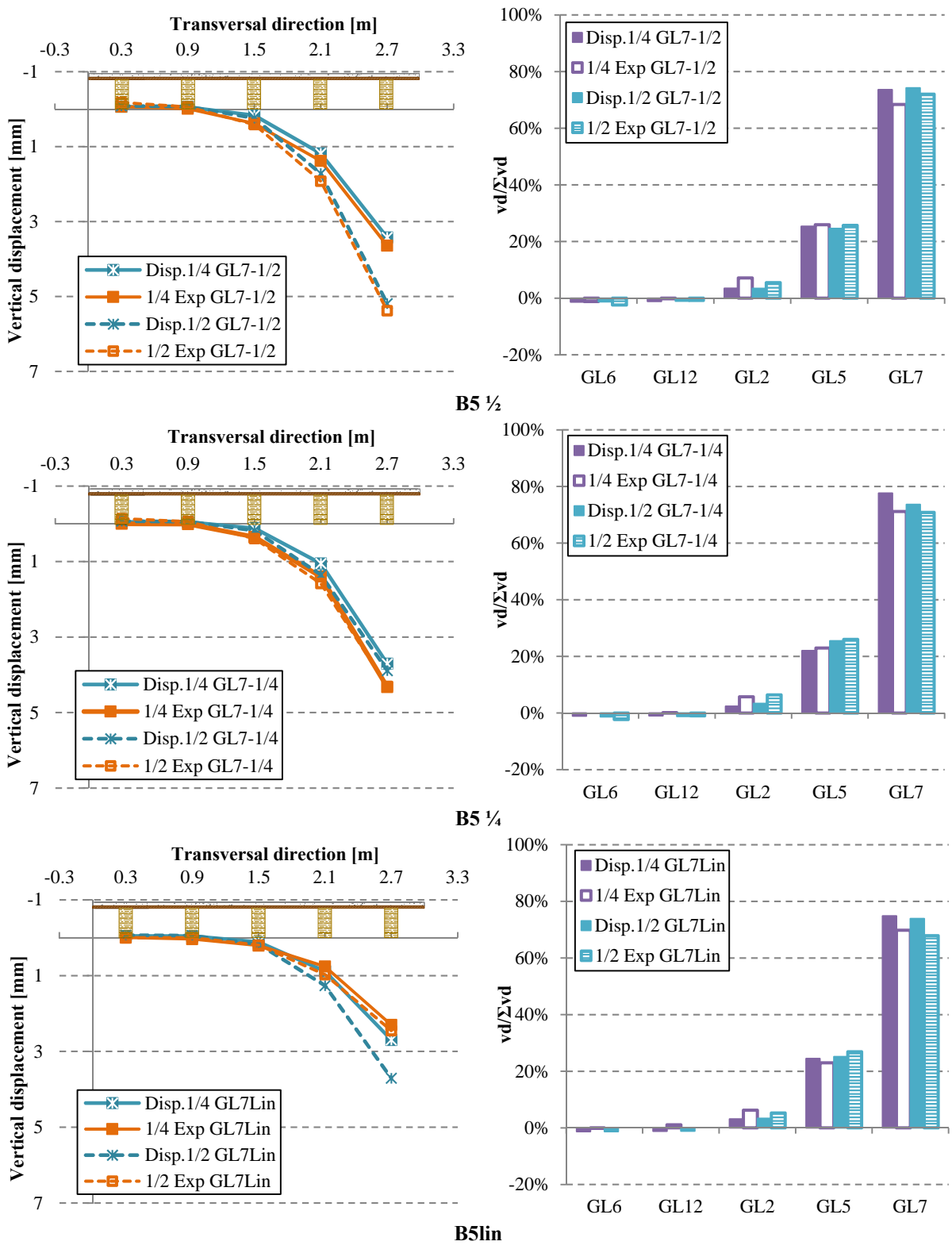


Fig. B.106 – S3-hc=0.03m: experimental and numerical vertical displacements when loaded at B5-GL7

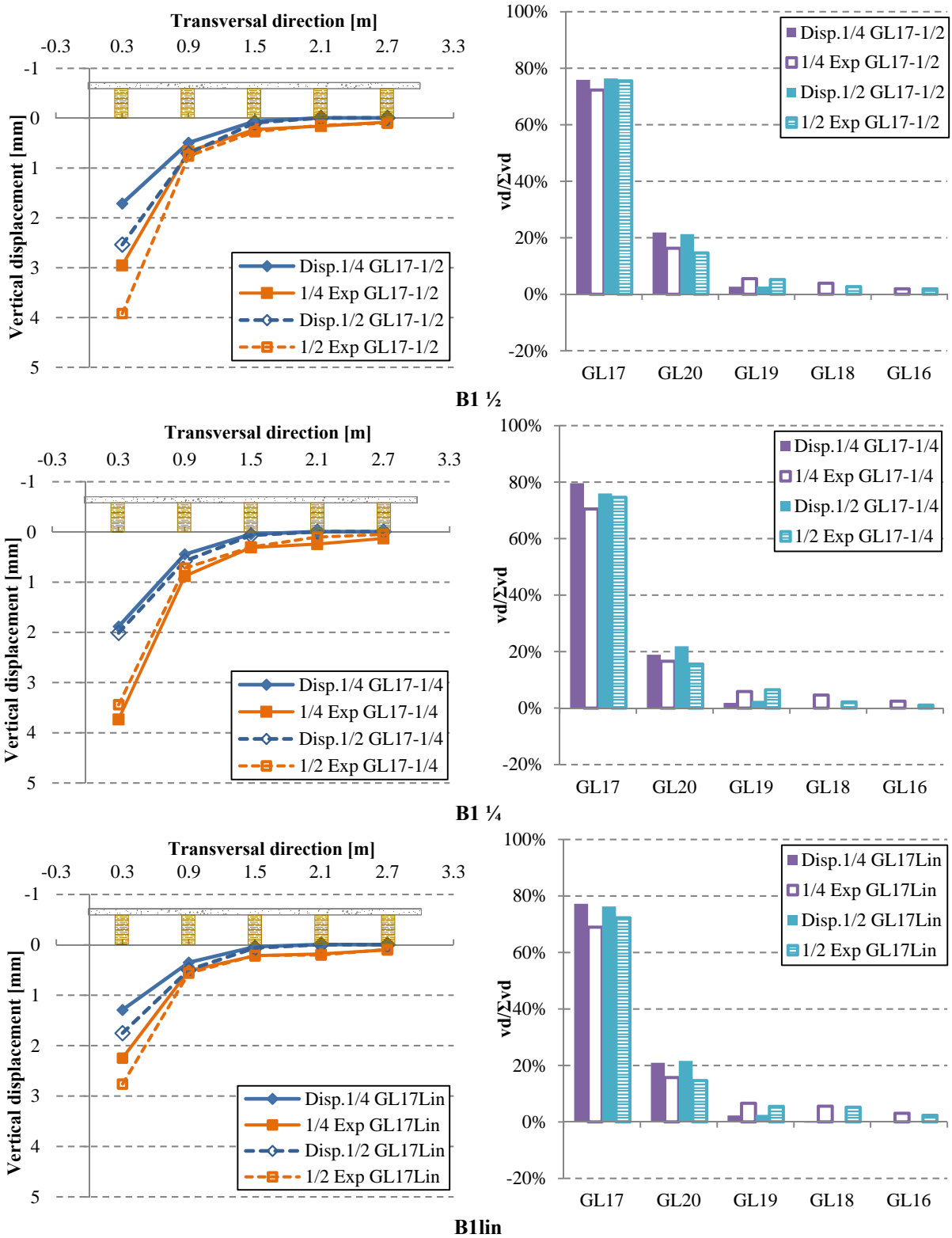


Fig. B.107 – S4-L=2.00m: experimental and numerical vertical displacements when loaded at B1-GL17

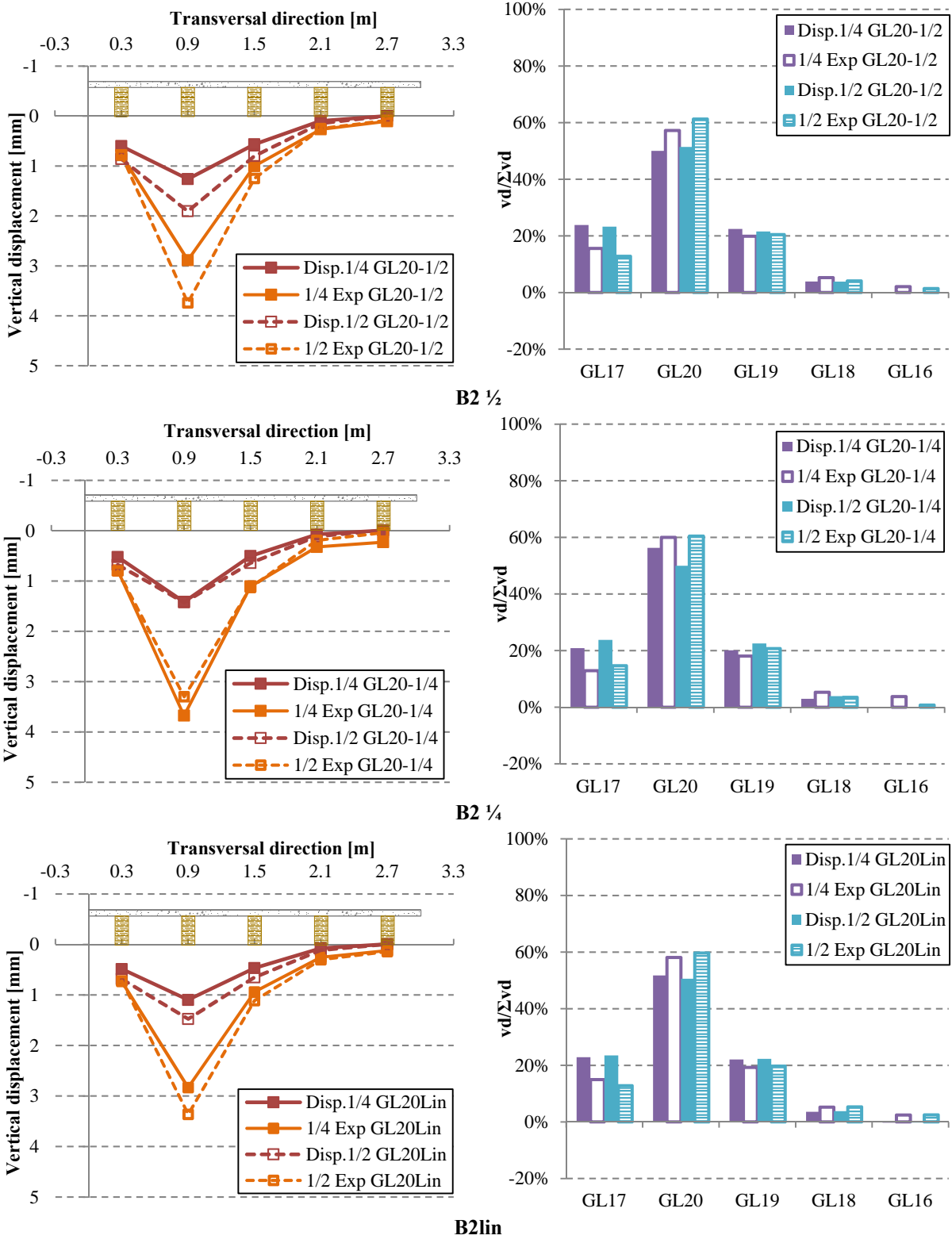


Fig. B.108 – S4-L=2.00m: experimental and numerical vertical displacements when loaded at B2-GL20

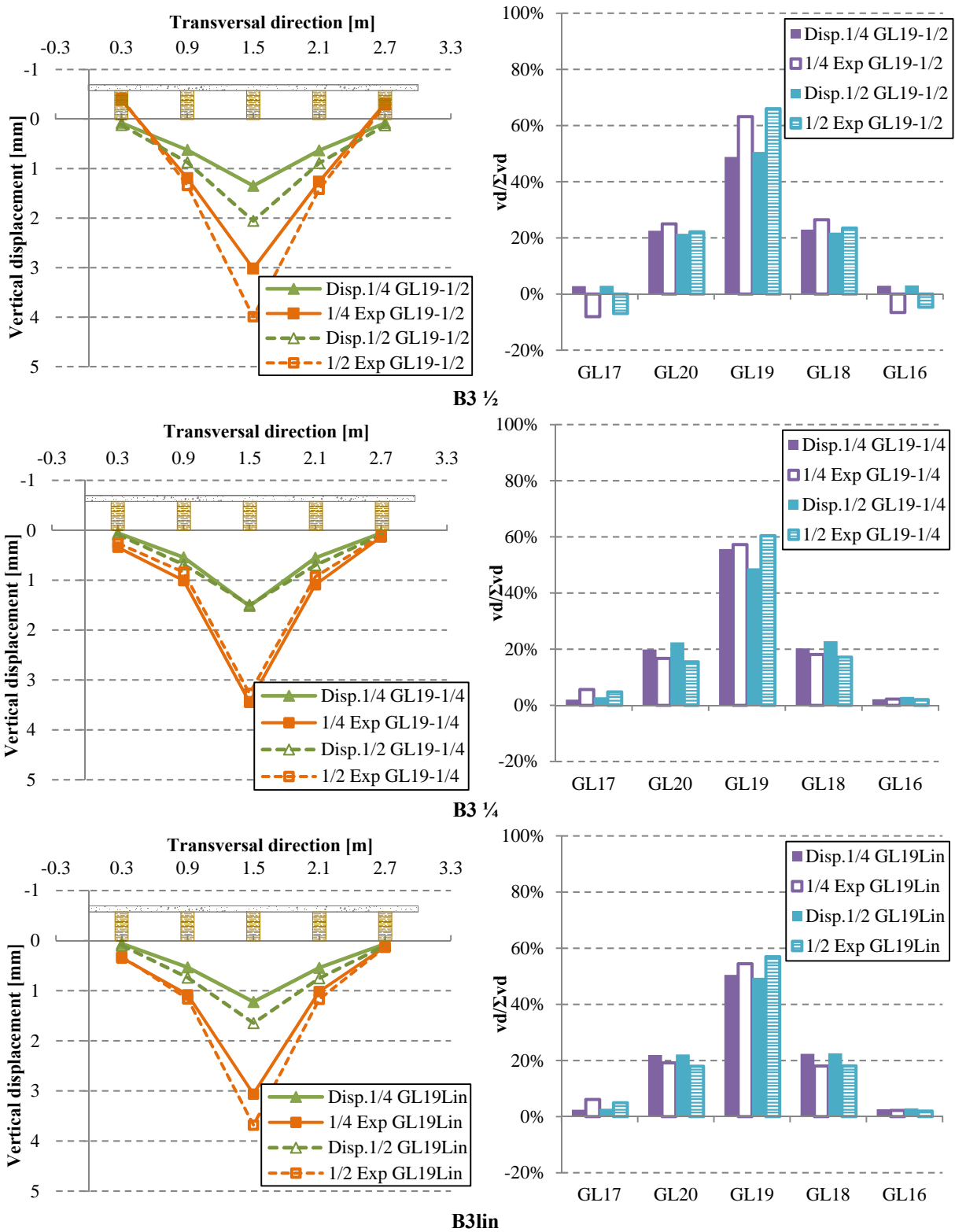


Fig. B.109 – S4-L=2.00m: experimental and numerical vertical displacements when loaded at B3-GL19

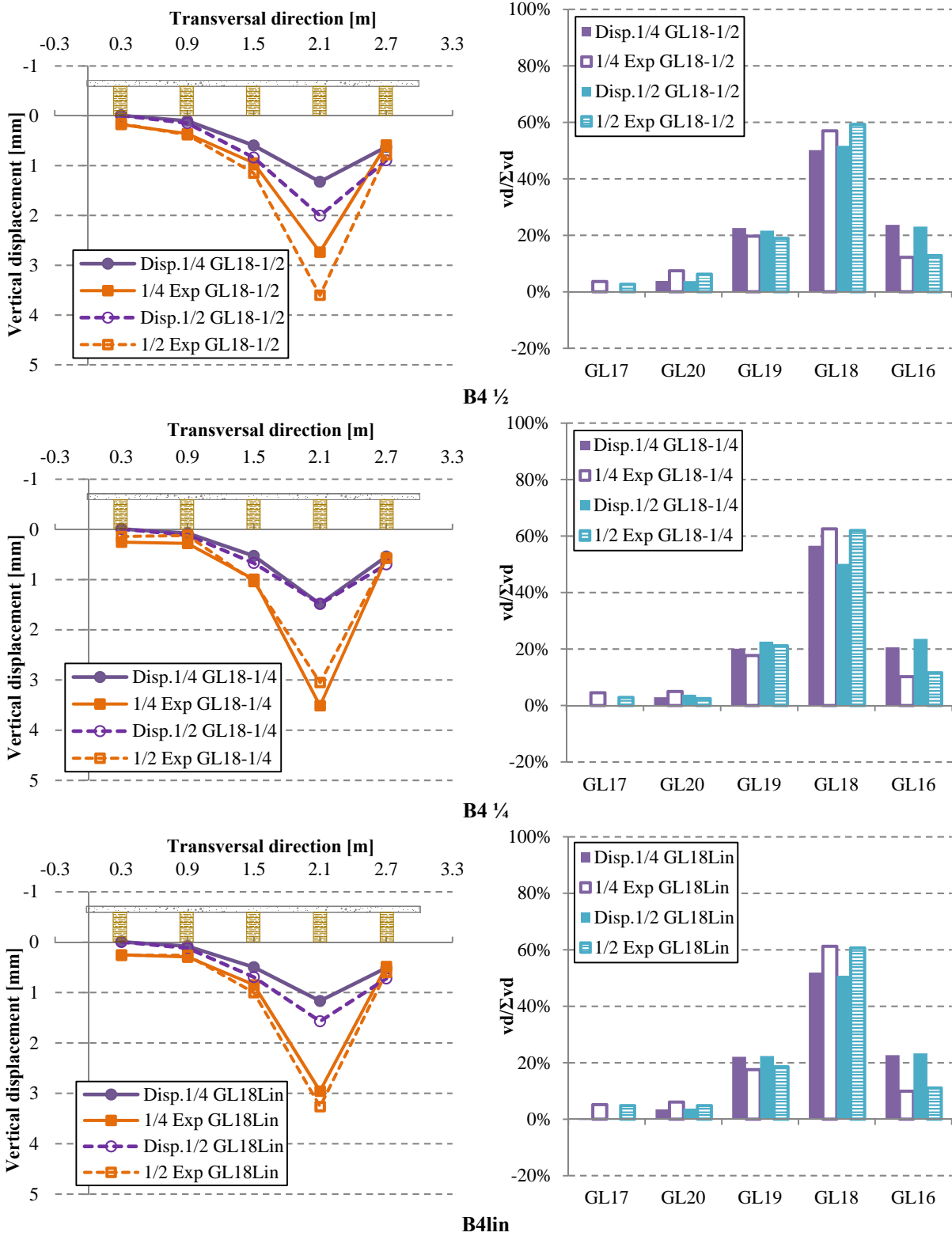


Fig. B.110 – S4-L=2.00m: experimental and numerical vertical displacements when loaded at B4-GL18

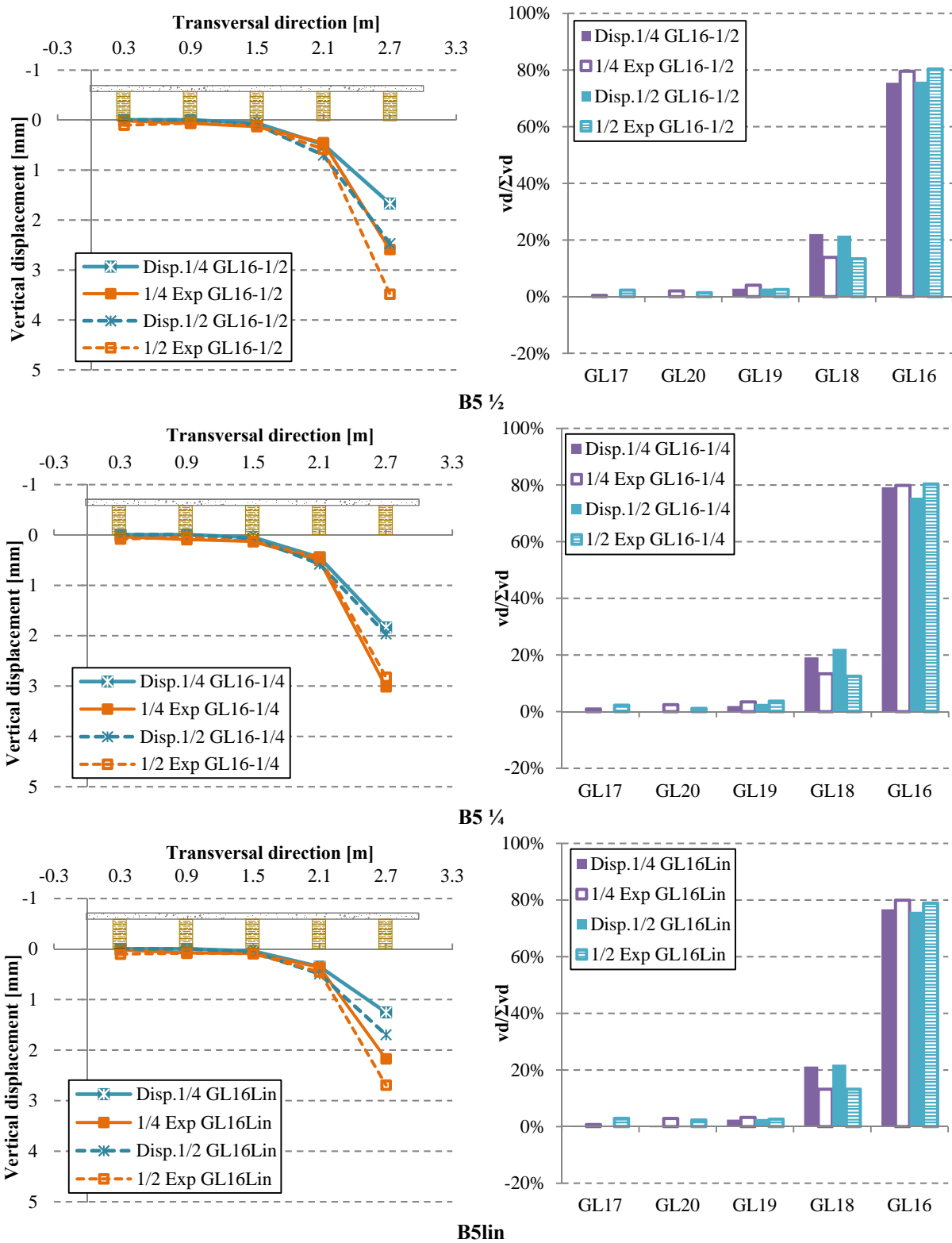


Fig. B.111 – S4-L=2.00m: experimental and numerical vertical displacements when loaded at B5-GL16

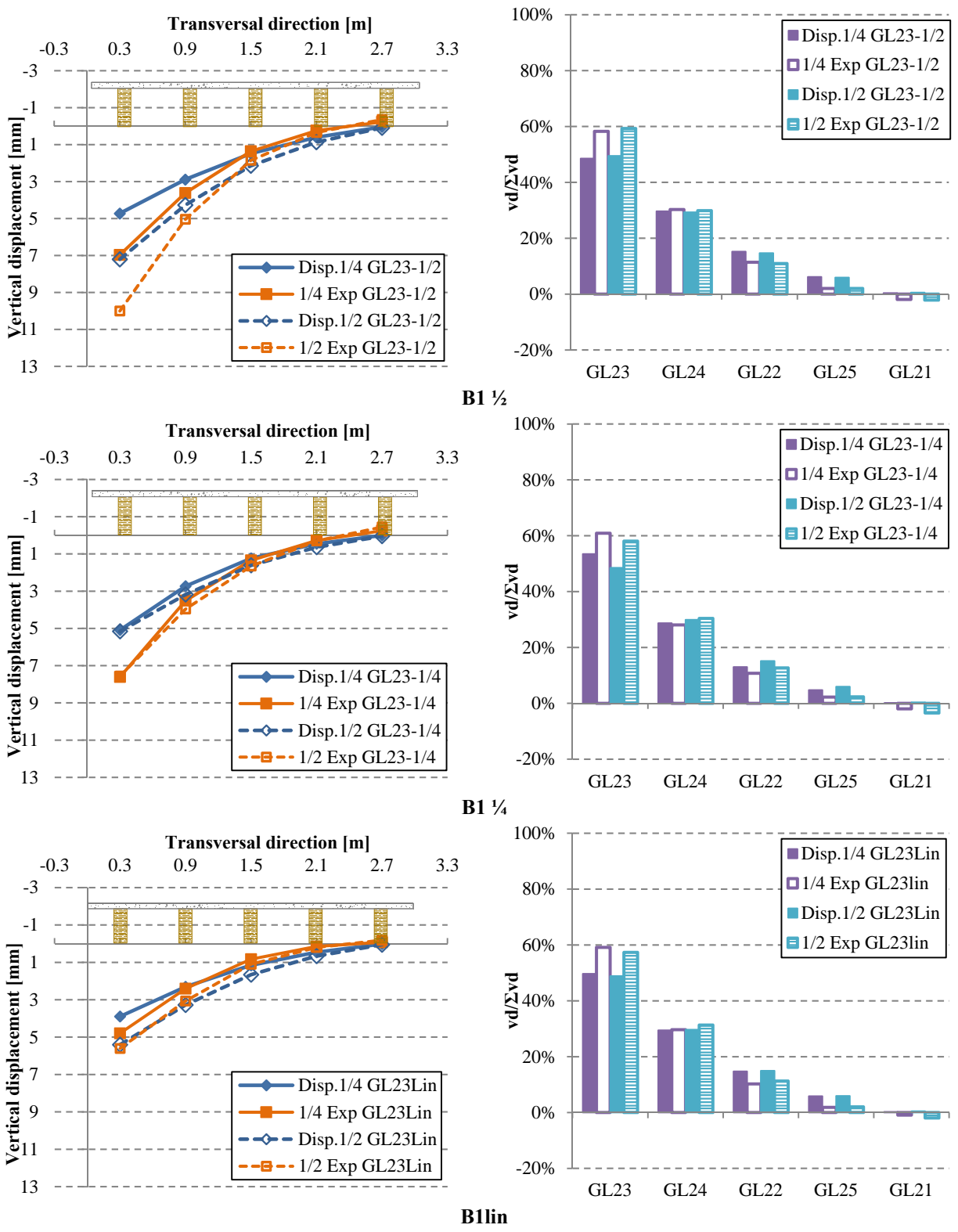


Fig. B.112 – S5-L=6.00m: experimental and numerical vertical displacements when loaded at B1-GL23

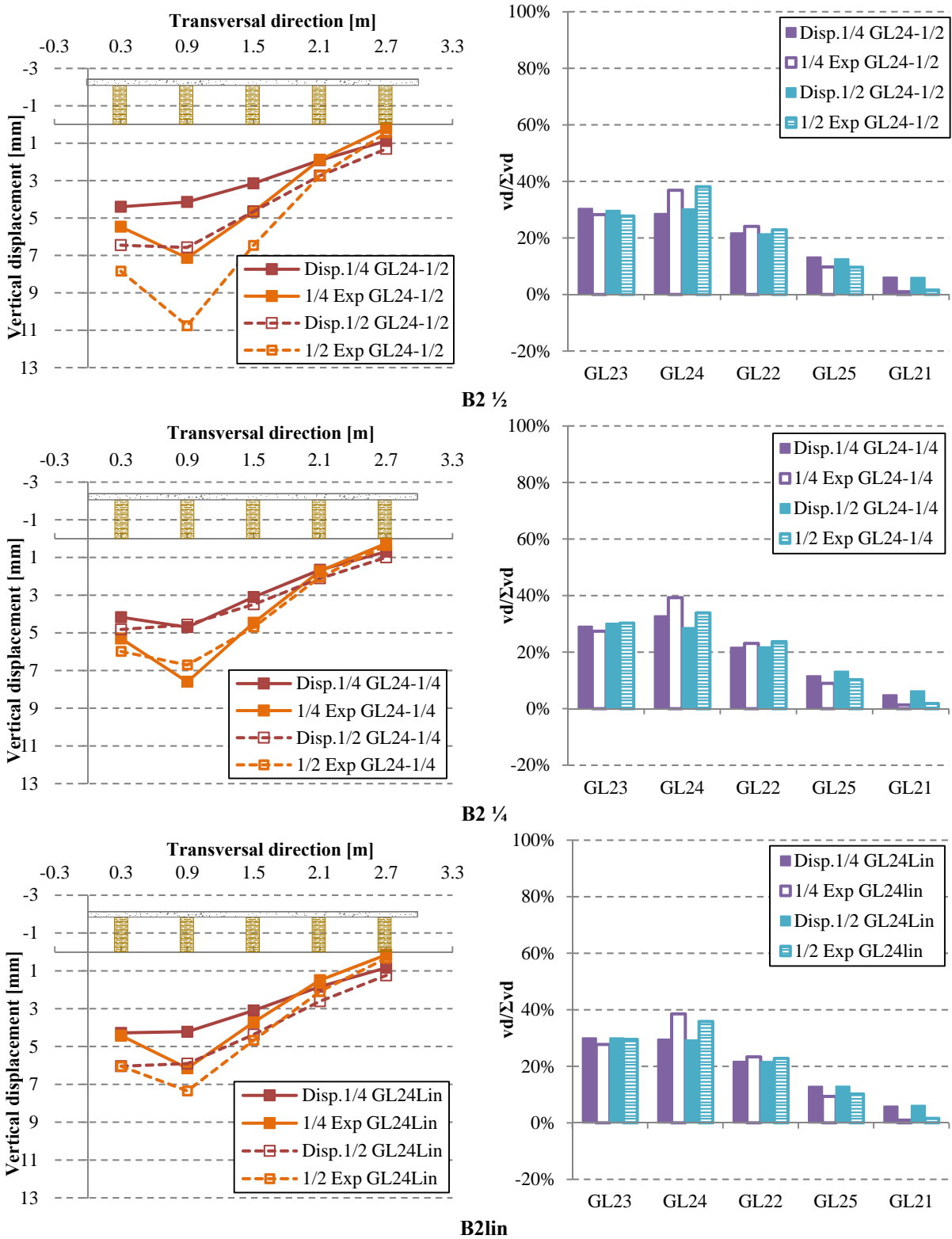


Fig. B.113 – S5-L=6.00m: experimental and numerical vertical displacements when loaded at B2-GL24

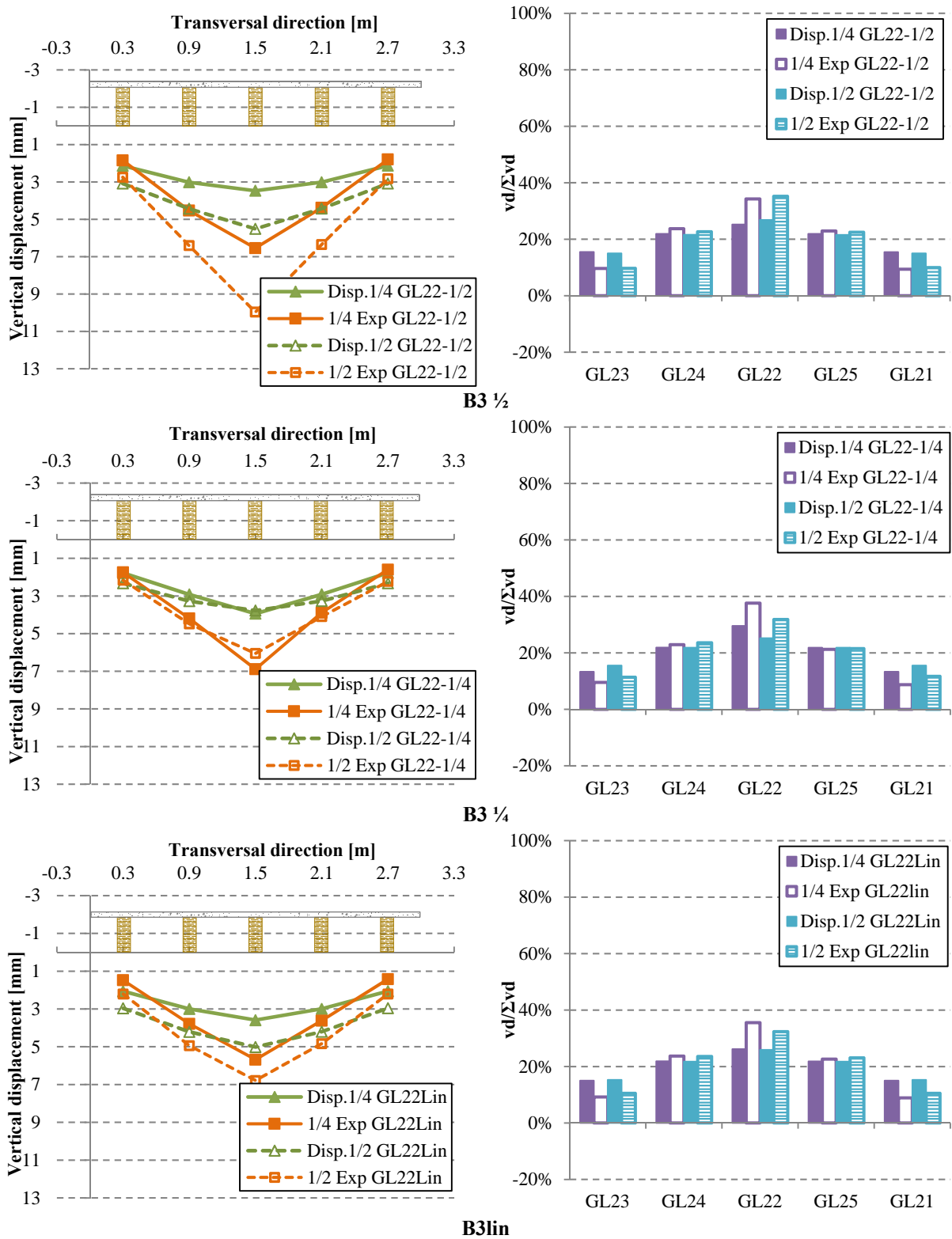


Fig. B.114 – S5-L=6.00m: experimental and numerical vertical displacements when loaded at B3-GL22

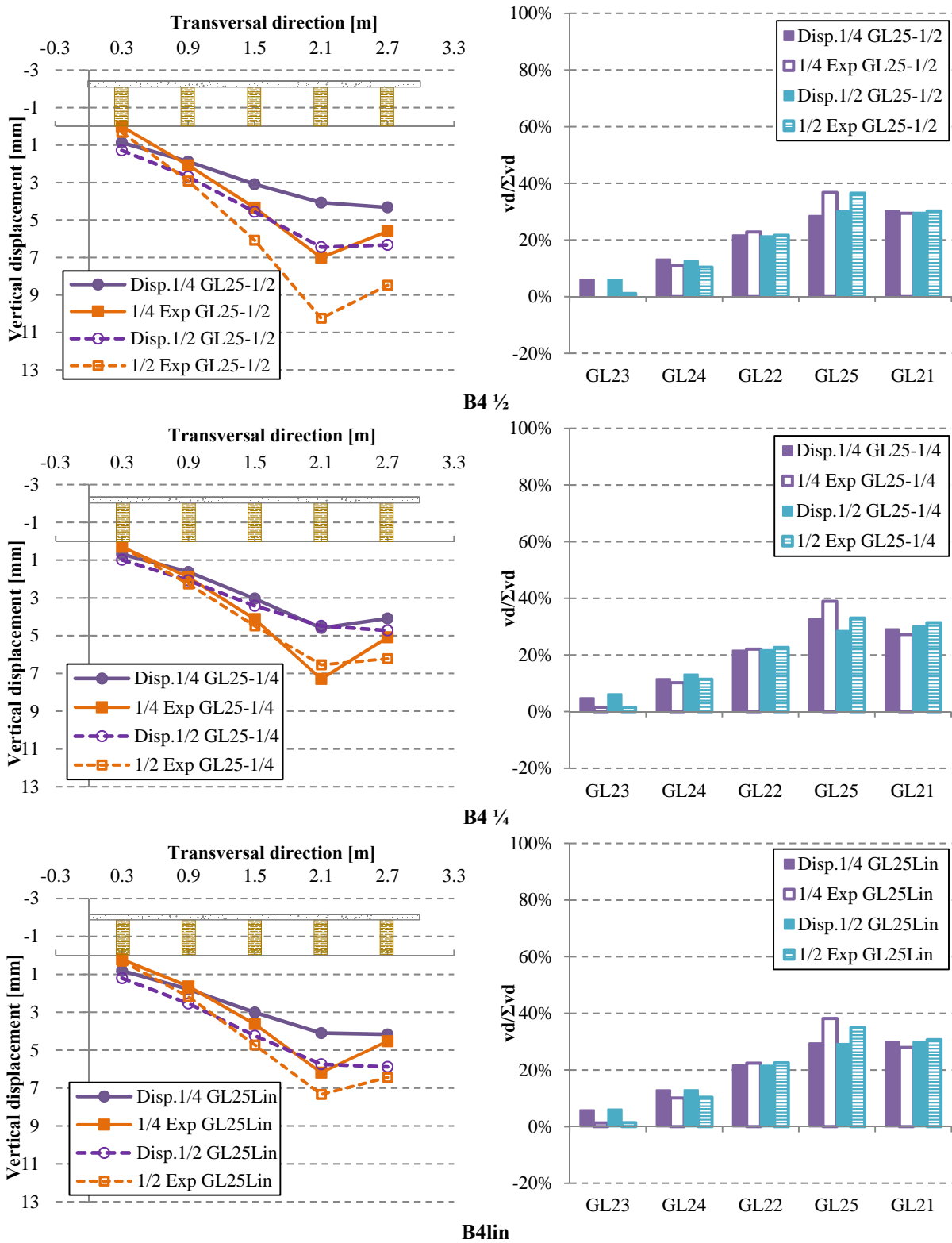


Fig. B.115 – S5-L=6.00m: experimental and numerical vertical displacements when loaded at B4-GL25

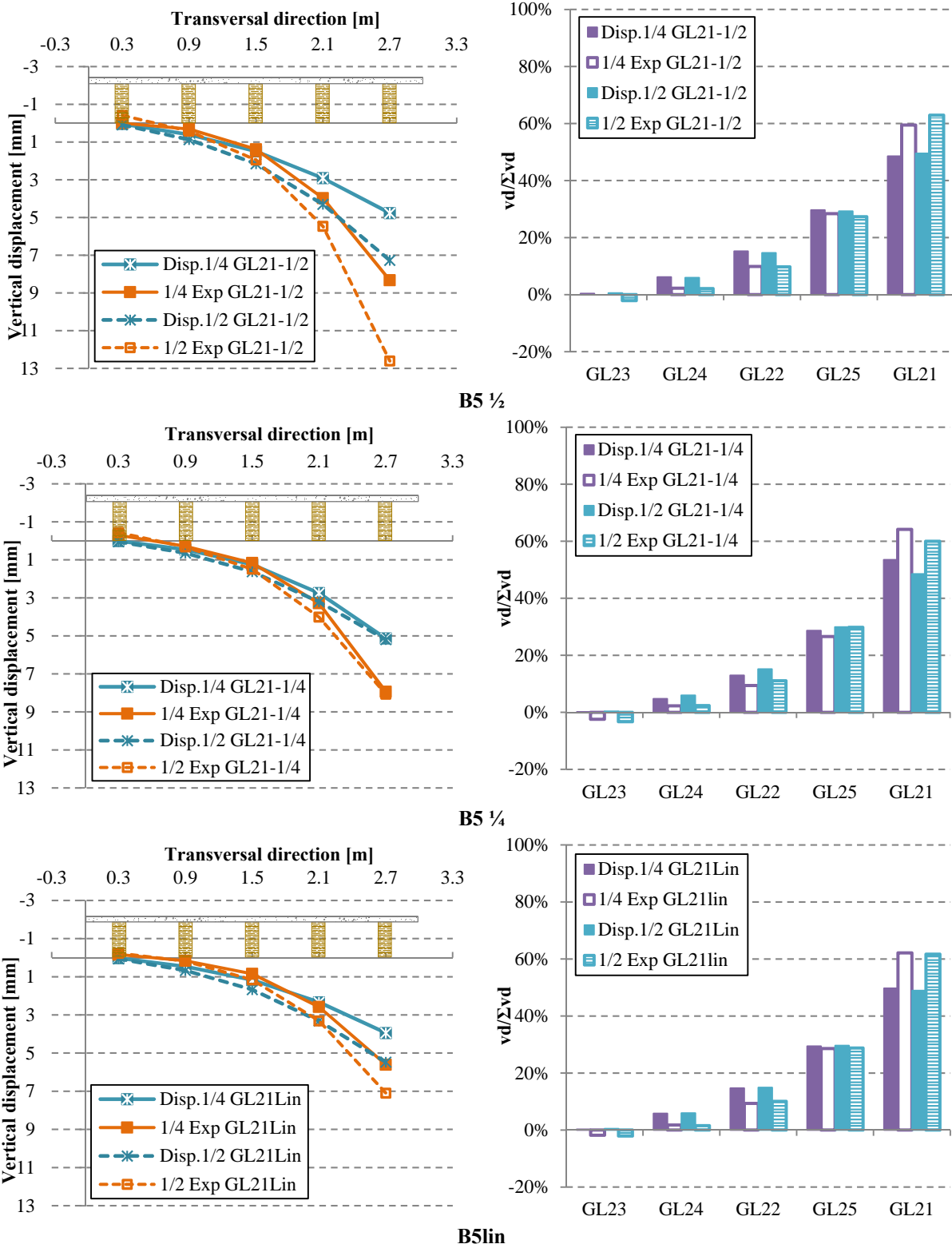


Fig. B.116 – S5-L=6.00m: experimental and numerical vertical displacements when loaded at B5-GL21

Table B.12 – Numerical distribution of vertical displacements [%]

Floor specimen	Load case	Measuring location	Beam position					Floor specimen	Load case	Measuring location	Beam position						
			B1	B2	B3	B4	B5				B1	B2	B3	B4	B5		
S1-BSp	B1 ½	¼	54	29	13	4	0	S4- L=2.00m	B1 ½	¼	76	22	3	0	0		
		½	55	29	12	4	0			½	76	21	3	0	0		
	B2 ½	¼	31	31	22	12	4		B2 ½	¼	24	50	22	4	0		
		½	30	33	22	11	4			½	23	51	22	4	0		
	B3 ½	¼	13	23	28	23	13		B3 ½	¼	3	23	49	23	3		
		½	13	22	30	22	13			½	3	21	51	22	3		
	B4 ½	¼	4	12	22	31	30		B4 ½	¼	0	4	23	50	24		
		½	4	11	22	33	30			½	0	4	22	52	23		
	B5 ½	¼	0	4	13	29	54		B5 ½	¼	0	0	3	22	75		
		½	0	4	12	29	55			½	0	0	3	22	76		
	B1 ¼	¼	59	27	10	3	0		B1 ¼	¼	80	19	2	0	0		
		½	54	30	13	4	0			½	76	22	3	0	0		
	B2 ¼	¼	29	36	22	10	3		B2 ¼	¼	21	56	20	3	0		
		½	30	31	22	12	4			½	24	50	23	4	0		
	B3 ¼	¼	11	22	34	22	11		B3 ¼	¼	2	20	56	20	2		
		½	13	23	28	23	13			½	3	22	49	23	3		
	B4 ¼	¼	3	10	22	36	29		B4 ¼	¼	0	3	20	57	21		
		½	4	12	22	31	30			½	0	4	23	50	24		
	B5 ¼	¼	0	3	10	27	59		B5 ¼	¼	0	0	2	19	79		
		½	0	4	13	30	54			½	0	0	3	22	76		
	B1lin	¼	59	27	10	3	0		B1lin	¼	77	21	2	0	0		
		½	54	30	13	4	0			½	76	22	3	0	0		
	B2lin	¼	29	36	22	10	3		B2lin	¼	23	52	22	4	0		
		½	30	31	22	12	4			½	24	51	22	4	0		
	B3lin	¼	11	22	34	22	11		B3lin	¼	2	22	51	22	3		
		½	13	23	28	23	13			½	3	22	49	23	3		
	B4lin	¼	3	10	22	36	29		B4lin	¼	0	4	22	52	23		
		½	4	12	22	31	30			½	0	4	22	51	23		
	B5lin	¼	0	3	10	27	59		B5lin	¼	0	0	2	21	77		
		½	0	4	13	30	54			½	0	0	3	22	76		
	S2-LWAC	B1 ½	¼	52	29	14	5		0	S5- L=6.00m	B1 ½	¼	49	30	15	6	0
			½	53	29	13	5		0			½	49	29	15	6	1
B2 ½		¼	31	30	22	12	5	B2 ½	¼		30	29	22	13	6		
		½	30	32	22	12	5		½		30	30	21	13	6		
B3 ½		¼	14	22	27	22	14	B3 ½	¼		15	22	25	22	15		
		½	14	22	29	22	14		½		15	22	27	22	15		

Table B.12 – Numerical distribution of vertical displacements [%] (cont.)

Floor specimen	Load case	Measuring location	Beam position					Floor specimen	Load case	Measuring location	Beam position				
			B1	B2	B3	B4	B5				B1	B2	B3	B4	B5
S2-LWAC	B4 ½	¼	5	12	22	30	31	S5- L=6.00m	B4 ½	¼	6	13	22	29	30
		½	5	12	22	32	30			½	6	13	21	30	30
	B5 ½	¼	0	5	14	29	52		B5 ½	¼	0	6	15	30	49
		½	0	5	13	29	53			½	1	6	15	29	50
	B1 ¼	¼	57	28	12	4	0		B1 ¼	¼	53	29	13	5	0
		½	52	30	14	5	0			½	49	30	15	6	0
	B2 ¼	¼	29	34	22	11	4		B2 ¼	¼	29	33	22	12	5
		½	30	30	22	12	5			½	30	29	22	13	6
	B3 ¼	¼	12	22	32	22	12		B3 ¼	¼	13	22	30	22	13
		½	14	22	27	22	14			½	16	22	25	22	16
	B4 ¼	¼	4	11	22	34	29		B4 ¼	¼	5	12	22	33	29
		½	5	12	22	30	30			½	6	13	22	29	30
	B5 ¼	¼	0	4	12	28	57		B5 ¼	¼	0	5	13	29	54
		½	0	5	14	30	52			½	0	6	15	30	49
	B1lin	¼	53	29	13	5	0		B1lin	¼	50	29	15	6	0
		½	52	29	13	5	0			½	49	30	15	6	0
	B2lin	¼	30	31	22	12	5		B2lin	¼	30	30	22	13	6
		½	30	31	22	12	5			½	30	29	22	13	6
	B3lin	¼	14	22	28	22	14		B3lin	¼	15	22	26	22	15
		½	14	22	28	22	14			½	15	22	26	22	15
	B4lin	¼	5	12	22	31	30		B4lin	¼	6	13	22	30	30
		½	5	12	22	31	30			½	6	13	22	29	30
	B5lin	¼	0	5	13	29	53		B5lin	¼	0	6	15	29	50
		½	0	5	13	29	52			½	0	6	15	30	49
S3- hc=0.03m	B1 ½	¼	73	25	4	-1	-1		B1 ½	¼	73	25	4	-1	-1
		½	74	25	3	-1	-1			½	74	25	3	-1	-1
	B2 ½	¼	27	46	24	5	-1		B2 ½	¼	27	46	24	5	-1
		½	26	48	23	5	-1			½	26	48	23	5	-1
	B3 ½	¼	4	25	44	24	4		B3 ½	¼	4	25	44	24	4
		½	4	24	46	23	4			½	4	24	46	23	4
	B4 ½	¼	-1	5	24	46	27		B4 ½	¼	-1	5	23	48	26
		½	-1	5	23	48	26			½	-1	5	23	48	26
	B5 ½	¼	-1	-1	4	25	74		B5 ½	¼	-1	-1	4	25	74
		½	-1	-1	3	25	74			½	-1	-1	3	25	74
B1 ¼	¼	77	22	2	-1	-1	B1 ¼	¼	77	22	2	-1	-1		
	½	73	26	3	-1	-1		½	73	26	3	-1	-1		

Table B.13 – Difference between experimental and numerical distribution of vertical displacements [%]

Floor specimen	Load case	Measuring location	Beam position					Floor specimen	Load case	Measuring location	Beam position				
			B1	B2	B3	B4	B5				B1	B2	B3	B4	B5
S1-BSp	B1 ½	¼	10	-1	-4	-3	-2	S4- L=2.00m	B1 ½	¼	-4	-6	3	4	2
		½	8	1	-4	-3	-2			½	-1	-7	2	3	2
	B2 ½	¼	-3	8	1	-2	-4		B2 ½	¼	-8	7	-3	1	2
		½	-2	8	-1	-2	-4			½	-11	10	-1	0	2
	B3 ½	¼	-8	1	11	2	-6		B3 ½	¼	-11	2	14	4	-10
		½	-7	0	11	1	-6			½	-10	1	15	2	-8
	B4 ½	¼	-4	-2	1	6	-1		B4 ½	¼	4	4	-3	7	-12
		½	-4	-2	2	5	-1			½	3	2	-3	8	-10
	B5 ½	¼	-1	-3	-4	-3	11		B5 ½	¼	1	2	1	-8	4
		½	-1	-3	-4	-2	9			½	3	2	0	-8	4
	B1 ¼	¼	7	0	-3	-2	-2		B1 ¼	¼	-9	-2	4	5	3
		½	8	1	-4	-3	-3			½	-1	-6	4	2	1
	B2 ¼	¼	-1	3	1	0	-3		B2 ¼	¼	-6	4	-2	2	4
		½	1	3	1	-1	-4			½	-9	10	-2	0	1
	B3 ¼	¼	-3	0	6	1	-5		B3 ¼	¼	4	-3	2	-2	0
		½	-4	0	7	1	-4			½	2	-7	12	-6	-1
	B4 ¼	¼	-2	0	1	2	-1		B4 ¼	¼	5	2	-2	6	-10
		½	-3	-1	1	2	1			½	3	-1	-1	12	-12
	B5 ¼	¼	0	-1	-4	-5	9		B5 ¼	¼	1	3	1	-6	1
		½	-1	-2	-6	-2	11			½	2	1	1	-10	5
	B1 4P	¼	14	-5	-6	-3	0		B1lin	¼	-8	-5	4	6	3
		½	15	-4	-7	-3	-1			½	-4	-7	3	5	3
	B2 4P	¼	-4	7	2	-1	-4		B2lin	¼	-8	6	-3	2	3
		½	-3	9	1	-2	-4			½	-11	9	-3	2	3
	B3lin	¼	-10	1	16	1	-7		B3lin	¼	4	-3	4	-4	0
		½	-9	1	14	2	-7			½	2	-4	8	-4	-1
	B3 4P	¼	-9	2	14	2	-9		B4lin	¼	5	3	-5	9	-13
		½	-9	1	16	2	-9			½	5	1	-4	10	-12
B4lin	¼	-3	-1	1	7	-4	B5lin	¼	1	3	1	-8	3		
	½	-4	-1	1	8	-4		½	3	3	0	-9	3		
B4 4P	¼	-4	-2	2	7	-3	B5 4P	¼	-1	-3	-5	-4	13		
	½	-4	-3	1	9	-3		½	-1	-2	-6	-3	13		
B5lin	¼	-1	-1	-5	-3	10									
	½	0	-1	-4	-1	6									
B5 4P	¼	-1	-3	-5	-4	13									
	½	-1	-2	-6	-3	13									

**Table B.13 – Difference between experimental and numerical distribution of vertical displacements [%]
(cont.)**

Floor specimen	Load case	Measuring location	Beam position					Floor specimen	Load case	Measuring location	Beam position				
			B1	B2	B3	B4	B5				B1	B2	B3	B4	B5
S2-LWAC	B1 ½	¼	20	-6	-8	-5	-1	S5- L=6.00m	B1 ½	¼	10	1	-4	-4	-2
		½	19	-5	-8	-4	-1			½	10	1	-4	-4	-3
	B2 ½	¼	-7	15	1	-4	-6		B2 ½	¼	-2	8	2	-3	-5
		½	-6	16	1	-4	-6			½	-2	8	1	-3	-4
	B3 ½	¼	-14	2	24	2	-15		B3 ½	¼	-6	2	9	1	-6
		½	-13	1	25	0	-14			½	-5	1	8	1	-5
	B4 ½	¼	-6	-5	3	17	-9		B4 ½	¼	-6	-2	1	8	-1
		½	-6	-5	2	19	-9			½	-5	-2	0	6	1
	B5 ½	¼	-1	-5	-9	-8	22		B5 ½	¼	0	-4	-5	-1	11
		½	-2	-4	-9	-7	22			½	-3	-4	-5	-2	13
	B1 ¼	¼	17	-6	-8	-4	0		B1 ¼	¼	7	-1	-2	-3	-2
		½	19	-4	-9	-5	0			½	10	0	-2	-4	-4
	B2 ¼	¼	-10	19	-1	-5	-4		B2 ¼	¼	-2	6	1	-3	-4
		½	-7	18	0	-6	-5			½	0	5	2	-3	-4
	B3 ¼	¼	-11	-1	23	0	-11		B3 ¼	¼	-4	1	8	-1	-5
		½	-12	0	24	1	-13			½	-4	2	7	0	-4
	B4 ¼	¼	-4	-5	-1	19	-9		B4 ¼	¼	-3	-1	0	6	-2
		½	-6	-6	1	19	-8			½	-5	-2	1	4	1
	B5 ¼	¼	0	-3	-7	-7	18		B5 ¼	¼	-2	-3	-4	-2	11
		½	-1	-4	-9	-5	20			½	-4	-4	-4	0	11
	B1lin	¼	17	-5	-9	-4	0		B1lin	¼	9	0	-5	-4	-1
		½	16	-2	-9	-5	0			½	8	2	-4	-4	-2
	B2lin	¼	-8	15	2	-5	-4		B2lin	¼	-2	9	2	-4	-5
		½	-6	13	2	-5	-5			½	0	7	1	-3	-5
	B3lin	¼	-12	0	22	1	-10		B3lin	¼	-6	2	9	1	-6
		½	-12	1	21	1	-11			½	-5	2	6	1	-5
	B4lin	¼	-5	-5	1	16	-7		B4lin	¼	-5	-3	1	9	-2
		½	-5	-5	1	17	-7			½	-5	-3	1	6	1
B5lin	¼	0	-2	-8	-9	20	B5lin	¼	-2	-4	-5	-1	12		
	½	-1	-3	-9	-7	20		½	-3	-4	-5	-1	13		
S3- hc=0.03m	B1 ½	¼	3	-5	1	1	0		B1 ½	¼	3	-5	1	1	0
		½	4	-5	0	1	-1			½	4	-5	0	1	-1
	B2 ½	¼	-5	2	-1	3	1		B2 ½	¼	-5	2	-1	3	1
		½	-4	3	-2	2	0			½	-4	3	-2	2	0

**Table B.13 – Difference between experimental and numerical distribution of vertical displacements [%]
(cont.)**

Floor specimen	Load case	Measuring location	Beam position					Floor specimen	Load case	Measuring location	Beam position														
			B1	B2	B3	B4	B5				B1	B2	B3	B4	B5										
S3- hc=0.03m	B3 ½	¼	-1	-1	0	1	1																		
		½	-1	0	0	0	0	1																	
	B4 ½	¼	0	0	1	0	-1																		
		½	0	0	0	1	-1																		
	B5 ½	¼	0	1	4	1	-5																		
		½	-1	0	2	1	-2																		
	B1 ¼	¼	1	-4	1	1	0																		
		½	3	-5	1	0	0																		
	B2 ¼	¼	-5	1	0	2	2																		
		½	-4	3	-1	0	2																		
	B3 ¼	¼	0	-2	-1	1	2																		
		½	-1	-2	-1	0	3																		
	B4 ¼	¼	1	1	0	-1	-1																		
		½	0	0	0	0	1																		
	B5 ¼	¼	1	1	3	1	-6																		
		½	-1	0	3	1	-3																		
	B1lin	¼	2	-5	1	1	1																		
		½	3	-4	0	2	0																		
	B2lin	¼	-6	2	0	2	3																		
		½	-3	0	0	2	2																		
	B3lin	¼	-1	-2	-2	1	4																		
		½	0	-1	-5	2	4																		
	B4lin	¼	1	2	-1	-4	3																		
		½	1	1	-1	-4	2																		
B5lin	¼	1	2	3	-1	-5																			
	½	1	1	2	2	-6																			

½ - mid-span; ¼ - quarter-span; lin - line load; 4P - 4-point load

B.3.2 Support reactions

Fig. B.117 to Fig. B.141 present the support reaction distribution obtained with the numerical model, for the five beams of each specimen for the three loading cases. Table B.14 summarizes the support reaction distribution, obtained both experimentally as numerically for easy comparison, and Table B.15 presents the differences found between experimental and numerical results.

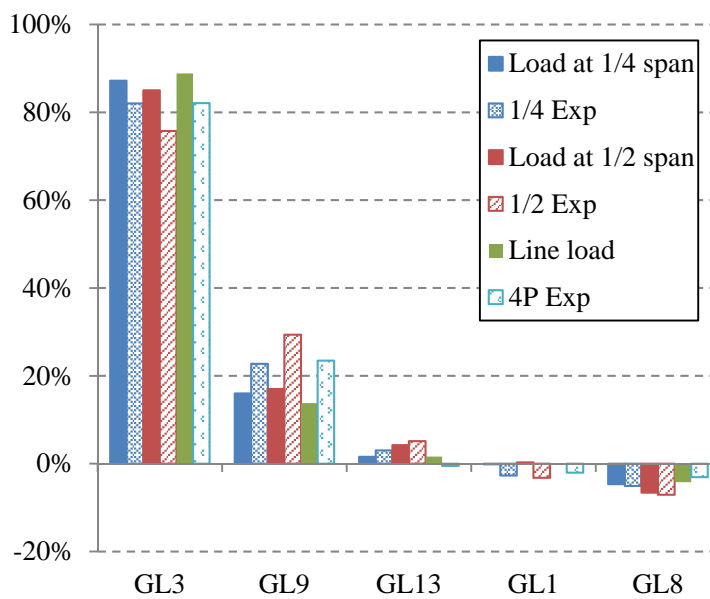


Fig. B.117 – S1-BSp: experimental and numerical distribution of support reactions when loaded at B1-GL3

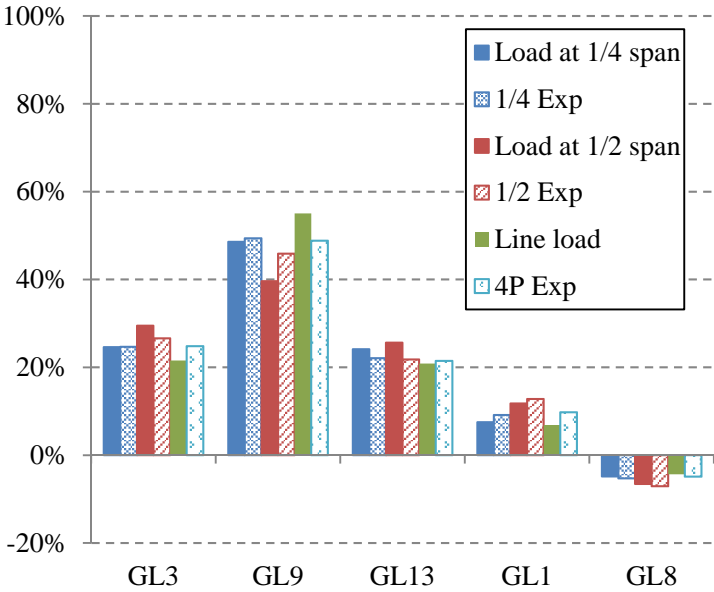


Fig. B.118 – S1-BSp: experimental and numerical distribution of support reactions when loaded at B2-GL9

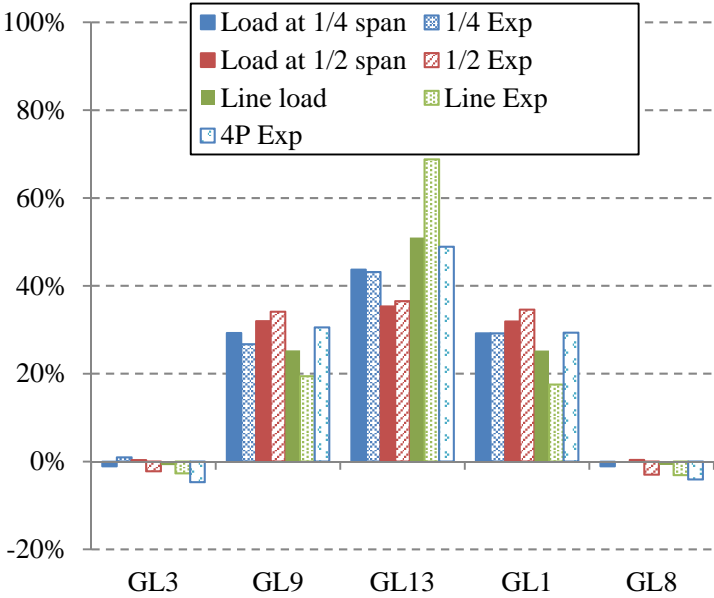


Fig. B.119 – S1-BSp: experimental and numerical distribution of support reactions when loaded at B3-GL13

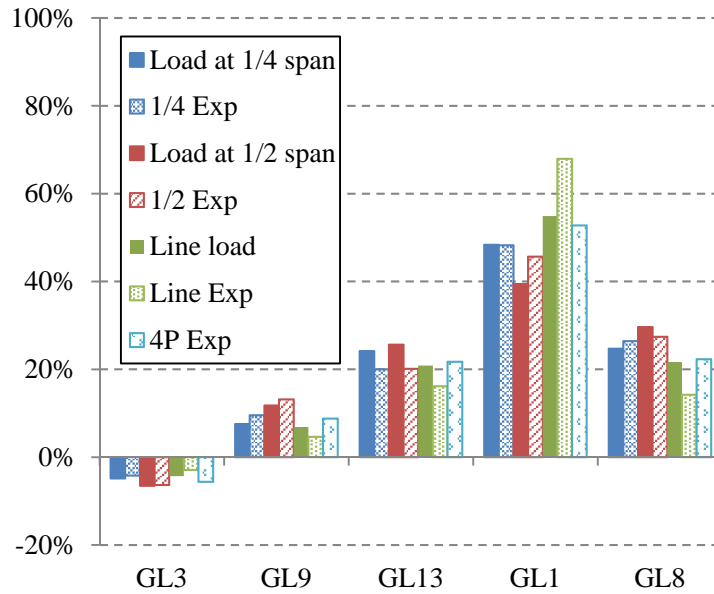


Fig. B.120 – S1-BSp: experimental and numerical distribution of support reactions when loaded at B4-GL1

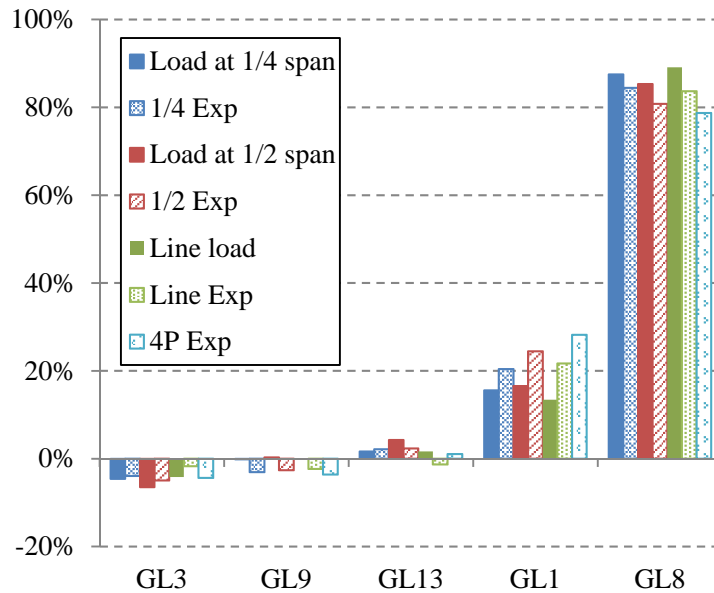


Fig. B.121 – S1-BSp: experimental and numerical distribution of support reactions when loaded at B5-GL8

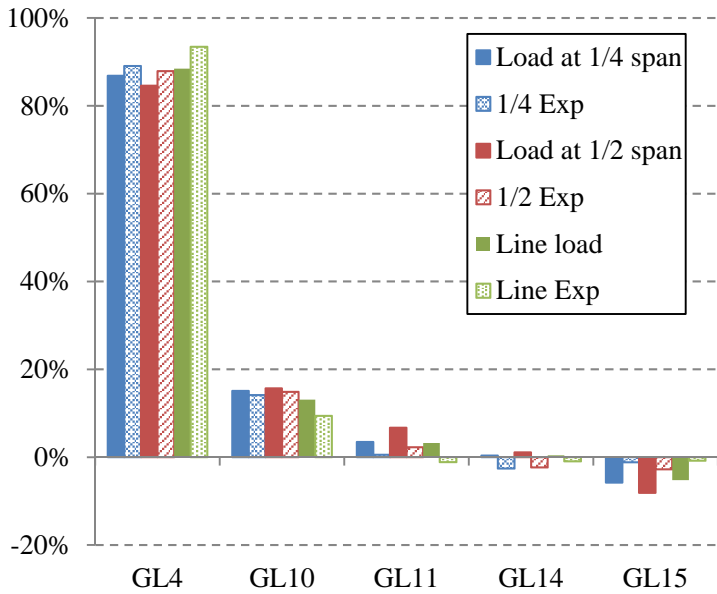


Fig. B.122 – S2-LWAC: experimental and numerical distribution of support reactions when loaded at B1-GL4

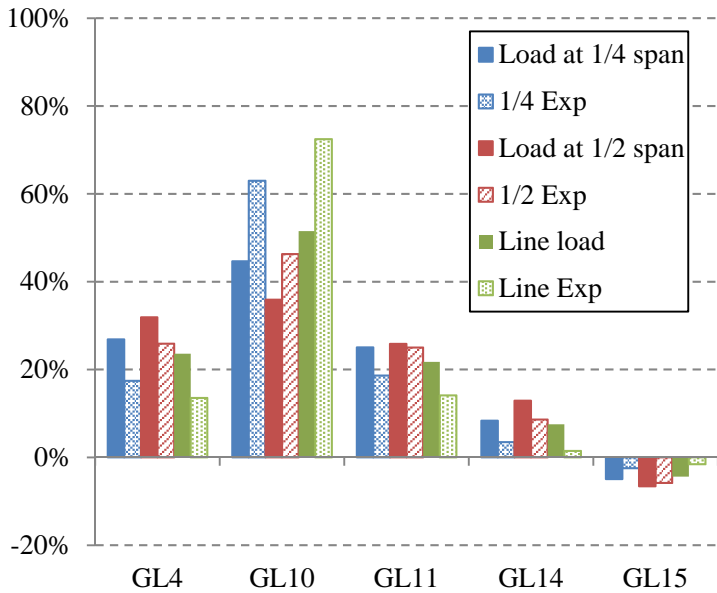


Fig. B.123 – S2-LWAC: experimental and numerical distribution of support reactions when loaded at B2-GL10

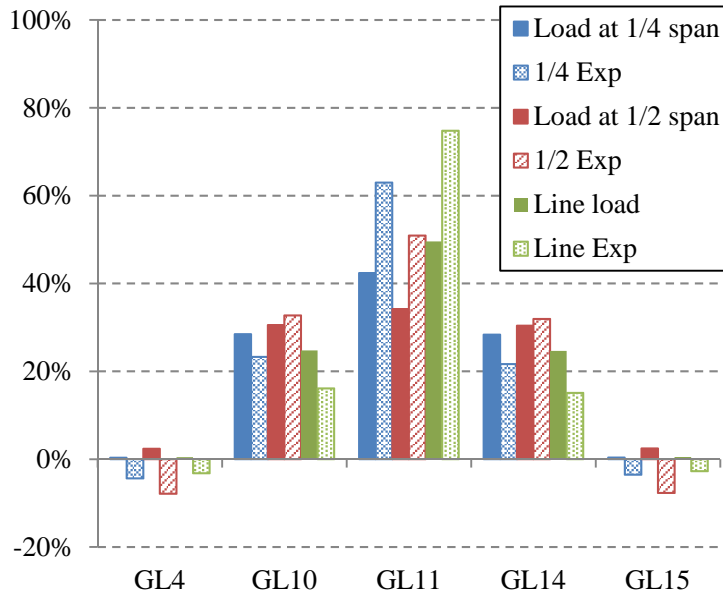


Fig. B.124 – S2-LWAC: experimental and numerical distribution of support reactions when loaded at B3-GL11

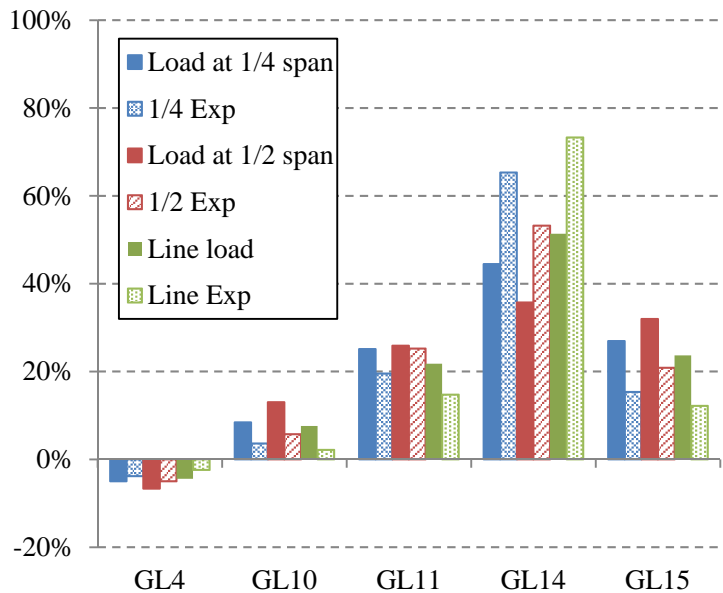


Fig. B.125 – S2-LWAC: experimental and numerical distribution of support reactions when loaded at B4-GL14

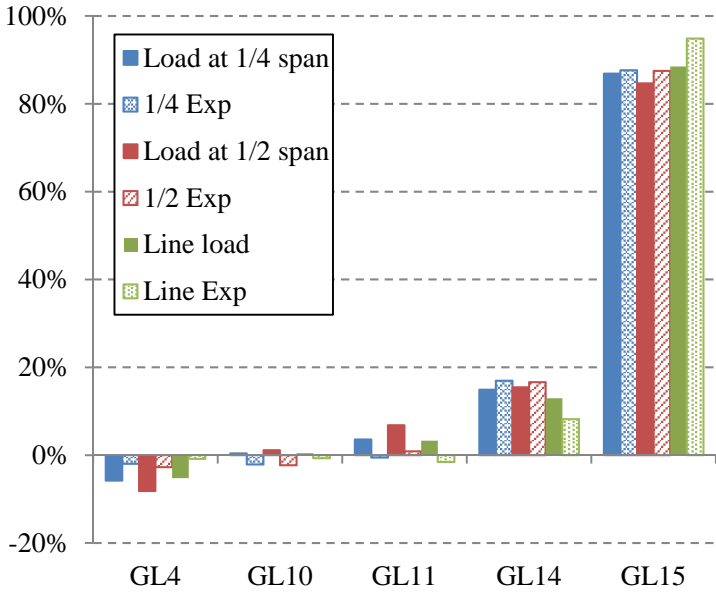


Fig. B.126 – S2-LWAC: experimental and numerical distribution of support reactions when loaded at B5-GL15

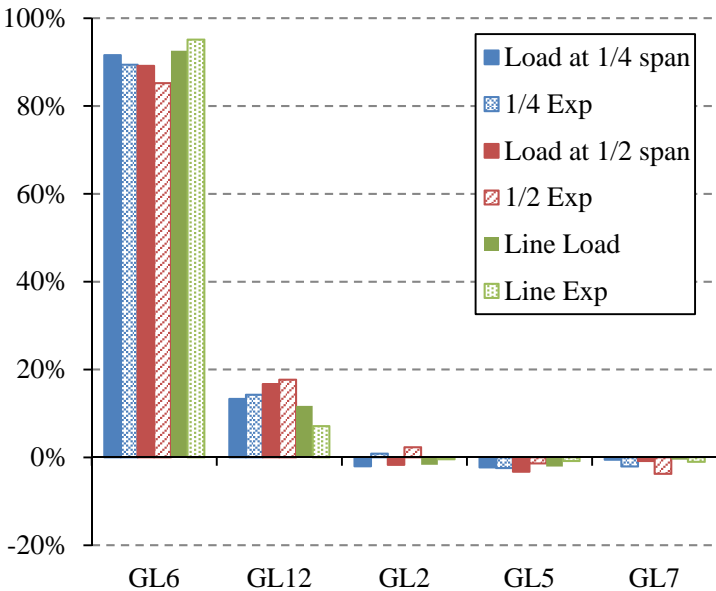


Fig. B.127 – S3-hc=0.03m: experimental and numerical distribution of support reactions when loaded at B1-GL6

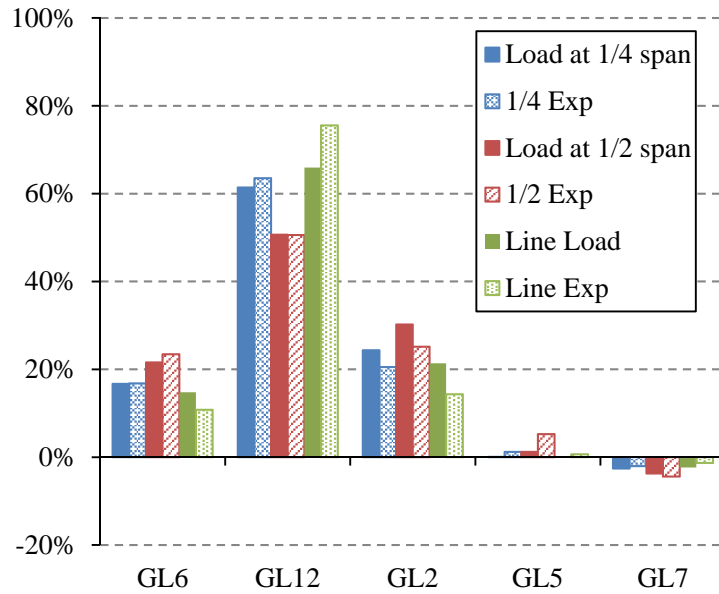


Fig. B.128 – S3-hc=0.03m: experimental and numerical distribution of support reactions when loaded at B2-GL12

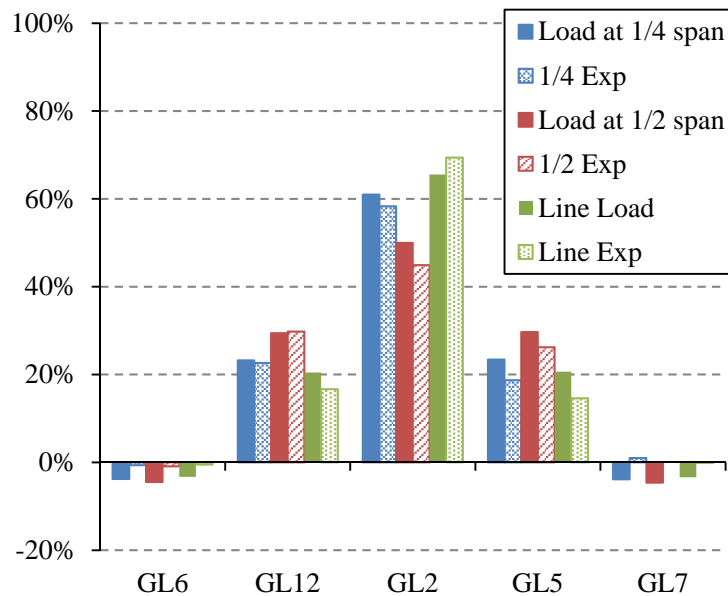


Fig. B.129 – S3-hc=0.03m: experimental and numerical distribution of support reactions when loaded at B3-GL2

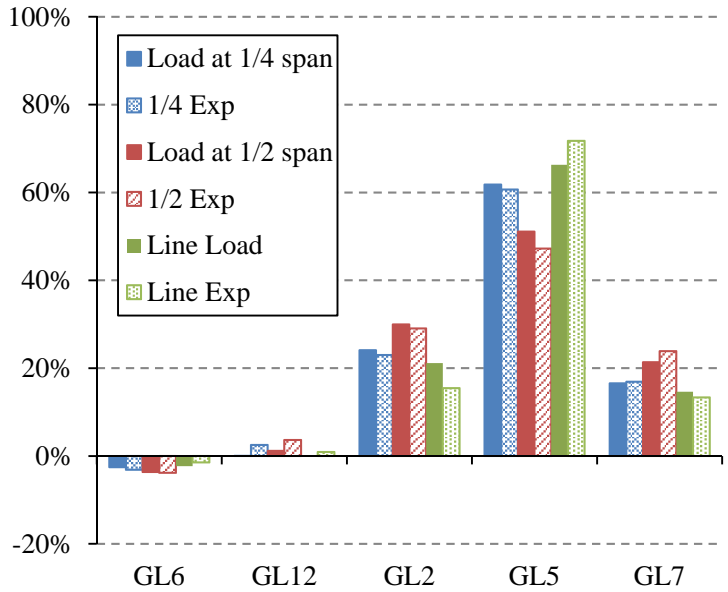


Fig. B.130 – S3-hc=0.03m: experimental and numerical distribution of support reactions when loaded at B4-GL5

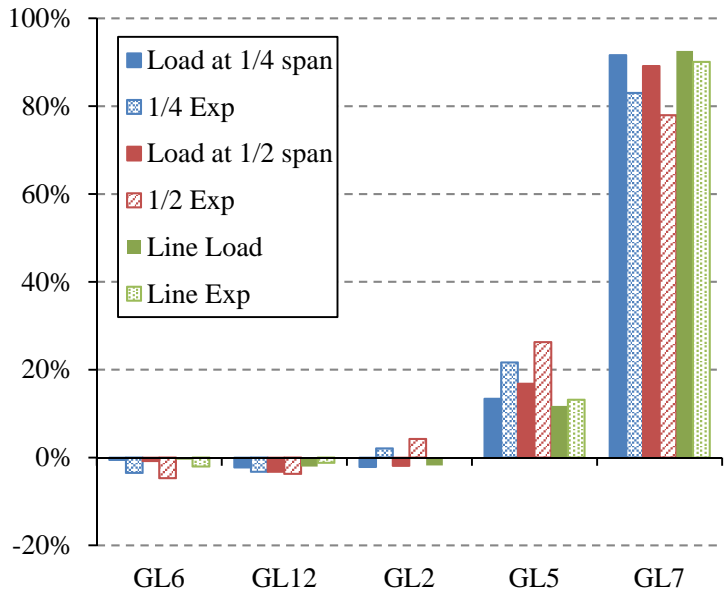


Fig. B.131 – S3-hc=0.03m: experimental and numerical distribution of support reactions when loaded at B5-GL7

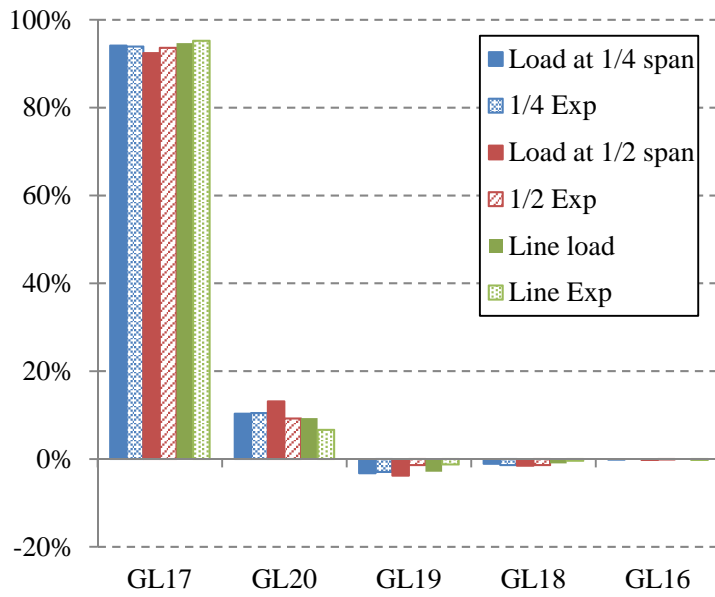


Fig. B.132 – S4-L=2.00m: experimental and numerical distribution of support reactions when loaded at B1-GL17

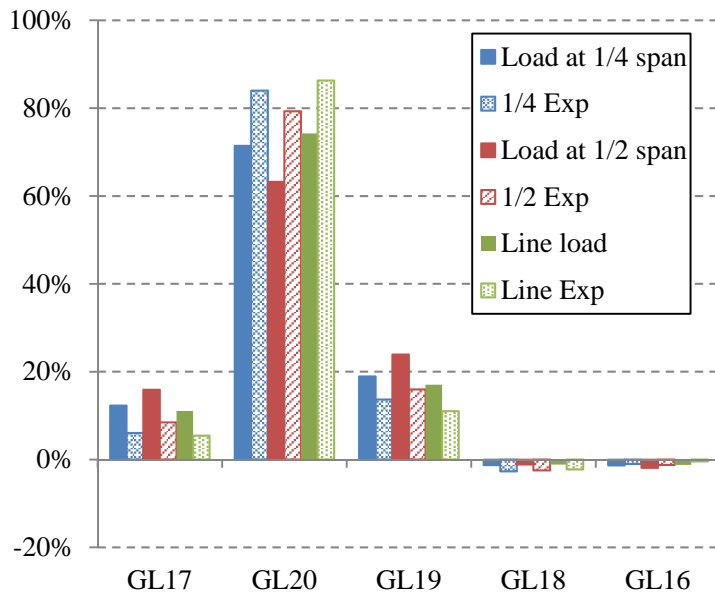


Fig. B.133 – S4-L=2.00m: experimental and numerical distribution of support reactions when loaded at B2-GL20

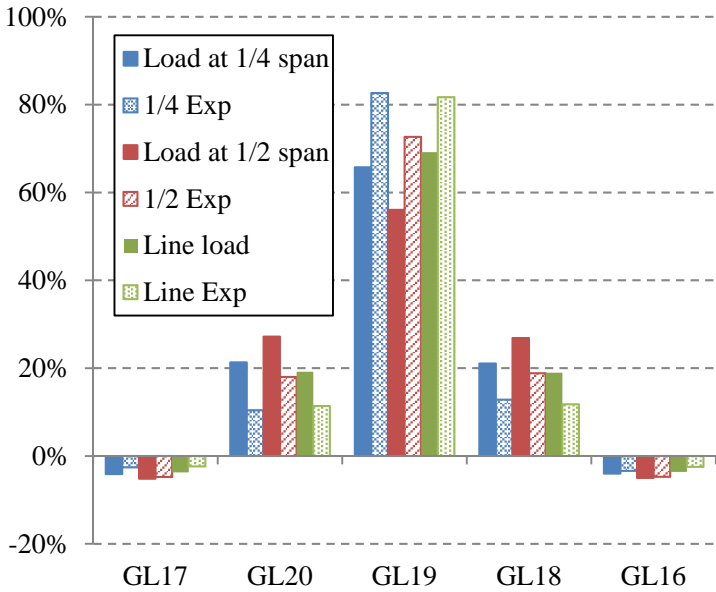


Fig. B.134 – S4-L=2.00m: experimental and numerical distribution of support reactions when loaded at B3-GL19

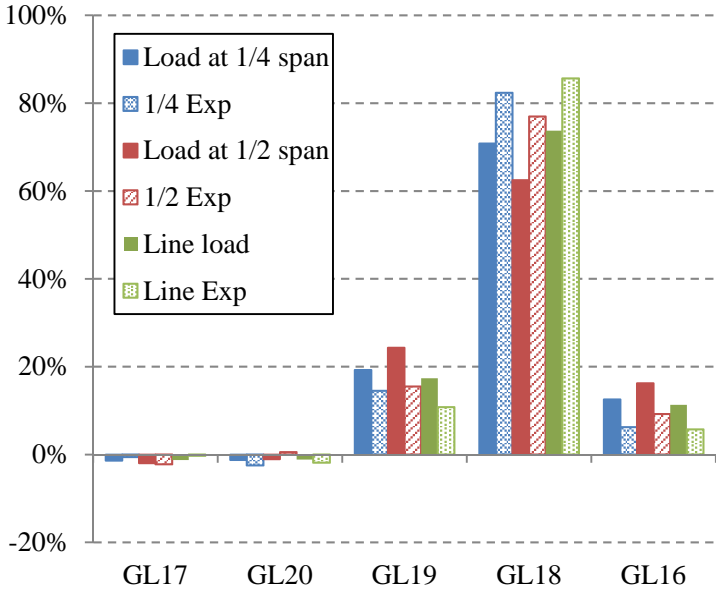


Fig. B.135 – S4-L=2.00m: experimental and numerical distribution of support reactions when loaded at B4-GL18

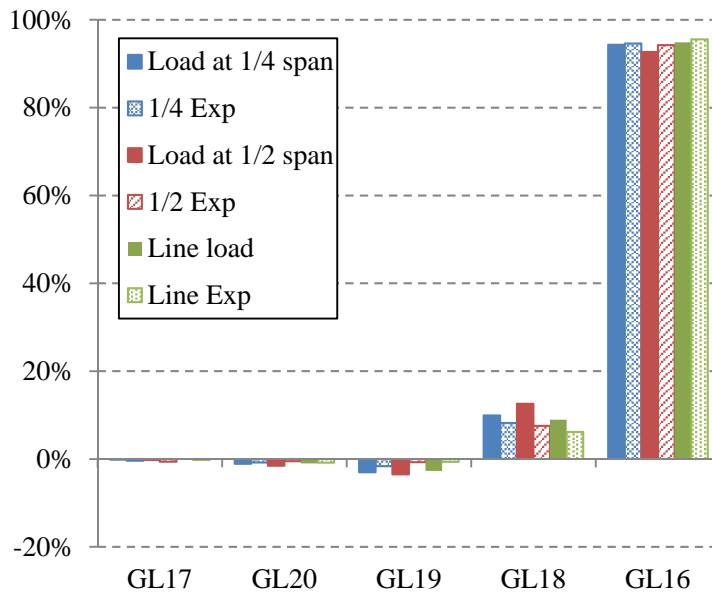


Fig. B.136 – S4-L=2.00m: experimental and numerical distribution of support reactions when loaded at B5-GL16

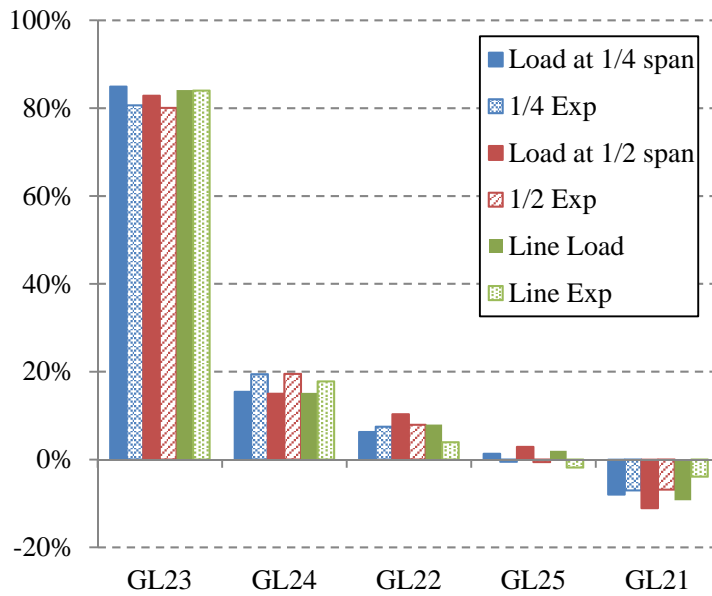


Fig. B.137 – S5-L=6.00m: experimental and numerical distribution of support reactions when loaded at B1-GL23

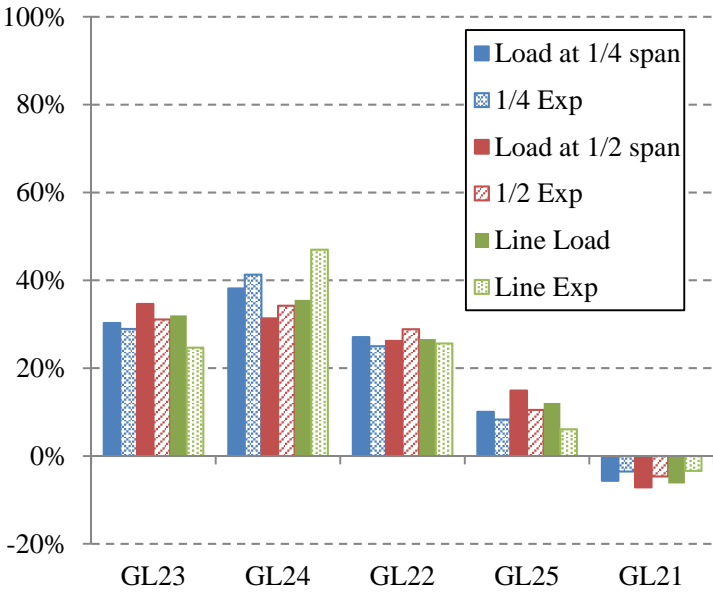


Fig. B.138 – S5-L=6.00m: experimental and numerical distribution of support reactions when loaded at B2-GL24

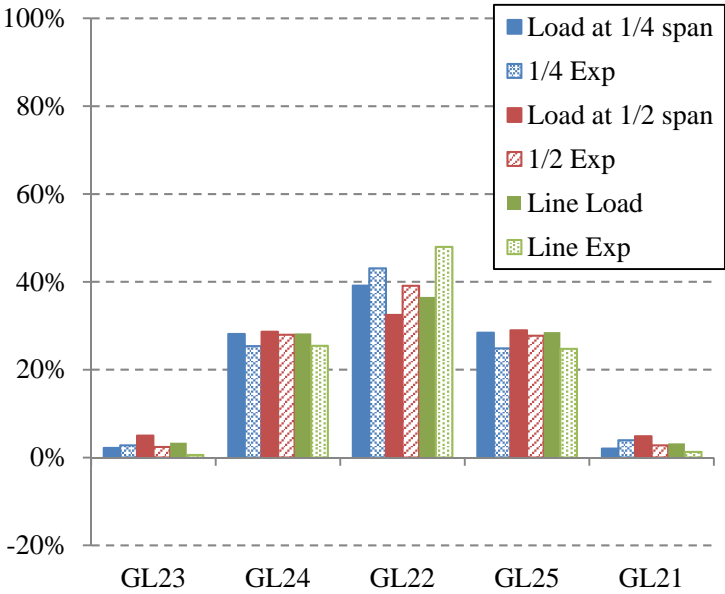


Fig. B.139 – S5-L=6.00m: experimental and numerical distribution of support reactions when loaded at B3-GL22

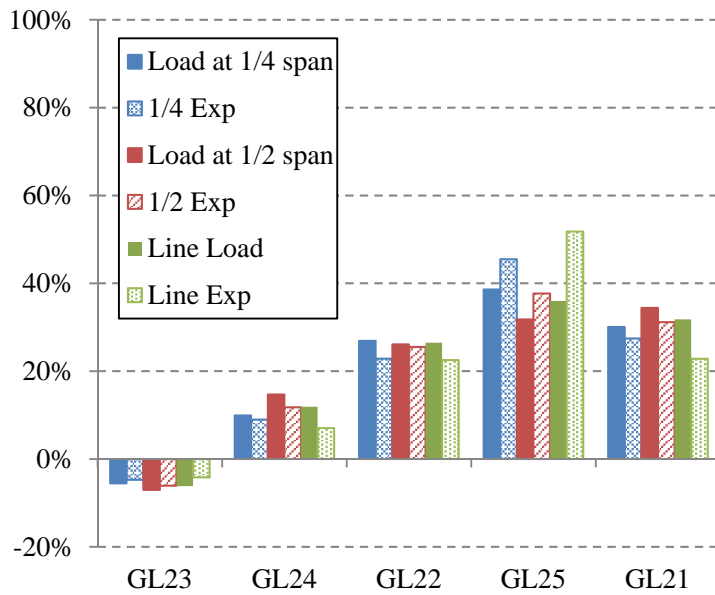


Fig. B.140 – S5-L=6.00m: experimental and numerical distribution of support reactions when loaded at B4-GL25

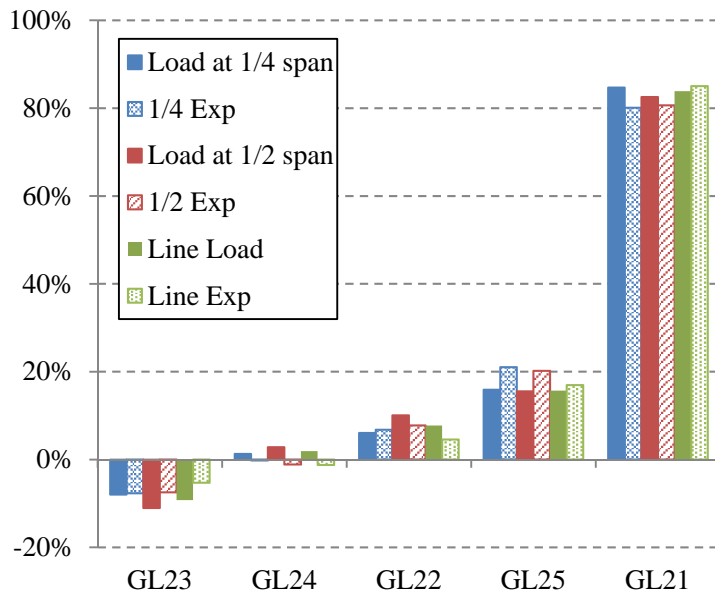


Fig. B.141 – S5-L=6.00m: experimental and numerical distribution of support reactions when loaded at B5-GL21

Table B.14 – Experimental and numerical support reaction distribution [%]

Floor specimen	Load case	Experimental					Numerical				
		Beam position									
		B1	B2	B3	B4	B5	B1	B2	B3	B4	B5
S1-BSp	B1 ½	76	29	5	-3	-7	85	17	4	0	-7
	B2 ½	27	46	22	13	-7	30	40	26	12	-7
	B3 ½	-2	34	37	35	-3	0	32	35	32	0
	B4 ½	-6	13	20	46	27	-7	12	26	39	30
	B5 ½	-5	-3	2	24	81	-7	0	4	17	85
	B1 ¼	82	23	3	-3	-5	87	16	2	0	-5
	B2 ¼	25	49	22	9	-5	25	49	24	8	-5
	B3 ¼	1	27	43	29	0	-1	29	44	29	-1
	B4 ¼	-4	10	20	48	26	-5	8	24	48	25
	B5 ¼	-4	-3	2	20	84	-5	0	2	16	88
	B1 4P	82	23	0	-2	-3	89	14	2	0	-4
	B2 4P	25	49	21	10	-5	22	55	21	7	-4
	B3lin	-3	19	69	18	-3	-1	25	51	25	-1
	B3 4P	-5	31	49	29	-4	-4	7	21	55	22
	B4lin	-3	5	16	68	14	-4	0	2	13	89
	B4 4P	-6	9	22	53	22	-4	0	2	13	89
B5lin	-2	-2	-1	22	84	-4	0	2	13	89	
B5 4P	-4	-4	1	28	79	-4	0	2	13	89	
S2-LWAC	B1 ½	88	15	2	-2	-3	85	16	7	1	-8
	B2 ½	26	46	25	9	-6	32	36	26	13	-7
	B3 ½	-8	33	51	32	-8	2	31	34	30	2
	B4 ½	-5	6	25	53	21	-7	13	26	36	32
	B5 ½	-3	-2	1	17	88	-8	1	7	15	85
	B1 ¼	89	14	1	-3	-1	87	15	3	0	-6
	B2 ¼	17	63	19	3	-2	27	45	25	8	-5
	B3 ¼	-4	23	63	22	-4	0	28	42	28	0
	B4 ¼	-4	4	20	65	15	-5	8	25	44	27
	B5 ¼	-2	-2	-1	17	88	-6	0	4	15	87
	B1lin	93	9	-1	-1	-1	88	13	3	0	-5
	B2lin	14	72	14	1	-2	24	52	22	8	-4
	B3lin	-3	16	75	15	-3	0	25	50	25	1
	B4lin	-2	2	15	73	12	-4	8	22	51	24
	B5lin	-1	-1	-2	8	95	-5	0	3	13	89

Table B.14 – Experimental and numerical support reaction distribution [%] (cont.)

Floor specimen	Load case	Experimental					Numerical				
		Beam position									
		B1	B2	B3	B4	B5	B1	B2	B3	B4	B5
S3-hc=0.03m	B1 ½	85	18	2	-1	-4	89	17	-2	-3	-1
	B2 ½	23	51	25	5	-4	22	51	30	1	-4
	B3 ½	-1	30	45	26	0	-4	29	50	30	-5
	B4 ½	-4	4	29	47	24	-4	1	30	51	21
	B5 ½	-5	-4	4	26	78	-1	-3	-2	17	89
	B1 ¼	89	14	1	-2	-2	92	13	-2	-2	-1
	B2 ¼	17	64	21	1	-2	17	61	24	0	-3
	B3 ¼	-1	23	58	19	1	-4	23	61	23	-4
	B4 ¼	-3	3	23	61	17	-3	0	24	62	17
	B5 ¼	-3	-3	2	22	83	-1	-2	-2	13	92
	B1lin	95	7	0	-1	-1	93	12	-2	-2	-1
	B2lin	11	76	14	1	-1	15	66	21	0	-2
	B3lin	0	17	69	15	0	-3	20	66	21	-3
	B4lin	-1	1	15	72	13	-2	0	21	66	15
B5lin	-2	-1	0	13	90	-1	-2	-2	12	93	
S4-L=2.00m	B1 ½	94	9	-1	-1	0	92	13	-4	-2	0
	B2 ½	8	79	16	-2	-1	16	63	24	-1	-2
	B3 ½	-5	18	73	19	-5	-5	27	56	27	-5
	B4 ½	-2	1	15	77	9	-2	-1	24	62	16
	B5 ½	-1	0	-1	8	94	0	-2	-3	13	93
	B1 ¼	94	10	-3	-1	0	94	10	-3	-1	0
	B2 ¼	6	84	14	-3	-1	12	71	19	-1	-1
	B3 ¼	-3	10	83	13	-3	-4	21	66	21	-4
	B4 ¼	-1	-2	14	82	6	-1	-1	19	71	13
	B5 ¼	0	-1	-2	8	95	0	-1	-3	10	94
	B1lin	95	7	-1	0	0	95	9	-3	-1	0
	B2lin	5	86	11	-2	0	11	74	17	-1	-1
	B3lin	-2	11	82	12	-2	-4	19	69	19	-4
	B4lin	0	-2	11	86	6	-1	-1	17	74	11
B5lin	0	-1	-1	6	96	0	-1	-3	9	95	
S5-L=6.00m	B1 ½	80	19	8	-1	-7	83	15	10	3	-11
	B2 ½	31	34	29	11	-5	35	31	26	15	-7
	B3 ½	2	28	39	28	3	5	29	32	29	5
	B4 ½	-6	12	26	38	31	-7	15	26	32	34
	B5 ½	-7	-1	8	20	81	-11	3	10	16	83

Table B.14 – Experimental and numerical support reaction distribution [%] (cont.)

Floor specimen	Load case	Experimental					Numerical				
		Beam position									
		B1	B2	B3	B4	B5	B1	B2	B3	B4	B5
S5-L=6.00m	B1 ¼	81	19	7	-1	-7	85	15	6	1	-8
	B2 ¼	29	41	25	8	-4	30	38	27	10	-6
	B3 ¼	3	25	43	25	4	2	28	39	28	2
	B4 ¼	-5	9	23	45	27	-6	10	27	39	30
	B5 ¼	-8	0	7	21	80	-8	1	6	16	85
	B1lin	84	18	4	-2	-4	84	15	8	2	-9
	B2lin	25	47	26	6	-3	32	36	27	12	-6
	B3lin	1	25	48	25	1	3	28	37	29	3
	B4lin	-4	7	23	52	23	-6	12	26	36	32
	B5lin	-5	-1	5	17	85	-9	2	8	16	84

½ - mid-span; ¼ - quarter-span; lin - line load; 4P - 4-point load

Table B.15 – Difference between experimental and numerical support reaction distribution [%]

Floor specimen	Load case	Beam position					Floor specimen	Load case	Beam position				
		B1	B2	B3	B4	B5			B1	B2	B3	B4	B5
S1-BSp	B1 ½	-9	12	1	-4	0	S4-L=2.00m	B1 ½	1	-4	2	0	0
	B2 ½	-3	6	-4	1	-1		B2 ½	-7	16	-8	-1	1
	B3 ½	-3	2	1	3	-3		B3 ½	0	-9	17	-8	0
	B4 ½	0	1	-6	6	-2		B4 ½	0	2	-9	14	-7
	B5 ½	2	-3	-2	8	-5		B5 ½	0	1	3	-5	2
	B1 ¼	-5	7	1	-3	0		B1 ¼	0	0	0	0	0
	B2 ¼	0	1	-2	2	0		B2 ¼	-6	13	-5	-1	0
	B3 ¼	2	-3	-1	0	1		B3 ¼	2	-11	17	-8	1
	B4 ¼	1	2	-4	0	2		B4 ¼	1	-1	-5	12	-6
	B5 ¼	1	-3	0	5	-3		B5 ¼	0	0	1	-2	0
	B1 4P	-7	10	-2	-2	1		B1lin	1	-3	2	1	0
	B2 4P	3	-6	1	3	-1		B2lin	-6	12	-6	-1	1
	B3lin	-2	-6	18	-8	-2		B3lin	1	-8	13	-7	1
	B3 4P	-4	31	49	29	-4		B4lin	1	-1	-7	12	-6
	B4lin	1	-2	-5	13	-7		B5lin	0	0	2	-3	1
	B4 4P	-1	2	1	-2	1							
B5lin	2	-2	-3	8	-5								
B5 4P	0	-4	-1	15	-10								

Table B.15 – Difference between experimental and numerical support reaction distribution [%]

Floor specimen	Load case	Beam position					Floor specimen	Load case	Beam position				
		B1	B2	B3	B4	B5			B1	B2	B3	B4	B5
S2-LWAC	B1 ½	3	-1	-4	-3	5	S5-L=6.00m	B1 ½	-3	4	-2	-3	4
	B2 ½	-6	10	-1	-4	1		B2 ½	-4	3	3	-4	2
	B3 ½	-10	2	17	2	-10		B3 ½	-3	-1	7	-1	-2
	B4 ½	2	-7	-1	17	-11		B4 ½	1	-3	-1	6	-3
	B5 ½	5	-3	-6	1	3		B5 ½	4	-4	-2	5	-2
	B1 ¼	2	-1	-3	-3	5		B1 ¼	-4	4	1	-2	1
	B2 ¼	-9	18	-6	-5	2		B2 ¼	-1	3	-2	-2	2
	B3 ¼	-5	-5	21	-7	-4		B3 ¼	1	-3	4	-4	2
	B4 ¼	1	-5	-6	21	-12		B4 ¼	1	-1	-4	7	-3
	B5 ¼	4	-3	-4	2	1		B5 ¼	0	-2	1	5	-5
	B1lin	5	-4	-4	-1	4		B1lin	0	3	-4	-4	5
	B2lin	-10	21	-8	-6	3		B2lin	-7	11	-1	-6	3
	B3lin	-4	-9	25	-10	-3		B3lin	-3	-3	11	-4	-2
	B4lin	2	-5	-7	22	-12		B4lin	2	-5	-4	16	-9
	B5lin	4	-1	-5	-5	6		B5lin	4	-3	-3	1	1
S3-hc=0.03m	B1 ½	-4	1	4	2	-3		B1 ½	-4	1	4	2	-3
	B2 ½	2	0	-5	4	-1		B2 ½	2	0	-5	4	-1
	B3 ½	4	0	-5	-3	5		B3 ½	4	0	-5	-3	5
	B4 ½	0	2	-1	-4	2		B4 ½	0	2	-1	-4	2
	B5 ½	-4	0	6	9	-11		B5 ½	-4	0	6	9	-11
	B1 ¼	-2	1	3	0	-2		B1 ¼	-2	1	3	0	-2
	B2 ¼	0	2	-4	1	1		B2 ¼	0	2	-4	1	1
	B3 ¼	3	-1	-3	-5	5		B3 ¼	3	-1	-3	-5	5
	B4 ¼	-1	2	-1	-1	0		B4 ¼	-1	2	-1	-1	0
	B5 ¼	-3	-1	4	8	-9		B5 ¼	-3	-1	4	8	-9
	B1lin	3	-5	1	1	0		B1lin	3	-5	1	1	0
	B2lin	-4	10	-7	0	1		B2lin	-4	10	-7	0	1
	B3lin	3	-4	4	-6	3		B3lin	3	-4	4	-6	3
	B4lin	1	1	-6	5	-1		B4lin	1	1	-6	5	-1
	B5lin	-2	1	2	1	-3		B5lin	-2	1	2	1	-3

½ - mid-span; ¼ - quarter-span; lin - line load; 4P - 4-point load

B.3.3 Stresses

Table B.16 gathers the stresses computed with the mean experimental strains recorded for the loaded beam, together with the stresses obtained with the numerical model. Also the percentage difference computed relatively to the experimental values is presented.

Table B.16 – Stresses comparison [MPa]

Floor specimen	Beam position	Experimental			Numerical			Relative difference [%]		
		Load case								
		½	¼	lin/4P	½	¼	lin	½	¼	lin/4P
S1-BSp	B1	5.63	2.08	6.18 (4P)	6.35	2.26	3.06	-13	-9	51
	B2	4.91	1.11	5.46 (4P)	6.37	1.78	3.13	-30	-61	43
	B3	6.11	1.28	1.42	6.35	1.47	3.15	-4	-15	-122
	B4	5.98	1.48	2.09	6.36	1.77	3.12	-6	-20	-49
	B5	2.12	2.33	1.38	6.35	2.28	3.09	-200	2	-124
S2-LWAC	B1	7.12	3.03	1.12	6.81	2.46	3.33	4	19	-197
	B2	8.18	3.15	2.50	6.79	1.95	3.30	17	38	-32
	B3	9.51	3.57	2.79	6.82	1.72	3.35	28	52	-20
	B4	8.64	3.06	3.45	6.77	1.94	3.29	22	37	4
	B5	9.20	3.82	1.49	6.82	2.47	3.30	26	35	-122
S3-hc=0.03m	B1	5.57	2.70	0.65	6.23	2.49	2.98	-12	8	-358
	B2	6.20	2.11	1.47	6.33	1.64	3.11	-2	22	-112
	B3	5.48	1.90	1.24	6.31	1.79	3.09	-15	5	-148
	B4	3.91	1.19	0.92	6.35	1.61	3.13	-62	-35	-239
	B5	4.75	2.10	0.97	6.24	2.49	2.97	-31	-19	-206
S4-L=2.00m	B1	3.92	2.28	1.85	6.56	3.19	3.25	-67	-40	-76
	B2	6.64	3.65	4.20	6.57	2.53	3.30	1	31	21
	B3	6.18	3.20	4.47	6.59	2.39	3.31	-7	25	26
	B4	4.71	2.45	2.84	6.57	2.59	3.29	-40	-6	-16
	B5	6.50	3.48	3.91	6.55	3.16	3.25	-1	9	17
S5-L=6.00m	B1	5.91	2.41	1.66	6.23	2.15	2.98	-5	11	-79
	B2	6.37	1.55	1.82	6.23	1.60	3.06	2	-3	-68
	B3	7.66	1.90	2.16	6.23	1.50	3.05	19	21	-42
	B4	7.89	2.00	2.40	6.23	1.62	3.06	21	19	-27
	B5	8.49	3.33	2.57	6.23	2.14	2.98	27	36	-16

½ - mid-span; ¼ - quarter-span; lin - line load; 4P - 4-point load

APPENDIX C

C.1 First phase numerical analysis

The following sections summarize the results obtained with the preliminary numerical analysis for the various load cases. They complement the information referred in 3.6 *Preliminary numerical analysis* section and presented in more detail in 5.2 *Parametric study*.

The various modeling cases were obtained based on *BS* (Base simulation) by changing a parameter. Table C.1 gathers the characteristics of the first phase modeling.

Table C.1 – First phase modeling

Denomination	Description	Variation	Span L [m]	Width b_{slab} [m]	Interlayer h_i [m]	Connection stiffness K [kN/m]	Beams			Concrete height h_c [m]	Timber EN 338	Concrete EC 2	Support conditions S_c	Loads EC 1		
							Spacing s_b [m]	Width b_t [m]	Section h_t, \varnothing [m]							
B_s	Base simulation	-	4.00	4.00	0.02	12000	0.60	0.10	0.07	C24	C25/ 30	S_s	sw, Pt, Ln			
B_{si}	B_s - interlayer	Interlayer, h_i			0.00								$Rt, 0.20$	Pt, Ln		
B_{silA}	B_s + Imposed load	Imposed load (Il)			0.02								3000	A		
B_{silC4}	B_s + Imposed load	Il + Beam height, h_t													$Rt, 0.25$	C4
B_{s-IK}	B_s + Low stiffness	Connection stiffness, K													100000	Pt, Ln
B_{s-hK}	B_s + High stiffness				12000								$Rt, 0.20$			
B_{s-fx}	B_s + Fx	Support conditions (S_c)												Fx	Pt, Ln	
B_{s4sup}	B_s + Sae													Sae		
B_{sjb01}	B_s + $s_b = 0.00$	Juxtaposed beams, $s_b = 0.00$ m			0.00								S_s			

Table C.1 – First phase modeling (cont.)

Denomination	Description	Variation	Span	Width	Interlayer	Connection stiffness	Beams			Concrete height	Timber	Concrete	Support conditions	Loads	
							Spacing	Width	Section						
							L [m]	b_{slab} [m]	h_i [m]						K [kN/m]
Bsjb06	$B_s + s_b = 0.00 + b_t$	Juxtaposed beams + Beam width, b_t	4.00	4.00	0.02	12000	0.60	0.60	0.07	C24	C25/30	S_s	P_t, L_n		
Bsl2	$B_s + L = 2.00$	Span, L	2.00												
Bsl5	$B_s + L = 5.00$		5.00												
Bsl8ht	$B_s + L = 8.00$	$L + h_t$	8.00											$R_t, 0.20$	
sb040	$B_s + s_b = 0.40$	Beam spacing, s_b	4.00											0.40	$R_t, 0.25$
sb075	$B_s + s_b = 0.75$													0.75	
Bstc2	$B_s + h_c = 0.02$	Concrete height, h_c	4.00											0.10	0.02
Bstc3	$B_s + h_c = 0.03$														0.03
Bstc5	$B_s + h_c = 0.05$														0.05
Bstc10	$B_s + h_c = 0.10$														$R_t, 0.20$
3×4Bstc3	$b_{slab} = 3.00 + h_c = 0.03$	Width, $b_{slab} + h_c$	3.00	0.60	0.03										
3×4Bstc5	$b_{slab} = 3.00 + h_c = 0.05$				0.05										
3×4Bstc7	$b_{slab} = 3.00 + h_c = 0.07$	b_{slab}			0.07										

Table C.1 – First phase modeling (cont.)

Denomination	Description	Variation	Span	Width	Interlayer	Connection stiffness	Beams			Concrete height	Timber	Concrete	Support conditions	Loads										
							Spacing	Width	Section															
							L [m]	b_{slab} [m]	h_i [m]						K [kN/m]	s_b [m]	b_t [m]	h_t, \emptyset [m]	h_c [m]	EN 338	EC 2	S_c	EC 1	
3×6Bstc5	$b_{slab} = 3.00 + L = 6.00 + h_c = 0.05$	$b_{slab} + L + h_c$	6.00	3.00																				
4×6Bstc5	$B_s + L = 6.00 + h_c = 0.05$	$L + h_c$													0.10	$R_t, 0.20$	0.05	C24	C25/ 30					
Bsfi15	$B_s + \emptyset 15$	Round section beams																						
Bsfi25	$B_s + \emptyset 25$		O, 0.25																					
BsiOSB	$B_s + OSB + LVL + I$ -shaped	Timber + I-shaped beams																						
BsiKertoS	$B_s + LVL + I$ -shaped															I, 0.059, 0.406	OSB							
BsC16-20	$B_s + C16/20$	Concrete	4.00	4.00	0.02	12000	0.60																	
BsC40-50	$B_s + C40/50$															C24	C16/ 20							
BsLC16-18	$B_s + LC16/18$																	C40/ 50						
BsLC35-38	$B_s + LC35/38$																		LC 16/18					
BsC14	$B_s + C14$																	BsLC 35-38						
BsD60	$B_s + D60$	Timber																						
BsGL24	$B_s + GL24h$															C14								
BsGL32	$B_s + GL32h$															D60								
BsKertoS	$B_s + LVL$															GL 24h								
BsCLT	$B_s + CLTdeck$															GL 32h								
		Timber + h_i																						

Table C.1 – First phase modeling (cont.)

Denomination	Description	Variation	Span	Width	Interlayer	Connection stiffness	Beams			Concrete height	Timber	Concrete	Support conditions	Loads		
							Spacing	Width	Section							
							L [m]	b_{slab} [m]	h_i [m]						K [kN/m]	s_b [m]
BsCLTfx	$Bs +$ CLTdeck $+ Fx$	Timber + $h_i + S_c$	4.00	4.00	0.00	12000	-	4.00	Deck, 0.169	CLT	C25/ 30	S_c	F_x			
BsCLT4s	$Bs +$ CLTdeck $+ Sae$													Sae		
BsCLT5	$Bs +$ CLTdeck $+ h_c =$ 0.05	Timber + $h_i + h_c$		3.00										0.05	Deck, 0.120	
3BsCLT5	$Bs +$ CLTdeck $+ b_{slab} =$ $3.00 + h_c$ $= 0.05$	Timber + $b_{slab} + h_i$ $+ h_c$														Deck, 0.099
3BsCLT5_h 12	$Bs +$ CLTdeck $+ b_{slab} =$ $3.00 + h_c$ $= 0.05 +$ $h_t = 0.120$	Timber + b $+ h_i + h_c +$ h_t														
3BsCLT5_h 9.9	$Bs +$ CLTdeck $+ b_{slab} =$ $3.00 + h_c =$ 0.05 + $h_t = 0.099$															

The results of the numerical analysis were processed with a spreadsheet using all the decimal places. The percentages presented for a modeling were computed by dividing the value obtained for the corresponding beam by the sum of the values associated with all the beams. Therefore, the sum of percentages associated with a modeling is equal to 100 %. However, since the percentages presented in the tables were rounded to the closest unit value,

in some cases the sum associated to each modeling may be slightly different from 100. The following tables present the results, in terms of displacements, support reactions and bending moments, for two specific load cases: the central beam loaded at mid-span with a point load, and the same beam loaded with a linear load.

As mentioned in section 5. *NUMERICAL ANALYSIS*, some modeling cases have different number of beams, either by having a different slab width (3.00 m rather than 4.00 m) or by having a different beam spacing. In the case where the beam spacing changes from 0.60 m to 0.75 m (*sb075*) the number of beams decreases, while when it changes from 0.60 to 0.40 m (*sb040*) the number of beams increases. Considering specifically the results presented for the *sb040* modeling, for those designated “when the load is applied at B3” and “when the load is applied at B4” (marked with *), in fact they do not correspond to the loading over B3 and B4 in the slab under consideration. The slab modeled as *sb040* is composed by eleven beams, while most of the remaining modeling have only seven. Therefore, it was chosen to present respectively the results when the load is applied at B5 and B6. With B6 being the central beam at *sb040* and B5 the immediately adjacent one. This allows a better comparison with the remaining modeling.

As for the cases where the slabs are composed by five beams, the results designated as “when the load is applied at B3” do really correspond to the B3 beam, which matches to the central beam. For these modeling, the results correspondent to the loading of B4 beam are not presented because there are symmetrical to those obtained when the load is applied to B2 beam.

The symbology is the same as that presented in the section 3.6 *Preliminary numerical analysis*, as well as the identification in each modeling of the values corresponding to the central beam, when loaded, using bold characters.

It should be noted that, for modeling where the width was 3.00 m or where the beam spacing was different from 0.60 m the number of beams was different from seven. In the table, the results in bold identify those corresponding to the central beam. Since the central beam is the loaded one, the percentages of displacements are symmetrically relatively to it, as it would be expected, with the loaded beam receiving the highest percentage.

C.1.1 Vertical displacement at each beam mid-span

Table C.2 – Vertical displacements at $\frac{1}{2} L$, when the load is applied at $B1 \frac{1}{2} L$ [%]

Modeling denomination	Load case													
	Point load at the central beam mid-span							Line load along the central beam longitudinal axis						
	Beam position							Beam position						
	B1	B2	B3	B4	B5	B6	B7	B1	B2	B3	B4	B5	B6	B7
<i>Bs</i>	47	28	15	7	3	1	0	46	28	15	7	3	1	0
<i>Bsi</i>	45	28	15	8	3	1	0	44	28	16	8	3	1	0
<i>Bs-lK</i>	40	26	16	9	5	2	1	40	27	16	9	5	2	1
<i>Bs-hK</i>	52	29	14	5	1	0	-1	51	30	14	5	1	0	-1
<i>Bs-fx</i>	57	29	12	3	0	-1	-1	56	30	12	3	0	-1	-1
<i>Bs4sup</i>	45	28	15	8	3	1	0	44	28	16	8	3	1	0
<i>Bsjb01</i>	53	28	12	5	2	0	0	53	28	12	5	2	0	0
<i>Bsjb06</i>	48	27	14	7	3	1	1	48	27	14	6	3	1	1
<i>Bsl2</i>	65	26	8	2	0	0	0	65	26	8	2	0	0	0
<i>Bsl5</i>	41	27	16	9	5	2	0	40	27	17	9	5	2	0
<i>Bsl8ht</i>	34	25	18	12	7	4	1	33	25	18	12	7	4	1
<i>sb040</i>	38	26	17	10	6	3	1	37	26	17	10	6	3	1
<i>sb075</i>	51	29	13	5	1			51	29	14	5	1		
<i>Bstc2</i>	78	22	3	0	0	0	-1	77	22	2	0	0	0	-1
<i>Bstc3</i>	67	27	7	1	0	-1	0	66	27	7	1	-1	-1	0
<i>Bstc5</i>	54	29	13	4	1	0	-1	53	29	13	4	1	0	-1
<i>Bstc10</i>	40	26	16	9	5	3	1	39	26	16	9	5	3	1
<i>3×4Bstc3</i>	67	27	7	1	-1			66	27	7	0	-1		
<i>3×4Bstc5</i>	54	29	13	4	0			53	30	13	4	0		
<i>3×4Bstc7</i>	47	29	15	7	2			46	29	16	7	2		
<i>3×6Bstc5</i>	44	29	17	8	3			43	29	17	9	3		
<i>4×6Bstc5</i>	43	28	16	9	4	1	-1	42	28	17	9	4	1	-1
<i>Bsfi15</i>	42	27	16	9	4	2	1	41	27	16	9	5	2	0
<i>Bsfi25</i>	49	28	14	6	2	1	0	49	28	14	6	2	1	0
<i>BsiOSB</i>	54	30	13	5	1	-1	-1	53	30	14	5	1	-1	-1
<i>BsiKertoS</i>	52	29	14	5	1	0	-1	51	30	14	5	1	0	-1
<i>BsC16-20</i>	47	28	15	7	3	1	0	46	29	15	7	3	1	-1
<i>BsC40-50</i>	45	28	15	7	3	1	0	45	28	16	8	3	1	0
<i>BsLC16-18</i>	63	29	9	2	0	-1	-1	62	29	9	2	-1	-1	-1
<i>BsLC35-38</i>	47	28	15	7	3	1	0	46	29	15	7	3	1	-1
<i>BsC14</i>	44	28	15	8	4	1	0	44	28	16	8	4	1	0
<i>BsD60</i>	48	28	14	6	2	0	-1	48	29	15	7	2	0	-1
<i>BsGL24</i>	47	28	15	7	3	1	0	46	29	15	7	3	1	0
<i>BsGL32</i>	47	28	15	7	3	1	0	47	29	15	7	3	1	-1
<i>BsKertoS</i>	47	28	15	7	3	1	0	47	29	15	7	3	1	-1
<i>BsCLT</i>	39	28	19	12	6	1	-4	38	28	19	12	6	1	-4
<i>BsCLTfx</i>	45	30	19	10	4	-1	-6	44	30	19	11	4	-2	-6
<i>BsCLT4s</i>	21	21	20	17	12	7	2	12	20	22	20	15	9	2
<i>BsCLT5</i>	40	28	19	11	5	0	-5	39	29	19	12	6	0	-5
<i>3BsCLT5</i>	43	30	18	9	0			42	30	19	9	0		
<i>3BsCLT5_h12</i>	42	29	18	9	1			41	29	19	10	1		
<i>3BsCLT5_h9.9</i>	41	29	18	10	2			40	29	19	10	2		

Table C.3 – Vertical displacements at ½ L, when the load is applied at B2 ½ L [%]

Modeling denomination	Load case													
	Point load at the central beam mid-span							Line load along the central beam longitudinal axis						
	Beam position							Beam position						
	B1	B2	B3	B4	B5	B6	B7	B1	B2	B3	B4	B5	B6	B7
<i>Bs</i>	29	28	20	12	6	3	1	29	27	20	13	7	3	1
Bsi	29	28	20	12	7	3	1	29	27	20	13	7	4	1
Bs-1K	27	26	19	13	8	5	3	27	25	19	13	8	5	3
Bs-hK	30	31	21	12	5	2	0	30	29	21	12	6	2	0
Bs-fx	30	34	22	10	4	1	-1	31	32	22	11	4	1	-1
Bs4sup	29	28	20	12	7	3	1	29	27	20	13	7	4	1
Bsjb01	29	34	21	10	4	2	0	29	33	22	11	4	2	0
Bsjb06	28	30	20	11	6	3	1	28	29	21	12	6	3	1
Bsl2	27	41	22	8	2	0	0	28	40	23	8	2	0	0
Bsl5	28	26	19	13	8	4	2	28	25	19	13	8	4	2
Bsl8ht	26	23	18	14	10	6	4	26	22	18	14	10	7	4
sb040	27	24	18	13	8	5	3	27	23	18	13	9	5	3
sb075	29	32	22	12	5			29	31	22	12	6		
Bstc2	22	54	22	4	0	0	0	22	52	22	4	0	0	0
Bstc3	27	42	23	8	1	0	-1	28	40	24	8	1	0	-1
Bstc5	30	32	21	11	5	1	0	30	31	22	11	5	1	0
Bstc10	27	25	19	13	8	5	3	27	25	19	13	8	5	3
3×4Bstc3	27	42	23	8	1			27	40	24	8	1		
3×4Bstc5	30	33	22	11	4			30	31	22	12	4		
3×4Bstc7	29	29	21	13	7			29	28	21	14	8		
3×6Bstc5	29	28	21	14	9			29	27	21	14	9		
4×6Bstc5	29	27	20	13	7	4	1	29	26	20	13	8	4	1
Bsfi15	28	26	19	13	8	4	2	28	25	19	13	8	4	2
Bsfi25	29	31	21	11	6	2	1	29	29	21	12	6	2	1
BsiOSB	30	31	21	11	5	1	-1	31	30	21	12	5	1	-1
BsiKertoS	30	31	21	12	5	2	0	30	29	21	12	5	2	0
BsC16-20	29	29	20	12	6	3	1	29	28	20	12	7	3	1
BsC40-50	29	28	20	12	7	3	1	29	27	20	13	7	3	1
BsLC16-18	29	38	23	9	2	0	-1	30	36	23	9	3	0	-1
BsLC35-38	29	29	20	12	6	3	1	29	28	20	12	7	3	1
BsC14	29	27	20	12	7	4	1	29	26	20	13	7	4	1
BsD60	29	29	21	12	6	3	0	29	28	21	12	6	3	0
BsGL24	29	28	20	12	6	3	1	29	27	20	12	7	3	1
BsGL32	29	29	20	12	6	3	1	29	28	21	12	6	3	1
BsKertoS	29	29	20	12	6	3	1	29	28	21	12	6	3	1
BsCLT	29	25	19	13	9	5	1	29	24	19	13	9	5	1
BsCLTfx	32	27	20	13	7	3	-2	32	26	20	13	8	3	-2
BsCLT4s	7	22	23	20	15	9	3	6	19	23	22	17	10	3
BsCLT5	30	25	19	13	8	4	0	30	25	19	13	8	4	0
3BsCLT5	31	26	20	14	9			31	26	20	14	9		
3BsCLT5_h12	30	26	20	14	10			30	25	20	15	10		
3BsCLT5_h9.9	30	26	20	15	10			30	25	20	15	11		

Table C.4 – Vertical displacements at $\frac{1}{2} L$, when the load is applied at B3* $\frac{1}{2} L$ [%]

Modeling denomination	Load case													
	Point load at the central beam mid-span							Line load along the central beam longitudinal axis						
	Beam position							Beam position						
	B1	B2	B3	B4	B5	B6	B7	B1	B2	B3	B4	B5	B6	B7
<i>Bs</i>	16	20	24	18	12	7	3	16	21	23	19	12	7	3
<i>Bsi</i>	16	20	23	18	12	7	4	16	20	22	18	12	7	4
<i>Bs-lK</i>	17	19	21	17	12	8	5	17	19	21	17	12	8	5
<i>Bs-hK</i>	14	21	27	20	11	5	1	15	21	25	20	12	6	1
<i>Bs-fx</i>	12	22	31	21	10	4	0	12	22	29	21	11	4	0
<i>Bs4sup</i>	16	20	23	18	12	7	4	16	20	22	18	12	7	4
<i>Bsjb01</i>	13	21	30	20	10	4	2	13	22	29	20	10	4	2
<i>Bsjb06</i>	14	21	26	19	11	6	3	14	21	26	19	11	6	3
<i>Bsl2</i>	8	22	38	22	8	2	0	8	23	37	22	8	2	0
<i>Bsl5</i>	17	20	21	17	12	8	5	17	20	20	17	12	8	5
<i>Bsl8ht</i>	18	18	18	16	13	10	7	18	18	18	16	13	10	7
<i>sb040</i>	6	9	12	15	17	14	11	6	9	12	15	16	14	11
<i>sb075</i>	14	22	29	22	14			14	22	28	22	14		
<i>Bstc2</i>	3	22	51	21	4	0	0	3	22	50	22	4	0	0
<i>Bstc3</i>	7	23	40	22	7	1	0	7	24	38	23	8	1	-1
<i>Bstc5</i>	13	22	29	20	11	5	1	13	22	27	21	11	5	1
<i>Bstc10</i>	17	19	21	17	12	8	5	17	19	20	17	12	8	6
<i>3×4Bstc3</i>	7	23	40	23	7			7	24	38	24	7		
<i>3×4Bstc5</i>	13	22	30	22	13			13	22	29	22	13		
<i>3×4Bstc7</i>	16	21	26	21	16			16	21	25	21	16		
<i>3×6Bstc5</i>	17	21	24	21	17			17	21	23	21	17		
<i>4×6Bstc5</i>	17	20	22	18	12	7	4	17	20	21	18	12	8	4
<i>Bsfi15</i>	17	20	22	17	12	8	5	17	20	21	17	12	8	5
<i>Bsfi25</i>	14	21	27	19	11	6	2	14	21	26	20	11	6	2
<i>BsiOSB</i>	14	22	27	20	11	5	1	14	22	26	20	12	5	1
<i>BsiKertoS</i>	14	21	27	20	11	5	1	15	21	25	20	12	6	1
<i>BsC16-20</i>	16	21	24	19	12	6	3	16	21	23	19	12	7	3
<i>BsC40-50</i>	16	20	24	18	12	7	3	16	20	23	18	12	7	3
<i>BsLC16-18</i>	10	23	35	22	9	2	0	10	23	34	22	9	3	-1
<i>BsLC35-38</i>	15	21	24	19	12	6	3	16	21	23	19	12	7	3
<i>BsC14</i>	16	20	23	18	12	7	4	17	20	22	18	12	7	4
<i>BsD60</i>	15	21	25	19	12	6	2	15	21	24	19	12	6	2
<i>BsGL24</i>	16	21	24	19	12	6	3	16	21	23	19	12	7	3
<i>BsGL32</i>	15	21	25	19	12	6	3	16	21	24	19	12	7	3
<i>BsKertoS</i>	15	21	25	19	12	6	3	16	21	23	19	12	7	3
<i>BsCLT</i>	21	19	18	15	12	9	6	21	19	17	15	12	9	7
<i>BsCLTfx</i>	20	20	20	16	12	8	4	21	20	19	16	12	8	4
<i>BsCLT4s</i>	5	16	25	23	18	11	3	5	16	23	23	19	12	3
<i>BsCLT5</i>	21	19	18	15	12	9	6	21	19	18	15	12	9	6
<i>3BsCLT5</i>	19	20	21	20	19			20	20	20	20	20		
<i>3BsCLT5_h12</i>	19	20	21	20	19			20	20	20	20	20		
<i>3BsCLT5_h9.9</i>	19	20	21	20	19			20	20	20	20	20		

Table C.5 – Vertical displacements at $\frac{1}{2} L$, when the load is applied at B4* $\frac{1}{2} L$ [%]

Modeling denomination	Load case													
	Point load at the central beam mid-span							Line load along the central beam longitudinal axis						
	Beam position							Beam position						
	B1	B2	B3	B4	B5	B6	B7	B1	B2	B3	B4	B5	B6	B7
<i>Bs</i>	7	12	19	23	19	12	7	8	13	19	22	19	13	8
Bsi	8	13	18	22	18	13	8	8	13	18	21	18	13	8
Bs-lK	10	13	17	20	17	13	10	10	13	17	20	17	13	10
Bs-hK	6	12	20	26	20	12	6	6	12	20	25	20	12	6
Bs-fx	3	10	21	30	21	10	3	4	11	21	29	21	11	4
Bs4sup	8	13	18	22	18	13	8	8	13	18	21	18	13	8
Bsjb01	5	10	20	29	20	10	5	5	11	20	28	20	11	5
Bsjb06	7	12	19	26	19	12	7	7	12	19	25	19	12	7
Bsl2	2	8	22	38	22	8	2	2	8	22	37	22	8	2
Bsl5	10	13	17	20	17	13	10	10	13	17	19	17	13	10
Bsl8ht	12	14	16	17	16	14	12	12	14	16	16	16	14	12
sb040	3	5	8	11	14	17	14	3	5	8	11	14	16	14
sb075														
Bstc2	0	4	21	51	21	4	0	0	4	22	50	22	4	0
Bstc3	1	8	22	39	22	8	1	1	8	23	38	23	8	1
Bstc5	5	11	20	28	20	11	5	5	11	21	27	21	11	5
Bstc10	10	13	17	20	17	13	10	10	13	17	19	17	13	10
3×4Bstc3														
3×4Bstc5														
3×4Bstc7														
3×6Bstc5														
4×6Bstc5	9	13	18	21	18	13	9	9	13	18	20	18	13	9
Bsfi15	9	13	17	21	17	13	9	9	13	17	20	17	13	9
Bsfi25	6	12	19	26	19	12	6	6	12	20	25	20	12	6
BsiOSB	5	12	20	27	20	12	5	5	12	20	25	20	12	5
BsiKertoS	5	12	20	26	20	12	5	6	12	20	25	20	12	6
BsC16-20	7	12	19	24	19	12	7	7	13	19	22	19	13	7
BsC40-50	8	12	18	23	18	12	8	8	13	18	22	18	13	8
BsLC16-18	2	9	22	35	22	9	2	2	9	22	33	22	9	2
BsLC35-38	7	12	19	24	19	12	7	7	13	19	22	19	13	7
BsC14	8	13	18	22	18	13	8	8	13	18	21	18	13	8
BsD60	7	12	19	24	19	12	7	7	12	19	23	19	12	7
BsGL24	7	12	19	23	19	12	7	8	13	19	22	19	13	8
BsGL32	7	12	19	24	19	12	7	7	13	19	23	19	13	7
BsKertoS	7	12	19	24	19	12	7	7	13	19	23	19	13	7
BsCLT	13	14	15	16	15	14	13	13	14	15	16	15	14	13
BsCLTfx	11	13	16	19	16	13	11	12	14	16	17	16	14	12
BsCLT4s	4	13	21	26	21	13	4	4	13	21	24	21	13	4
BsCLT5	13	14	15	16	15	14	13	13	14	15	16	15	14	13
3BsCLT5														
3BsCLT5_h12														
3BsCLT5_h9.9														

C.1.2 Support reactions at each beam

Table C.6 – Support reactions at each beam, when the load is applied at B1 ½ L [%]

Modeling denomination	Load case													
	Point load at the central beam mid-span							Line load along the central beam longitudinal axis						
	Beam position							Beam position						
	B1	B2	B3	B4	B5	B6	B7	B1	B2	B3	B4	B5	B6	B7
<i>Bs</i>	84	14	8	1	-1	-1	-4	87	12	4	0	-1	-1	-2
<i>Bsi</i>	84	13	8	1	-1	0	-4	88	12	4	0	-1	0	-3
<i>Bs-lK</i>	86	9	8	2	0	1	-5	89	9	4	1	0	0	-3
<i>Bs-hK</i>	83	16	7	0	-2	-1	-2	87	14	4	-1	-1	-1	-1
<i>Bs-fx</i>	72	26	7	-1	-2	-1	-1	80	20	3	-1	-1	-1	0
<i>Bs4sup</i>	9	44	29	13	4	1	-1	51	33	10	4	1	0	0
<i>Bsjb01</i>	89	14	1	-2	-1	0	-1	91	12	0	-1	-1	0	0
<i>Bsjb06</i>	87	16	2	-1	-1	0	-1	89	14	0	-1	-1	0	-1
<i>Bsl2</i>	91	13	-1	-2	-1	0	0	93	10	-1	-1	-1	0	0
<i>Bsl5</i>	81	13	10	3	0	1	-8	85	12	6	2	0	0	-5
<i>Bsl8ht</i>	75	12	14	8	4	5	-18	80	12	9	5	2	3	-11
<i>sb040</i>	73	20	10	4	0	-1	-1	79	18	6	2	0	-1	-1
<i>sb075</i>	88	11	6	2	-7			91	10	3	1	-4		
<i>Bstc2</i>	92	14	-4	-2	0	0	0	95	9	-3	-1	0	0	0
<i>Bstc3</i>	89	16	0	-3	-1	0	0	92	12	-1	-2	-1	0	0
<i>Bstc5</i>	85	15	6	-1	-2	-1	-1	89	13	3	-1	-1	-1	-1
<i>Bstc10</i>	83	13	8	2	0	1	-7	86	13	4	1	0	0	-4
<i>3x4Bstc3</i>	89	16	0	-3	-2			92	12	-1	-2	-1		
<i>3x4Bstc5</i>	86	15	6	1	-7			89	12	3	0	-5		
<i>3x4Bstc7</i>	85	13	9	5	-11			88	12	5	3	-7		
<i>3x6Bstc5</i>	81	13	12	9	-16			86	13	7	5	-11		
<i>4x6Bstc5</i>	80	14	11	3	-1	0	-7	85	13	6	1	-1	0	-4
<i>Bsfi15</i>	85	11	8	2	0	0	-5	88	10	5	1	0	0	-3
<i>Bsfi25</i>	86	15	4	-1	-2	-1	-2	89	13	2	-1	-1	-1	-1
<i>BsiOSB</i>	81	18	8	0	-2	-2	-2	86	15	4	-1	-2	-1	-1
<i>BsiKertoS</i>	82	17	8	0	-2	-2	-2	87	14	4	-1	-1	-1	-2
<i>BsC16-20</i>	84	14	8	1	-1	-1	-3	87	12	4	0	-1	-1	-2
<i>BsC40-50</i>	84	13	8	1	-1	-1	-4	87	12	4	0	-1	0	-3
<i>BsLC16-18</i>	87	17	2	-3	-2	-1	0	91	12	0	-2	-1	-1	0
<i>BsLC35-38</i>	84	14	8	1	-1	-1	-3	87	12	4	0	-1	-1	-2
<i>BsC14</i>	83	14	8	1	-1	0	-5	87	13	4	0	-1	0	-3
<i>BsD60</i>	84	14	7	0	-2	-1	-3	88	12	4	0	-1	-1	-2
<i>BsGL24</i>	84	14	8	1	-1	-1	-4	88	12	4	0	-1	-1	-2
<i>BsGL32</i>	84	14	8	0	-1	-1	-3	88	12	4	0	-1	-1	-2
<i>BsKertoS</i>	84	14	8	0	-1	-1	-3	88	12	4	0	-1	-1	-2
<i>BsCLT</i>	57	28	18	11	5	-1	-19	65	27	13	7	3	-2	-12
<i>BsCLTfx</i>	52	32	21	11	3	-4	-16	66	27	13	5	1	-3	-9
<i>BsCLT4s</i>	-13	1	23	37	33	19	0	43	26	14	9	5	3	0
<i>BsCLT5</i>	56	29	19	11	5	-2	-18	65	27	13	6	2	-2	-12
<i>3BsCLT5</i>	66	30	19	8	-23			72	27	13	4	-16		
<i>3BsCLT5_h12</i>	68	28	18	9	-23			74	25	12	5	-16		
<i>3BsCLT5_h9.9</i>	69	26	18	10	-23			75	23	12	6	-16		

Table C.7 – Support reactions at each beam, when the load is applied at B2 ½ L [%]

Modeling denomination	Load case													
	Point load at the central beam mid-span							Line load along the central beam longitudinal axis						
	Beam position							Beam position						
	B1	B2	B3	B4	B5	B6	B7	B1	B2	B3	B4	B5	B6	B7
<i>Bs</i>	36	30	23	11	3	2	-5	28	45	21	6	2	1	-3
<i>Bsi</i>	37	29	22	11	4	2	-5	28	44	21	7	2	1	-3
<i>Bs-lK</i>	39	27	22	11	4	3	-6	30	43	20	7	2	2	-4
<i>Bs-hK</i>	35	32	24	10	2	1	-4	26	48	21	6	1	0	-3
<i>Bs-fx</i>	31	36	24	9	2	-1	-2	23	53	20	5	1	0	-1
<i>Bs4sup</i>	8	36	31	17	7	2	-1	11	51	25	9	3	1	0
<i>Bsjb01</i>	25	48	25	5	-1	0	-1	19	59	22	2	-1	0	-1
<i>Bsjb06</i>	29	41	26	6	0	0	-2	22	53	22	4	0	0	-1
<i>Bsl2</i>	22	52	26	2	-1	-1	0	16	64	20	1	-1	0	0
<i>Bsl5</i>	40	25	21	12	6	4	-8	31	40	20	8	3	3	-5
<i>Bsl8ht</i>	46	17	18	13	9	9	-13	37	32	19	10	6	6	-8
<i>sb040</i>	41	24	19	12	6	2	0	33	37	20	8	3	1	0
<i>sb075</i>	32	36	25	12	-6			24	52	21	7	-4		
<i>Bstc2</i>	16	61	26	-2	-2	0	0	11	74	18	-2	-1	0	0
<i>Bstc3</i>	23	49	28	3	-1	-1	0	16	63	21	1	-1	-1	0
<i>Bstc5</i>	31	37	25	9	1	0	-3	23	52	21	5	1	0	-2
<i>Bstc10</i>	41	25	20	11	5	4	-7	32	39	20	7	3	2	-4
<i>3×4Bstc3</i>	23	49	28	5	-5			16	64	21	2	-3		
<i>3×4Bstc5</i>	31	37	26	13	-6			23	52	21	7	-4		
<i>3×4Bstc7</i>	36	31	24	16	-6			28	46	21	10	-4		
<i>3×6Bstc5</i>	39	26	23	19	-7			30	42	21	12	-5		
<i>4×6Bstc5</i>	39	25	21	12	5	4	-8	30	41	20	8	3	2	-5
<i>Bsfi15</i>	39	27	22	11	4	3	-6	30	43	20	7	2	2	-4
<i>Bsfi25</i>	31	37	25	8	1	0	-3	24	50	22	5	1	0	-2
<i>BsiOSB</i>	35	31	24	11	3	0	-4	26	47	21	6	2	0	-3
<i>BsiKertoS</i>	35	32	24	11	3	1	-4	26	48	21	6	1	0	-3
<i>BsC16-20</i>	36	31	23	11	3	2	-5	27	46	21	6	2	1	-3
<i>BsC40-50</i>	37	30	22	11	4	2	-5	28	45	21	7	2	1	-3
<i>BsLC16-18</i>	26	44	27	5	-1	-1	-1	19	60	21	3	-1	-1	-1
<i>BsLC35-38</i>	36	31	23	11	3	2	-5	27	46	21	6	2	1	-3
<i>BsC14</i>	38	28	22	11	4	2	-5	29	43	21	7	2	1	-4
<i>BsD60</i>	35	32	23	10	3	1	-4	26	47	21	6	2	1	-3
<i>BsGL24</i>	36	30	23	11	3	2	-5	27	46	21	6	2	1	-3
<i>BsGL32</i>	36	31	23	10	3	1	-5	27	46	21	6	2	1	-3
<i>BsKertoS</i>	36	31	23	10	3	1	-5	27	46	21	6	2	1	-3
<i>BsCLT</i>	42	23	17	13	9	4	-9	36	32	19	11	6	2	-6
<i>BsCLTfx</i>	37	27	20	14	8	3	-9	30	40	19	10	5	1	-6
<i>BsCLT4s</i>	-6	9	23	30	28	17	0	8	38	25	15	9	4	0
<i>BsCLT5</i>	42	24	18	13	9	4	-9	36	32	19	11	6	2	-6
<i>3BsCLT5</i>	44	24	18	13	0			38	32	19	11	-1		
<i>3BsCLT5_h12</i>	45	23	18	14	-1			38	33	19	12	-1		
<i>3BsCLT5_h9.9</i>	46	22	18	15	-1			38	33	19	12	-1		

Table C.8 – Support reactions at each beam, when the load is applied at B3* ½ L [%]

Modeling denomination	Load case													
	Point load at the central beam mid-span							Line load along the central beam longitudinal axis						
	Beam position							Beam position						
	B1	B2	B3	B4	B5	B6	B7	B1	B2	B3	B4	B5	B6	B7
<i>Bs</i>	7	28	30	23	12	6	-6	4	24	44	21	7	4	-4
Bsi	9	27	29	23	12	7	-6	4	24	43	21	7	4	-4
Bs-1K	10	26	28	22	12	8	-6	5	23	43	20	7	5	-4
Bs-hK	6	29	30	24	11	5	-5	2	24	46	21	7	3	-4
Bs-fx	6	27	33	25	10	2	-3	3	21	52	20	6	1	-2
Bs4sup	3	24	31	25	13	5	0	1	22	45	22	7	3	0
Bsjb01	-2	29	44	25	5	1	-3	-2	24	56	21	3	0	-2
Bsjb06	0	30	38	26	7	2	-4	-1	25	51	22	4	1	-2
Bsl2	-3	29	48	26	2	-1	-1	-3	22	61	20	1	-1	-1
Bsl5	13	25	25	21	13	10	-7	7	23	39	20	9	6	-4
Bsl8ht	22	20	19	17	14	14	-6	13	21	32	19	10	9	-5
sb040	-4	9	14	19	21	19	13	-3	6	10	20	34	20	9
sb075	3	30	35	30	3			1	24	50	24	1		
Bstc2	-6	28	55	26	-2	-2	0	-4	19	70	18	-2	-1	0
Bstc3	-4	32	44	28	3	-1	-2	-3	23	60	21	1	-1	-1
Bstc5	2	30	34	25	10	3	-5	1	25	49	21	5	2	-3
Bstc10	13	24	26	21	13	8	-6	7	23	39	21	8	5	-4
3x4Bstc3	-4	32	44	32	-4			-3	23	60	23	-3		
3x4Bstc5	2	31	35	31	2			0	25	50	25	0		
3x4Bstc7	6	28	31	28	6			3	25	45	25	3		
3x6Bstc5	10	27	27	27	10			5	25	41	25	5		
4x6Bstc5	11	26	25	21	13	10	-7	6	24	40	20	9	6	-5
Bsfi15	10	26	28	22	12	8	-6	5	24	42	21	7	5	-4
Bsfi25	2	30	35	25	9	3	-5	0	25	48	22	5	2	-3
BsiOSB	6	28	29	24	12	5	-6	3	24	45	21	7	3	-4
BsiKertoS	6	29	30	24	12	5	-6	3	24	46	21	7	3	-4
BsC16-20	7	28	30	23	12	6	-6	3	24	44	21	7	4	-4
BsC40-50	8	27	29	23	12	7	-6	4	24	43	21	7	4	-4
BsLC16-18	-2	32	40	27	6	0	-3	-2	24	56	21	3	0	-2
BsLC35-38	7	28	30	23	12	6	-6	3	24	44	21	7	4	-4
BsC14	9	27	28	22	12	7	-6	5	24	42	21	8	4	-4
BsD60	6	29	31	24	11	6	-6	3	24	46	21	7	3	-4
BsGL24	7	28	30	23	12	6	-6	4	24	44	21	7	4	-4
BsGL32	7	28	30	23	11	6	-6	3	24	45	21	7	4	-4
BsKertoS	7	28	30	23	11	6	-6	3	24	45	21	7	4	-4
BsCLT	27	19	16	14	13	10	1	19	20	26	17	11	7	0
BsCLTfx	22	21	19	16	13	9	-1	14	20	35	17	10	6	-1
BsCLT4s	-3	12	22	27	25	16	0	2	18	36	23	14	7	0
BsCLT5	27	19	16	14	12	10	1	19	20	27	17	11	6	0
3BsCLT5	22	19	18	19	22			16	20	28	20	16		
3BsCLT5_h12	22	19	18	19	22			16	20	30	20	16		
3BsCLT5_h9.9	22	19	18	19	22			15	19	30	19	15		

Table C.9 – Support reactions at each beam, when the load is applied at B4* ½ L [%]

Modeling denomination	Load case													
	Point load at the central beam mid-span							Line load along the central beam longitudinal axis						
	Beam position							Beam position						
	B1	B2	B3	B4	B5	B6	B7	B1	B2	B3	B4	B5	B6	B7
<i>Bs</i>	-4	15	24	29	24	15	-4	-3	10	21	44	21	10	-3
<i>Bsi</i>	-3	16	23	28	23	16	-3	-2	10	21	43	21	10	-2
<i>Bs-lK</i>	-2	16	23	28	23	16	-2	-2	10	21	42	21	10	-2
<i>Bs-hK</i>	-4	15	25	30	25	15	-4	-3	9	22	45	22	9	-3
<i>Bs-fx</i>	-3	11	25	33	25	11	-3	-2	6	20	51	20	6	-2
<i>Bs4sup</i>	0	12	23	29	23	12	0	0	7	21	43	21	7	0
<i>Bsjb01</i>	-5	7	25	44	25	7	-5	-3	4	22	55	22	4	-3
<i>Bsjb06</i>	-5	10	27	37	27	10	-5	-3	6	23	50	23	6	-3
<i>Bsl2</i>	-3	4	26	48	26	4	-3	-2	2	20	61	20	2	-2
<i>Bsl5</i>	-1	17	22	25	22	17	-1	-1	11	21	39	21	11	-1
<i>Bsl8ht</i>	4	18	18	19	18	18	4	2	13	19	31	19	13	2
<i>sb040</i>	-5	5	8	13	19	21	19	-4	3	5	9	20	34	20
<i>sb075</i>														
<i>Bstc2</i>	-2	-2	26	55	26	-2	-2	-1	-1	18	70	18	-1	-1
<i>Bstc3</i>	-4	5	28	43	28	5	-4	-3	2	21	60	21	2	-3
<i>Bstc5</i>	-5	13	26	34	26	13	-5	-4	7	21	49	21	7	-4
<i>Bstc10</i>	-1	16	22	26	22	16	-1	-1	10	21	39	21	10	-1
<i>3×4Bstc3</i>														
<i>3×4Bstc5</i>														
<i>3×4Bstc7</i>														
<i>3×6Bstc5</i>														
<i>4×6Bstc5</i>	-2	18	22	25	22	18	-2	-2	12	21	40	21	12	-2
<i>Bsfi15</i>	-3	16	23	28	23	16	-3	-2	10	21	42	21	10	-2
<i>Bsfi25</i>	-5	12	26	34	26	12	-5	-4	7	22	48	22	7	-4
<i>BsiOSB</i>	-4	15	25	29	25	15	-4	-3	9	22	45	22	9	-3
<i>BsiKertoS</i>	-4	15	25	30	25	15	-4	-3	9	21	45	21	9	-3
<i>BsC16-20</i>	-4	15	24	29	24	15	-4	-3	9	21	44	21	9	-3
<i>BsC40-50</i>	-3	16	23	29	23	16	-3	-3	10	21	43	21	10	-3
<i>BsLC16-18</i>	-5	8	27	40	27	8	-5	-3	4	21	56	21	4	-3
<i>BsLC35-38</i>	-4	15	24	29	24	15	-4	-3	9	21	44	21	9	-3
<i>BsC14</i>	-3	16	23	28	23	16	-3	-2	10	21	42	21	10	-2
<i>BsD60</i>	-4	15	24	30	24	15	-4	-3	9	21	45	21	9	-3
<i>BsGL24</i>	-4	15	24	29	24	15	-4	-3	9	21	44	21	9	-3
<i>BsGL32</i>	-4	15	24	30	24	15	-4	-3	9	21	45	21	9	-3
<i>BsKertoS</i>	-4	15	24	30	24	15	-4	-3	9	21	45	21	9	-3
<i>BsCLT</i>	13	15	15	14	15	15	13	8	12	17	25	17	12	8
<i>BsCLTfx</i>	9	16	17	17	17	16	9	5	12	17	34	17	12	5
<i>BsCLT4s</i>	-1	15	23	26	23	15	-1	0	10	21	36	21	10	0
<i>BsCLT5</i>	13	15	15	14	15	15	13	8	12	17	26	17	12	8
<i>3BsCLT5</i>														
<i>3BsCLT5_h12</i>														
<i>3BsCLT5_h9.9</i>														

C.2.1 Longitudinal bending moment at the mid-span section of each beam

Table C.10 – Longitudinal bending moment at $\frac{1}{2} L$, when the load is applied at B1 $\frac{1}{2} L$ [%]

Modeling denomination	Load case													
	Point load at the central beam mid-span							Line load along the central beam longitudinal axis						
	Beam position							Beam position						
	B1	B2	B3	B4	B5	B6	B7	B1	B2	B3	B4	B5	B6	B7
<i>Bs</i>	58	24	11	5	2	1	0	43	29	16	8	3	1	0
<i>Bsi</i>	55	24	12	6	2	1	0	42	29	17	8	4	1	0
<i>Bs-lK</i>	50	24	13	7	4	2	1	37	27	17	10	5	3	1
<i>Bs-hK</i>	63	23	10	4	1	0	-1	49	30	15	6	2	0	-1
<i>Bs-fx</i>	67	23	8	2	0	0	0	52	31	14	4	1	-1	-1
<i>Bs4sup</i>	64	18	9	5	3	1	0	7	28	28	20	11	5	1
<i>Bsjb01</i>	68	19	8	3	1	0	0	49	30	14	5	2	0	0
<i>Bsjb06</i>	52	25	12	6	3	1	1	37	31	17	8	4	2	1
<i>Bsl2</i>	70	22	6	1	0	0	0	61	29	9	2	0	0	0
<i>Bsl5</i>	54	23	12	6	3	1	0	38	27	18	10	5	2	0
<i>Bsl8ht</i>	48	23	13	8	5	2	1	32	25	18	12	8	4	1
<i>sb040</i>	51	23	13	7	4	2	1	34	26	18	11	6	3	2
<i>sb075</i>	62	24	10	4	1			48	30	15	6	1		
<i>Bstc2</i>	83	16	2	0	0	0	0	74	25	3	0	-1	-1	-1
<i>Bstc3</i>	75	20	5	1	0	0	0	62	30	8	1	-1	-1	-1
<i>Bstc5</i>	65	23	9	3	1	0	0	50	31	14	5	1	0	-1
<i>Bstc10</i>	51	23	13	7	4	2	1	37	27	17	10	6	3	1
<i>3×4Bstc3</i>	75	20	5	1	-1			62	30	8	1	-1		
<i>3×4Bstc5</i>	64	23	9	3	0			50	31	14	5	0		
<i>3×4Bstc7</i>	57	24	12	5	2			43	29	17	8	3		
<i>3×6Bstc5</i>	57	24	12	6	2			40	29	18	9	3		
<i>4×6Bstc5</i>	57	23	12	6	3	1	0	40	28	18	9	4	1	-1
<i>Bsfi15</i>	55	23	12	6	3	1	0	38	27	17	10	5	2	1
<i>Bsfi25</i>	59	23	11	5	2	1	0	44	30	16	7	3	1	0
<i>BsiOSB</i>	62	25	10	3	1	0	-1	51	31	14	5	1	-1	-1
<i>BsiKertoS</i>	60	25	11	4	1	0	-1	49	30	15	6	1	0	-1
<i>BsC16-20</i>	58	24	11	5	2	0	0	44	29	16	8	3	1	0
<i>BsC40-50</i>	57	24	11	5	2	1	0	42	29	17	8	4	1	0
<i>BsLC16-18</i>	72	22	7	1	0	-1	-1	59	31	11	2	-1	-1	-1
<i>BsLC35-38</i>	58	24	11	5	2	0	0	44	29	16	8	3	1	0
<i>BsC14</i>	56	23	12	6	3	1	0	41	28	17	9	4	1	0
<i>BsD60</i>	59	24	11	5	2	0	0	45	30	16	7	3	0	-1
<i>BsGL24</i>	58	24	11	5	2	1	0	43	29	16	8	3	1	0
<i>BsGL32</i>	58	24	11	5	2	0	0	44	29	16	8	3	1	0
<i>BsKertoS</i>	58	24	11	5	2	0	0	44	29	16	8	3	1	0
<i>BsCLT</i>	60	20	12	7	3	0	-2	38	28	19	12	6	1	-4
<i>BsCLTfx</i>	69	19	10	5	1	-1	-3	46	31	19	10	3	-2	-7
<i>BsCLT4s</i>	83	8	4	3	2	1	0	23	17	19	18	13	8	2
<i>BsCLT5</i>	61	21	12	7	3	0	-3	40	29	19	12	5	0	-5
<i>3BsCLT5</i>	62	21	12	5	0			42	30	19	9	0		
<i>3BsCLT5_h12</i>	62	20	11	5	1			41	29	19	10	2		
<i>3BsCLT5_h9.9</i>	62	20	11	6	1			40	28	19	10	3		

Table C.11 – Longitudinal bending moment at ½ L, when the load is applied at B2 ½ L [%]

Modeling denomination	Load case													
	Point load at the central beam mid-span							Line load along the central beam longitudinal axis						
	Beam position							Beam position						
	B1	B2	B3	B4	B5	B6	B7	B1	B2	B3	B4	B5	B6	B7
Bs	24	42	18	9	5	2	1	29	26	20	13	7	3	1
Bsi	24	40	18	9	5	2	1	29	26	20	13	8	4	1
Bs-1K	24	36	18	10	6	4	2	27	24	19	13	8	5	3
Bs-hK	23	46	17	8	4	1	0	31	28	21	12	6	2	0
Bs-fx	23	49	17	7	3	1	0	31	30	22	12	5	1	0
Bs4sup	9	51	20	11	6	3	1	7	24	27	21	13	6	1
Bsjb01	20	55	15	6	3	1	0	30	30	22	11	5	2	1
Bsjb06	20	44	18	10	5	3	1	25	28	22	13	7	4	2
Bsl2	23	52	18	6	2	0	0	29	36	23	9	2	0	0
Bsl5	24	39	17	10	5	3	1	28	24	19	14	9	5	2
Bsl8ht	23	36	17	10	7	4	2	25	22	18	14	10	7	4
sb040	24	35	17	10	6	4	2	26	22	18	13	9	6	3
sb075	23	47	18	8	4			30	29	22	13	6		
Bstc2	16	66	15	3	0	0	0	25	48	23	4	0	0	-1
Bstc3	20	57	17	5	1	0	0	30	36	24	9	2	0	-1
Bstc5	23	48	17	8	3	1	0	31	29	22	12	5	2	0
Bstc10	24	37	17	10	6	4	2	27	24	19	13	9	5	3
3×4Bstc3	20	57	17	5	1			29	37	24	9	1		
3×4Bstc5	23	48	18	8	3			31	29	22	12	5		
3×4Bstc7	24	43	18	10	6			29	27	21	14	9		
3×6Bstc5	24	43	18	10	6			29	26	21	15	10		
4×6Bstc5	23	42	17	9	5	2	1	28	25	20	14	8	4	1
Bsfi15	23	41	17	9	5	3	2	28	24	19	13	8	5	2
Bsfi25	23	45	17	9	4	2	1	29	27	21	13	6	3	1
BsiOSB	26	42	19	9	4	1	0	31	29	21	12	6	2	-1
BsiKertoS	26	41	19	9	4	1	0	31	28	21	12	6	2	0
BsC16-20	24	42	18	9	4	2	1	29	26	20	13	7	3	1
BsC40-50	24	41	18	9	5	2	1	29	26	20	13	7	4	1
BsLC16-18	22	53	17	6	2	0	-1	31	34	23	10	3	0	-1
BsLC35-38	24	42	18	9	4	2	1	29	26	20	13	7	3	1
BsC14	24	41	17	9	5	2	1	29	25	20	13	8	4	2
BsD60	24	43	18	9	4	2	0	30	27	21	13	7	3	1
BsGL24	24	42	18	9	5	2	1	29	26	20	13	7	3	1
BsGL32	24	43	18	9	4	2	1	29	26	20	13	7	3	1
BsKertoS	24	42	18	9	4	2	1	29	26	20	13	7	3	1
BsCLT	21	48	14	9	5	3	1	28	26	18	13	9	5	1
BsCLTfx	20	55	13	7	4	1	-1	31	29	19	13	7	3	-1
BsCLT4s	5	68	12	7	5	3	1	3	27	22	20	16	10	2
BsCLT5	22	48	14	9	5	2	0	29	26	19	13	8	4	0
3BsCLT5	21	49	15	9	6			29	27	20	14	10		
3BsCLT5_h12	20	50	14	9	6			29	27	20	15	10		
3BsCLT5_h9.9	20	51	14	9	6			28	27	20	15	11		

Table C.12 – Longitudinal bending moment at $\frac{1}{2} L$, when the load is applied at B3* $\frac{1}{2} L$ [%]

Modeling denomination	Load case													
	Point load at the central beam mid-span							Line load along the central beam longitudinal axis						
	Beam position							Beam position						
	B1	B2	B3	B4	B5	B6	B7	B1	B2	B3	B4	B5	B6	B7
<i>Bs</i>	12	18	39	16	9	5	2	17	20	21	18	12	7	4
<i>Bsi</i>	12	18	37	16	9	5	3	17	20	21	18	12	8	4
<i>Bs-lK</i>	13	18	33	16	10	6	4	18	19	19	17	13	9	6
<i>Bs-hK</i>	10	17	44	16	8	4	1	16	21	24	20	12	6	2
<i>Bs-fx</i>	9	17	47	17	7	3	0	14	22	26	21	12	5	1
<i>Bs4sup</i>	4	16	46	19	10	5	1	5	19	26	24	16	9	2
<i>Bsjb01</i>	8	15	53	14	6	3	1	15	22	26	20	11	5	2
<i>Bsjb06</i>	10	18	40	16	9	5	3	14	21	23	19	12	7	4
<i>Bsl2</i>	7	18	50	17	6	2	0	10	23	34	22	9	2	0
<i>Bsl5</i>	13	18	36	16	9	6	3	18	19	19	17	13	9	5
<i>Bsl8ht</i>	14	17	32	15	10	7	5	19	18	17	15	13	10	8
<i>sb040</i>	4	6	9	15	30	14	9	7	9	12	14	15	14	11
<i>sb075</i>	10	18	45	18	10			15	22	26	22	15		
<i>Bstc2</i>	2	15	65	15	3	0	0	4	23	46	23	4	0	0
<i>Bstc3</i>	5	16	56	16	5	1	0	9	24	34	23	9	2	0
<i>Bstc5</i>	9	17	45	16	8	3	1	15	22	25	20	12	5	1
<i>Bstc10</i>	13	18	34	16	10	6	4	18	19	19	16	13	9	6
<i>3×4Bstc3</i>	5	16	56	16	5			9	24	35	24	9		
<i>3×4Bstc5</i>	9	18	46	18	9			15	22	26	22	15		
<i>3×4Bstc7</i>	12	18	40	18	12			17	21	23	21	17		
<i>3×6Bstc5</i>	12	18	40	18	12			18	21	22	21	18		
<i>4×6Bstc5</i>	12	17	39	16	9	5	3	18	20	20	17	13	8	5
<i>Bsfi15</i>	12	17	38	15	9	5	3	18	19	20	17	13	8	5
<i>Bsfi25</i>	11	17	42	16	8	4	2	16	21	23	19	12	6	3
<i>BsiOSB</i>	11	19	39	18	9	4	1	15	21	24	20	12	6	1
<i>BsiKertoS</i>	11	19	38	18	9	4	1	16	21	24	20	12	6	2
<i>BsC16-20</i>	11	18	40	16	9	4	2	17	20	22	18	12	7	3
<i>BsC40-50</i>	12	18	38	16	9	5	3	17	20	21	18	12	7	4
<i>BsLC16-18</i>	7	17	51	17	6	2	0	11	23	31	22	10	3	0
<i>BsLC35-38</i>	11	18	40	16	9	4	2	17	20	22	18	12	7	3
<i>BsC14</i>	12	18	38	16	9	5	3	17	20	21	18	13	8	4
<i>BsD60</i>	11	18	40	16	8	4	2	17	21	22	19	12	7	3
<i>BsGL24</i>	12	18	39	16	9	5	2	17	20	21	18	12	7	4
<i>BsGL32</i>	11	18	40	16	9	4	2	17	20	22	18	12	7	3
<i>BsKertoS</i>	11	18	40	16	9	4	2	17	20	22	18	12	7	3
<i>BsCLT</i>	13	14	44	12	8	6	4	20	19	19	15	12	9	7
<i>BsCLTfx</i>	11	14	51	11	7	4	2	20	19	22	15	11	8	5
<i>BsCLT4s</i>	2	10	63	13	7	4	1	3	15	29	22	18	11	2
<i>BsCLT5</i>	13	15	44	12	8	5	3	20	19	20	15	12	9	6
<i>3BsCLT5</i>	12	15	46	15	12			19	20	22	20	19		
<i>3BsCLT5_h12</i>	12	15	48	15	12			19	20	23	20	19		
<i>3BsCLT5_h9.9</i>	12	14	48	14	12			19	20	23	20	19		

Table C.13 – Longitudinal bending moment at ½ L, when the load is applied at B4* ½ L [%]

Modeling denomination	Load case													
	Point load at the central beam mid-span							Line load along the central beam longitudinal axis						
	Beam position							Beam position						
	B1	B2	B3	B4	B5	B6	B7	B1	B2	B3	B4	B5	B6	B7
<i>Bs</i>	5	9	16	39	16	9	5	9	13	18	21	18	13	9
Bsi	6	10	16	36	16	10	6	9	13	18	20	18	13	9
Bs-lK	8	10	16	32	16	10	8	10	14	17	18	17	14	10
Bs-hK	4	8	16	43	16	8	4	6	12	20	23	20	12	6
Bs-fx	3	7	17	47	17	7	3	5	12	21	25	21	12	5
Bs4sup	2	8	18	44	18	8	2	3	13	21	25	21	13	3
Bsjb01	3	6	14	53	14	6	3	6	11	20	25	20	11	6
Bsjb06	5	9	16	39	16	9	5	7	13	19	22	19	13	7
Bsl2	2	6	17	50	17	6	2	2	9	22	33	22	9	2
Bsl5	7	10	16	35	16	10	7	11	14	17	18	17	14	11
Bsl8ht	8	11	15	31	15	11	8	13	14	15	16	15	14	13
sb040	2	4	6	9	14	30	14	4	6	8	11	14	14	14
sb075														
Bstc2	0	3	15	65	15	3	0	0	4	23	46	23	4	0
Bstc3	1	5	16	56	16	5	1	1	9	23	34	23	9	1
Bstc5	3	8	16	45	16	8	3	6	12	20	24	20	12	6
Bstc10	8	10	16	33	16	10	8	11	14	17	18	17	14	11
3x4Bstc3														
3x4Bstc5														
3x4Bstc7														
3x6Bstc5														
4x6Bstc5	6	9	16	38	16	9	6	10	14	17	19	17	14	10
Bsfi15	7	9	15	37	15	9	7	10	13	17	19	17	13	10
Bsfi25	5	8	16	41	16	8	5	8	12	19	22	19	12	8
BsiOSB	4	9	18	39	18	9	4	5	12	20	24	20	12	5
BsiKertoS	4	9	18	38	18	9	4	6	12	20	23	20	12	6
BsC16-20	5	9	16	39	16	9	5	8	13	18	21	18	13	8
BsC40-50	6	9	16	38	16	9	6	9	13	18	20	18	13	9
BsLC16-18	2	6	17	51	17	6	2	2	10	22	30	22	10	2
BsLC35-38	5	9	16	39	16	9	5	8	13	18	21	18	13	8
BsC14	6	9	16	37	16	9	6	9	13	18	20	18	13	9
BsD60	5	9	16	40	16	9	5	8	13	19	21	19	13	8
BsGL24	5	9	16	39	16	9	5	8	13	18	21	18	13	8
BsGL32	5	9	16	39	16	9	5	8	13	18	21	18	13	8
BsKertoS	5	9	16	39	16	9	5	8	13	18	21	18	13	8
BsCLT	8	9	12	43	12	9	8	13	14	15	18	15	14	13
BsCLTfx	6	8	11	50	11	8	6	11	13	15	20	15	13	11
BsCLT4s	1	6	12	61	12	6	1	3	13	20	29	20	13	3
BsCLT5	8	9	12	43	12	9	8	13	14	15	18	15	14	13
3BsCLT5														
3BsCLT5_h12														
3BsCLT5_h9.9														

C.1.4 Self-weight and imposed loads

Table C.14 – Self-weight and imposed load cases

Modeling denomination	Load case	Beam position							Quantity
		B1	B2	B3	B4	B5	B6	B7	
<i>Bs</i>	<i>sw</i>	14	14	15	15	15	14	14	Vertical displacement
		13	15	15	15	15	15	13	Support reaction
		14	14	14	15	14	14	14	Bending moment
BsilA	<i>II, A Cat., 2 kN/m²</i>	14	14	15	15	15	14	14	Vertical displacement
		13	15	15	15	15	15	13	Support reaction
		14	14	14	15	14	14	14	Bending moment
BsilC4	<i>II, C4 Cat., 7 kN/m²</i>	14	14	14	15	14	14	14	Vertical displacement
		13	14	15	15	15	14	13	Support reaction
		14	14	14	15	14	14	14	Bending moment

C.1.5 Analysis of the parameters effects

The following tables summarize the findings on the parameters effects for the first phase numerical analysis.

Results are summarized in tables per quantity analyzed: vertical displacement, support reaction and longitudinal bending moment; and loaded beam. Most of the times, the loaded beam is the one receiving the biggest percentage of displacement, support reaction or bending moment, when compared with the remaining beams. Nevertheless, this was not that common when B2 was loaded. Most of the times, for this load case, the first beam was the one receiving the biggest share.

As already presented, not all the modeling had the same number of beams. Therefore, it was decided to present the results corresponding to the central beam in the same table for all modeling that was considered. For the cases where the central beam is the B3 beam, the corresponding cells are not filled in the table corresponding to the cases “when B3 is loaded” but in those “when B4 is loaded”.

Concerning the concrete thickness, two separate analyses were made: one considering all the thicknesses and another selecting only those thicknesses that were considered to be the most commonly used in practice (0.03 m and 0.05 m, designated as h_c exp).

As presented in section 5.2 *Parametric study* all the comparisons were performed using the percentage associated to the loaded beam, but not all were computed using *Bs* as the “comparing modeling”. To identify the comparisons performed between different modeling a color code was adopted. In the following tables, the third row from the end (beige), intends to evaluate the effect that support conditions may have in a composite floor with a lower deck of

CLT. Therefore, the comparisons were made relatively to *BSCLT* modeling, instead of *Bs*, which was simply supported in two ends. The compared modeling represent, at a time, those two sides fixed and the four sides simply supported.

The penultimate row of the following tables presents the comparison between the CTLdeck heights (light grey). Therefore, the comparison was performed relatively to the *3BsCLT5* modeling. This corresponds to a slab with a CLTdeck instead of timber beams, whose thickness was assumed to be equal to h_t in *Bs* modeling (0.20 m), a width equal to 3.00 m and a concrete thickness of 0.05 m.

The last row of the following tables presents the comparison between the effects of the span equal to 6.00 m with a concrete thickness of 0.05 m and the floor width, " $L = 6.00 \text{ m} + h_c = 0.05 \text{ m}$ " (grey). Given that, in *Bs* modeling, the beams were 4.00 m long and the concrete layer 0.07 m thick. The modeling chosen to perform the comparison were *Bstc5* and $3 \times 4Bstc5$. These modeling have a concrete layer with the same thickness (0.05 m) and a different span (4.00 m), the first was used to compare with $4 \times 6Bstc5$ and the last with $3 \times 6Bstc5$.

Table C.15 – Deviation between *Bs* and the remaining modeling considering the vertical displacement, when B1 is loaded [%]

Comparison modeling								
<i>Bs</i>	47	46						
BsCLT	39	38						
3BsCLT5	43	42						
Bstc5	54	53						
3×4Bstc5	54	53						
Load case	Pt at B1	Ln at B1	Description	Pt at B1	Ln at B1	Description	Pt at B1	Ln at B1
Variation	Minimum			Maximum			Max. difference	
Beam spacing	38	37	0.40 m	51	51	0.75 m	9	9
Connection stiffness	40	40	low	52	51	high	6	6
Support conditions	45	44	<i>Sae</i>	57	56	<i>Fx</i>	10	10
Span	34	33	8.00 m	65	65	2.00 m	18	19
h_c	40	39	0.10 m	78	77	0.02 m	31	31
h_c exp	54	53	0.05 m	67	66	0.03 m	20	21
\emptyset	42	41	0.15 m	49	49	0.25 m	5	5
I-section	52	51	Kerto-S	54	53	OSB+LVL	7	7
Concrete	45	45	C40/50	63	62	LC16/18	16	17
Timber	44	44	C14	48	48	D60	2	2
CLTdeck vs. Juxtaposed beams	39	38	CLTdeck	53	53	Juxtaposed beams	8	8
CLTdeck supports	21	12	<i>Sae</i>	45	44	<i>Fx</i>	18	26
CLT height	41	40	0.099	42	41	0.120	2	3
$L = 6.00 \text{ m} + h_c = 0.05 \text{ m}$	43	42	4×6	44	43	3×6	11	11

Table C.16 – Deviation between B_s and the remaining modeling considering the vertical displacement, when B2 is loaded [%]

Comparison modeling								
B_s	28	27						
BsCLT	25	24						
3BsCLT5	26	26						
Bstc5	32	31						
3×4Bstc5	33	31						
Load case	Pt at B2	Ln at B2	Description	Pt at B2	Ln at B2	Description	Pt at B2	Ln at B2
Variation	Minimum			Maximum			Max. difference	
Beam spacing	24	23	0.40 m	32	31	0.75 m	4	4
Connection stiffness	26	25	low	31	29	high	3	2
Support conditions	28	27	Sae	34	32	Fx	6	5
Span	23	22	8.00 m	41	40	2.00 m	12	12
h_c	25	25	0.10 m	54	52	0.02 m	25	25
h_c exp	32	31	0.05 m	42	40	0.03 m	13	13
\emptyset	26	25	0.15 m	31	29	0.25 m	2	2
I-section	31	29	Kerto-S	31	30	OSB+LVL	3	3
Concrete	28	27	C40/50	38	36	LC16/18	9	9
Timber	27	26	C14	29	28	D60	1	1
CLTdeck vs. Juxtaposed beams	25	24	CLTdeck	34	33	Juxtaposed beams	5	5
CLTdeck supports	22	19	Sae	27	26	Fx	3	5
CLT height	26	25	0.099	26	25	0.120	0	1
$L = 6.00$ m + $h_c = 0.05$ m	27	26	4×6	28	27	3×6	6	5

Table C.17 – Deviation between B_s and the remaining modeling considering the vertical displacement when B3 is loaded [%]

Comparison modeling								
B_s	24	23						
BsCLT	18	17						
3BsCLT5								
Bstc5	29	27						
3×4Bstc5								
Load case	Pt at B3	Ln at B3	Description	Pt at B3	Ln at B3	Description	Pt at B3	Ln at B3
Variation	Minimum			Maximum			Max. difference	
Beam spacing				17	16	0.40 m	7	7
Connection stiffness	21	21	low	27	25	high	3	2
Support conditions	23	22	Sae	31	29	Fx	7	6
Span	18	18	8.00 m	38	37	2.00 m	14	14
h_c	21	20	0.10 m	51	50	0.02 m	27	27
h_c exp	29	27	0.05 m	40	38	0.03 m	15	15
\emptyset	22	21	0.15 m	27	26	0.25 m	3	3
I-section	27	26	Kerto-S/ OSB+LVL	27	25	OSB+LVL/ Kerto-S	3	2
Concrete	24	23	C40/50	35	34	LC16/18	11	11
Timber	23	22	C14	25	24	D60	1	1
CLTdeck vs. Juxtaposed beams	18	17	CLTdeck	30	29	Juxtaposed beams	6	6
CLTdeck supports	20	19	Fx	25	23	Sae	7	6
CLT height								
$L = 6.00 \text{ m} + h_c = 0.05 \text{ m}$				22	21	4×6	7	6

Table C.18 – Deviation between the B_s and the remaining modeling considering the vertical displacement when the central beam is loaded [%]

Comparison modeling								
B_s	23	22						
BsCLT	16	16						
3BsCLT5	21	20						
Bstc5	28	27						
3×4Bstc5	30	29						
Load case	Pt at B4	Ln at B4	Description	Pt at B4	Ln at B4	Description	Pt at B4	Ln at B4
Variation	Minimum			Maximum			Max. difference	
Beam spacing	17	16	0.40 m	29	28	0.75 m	7	7
Connection stiffness	20	20	low	26	25	high	3	3
Support conditions	22	21	Sae	30	29	Fx	7	6
Span	17	16	8.00 m	38	37	2.00 m	15	15
h_c	20	19	0.10 m	51	50	0.02 m	28	28
h_c exp	28	27	0.05 m	39	38	0.03 m	16	15
ϕ	21	20	0.15 m	26	25	0.25 m	3	3
I-section	26	25	Kerto-S	27	25	OSB+LVL	3	3
Concrete	23	22	C40/50	35	33	LC16/18	11	11
Timber	22	21	C14	24	23	D60	1	1
CLTdeck vs. Juxtaposed beams	16	16	CLTdeck	29	28	Juxtaposed beams	7	7
CLTdeck supports	19	17	Fx	26	24	Sae	9	9
CLT height	21	20	0.120	21	20	0.099	0	0
$L = 6.00$ m + $h_c = 0.05$ m	21	20	4×6	24	23	3×6	7	7

Table C.19 – Deviation between the B_s and the remaining modeling considering the support reactions when B1 is loaded [%]

Comparison modeling								
B_s	84	87						
BsCLT	57	65						
3BsCLT5	66	72						
Bstc5	85	89						
3×4Bstc5	86	89						
Load case	P_t at B1	L_n at B1	Description	P_t at B1	L_n at B1	Description	P_t at B1	L_n at B1
Variation	Minimum			Maximum			Max. difference	
Beam spacing	73	79	0.40 m	88	91	0.75 m	10	8
Connection stiffness	83	87	high	86	89	low	2	1
Support conditions	9	51	<i>Sae</i>	72	80	<i>Fx</i>	75	37
Span	75	80	8.00 m	91	93	2.00 m	9	7
h_c	83	86	0.10 m	92	95	0.02 m	8	7
h_c exp	85	89	0.05 m	89	92	0.03 m	5	5
\emptyset	85	88	0.15 m	86	89	0.25 m	2	2
I-section	81	86	OSB+LVL	82	87	Kerto-S	3	2
Concrete	84	87	C40/50	87	91	LC16/18	3	3
Timber	83	87	C14	84	88	D60	1	1
CLTdeck vs. Juxtaposed beams	57	65	CLTdeck	89	91	Juxtaposed beams	27	22
CLTdeck supports	-13	43	<i>Sae</i>	52	66	<i>Fx</i>	70	22
CLT height	68	75	0.120/0.099	69	74	0.099/0.120	3	2
$L = 6.00 \text{ m} + h_c = 0.05 \text{ m}$	80	85	4×6	81	86	3×6	5	4

Table C.20 – Deviation between the B_s and the remaining modeling considering the support reactions when B2 is loaded [%]

Comparison modeling								
B_s	30	45						
BsCLT	23	32						
3BsCLT5	24	32						
Bstc5	37	52						
3×4Bstc5	37	52						
Load case	P_t at B2	L_n at B2	Description	P_t at B2	L_n at B2	Description	P_t at B2	L_n at B2
Variation	Minimum			Maximum			Max. difference	
Beam spacing	24	37	0.40 m	36	52	0.75 m	6	9
Connection stiffness	27	43	low	32	48	high	3	3
Support conditions	36	51	Sae	36	53	F_x	6	8
Span	17	32	8.00 m	52	64	2.00 m	22	19
h_c	25	39	0.10 m	61	74	0.02 m	31	28
h_c exp	37	52	0.05 m	49	63	0.03 m	18	18
\varnothing	27	43	0.15 m	37	50	0.25 m	7	5
I-section	31	47	OSB+LVL	32	48	Kerto-S	1	2
Concrete	30	45	C40/50	44	60	LC16/18	14	14
Timber	28	43	C14	32	47	D60	2	2
CLTdeck vs. Juxtaposed beams	23	32	CLTdeck	48	59	Juxtaposed beams	18	14
CLTdeck supports	9	38	Sae	27	40	F_x	15	8
CLT height	22	33	0.099/0.120	23	33	0.120/0.099	2	1
$L = 6.00$ m + $h_c = 0.05$ m	25	41	4×6	26	42	3×6	11	11

Table C.21 – Deviation between the B_s and the remaining modeling considering the support reactions when B3 is loaded [%]

Comparison modeling								
B_s	30	44						
BsCLT	16	26						
3BsCLT5								
Bstc5	34	49						
3×4Bstc5								
Load case	Pt at B3	Ln at B3	Description	Pt at B3	Ln at B3	Description	Pt at B3	Ln at B3
Variation	Minimum			Maximum			Max. difference	
Beam spacing				21	34	0.40 m	8	10
Connection stiffness	28	43	low	30	46	high	2	2
Support conditions	31	45	Sae	33	52	Fx	4	8
Span	19	32	8.00 m	48	61	2.00 m	19	17
h_c	26	39	0.10 m	55	70	0.02 m	26	26
h_c exp	34	49	0.05 m	44	60	0.03 m	14	16
\emptyset	28	42	0.15 m	35	48	0.25 m	6	4
I-section	29	45	OSB+LVL	30	46	Kerto-S	0	2
Concrete	29	43	C40/50	40	56	LC16/18	10	12
Timber	28	42	C14	31	46	D60	1	2
CLTdeck vs. Juxtaposed beams	16	26	CLTdeck	44	56	Juxtaposed beams	15	18
CLTdeck supports	19	35	Fx	22	36	Sae	6	10
CLT height								
$L = 6.00 \text{ m} + h_c = 0.05 \text{ m}$				25	40	4×6	9	10

Table C.22 – Deviation between the B_s and the remaining modeling considering the support reactions when the central beam is loaded [%]

Comparison modeling								
B_s	29	44						
BsCLT	14	25						
3BsCLT5	18	28						
Bstc5	34	49						
3×4Bstc5	35	50						
Load case	P_t at B4	L_n at B4	Description	P_t at B4	L_n at B4	Description	P_t at B4	L_n at B4
Variation	Minimum			Maximum			Max. difference	
Beam spacing	21	34	0.40 m	35	50	0.75 m	8	10
Connection stiffness	28	42	low	30	45	high	2	2
Support conditions	29	43	Sae	33	51	Fx	4	8
Span	19	31	8.00 m	48	61	2.00 m	19	17
h_c	26	39	0.10 m	55	70	0.02 m	26	26
h_c exp	34	49	0.05 m	43	60	0.03 m	14	16
\emptyset	28	42	0.15 m	34	48	0.25 m	5	4
I-section	29	45	OSB+LVL	30	45	Kerto-S	1	2
Concrete	29	43	C40/50	40	56	LC16/18	11	13
Timber	28	42	C14	30	45	D60	1	2
CLTdeck vs. Juxtaposed beams	14	25	CLTdeck	44	55	Juxtaposed beams	15	18
CLTdeck supports	17	34	Fx	26	36	Sae	11	11
CLT height	18	30	0.120	18	30	0.099	0	2
$L = 6.00 \text{ m} + h_c = 0.05 \text{ m}$	25	40	4×6	27	41	3×6	9	10

Table C.23 – Deviation between the B_s and the remaining modeling considering the bending moment when B1 is loaded [%]

Comparison modeling								
B_s	58	43						
BsCLT	60	38						
3BsCLT5	62	42						
Bstc5	65	50						
3×4Bstc5	64	50						
Load case	P_t at B1	L_n at B1	Description	P_t at B1	L_n at B1	Description	P_t at B1	L_n at B1
Variation	Minimum			Maximum			Max. difference	
Beam spacing	51	34	0.40 m	62	48	0.75 m	7	9
Connection stiffness	50	37	low	63	49	high	8	6
Support conditions	64	7	Sae	67	52	F_x	9	36
Span	48	32	8.00 m	70	61	2.00 m	13	18
h_c	51	37	0.10 m	83	74	0.02 m	25	31
h_c exp	65	50	0.05 m	75	62	0.03 m	17	19
\varnothing	55	38	0.15 m	59	44	0.25 m	3	5
I-section	60	49	Kerto-S	62	51	OSB+LVL	4	8
Concrete	57	42	C40/50	72	59	LC16/18	14	16
Timber	56	41	C14	59	45	D60	2	2
CLTdeck vs. Juxtaposed beams	60	38	CLTdeck	68	49	Juxtaposed beams	11	6
CLTdeck supports	69	23	F_x/Sae	83	46	Sae/F_x	23	15
CLT height	62	40	0.099	62	41	0.120	0	2
$L = 6.00$ m + $h_c = 0.05$ m	57	40	4×6	57	40	3×6	8	10

Table C.24 – Deviation between the B_s and the remaining modeling considering the bending moment when B2 is loaded [%]

Comparison modeling								
B_s	42	26						
BsCLT	48	26						
3BsCLT5	49	27						
Bstc5	48	29						
3×4Bstc5	48	29						
Load case	P_t at B2	L_n at B2	Description	P_t at B2	L_n at B2	Description	P_t at B2	L_n at B2
Variation	Minimum			Maximum			Max. difference	
Beam spacing	35	22	0.40 m	47	29	0.75 m	7	4
Connection stiffness	36	24	low	46	28	high	6	2
Support conditions	49	24	F_x/S_{ae}	51	30	S_{ae}/F_x	9	4
Span	36	22	8.00 m	52	36	2.00 m	9	10
h_c	37	24	0.10 m	66	48	0.02 m	24	22
h_c exp	48	29	0.05 m	57	36	0.03 m	15	10
\emptyset	41	24	0.15 m	45	27	0.25 m	3	2
I-section	41	28	Kerto-S	42	29	OSB	1	2
Concrete	41	26	C40/50	53	34	LC16/18	11	8
Timber	41	25	C14	43	27	D60	1	1
CLTdeck vs. Juxtaposed beams	48	26	CLTdeck	55	30	Juxtaposed beams	13	4
CLTdeck supports	55	27	F_x/S_{ae}	68	29	S_{ae}/F_x	21	3
CLT height	51	27	0.099	50	27	0.120	1	0
$L = 6.00 \text{ m} + h_c = 0.05 \text{ m}$	42	25	4×6	43	26	3×6	6	4

Table C.25 – Deviation between the B_s and the remaining modeling considering the bending moment when B3 is loaded [%]

Comparison modeling								
B_s	39	21						
BsCLT	44	19						
3BsCLT5								
Bstc5	45	25						
3×4Bstc5								
Load case	P_t at B3	L_n at B3	Description	P_t at B3	L_n at B3	Description	P_t at B3	L_n at B3
Variation	Minimum			Maximum			Max. difference	
Beam spacing				30	15	0.40 m	9	7
Connection stiffness	33	19	low	44	24	high	6	2
Support conditions	46	26	Sae	47	26	Fx	8	4
Span	32	17	8.00 m	50	34	2.00 m	11	12
h_c	34	19	0.10 m	65	46	0.02 m	26	25
h_c exp	45	25	0.05 m	56	34	0.03 m	17	13
\emptyset	38	20	0.15 m	42	23	0.25 m	3	2
I-section	38	24	Kerto-S	39	24	OSB+LVL	1	3
Concrete	38	21	C40/50	51	31	LC16/18	12	9
Timber	38	21	C14	40	22	D60	1	1
CLTdeck vs. Juxtaposed beams	44	19	CLTdeck	53	26	Juxtaposed beams	14	5
CLTdeck supports	51	22	Fx	63	29	Sae	19	9
CLT height								
$L = 6.00 \text{ m} + h_c = 0.05 \text{ m}$				39	20	4×6	6	5

Table C.26 – Deviation between the B_s and the remaining modeling considering the bending moment when the central beam is loaded [%]

Comparison modeling								
B_s	39	21						
BsCLT	43	18						
3BsCLT5	46	22						
Bstc5	45	24						
3×4Bstc5	46	26						
Load case	P_t at B4	L_n at B4	Description	P_t at B4	L_n at B4	Description	P_t at B4	L_n at B4
Variation	Minimum			Maximum			Max. difference	
Beam spacing	30	14	0.40 m	45	26	0.75 m	9	6
Connection stiffness	32	18	low	43	23	high	6	3
Support conditions	44	25	Sae	47	25	Fx	8	5
Span	31	16	8.00 m	50	33	2.00 m	11	13
h_c	33	18	0.10 m	65	46	0.02 m	27	26
h_c exp	45	24	0.05 m	56	34	0.03 m	17	13
\varnothing	37	19	0.15 m	41	22	0.25 m	3	2
I-section	38	23	Kerto-S	39	24	OSB+LVL	1	3
Concrete	38	20	C40/50	51	30	LC16/18	13	10
Timber	37	20	C14	40	21	D60	1	1
CLTdeck vs. Juxtaposed beams	43	18	CLTdeck	53	25	Juxtaposed beams	14	5
CLTdeck supports	50	20	Fx	61	29	Sae	19	12
CLT height	48	23	0.120	48	23	0.099	2	0
$L = 6.00 \text{ m} + h_c = 0.05 \text{ m}$	38	19	4×6	40	22	3×6	7	6

C.2 Second phase numerical analysis

The following tables gather the characteristics of the second phase of modeling (Table C.27) and the results obtained with this numerical analysis, in terms of vertical displacement, support reactions and longitudinal bending moments. This analysis focus in the effect that the concrete thickness and the span length have in the transversal distribution of load. Among the span influence, also the design considerations were taken into account, specifically the use of undersized, oversized or “tight-fitting” sections, according to the EC5 recommendations. Complementary information can be found in 5.2 *Parametric study*.

Table C.27 – Second phase modeling

Denomination	Description	Variation	Span	Interlayer	Connection stiffness	Beams		Concrete height	FE mesh
			L	h_i	$K (s)$	Width	Section	h_c	-
			[m]	[m]	[kN/m]	b_t	h_t	[m]	[m]
B_s	Base simulation	-	4.00	0.02	12000 (0.10 m)	0.10	R_t , 0.20	0.07	0.10 × 0.10
Bstc12	$B_s + h_c = 0.12$	Concrete height, h	4.00	0.02	12000 (0.10 m)	0.10	R_t , 0.20	0.12	0.10 × 0.10
Bstc15	$B_s + h_c = 0.15$							0.15	
Bstc20	$B_s + h_c = 0.20$							0.20	
Bsl8un	$B_s + L = 8.00$	Span, L	8.00	0.00	12000 (0.05 m)	0.32	R_t , 0.40	0.07	0.05 × 0.05
Bsl12un	$B_s + L = 12.00$		12.00						
Bsl16un	$B_s + L = 16.00$		16.00						
L16ov	$B_s + L = 16.00 + h_i = 0.00 + b_t = 0.32 + h_t = 0.40 + s = 0.05 +$ FE mesh	$L + h_i + b_t + h_t + s +$ FE mesh	16.00	0.00	12000 (0.05 m)	0.32	R_t , 0.40	0.07	0.05 × 0.05
L12ov	L16od + $L = 12.00$		12.00						
L8ov	L16od + $L = 8.00$		8.00						

Table C.27 – Second phase modeling (cont.)

Denomination	Description	Variation	Span	Interlayer	Connection stiffness	Beams		Concrete height	FE mesh			
			L	h_i	$K (s)$	Width	Section					
			[m]	[m]	[kN/m]	b_t	h_t	h_c	-			
L4ov	L16od + $L = 4.00$	$L + h_i + b_t + h_t + s + \text{FE mesh}$	4.00	0.00	12000 (0.05 m)	0.32	R_t , 0.40	0.07	0.05×0.05			
L2ov	L16od + $L = 2.00$		2.00									
L16	$Bs +$ $L = 16.00 +$ $h_i = 0.00 +$ $b_t = 0.24 +$ $h_t = 0.36 +$ $s = 0.05 +$ FE mesh		16.00									
L12	$Bs +$ $L = 12.00 +$ $h_i = 0.00 +$ $b_t = 0.16 +$ $h_t = 0.32 +$ $s = 0.05 +$ FE mesh	$L + h_i + b_t + h_t + s + \text{FE mesh}$	12.00									
L4	$Bs +$ $h_i = 0.00 +$ $h = 0.03$	$h_i + h_c$	4.00			12000 (0.10 m)	0.10			R_t , 0.20	0.03	0.10×0.10
L2	$Bs +$ $L = 2.00 +$ $h_i = 0.00 +$ $b_t = 0.08 +$ $h_t = 0.16 +$ $h = 0.03$	$L + h_i + b_t + h_t + h_c$	2.00									
L4un	$Bs +$ $h_i = 0.00 +$ $b_t = 0.05 +$ $h_t = 0.15 +$ $h = 0.03$	$h_i + b_t + h_t + h_c$	4.00									
L2un	L4un + $L = 2.00$	$L + h_i + b_t + h_t + h_c$	2.00									

s - connector spacing; un - For these cases, cross sections and material characteristics used do not guarantee, deliberately, the design requirements of EC5 (EN1995 2004a).

C.2.1 Vertical displacement at each beam mid-span

Table C.28 – $vd \frac{1}{2} L$ when the load is applied at $B1 \frac{1}{2} L$ [%]

Modeling denomination	Load case													
	$\frac{1}{2} L$							<i>lin</i>						
	Beam position													
	B1	B2	B3	B4	B5	B6	B7	B1	B2	B3	B4	B5	B6	B7
Bstc12	37	25	16	10	6	3	2	37	26	17	10	6	3	2
Bstc15	35	24	16	11	7	4	3	34	25	17	11	7	4	3
Bstc20	33	24	16	11	8	5	3	33	24	17	11	7	5	3
Bsl8un	31	24	17	12	8	5	2	30	24	18	13	8	5	2
Bsl12un	24	20	17	14	11	8	6	24	20	17	14	11	9	6
Bsl16un	21	18	16	14	12	10	9	20	18	16	14	12	11	9
L16ov	24	20	16	13	11	9	7	23	20	16	13	11	9	7
L12ov	29	22	17	12	9	6	5	29	22	17	12	9	6	5
L8ov	40	27	16	9	5	2	1	40	27	16	9	5	2	1
L4ov	66	27	7	1	0	0	0	66	27	7	1	0	0	0
L2ov	89	13	-2	0	0	0	0	90	13	-2	0	0	0	0
L16	25	20	17	13	11	8	6	24	20	17	13	11	8	6
L12	31	24	18	13	8	5	2	30	24	18	13	9	5	2
L4	67	28	7	0	-1	-1	-1	67	28	7	0	-1	-1	-1
L2	81	19	1	-1	0	0	0	45	55	0	-1	0	0	0
L4un	59	30	11	3	0	-1	-1	58	30	12	3	-1	-1	-1
L2un	78	21	2	-1	0	0	0	78	22	2	-1	0	0	0

Table C.29 – $vd \frac{1}{2} L$ when the load is applied at B2 $\frac{1}{2} L$ [%]

Modeling denomination	Load case													
	$\frac{1}{2} L$							<i>lin</i>						
	Beam position							Beam position						
	B1	B2	B3	B4	B5	B6	B7	B1	B2	B3	B4	B5	B6	B7
Bstc12	26	24	18	13	9	6	4	26	23	18	13	9	6	4
Bstc15	26	23	18	13	9	7	5	25	22	18	13	9	7	5
Bstc20	25	22	17	13	10	7	5	25	22	18	13	10	7	5
Bsl8un	24	22	18	14	10	8	5	24	21	18	14	11	8	5
Bsl12un	20	19	16	14	12	10	8	20	18	16	14	12	10	9
Bsl16un	18	17	16	14	13	12	10	18	17	16	14	13	12	11
L16ov	20	19	16	14	12	10	9	20	18	16	14	12	10	9
L12ov	22	21	17	14	11	8	6	22	21	17	14	11	8	7
L8ov	27	26	20	13	8	4	2	27	26	20	13	8	5	2
L4ov	27	41	23	8	2	0	0	27	40	24	8	2	0	0
L2ov	13	70	18	-1	-1	0	0	13	70	19	-1	-1	0	0
L16	21	19	16	14	12	10	8	20	19	16	14	12	10	8
L12	24	21	18	14	11	8	5	24	21	18	14	11	8	5
L4	28	41	23	8	1	0	-1	28	39	24	8	1	0	-1
L2	20	58	21	2	0	0	0	20	57	22	2	0	0	0
L4un	31	34	22	11	4	0	-1	31	32	22	11	4	1	-1
L2un	22	53	22	3	0	0	0	23	51	23	4	0	0	0

Table C.30 – $vd \frac{1}{2} L$ when the load is applied at B3 $\frac{1}{2} L$ [%]

Modeling denomination	Load case													
	$\frac{1}{2} L$							<i>lin</i>						
	Beam position													
	B1	B2	B3	B4	B5	B6	B7	B1	B2	B3	B4	B5	B6	B7
Bstc12	17	19	20	16	12	9	6	18	19	19	16	13	9	7
Bstc15	18	18	19	16	12	10	7	18	18	18	16	13	10	8
Bstc20	18	18	18	15	13	10	8	18	18	18	16	13	10	8
Bsl8un	18	18	17	15	13	10	8	18	18	17	15	13	11	9
Bsl12un	17	16	16	15	13	12	11	17	16	15	14	13	12	11
Bsl16un	16	16	15	14	14	13	12	16	16	15	14	14	13	12
L16ov	16	16	16	15	13	12	11	16	16	16	15	13	12	11
L12ov	17	17	18	16	13	11	9	17	17	17	16	13	11	9
L8ov	16	20	22	17	12	8	5	16	20	21	18	12	8	5
L4ov	7	23	39	22	8	2	0	7	24	38	23	8	2	0
L2ov	-2	18	68	18	-1	-1	0	-2	19	66	19	-1	-1	0
L16	17	17	16	15	13	12	11	17	16	16	15	13	12	11
L12	18	18	17	15	13	11	9	18	18	17	15	13	11	9
L4	7	23	39	23	8	1	-1	7	24	37	23	8	1	-1
L2	1	21	56	21	2	0	0	1	22	55	21	2	0	0
L4un	12	22	30	21	11	4	0	12	23	29	22	11	4	0
L2un	2	22	51	22	3	0	0	2	23	50	23	4	0	0

Table C.31 – $vd \frac{1}{2} L$ when the load is applied at $B4 \frac{1}{2} L$ [%]

Modeling denomination	Load case													
	$\frac{1}{2} L$							<i>lin</i>						
	Beam position													
	B1	B2	B3	B4	B5	B6	B7	B1	B2	B3	B4	B5	B6	B7
Bstc12	11	13	16	19	16	13	11	12	14	16	17	16	14	12
Bstc15	12	14	16	18	16	14	12	12	14	16	17	16	14	12
Bstc20	12	14	16	17	16	14	12	10	13	17	19	17	13	10
Bsl8un	13	14	15	16	15	14	13	10	13	17	19	17	13	10
Bsl12un	14	14	15	15	15	14	14	14	14	14	14	14	14	14
Bsl16un	14	14	14	15	14	14	14	0	-1	19	66	19	-1	0
L16ov	13	14	15	16	15	14	13	-1	2	21	55	21	2	-1
L12ov	12	14	16	17	16	14	12	13	14	15	15	15	14	13
L8ov	9	13	17	21	17	13	9	12	14	16	16	16	14	12
L4ov	1	8	22	38	22	8	1	9	13	18	20	18	13	9
L2ov	0	-1	18	67	18	-1	0	1	8	23	37	23	8	1
L16	13	14	15	15	15	14	13	-1	4	23	50	23	4	-1
L12	13	14	15	16	15	14	13	14	14	15	15	15	14	14
L4	0	8	23	38	23	8	0	13	14	15	16	15	14	13
L2	-1	2	21	56	21	2	-1	0	8	23	37	23	8	0
L4un	3	11	21	30	21	11	3	14	14	14	15	14	14	14
L2un	-1	3	22	51	22	3	-1	3	11	22	29	22	11	3

Table C.32 – $vd \frac{1}{2} L$ received by the loaded beam [%]

Modeling denomination	Load case							
	$\frac{1}{2} L$				<i>lin</i>			
	Beam position							
	B1	B2	B3	B4	B1	B2	B3	B4
<i>Bs</i>	47	28	24	23	46	27	23	22
Bsl2	65	41	38	38	65	40	37	37
Bsl8un	31	22	17	16	30	30	17	19
Bsl8ht	34	23	18	17	33	22	18	16
Bsl12un	24	19	16	15	24	18	15	14
Bsl16un	21	17	15	15	20	17	15	66
L2ov	89	70	68	67	90	70	66	37
L4ov	66	41	39	38	66	40	38	20
L8ov	40	26	22	21	40	26	21	16
L12ov	29	21	18	17	29	21	17	15
L16ov	24	19	16	16	23	18	16	55
L2	81	58	56	56	45	57	55	37
L4	67	41	39	38	67	39	37	16
L12	31	21	17	16	30	21	17	15
L16	25	19	16	15	24	19	16	50

Table C.32 – vd $\frac{1}{2}$ L received by the loaded beam [%] (cont.)

Modeling denomination	Load case							
	$\frac{1}{2}$ L				<i>lin</i>			
	Beam position							
	B1	B2	B3	B4	B1	B2	B3	B4
L2un	78	53	51	51	78	51	50	29
L4un	59	34	30	30	58	32	29	15
Bstc2	78	54	51	51	77	52	50	50
Bstc3	67	42	40	39	66	40	38	38
Bstc5	54	32	29	28	53	31	27	27
Bstc10	40	25	21	20	39	25	20	18
Bstc12	37	24	20	19	37	23	19	17
Bstc15	35	23	19	18	34	22	18	17
Bstc20	33	22	18	17	33	22	18	19

C.2.2 Support reactions at each beam

Table C.33 – sr when the load is applied at B1 $\frac{1}{2}$ L [%]

Modeling denomination	Load case													
	$\frac{1}{2}$ L							<i>lin</i>						
	Beam position													
	B1	B2	B3	B4	B5	B6	B7	B1	B2	B3	B4	B5	B6	B7
Bstc12	82	14	7	3	1	1	-8	85	14	4	1	0	0	-5
Bstc15	80	17	6	3	2	1	-8	82	18	3	1	1	0	-5
Bstc20	75	22	7	3	1	0	-8	77	23	5	1	0	0	-5
Bsl8un	76	9	13	9	6	8	-21	81	10	9	5	3	5	-13
Bsl12un	74	5	14	12	10	16	-32	78	8	11	8	6	10	-22
Bsl16un	74	3	14	13	13	21	-38	77	6	11	9	8	14	-27
L16ov	79	9	9	7	7	9	-20	81	12	6	4	4	5	-13
L12ov	82	11	7	4	3	4	-12	84	14	5	2	1	3	-8
L8ov	83	15	6	1	-1	0	-4	86	15	3	0	-1	0	-3
L4ov	88	18	-2	-3	-1	0	0	91	14	-2	-2	-1	0	0
L2ov	95	10	-5	-1	0	0	0	96	8	-4	0	0	0	0
L16	76	8	11	10	9	12	-26	79	11	8	6	5	7	-18
L12	72	11	14	10	7	9	-24	78	13	10	6	4	5	-16
L4	87	17	1	-3	-2	-1	0	91	13	0	-2	-1	0	0
L2	94	11	-3	-1	0	0	0	96	7	-2	-1	0	0	0
L4un	81	19	7	-2	-3	-2	-1	87	14	4	-1	-2	-1	-1
L2un	93	12	-3	-2	0	0	0	95	8	-2	-1	0	0	0

Table C.34 – *sr* when the load is applied at B2 ½ L [%]

Modeling denomination	Load case													
	½ L							<i>lin</i>						
	Beam position													
	B1	B2	B3	B4	B5	B6	B7	B1	B2	B3	B4	B5	B6	B7
Bstc12	42	24	19	12	6	4	-7	34	36	20	8	4	2	-4
Bstc15	43	23	18	12	7	4	-7	36	34	20	9	4	2	-5
Bstc20	43	24	17	11	7	3	-6	38	31	19	10	5	2	-4
Bsl8un	48	15	17	13	10	11	-14	39	29	18	10	6	7	-9
Bsl12un	52	9	15	14	12	17	-19	44	22	17	11	9	11	-13
Bsl16un	54	7	14	14	13	19	-21	47	18	16	12	10	13	-15
L16ov	47	16	16	13	11	12	-15	39	29	18	10	7	7	-10
L12ov	42	23	19	12	8	7	-11	34	35	20	9	5	4	-7
L8ov	35	32	23	10	4	2	-6	28	43	22	7	2	1	-4
L4ov	24	48	28	3	-2	-1	0	18	60	23	2	-1	-1	0
L2ov	11	72	21	-4	-1	0	0	9	78	17	-3	-1	0	0
L16	49	13	15	14	13	14	-17	41	26	18	11	8	9	-12
L12	48	15	16	14	11	12	-16	39	28	18	11	7	8	-11
L4	25	45	28	5	-1	-1	-1	18	61	21	2	-1	-1	0
L2	14	66	23	-2	-1	0	0	10	77	16	-2	-1	0	0
L4un	33	33	25	10	2	-1	-3	24	51	20	6	1	0	-2
L2un	17	61	24	-1	-1	0	0	11	74	17	-1	-1	0	0

Table C.35 – *sr* when the load is applied at B3 ½ L [%]

Modeling denomination	Load case													
	½ L							<i>lin</i>						
	Beam position													
	B1	B2	B3	B4	B5	B6	B7	B1	B2	B3	B4	B5	B6	B7
Bstc12	15	23	25	20	13	9	-5	9	23	36	21	9	5	-4
Bstc15	17	22	23	20	14	8	-4	11	23	33	21	10	5	-3
Bstc20	19	21	22	19	14	8	-3	13	22	29	21	11	5	-3
Bsl8un	24	18	18	17	14	15	-6	15	20	30	18	11	10	-4
Bsl12un	32	13	15	14	14	16	-4	22	17	25	17	12	12	-4
Bsl16un	34	11	14	14	14	17	-3	25	15	22	16	12	13	-4
L16ov	21	19	20	18	16	15	-8	14	21	30	20	12	10	-6
L12ov	14	23	25	21	15	11	-8	9	23	35	21	10	7	-6
L8ov	6	28	31	24	12	6	-6	3	25	42	22	8	4	-4
L4ov	-4	31	44	28	3	-1	-2	-3	25	57	22	2	-1	-1
L2ov	-5	21	67	21	-4	-1	0	-4	17	74	17	-3	-1	0
L16	26	16	17	16	15	16	-7	17	19	27	18	12	11	-5
L12	26	17	17	16	15	15	-6	16	20	29	18	11	10	-5
L4	-3	32	41	28	5	-1	-2	-2	23	58	21	3	0	-2
L2	-5	25	61	23	-2	-1	0	-3	17	74	16	-2	-1	0
L4un	4	30	31	26	11	4	-5	2	24	49	21	6	2	-3
L2un	-5	27	56	25	-1	-1	0	-3	18	70	17	-1	-1	0

Table C.36 – *sr* when the load is applied at B4 ½ L [%]

Modeling denomination	Load case													
	½ L							<i>lin</i>						
	Beam position													
	B1	B2	B3	B4	B5	B6	B7	B1	B2	B3	B4	B5	B6	B7
Bstc12	1	16	21	24	21	16	1	0	11	22	36	22	11	0
Bstc15	3	15	21	23	21	15	3	1	11	22	33	22	11	1
Bstc20	5	14	20	22	20	14	5	2	12	22	30	22	12	2
Bsl8un	7	17	17	18	17	17	7	3	13	19	30	19	13	3
Bsl12un	13	15	15	15	15	15	13	7	13	17	25	17	13	7
Bsl16un	15	14	14	14	14	14	15	10	13	16	22	16	13	10
L16ov	3	18	19	20	19	18	3	1	14	20	30	20	14	1
L12ov	-1	17	22	24	22	17	-1	-2	12	22	35	22	12	-2
L8ov	-5	15	25	30	25	15	-5	-4	10	23	42	23	10	-4
L4ov	-4	5	28	43	28	5	-4	-3	2	22	56	22	2	-3
L2ov	-1	-4	21	67	21	-4	-1	0	-3	17	74	17	-3	0
L16	7	17	17	17	17	17	7	4	14	19	27	19	14	4
L12	8	17	17	17	17	17	8	4	14	19	28	19	14	4
L4	-5	7	28	40	28	7	-5	-3	4	21	58	21	4	-3
L2	-1	-2	23	61	23	-2	-1	-1	-2	16	74	16	-2	-1
L4un	-5	14	26	31	26	14	-5	-3	8	21	49	21	8	-3
L2un	-2	0	25	56	25	0	-2	-1	-1	17	70	17	-1	-1

Table C.37 – *sr* received by the loaded beam [%]

Modeling denomination	Load case							
	½ L				<i>lin</i>			
	Beam position							
	B1	B2	B3	B4	B1	B2	B3	B4
Bs	84	30	30	29	87	45	44	44
Bsl2	91	52	48	48	93	64	61	61
Bsl8un	76	15	18	18	81	29	30	30
Bsl8ht	75	17	19	19	80	32	32	31
Bsl12un	74	9	15	15	78	22	25	25
Bsl16un	74	7	14	14	77	18	22	22
L2ov	95	72	67	67	96	78	74	74
L4ov	88	48	44	43	91	60	57	56
L8ov	83	32	31	30	86	43	42	42
L12ov	82	23	25	24	84	35	35	35
L16ov	79	16	20	20	81	29	30	30
L2	94	66	61	61	96	77	74	74
L4	87	45	41	40	91	61	58	58
L12	72	15	17	17	78	28	29	28
L16	76	13	17	17	79	26	27	27

Table C.37 – *sr* received by the loaded beam [%] (cont.)

Modeling denomination	Load case							
	$\frac{1}{2} L$				<i>lin</i>			
	Beam position							
	B1	B2	B3	B4	B1	B2	B3	B4
L2un	93	61	56	56	95	74	70	70
L4un	81	33	31	31	87	51	49	49
Bstc2	92	61	55	55	95	74	70	70
Bstc3	89	49	44	43	92	63	60	60
Bstc5	85	37	34	34	89	52	49	49
Bstc10	83	25	26	26	86	39	39	39
Bstc12	82	24	25	24	85	36	36	36
Bstc15	80	23	23	23	82	34	33	33
Bstc20	75	24	22	22	77	31	29	30

C.2.3 Longitudinal bending moment at the mid-span section of each beam

Table C.38 – *bm* when the load is applied at B1 $\frac{1}{2} L$ [%]

Modeling denomination	Load case													
	$\frac{1}{2} L$							<i>lin</i>						
	Beam position													
	B1	B2	B3	B4	B5	B6	B7	B1	B2	B3	B4	B5	B6	B7
Bstc12	48	23	13	8	5	3	1	34	25	17	11	7	4	2
Bstc15	45	22	14	9	5	3	2	32	24	17	12	7	5	3
Bstc20	42	22	14	9	6	4	3	29	23	17	12	8	6	4
Bsl8un	45	22	13	9	6	3	2	29	23	18	13	9	6	3
Bsl12un	38	20	14	10	8	6	4	23	20	17	14	11	9	7
Bsl16un	33	19	14	11	9	7	6	19	18	16	14	13	11	9
L16ov	36	19	14	10	8	7	6	22	19	16	14	11	10	8
L12ov	41	20	14	9	7	5	4	26	22	17	13	10	7	6
L8ov	51	23	13	7	4	2	1	35	27	18	10	6	3	1
L4ov	70	22	7	1	0	0	0	60	30	9	2	0	0	0
L2ov	89	12	-1	0	0	0	0	86	16	-1	-1	0	0	0
L16	37	20	14	10	8	6	5	23	20	17	14	11	9	7
L12	44	22	14	9	6	3	1	29	23	18	13	9	5	2
L4	75	21	5	0	-1	-1	0	64	30	8	0	-1	-1	-1
L2	85	15	1	-1	0	0	0	79	21	1	-1	0	0	0
L4un	70	23	8	2	0	-1	-1	56	31	12	3	-1	-1	-1
L2un	83	17	1	-1	0	0	0	76	24	2	-1	0	0	0

Table C.39 – *bm* when the load is applied at B2 ½ L [%]

Modeling denomination	Load case													
	½ L							<i>lin</i>						
	Beam position													
	B1	B2	B3	B4	B5	B6	B7	B1	B2	B3	B4	B5	B6	B7
Bstc12	24	35	17	11	7	4	3	26	23	18	14	9	6	4
Bstc15	23	33	17	11	7	5	4	25	22	18	14	10	7	5
Bstc20	23	31	17	11	8	6	5	24	21	17	14	10	8	6
Bsl8un	23	34	17	11	7	5	4	23	20	17	14	11	8	6
Bsl12un	21	29	16	12	9	7	6	20	18	16	14	12	11	9
Bsl16un	19	26	16	12	10	9	8	18	17	15	14	13	12	11
L16ov	19	29	16	12	9	8	7	19	18	16	14	12	11	10
L12ov	20	33	16	11	8	6	5	21	20	17	14	11	9	8
L8ov	22	39	17	10	6	4	2	26	24	19	14	9	5	3
L4ov	22	52	18	7	2	0	0	29	36	24	9	2	0	0
L2ov	12	74	14	0	0	0	0	16	64	21	0	-1	0	0
L16	20	29	16	12	9	7	6	20	18	16	14	12	11	9
L12	22	33	17	11	8	5	4	23	20	17	14	11	8	6
L4	21	55	18	6	1	0	0	30	36	24	9	2	0	-1
L2	15	67	16	2	0	0	0	22	54	23	2	0	0	0
L4un	23	50	18	7	3	0	-1	32	31	22	12	4	1	-1
L2un	17	64	17	3	0	0	0	24	49	24	4	0	0	0

Table C.40 – *bm* when the load is applied at B3 ½ L [%]

Modeling denomination	Load case													
	½ L							<i>lin</i>						
	Beam position													
	B1	B2	B3	B4	B5	B6	B7	B1	B2	B3	B4	B5	B6	B7
Bstc12	14	17	31	16	10	7	5	18	19	18	16	13	10	7
Bstc15	14	17	29	15	10	8	6	18	18	17	15	13	10	8
Bstc20	15	17	28	15	11	8	7	18	18	17	15	13	11	9
Bsl8un	14	17	31	15	10	7	6	18	17	16	15	13	11	9
Bsl12un	14	16	26	15	11	9	8	17	16	15	14	13	12	12
Bsl16un	14	16	24	15	12	10	9	16	15	15	14	14	13	13
L16ov	14	16	27	15	11	9	8	16	16	15	15	14	13	12
L12ov	13	16	30	15	10	8	7	17	17	16	15	13	11	10
L8ov	13	17	36	15	9	6	4	18	19	19	17	13	9	6
L4ov	7	18	50	17	6	2	0	10	23	33	23	9	2	0
L2ov	-1	14	73	14	0	0	0	-1	20	61	20	0	-1	0
L16	14	16	27	15	11	9	8	17	16	15	15	13	12	11
L12	14	17	30	15	10	8	6	18	17	16	15	13	11	9
L4	5	17	54	17	6	1	-1	9	24	34	24	9	2	-1
L2	1	16	66	16	2	0	0	1	23	52	22	2	0	0
L4un	8	18	48	17	7	3	0	13	23	27	22	12	4	0
L2un	1	17	63	16	3	0	0	2	24	47	23	4	0	0

Table C.41 – *bm* when the load is applied at B4 ½ L [%]

Modeling denomination	Load case													
	½ L							<i>lin</i>						
	Beam position													
	B1	B2	B3	B4	B5	B6	B7	B1	B2	B3	B4	B5	B6	B7
Bstc12	8	11	16	31	16	11	8	12	14	16	17	16	14	12
Bstc15	9	11	15	29	15	11	9	12	14	16	16	16	14	12
Bstc20	10	12	15	27	15	12	10	13	14	15	16	15	14	13
Bsl8un	9	11	15	30	15	11	9	13	14	15	15	15	14	13
Bsl12un	10	12	15	26	15	12	10	14	14	14	14	14	14	14
Bsl16un	11	12	15	23	15	12	11	14	14	14	14	14	14	14
L16ov	11	12	15	26	15	12	11	14	14	15	15	15	14	14
L12ov	10	11	15	30	15	11	10	13	14	15	15	15	14	13
L8ov	7	10	15	35	15	10	7	11	14	17	18	17	14	11
L4ov	2	6	17	50	17	6	2	2	9	22	33	22	9	2
L2ov	0	0	14	73	14	0	0	-1	0	20	61	20	0	-1
L16	10	12	15	26	15	12	10	14	14	15	15	15	14	14
L12	9	11	15	29	15	11	9	13	14	15	15	15	14	13
L4	0	6	17	54	17	6	0	1	9	24	34	24	9	1
L2	-1	2	16	66	16	2	-1	-1	2	22	52	22	2	-1
L4un	2	7	17	47	17	7	2	3	12	22	27	22	12	3
L2un	-1	3	16	63	16	3	-1	-1	4	23	47	23	4	-1

Table C.42 – *bm* received by the loaded beam [%]

Modeling denomination	Load case							
	½ L				<i>lin</i>			
	Beam position							
	B1	B2	B3	B4	B1	B2	B3	B4
Bs	58	42	39	39	43	26	21	21
Bsl2	70	52	50	50	61	36	34	33
Bsl8un	45	34	31	30	29	20	16	15
Bsl8ht	48	36	32	31	32	22	17	16
Bsl12un	38	29	26	26	23	18	15	14
Bsl16un	33	26	24	23	19	17	15	14
L2ov	89	74	73	73	86	64	61	61
L4ov	70	52	50	50	60	36	33	33
L8ov	51	39	36	35	35	24	19	18
L12ov	41	33	30	30	26	20	16	15
L16ov	36	29	27	26	22	18	15	15
L2	85	67	66	66	79	54	52	52
L4	75	55	54	54	64	36	34	34
L12	44	33	30	29	29	20	16	15
L16	37	29	27	26	23	18	15	15

Table C.42 – *bm* received by the loaded beam [%] (cont.)

Modeling denomination	Load case							
	$\frac{1}{2} L$				<i>lin</i>			
	Beam position							
	B1	B2	B3	B4	B1	B2	B3	B4
L2un	83	64	63	63	76	49	47	47
L4un	70	50	48	47	56	31	27	27
Bstc2	83	66	65	65	74	48	46	46
Bstc3	75	57	56	56	62	36	34	34
Bstc5	65	48	45	45	50	29	25	24
Bstc10	51	37	34	33	37	24	19	18
Bstc12	48	35	31	31	34	23	18	17
Bstc15	45	33	29	29	32	22	17	16
Bstc20	42	31	28	27	29	21	17	16

C.3 Results from the development of an expeditious tool

The tables and graphs in this section present the results obtained on the seeking of the simplified equation to predict the load distribution in timber-concrete composite floors, specifically: results from modeling of the Bs set when the load was applied at $\frac{1}{4}$ L; approximation attempts to adjust the *bm* numerical distribution together with the comparison between numerical and experimental results vs. simplified prediction. Complementary information can be found in 5.3 *Development of an expeditious tool*.

C.3.1 Longitudinal bending moment at the quarter-span section of each beam

Table C.43 – Numerical analysis: *bm*, when the load is applied at B1 $\frac{1}{4}$ L [%]

Modeling denomination	Load case						
	$\frac{1}{4}$ L						
	Beam position						
	B1	B2	B3	B4	B5	B6	B7
Bs	37	31	19	9	4	1	0
Bsl2	58	31	9	2	0	0	0
Bsl5	32	28	20	12	6	2	0
Bsl8ht	24	22	19	15	10	6	3
Bsl12un	19	18	17	15	13	10	8
Bsl16un	17	16	16	15	14	12	11
Bstc2	70	28	4	0	-1	-1	-1
Bstc3	57	34	10	1	-1	-1	-1
Bstc5	44	34	17	6	1	0	-1
Bstc10	31	27	19	12	6	3	1
Bstc12	29	26	19	12	7	4	2
Bstc15	27	24	19	13	8	5	3
Bstc20	25	23	19	13	9	6	4

Table C.44 – Numerical analysis: *bm*, when the load is applied at B2 ¼ L [%]

Modeling denomination	Load case						
	¼ L						
	Beam position						
	B1	B2	B3	B4	B5	B6	B7
Bs	31	20	21	15	8	4	1
Bsl2	32	31	25	9	2	0	0
Bsl5	28	20	19	15	10	6	2
Bsl8ht	22	18	16	15	12	9	7
Bsl12un	18	17	15	14	13	12	10
Bsl16un	16	16	15	14	14	13	12
Bstc2	28	41	27	5	0	0	-1
Bstc3	34	27	28	10	2	0	-1
Bstc5	34	21	23	14	6	2	0
Bstc10	27	20	19	15	10	6	3
Bstc12	26	19	18	15	11	7	5
Bstc15	24	19	17	15	11	8	6
Bstc20	23	18	17	15	11	9	7

Table C.45 – Numerical analysis: *bm*, when the load is applied at B3 ¼ L [%]

Modeling denomination	Load case						
	¼ L						
	Beam position						
	B1	B2	B3	B4	B5	B6	B7
Bs	20	21	15	18	14	8	4
Bsl2	10	25	28	25	9	2	0
Bsl5	21	19	14	16	14	10	6
Bsl8ht	19	16	14	14	14	12	11
Bsl12un	17	15	14	14	14	13	13
Bsl16un	16	15	14	14	14	14	14
Bstc2	4	26	39	26	5	0	-1
Bstc3	10	27	25	27	10	2	0
Bstc5	17	23	16	22	14	6	2
Bstc10	20	19	14	16	14	10	7
Bstc12	20	18	14	15	14	11	8
Bstc15	20	18	14	15	14	11	9
Bstc20	19	17	14	14	14	12	10

Table C.46 – Numerical analysis: bm , when the load is applied at B4 $\frac{1}{4}$ L [%]

Modeling denomination	Load case						
	$\frac{1}{4}$ L						
	Beam position						
	B1	B2	B3	B4	B5	B6	B7
Bs	10	15	18	14	18	15	10
Bsl2	2	9	25	28	25	9	2
Bsl5	12	16	16	12	16	16	12
Bsl8ht	15	15	14	12	14	15	15
Bsl12un	15	15	14	13	14	15	15
Bsl16un	15	14	14	14	14	14	15
Bstc2	0	5	26	38	26	5	0
Bstc3	1	10	26	24	26	10	1
Bstc5	6	14	22	16	22	14	6
Bstc10	12	15	16	13	16	15	12
Bstc12	13	15	15	13	15	15	13
Bstc15	14	15	15	13	15	15	14
Bstc20	14	15	14	13	14	15	14

Table C.47 – bm received by the loaded beam [%]

Modeling denomination	Load case			
	$\frac{1}{4}$ L			
	Beam position			
	B1	B2	B3	B4
Bs	37	20	15	14
Bsl2	58	31	28	28
Bsl5	32	20	14	12
Bsl8ht	24	18	14	12
Bsl12un	19	17	14	13
Bsl16un	17	16	14	14
Bstc2	70	41	39	38
Bstc3	57	27	25	24
Bstc5	44	21	16	16
Bstc10	31	20	14	13
Bstc12	29	19	14	13
Bstc15	27	19	14	13
Bstc20	25	18	14	13

C.3.2 Adjustment of *bm* distribution through polynomial equations

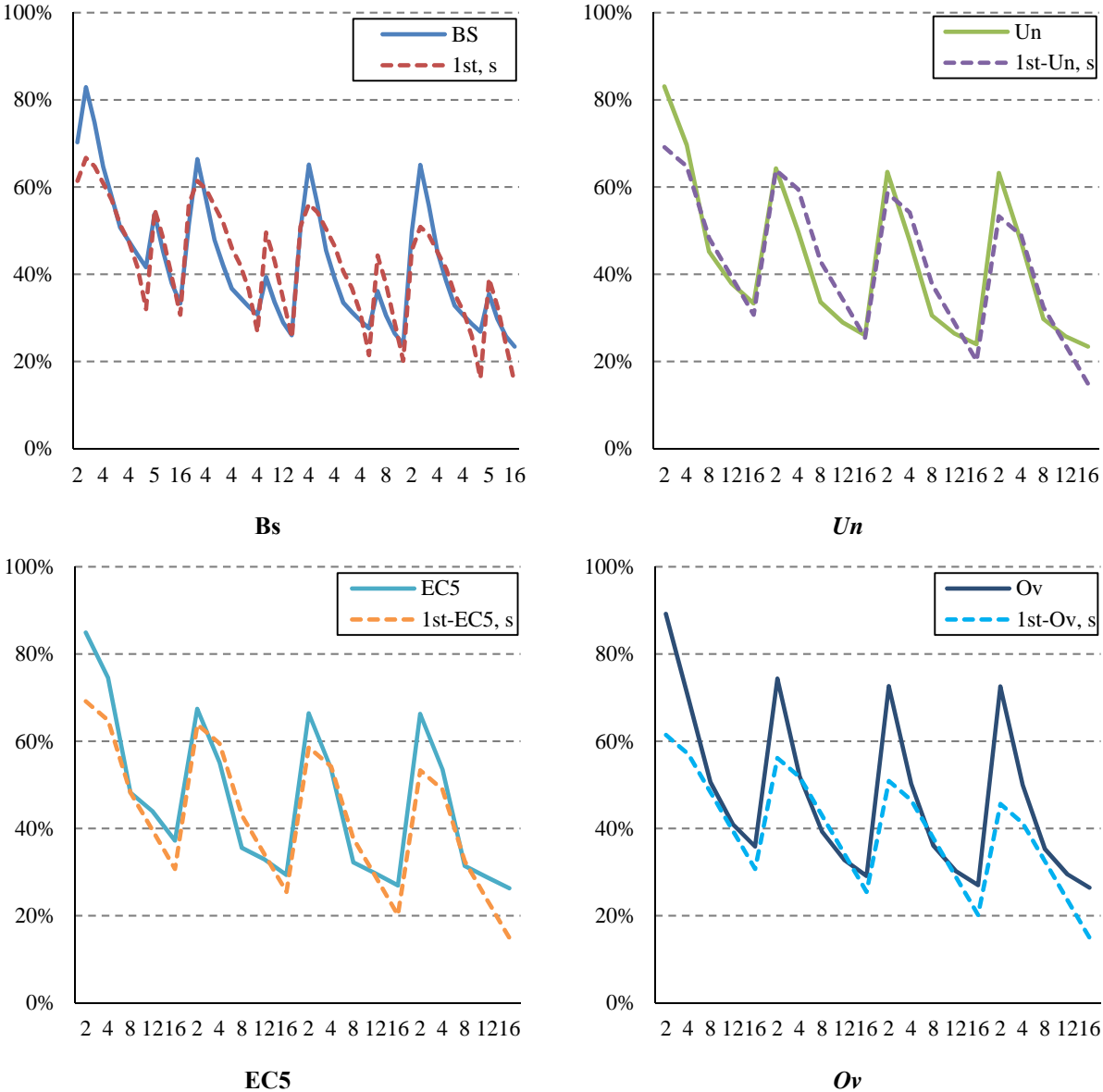


Fig. C.1 – *bm* distribution for 1/2 L loading vs. 1st degree polynomial, simple

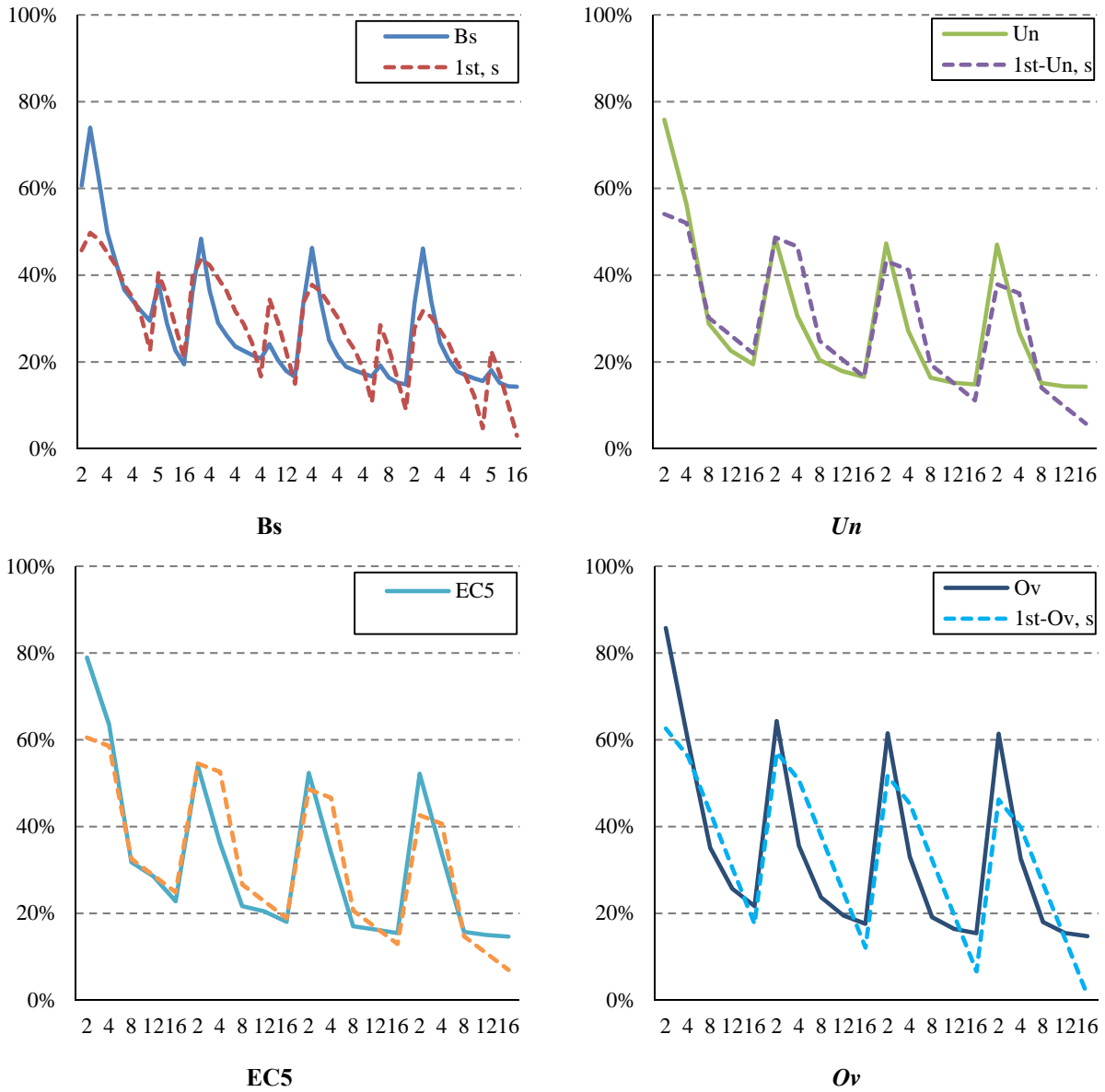


Fig. C.2 – bm distribution for lin loading vs. 1st degree polynomial, simple

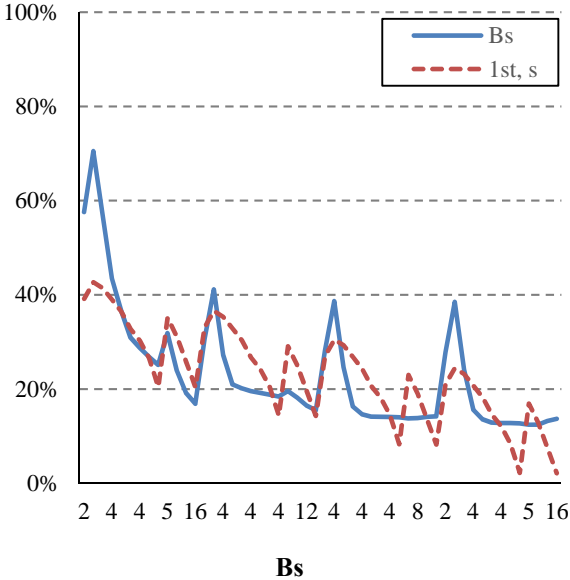


Fig. C.3 – *bm* distribution for ¼ L loading vs. 1st degree polynomial, simple

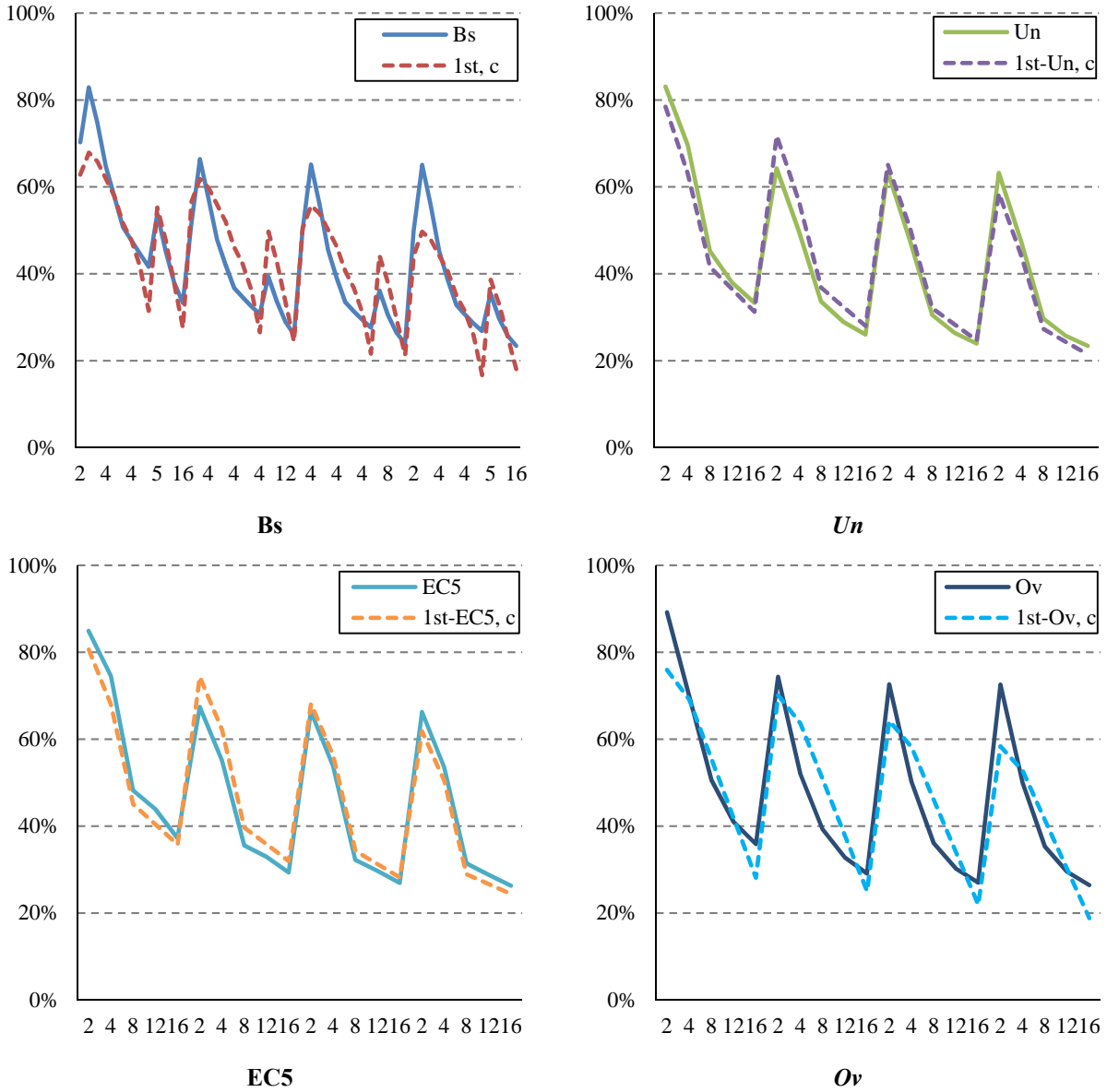


Fig. C.4 – *bm* distribution for $\frac{1}{2}$ L loading vs. 1st degree polynomial, crossed terms

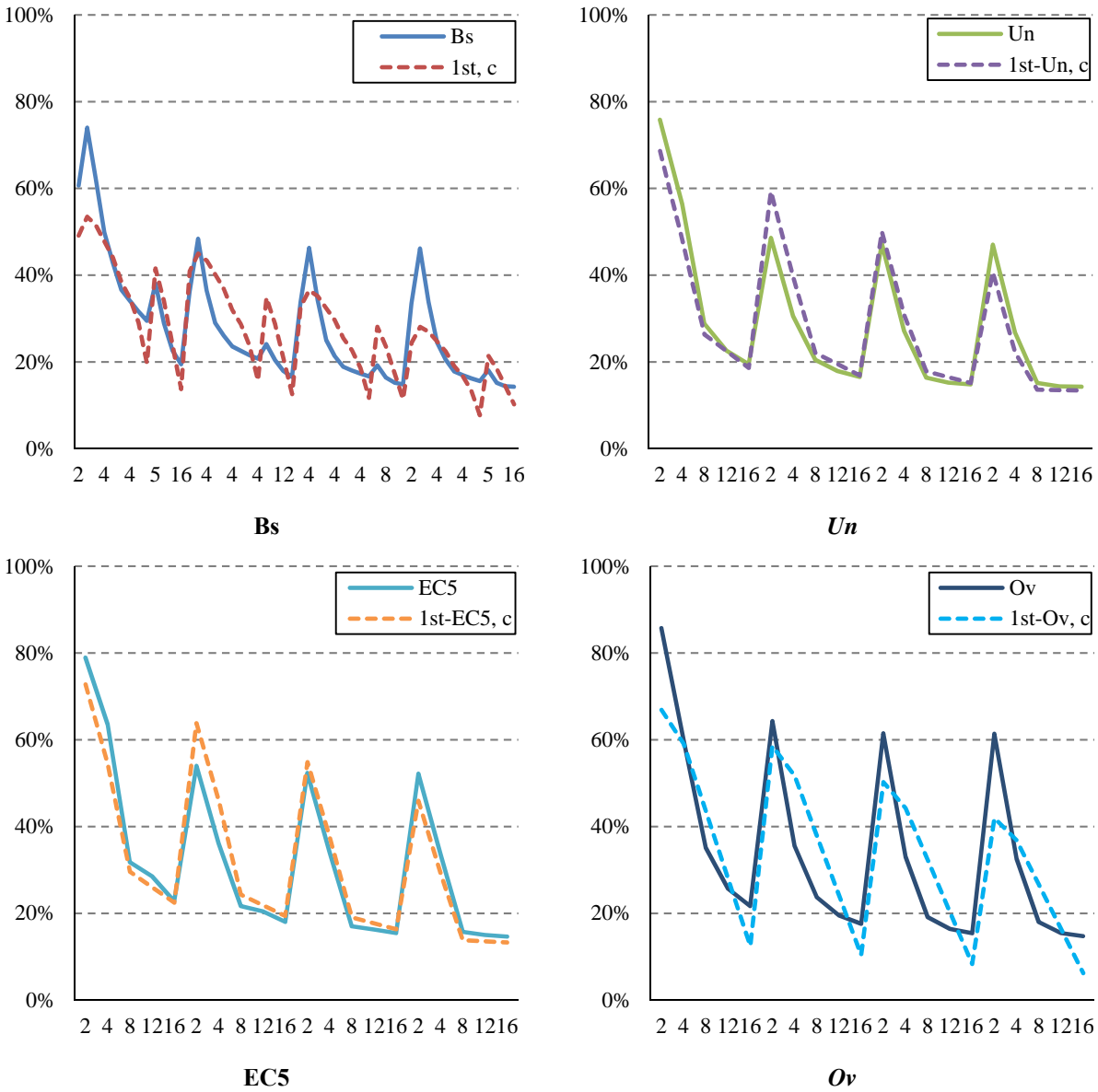


Fig. C.5 – bm distribution for lin loading vs. 1st degree polynomial, crossed terms

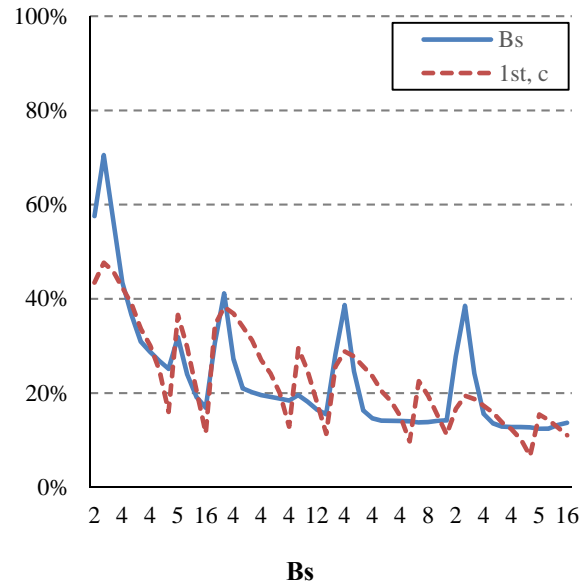


Fig. C.6 – *bm* distribution for ¼ L loading vs. 1st degree polynomial, crossed terms

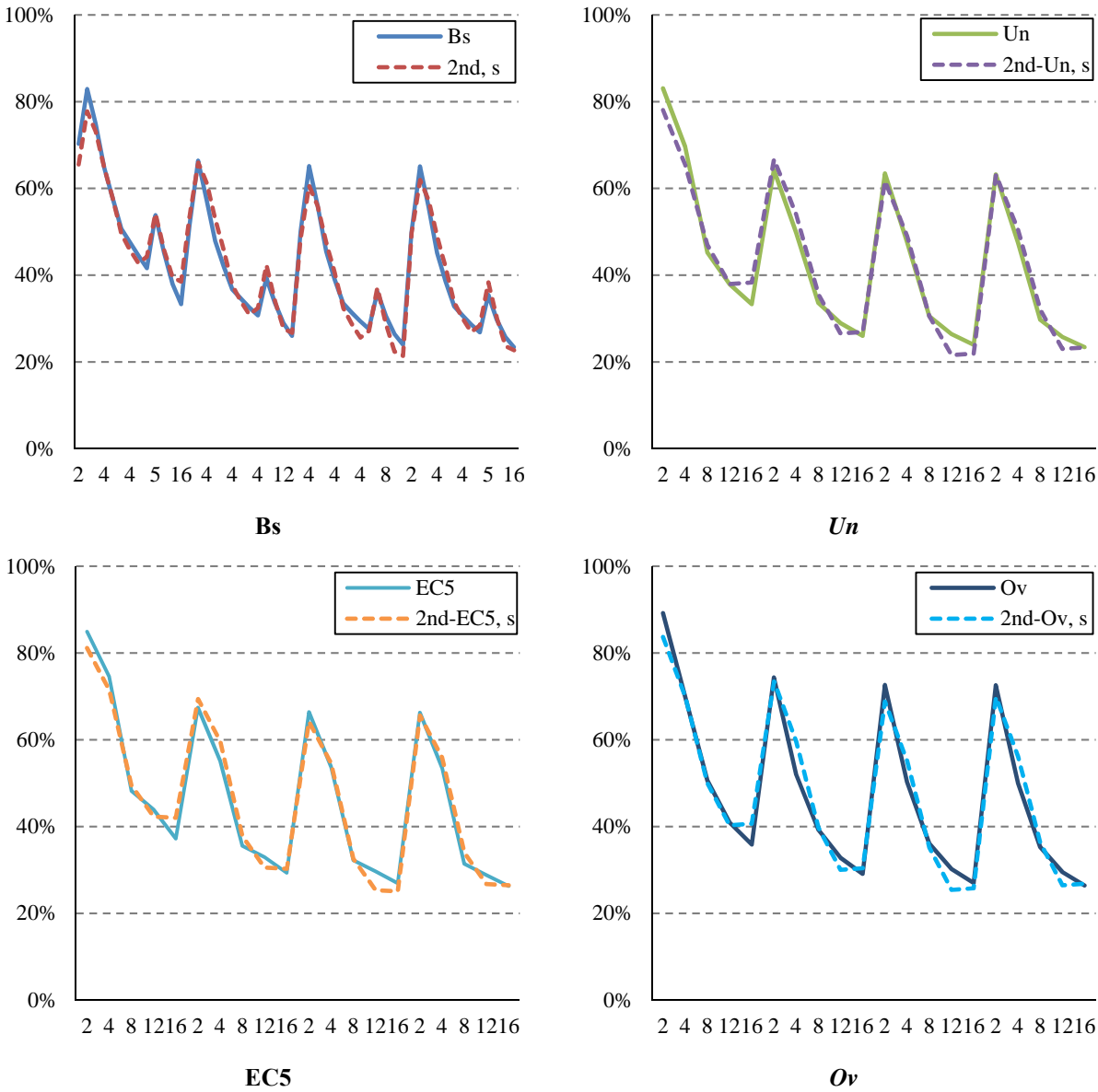


Fig. C.7 – bm distribution for $\frac{1}{2} L$ loading vs. 2nd degree polynomial, simple

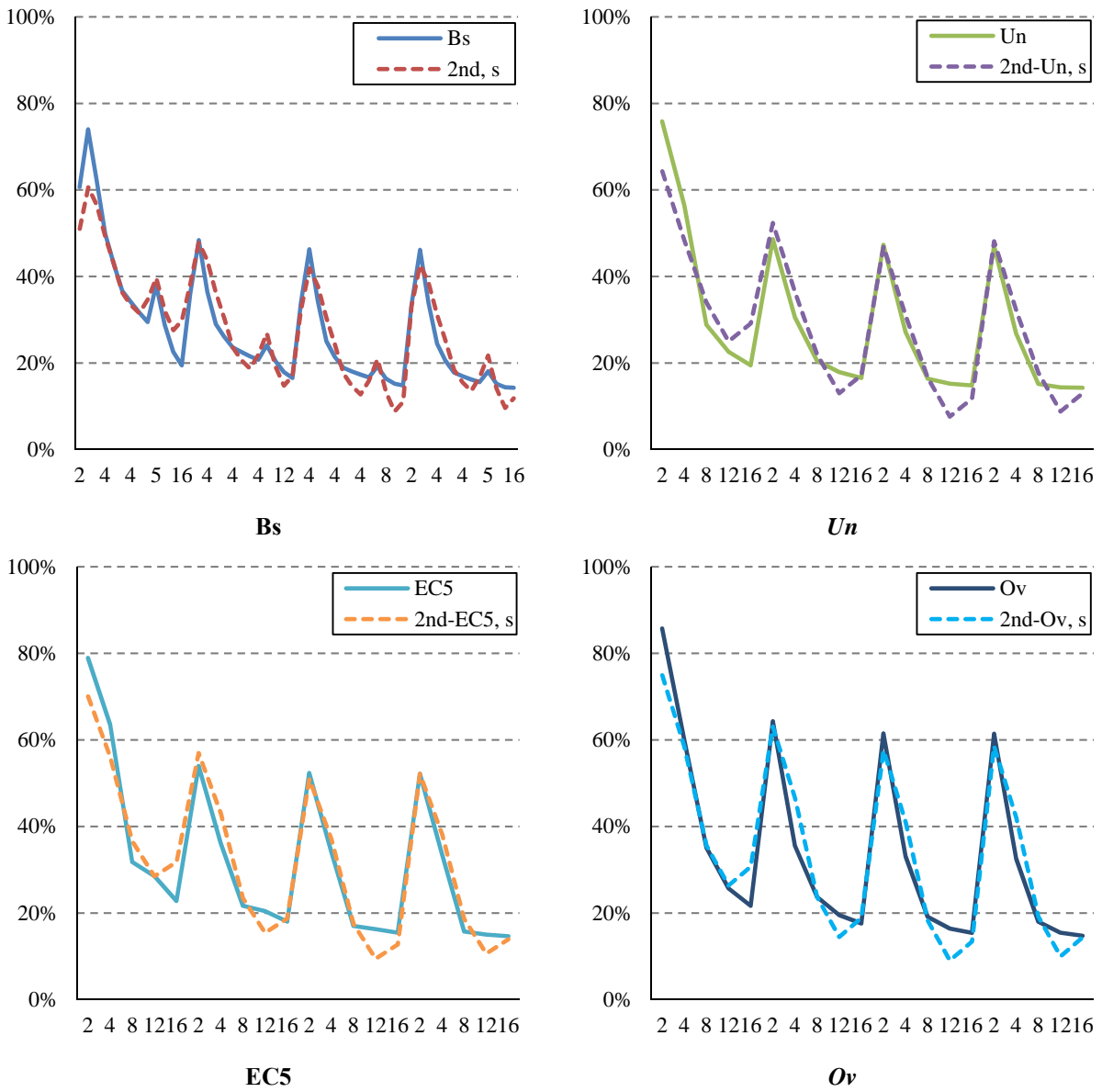


Fig. C.8 – *bm* distribution for *lin* loading vs. 2nd degree polynomial, simple

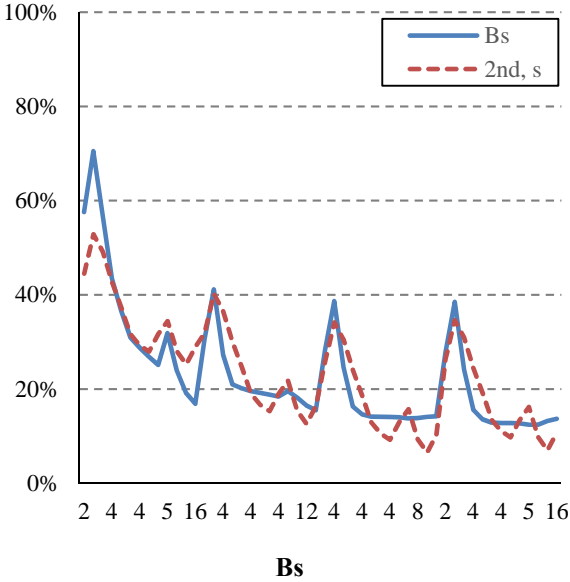


Fig. C.9 – *bm* distribution for 1/4 L loading vs. 2nd degree polynomial, simple

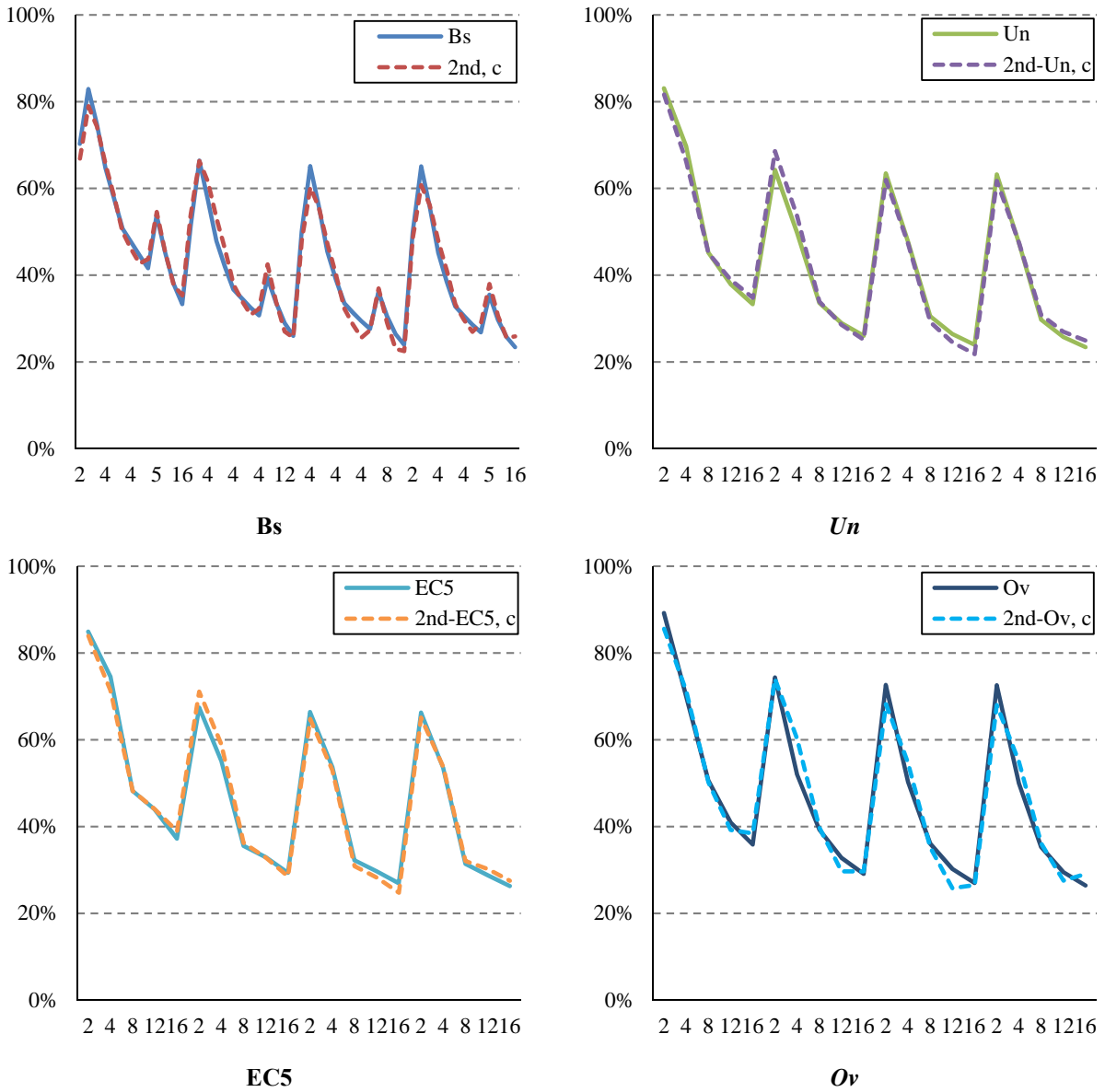


Fig. C.10 – *bm* distribution for 1/2 L loading vs. 2nd degree polynomial, crossed terms

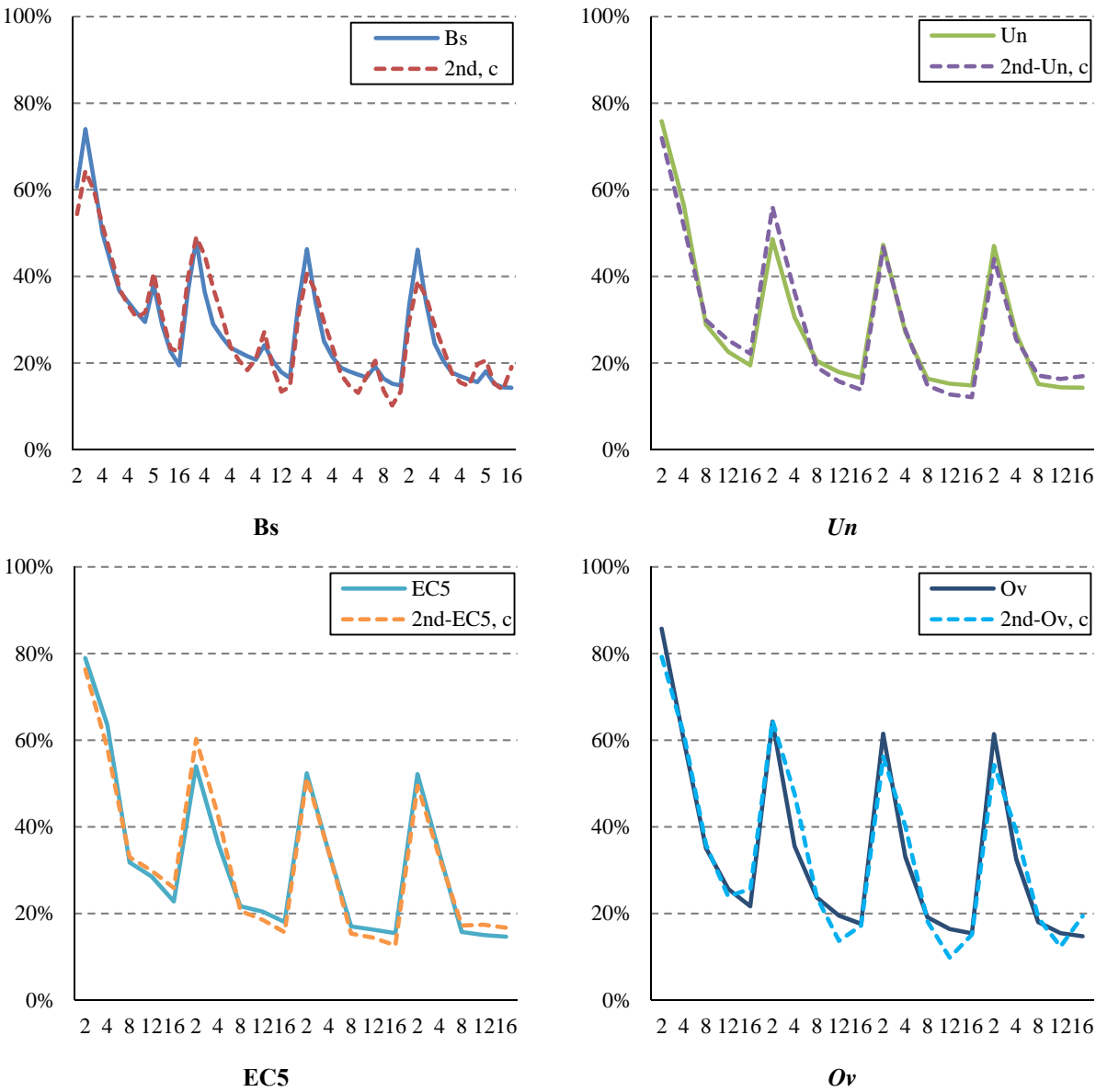


Fig. C.11 – *bm* distribution for *lin* loading vs. 2nd degree polynomial, crossed terms

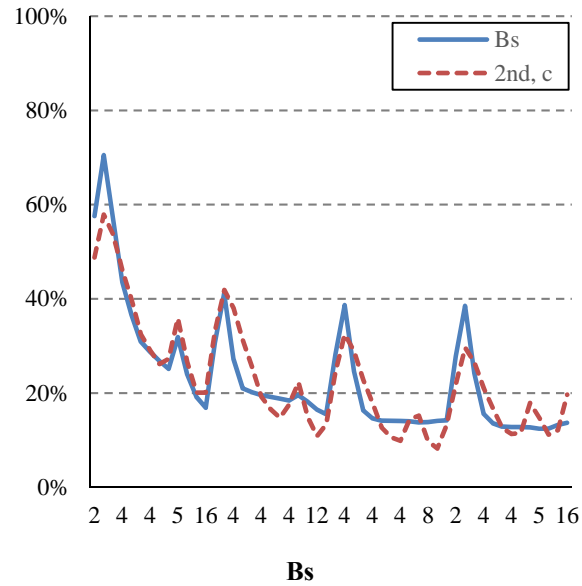


Fig. C.12 – *bm* distribution for $\frac{1}{4}$ L loading vs. 2nd degree polynomial, crossed terms

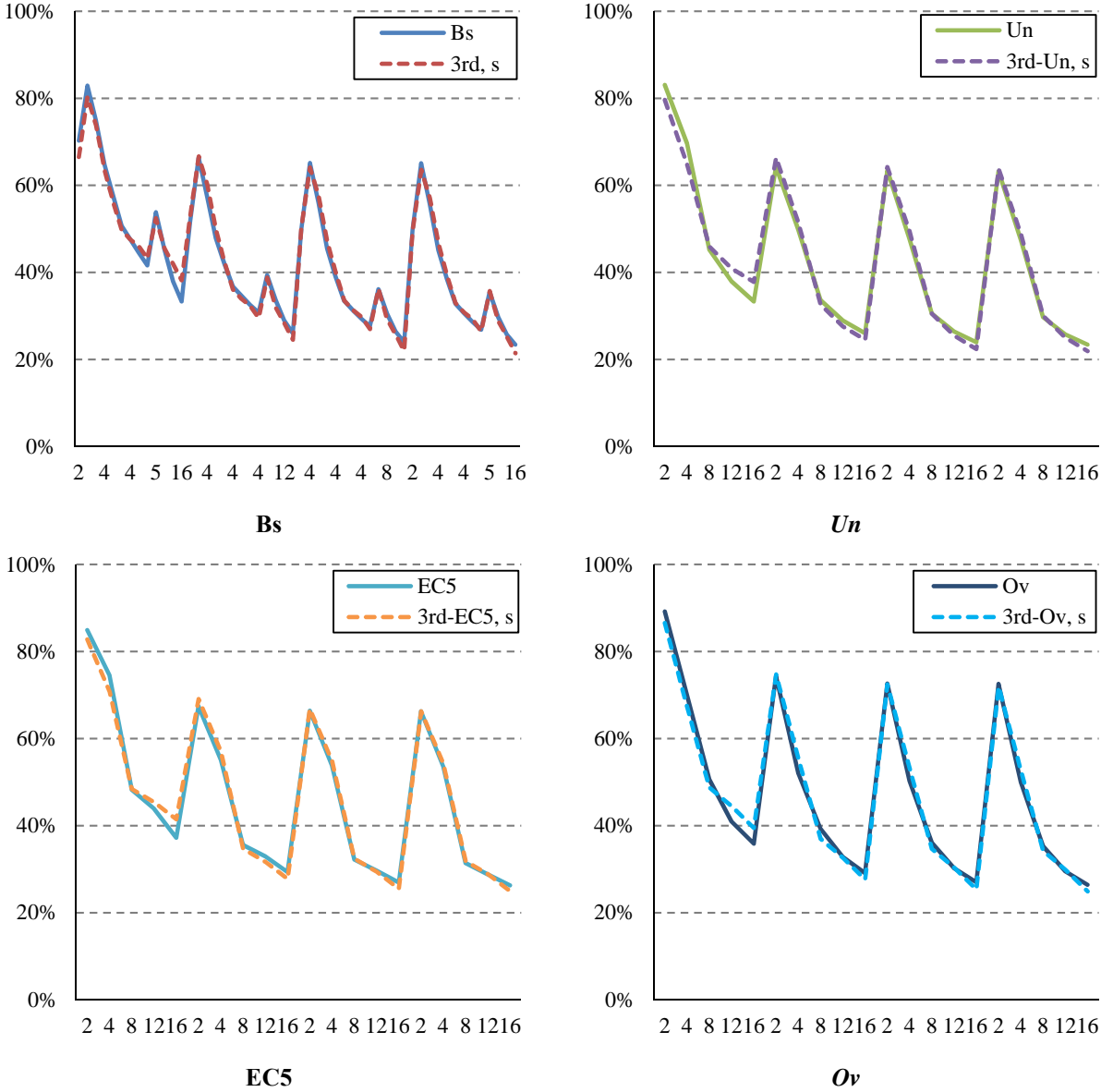


Fig. C.13 – bm distribution for $\frac{1}{2}L$ loading vs. 3rd degree polynomial, simple

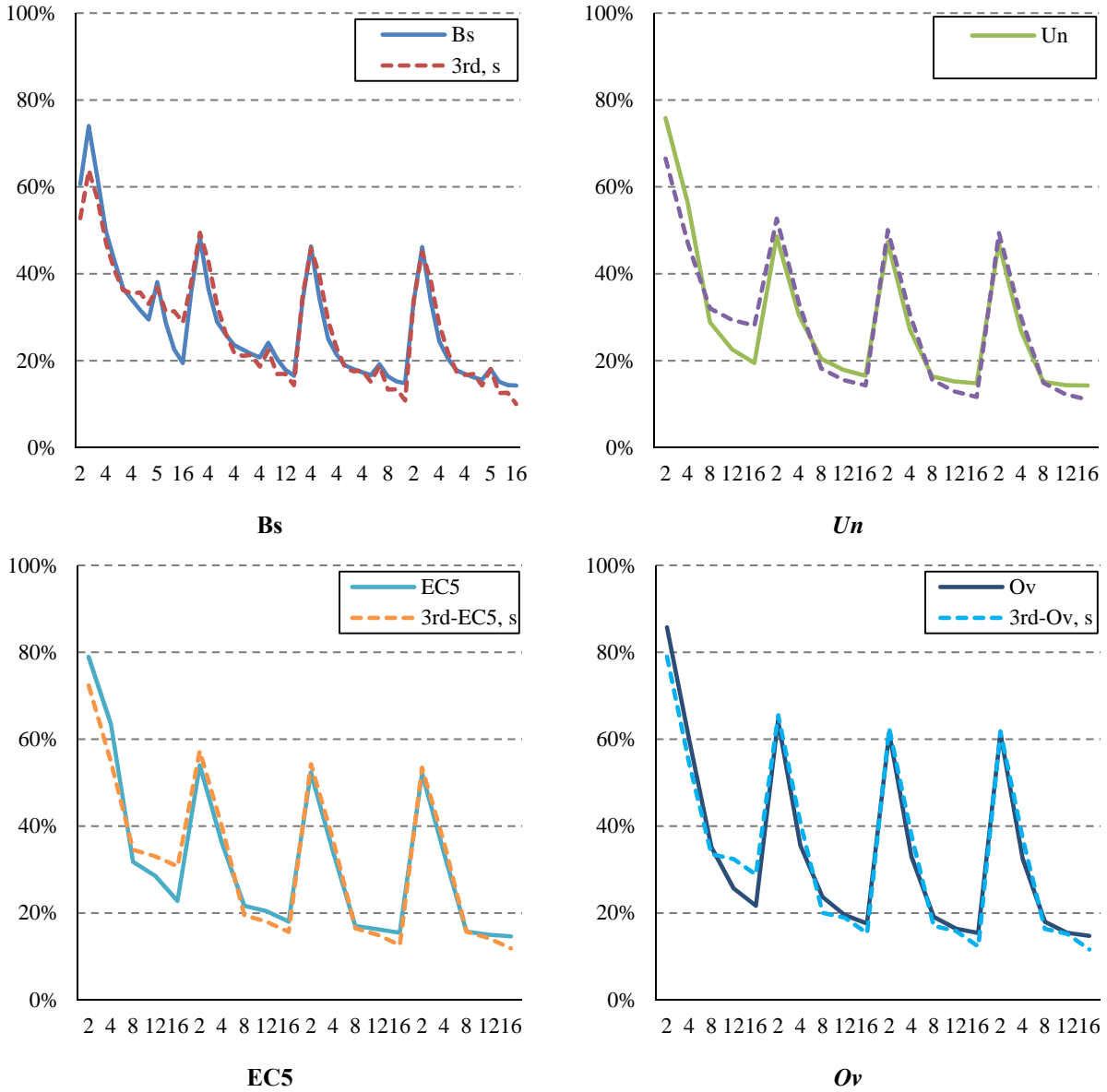


Fig. C.14 – *bm* distribution for *lin* loading vs. 3rd degree polynomial, simple

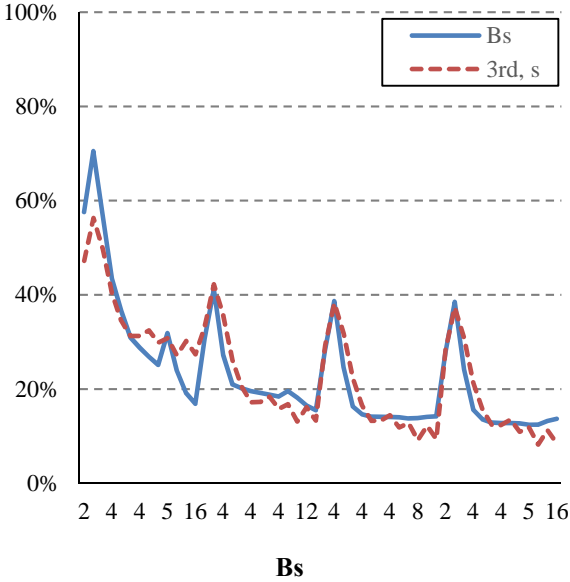


Fig. C.15 – *bm* distribution for ¼ L loading vs. 3rd degree polynomial, simple

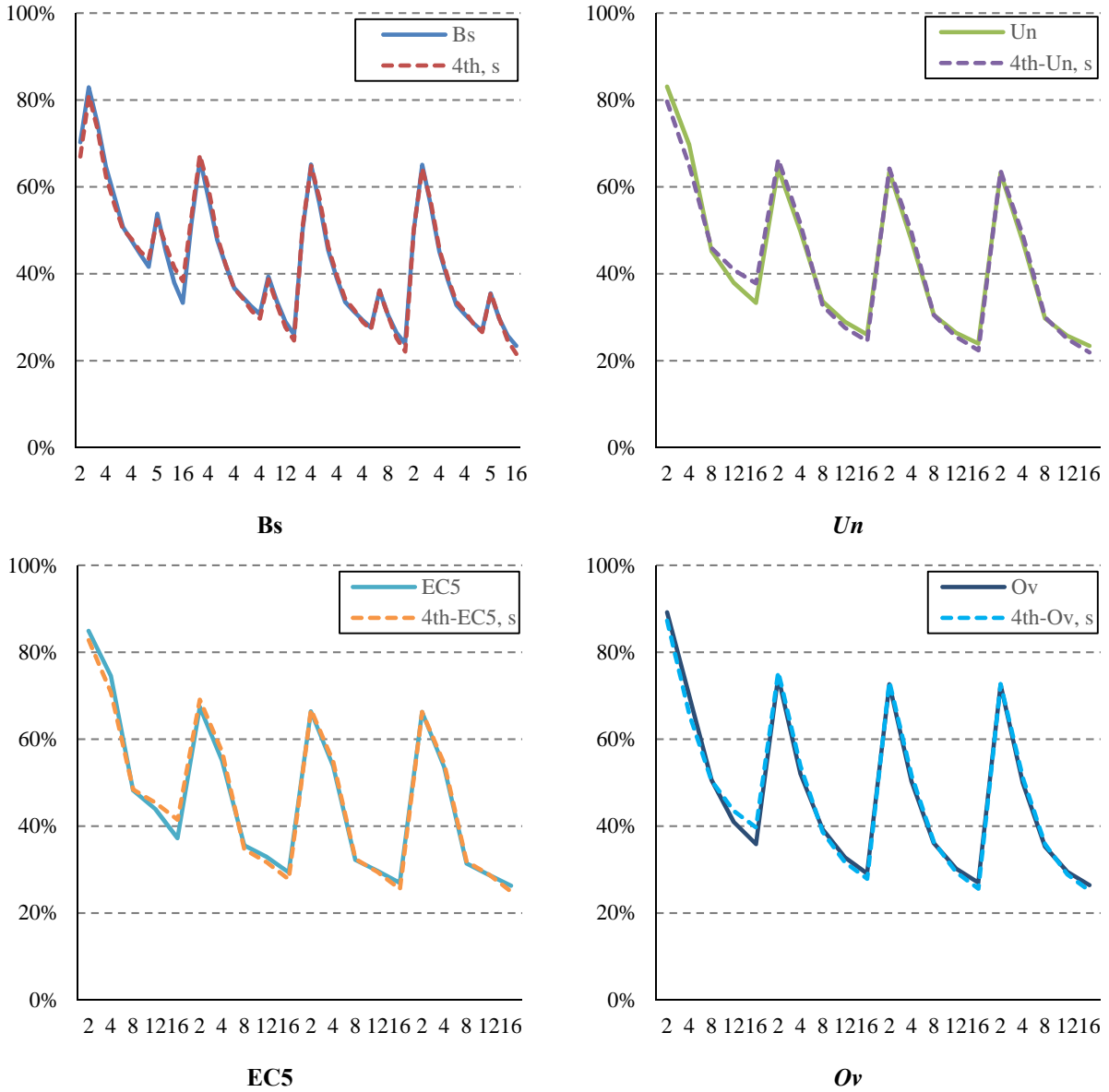


Fig. C.16 – *bm* distribution for 1/2 L loading vs. 4th degree polynomial, simple

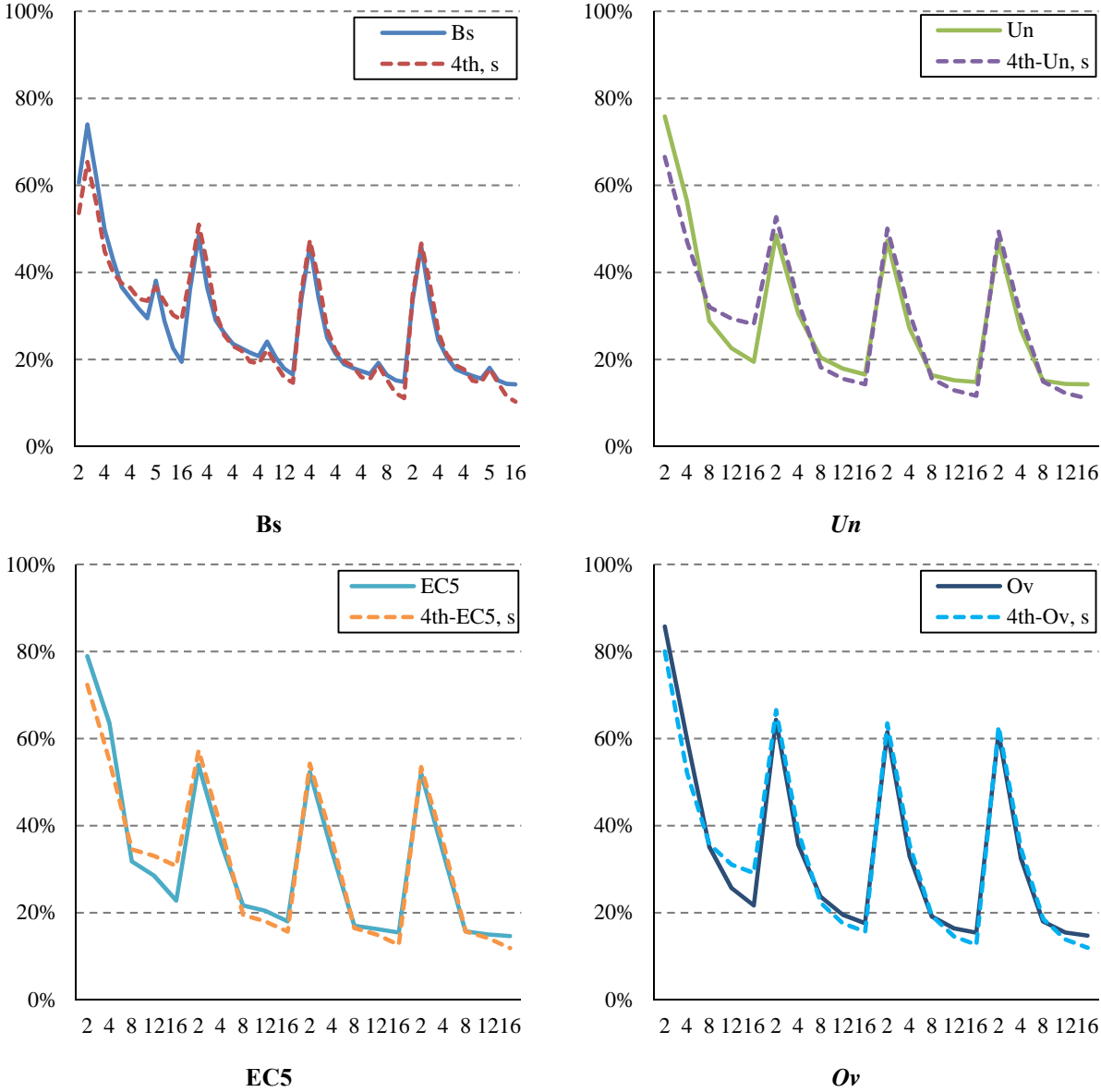


Fig. C.17 – *bm* distribution for *lin* loading vs. 4th degree polynomial, simple

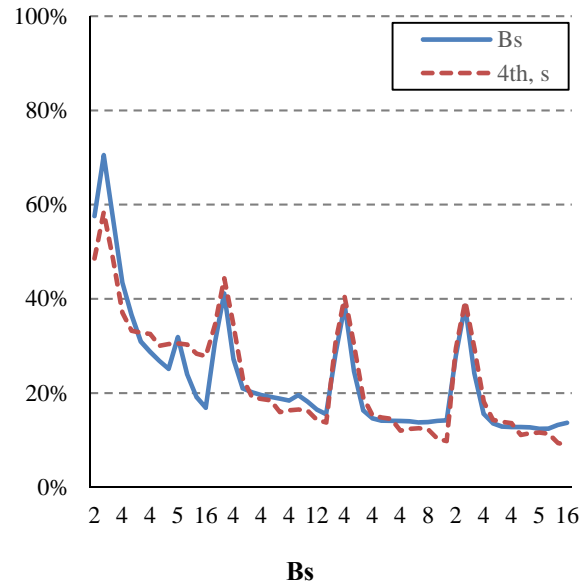


Fig. C.18 – *bm* distribution for $\frac{1}{4}$ L loading vs. 4th degree polynomial, simple

C.3.3 Comparison between experimental and polynomial predictions for S1 to S5

Table C.48 – Experimental vs. *Pr* polynomial predictions for *vd* ½ L: S1 to S5

Specimen	Beam	x_1	x_2	x_3	<i>vd</i> ½ L			Differences			
					Experimental			<i>Pr</i>	<i>Pr</i> vs. ½ L	<i>Pr</i> vs. ¼ L	<i>Pr</i> vs. <i>lin</i>
		Loading									
		<i>L</i>	<i>b_l</i>	<i>h_c</i>	½ L	¼ L	<i>lin</i>				
[m]				[%]							
S1	B1	4.00	0.00	0.05	63	62	69	52	-11	-10	-17
	B2		0.50		41	35	41	36	-5	1	-5
	B3		1.00		41	35	43	35	-6	0	-8
	B4		0.50		38	34	40	36	-2	2	-4
	B5		0.00		64	65	61	52	-12	-13	-9
S2	B1	4.00	0.00	0.05	72	71	69	52	-20	-19	-17
	B2		0.50		47	48	44	36	-11	-12	-8
	B3		1.00		54	51	49	35	-19	-16	-14
	B4		0.50		51	49	47	36	-15	-13	-11
	B5		0.00		75	72	72	52	-23	-20	-20
S3	B1	4.00	0.00	0.03	78	77	76	60	-18	-17	-16
	B2		0.50		51	49	46	44	-7	-5	-2
	B3		1.00		46	43	39	42	-4	-1	3
	B4		0.50		49	46	43	44	-5	-2	1
	B5		0.00		72	71	68	60	-12	-11	-8
S4	B1	2.00	0.00	0.05	76	75	72	60	-16	-15	-12
	B2		0.50		61	60	60	44	-17	-16	-16
	B3		1.00		66	60	57	43	-23	-17	-14
	B4		0.50		59	62	61	44	-15	-18	-17
	B5		0.00		80	80	79	60	-20	-20	-19
S5	B1	6.00	0.00	0.05	59	58	57	46	-13	-12	-11
	B2		0.50		38	34	36	30	-8	-4	-6
	B3		1.00		35	32	32	29	-6	-3	-3
	B4		0.50		37	33	35	30	-7	-3	-5
	B5		0.00		63	60	62	46	-17	-14	-16

Table C.49 – Experimental vs. *Pr* polynomial predictions for $vd \frac{1}{4} L$: S1 to S5

Specimen	Beam	x_1	x_2	x_3	$vd \frac{1}{4} L$			Differences			
					Experimental			<i>Pr</i>	<i>Pr</i> vs. $\frac{1}{2} L$	<i>Pr</i> vs. $\frac{1}{4} L$	<i>Pr</i> vs. <i>lin</i>
		Loading			$\frac{1}{2} L$	$\frac{1}{4} L$	<i>lin</i>				
		<i>L</i>	<i>b_l</i>	<i>h_c</i>	$\frac{1}{2} L$	$\frac{1}{4} L$	<i>lin</i>				
[m]			[%]								
S1	B1	4.00	0.00	0.05	64	66	70	52	-12	-14	-18
	B2		0.50		39	39	40	36	-3	-3	-4
	B3		1.00		40	40	45	35	-5	-5	-10
	B4		0.50		37	38	40	36	-1	-2	-4
	B5		0.00		65	69	65	52	-13	-17	-13
S2	B1	4.00	0.00	0.05	72	74	70	52	-20	-22	-18
	B2		0.50		45	54	46	36	-9	-18	-10
	B3		1.00		51	55	50	35	-16	-20	-15
	B4		0.50		48	54	47	36	-12	-18	-11
	B5		0.00		74	75	73	52	-22	-23	-21
S3	B1	4.00	0.00	0.03	76	79	77	60	-16	-19	-17
	B2		0.50		47	54	49	44	-3	-10	-5
	B3		1.00		44	49	43	42	-2	-7	-1
	B4		0.50		46	52	43	44	-2	-8	1
	B5		0.00		68	71	70	60	-8	-11	-10
S4	B1	2.00	0.00	0.05	72	70	69	60	-12	-10	-9
	B2		0.50		57	60	58	44	-13	-16	-14
	B3		1.00		63	57	54	43	-20	-14	-11
	B4		0.50		57	63	61	44	-13	-19	-17
	B5		0.00		80	80	80	60	-20	-20	-20
S5	B1	6.00	0.00	0.05	58	61	59	46	-12	-15	-13
	B2		0.50		37	39	39	30	-7	-9	-9
	B3		1.00		34	38	36	29	-5	-9	-7
	B4		0.50		37	39	38	30	-7	-9	-8
	B5		0.00		59	64	62	46	-13	-18	-16

Table C.50 – Experimental vs. *Pr* polynomial predictions for *sr*: S1 to S5

Specimen	Beam	x_1	x_2	x_3	<i>sr</i>			Differences			
					Experimental			<i>Pr</i>	<i>Pr</i> vs. ½ L	<i>Pr</i> vs. ¼ L	<i>Pr</i> vs. <i>lin</i>
		Loading									
		<i>L</i>	<i>b_l</i>	<i>h_c</i>	½ L	¼ L	<i>lin</i>				
[m]				[%]							
S1	B1	4.00	0.00	0.05	76	82	82	52	-23	-30	-30
	B2		0.50		46	49	49	36	-10	-13	-13
	B3		1.00		37	43	69	35	-2	-8	-34
	B4		0.50		46	48	68	36	-9	-12	-32
	B5		0.00		81	84	84	52	-28	-32	-31
S2	B1	4.00	0.00	0.05	88	89	93	52	-36	-37	-41
	B2		0.50		46	63	72	36	-10	-27	-36
	B3		1.00		51	63	75	35	-16	-28	-40
	B4		0.50		53	65	73	36	-17	-29	-37
	B5		0.00		88	88	95	52	-35	-35	-43
S3	B1	4.00	0.00	0.03	85	89	95	60	-25	-30	-35
	B2		0.50		51	64	76	44	-7	-20	-32
	B3		1.00		45	58	69	42	-2	-16	-27
	B4		0.50		47	61	72	44	-4	-17	-28
	B5		0.00		78	83	90	60	-18	-23	-30
S4	B1	2.00	0.00	0.05	94	94	95	60	-34	-34	-35
	B2		0.50		79	84	86	44	-36	-40	-43
	B3		1.00		73	83	82	43	-30	-40	-39
	B4		0.50		77	82	86	44	-33	-39	-42
	B5		0.00		94	95	96	60	-34	-35	-36
S5	B1	6.00	0.00	0.05	80	81	84	46	-34	-34	-38
	B2		0.50		34	41	47	30	-4	-11	-17
	B3		1.00		39	43	48	29	-10	-14	-19
	B4		0.50		38	45	52	30	-7	-15	-22
	B5		0.00		81	80	85	46	-34	-34	-39

Table C.51 – Experimental vs. $cf_{vd} \cdot Pr$ predictions for vd at $\frac{1}{2} L$: S1 to S5

Specimen	Beam	$vd \frac{1}{2} L$				Differences		
		Experimental			$cf_{vd} \cdot Pr$	$cf_{vd} \cdot Pr$	$cf_{vd} \cdot Pr$	$cf_{vd} \cdot Pr$
		Loading				vs.	vs.	vs.
		$\frac{1}{2} L$	$\frac{1}{4} L$	lin	$\frac{1}{2} L$	$\frac{1}{4} L$	lin	
[%]								
S1	B1	63	62	69	65	2	3	-4
	B2	41	35	41	45	4	10	4
	B3	41	35	43	44	3	9	1
	B4	38	34	40	45	7	11	5
	B5	64	65	61	65	1	0	4
S2	B1	72	71	69	65	-7	-6	-4
	B2	47	48	44	45	-2	-3	1
	B3	54	51	49	44	-10	-7	-5
	B4	51	49	47	45	-6	-4	-2
	B5	75	72	72	65	-10	-7	-7
S3	B1	78	77	76	75	-3	-2	-1
	B2	51	49	46	54	3	5	8
	B3	46	43	39	53	7	10	14
	B4	49	46	43	54	5	8	11
	B5	72	71	68	75	3	4	7
S4	B1	76	75	72	75	-1	0	3
	B2	61	60	60	55	-6	-5	-5
	B3	66	60	57	53	-13	-7	-4
	B4	59	62	61	55	-4	-7	-6
	B5	80	80	79	75	-5	-5	-4
S5	B1	59	58	57	58	-1	0	1
	B2	38	34	36	38	0	4	2
	B3	35	32	32	36	1	4	4
	B4	37	33	35	38	1	5	3
	B5	63	60	62	58	-5	-2	-4

Table C.52 – Experimental vs. $cf_{vd} \cdot Pr$ predictions for $vd \frac{1}{4} L$: S1 to S5

Specimen	Beam	$vd \frac{1}{4} L$				Differences		
		Experimental			$cf_{vd} \cdot Pr$	$cf_{vd} \cdot Pr$	$cf_{vd} \cdot Pr$	$cf_{vd} \cdot Pr$
		Loading				vs.	vs.	vs.
		$\frac{1}{2} L$	$\frac{1}{4} L$	<i>lin</i>		$\frac{1}{2} L$	$\frac{1}{4} L$	<i>lin</i>
[%]								
S1	B1	64	66	70	65	1	-1	-5
	B2	39	39	40	45	6	6	5
	B3	40	40	45	44	4	4	-1
	B4	37	38	40	45	8	7	5
	B5	65	69	65	65	0	-4	0
S2	B1	72	74	70	65	-7	-9	-5
	B2	45	54	46	45	0	-9	-1
	B3	51	55	50	44	-7	-11	-6
	B4	48	54	47	45	-3	-9	-2
	B5	74	75	73	65	-9	-10	-8
S3	B1	76	79	77	75	-1	-4	-2
	B2	47	54	49	54	7	0	5
	B3	44	49	43	53	9	4	10
	B4	46	52	43	54	8	2	11
	B5	68	71	70	75	7	4	5
S4	B1	72	70	69	75	3	5	6
	B2	57	60	58	55	-2	-5	-3
	B3	63	57	54	53	-10	-4	-1
	B4	57	63	61	55	-2	-8	-6
	B5	80	80	80	75	-5	-5	-5
S5	B1	58	61	59	58	0	-3	-1
	B2	37	39	39	38	1	-1	-1
	B3	34	38	36	36	2	-2	0
	B4	37	39	38	38	1	-1	0
	B5	59	64	62	58	-1	-6	-4

Table C.53 – Experimental vs. $cf_{sr} \cdot Pr$ predictions for sr : S1 to S5

Specimen	Beam	sr				Differences		
		Experimental			$cf_{sr} \cdot Pr$	$cf_{sr} \cdot Pr$	$cf_{sr} \cdot Pr$	$cf_{sr} \cdot Pr$
		Loading				vs.	vs.	vs.
		$\frac{1}{2} L$	$\frac{1}{4} L$	lin	$\frac{1}{2} L$	$\frac{1}{4} L$	lin	
[%]								
S1	B1	76	82	82	84	8	2	2
	B2	46	49	49	58	12	9	9
	B3	37	43	69	56	19	13	-13
	B4	46	48	68	58	12	10	-10
	B5	81	84	84	84	3	-1	0
S2	B1	88	89	93	84	-4	-5	-10
	B2	46	63	72	58	12	-5	-15
	B3	51	63	75	56	5	-7	-19
	B4	53	65	73	58	5	-7	-15
	B5	88	88	95	84	-4	-4	-11
S3	B1	85	89	95	96	10	6	0
	B2	51	64	76	70	19	6	-6
	B3	45	58	69	68	23	10	-2
	B4	47	61	72	70	23	9	-2
	B5	78	83	90	96	18	13	5
S4	B1	94	94	95	96	2	2	1
	B2	79	84	86	70	-9	-14	-16
	B3	73	83	82	68	-4	-14	-14
	B4	77	82	86	70	-7	-12	-16
	B5	94	95	96	96	2	1	0
S5	B1	80	81	84	74	-6	-7	-10
	B2	34	41	47	48	14	7	1
	B3	39	43	48	46	7	3	-2
	B4	38	45	52	48	11	3	-3
	B5	81	80	85	74	-7	-6	-11

C.3.4 Comparison between experimental and polynomial predictions for CSGL and CSTL

Table C.54 – Experimental vs. Pr polynomial predictions for $vd \frac{1}{2} L$: CSGL and CSTL

Specimen	Beam	x_1	x_2	x_3	$vd \frac{1}{2} L$			Differences	
					Experimental Loading		Pr	Pr vs. $\frac{1}{2} L$	Pr vs. $\frac{1}{4} L$
		L	b_l	h_c	$\frac{1}{2} L$	$\frac{1}{4} L$			
		[m]				[%]			
CSGL	B1	3.30	0.00	0.05	72	80	55	-18	-25
	B2		0.50		43	46	39	-4	-7
	B3		1.00		40	42	37	-3	-5
	B4		0.50		41	42	39	-3	-3
	B5		0.00		73	73	55	-18	-18
CSTL	B1	4.00	0.00	0.05	62	64	55	-7	-9
	B2		0.33		45	44	42	-3	-2
	B3		0.67		44	40	37	-8	-4
	B4		1.00		47	38	37	-9	0
	B5		0.67		42	39	37	-5	-2
	B6		0.33		43	43	42	0	-1
	B7		0.00		66	63	55	-11	-9

Table C.55 – Experimental vs. Pr polynomial predictions for $vd \frac{1}{4} L$: CSGL and CSTL

Specimen	Beam	x_1	x_2	x_3	$vd \frac{1}{4} L$			Differences	
					Experimental Loading		Pr	Pr vs. $\frac{1}{2} L$	Pr vs. $\frac{1}{4} L$
		L	b_l	h_c	$\frac{1}{2} L$	$\frac{1}{4} L$			
		[m]				[%]			
CSGL	B1	3.30	0.00	0.05	72	88	55	-17	-33
	B2		0.50		46	51	39	-7	-12
	B3		1.00		43	47	37	-6	-10
	B4		0.50		43	48	39	-5	-9
	B5		0.00		74	75	55	-20	-20
CSTL	B1	4.00	0.00	0.05	59	69	55	-5	-14
	B2		0.33		40	50	42	3	-8
	B3		0.67		42	47	37	-5	-10
	B4		1.00		47	47	37	-10	-9
	B5		0.67		37	44	37	-1	-8
	B6		0.33		41	52	42	1	-10
	B7		0.00		64	68	55	-9	-13

Table C.56 – Experimental vs. *Pr* polynomial predictions for *sr*: CSGL and CSTL

Specimen	Beam	x_1	x_2	x_3	<i>sr</i>			Differences	
					Experimental Loading		<i>Pr</i>	<i>Pr</i> vs. ½ L	<i>Pr</i> vs. ¼ L
		<i>L</i>	b_l	h_c	½ L	¼ L			
		[m]				[%]			
CSGL	B1	3.30	0.00	0.05	83	87	55	-28	-32
	B2		0.50		43	58	39	-4	-20
	B3		1.00		40	53	37	-2	-15
	B4		0.50		41	56	39	-3	-17
	B5		0.00		81	86	55	-27	-31
CSTL	B1	4.00	0.00	0.05	80	91	55	-26	-36
	B2		0.33		52	58	42	-10	-15
	B3		0.67		48	58	37	-11	-22
	B4		1.00		45	57	37	-8	-20
	B5		0.67		48	59	37	-11	-23
	B6		0.33		54	64	42	-12	-22
	B7		0.00		78	80	55	-23	-25

Table C.57 – Average partial differences: experimental vs. *Pr* for CSGL and CSTL

Specimen	Average partial differences					
	<i>vd</i> ½ L		<i>vd</i> ¼ L		<i>sr</i>	
	<i>Pr</i> vs. ½ L	<i>Pr</i> vs. ¼ L	<i>Pr</i> vs. ½ L	<i>Pr</i> vs. ¼ L	<i>Pr</i> vs. ½ L	<i>Pr</i> vs. ¼ L
	[%]					
	CSGL	-9	-12	-11	-17	-13
CSTL	-6	-4	-4	-10	-14	-23

Table C.58 – Experimental vs. $cf_{vd} \cdot Pr$ predictions for vd at $\frac{1}{2} L$: CSGL and CSTL

Specimen	Beam	$vd \frac{1}{2} L$			Differences	
		Experimental		$cf_{vd} \cdot Pr$	$cf_{vd} \cdot Pr$ vs. $\frac{1}{2} L$	$cf_{vd} \cdot Pr$ vs. $\frac{1}{4} L$
		Loading				
		$\frac{1}{2} L$	$\frac{1}{4} L$	[%]		
CSGL	B1	72	80	68	-4	-11
	B2	43	46	48	6	3
	B3	40	42	47	6	5
	B4	41	42	48	7	7
	B5	73	73	68	-5	-4
CSTL	B1	62	64	68	7	5
	B2	45	44	53	7	8
	B3	44	40	46	2	6
	B4	47	38	47	0	9
	B5	42	39	46	4	7
	B6	43	43	53	10	10
	B7	66	63	68	2	5

Table C.59 – Experimental vs. $cf_{vd} \cdot Pr$ predictions for vd at $\frac{1}{4} L$: CSGL and CSTL

Specimen	Beam	$vd \frac{1}{4} L$			Differences	
		Experimental		$cf_{vd} \cdot Pr$	$cf_{vd} \cdot Pr$ vs. $\frac{1}{2} L$	$cf_{vd} \cdot Pr$ vs. $\frac{1}{4} L$
		Loading				
		$\frac{1}{2} L$	$\frac{1}{4} L$	[%]		
CSGL	B1	72	88	68	-3	-19
	B2	46	51	48	3	-3
	B3	43	47	47	4	-1
	B4	43	48	48	5	0
	B5	74	75	68	-6	-6
CSTL	B1	59	69	68	9	-1
	B2	40	50	53	13	3
	B3	42	47	46	4	-1
	B4	47	47	47	0	0
	B5	37	44	46	8	1
	B6	41	52	53	12	1
	B7	64	68	68	5	1

Table C.60 – Experimental vs. $cf_{sr} \cdot Pr$ predictions for sr : CSHL and CSTL

Specimen	Beam	sr			Differences	
		Experimental		$cf_{sr} \cdot Pr$	$cf_{sr} \cdot Pr$	$cf_{sr} \cdot Pr$
		Loading			vs.	vs.
		1/2 L	1/4 L	1/2 L	1/4 L	
[%]						
CSHL	B1	83	87	88	5	1
	B2	43	58	62	19	3
	B3	40	53	60	20	7
	B4	41	56	62	21	6
	B5	81	86	88	6	2
CSTL	B1	80	91	88	7	-4
	B2	52	58	68	15	10
	B3	48	58	59	11	0
	B4	45	57	60	15	3
	B5	48	59	59	11	-1
	B6	54	64	68	14	3
	B7	78	80	88	10	8

